Novel design tools enabling to predict the quality of transmission and to design optical networks modulated at 10, 40, and 100Gb/s

Jean-Christophe Antona

▶ **To cite this version:**

Jean-Christophe Antona. Novel design tools enabling to predict the quality of transmission and to design optical networks modulated at 10, 40, and 100Gb/s. Optics / Photonic. Télécom ParisTech, 2011. English. NNT : . pastel-00678415

HAL Id: pastel-00678415
https://pastel.hal.science/pastel-00678415

Submitted on 12 Mar 2012

HAL is a multi-disciplinary open access archive for the deposit and dissemination of scientific research documents, whether they are published or not. The documents may come from teaching and research institutions in France or abroad, or from public or private research centers.

L'archive ouverte pluridisciplinaire **HAL**, est destinée au dépôt et à la diffusion de documents scientifiques de niveau recherche, publiés ou non, émanant des établissements d'enseignement et de recherche français ou étrangers, des laboratoires publics ou privés.

ParisTech
INSTITUT DES SCIENCES ET TECHNOLOGIES
PARIS INSTITUTE OF TECHNOLOGY

TELECOM ParisTech

Doctorat ParisTech

T H È S E

pour obtenir le grade de docteur délivré par

Télécom ParisTech
Spécialité " Electronique et Communications "

présentée et soutenue publiquement par

Jean-Christophe ANTONA

le 29 septembre 2011

Nouveaux outils pour l'estimation de la qualité de transmission et l'optimisation de réseaux optiques modulés à 10, 40 et 100Gb/s

Directeur de thèse : **Yves JAOUEN**
Co-encadrement de la thèse : **Sébastien BIGO**

Jury

M. Badr-Eddine BENKELFAT, Professeur, Télécom SudParis, Evry	Président
M. Christophe FINOT, Professeur, Université de Bourgogne, Dijon	Rapporteur
M. Michel JOINDOT, Professeur associé, ENSSAT, Lannion	Rapporteur
M. Alberto BONONI, Professeur, Università di Parma, Italie	Examinateur
M. Sébastien BIGO, Directeur de laboratoire, Alcatel-Lucent Bell-Labs	Examinateur
M. Yves JAOUEN, Professeur, Télécom ParisTech, Paris	Directeur de thèse
M. Erwan PINCEMIN, Ingénieur de recherche, Orange Labs, Lannion	Invité

T H È S E

Télécom ParisTech
Grande école de l'Institut Télécom – membre fondateur de ParisTech
46, rue Barrault – 75634 Paris Cedex 13 – Tél. + 33 (0)1 45 81 77 77 – www.telecom-paristech.fr

CONTENTS

RESUME

En seulement quelques années, nos moyens de communications ont changé de manière drastique. La révolution des télécommunications a vu le développement massif des communications mobiles, complété par celui des communications fixes, de l'internet, de la télévision numérique, le tout combiné sous forme d'offres triples ou quadruples et allant de pair avec une croissance perpétuelle des bandes passantes offertes. A titre d'exemple, les débits d'information typiques dont pouvait bénéficier l'utilisateur final étaient de 25 à 55kb/s il y a seulement 15 ans, alors qu'ils peuvent atteindre aujourd'hui jusqu'à 100Mb/s. Dans le réseau de transport, la quantité de trafic de données croît à un rythme de de +50% par an depuis plus de 20 ans, et cette croissance est aujourd'hui soutenue par l'émergence d'applications gourmandes en bande passante, telles que les services de vidéo haute-définition.

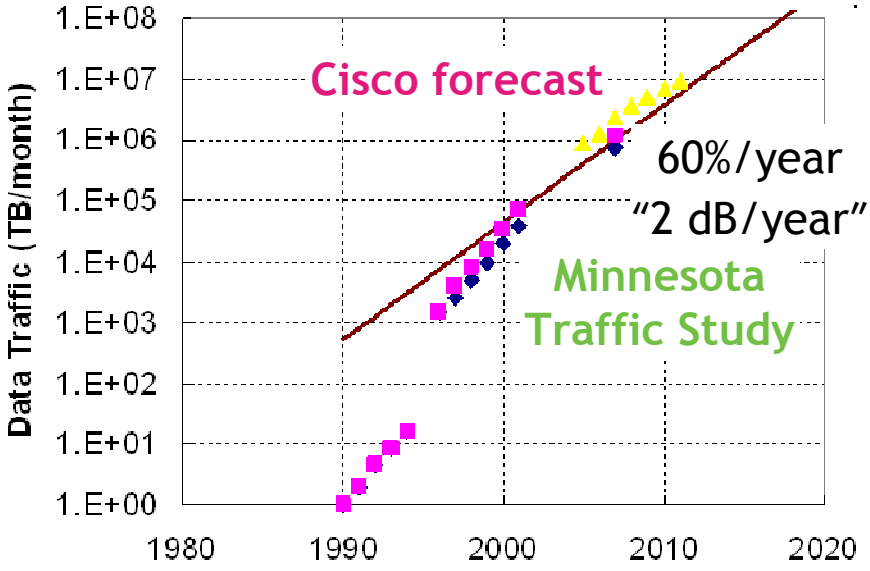

Figure A : Etude montrant l'évolution du traffic internet en Amérique du Nord (traffic mesuré et prédit) entre 1990 et 2012.
(D'après: R.W. Tkach, Bell-Labs Technical Journal, 14(4), 3-10, 2010)

Dans ce contexte, la fibre optique monomode s'est révélée être un support de transport des informations sans équivalent pour faire face à l'explosion du trafic. Le principal avantage de ce matériau réside dans son aptitude à guider de la lumière avec une atténuation très faible (<0.3dB/km) tout en offrant une bande passante très généreuse de l'ordre de 60THz pour des longueurs d'onde comprises entre 1.3 et 1.6μm. L'avènement des amplificateurs à fibre dopée à l'erbium à la fin des années 1980 a constitué l'un des tournants de l'histoire des systèmes de transmission sur fibre : ces derniers permettent en effet l'amplification optique simultanée de signaux optiques sur une fenêtre spectrale de 4THz, petite au regard des 60THz mais néanmoins immense au regard des autres moyens de transport d'information. Cette fenêtre spectrale est généralement remplie à l'aide d'une multitude de lasers opérants à différentes longueurs d'onde (jusqu'à ~100 typiquement) et modulés de manière indépendante par des informations à des débits allant de 2.5 à 10, 40 voire 100Gb/s aujourd'hui. La capacité de transport de tels systèmes de transmission sur fibres est alors

donnée par la somme des débits portés par chacun des lasers. De tels systèmes sont dits multiplexés en longueurs d'onde (ou WDM, Wavelength Division Multiplex).

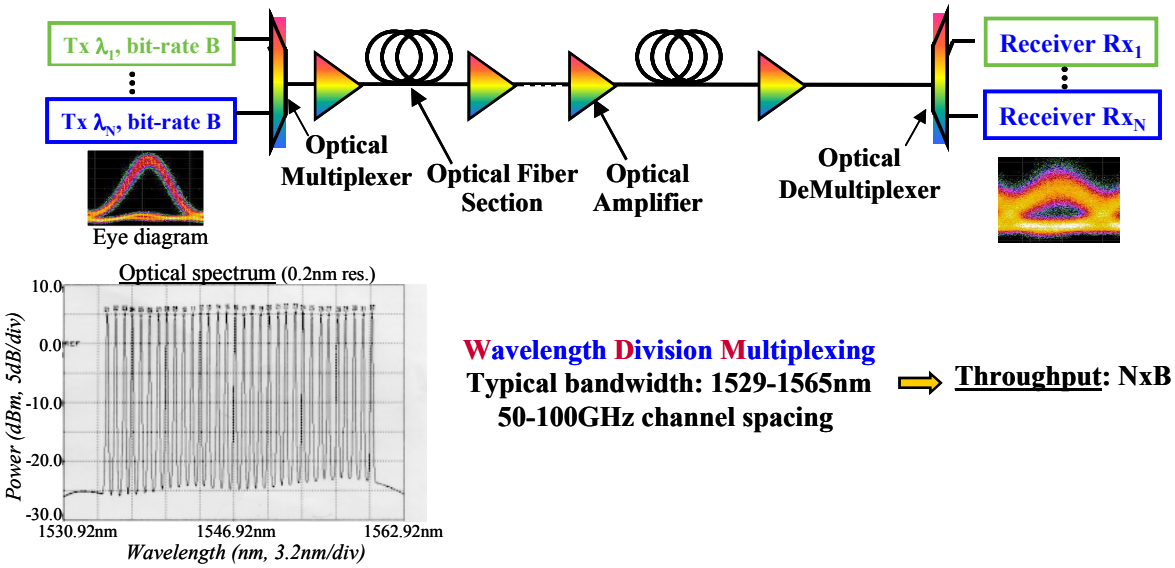

Figure B : Système de transmission WDM typique

Ils permettent de transporter cette capacité sur des milliers de kilomètres et de traverser de multiples nœuds de transit sans traitement optoélectronique. Ce faisant, les systèmes WDM ont permis de réduire de manière considérable le coût et la consommation électrique du bit d'information transmis, à tels point que la fibre optique est devenu le support de transport privilégié dans tous les segments des réseaux de télécommunications, des systèmes sous-marins transocéaniques aux réseaux dorsaux terrestres entre villes et régions, aux réseaux métropolitains (intra-région) et même jusque chez l'abonné.

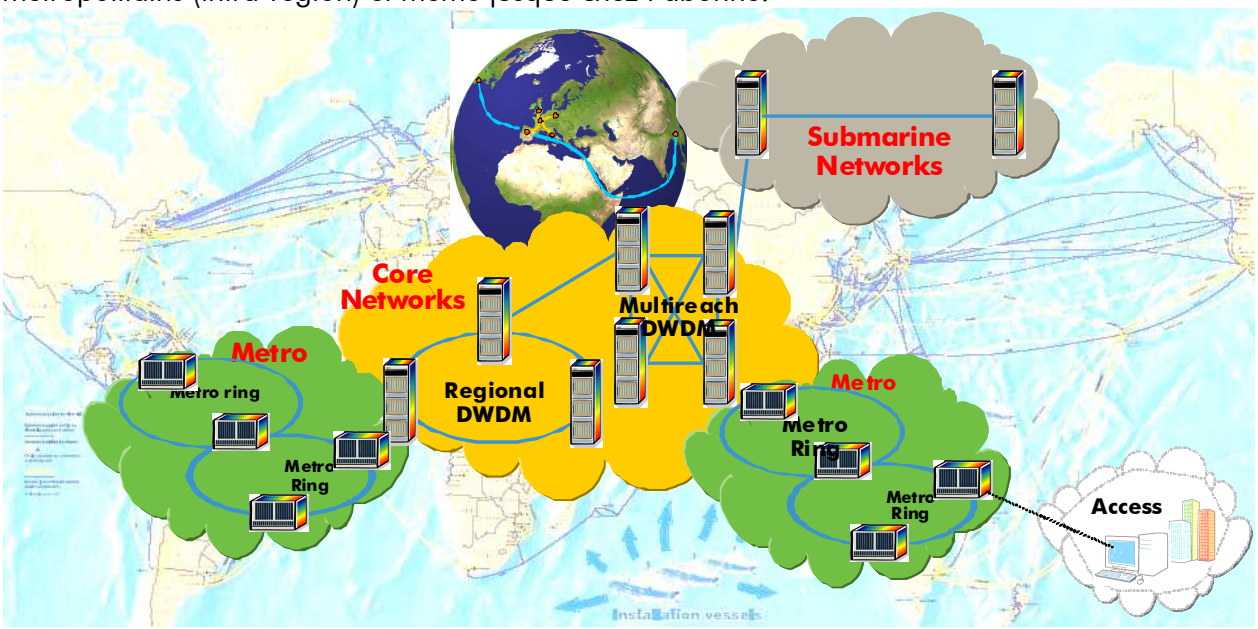

Figure C: Utilisation de la fibre optique sur les differents segments des réseaux de télécommunication

Depuis cette première étape, les voies d'amélioration des réseaux optiques WDM sont principalement les quatre suivantes : l'augmentation de la portée optique, c'est-à-dire la distance de transmission atteignable sans régénération optoélectronique du signal, y compris

lors de la traversée de nœuds intermédiaires ; l'augmentation des capacités de transport offerte, pour faire face à l'explosion du trafic ; davantage de flexibilité grâce à des reconfigurations automatiques ou à distance ; et une réduction de la consommation électrique et du coût du bit transporté.
La notion de portée est capitale pour un fournisseur d'équipements : si une connexion entre deux points distants d'un réseau n'est pas réalisable de manière toute-optique, il sera nécessaire d'installer le long du chemin parcouru des points de régénération optoélectronique du signal, au détriment du coût et de la consommation d'énergie. La portée dépend bien évidemment en tout premier lieu des avancées obtenues dans chacun des composants et technologies déployés dans de tels réseaux. Mais au delà de la qualité de ces technologies et composants, la performance effective d'un système déployé dépend également de la manière de combiner intelligemment tous ces dispositifs pour que la configuration globale soit optimisée ; enfin, la performance et le coût d'un système sont limités par les portées attendues, lesquelles sont liées aux **prédictions de performance** qui seront réalisées ainsi qu'à l'estimation de la précision qui est associée à ces prédictions.
Ces deux dernières problématiques peuvent se révéler particulièrement délicates en raison de la **complexité** sous-jacente à un réseau optique et sont particulièrement étudiées dans ce manuscrit. Cette complexité est tout d'abord liée à la multiplicité des dispositifs installés : émetteurs et récepteurs optoélectroniques, sections de fibre optique séparées par des amplificateurs otiques, nœuds d'aiguillage optique en ligne, égaliseurs de puissance optique, filtres optiques… En outre, les signaux optiques se propageant sont affectés par de multiples phénomènes physiques (atténuation, dispersion de vitesse de groupe, effets non-linéaires de type Kerr intra- et inter-canal, dispersion modale de polarisation, filtrage en ligne, diffusion Raman stimulée…) et sont impactés par l'accumulation de bruit optique (diaphotie lors la traversée de nœuds, bruit d'émission spontanée amplifiée).

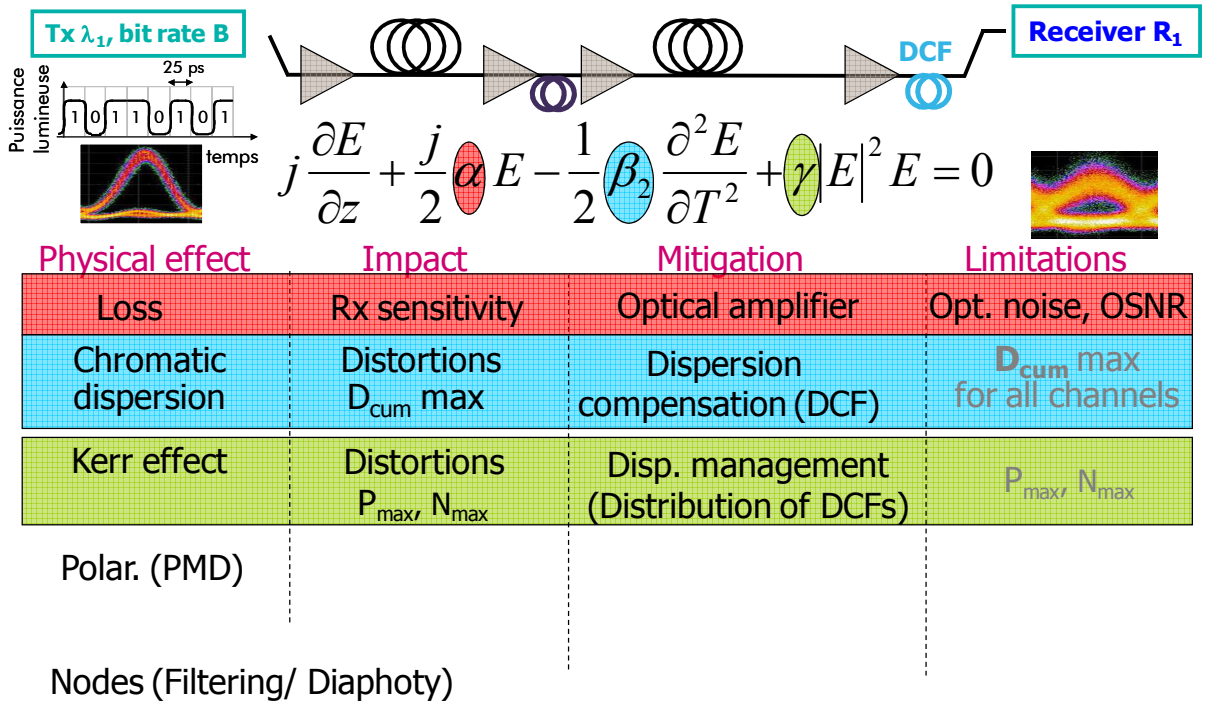

Figure D: Principaux effets de propagation et leur impact

La complexité d'un réseau optique provient également de sa nature. Lors de la conception de systèmes de transmissions sous-marines à ultra-longue distance, les distances à atteindre sont si grandes que les liens sont conçus de manière optimale, proche des conditions que l'on peut

retrouver dans un laboratoire, et la complexité du système est réduite de par son homogénéité : toutes les sections de fibre ainsi que les amplificateurs optiques déployés sont identiques et leurs caractéristiques sont optimisées, tel que l'espacement entre amplificateurs compris entre 40 et 80km en fonction des portées à atteindre.
En revanche, la complexité inhérente à un **réseau optique terrestre** est renforcée par l'**hétérogénéité** du système. Tout d'abord, la distribution spatiale des amplificateurs optiques et des nœuds ne peut généralement pas être optimisée mais est plutôt imposée par des contraintes topologiques, géographiques ou démographiques : ainsi l'espacement entre amplificateurs n'est pas constant le long d'un chemin optique entre un émetteur et un récepteur mais varie d'un amplificateur à l'autre dans une plage comprise entre 10 et 150km. En outre, un des éléments caractéristiques d'un réseau terrestre est la propension très grande à réutiliser les infrastructures préexistantes lors d'un déploiement d'un nouveau réseau, en particulier les fibres installées. En conséquence, les activités de systémier et de fabriquant de fibre deviennent indépendantes : le systémier cherchera bâtir un réseau optique de grande performance à partir d'une infrastructure fibrée existante qu'il ne peut modifier (sauf peut-être de manière localisée au niveau des sites d'amplification) et dont les caractéristiques ne sont que partiellement connues. De manière plus large, un environnement terrestre est beaucoup plus contraint qu'un environnement sous-marin, et le degré de **connaissance des caractéristiques des éléments traversés** y est bien plus faible. De plus, le développement progressif de réseaux toujours plus gros et permettant de transporter toujours plus d'informations a une contrepartie : une hétérogénéité possible et même très fréquente dans les types de fibres déployées sur un même réseau marquée par des caractéristiques potentiellement très différentes, notamment en matière de dispersion de vitesse de groupe (pouvant varier de plus d'un ordre de grandeur) et par ricochet en matière de tolérance aux effets non-linéaires de type Kerr. Enfin, l'hétérogénéité d'un réseau terrestre se manifeste également en termes de types de modulations ainsi que de débits transmis entre émetteurs et récepteurs.
Dans ce contexte de réseaux terrestres, la conception intelligente de tels systèmes ainsi que la prédiction de leur performance sont des activités particulièrement délicates. En particulier, **la performance effective d'un réseau optique est généralement bornée par la performance prédite** : en effet, la phase de conception du système est planifiée avant son installation et donc avant que d'hypothétiques mesures puissent être réalisées sur le terrain. La précision associée à une prédiction de la faisabilité physique d'une connexion toute optique a donc un impact direct sur le nombre et la localisation des dispositifs de régénération optoélectronique du signal ; elle a donc un impact direct sur le coût et la consommation énergétique du réseau. En conséquence, un équipementier télécom cherchera à **réaliser des prédictions de performance avec la précision la plus fine possible**, dans les limites imposées par le degré de connaissance des caractéristiques de l'infrastructure de manière à minimiser l'utilisation de marges systèmes et le surdimensionnement en dispositifs de régénération qui permettent d'éviter le déploiement de connexions non viables physiquement. Cependant, la précision n'est pas le seul critère à prendre en compte pour rendre un outil d'estimation de la performance physique compatible avec une exploitation dans un réseau optique : la **complexité** ainsi que le **temps de calcul** de l'outil sont des paramètres qu'il convient de ne pas négliger, ce qui implique de trouver des compromis. En effet, contrairement à un lien de transmission point à point, il n'est la plupart du temps pas possible d'utiliser des expériences ou même des simulations numériques dédiées pour prédire la qualité de transmission dans un réseau optique de toutes les connexions entre nœuds possibles, d'autant que l'infrastructure est hétérogène et doit également être optimisée. Enfin, il convient de garder à l'esprit que la tâche consistant à prédire la performance physique d'une connexion n'est qu'une des composantes de la phase de dimensionnement du réseau qui comprend en outre les étapes de routage du trafic et du dimensionnement des ressources à allouer. Cette phase intervient généralement lors de la planification du réseau préalable à l'établissement d'une offre d'un équipementier vers un opérateur et donc à l'installation. Cette

même phase peut également intervenir pendant la vie du réseau pour permettre une reconfiguration rapide du réseau de manière à répondre à l'arrivée d'une nouvelle demande de connexion ou à l'irruption d'une panne dans le réseau. Dans ces conditions, nous pouvons donc comprendre que le temps de calcul d'un outil de prédiction de performance soit également un critère important et que des compromis entre précision, temps et complexité de calcul doivent être recherchés, en se basant sur des modèles issus d'une connaissance fine de la physique et d'observations expérimentales.

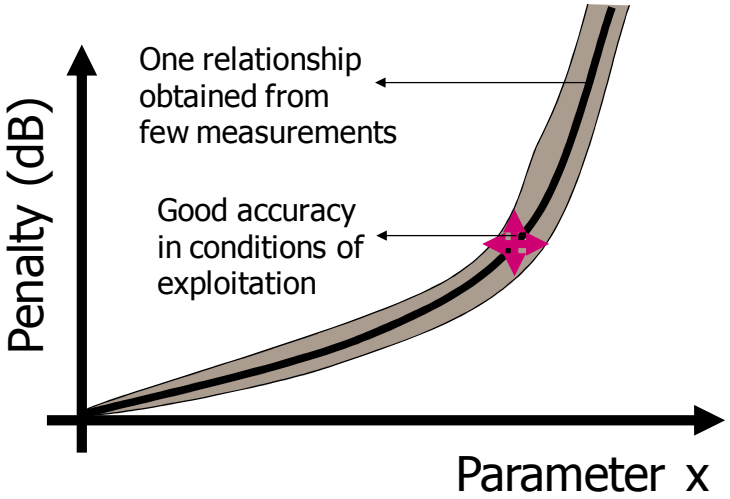

Figure E:Illustration de la quête d'un paramètre X, simple, synthétique, cumulatif qui puisse être relié à la pénalité de transmission et qui permette (après quelques calibrations) de prédire la performance physique avec précision malgré la complexité d'un système de transmission terrestre

Le présent manuscrit est donc une plongée dans cette problématique : m'appuyant sur des études originales permettant de comprendre et de quantifier l'accumulation de non-linéarités optiques de type Kerr, l'objectif est ici d'introduire tout à la fois de nouveaux outils permettant une estimation rapide et précise à la fois de la qualité de transmission dans un contexte de réseaux hétérogènes et également de proposer des guides pour concevoir et régler de tels systèmes (relatifs notamment à la distribution de la dispersion chromatique le long de la ligne ou au réglage des puissances de sorties des amplificateurs optiques).
Ce manuscrit correspond à des travaux que j'ai essentiellement conduits ou supervisés entre 2000 et 2011 dans les laboratoires du domaine de recherche Réseaux Optiques au sein du centre de recherche d'Alcatel, aujourd'hui Alcatel-Lucent Bell-Labs. Pendant ces années, mon statut dans ces laboratoires a évolué d'ingénieur de recherche à responsable de projet et puis à celui de directeur d'un groupe de recherche de 12 personnes étudiant les aspects physiques et logiques de réseaux optiques dynamiques. La plupart des travaux présentés dans ce document ont trait aux activités de recherches auxquelles j'ai le plus contribué avant d'occuper mon poste de responsable d'un groupe de recherche, c'est-à-dire aux systèmes de transmission modulés à 10 et 40Gb/s utilisant des techniques de détection non- cohérente. Lors du dernier chapitre de ce document, ces travaux sont mis en perspective par rapport à des études plus récentes de mon groupe traitant de systèmes modulés à 100Gb/s et basés sur de la détection cohérente. J'ai contribué à ces derniers travaux principalement au travers de l'encadrement d'un étudiant en thèse, Edouard Grellier.

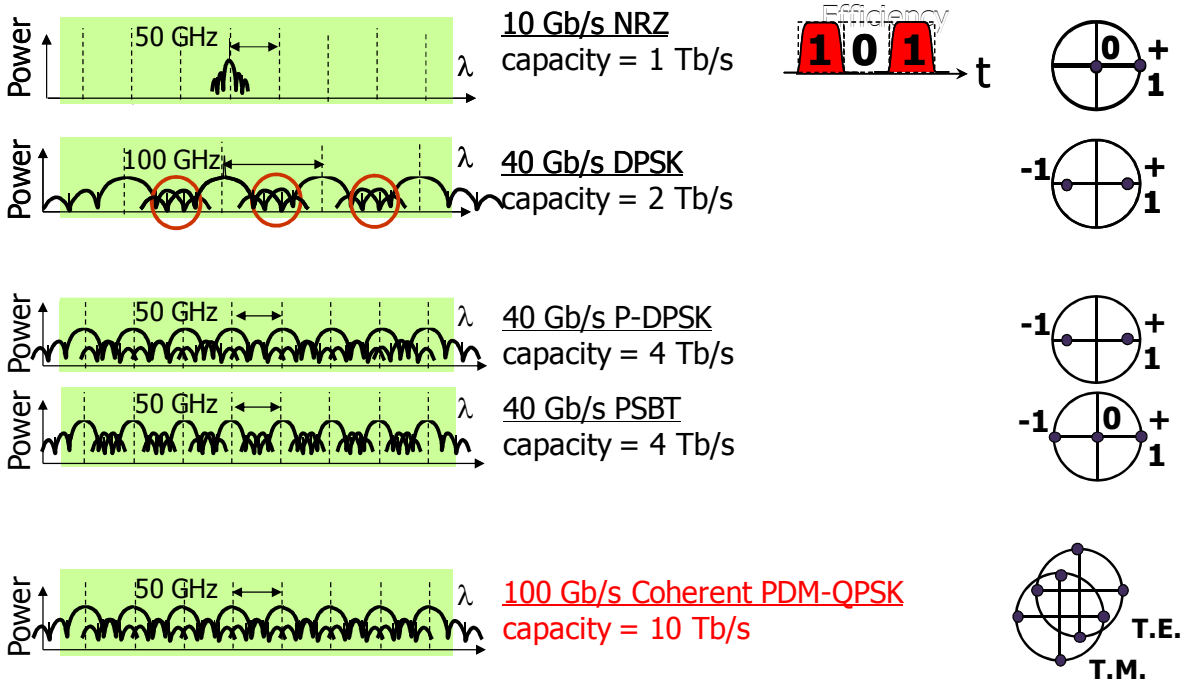

Figure F: Modulations et débits considérés dans ce manuscrit

Par rapport à l'état de l'art, le point de départ de cette aventure a consisté à démontrer, en 2001, au moyen d'une kyrielle de simulations numériques, qu'un paramètre aussi simple que la phase non-linéaire servant à décrire le pur effet Kerr puisse être un excellent candidat pour décrire l'impact de tous les effets non-linéaires d'importance notable pour les systèmes de transmissions usuels dégradés simultanément par une multitude d'effets physiques tels que la dispersion chromatique. Nous avons ensuite étudié en profondeur les limites d'un tel modèle et proposé des adaptations afin de tenir compte de l'hétérogénéité des systèmes. Par la suite, nous avons déduit de ces travaux un certain nombre d'outils simples permettant d'estimer rapidement, mais aussi avec une précision suffisante, la qualité de transmission à partir d'un nombre limité de paramètres synthétiques, l'objectif avoué étant que ces outils puissent être utilisés lors de l'opération de réseaux optiques basés notamment sur une couche de control GMPLS (Generalized Multi Protocol Label Switching). Enfin, nous avons proposé des guides permettant de régler les puissances de sorties des amplificateurs optiques dans ce conexte de réseaux hétérogènes.

Le manuscrit est ainsi organisé de la façon suivante.

Le **Chapitre 1** pose les bases des systèmes de transmissions optiques et des réseaux optiques multiplexés en longueur d'onde (WDM, Wavelength Division Multiplex), puis décrit les principaux effets physiques en jeu, ainsi que les méthodes utilisées pour émuler ou caractériser de tels systèmes.

Ensuite, la caractérisation non-linéaire de systèmes débute par le biais de mesures expérimentales du coefficient non-linéaire d'un échantillon représentatif des fibres les plus répandues. Ces travaux ont été réalisés en générant du mélange à 4 ondes issu de deux ondes continues incidentes à des longueurs d'ondes dans les matériaux à mesurer.

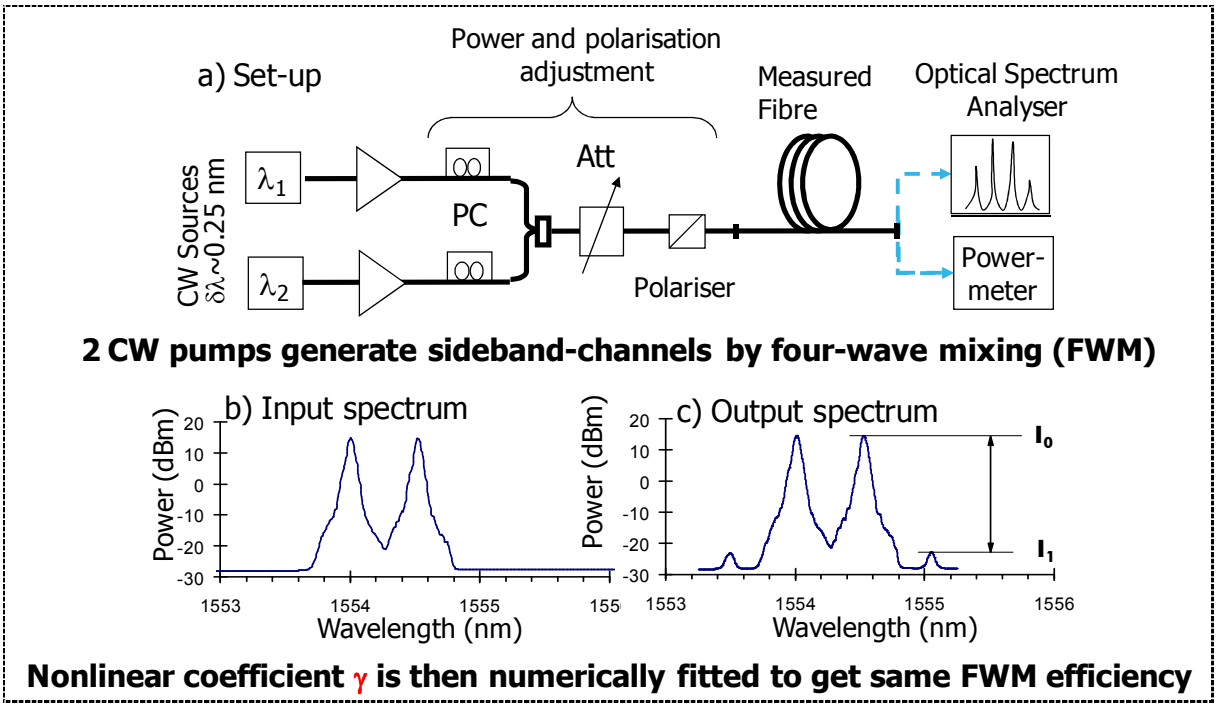

Figure G:Protocole expérimental servant à déterminer le coefficient non-linéaire d'une fibre par mélange à quatre ondes.

De telles mesures, publiées à la conférence ECOC en 2001, ont servi de base pour toutes les simulations numériques que j'ai réalisées par la suite.

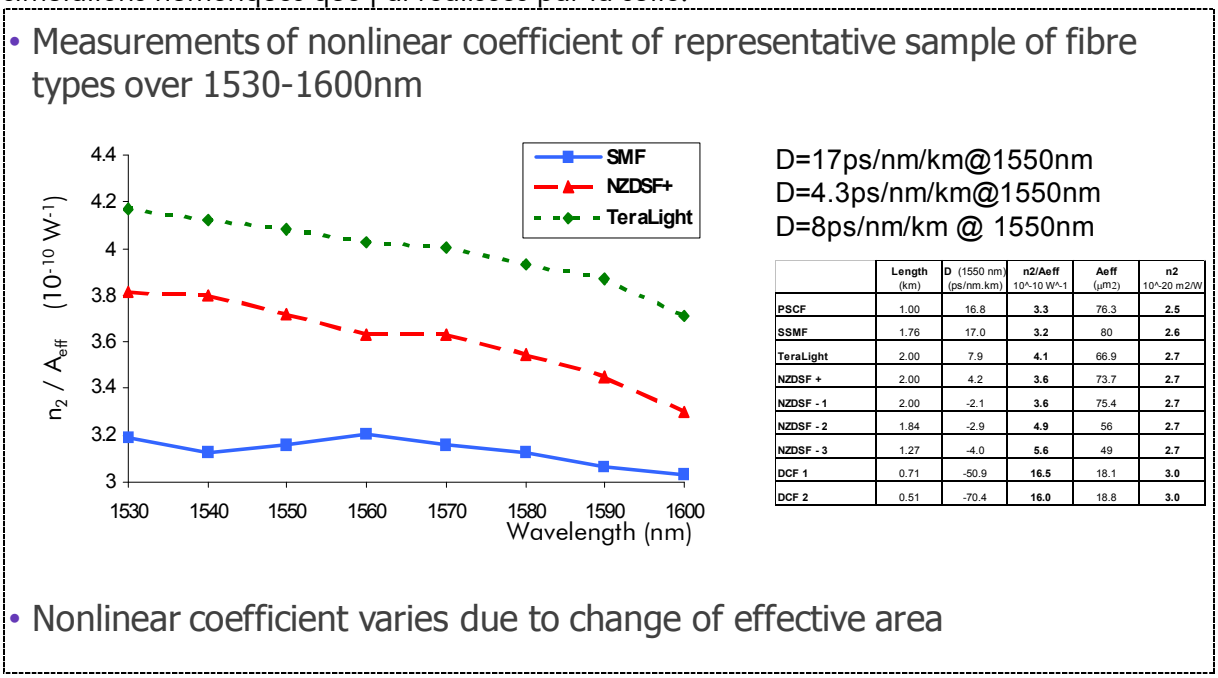

	Length (km)	D (1550 nm) (ps/nm.km)	n2/Aeff 10^-10 W^-1	Aeff (μm2)	n2 10^-20 m2/W
PSCF	1.00	16.8	**3.3**	76.3	**2.5**
SSMF	1.76	17.0	**3.2**	80	**2.6**
TeraLight	2.00	7.9	**4.1**	66.9	**2.7**
NZDSF +	2.00	4.2	**3.6**	73.7	**2.7**
NZDSF - 1	2.00	-2.1	**3.6**	75.4	**2.7**
NZDSF - 2	1.84	-2.9	**4.9**	56	**2.7**
NZDSF - 3	1.27	-4.0	**5.6**	49	**2.7**
DCF 1	0.71	-50.9	**16.5**	18.1	**3.0**
DCF 2	0.51	-70.4	**16.0**	18.8	**3.0**

Figure H: Mesures de coefficients non-linéaires des fibres les plus répandues dans les systèmes de transmission terrestres et sous-marins. Publié à ECOC 2001.

Nous décrivons enfin également la méthode utilisée pour conduire les études lors des chapitres suivants dans notre quête d'un critère simple permettant de prédire les distorsions du signal induites par les effets non-linéaires dans un environnement complexe et hétérogène : nous sommes en effet à la recherche d'un paramètre simple, cumulatif, qui puisse être relié la pénalité de transmission par une relation déductible d'un nombre limité de mesures et tel

que cette relation offre une bonne précision dans les conditions d'exploitation des systèmes de transmission, , sachant que la tâche n'est pas aisée de prime abord.

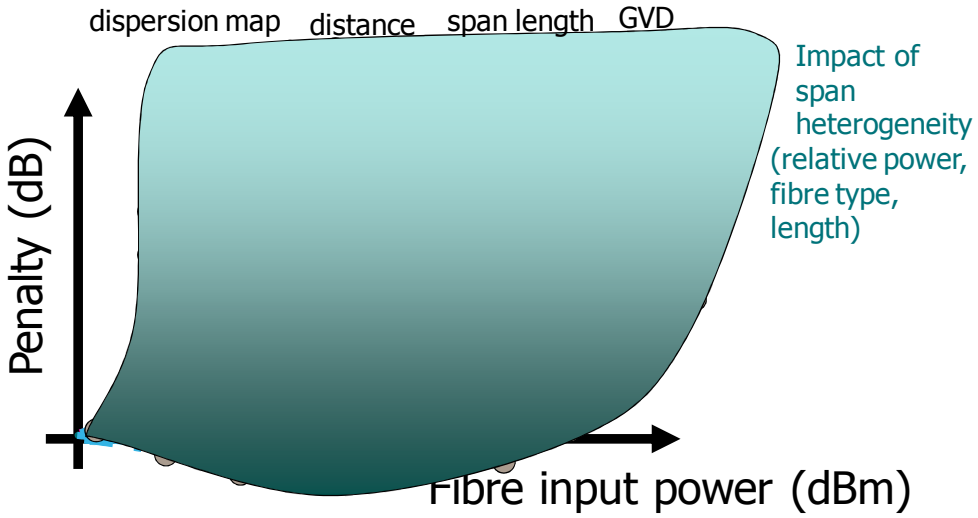

Figure I: Illustration de l'inadéquation d'utiliser la seule puissance optique injectée dans les fibres pour prédire la pénalité de transmission dans un environnement terrestre typique.

Pour ce faire nous fixons un certain nombre de contraintes externes, telles que la stratégie de gestion de la dispersion chromatique le long des lignes, mais recherchons une relation capable de gérer un certain nombre de paramètres libres tels que la distance, la puissance optique injectée dans une fibre, le type de fibre, la longueur des fibres entre amplificateurs, le tout dans un cadre hétérogène.

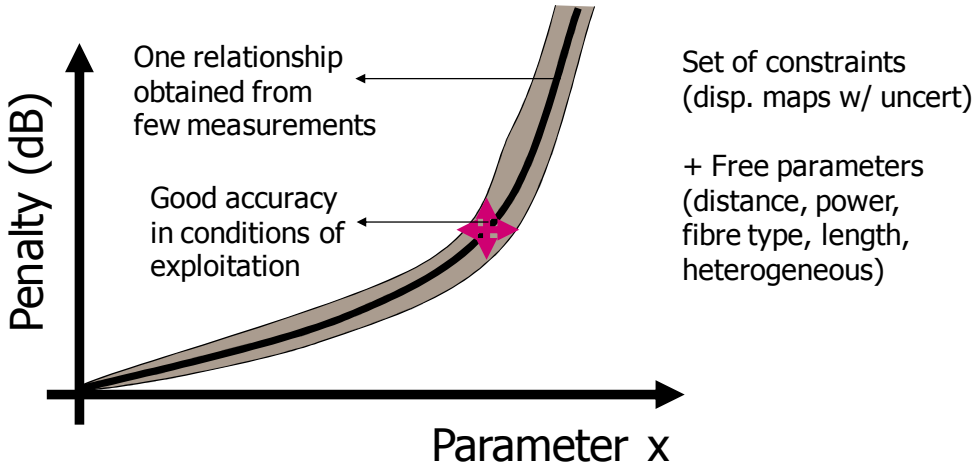

Figure J:Illustration de la quête d'un paramètre X servant à prédire la performance à partir de quelques calibrations, autorisant un certain nombre de paramètres libres et considérant comme fixes quelques contraintes telles que la stratégie de dispersion ou le type de fibre de transmission.

La démarche suivie au cours des chapitres suivants consiste alors à proposer de tels critères en allant des systèmes les plus simples, idéaux, homogènes, vers les cas complexes, pratiques, hétérogènes. Les chapitres 2 à 5 sont relatifs aux seuls systèmes de transmission modulés à 10 et 40Gb/s, alors que le chapitre 6 est une plongée vers les systèmes modulés en phase et en polarisation à 100Gb/s et exploitant la détection cohérente.
Le Chapitre 2 a pour but de construire un outil qui prédise l'impact de l'effet Kerr sur la qualité du signal avec une précision et un temps de calcul raisonnables. Nous revisitons ici tout d'abord le paramètre phase non-linéaire $\overline{\Phi}_{NL}(L) = \int_0^L \gamma \overline{|E|^2}(z) dz$ (ou E est l'enveloppe du

signal optique et γ est le coefficient non-linéaire à la distance z) censé décrire l'effet Kerr moyenné dans le temps en absence d'autre effet de propagation. Nous démontrons de manière numérique qu'il est possible de construire une relation localement bijective entre la pénalité de transmission et la phase non-linéaire moyenne avec une précision remarquable dans le cadre de systèmes terrestres WDM périodiques impactés simultanément par la dispersion chromatique et l'effet Kerr quels que soient les distances de transmissions ou les puissances d'injection du signal dans les fibres, moyennant l'hypothèse d'une gestion de dispersion optimisée (c'est-à-dire une optimisation de la distribution de la dispersion chromatique le long du système par l'entremise de modules de compensation de dispersion, DCF).

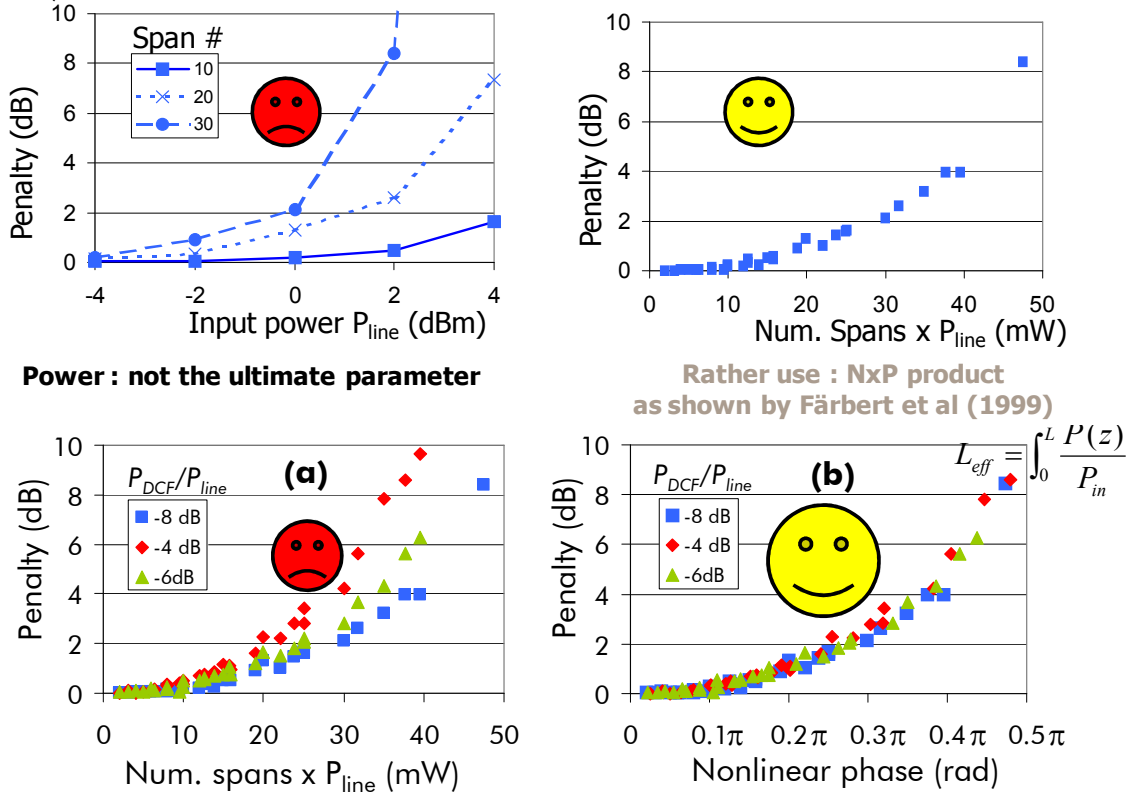

Figure K: Simulations numériques WDM réalisées à 40Gb/s (9 canaux RZ espacés de 100GHz), propagation sur un nombre variable de sections de fibre SMF gérée en dispersion (par le biais de l'utilisation périodique de fibres à compensation de dispersion, DCF, et pour des puissances d'injections dans les fibres variables. A chaque point correspond une gestion de dispersion optimisée. Les figures représentent l'évolution de la pénalité de transmission en fonction de divers paramètres (puissance, produit puissance et nombre de section de fibre de transmission, phase non-linéaire). Figures du haut/bas : absence/ présence de non-linéarités dans la DCF. La figure en bas à droite illustre la pertinence du paramètre phase non-linéaire, relié de manière quasi-bijective à la pénalité quels que soient les 105 configurations de puissances et distances (issus de plus de 300 000 simulations).

Une telle relation dépend également de la dispersion locale de la fibre de transmission, des caractéristiques du couple transmetteur / récepteur (notamment le débit et le format de modulation) et de l'espacement spectral entre canaux WDM. Nous définissons alors le critère phase non-linéaire comme l'aptitude à prédire les pénalités de transmission en fonction du seul paramètre phase non-linéaire (après une rapide calibration de la relation), ainsi que les notions de pénalité seuil, de seuil non-linéaire (NLT) et de précision associés.

Nonlinear phase criterion and accuracy

- Calibration curve from few measurements, eg constant power and variable distance

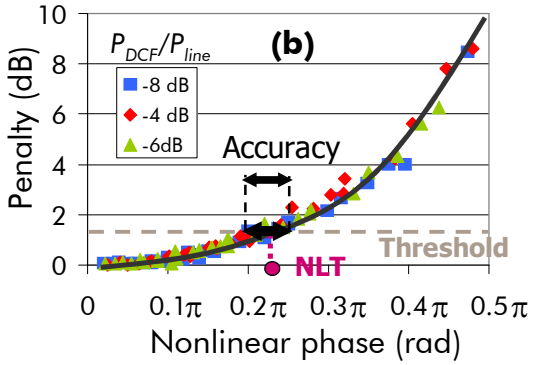

$Pen_{est,dB}(\phi_{nl}) = 38.5\ \phi_{nl}^2 - 2.5\ \phi_{nl}$

- Differences between estimated penalty and measured penalty : 0.3dB RMS

Nonlinear phase criterion:

- use ϕ_{nl} as the metrics to predict system penalty

Penalty threshold: typically 1.5dB at 40Gb/s. (1dB/dB slope is remarkable)

Nonlinear threshold (NLT): Φ_{nl} yielding penalty threshold. Here ~ 0.23π.

Accuracy: Ratio of max and min possible values of nonlinear phase leading to a penalty threshold, and expressed in dB. Acceptable if lower than 1.5dB. Here 0.9dB.

Different relationships depending on format, bit-rate, fiber type, ch. spacing

Figure L: Illustration du critère phase non-linéaire et des notions de précision et seuil-non-linéaire.

Le chapitre s'ouvre alors sur une investigation d'outils analytiques plus sophistiqués issus de modèles petit-signal ou d'approches perturbatrices de l'équation de propagation non-linéaire et sur une étude de leur aptitude à prédire les distorsions du signal induites par l'effet conjoint de la dispersion chromatique et de l'effet Kerr. Nous montrons qu'ils permettent d'acquérir une connaissance plus fine de la physique des systèmes en jeu, de simplifier l'optimisation de la gestion de la dispersion chromatique, mais qu'ils n'offrent pas une meilleure précision que ne peut l'offrir un outil simple de prédiction basé sur la phase non-linéaire, malgré une augmentation très substantielle de la complexité de calcul. Cependant, ces modèles analytiques nous confirment qu'il est possible de modéliser l'accumulation des distorsions du signal comme une combinaison linéaire des phases non-linéaires provenant de chaque section de fibre, combinaison qui s'avère entièrement compatible avec le critère phase non-linéaire moyennant certaines hypothèses de débit et de gestion de dispersion. Enfin, ces modèles analytiques nous permettent de pressentir le domaine de validité du critère phase non-linéaire et serviront à renforcer/étendre le critère phase non-linéaire dans un contexte de système de transmission terrestre hétérogène dans le chapitre 3.

Après avoir considéré des systèmes de transmissions terrestres homogènes, périodiques et bénéficiant de conditions d'opération optimales (notamment en matière de gestion de dispersion), le **Chapitre 3** a maintenant pour but d'investiguer le domaine de validité de notre outil de prédiction basé sur la phase non-linéaire dans des conditions d'utilisations exotiques tout autant que réalistes, avant de proposer une généralisation de l'outil à des systèmes hétérogènes.

Nous établissons en premier lieu la précision du critère phase non-linéaire dans des conditions homogènes à 10 et 40Gb/s à partir de simulations numériques tout autant que d'expériences. Dans un premier temps, nous établissons que ce critère ne permet pas de prédire la performance de systèmes basés sur une seule section de fibre à partir d'une relation

valable pour plusieurs sections de fibres. Ensuite, nous étudions l'impact sur a précision du critère des puissances optiques injectées dans les fibres (les fibres de transmission ainsi que les modules de compensation de dispersion) bien au delà des conditions typiques d'opération. Dans un troisième temps, nous établissons la dépendance de la précision du critère en fonction de la longueur des sections de fibre et confirmons que la relation liant la pénalité et la phase non-linéaire ne dépend pas que de la valeur de dispersion chromatique locale de la fibre de transmission, mais plutôt de son produit avec la longueur effective d'atténuation de la fibre ainsi que du carré de la fréquence de modulation, en accord avec les modèles analytiques développés au chapitre 2. Dans un quatrième temps, nous investiguons l'impact de la gestion de dispersion sur la précision du critère, au travers de stratégies de gestion de dispersion non idéales, mais plus typiques de cas réels, nous apprenant que dans la mesure où le produit entre dispersion chromatique cumulée en ligne et carré de la fréquence de modulation restent faibles à 10 et 40Gb/s, le critère reste suffisamment précis. A 40Gb/s, pour des systèmes non-cohérents modulés à 2 niveaux d'intensité ou de phase, ceci est notamment dû au fait que les valeurs maximales souhaitables de dispersion cumulée en ligne doivent rester suffisamment faibles pour que les effets non-linéaires n'aient un impact trop significatif. L'ensemble de ces études nous permet de garantir que dans les conditions typiques d'utilisation, la précision du critère reste meilleure que 1.5dB, moyennant le couplage entre dispersion et longueur de fibre.
Enfin, nous étudions la problématique de l'hétérogénéité de fibre de transmission en termes de dispersion chromatique, ce qui est typique des systèmes déployés. Dans la mesure où nous avions précédemment établi que la relation liant pénalité et phase non-linéaire dépendait de la dispersion chromatique de la fibre de transmission, le critère phase non-linéaire n'apparait plus comme adapté et sa précision se dégrade singulièrement, dépassant parfois les 5dB. Nous appuyant alors sur les modèles analytiques du chapitre 2 laissant espérer qu'il est possible de modéliser l'accumulation des distorsions du signal comme une combinaison linéaire des phases non-linéaires provenant de chaque section de fibre, nous généralisons alors le concept de phase non-linéaire au concept de phase non-linéaire pondérée. Celui-ci est basé sur l'utilisation pour chaque section de fibre de la phase non-linéaire issue de cette section, normalisée par le seuil non-linéaire (associé à une valeur seuil de pénalité, typiquement 1.5dB) correspondant à ce type de fibre, et de sommer ces contributions normalisées pour en déduire une valeur de phase non-linéaire pondérée totale. Nous avons alors démontré, tant numériquement qu'expérimentalement, que le critère phase non-linaire pondérée ainsi obtenu nous garantit maintenant une très bonne précision dans les configurations hétérogènes et qu'une valeur de phase pondérée inférieure à 100% nous garantissait également une pénalité inférieur à la pénalité seuil. L'outil ainsi dérivé est alors compatible avec une utilisation pour des systèmes déployés, et non plus seulement avec des expériences de laboratoire.

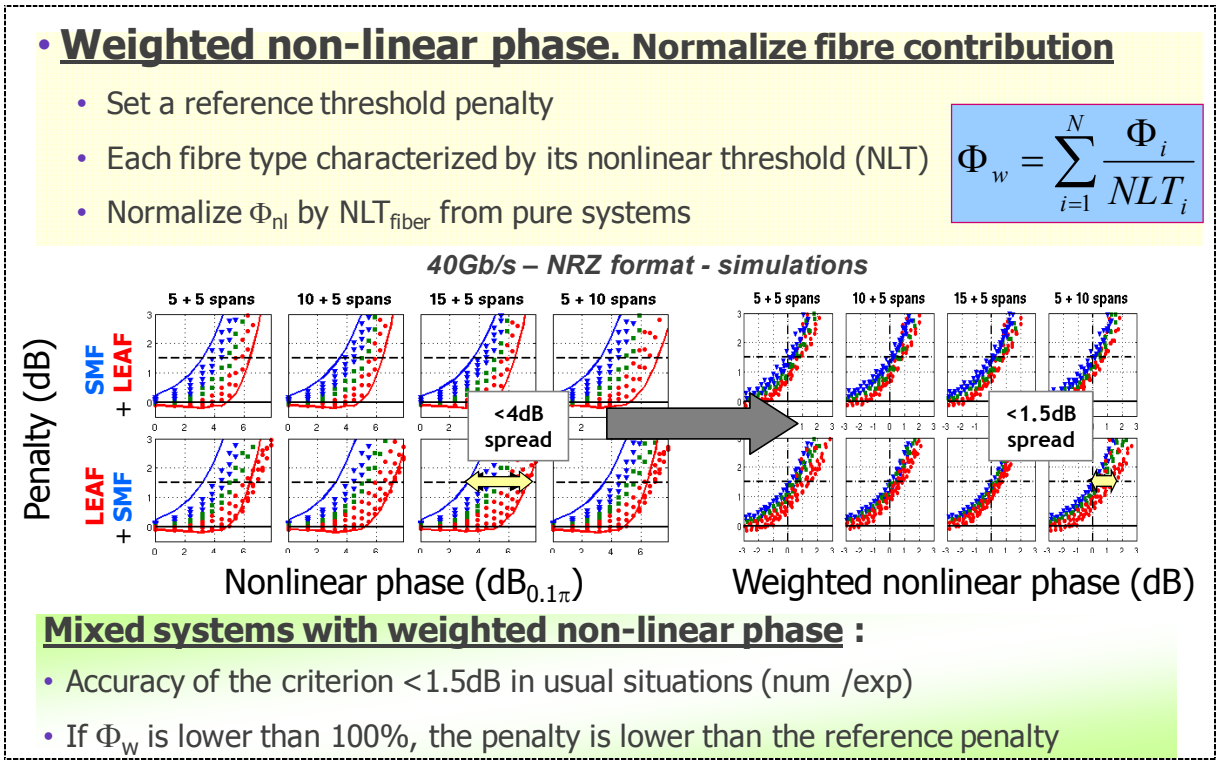

Figure M: Illustration du critère phase non-linéaire pondérée et de sa précision pour un système hybride à base de fibre LEAF et SMF et basé sur une modulation NRZ à 40Gb/s (9 canaux espacés de 100GHz). Simulations numériques.

Dans les deux chapitres suivants, nous exploitons cette aptitude à prédire les pénalités induites par l'effet Kerr avec une précision acceptable grâce à la phase non-linéaire (pondérée). Nous élaborons alors des estimateurs de la qualité de transmission prenant en compte d'autres effets de propagation que les non-linéarités Kerr ou la dispersion chromatique.

Le **chapitre 4** est ainsi dédié à la méthode que nous avons employée pour élaborer un outil prédisant la qualité de transmission (QoT, Quality of Transmission) de signaux impactés par de multiples effets de propagation et de multiples sources de dégradation du signal (tels que les bruit des amplificateurs optiques, l'effet Kerr, la dispersion chromatique, les effets de polarisation, l'impact du filtrage en ligne, de la diaphotie). Une attention particulière est donnée à la recherche d'outils à la fois simples et précis, l'objectif étant de permettre d'estimer si une connexion est faisables de manière toute-optique entre deux points d'un réseau maillé, lors de la phase de planification aussi bien qu'en phase d'opération.

Le **chapitre 5** propose la construction d'un estimateur de la qualité de transmission plus simple, focalisé sur les compromis entre effets Kerr et accumulation du bruit qui fixent souvent les distances de transmission atteignables de manière toute-optique. La motivation est ici de déduire des études précédentes des expressions très simples pour prédire la portée de systèmes tout en permettant d'identifier et d'isoler l'impact sur cette portée du couple émetteur/récepteur, de la chaine d'amplification ou des fibres traversées. Ces règles simples permettent alors d'optimiser quelques éléments individuellement pour maximiser la portée du système complet. Par ailleurs, ces règles permettent également d'optimiser les puissances optiques injectées dans les fibres, quelle que soit l'hétérogénéité du système en termes de types ou longueurs de fibres. Toutes ces règles s'appuient sur l'identification d'un couple singulier « phase non-linéaire pondérée et pénalité » correspondant au point de fonctionnement ultime du système. Dans ce chapitre, une illustration de l'utilité de telles règles est donnée à travers l'optimisation d'un schéma d'amplification optique hybride Raman + Erbium qui a servi de configuration de référence pour la conception d'expériences de très

longues distances présentées en session post-deadline lors de conférences majeures entre 2001 et 2003.

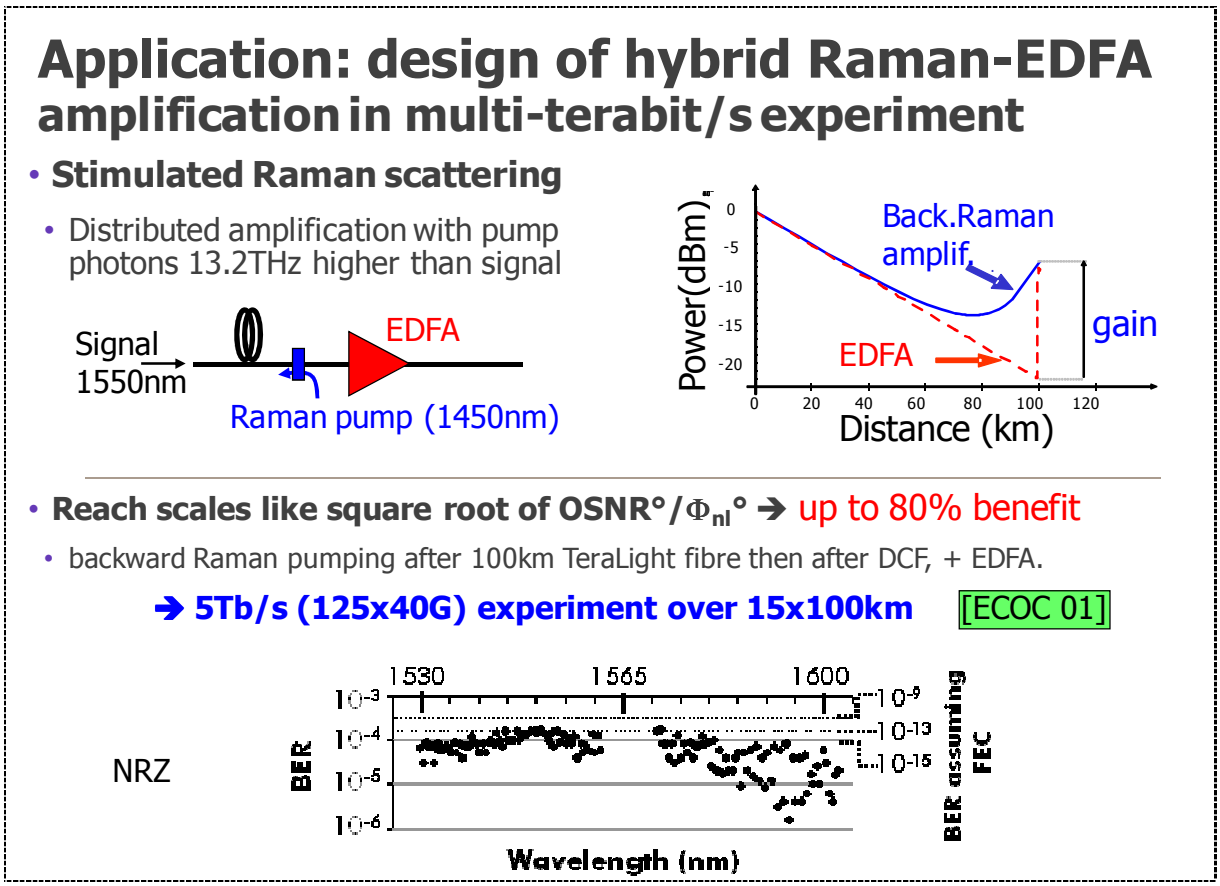

Figure N:application des règles définies au chapitre 5 pour estimer simplement la portée d'un système au cas de l'optimisation d'un schéma hybride d'amplification optique Erbium et Raman en maximisant le ratio entre phase non-linéaire et dégradation de l'OSNR sur un tronçon de fibre de transmission amplifié, et application à une des première expériences de transmission longue distance à 40Gb/s présentée à ECOC en 2001 en session postdeadline, permettant la transmission de 125 canaux NRZ modulés à 40Gb/s sur 12 puis 15 sections de 100km de fibre TeraLight Ultra avec un taux d'erreurs binaire meilleur que 2 10^{-4}.

Finalement, dans le **Chapitre 6**, nous revisitons brièvement les concepts proposés dans le contexte des systèmes de transmissions apparus récemment, c'est-à-dire exploitant des formats de modulation multi-niveaux à 40-100Gb/s associés à de la détection cohérente assitée par traitement numérique du signal. Nous montrons tout d'abord que les concepts proposés jusqu'à présent s'appliquent avec une précision équivalente si l'on conserve les infrastructures et stratégies de gestion de dispersion traditionnelles. Cependant, nous montrons aussi que la tolérance à l'effet Kerr peut être grandement améliorée hors des conditions d'utilisation classiques, favorisant alors des régimes fortement dispersifs pour lesquelles la dispersion cumulée en ligne totale est typiquement 1 à 2 ordres de grandeur plus importantes que pour les architectures traditionnelles. Dans ces nouvelles conditions, la phase non-linéaire ne suffit plus à prédire la pénalité de transmission quelles que soient la distance ou la puissance optique, et le critère phase non-linéaire (pondérée) doit être adapté, ce qui semble en accord avec les limites pressenties en étudiant les modèles analytiques du chapitre 2.

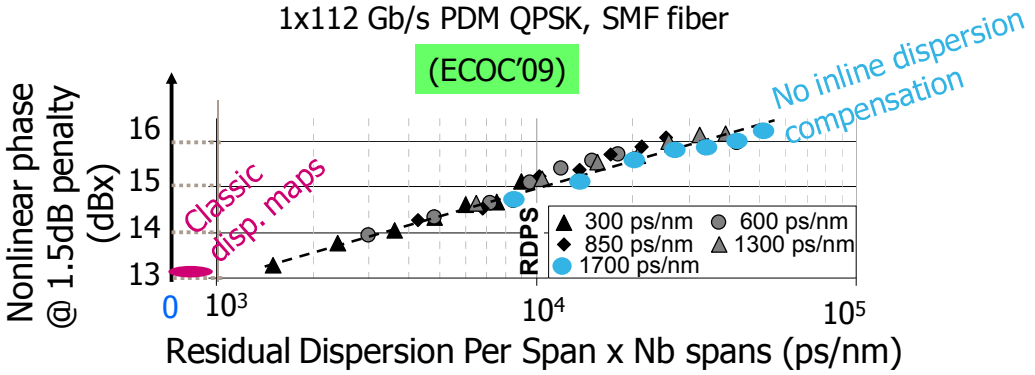

Figure O:Simulation numérique de transmission d'un canal modulé à 112Gb/s (28 Gbaud PDM-QPSK, détection cohérente). Evolution du seuil non-linéaire (phase non-linéaire correspondant à 1.5dB de pénalité) en fonction de la dispersion cumulée en ligne (produit entre nombre de sections de fibre de ligne et dispersion résiduelle par section de fibre de ligne gérée en dispersion), pour différentes valeurs de dispersion résiduelle par section et différentes distances. Il apparait que pour les cartes de dispersion classiques, ce seuil est indépendant de la distance, en accord avec le critère phase non-linéaire développé précédemment ; par ailleurs, les régimes de propagation fortement semblent bien plus performants, mais dans ces régimes, le seuil non-linéaire dépend fortement de la distance, indiquant que le critère phase non-linéaire n'est plus adapté.

Nous proposons alors deux adaptations au critère, l'une légère mais pertinente (et permettant d'adapter les réglages de puissance), et l'autre plus profonde, basée sur la découverte par mon équipe que dans ces régimes de dispersion, les distorsions du signal induites par les effets conjoints des non-linéarités et de la dispersion chromatique cumulée sont assimilables à du bruit Gaussien avec une excellente précision, y compris dans le récepteur, juste avant la phase d'identification des symboles.

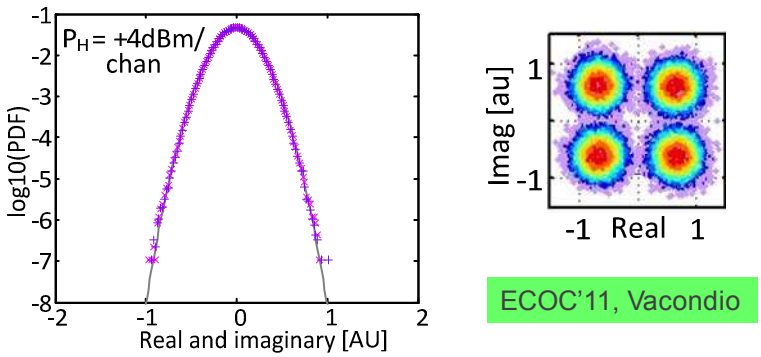

Figure P: Graphe de gauche : distributions mesurées dans le récepteur des parties réelle et imaginaire de la différence entre l'enveloppe reçue d'un signal PDM-QPSK 100Gb/s (2 polarisations confondues) et attendue à l'instant d'échantillonnage, après 15x100km de propagation sur fibre SMF sans compensation de dispersion en ligne, et dans un régime de propagation fortement non-linéaire. Courbe en trait plein : fit Gaussien.
Graphe de droite : superposition des points de mesures du signal reçu à l'instant d'échantillonnage avant identification des symboles.

Dans ces conditions, caractériser la manière dont s'accumulent ces distorsions revient à caractériser comment varie et s'accumule la variance de ce bruit optique non-linéaire. Nous avons pu établir qu'elle était proportionnelle au carré de la puissance optique du signal injecté dans les fibres, et que dans le cas de ces systèmes fortement dispersifs, la corrélation du bruit non-linéaire issu de différentes sections de fibre est négligeable. La variance totale après transmission est donc égale à la somme des variances des différentes sections de fibre.

Cette variance varie toutefois de manière supra-linéaire avec la distance dans la mesure où elle dépend également, pour chaque section de fibre de la dispersion chromatique cumulée à l'entrée de celle-ci.

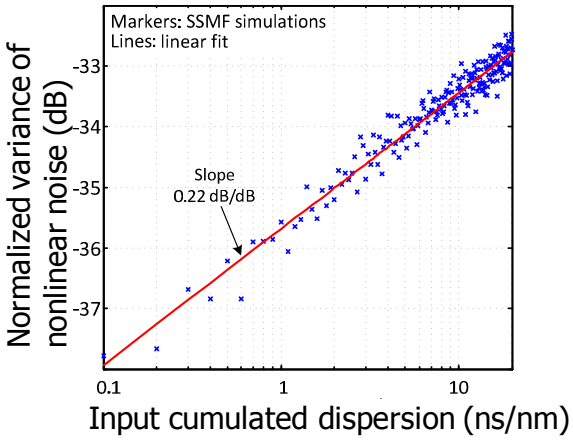

Figure Q: Evolution de la variance du bruit optique non-linéaire généré par une section de fibre optique SMF avec la dispersion cumulée en entrée de fibre, pour une puissance fixe d'entrée dans la fibre. Simulations numériques, 11 canaux PDM-QPSK modulés à 112 Gb/s.

Enfin, nous notons que l'utilisation d'un tel modèle de bruit non-linéaire Gaussien lié à ces nouvelles conditions de gestion de dispersion et au type de récepteur (cohérent) nous permet de déterminer analytiquement les pénalités, taux d'erreurs binaires et seuils non-linéaires, en accord remarquable avec les observations numériques et expérimentales.

En conclusion ce manuscrit couvre la plupart des aspects des modèles imaginés au cours de ces dix dernières années pour décrire l'accumulation des non-linéarités et prédire la performance dans le cadre de systèmes 10-40Gb/s fortement gérés en dispersion dans un premier temps, puis dans le cadre de systèmes faiblement gérés en dispersion typiques des systèmes cohérents modulés à 100Gb/s. Après avoir réalisé des expériences de mesures des coefficients non-linéaires de fibres optiques, j'ai proposé un certain nombre de modèles pour prédire la manière dont les effets non-linéaires s'accumulent, tels que les critères phase non-linéaire (pondérée) pour les systèmes (hétérogènes) modulés à 10 et 40Gb/s, puis j'ai sondé les limites de ces critères, et déduit des outils d'optimisation de la ligne de transmission et de prédiction de performance adaptés à un réseau optique reconfigurable. Enfin, j'ai relaté un certain nombre de travaux réalisés avec mon équipe autour des systèmes modulés à 100Gb/s et exploitant la détection cohérente, et notamment l'impact de la gestion de dispersion, la nécessaire adaptation des outils précédemment nommés ainsi que l'élaboration d'une nouvelle métrique pour l'accumulation des effets non-linéaires, basée sur une assimilation à unbruit Gaussien, et permettant de déduire analytiquement des estimations encore plus précises de performance tout en recourant à moins d'étapes de calibration.
Ces travaux ont fait l'objet de 59 publications dans des revues scientifiques et conférences internationales, ont donné lieu à la soumission de 13 brevets, et se sont concrétisés par un certain nombre de transferts industriels pour les compagnies Alcatel-Lucent et Draka (outils de prédiction de l'accumulation des non-linéarités, règles de gestion de la dispersion chromatique et de la puissance, outils de prédiction de performance en environnement hétérogène, dans le cas de systèmes gérés en dispersion et...).

TABLE OF ACRONYMS

Acronym	Meaning
ADC	Analog to Digital Converter
ASE	Amplified Spontaneous Emission of optical noise
BER	Bit Error Rate
C-band	Wavelength window around [1529-1565] nm
CRZ	Chirped RZ
CSRZ	Carrier-Suppressed RZ
DCF	Dispersion Compensating Fibre
DCM	Dispersion Compensating Module
DGD	Differential Group Delay (between PSPs of a birefringent section)
DM	Dispersion-Management
DBPSK	Differential Binary Phase Shift Keying, identical to DPSK
DFB	Distributed FeedBack laser
DPSK	Differential Phase Shift Keying
DGE	Dynamic Gain Equalizer
DQPSK	Differential Quadrature Phase Shift Keying
DSF	Dispersion Shifted Fibre
DSP	Digital Signal Processing
EDFA	Erbium-Doped Fibre Amplifiers
EO	Eye opening
EPSBT	Enhanced PSBT
FEC	Forward Error Correction
FFT	Fast Fourier Transform
FWHM	Full Width at Half Max
FWM	Four-Wave Mixing
GMPLS	Generalized Multi-Protocol Label Switching
GVD	Group Velocity Dispersion
ITU-T	International Telecommunication Union- Telecommunication standardization body
LCOS	Liquid Crystal On Silicon
LEAF™	Large-Effective Area Fibre (with 4.2 ps/nm/km GVD @1550nm)
MEM	Micro-Electro-mechanical Mirror
mNLT	Minimum Non-Linear Threshold
MZ	Mach-Zehnder
n_2	Nonlinear Kerr index
NF	Amplifier Noise Figure

NLSE	Non-Linear Schrödinger equation
NLT	Non-Linear Threshold
NRZ	Non-Return to Zero
NZDSF	Non-Zero Dispersion-Shifted Fibre
OOK	On-Off Keying (intensity modulated format, such as NRZ or PSBT)
OSNR	Optical Signal to Noise Ratio
OFDM	Orthogonal Frequency Division Multiplexing
PDF	Probability Density Function
PDL	Polarization Dependent Loss
PDM	Or PolMux, or DualPol : Polarization Division Multiplexing
PIC	Phase to Intensity Conversion
PMD	Polarization Mode Dispersion
PRBS	Pseudo Random Binary Sequence
PSCF	Pure Silica Core Fibre
PSK	Phase Shift Keying
PSP	Principal State of Polarization
PSBT	Phase-Shaped Binary Transmission
Q factor	Factor to express the quality of a transmission link. Linked with BER
Q' factor	Geometric eye opening
QPSK	Quadrature Phase Shift Keying
RDPS	Residual dispersion per span (also named Dres/span)
RDPSub	Residual dispersion per subdivision
ROADM	Reconfigurable Optical Add/Drop Multiplexer
RZ	Return to Zero (modulation format or additional pulse carving when used with other format)
SBS	Stimulated Brillouin Scattering
SRS	Stimulated Raman Scattering
SI-SRS	Self-Induced Stimulated Raman Scattering
SMF	Standard Single Mode Fibre
SPM	Self-Phase Modulation
SSFM	Split Step Fourier Method
TeraLight™	Medium Dispersion Fibre (around 8ps/nm/km GVD @1550nm)
WDM	Wavelength Division Multiplexing
WNLT	Weighted Non-Linear Threshold
WSS	Wavelength-Selective Switch
XPM	Cross-Phase Modulation
XPolM	Cross-Polarization Modulation

FOREWORD

In just a few years, a revolution has taken place in the ways we communicate to each other. This revolution includes the massive expansion of mobile voice communications, complementing fixed voice communications, of internet, of digital television, all possibly mixed in triple-play or quadruple-play offers with gradually increasing bandwidth. As an example, a typical data rate brought to the end user was 32-55kb/s 15 years ago. Today, it can reach up to 100Mbit/s in dedicated areas. In the core of the network, the overall data traffic has been growing by more than +50% per year for more than 20 years, as a result of the introduction of new bandwidth-hungry applications, such as high-definition video services.

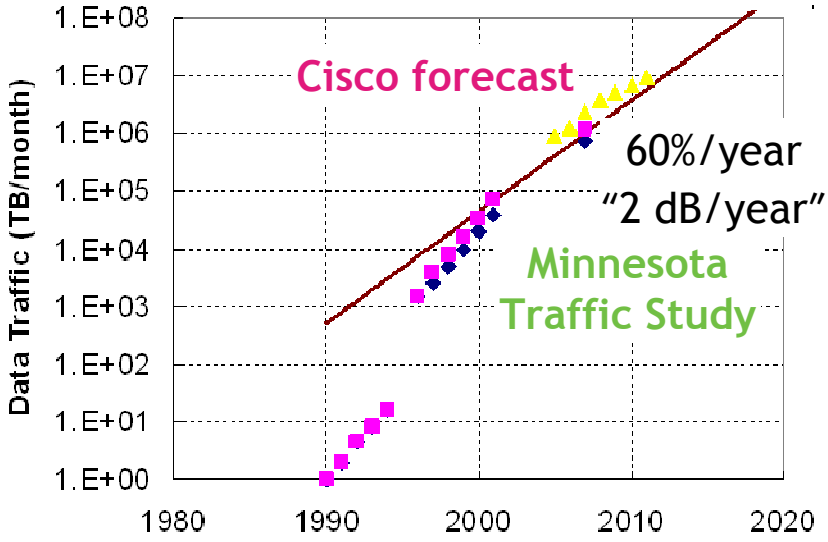

Figure 0-1 : Minnesota internet traffic study showing the measured and forecast yearly traffic in North America over the period 1990 to 2012.
(After: R.W. Tkach, Bell-Labs Technical Journal, 14(4), 3-10, 2010)

In this context, the optical fibre has proven unrivalled for coping with the explosion of capacity demand. The key advantage of the optical fibre resides in its ability to guide light with very low attenuation (<0.3dB/km) over a wide bandwidth of about 60THz. One key step in the history of fibre systems is the introduction of erbium-doped fibre amplifiers, in the late 1980s. They cannot operate over the entire 60THz bandwidth, but over an already-huge 4THz window. This window is generally filled with a set of lasers, each at a different wavelength (up to ~100) and modulated at 2.5Gb/s, at 10Gb/s, at 40Gb/s or now at 100Gb/s bit-rates. The total capacity of such fibre systems is then given by the number of lasers times the bit-rate carried by each of them. They are generally referred to as wavelength-division multiplexed (WDM) systems. Their capacity can be transmitted over several thousands of kilometres and over several transit nodes without optoelectronic regeneration. With WDM, optics has helped to drastically reduce the cost and the energy per transmitted bit of information. As a result, the optical fibre has been spreading across all the segments of telecommunication networks, from transoceanic submarine systems, to (inter-city) backbone systems, to (intra-city) metropolitan systems, and even to the end-user.

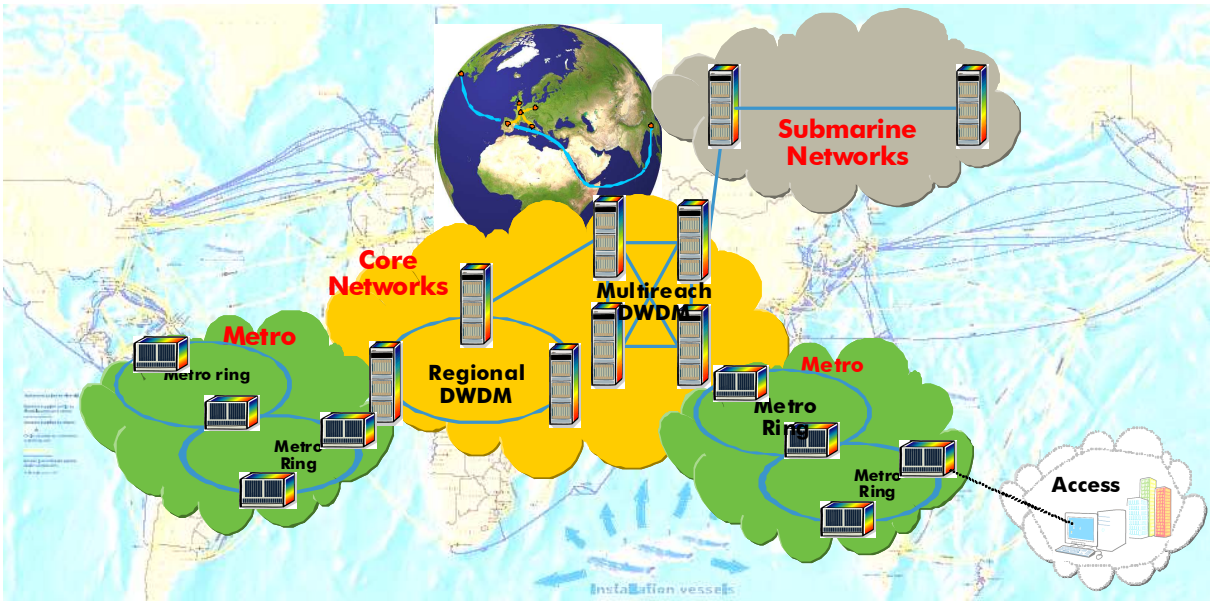

Figure 0-2: Utilization of optical fibre over the different telecommunication network segments

Once installed, optical fibre networks have been or can be improved along four main directions: (1) to achieve longer distances without optoelectronic regeneration across nodes (2) to be more flexible thanks to remote/automatic reconfiguration (3) to deliver more capacity and (4) to require less power consumption at lower cost per bit.

The notion of reach is key for a system vendor: if a connection between two distant points is not feasible all optically, intermediate optoelectronic regeneration of the signals will be necessary, most often at the expense of cost and energy consumption. Beyond the advances in the individual technologies and components that can be used over such networks, the effective performance (or reach) of a whole system strongly depends on the ability to smartly assemble all those components so as to obtain the best overall configuration and on the expectations of reach (that are related to the predictions of performance that can be made and to the estimated accuracy of such predictions).

Those issues can be very delicate to handle owing to the complexity of an optical network. This complexity stems first from the multiplicity of the devices that can be used: optoelectronic transmitters and receivers, sections of optical fibres separated by optical amplifiers, inline optical nodes, power equalizers, optical filters. In turn, the propagating signals experience a multiplicity of physical effects (attenuation, Group Velocity Dispersion, intra- and inter-channel nonlinear Kerr effects, Polarization Mode Dispersion, inline filtering, in-band crosstalk, Stimulated Raman Scattering…) and suffer from the accumulation of optical noise.

In submarine ultra-long haul systems, the distances to be bridged are so long that the links can benefit from an optimal design, close to lab conditions and the system complexity is dealt with by the homogeneity of the link: all fibre sections and amplifiers are alike and the characteristics of each family are optimized, such as the amplifier spacing around 40 to 80km depending on the reach of the system.

Conversely, in terrestrial optical networks, the inherent system complexity is enhanced by the high heterogeneity of the system. To begin with, the spatial distribution of inline amplifiers and nodes is generally not optimized but imposed by topological, geographical or demographic constraints: for instance, the amplifier spacing is not constant along an optical path from one transmitter to one receiver but varies from one amplifier to the other over a range between 10 and 150km. Moreover, in the terrestrial segment, one key element is the ability to reuse the already deployed infrastructures when deploying a new network, and particularly the installed

fibres. Thus, the activities of system vendor and fibre manufacturer are independent. As a result, the system vendor will aim to build a high performance optical network from a fibre infrastructure that can not be changed (except locally within amplifier sites) and which characteristics are partially known. To a largest extent, a terrestrial environment is much more constrained than a submarine environment, and the degree of knowledge of the characteristics of the links is much lower. In addition to that, the progressive growth of networks over years also implies heterogeneity in the types of optical fibres deployed over a single optical network with very significant discrepancies in fibre characteristics such as Group Velocity Dispersion (an thus in terms of tolerance to nonlinear effects). Eventually, the progressive growth of networks over years also implies heterogeneity in the types and bit-rates of the transmitters and receivers. The high degree of heterogeneity of a terrestrial system therefore greatly amplifies the complexity of the transmission.

In that context of terrestrial networks, optimizing the design of such systems and predicting their performance become very challenging. In particular, the effective performance of an optical network is generally upper-bounded by the predicted performance, because the system design is planned before the installation and before some inline, hypothetic, measurements can be performed. The accuracy of the predictions of all-optical connection feasibility has a direct impact on the number and on the location of devices enabling optoelectronic regeneration of the signal, thus a direct impact on the cost and the energy consumption of the optical network. A performance prediction has therefore to be as accurate as possible, as good as allowed by the degree of knowledge of the characteristics of the infrastructure, otherwise resulting in margins and over-provisioning of regeneration resources to avoid failures when deploying connections. But accuracy is not enough to make a performance prediction tool suitable for optical networks: complexity and computation time become important matters as well, leading to necessary trade-offs. Indeed, as opposed to point-to-point transmission links, it is generally not conceivable to predict the quality of transmission in a mesh optical network for all the possible connections between any node to any distant node with dedicated experiments or even with dedicated numerical simulations, all the more as the heterogeneous transmission link itself has to be optimized. Besides, physical performance prediction is only one of the tasks of network planning, dimensioning and allocation of resources; and time is an important issue for this task, whatever a utilization during the network planning phase before installation to make a bid to an operator or during the operation phase when the network needs fast reconfiguration when a new connection demand arrives or when a failure arises. To cope with such complexity and time constraints, models derived from physics laws and observations are necessary to enable to predict the quality of transmission of such complex systems with trade-offs between accuracy, complexity and speed.

This manuscript particularly addresses those issues: based on studies to understand and quantify the accumulation of Kerr nonlinearities, it aims to introduce novel tools that rapidly and accurately predict the quality of transmission of heterogeneous terrestrial networks and to propose guidelines that can help optimizing the system design (such as the distribution of chromatic dispersion along links or the settings of optical amplifiers).

The manuscript corresponds to studies that I have essentially conducted or supervised in the period 2000-2010 within the Optical Networks domain of Alcatel Corporate Research Centre, subsequently renamed as Research & Innovation before becoming Alcatel-Lucent Bell-Labs. Over these years, my position in the company has evolved from that of a research engineer to that of a project leader then to that of a research manager of 12 researchers investigating the physical and logical aspects of dynamic optical networks. Most of the studies that will be presented concern the research activities where I had most contributed in, prior to my current position of research manager, i.e. transmission systems modulated at 10 and 40Gb/s with

non-coherent detection schemes. At the end of this manuscript, I will put those studies in perspective with more recent studies I have contributed to, dealing with 100Gb/s-modulated systems using coherent detection, essentially when supervising a PhD student, Edouard Grellier.

With respect to the prior art, the starting point of the studies described in the following chapters was to demonstrate through a myriad of numerical simulations that a parameter as simple as the nonlinear phase shift describing the pure Kerr effect could be a reliable candidate to describe the impact of all meaningful nonlinear effects in usual transmission systems simultaneously impaired by multiple propagation effects such as Group Velocity Dispersion. We thoroughly investigated the limits of such a model and proposed adaptations to deal with the heterogeneity of transmission systems. Then we derived tools to predict simple yet accurate quality of transmission estimators based on a few synthetic parameters, such that they could be used for the operation of optical networks based for instance on a GMPLS (Generalized Multi-Protocol Label Switching) control-plane. Eventually we proposed guidelines to set the optical amplifiers and the fibre input powers in this context of network heterogeneity.

The manuscript is then organized as follows:

In Chapter 1, we describe the basics of optical transmission systems and networks, the fundamentals about the propagation effects into play and the methods used to characterize or emulate such systems. We also describe the method used in the studies conducted in the subsequent chapters. We start the characterization of systems by experimental measurements of the nonlinear coefficients of a representative sample of the most widespread optical fibres. Such measurements will be the basis for all the numerical simulations and the models detailed in the following chapters.

In Chapter 2 to 5, we will only consider 10 and 40Gb/s-modulated transmission systems without coherent detection.

Chapter 2 aims to build a tool that predicts the impact of nonlinear Kerr effect on signal quality with reasonable accuracy and computation time. We first revisit the nonlinear cumulated phase parameter and numerically demonstrate that we can build a locally bi-univocal relationship with excellent accuracy between transmission penalties and the nonlinear phase for a terrestrial WDM periodic system impacted by Group Velocity Dispersion and Kerr effects whatever the fibre input powers and distance, provided optimized dispersion management (i.e. the distribution of dispersion compensation along the system). Such relationship additionally depends on the transmission fibre local dispersion, on the transmitter/receiver pair and on the channel spacing. We define the nonlinear phase criterion as this ability to predict penalties as a function of the single nonlinear phase parameter. Then we investigate more sophisticated analytical small-signal models and perturbative approaches from the propagation equation and their ability to predict nonlinear / dispersion induced signal distortions system performance. We show that they enable to get more insight into physics, to simplify the optimization of the dispersion management but do not appear particularly more accurate than the simple nonlinear phase-based prediction tool, despite a substantial increase in the computation complexity. Yet they confirm that the signal distortions could vary as a function of a linear combination of the nonlinear phases stemming from each fibre section, which can be further simplified under certain assumptions of bit-rate and of dispersion management so as to comfort the nonlinear phase criterion. Moreover these perturbative models enable to identify the domain of validity of the nonlinear phase criterion, and will enable to enhance it in the conditions of a deployed heterogeneous terrestrial system in the Chapter 3.

After addressing homogeneous and periodic terrestrial systems with optimal conditions of operation in Chapter 2, Chapter 3 aims to investigate the domain of validity of the nonlinear phase-based prediction tool in exotic as well as real-life conditions, before proposing a generalization of this tool to heterogeneous conditions. In a first step we establish the accuracy of the nonlinear phase criterion in homogeneous conditions. We first establish that the nonlinear phase criterion is not meant to predict performance for single-fibre and multi-fibre systems at the same time. Then we investigate the impact of the input powers into the transmission fibres and the dispersion compensating fibres far beyond the usual conditions of operation. Thirdly we establish the accuracy of the nonlinear phase criterion depending on fibre length and confirm that, in agreement with the perturbative theories, the penalty versus nonlinear phase relationship depends not only on transmission fibre local group velocity dispersion but rather on its product with a fibre section effective length and the square of symbol rate. Fourthly, we investigate the impact of typical yet non-ideal dispersion management schemes. Eventually we address the issue of line fibre heterogeneity in terms of dispersion heterogeneity and come up with a proposal of generalized nonlinear phase, referred to as weighted nonlinear phase.

In the two following chapters, we exploit this ability to predict nonlinear induced penalties based on the (weighted) nonlinear phase with a reasonable accuracy so as to elaborate quality of transmission estimators accounting for other propagation effects than nonlinearities or group velocity dispersion.

Chapter 4 is dedicated to the method to elaborate a tool predicting the quality of transmission for signals impaired by multiple propagation effects and sources of impairments (such as amplifier noise, Kerr effect, Group Velocity dispersion, polarization issues, filtering issues, and crosstalk issues). A special focus will be given on the search for simple yet accurate models. The aim of such a tool is primarily to predict the optical feasibility of a connection between distant nodes in a mesh network, at the planning phase or in the operation phase.

Chapter 5 proposes to build a simpler quality of transmission estimator, focused on capturing the tradeoffs between Kerr effects and noise accumulation that often fix the transmission distance that can be bridged. The motivation is here to derive from the previous chapters some very simple expressions predicting the reach of systems such that they enable to isolate the impact of the transmitter/receiver scheme, the impact of the amplifier scheme or the impact of the fibres. They will enable to optimize some individual elements so as to maximize the reach of a whole system. Additionally the derived rules will enable to optimize the input powers into fibre sections, whatever the system heterogeneity in terms of line fibre section length or type. Those rules are then applied to optimize a Raman + Erbium optical amplification scheme and serve as the reference design for the ultra-long reach experiment that had presented at the post-deadline session of ECOC conference in 2001.

Eventually, in Chapter 6, we briefly revisit the proposed concepts for the recently 40-100Gb/s introduced multi-level modulation formats associated with coherent detection schemes. We particularly show that the proposed concepts essentially apply to the existing physical infrastructures including chromatic dispersion management, while in absence of dispersion management such concepts can be slightly adapted or totally renewed.

Chapter 1 : INTRODUCTION TO OPTICAL TRANSMISSION SYSTEMS AND THEIR MODELLING

This chapter aims to describe the basics of optical transmission systems as well as the experimental and numerical methods used in the following chapters.

In a first step, we introduce the optical transmission systems and optical networks, starting from their main architectures and features as well as the usual tools enabling to characterize the physical performance of such systems. We then describe the main physical effects that might impair the quality of the transmitted signals as well as usual ways to circumvent them. Eventually, we describe in more details the main building blocks of optical networks.

In a second step, we describe usual numerical and experimental tools able to emulate optical transmission systems. We then explain the chosen methodology applied in this manuscript to characterize optical networks impacted by multiple sources of impairments, and which is based on the principle of the separation of effects.

Eventually, we initiate in the Appendix the characterization of optical transmission systems by an experimental characterization of the nonlinear coefficient and the nonlinear Kerr index of typical optical fibres. The knowledge of such values is key to further numerically model transmission systems and to build efficient design and performance prediction tools.

1.I. Optical transmission systems architectures

I.1. Optical fibre for the transport of digital data

Optical fibre is by far the preferred medium for the transport of high volumes of data over distances ranging from a few kilometres up to more than ten thousand kilometres [1][2]. Such a success stems from the unique properties of glass optical fibre as an extremely low attenuation waveguide to light-waves operated over a very wide range of wavelengths, in combination with the availability of complementary technologies such as laser diodes and wide-band optical amplifiers in this range of wavelengths.

I.1.1. Optical Glass Fibre Main Characteristics

Optical fibre can first be seen as a very thin, flexible and long cylinder made of concentric layers of silica (SiO_2). The subtle addition of doping elements (such as Germanium) to those layers enables to modulate the radial refractive index of the fibre with highest values at the core of the fibre in such a way that light can be guided. Typical optical fibres are operated in a single-mode propagation regime at wavelengths higher than 1300nm for transport networks.

Secondly, optical fibre is made of so pure glass that the material is dramatically transparent to the propagation of lightwaves for a huge range of wavelengths. Typical attenuation of light can be typically as low as 0.2dB/km around 1550nm. As a result, it takes 50km fibre propagation before the signal power is reduced by 10. Besides, as illustrated by Figure 1-1, the potential transport capacity is huge compared to the radio spectrum: we could dream of a typically 50THz-wide available spectral window for telecommunications, for wavelengths ranging within 1300-1600nm with an attenuation lower than 0.3dB/km (should we overcome the attenuation peak due to absorption of light by OH^-). In practice, we operate today optical fibre over a 4-5THz bandwidth thanks to the use of Erbium Doped Fibre Amplifiers.

The limitations to the attenuation for low values of wavelength essentially come from Rayleigh scattering [6]. This effect is caused by the interaction of light with molecules that scatter

photons in an isotropic way. It essentially results in an attenuation of the transmitted lightwave at wavelength λ, proportional to $1/\lambda^4$. The backscattered signal can be measured to monitor the attenuation along the fibre(s) by optical time domain reflectometry techniques.

Note that double Rayleigh backscattering may cause some crosstalk co-propagating with the incident ligthwave: system impact is generally negligible except in case of distributed Raman amplification of the fibre (cf Chapter 5).

The limitations to the attenuation for high values of wavelength essentially stems from bending loss.

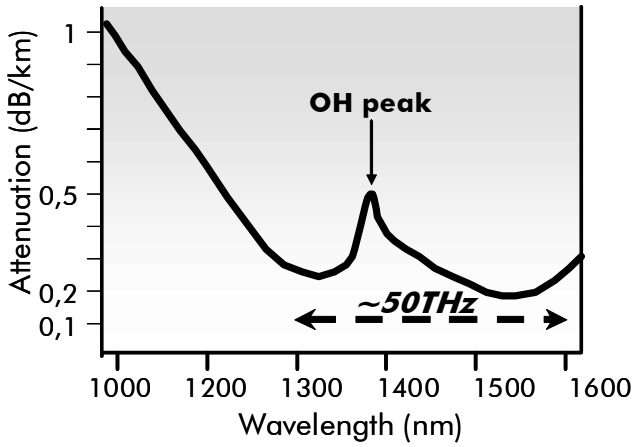

Figure 1-1 : Typical optical fibre attenuation as a function of wavelength

I.1.2. High-capacity digital optical transmission transmission systems

A digital single-channel optical transmission system basically consists of an optoelectronic transmitter followed by an optical transmission link, and by an optoelectronic receiver. The transmitter converts binary data into a modulated optical signal at a given bit-rate on a given optical carrier wavelength (usually denoted as a channel), that is sent into an optical transmission link. The transmission link is primarily composed of a concatenation of sections of single-mode optical fibres and optical amplifiers, and conveys the signal to an optoelectronic receiver, which recovers the binary information after photo-detection around the carrier wavelength and signal sampling.

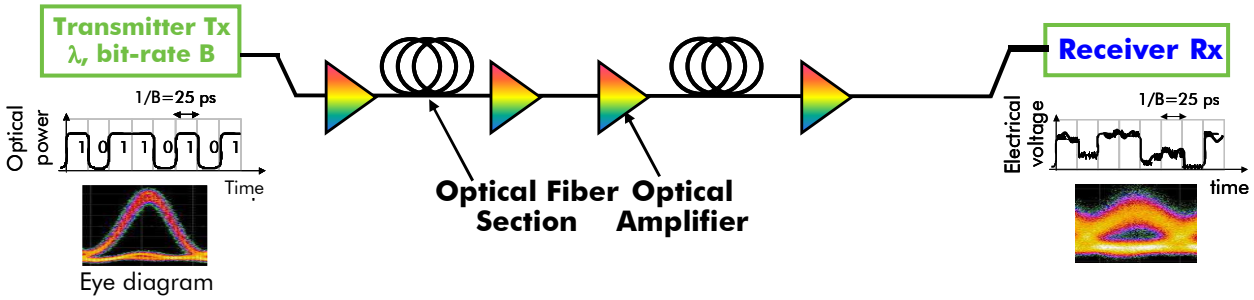

Figure 1-2 : single-channel optical transmission system

The periodic presence of optical amplifiers allows coping with fibre attenuation such that all optical signal propagation is possible over long distances without optoelectronic signal regeneration, typically more than a thousand of kilometres for 100Gb/s modulated signals. Another crucial element to enable long reaches is the use of Error Correction Techniques. Provided the periodic use of redundancy bits in addition to the useful data, the receiver can

correct most errors occurring at the detection level when interpreting the transmitted bits from the received optical signal. Typical techniques allow error-free transmission when the error rates does not exceed 4 errors every thousand bits, with a 7% overhead, such that the transported bit rate is 7% higher than the effective data-rate [10]. Mode details will be given in section IV.1.3.

One important aspect is the transported capacity. We define it as the total transported bit-rate.

In the abovementioned configuration, the transported capacity corresponds to the bit rate of the transmitter. Commercial transmitters and receivers for long-haul transmission support data-rates up to 100Gb/s. To do so, the transmitters periodically convert incoming blocks of binary data into symbols and modulate the light accordingly. The receivers then detect the transmitted symbols and recover the binary data. We can thus make a distinction between the data-rate (or bit-rate, expressed in bit/s) and the lower modulation frequency (or symbol rate, expressed in baud).

For deployed transmission systems with bit-rates up to 10Gb/s, to each bit 1 or 0 is associated one symbol and the modulation frequency is equal to the bit-rate. For such systems, the modulation of light is basic and is referred to as on/off keying or non-return to zero: as illustrated by Figure 1-2, the optical signal is a copy of the electrical binary signal and a symbol "0" will is coded by a low intensity signal while a symbol "1" is coded by a high intensity signal. Beyond 40Gb/s, multilevel modulations can be considered: a symbol can correspond to a set of n consecutive bits, with n being a power of 2. For instance, a quaternary modulation consists in transmitting two bits per symbol, with optical symbols of complex amplitude (a_1, a_2, a_3, a_4) respectively corresponding to bits (00, 01, 10, 11). Symbols can be all real with different amplitude (multilevel amplitude modulation) or with a constant intensity and various phases such as (0, $\pi/2$, π, $3\pi/2$) for Quaternary Phase Shift Keying. With a multilevel modulation with $n=2^k$ bits per symbol, the bit rate is equal to the product between modulation rate and k. In doing so, the bit rate can be increased while relaxing constraints on electrical devices. Some recent 40 and 100Gb/s industrial systems involve binary or quaternary modulation of the phase of light per polarization.

The capacity transported can be significantly improved by multiplexing the signals stemming from different transmitters on the same fibre.

The most usual way to do so is called WDM: **Wavelength Division Multiplexing**.

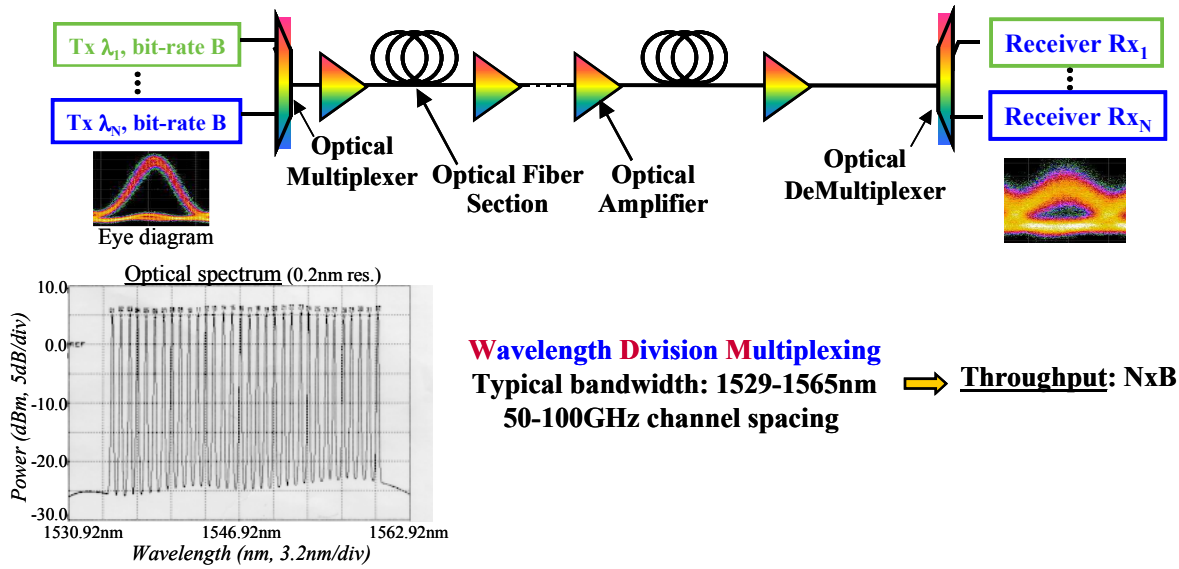

Figure 1-3: Basic WDM transmission system with N electro-optic transmitters (Tx) modulating light signals at bit rate B over wavelengths $\lambda_1 \ldots \lambda_N$, an optical multiplexer, a concatenation of fibre and optical amplifier sections, an optical demultiplexer and N opto-electronic receivers (Rx)

This technique is based upon combining (multiplexing) into the same fibre N modulated channels, each being at a different carrier wavelength. The total throughput is the sum of the individual channel bit rates, which are usually identical (e.g. throughput=Nx10Gb/s). At receiver side, each channel is filtered and recovered separately, so that any limitations on fibre propagation arising from linear effects in the fibre, such as noise sensitivity, Group Velocity Dispersion and Polarization Mode Dispersion (PMD), are only related to the bit rate of each individual channel. The role of the optical amplifiers is here to amplify the signals corresponding to multiple wavelengths at the same time, whatever their bit rate and modulation type. WDM is therefore a very efficient and common way to exploit the large fibre bandwidth [8], and allow high-capacity and distance transmissions without intermediate optoelectronic signal processing. Typical wide-band optical amplifiers such as Erbium-Doped Fibre Amplifiers (EDFA) provide amplification of light over a 4.5THz-wide spectral range, the so-called C-band between 1529 and 1565nm. This can be compared to the spectral occupancy of today's 100Gb/s modulated signals, below 50GHz [53].

One useful concept is thus the so-called **information spectral density**, or **spectral efficiency**, which refers to the transported capacity per unit frequency; it generally corresponds to the channel bit-rate divided by the inter-channel frequency spacing and is expressed in b/s/Hz.

Today's most deployed terrestrial long-haul WDM transmission systems consist of 10Gb/s-modulated channels (with basic non-return to zero modulation format, as illustrated in Figure 1-2) spread over the C-band and separated by 100 or 50GHz. This amounts to a maximum of about 80-90 channels, thus about 800-900Gb/s total capacity with a spectral efficiency of up to 0.2b/s/Hz. The recent introduction of 40 and 100Gb/s technologies have enabled to increase the transported capacities by a factor of ten while keeping the same channel spacing, leading to a spectral efficiency of 2b/s/Hz.

A second technique of multiplexing is **polarization multiplexing**. It consists in sending two independent data streams on orthogonal transverse polarization states into the fibre, and recovering each data stream at fibre output after separation of polarizations. Such technique that had been widely used in lab experiments to demonstrate high capacities, is not practically usable for most deployed 10Gb/s systems today (based on direct or differential detection)

because of difficulties to track the polarizations of modulation at transmission output and of the associated signal impairments. However, the most recent commercial 40-100Gb/s transmission systems based on coherent detection and high speed digital signal processing exploit this technique to double the transported capacity.

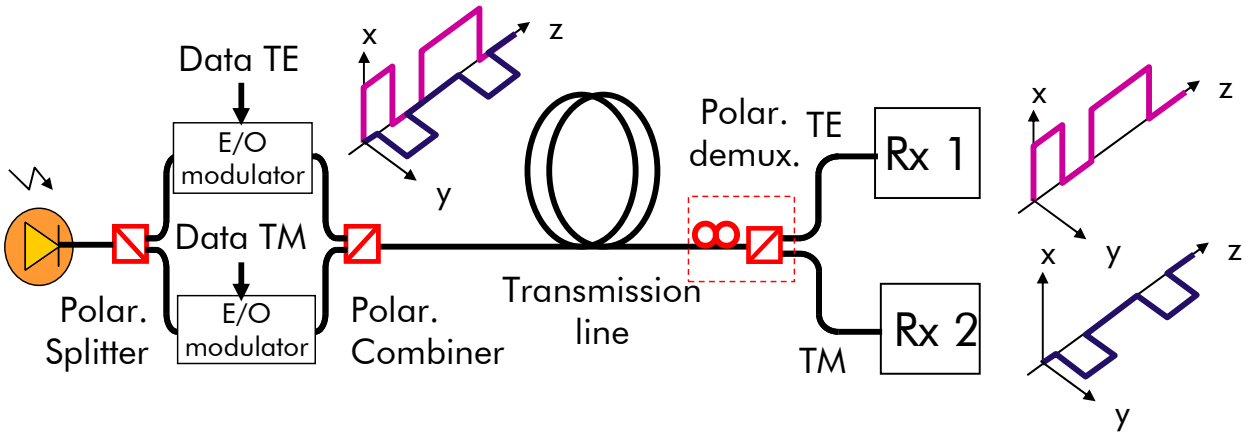

Figure 1-4 : Principle of polarization multiplexing

Eventually, a third technique of multiplexing is **spatial multiplexing**. It consists in sending independent data streams on different fibres in parallel, or on different spatial modes of a multimode fibre, or different cores of a multi-core fibre. While the first technique is trivial and used since it just consists in replicating the transmission systems, the latter techniques have recently emerged at the research level. The interest for such techniques has been renewed by the advent of coherent detection technologies assisted by digital signal processing since they could enable MIMO (multiple inputs multiple outputs) processing.

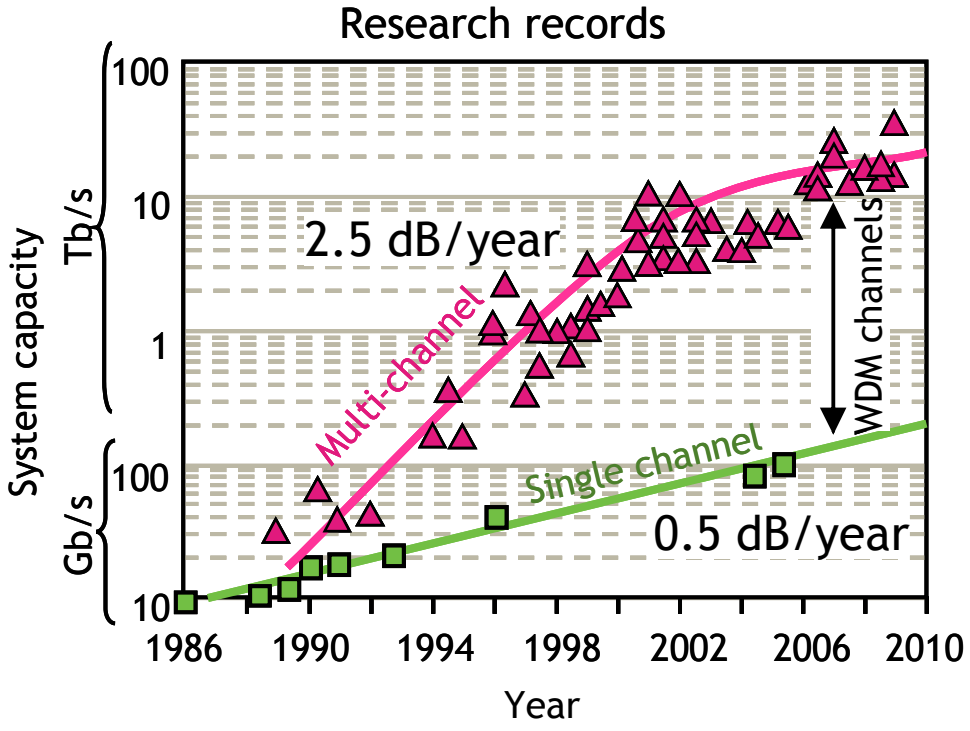

Figure 1-5 : Evolution of the achieved transported capacity

To conclude on the benefits brought by those techniques of modulation and multiplexing, Figure 1-5 depicts the evolution of capacity records achieved in research labs over the past 25 years, up to 2010. It clearly shows the explosion of capacity with the introduction of WDM in the late 80s , and the growth rate of 2.5dB improvement per year up to the beginning of the XXIst century with the evolution of channel spacing down to 50GHz and the increase of bit-rate up to 40Gb/s per polarization. In the first decade of XXIst century, the spectral efficiency and the bit rate per 50GHz slot improved with the use of multilevel modulations and coherent detection techniques in combination with digital signal processing. The average growth rate over the past decade has slowed down to 1dB/year when considering the latest records of 2011 over single-mode, few-modes or multi-core fibres. Today's record lab experiments report the transmission of up to 198 channels modulated at 100Gb/s over 6860km, which corresponds to a capacity x distance product of 136Pbit/s.km [3]. As far as the sole ultimate transported capacity is concerned, the transmission of 101.7Tb/s has been achieved over 165km single-mode fibre in 2011 with 370 OFDM (optical Orthogonal Frequency Division Multiplexed) channels [3]. Note that the current capacity record has been achieved also in 2011 over a multi-core fibre with 109Tb/s [5].

In the manuscript, we consider 10Gb/s and 40Gb/s modulated WDM systems with 2 level modulation of the intensity or the phase from Chapter 2 to 5, and 100Gb/s WDM systems with quaternary phase modulation and polarization multiplexing in Chapter 6.

I.1.3. Transparent Optical Networks

Terrestrial optical transmission systems are not only designed to establish a predefined connection between two distant points but are also part of a reconfigurable transport network. The physical infrastructure of such a network is composed of optical links, nodes and of optoelectronic transmitters and receivers. This network aims to establish semi-permanent connections between any node to any node in the network in order to cope with the traffic demands arising from the IP routers. This connection will be established by propagating one or several modulated channels over intermediate links and nodes. Until recently, such transport networks have been opaque: this means that a modulated optical signal cannot cross a node optically and that a connection between distant nodes must be split in connections between adjacent nodes, so that the signal is electrically processed at each intermediate node. The recent advent of ROADMs (Reconfigurable Add/Drop Multiplexers) has enabled to introduce optical transparency in the transport networks: an optical signal carried by a wavelength can traverse such a node to any output direction without electronic processing, provided the quality of the signal is good enough, as illustrated by Figure 1-6. Today's key element for such ROADMs is the Wavelength Selective Switch. It will be described in section IV.4. along with the typical ROADM architecture.

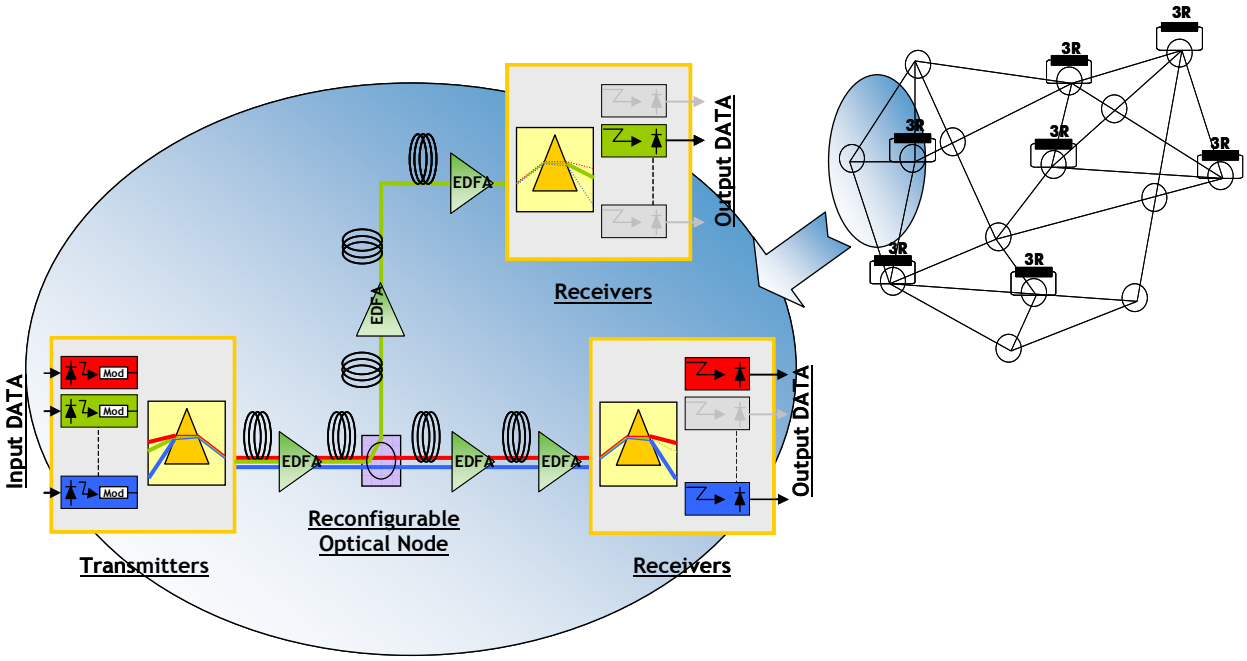

Figure 1-6 : transparent optical network with ROADMs enabling to route wavelengths to different directions without optoelectronic signal processing

1.II. Characterization of optical transmission systems

We introduce here usual criteria and methods to describe the signal quality. We first describe the Bit Error Rate, which is the most meaningful criterion accounting for the quality of the communication. Then we introduce the Q factor as another way to express the Bit Error Rate as well as an analytic criterion. Eventually we describe geometric ways to represent the signal and its quality such as the use of the eye diagram and the derived eye opening.

II.1. Bit-Error Rate

We usually measure the quality of a transmission system using the Bit-Error Rate (BER), which is the ratio of erroneously transmitted bits over the total number of transmitted bits.

$$BER = \frac{\text{Number of erroneously detected bits}}{\text{Number of transmitted bits}}$$

Errors stem from signal distortions and optical / electrical noise. In presence of optical amplifiers, the main source of noise is due to the amplified spontaneous emission (ASE) generated by the optical amplifiers. In the electrical domain, after passing the signal and the ASE into a photodiode converting the total optical power into electrical voltages, the noise contributions are usually related to the dominant beatings between signal and ASE and the beating between the ASE and itself.

Optical links are usually expected to convey data with BER as low as 10^{-13}. This has become possible over several thousands of kilometres owing to the use of Forward Error Correction devices, generally able to bring BERs as high as 2 10^{-3} before correction down to 10^{-13} BER after correction, with information redundancy of only ~7% [10]. Measurements of BER are

obtained by sending and receiving some known pseudo-random data, or by exploiting the error counters of the Forward Error Correction devices.

II.2. Q factor

This BER is often expressed in terms of Q factor, using the following conversion relationship [8][11][12]:

$$BER = \frac{1}{2} Erfc\left(\frac{Q}{\sqrt{2}}\right) \approx \frac{1}{\sqrt{2\pi}} \frac{e^{-\frac{Q^2}{2}}}{Q}, \qquad (1\text{-}1)$$

where Erfc() is the complementary error function $Erfc(x) = \frac{2}{\sqrt{\pi}} \int_x^{+\infty} e^{-y^2} dy$. Q factor itself is generally expressed in dB scale, with $Q^2{}_{dB} = 20\,Log_{10}(Q)$. This expression in dB scale is used to maintain consistency with the linear noise accumulation model. For example, a 3dB increase in the average launch power in all of the fibre spans results in "almost" 3dB increase in Q-factor, assuming that signal-spontaneous beat noise dominates and ignoring signal decay and fibre nonlinearity. We will see in Chapter 4 how we can interpret and handle this "almost" 3dB increase.

Typical values of BER and corresponding Q factor are worthwhile. A usual BER target for error free transmission system is 10^{-9}, this corresponds to a Q of 15.6dB. Since transmission systems utilize Forward Error Correction, a typical value of target BER before correction in begin of life conditions is 10^{-5}, this corresponds to a Q of 12.6dB. Eventually, 10 and 40G systems usually tolerate BER as high as 4. 10^{-3} before correction, this corresponds to a Q of 8.5dB.

When the received noisy symbols follow Gaussian distributions, the Q factor becomes more meaningful since it can be analytically related to the characteristics of the received signal: assuming basic Non-Return to Zero format, with possible marks "1" or spaces "0" detected, mean intensities I_1 and I_0 respectively, and standard deviations σ_1 and σ_0 respectively, then the Q factor is:

$$Q = \frac{I_1 - I_0}{\sigma_1 + \sigma_0} \qquad (1\text{-}2)$$

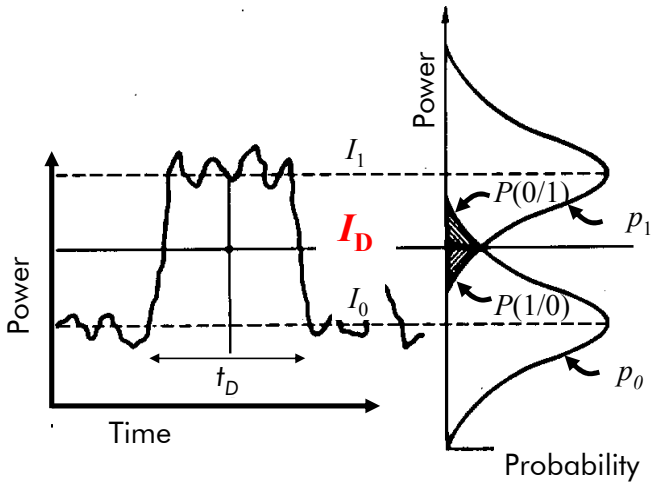

Figure 1-7 : Left : temporal trace of signal power over several bit times, with mean powers I_1 and I_0 respectively for marks and spaces around decision time, and descision power threshold I_D. Right: probability density functions p_1 and p_0 of detected powers for marks and spaces.

A demonstration of such relationship is detailed below:

Let I_D be the threshold intensity enabling to decide whether the detected symbol at detection time is a "0" or "1" depending on its intensity being respectively lower or higher than I_D. The BER is the sum of the probabilities to mistake a "1" for a "0" and vice versa, weighted by the probabilities p_1 and p_2 to send a "1" or a "0".

BER = p_1 P (0/1) + p_0 P(1/0)

Usually, $p_1 = p_0 = 0.5$.

$$P(1/0) = P(I > I_D / 0) = \int_{I_D}^{+\infty} \frac{1}{\sqrt{2\pi}.\sigma_0} e^{-\frac{(I-I_0)^2}{2\sigma_0^2}} .dI = \int_{\frac{I_D - I_0}{\sigma_0}}^{+\infty} \frac{1}{\sqrt{2\pi}} e^{-\frac{x^2}{2}} .dx$$

$$P(0/1) = P(I < I_D / 1) = \int_{-\infty}^{I_D} \frac{1}{\sqrt{2\pi}.\sigma_0} e^{-\frac{(I-I_1)^2}{2\sigma_0^2}} .dI = \int_{\frac{I_1 - I_D}{\sigma_1}}^{+\infty} \frac{1}{\sqrt{2\pi}} e^{-\frac{x^2}{2}} .dx$$

It can be shown that the optimum value for I_D is close to

$$I_{D,opt} \approx \frac{I_1.\sigma_0 + I_0.\sigma_1}{\sigma_0 + \sigma_1}$$

Then $P(0/1) = P(1/0) = \int_{\frac{I_1 - I_0}{\sigma_1 + \sigma_0}}^{+\infty} \frac{1}{\sqrt{2\pi}} e^{-\frac{x^2}{2}} .dx$

and

$$BER = \int_{Q}^{+\infty} \frac{1}{\sqrt{2\pi}} e^{-\frac{x^2}{2}} .dx \qquad with \;\; Q = \frac{I_1 - I_0}{\sigma_1 + \sigma_0}$$

Then

$$BER = \frac{1}{2} ercf(\frac{Q}{\sqrt{2}}) \;\; with \;\; erfc(x) = \frac{1}{\sqrt{\pi}} \int_{x}^{+\infty} e^{-x^2} .dx \, .$$

II.3. Signal representations and geometric criteria of quality

One way to represent the optical signal is to show a sample of the recorded temporal trace of the signal via an oscilloscope. It is thus possible to get an idea of the distortions that a binary sequence can undergo, as illustrated by Figure 1-8a.

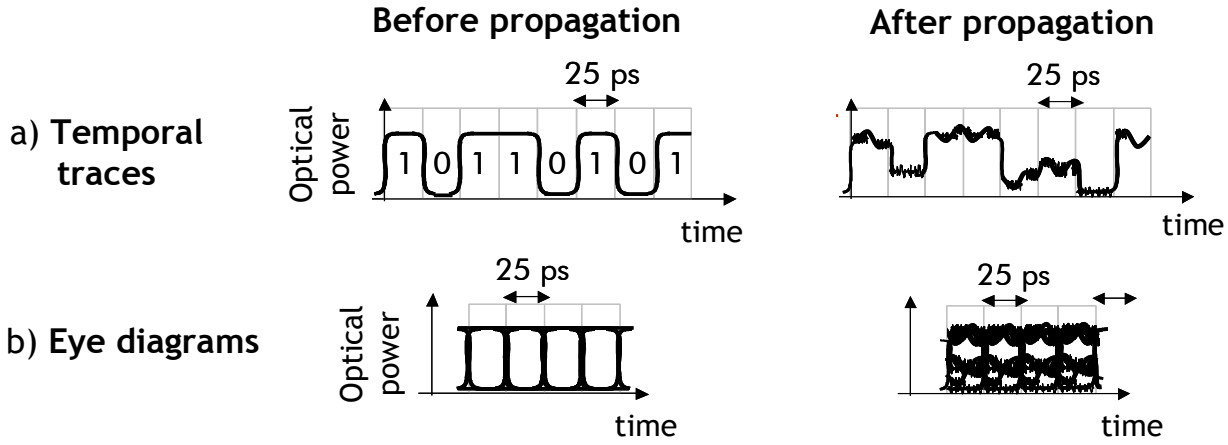

Figure 1-8 : Typical temporal traces and eye diagrams of an NRZ-modulated signal, before and after propagation

In order to get a simpler overview of signal quality, a useful way to represent signal is the eye diagram: it consists of the superposition of the signal traces over the time modulo one or a few symbol times. As shown in Figure 1-8-b for basic non-return to zero modulation format, the traces corresponding to the one and zero symbols are well separated at the center of the bit time, before propagation (left plot): the eye is said to be open; after propagation (right plot), the distinction between ones and zeros becomes less obvious, and the eye is almost closed. The eye diagram thus gives us a rough estimate of the quality of the signal since it allows visualizing the distributions of symbols intensities around a possible decision time. The analysis of the eye diagram could thus lead to an estimate of the Q factor.

Some analytical criteria of the signal quality related to the notion of eye may be of use. They are usually referred to as eye opening.

Most of the time, for a two-level intensity modulated signal, the eye opening is defined as:

$$EO = \frac{P_1 - P_0}{2.P_{av}} \qquad (1\text{-}3)$$

Where $P_{1,0}$ refers to the power of bit 1 or 0 at best decision time, and P_{av} refers to the average signal power over time (which is usually different from the mean between P_1 and P_0).

The eye opening may be related to the average or worst traces for 1 and 0 when considering the eye diagram. It may also be related to noiseless or noisy propagations (such a distinction being possible only through a numerical emulation of the line). Considering the average case eye opening may be equivalent in noisy and noiseless propagations, such as the eye opening may represent the quality of the noiseless signal, and its evolution after propagation may be related to non-noise, signal penalties.

The eye opening can be expressed in dB scale as:

$$EO_{dB} = 20\log_{10}(EO) \qquad (1\text{-}4)$$

And the eye opening penalty can be defined as the difference (in dB) between the eye opening without fibre propagation and with fibre propagation:

$$EOP_{dB} = EO_{dB}(\text{no propagation}) - EO_{dB}(\text{after propagation}) \qquad (1\text{-}5)$$

Another definition of the eye opening exists in the literature: it is called geometric eye opening or Q' factor [31].

$$Q' = \frac{\sqrt{P_1} - \sqrt{P_0}}{\sqrt{2.P_{av}}} \qquad (1\text{-}6)$$

with the same abovementioned notations.

Like the usual eye opening, Q' quantifies the quality of the detected signal. Besides, when assuming Gaussian distributions of detected symbols 1 and 0 due to beatings between signal and optical amplifiers noise, Q' can be analytically related to the Q factor. Q factor is particularly shown to be proportional to Q' and the square root of the optical signal to noise ratio when the statistics of the detected signals are Gaussian. More details are shown in Chapter 4, they will serve as the starting point of the building of a quality of transmission estimator developed along that Chapter.

1.III. Physical effects occuring in Optical Transmission Networks, and Resulting Design Trade-offs

III.1. Propagation equation (NLSE)

Let us now briefly describe **the major physical impairments** and their influence on the design of usual transmission systems.

For this purpose, we will start with the description of the propagation equation into an optical fibre, the so-called Nonlinear Schrödinger Equation (NLSE) [6] (following the (kz-ωt) convention):

$$\frac{\partial A}{\partial z}(z,T) = -\frac{\alpha}{2}A - \frac{i}{2}\beta_2 \frac{\partial^2 A}{\partial T^2} + i\gamma|A|^2 A \qquad (1\text{-}7)$$

where A(z,T) is related to the complex envelop of the optical signal around carrier frequency ω, z refers to transmission distance, T refers to time in the retarded time frame (accounting for mean group velocity induced time shifts at distance z), α stands for fibre linear attenuation, β_2 for fibre Group-Velocity Dispersion, and γ for the nonlinear Kerr coefficient.

In the following subsections, we will describe the consequences of attenuation, Group-Velocity Dispersion and nonlinear Kerr effect, before addressing polarization-related effects as well as other nonlinear scattering effects.

III.2. Attenuation, Amplifiers and OSNR

III.2.1. Attenuation and optical amplifiers

One limitation to system reach comes from **fibre attenuation**. Despite very low values of attenuation for wavelengths around 1550nm, about 0.2dB/km, long-haul transmission, over a few hundreds of kilometers or more, is not feasible without optical amplification or regeneration. Therefore, inline optical amplifiers, mostly Erbium Doped Fibre Amplifiers (EDFA), are generally deployed along the transmission link, on average every 80km for terrestrial systems. They can amplify an optical field over a wide waveband such as the C-band (between 1530 and 1565nm) without optoelectronic regeneration, and therefore allow much longer transmission reach for all the transmitted channels in the amplified waveband, even though the amplifiers generate Amplified Spontaneous Emission (ASE) noise at the same time.

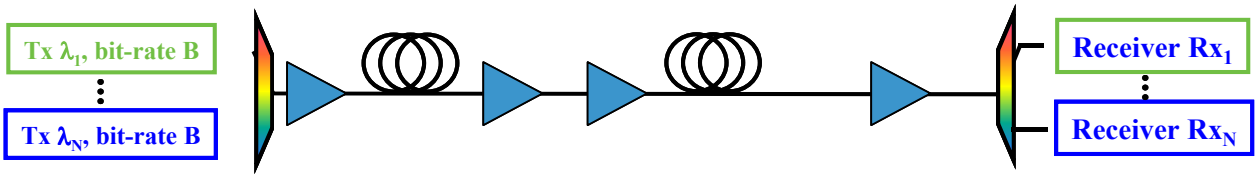

Figure 1-9: schematic of an optically amplified transmission line

III.2.2. Optical Signal to Noise Ratio and accumulation of noise

After transmission over an amplified link, the accumulated ASE becomes the dominant source of noise, and the **Optical signal to Noise Ratio** (OSNR) at receiver end is the most relevant parameter to characterize noise-related system degradation: it refers to the ratio of the channel signal power divided by the optical noise power (integrated over reference bandwidth, usually 0.1nm). The OSNR is a cumulative parameter since the inverses of the OSNR degradations of different parts of the system can be added to get the inverse of the overall OSNR **[8]**.

Let us briefly explain why: an optical amplifier generates wideband ASE, which power can be assessed in good approximation over a predefined spectral bandwidth B_{ref}, as:

$$P_{ase,B_{ref}} = NF.h.\nu.B_{ref}.G \qquad (1\text{-}8)$$

With G being the optical amplifier gain, h the Planck constant, ν the optical frequency of the emitted photon and NF the amplifier's noise figure. NF is usually expressed in dB scale (with NF_{dB} =10 log (NF)) and typical values for EDFAs range between 4 and 6dB.

With such an assumption, we can easily calculate the OSNR degradation when an incoming signal characterized by an input OSNR and a power P_{in} traverses an optical amplifier:

$$\frac{1}{OSNR_{out,Bref}} = \frac{1}{OSNR_{in,Bref}} + \frac{NF.h\nu.B_{ref}}{P_{in}} \qquad (1\text{-}9)$$

In the case of a cascade of amplifiers, the resulting OSNR simply becomes:

$$\frac{1}{OSNR_{out,Bref}} = \frac{1}{OSNR_{in,Bref}} + \sum_k \frac{NF_k.h\nu.B_{ref}}{P_{in,k}} \qquad (1\text{-}10)$$

The OSNR is usually expressed in dB scale as $OSNR_{dB}=10\log_{10}(OSNR)$. When cascading N identical amplifiers, the overall OSNR can be directly calculated in dB scale as a function of the amplifier input power in dBm:

$$OSNR_{dB,Bref} = P_{in,dBm} - NF_{dB} - 10\log_{10}(N) - K_{dBm} \qquad (1\text{-}11)$$

With $K_{dBm} = 10\log_{10}(\frac{h\nu.B_{ref}}{1mW}) = -58dBm$ when B_{ref}=0.1nm i.e. 12.5GHz around the wavelength $\lambda = c/\nu \approx 1.55\mu m$ (with c the celerity of light in the vacuum.

III.2.3. System tolerance to noise: sensitivities and penalties

Let us now focus on how to quantify system tolerance to noise: for that purpose we usually define the **OSNR sensitivity** as the required OSNR to guarantee a reference Bit-Error Rate. If we choose this reference BER equal to the one corresponding to the feasibility of optical connections, therefore an optical connection will hence be feasible as long as the actual OSNR at receiver end is higher than the OSNR sensitivity. To do so, a minimum input power into fibre sections is required. Typical OSNR sensitivity (assuming reference 0.1nm noise bandwidth) is about 13dB for a 10^{-5} BER in 10Gb/s Non-Return to Zero systems, and scales proportionally with the inverse of the bit-rate (with OSNR in linear scale).

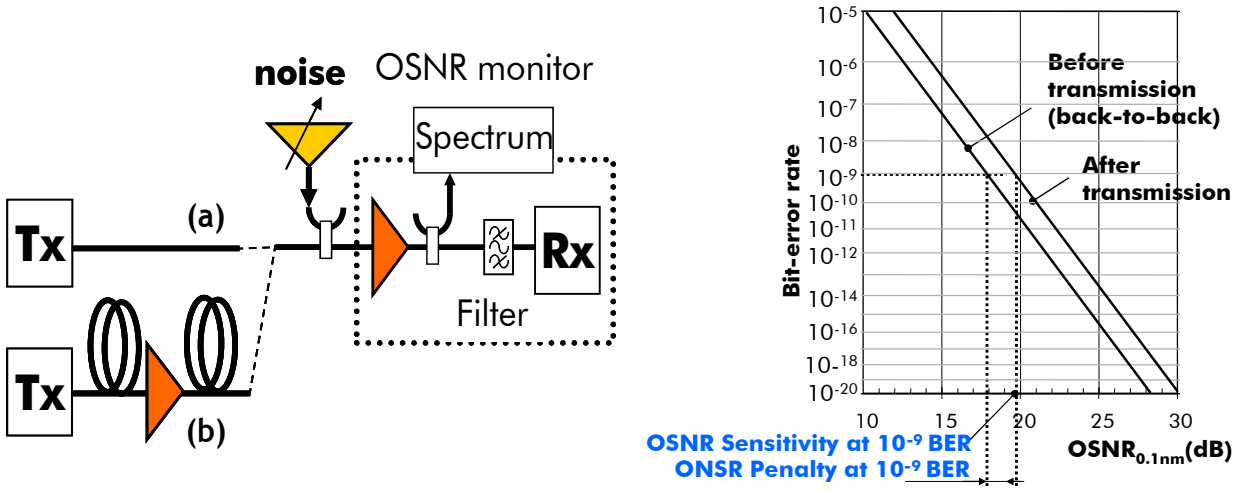

Figure 1-10 : Left: usual scheme to measure OSNR sensitivity in back-to-back (a) and after-transmission (b) configurations including addition of noise before receiver and measurements of OSNR and BER. Right: typical OSNR sensitivity curve representing the evolution of BER as a function of OSNR in back-to-back and after transmission conditions.

To account for non-noise system impairments, the notion of **OSNR penalty** is often used: for a reference BER, it represents the excess OSNR required after transmission to get this reference BER, with respect to the requirements in the so-called "back-to-back" configuration, i.e. when transmitter and receiver are directly connected without transmission. In other words, the OSNR penalty is the difference in sensitivity (in dB scale) after and before transmission for the same reference BER.

III.3. Chromatic dispersion, Compensation and Cumulated dispersion

Another limitation stems from Group Velocity Dispersion (GVD), also referred to as **chromatic dispersion**. In the following, for simplicity reasons, we will often refer to it as dispersion. GVD characterizes wavelength dependence of fibre refractive index n(λ). It is the linear phenomenon by which the spectral components of a signal are carried by guided modes which have different speeds. They therefore arrive delayed with respect to each other at the receiver end, thus distorting the original signal waveform and increasing the number of decision errors. Fibre GVD is usually characterized in the Optics community with the dispersion parameter D per unit length expressed in ps/(nm.km). D is particularly equal to the wavelength derivative of the inverse of group velocity, in the vicinity of a particular wavelength. In physics notations, GVD is rather described by the derivative of the inverse of group velocity with respect to angular frequency with the dispersion parameter β_2, expressed in ps^2/km. This latter notation is the one appearing in the NLSE in Equation (1-7). D and β_2 parameters are related by:

$$D = -\frac{2\pi c}{\lambda^2}\beta_2 \qquad (1\text{-}12)$$

In the following, in absence of a specific mention, we will describe GVD using the optics convention.

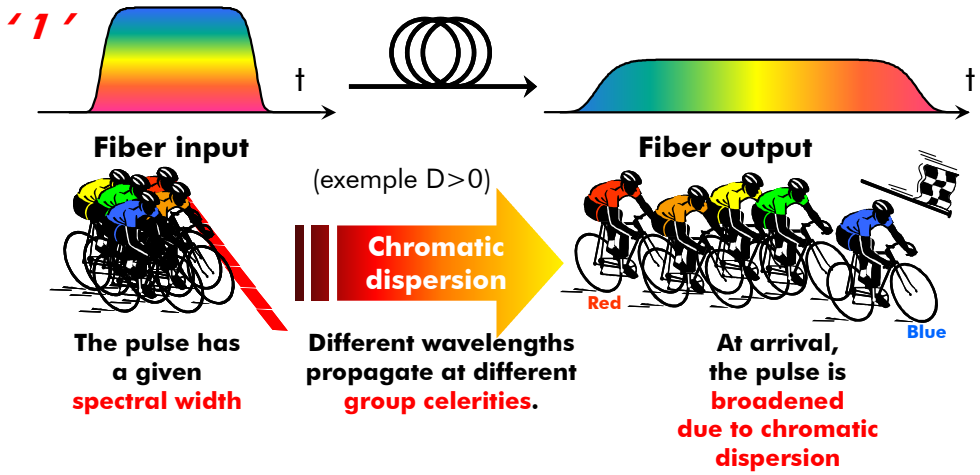

Figure 1-11: impact of group velocity dispersion on pulse broadening

Different categories of fibre exist depending on their GVD characteristics: standard SMF (Single-Mode Fibre, G652 type according to ITU-T, International Telecommunication Union-Telecommunication standardization body) was the first type of single-mode fibre to be installed and is still the most widespread fibre; it presents typical GVD values of 0ps/nm/km and 17ps/nm/km GVD around 1300nm and 1550nm respectively. GVD varies linearly with wavelength in good approximation with a slope of 0.054ps/nm^2/km. In order to alleviate the chromatic dispersion issue in the C-band (around 1550nm), a second generation of fibre has then been introduced, the Dispersion Shifted Fibre (G653 type) with 0 ps/nm/km GVD around 1550nm. However, this type of fibre revealed unpractical for WDM systems due to the perfect phase matching conditions enabling detrimental four-wave mixing between the different channels: this effect indeed causes energy and phase transfer from three wavelengths to a fourth wavelength that overlay and interfere with the original signal at this latter wavelength. In order to break the phase matching conditions, a third category of fibre has then been introduced, called NZDSF (Non-Zero Dispersion-Shifted Fibre, G655 type), presenting a low, but non-zero, value of GVD in the C-band. One of the most widespread fibres of such type is LEAF™ (Large Effective area fibre), presenting a GVD of 4.25ps.nm.km at 1550nm (2.6ps/(nm/km) at 1530nm).

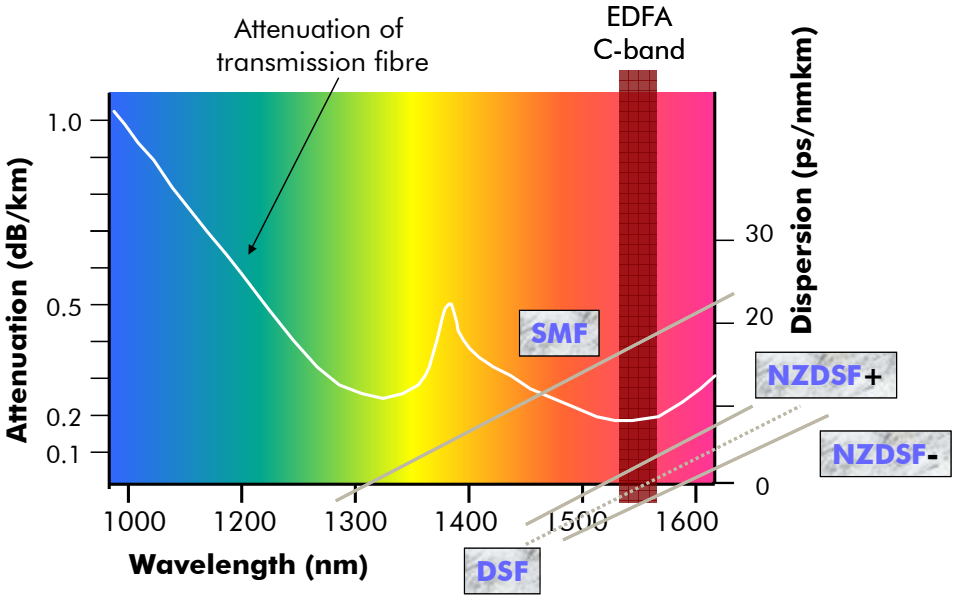

Figure 1-12 : Typical attenuation and GVD profiles with wavelength

The net impact of chromatic dispersion after propagation naturally depends on the **accumulated dispersion** (ps/nm) along all fibre sections.

Tolerance to accumulated dispersion can be defined as the range of accumulated dispersion leading to a penalty lower than a reference, e.g. 1dB. It typically scales like the inverse of the square of the symbol rate, and is about 1000ps/nm for usual 10Gb/s NRZ systems, which corresponds to about 60km SMF fibre or 240km LEAF fibre. At 100Gb/s, tolerance would fall down to 10ps/nm (600m SMF). Hence dispersion compensation is required, and is generally achieved with specific fibre sections called DCFs (Dispersion Compensating Fibres) exhibiting an opposite dispersion sign to the one of transmission fibre sections (also referred to as fibre spans) in the propagation waveband, so that the accumulated dispersion remains close to zero, thus enabling to minimize signal distortions. A more general term is the DCM for Dispersion Compensating Module, meaning that other solutions than DCF can be employed, such as Fibre Bragg Gratings. Those DCFs have typical dispersions of [-100; -250]ps/(nm/km) at 1550nm and are located regularly along the link, within the inline amplifiers, as illustrated in Figure 1-13: the optical pulses carrying the digital information tend to broaden but the succession of fibres with different dispersion signs limits the broadening, and then the resulting inter-symbol interference at the receiver side.

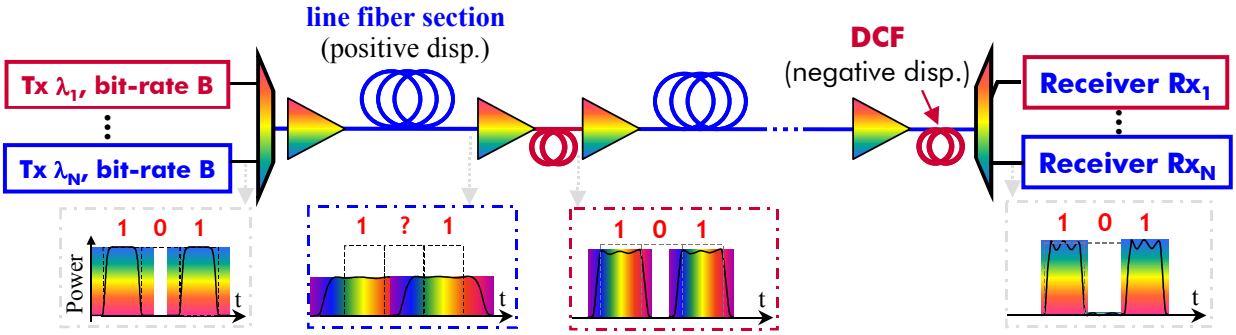

Figure 1-13: WDM transmission link with line fibre sections and Dispersion Compensating Fibres (DCF)

Since DCFs cannot compensate perfectly for the dispersion of a transmission fibre for every wavelength of the C-band at the same time, some accumulated dispersion remains uncompensated after transmission, and some adaptive, per channel, dispersion compensation might be required at receiver side, especially for symbol rates higher than 10Gb/s. Another reason why signal integrity cannot be fully recovered stems from optical nonlinear effects.

III.4. Nonlinear effects, dispersion-management

In the early days of lightwave systems, nonlinear phenomena were only considered as secondary by system designers. The main concern was to manufacture flat-gain amplifiers with maximum output power, for the optical signal-to-noise ratio in all channels to remain above some allowed limit. As capacities and distances increased, it progressively became apparent that upper-power limits should not be trespassed either, as a result of stronger nonlinear effects. Optimal system design thus requires that neither upper, nor lower power limits be approached or crossed during the entire operation life of the system.

Nonlinear phenomena can be divided into two categories, those stemming from electronic nonlinearities, namely Kerr effect, and those stemming from atomic/molecular/material nonlinearities, namely Stimulated Brillouin Scattering (SBS), core electrostriction, and inter-channel Self-Induced Stimulated Raman Scattering (SI-SRS). Kerr effect is today the most detrimental effect for signal propagation. Unexpectedly, these effects occur at relatively low

powers in the fibre (a few mWs or dBm), both because of the long integration distances (10-10000 km) and of the confinement of this power in a small region thus yielding high intensities (kW/cm2). This confinement is characterized by the effective area of the fibre, Aeff, which is fibre-type specific (80μm^2 for SMF, 72μm^2 for LEAF, 15-20μm^2 for DCFs around 1550nm).

III.4.1. Kerr effect

We focus here on Kerr effect, which translates the dependence of the instantaneous fibre refractive index n(z,t) on the signal intensity I(z,t). The intensity is simply related to the instantaneous power profile P(z,t) via I(z,t)=P(z,t)/Aeff. The magnitude of this effect is determined by the nonlinear coefficient n_2, according to the relation [6]:

$$n(z,t) = n_0 + n_2 \frac{P(z,t)}{A_{eff}} \qquad (1\text{-}13)$$

where n_0 is the linear part of the refractive index, while n_2 is expressed in m^2 /W . What actually determines the magnitude of fibre Kerr nonlinearity (regardless power) is more accurately determined by the ratio n_2/A_{eff} . While the parameter A_{eff} has become a common differentiating factor to qualify commercial fibres, the correct comparison between fibre types should only rely on the n_2/A_{eff} coefficient. Systematic experiments conducted so far have shown no large variation of n_2 with the type of fibre. The nonlinear index ranges between $n_2 = 2.5\ 10^{-20}$ and $3.0\ 10^{-20}$ m^2/W.

In the propagation equation (1-7), Kerr effect is accounted for by γ, the nonlinear coefficient, with

$$\gamma = \frac{2\pi}{\lambda}\frac{n_2}{A_{eff}} \qquad (1\text{-}14)$$

Kerr nonlinearities can be categorized into four types of physical phenomena:

- Self-Phase Modulation (SPM) whereby the signal phase of a given channel is modulated proportionally to its own power. At the receiver end, the photodiode is phase-insensitive, but GVD converts some of the phase modulation into intensity and phase modulations, causing detrimental signal distortions. SPM impact tends to increase with the absolute value of transmission fibre chromatic dispersion and symbol-rate.
- Cross-Phase Modulation (XPM), whereby the signal phase of a given channel is modulated proportionally to the power of the other channels, especially the close neighbours of this channel. Again, GVD converts some of the phase modulation into phase and intensity modulations, causing signal distortions. XPM impact tends to fade with high absolute values of transmission fibre chromatic dispersion, symbol-rate or channel spacing: the interaction time between bits carried by two different wavelengths will indeed be reduced due to the different group velocities and/or due to the reduced bit time.
- Four-wave mixing (FWM), whereby the interaction between three WDM channels at three different wavelengths results into the generation of an inter-modulation product at a fourth wavelength, which can fall on top of an existing fourth channel, producing detrimental crosstalk. FWM is particularly high for low absolute values of fibre chromatic dispersion and fades for higher values and/or high symbol rates [6].
- Signal-noise nonlinear interactions (referred to as Parametric-Gain or Modulation-Instability for intensity-modulated systems, nonlinear phase noise for phase-modulated

systems [6]), which strengthens or reduces the impact of amplifier noise, depending on the chromatic dispersion. They fade with high values of symbol rates.

SPM is the straightforward, self-induced Kerr effect. After propagation along a length L of fibre with attenuation α, the phase of a channel with power P(z,t) impaired by SPM can be simply derived from the propagation equation according to the well-known formula :

$$\Phi_{NL}(L,t) = \frac{2\pi}{\lambda}\int_0^L \frac{n_2(z)}{A_{eff}(z)} P(z,t)\,dt \qquad (1\text{-}15)$$

For typical WDM systems, the presence of amplifiers leads to the accumulation of SPM effects and phase shifts along the link.

SPM causes a broadening of the signal spectrum, since optical frequency shifts $\delta\omega = \partial\Phi_{NL}(L,t)/\partial t$ are generated on the pulse leading and trailing edges. Since this effect primarily concerns the signal phase, it does not affect intensity detection when chromatic dispersion is close to zero. In the case of non-zero chromatic dispersion, the interplay between SPM and chromatic dispersion results in a complicated phase-to-intensity conversion during signal propagation. Depending upon the chromatic dispersion sign, SPM is either beneficial, i.e. leading to pulse compression, or detrimental, i.e. leading to pulse broadening, distortion and irreversible breakup. The complex nature of the interplay between SPM and chromatic dispersion can also be intuitively understood since SPM generates phase modulation of the signal in the temporal domain, while chromatic dispersion meanwhile leads to phase modulation of the signal, but in the frequency domain, as it can be derived from the propagation equation (1-7).

When symbol rate increases, SPM-induced impairments tend to increase, while the impact of XPM, FWM and signal-noise nonlinear interaction tend to fade **[8]**. Similarly, the impact of SPM tends to increase with the absolute value of transmission fibre chromatic dispersion, while the impact of FWM and XPM fades for high absolute values of transmission fibre chromatic dispersion **[8]**.

III.4.2. Dispersion Management to mitigate Kerr and GVD effects

The outcome of the interaction between nonlinear and dispersive effects strongly depends on the distribution of dispersion compensation and signal power along a transmission link. In presence of nonlinearities, **Dispersion-Management [8][13][14][15]** consists in the clever distribution of dispersive elements along the link, so as to mitigate as much as possible nonlinear and dispersive effects at the same time. Practically, it is characterized by a Dispersion Map, representing the evolution of the accumulated dispersion with distance, such as illustrated by Figure 1-14:

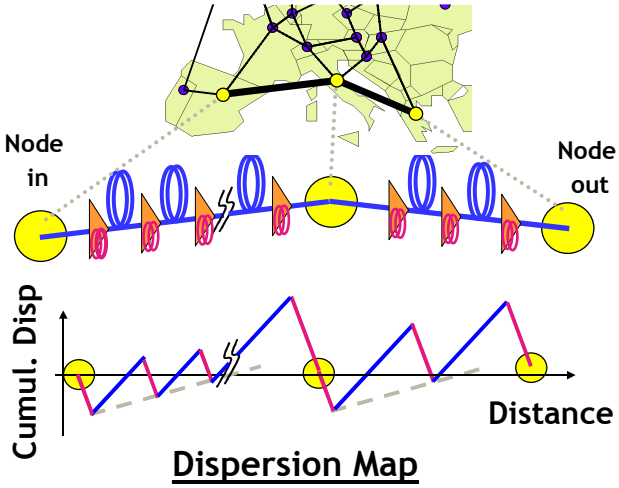

Figure 1-14: Dispersion map of a transmission link between two distant optical nodes of a European optical network

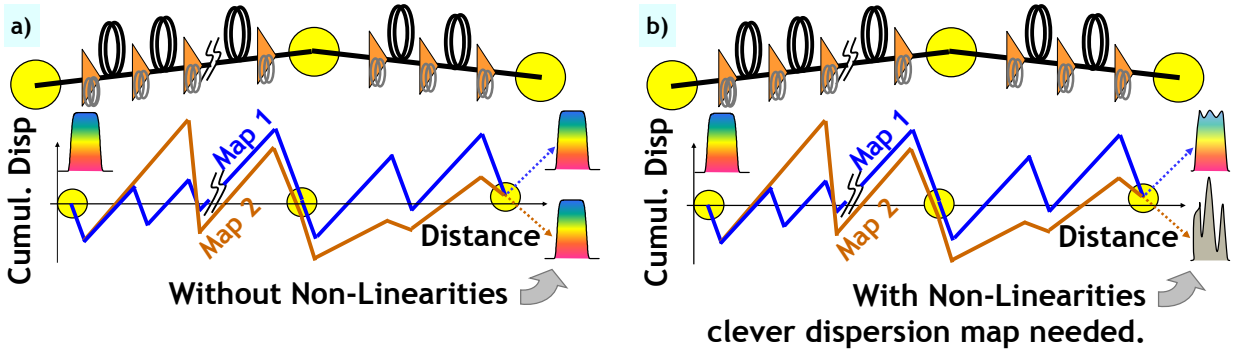

Figure 1-15: Impact of the dispersion map on the degradation a pulse propagating over an optical transmission systems, in absence (a) or in presence of Kerr nonlinear effect (b).

It must be noted that, in order to minimize signal degradation, zero accumulated dispersion at receiver is neither a sufficient solution (since dispersion management impact becomes critical, as illustrated by Figure 1-15) nor necessarily a good solution, since part of the accumulated dispersion has been practically compensated by nonlinearities. The construction of a dispersion map usually follows simple rules, so as to deal with a limited number of degrees of freedom. In principle, any DCF with any cumulated dispersion can be inserted within an optical repeater before/after a section of transmission fibre. To make it simpler, periodic patterns are usually considered.

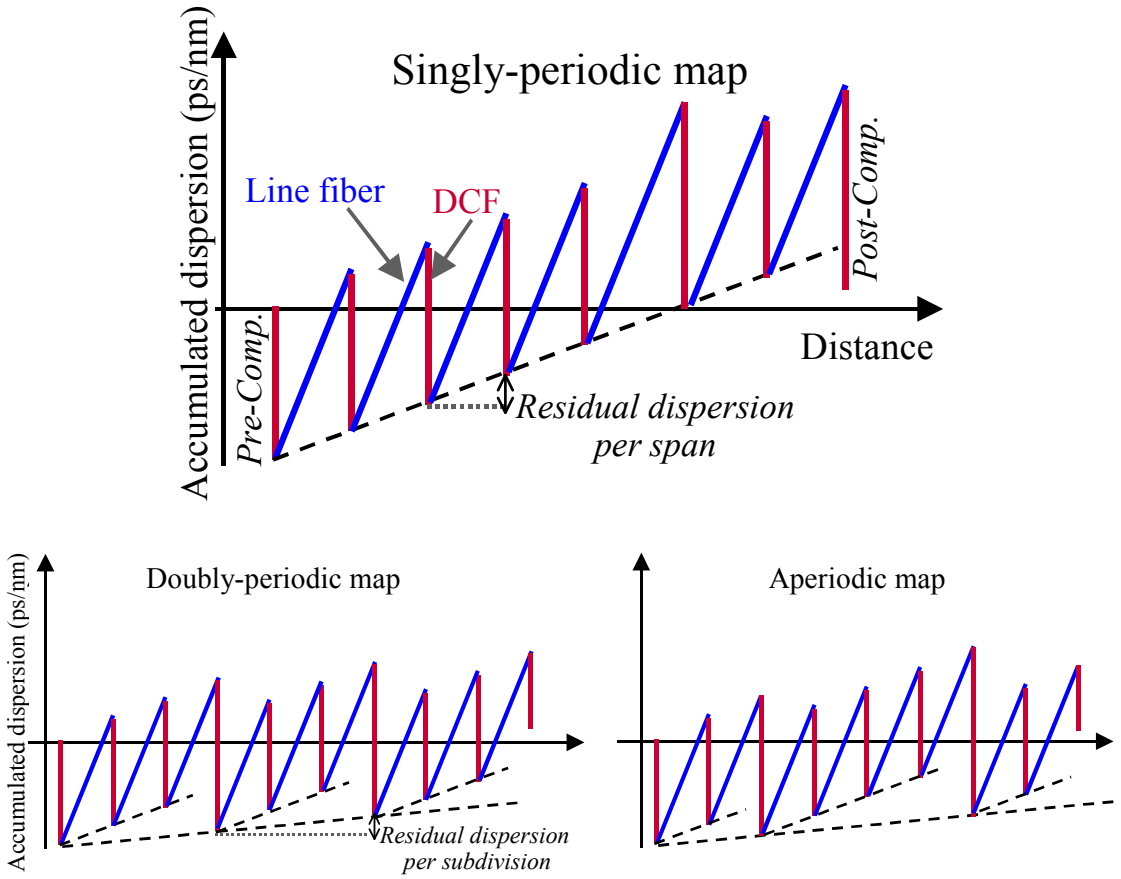

Figure 1-16: Typical dispersion management schemes: singly-periodic (top), doubly-periodic (bottom-left), aperiodic (bottom-right) maps.

The simplest class of dispersion map is referred to as **singly-periodic dispersion map[15]**. It is described by Figure 1-16-top: at transmission input, some DCM is inserted before the first section of transmission fibre. It is referred to as **pre-compensation DCF** and the corresponding cumulative dispersion is also referred to as pre-compensation. After each section of transmission fibre (also called span), some **inline DCF** is inserted at repeater site, so as to guarantee a constant cumulative dispersion from span to span (generally referred to as **Residual Dispersion Per Span**, RDPS). At transmission end, some **post-compensation DCF** can be used before the receiver; the corresponding amount of cumulative dispersion is usually referred to as post-compensation. The overall cumulative dispersion from the transmitter to the receiver is usually referred to as **residual dispersion**.

A second widespread class of dispersion map is called "**doubly-periodic dispersion map**"[16], as illustrated by Figure 1-16-bottom-left. It can be seen as a concatenation of subdivisions consisting of singly periodic maps of equal length (N spans), defined by their amount of pre-compensation, the residual dispersion per span, the **residual dispersion per subdivision** (RDPSub) of N spans, and a final post-compensation at receiver side.

In deployed optical networks, singly periodic maps or **aperiodic maps** derived from the doubly-periodic concepts are widely used. The specificity of singly periodic maps is that total cumulative dispersion from the transmitter node to the receiver node depends on the transmission distance, possibly requiring dedicated post-compensation at receiver on a per channel basis. Aperiodic maps are derived from doubly periodic maps, with subdivisions of unequal lengths, corresponding to node spacing. Most of the time, the target residual dispersion from node to node is set to be equal or close to zero (similar to Figure 1-14-

bottom-right), so that the accumulated dispersion of any channel at any node will not depend on the light-path, and reception without dedicated post-compensation might be possible.

Dispersion management is widely used in long-haul terrestrial and submarine systems, in backbone optical networks, for single-channel as well as WDM applications, in order to mitigate SPM but also XPM and FWM impairments. In Chapter 2 and 3, we will show that even in presence of dispersion management and especially for optimized dispersion maps, the accumulated nonlinear phase shift induced by SPM, as defined by (1-15), remains a relevant parameter to quantify the impact of all nonlinearities **[7]**. We will also show tools helping to optimize the dispersion management.

The impact of dispersion management compared to full dispersion compensation at terminals is far from negligible for simple two-level modulation formats as used for 10 and 40Gb/s since it increases the tolerance to nonlinearities by up to a factor of 10, which relaxes constraints on the maximal input power. Thus it enables to increase transmission reach significantly, by at least a factor of 3, as shown in Chapter 5. Dispersion-management has also replaced the former concepts of solitons **[6]**, taking benefit of fibres with alternate signs of dispersion to improve robustness to intra-channel and inter-channel nonlinear interactions while relaxing constraints on optical pulses powers and temporal widths. However, for the most recent 100Gb/s-modulated systems based on multilevel phase modulation, polarization multiplexing and coherent detection, non-dispersion managed schemes become very efficient (see Chapter 6).

III.4.3. Inelastic scattering processes: Stimulated Raman Scattering, and Stimulated Brillouin Scattering

Stimulated Raman scattering (SRS) and stimulated Brillouin scattering (SBS) are two significant nonlinear effects which origin lies in the interaction of the optical field with the silica molecules of the optical fibre [24].

III.4.3.1. *Stimulated Raman scattering (SRS)*

When a photon collides with a molecule of silica, it is normally scattered by Rayleigh scattering. The scattered photon then has the same energy as the incident one (elastic scattering) and no energy is therefore transferred to the silica molecule.

However, a partial transfer of energy from the photon to the molecule occurs for a small fraction of collisions between photons and silica molecules ($\sim 10^{-6}$). This is known as Raman scattering or Raman Effect and is referred to as non-elastic since the energy of the scattered photon is lower than that of incident one. The silica molecule moves to a higher-energy vibrational state through the absorption of a fraction of energy of the incident photon whereas a lower frequency (higher wavelength) photon is generated. The scattered photon/wave is referred to as Stokes photon/wave [11].

The maximum efficiency of SRS power transfer is found around 13.2 THz (~100 nm) lower than the original frequency [23]. This effect can be exploited to build Raman amplifiers. Raman amplification is further discussed in section IV.2. .

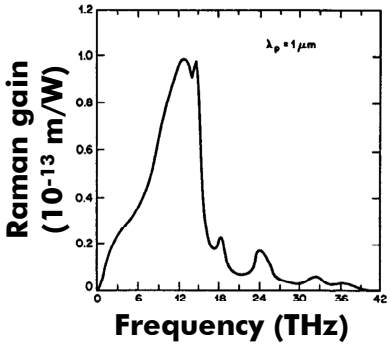

Figure 1-17 : typical Raman gain versus frequency offset

The same Raman gain that is beneficial for making amplifiers can be detrimental for WDM systems since it may result in unwanted crosstalk between different channels. In this case, a fraction of the energy of the shorter wavelength (higher frequency) channels is transferred to the longer wavelength (lower frequency) channels and can result in a time averaged [25] and in a bit-dependent SRS crosstalk [26].

Time-averaged SRS crosstalk results in gain-tilt in the WDM spectrum, as depicted in Figure 1-18. This gain tilt is well approximated as a linear power tilt in decibels, as shown experimentally [27] and analytically [28]. It is likely to cause OSNR issues to the lower wavelength-channels and Kerr-like issues to the higher-wavelength channels. The impact of gain-tilt can be mitigated by employing gain-tilt filters or dynamic gain equalisers (DGE) such as the spectral response of an amplified span or a section of several spans will be flat after equalization. The use of inline equalization can be coupled with channel power pre-emphasis at transmission input, corresponding to a partial or total pre-compensation of the tilt before the tilt-equalized section, as in [29], in order to equalize the wavelength-dependent signal degradations.

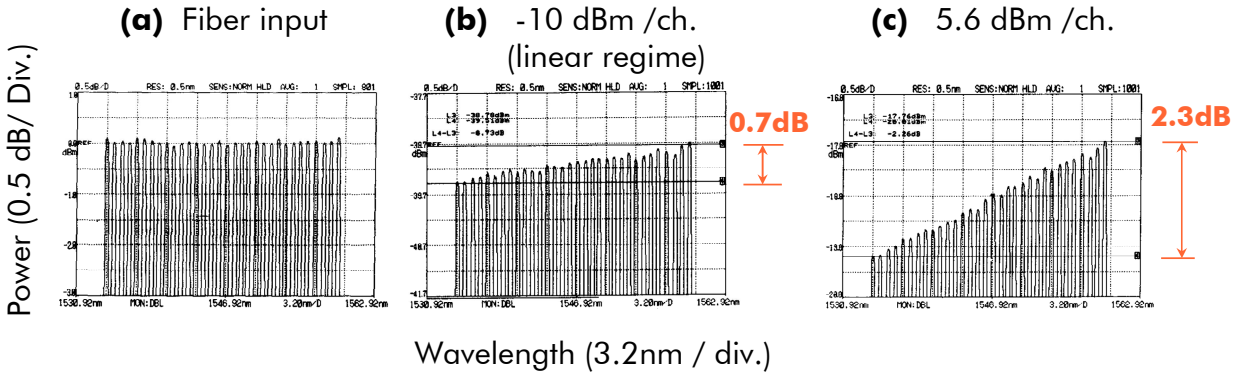

Figure 1-18 : Power tilt induced by SRS on a transmitted multiplex of 32 channels into a 100km section of NZDSF fibre: power spectrum at transmission input (a), at transmission output with a per channel power of -10dBm (b) and 5.6dBm (c), resulting in power tilts of 0.7 and 2.3dB respectively. Source: [27]

Bit-dependent SRS crosstalk is negligible when the channel spacing between the perturbing channel and the perturbed channel is low due to the very low Raman gain. It may become more significant for highly spaced channels but it is mitigated by the limited interaction time between bits. The impact tends then to fade for high value of chromatic dispersion and/or symbol rate, similar to XPM.

In the following, the impact of SRS will be overlooked, if not explicitly stated.

III.4.3.2. *Stimulated Brillouin Scattering (SBS)*

The mechanisms behind stimulated Brillouin scattering (SBS) are close to SRS. Nevertheless, stimulated Brillouin scattering arises from the interaction between photons and acoustical phonons. An optical wave propagating over an optical fibre generates an acoustic wave through the process of electrostriction. This acoustic wave in turn modulates periodically the refractive index of the fibre which results in a reflection grating. The incident light is then scattered through Bragg diffraction. As a result, a Stokes wave propagating backwards, counter-directionally to the optical signal at longer wavelength is generated. The frequency downshift caused by SBS (~10 GHz or ~0.08 nm) is much lower than SRS. The power reflected by SBS scales exponentially with the power of the incident field above the SBS threshold. SBS threshold depends on the spectral width of the incident field and its lowest value (~1 mW) is obtained for a continuous-wave (CW) or slowly modulated (pulses larger than 1 μs) incident field. The efficiency of SBS is strongly reduced when using short pulses (<10 ns) or phase-modulated signals [6]. Indeed, SBS can be neglected in transmission systems relying on phase-modulation beyond 1 Gb/s.

We will not consider it in the following.

III.5. Other sources of signal degradation

Other phenomena impair system propagation, such as Polarization Mode Dispersion (PMD), crosstalk, filtering due to optical nodes, are described in more details in **[18][19]**.

III.5.1. Polarization Mode Dispersion and Compensation

The origin of PMD lies in the weak residual birefringence of optical fibres.

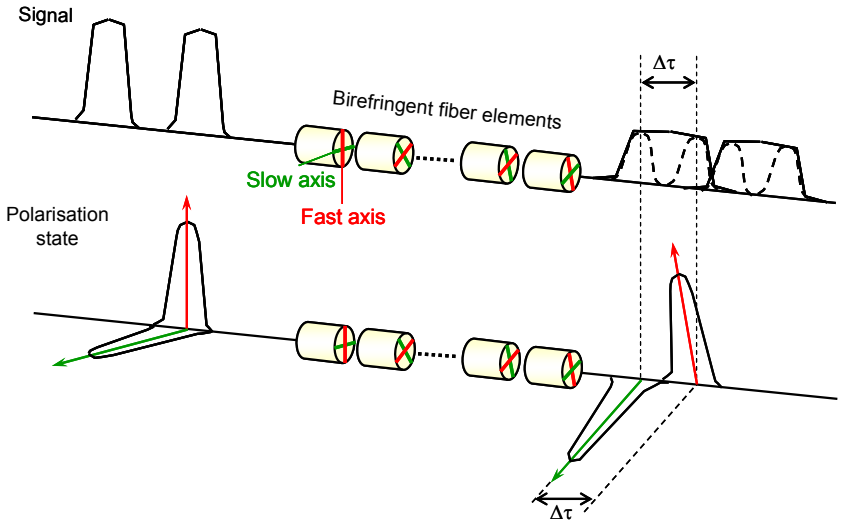

Figure 1-19 : Principle of the impact of the birefringence induced by optical fibre over an incoming modulated signal

The birefringent nature of a fibre causes the apparition of two principal states of polarization (PSP), along which the light propagates at different group velocities, leading to the concept of Differential Group Delay (DGD, which is the difference in group delay between two optical signals propagating over one principal state of polarization or the other). When transmitting information over such a birefringent material, the signal is split into two components aligned

with both PSP which propagate at different velocities, and which are thus delayed after transmission, leading to an overall signal distortion, and thus system performance degradation. Moreover, optical fibre is "weakly" birefringent, such that its birefringence is neither constant along the fibre, nor over time. An optical fibre can thus be modelled as a concatenation of small birefringent segments, each with different PSPs, leading to time variations of the overall PSPs and DGD, of stochastic nature.

The best statistics to describe the distribution of the DGD values over time is a Maxwellian law, characterized by the mean value of the DGD, also called PMD:

$$Pdf(\mathrm{DGD}) = \frac{32}{\pi^2}\frac{\mathrm{DGD}^2}{\mathrm{PMD}^3}\exp\left(-\frac{4}{\pi}\frac{\mathrm{DGD}^2}{\mathrm{PMD}^2}\right) \qquad (1\text{-}16)$$

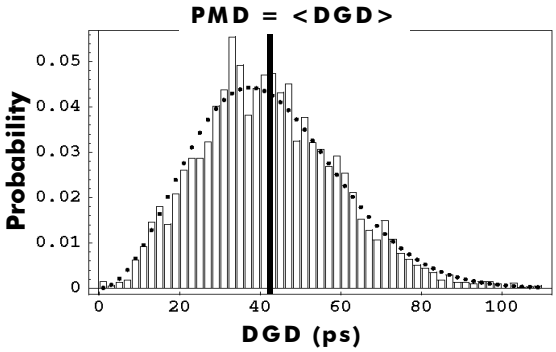

Figure 1-20 : Statistics of DGD over an installed link over a 6 months period.

The PMD of a fibre is usually given in ps (accumulated) or ps/km$^{1/2}$ (fibre features), and the accumulated PMD adds up quadratically when concatenating different fibre sections. Figure 1-20 shows the statistics of the measured DGD over an installed link (after a 6 months measurement period) (histogram curve), in agreement with the Maxwellian law (dots).

From a system point of view, DGD causes inter-symbol interference and then penalties. Figure 1-21 shows a typical measured penalty as a function of DGD, for a 10Gb/s NRZ signal (T_0 represents symbol duration). After such a measurement, we expect that, knowing the DGD of the birefringent material that supported transmission, we could derive the induced penalty.

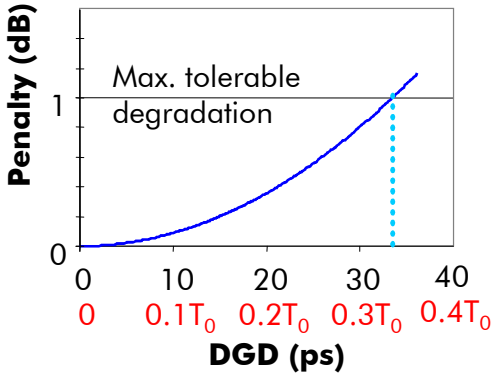

Figure 1-21: Typical OSNR penalty vs. DGD for 10Gb/s NRZ signal

However, it is impossible to predict accurately the penalty induced by PMD in an optical fibre, since DGD wanders around the mean value of the distribution. Therefore, since we know the

statistics of the DGD from the knowledge of the PMD of a link, we can estimate the maximum expectable value of the DGD combined with a cumulated probability. We can then define the outage probability (or unavailability rate) as the cumulated probability that the DGD of the link becomes higher than a given value, DGD_{out}.

A typical tolerated outage probability is 10^{-5}, which means that we tolerate DGD to become as high as possible in 1 over 10^5 possible configurations, which means 5 minutes per year. It also means that, with 99.999% probability, the DGD is upper-bounded. More precisely, if we calculate the maximum DGD threshold such that the cumulated probability of getting a higher DGD is 10^{-5} using the Maxwellian law and the knowledge of <DGD>, it amounts to DGD_{out}= 3.2 <DGD>. Therefore, with 99.999% probability, the DGD of the link is lower than 3.2 <DGD>.

With such an outage probability, it is common to estimate the tolerable amount of PMD such that in 99.999% of the cases, the induced penalty remains lower than a tolerable floor, for instance 1dB, which, in the case of NRZ systems, would correspond to 10% of symbol duration. Transmission systems are then considered feasible as long as the PMD of the link does not exceed the defined threshold, and 1dB penalty will be provisioned anyway, to assess performance.

Since PMD accumulates with square root of distance, system reach without PMD compensation scales like the square of the inverse of symbol rate, therefore becoming a very critical limitation for systems with symbol rates of 40Gb/s and above. Typical PMD of a transmission fibre is 0.1ps/km$^{1/2}$, and it can be as low as 0.04ps/km$^{1/2}$ for recent fibres. With such figures, reach would typically be limited to 10 000km at 10Gb/s, and to 600km at 40Gb/s.

Adaptive techniques exist to mitigate the impact of PMD, based on electronic or optical means [8]. For transmission systems relying on non-coherent detection techniques, such techniques basically enable to double the tolerated PMD value, thus to increase the reach by a maximum of 40%. For most recent systems relying on coherent detection assisted by digital signal processing, the PMD effect can be almost entirely compensated at receiver end owing to the use of adaptive equalization algorithms following a linear photo-receiver [24].

III.6. Polarization Dependent Loss

Most optical components present in optical transmission systems present some polarization-dependent loss (PDL). It refers to the fact that the attenuation of light depends on the polarization state at component input. The PDL of a given component is usually expressed as the ratio between the maximum and the minimum losses depending on the input polarization state. It is expressed in decibels [11].

PDL is essentially present in optical components such as optical isolators or amplifiers as well as optoelectronic modulators. PDL is therefore randomly distributed and translates into signal power fluctuations depending on the random evolution of the signal state of polarization. These power fluctuations cause OSNR variations and depolarization when PDL axes are not aligned with the birefringence axes.

III.7. Filtering and crosstalk issues when traversing ROADMs

Most optical networks today allow optical signals to cross several nodes (ROADMs, Reconfigurable Add/Drop Multiplexers) without optoelectronic regeneration. These nodes can block or let pass any wavelength coming from different input links.

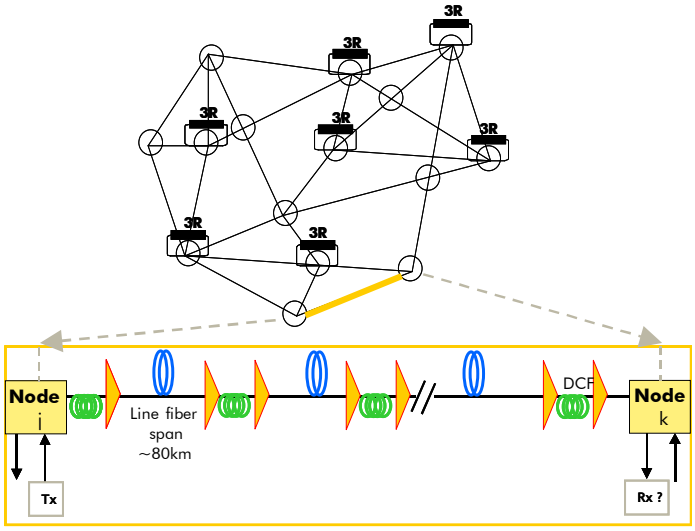

Figure 1-22 : Optical network with optical nodes with add/drop functions

As a result, they have an impact on signal through cascaded filtering functions when a light-path crosses several nodes. In addition, since the blocking functions cannot be perfect, when two incoming signals (at the same wavelength) enter one node and only one is supposed to pass through, some residual crosstalk remains on the output signal.

1.IV. Main building blocks of optical transmission

We describe here the main building blocks of optical transmission systems, starting by transmitters and receivers, then amplifiers

IV.1. Basics on transmitters and receivers

We describe here briefly the most usual transmitter and receiver types used in 10-100Gb/s transmission systems. The transmitters are essentially characterized by the choice of the modulation format [8][30], while receivers are mainly characterized by their photo-detection scheme. Particularly, we describe modulation formats such as 10G-typical intensity-modulated NRZ (Non Return to Zero) or RZ (Return to Zero), followed by modulation formats more dedicated to higher bit-rates such as PSBT (Phase-Shaped binary Transmission, similar to duobinary 3-level format) and phase-modulated signals like D-B-PSK (Differential-Binary Phase Shift Keying also simply referred to as DPSK, for Differential Phase Shift Keying in combination with the differential direct detection scheme, or BPSK when the detection scheme is coherent) and DQPSK (Differential Quaternary Phase Shift Keying, also simply referred to as QPSK when using the coherent detection scheme), based on the description from S. Bigo I have contributed to in [8]. Then we describe the following detection schemes: simple direct-detection, differential direct-detection, and coherent detection.

IV.1.1. Modulation Formats

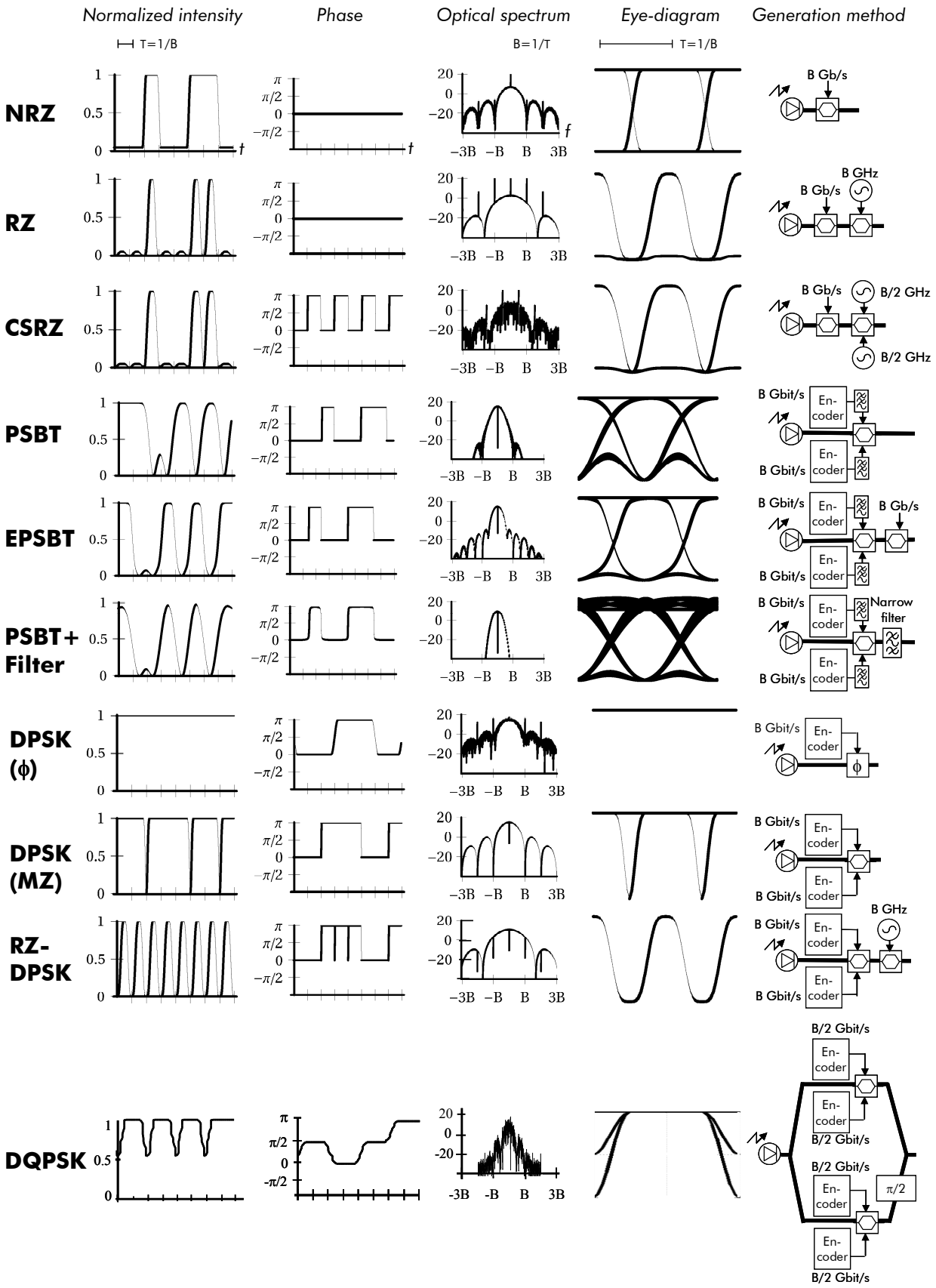

Figure 1-23 : Typical modulation formats proposed for optical transmission systems

IV.1.1.1. *NRZ modulation format for 10G systems*

In most deployed terrestrial transmission systems with bit rates equal to or lower than 10Gb/s, optical data are almost exclusively generated by intensity modulation with the non-return-to-zero (NRZ) format. NRZ is by far the simplest format. The optical signal is a copy of the electrical binary signal: a symbol "0" is encoded by a low intensity, and a symbol "1" is encoded by a high intensity signal. The format is called NRZ because the intensity of the signal remains constant at the transition between identical symbols. For bit rates as high as 10Gb/s, external modulation, as opposed to direct modulation of the laser, with the NRZ electrical signal is usually required. The generic transmitter is made of a cw laser source followed by a $LiNbO_3$ Mach-Zehnder (MZ) modulator driven by the electrical NRZ signal. An important feature of the NRZ signal is the power ratio between the "1" and the "0" symbols, namely the extinction ratio. It is typically between 10 and 13dB. The modulator will be preferably used in push-pull configuration in order to avoid additional phase modulation[30][8]. The reception of such a modulation format requires simple direct-detection.

As can be seen in Figure 1-23, the width of the main lobe of the signal spectrum is equal to twice the bit rate (i.e. 85GHz bandwidth for 42.7Gb/s-modulated signals, including 7% overhead for FEC); this makes NRZ compatible with 40G transmission with 100GHz channel spacing while not directly compatible with 50GHz channel spacing.

IV.1.1.2. *RZ modulation format [8]*

The return-to-zero format (RZ) [8] has often been viewed as a promising alternative to NRZ. With RZ, any "1" symbol is represented by a pulse, which can be of variable duration. It is customary to characterize this width with the duty cycle, i.e. the ratio of the average pulse power divided by the pulse peak power. In the example of Figure 1-23, the duty cycle has been set to 50%, meaning that the pulse width is close to one-half of the bit period (exactly one-half if the pulse envelope was square). RZ signals can be generated by cascading a NRZ generator with a second modulator driven by a near-sinusoidal clock (at data frequency). With respect to NRZ, two drawbacks of RZ are its broader spectral width and its lower resistance to GVD. Indeed, the narrower the pulses, the broader the spectral width and hence, the lower the GVD resistance (in dispersion-compensated transmission lines, however, the last argument is no more valid). On the advantages side, the OSNR sensitivity of RZ signals is generally better than NRZ. Additionally, RZ is known for higher tolerance to fibre nonlinearity.

Enhanced RZ formats have been proposed as alternatives to conventional RZ. They differ from each other by specific, non-uniform phase modulations. The carrier-suppressed RZ (CS-RZ) format was initially used in terrestrial links at 40Gbit/s channel rate. Two neighboring CS-RZ pulses have the particularity of having phases that differ by π. Such pulses can be simply generated by using a Mach-Zehnder modulator driven by a sinusoidal clock at half the information frequency and twice the conventional swing voltage as pulse shaper. The phase profile of CS-RZ format helps limit intersymbol interference and improve the tolerance to Kerr effects with respect to RZ. Variants exist such as chirped RZ (CRZ) format. It can be generated by concatenating an RZ data generator and a sinusoidally-driven phase modulator. Its superior resistance to nonlinearities has nonetheless been obtained at the expense of a larger channel spectral occupancy, which limits the maximum achievable information spectral density.

IV.1.1.3. *PSBT modulation format*

The Phase Shaped Binary Transmission (PSBT) modulation format is derived from duobinary coding [42][31]. Duobinary is basically a three-level coding scheme optimized to reduce the

channel spectral-width by half with respect to NRZ coding. It involves "0" symbols, as well as "+1" and "-1" symbols, which differ by optical π-phase shifts: "0" bits correspond to "0" symbols while "1" bits correspond to "+1" or "-1" symbols, such that the phase shit between two "1" bits is equal to π times the number of in-between "0" bits (modulo 2π). It requires an electronic device to precode the electrical data, but detection is performed with a conventional intensity-sensitive, direct-detection receiver. A practical way to implement duobinary coding is PSBT: it consists of passing a set of two complementary, precoded data into a low-pass Bessel electrical filter (fifth-order in fig.7.33) to drive a dual-input Mach-Zehnder modulator. This filter emulates the calculated, ideal duobinary filter, but has some surprising consequences on the phase of the coded optical data: a small fraction of light within "0" symbols incorporate π-phase shifts in their center. This results in a degraded sensitivity to OSNR as compared to NRZ or true duobinary coding but also in an increased tolerance to accumulated chromatic dispersion: indeed, this phase shaping prevents "1" bits to broaden over "0" bits as a result of chromatic dispersion owing to destructive interferences. This feature appeared of particular interest for transmission systems where chromatic dispersion compensation constraints could be relaxed. We can note that despite the lower spectral width, the true duobinary format does not bring any benefit in terms of tolerance to chromatic dispersion, contrary to widespread understanding [41].

However PSBT it is yet often referred to as mere duobinary modulation.

A main drawback of PSBT is that it requires an SNR approximately 3dB higher than NRZ. To address this issue, enhanced PSBT (EPSBT) has been proposed ([8][32][33]). It consists in superimposing an NRZ modulation to the PSBT modulation by cascading two modulators in series. This increases the tolerance to noise by improving the extinction ratio above the typical 7dB value of PSBT. However, the extinction ratio should not exceed a typical 13dB, otherwise the advantages of EPSBT are lost, and the EPSBT waveform behaves exactly like a conventional NRZ waveform. An alternative way to implement EPSBT is to pass the PSBT signal into a narrow optical filter: similar to chromatic dispersion, the filter will cause the symbols to overlap with destructive interferences over the "0" symbols and in turn reduce the fraction of energy within the "0" symbols. It is also called Bandwidth-Limited PSBT [34].

IV.1.1.4. *Phase-modulated modulation formats*

Binary Phase Shift Keying (BPSK) modulation format basically consists in encoding "1" and "0" bits into constant-intensity symbols differentiated by a phase of 0 or π. Owing to the difficulties to recover the absolute phase of an optical signal, the detection is usually differential: it is sensitive to the phase shifts between consecutive symbols. As a result, the data are also differentially encoded at transmitter side, with a precoder similar to the one used for PSBT. The modulation format is thus also named as DPSK or DBPSK, with D standing for differential. The generation of a DPSK signal most usually consists in sending the output of a cw laser into a LiNbO3 Mach-Zehnder modulator in push-pull configuration and driven by precoded electrical data. The main difference with an NRZ transmitter lies in the range of electrical signals driving the modulator, such that the amplitude modulation factor goes from $X/ER^{1/2}$ to X for NRZ and from –Y to +Y (with X and Y being real positive values and ER the extinction ratio). Note that if the DPSK could be generated using directly a phase modulator, the Mach-Zehnder-based technique is generally favored due to the better resistance of the signals to nonlinear effects induced by the slight intensity pulse shaping when transitioning from "0" to "π" symbols.

BPSK, even though formerly introduced in the 1980s, gained interest in 2002 when ultra-long distances were demonstrated at a modulation rate of 40Gb/s [35]. Indeed, when combined with differential detection and balanced photodiodes, the DPSK format yields significant improvements in OSNR sensitivity and tolerance to nonlinearities, by about 3dB, as compared

to NRZ format, thus allowing almost doubling of the reach. Transmission distances can be further increased with derived modulation formats including RZ-like additional pulse carving.

Nonetheless, the BPSK-based formats are not easily compatible with 50GHz channel spacing grid. To overcome such limitation, a derived format has been proposed more recently[30]: the so-called "Partial DPSK", involving pre-filtered DPSK, and adapted differential receiver achieving partial demodulation, to give DPSK better tolerance to filtering

Another way to reduce the channel spectral width is to perform multilevel modulation. One promising candidate is Quaternary Phase Shift Keying (**QPSK**). The coding consists of 4 possible symbols with constant intensities and phase shifts separated by $\pi/2$: 0, $\pi/2$, π, $3\pi/2$. As previously mentioned, each symbol corresponds to a pair of bits, and the modulation rate is here half of the bit-rate, such that the channel spectral width is reduced by half with respect to BPSK at constant bit-rate. Like BPSK, QPSK may require differential encoding and decoding, depending on the detection strategy. The QPSK modulator consists of a Mach-Zehnder interferometer composed of two independent BPSK modulators on the arms of the interferometer, one arm supporting an additional $\pi/2$ phase-shift. The detection of QPSK signals lies either on dual differential balanced photo-detectors or on coherent reception.

IV.1.2. Receiver schemes

We will give here an overview of the existing detection schemes, from the conventional direct-detection schemes used for 10G applications to polarization-diversity coherent receivers. The following description of each kind of receiver concerns one modulated channel at a given wavelength, which means that we consider signals after propagation and selection of one specific channel by optical filtering.

As explained earlier, Figure 1-24, direct-detection is used for usual 10G systems. It basically consists of a single-photodiode, sensitive to the intensity of the received light, followed by a simple decision gate. This kind of receiver is used for NRZ or PSBT formats at 40G.

To detect 2-level or 4-level phase-modulated signals such as Binary or Quaternary Phase Shift Keying, (B)PSK or QPSK respectively, a trick must be found to recover the data out of intensity-sensitive photodiodes.

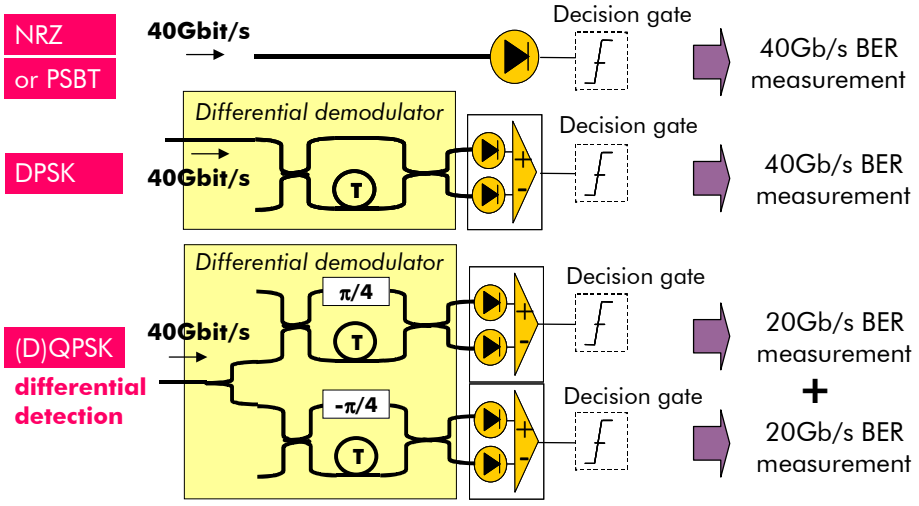

Figure 1-24 : direct detection schemes for intensity modulated signals (top), BPSK (middle) and QPSK (bottom)

Most of the time, the trick of **differential detection** is used (thus the "D" for differential in the acronyms DPSK or DQPSK): it basically consists of the comparison between the signal and itself with 1-symbol duration delay into an optical interferometer. For DPSK, only one

interferometer with one bit-delay is necessary, the outputs of which feed a "balanced-photodiode": one photodiode at each complementary output of the interferometer provides an electrical current dependent on the phase change from one symbol duration to the next (thus the "D" for differential in the acronyms); then the difference of each complementary photocurrent is used to enhance the tolerance to noise and other signal impairments. The resulting photocurrent eventually enters a decision gate. DQPSK can be recovered using two such interferometers and two balanced-photodiodes, each connected at the two complementary outputs of one interferometer, resulting in two receivers operated at half bit-rate. The abovementioned adapted differential detector for Partial DPSK consists of a standard differential detector but the delay between the two arms of the interferometer is only 66% of the bit time.

As for **coherent heterodyne** detection [9], it is basically obtained by mixing the optical signal with a local oscillator running at approximately the same optical frequency, before sending the combined optical field in a photodiode. At photodiode output, we get the beating terms between the optical signal and the local oscillator, and have then access to half information about the phase signal.

The full phase information can be recovered out of the interferences resulting from the mixing process onto a series of 4 photodiodes: the signal is split into 2 orthogonal polarizations, and for each polarization, an interferometer called coherent Mixer is used to mix the signal and the local oscillator, to get the in-phase and in-quadrature components of the signal at two photodiodes outputs. The following figure illustrates the principle of the coherent mixer. It can be noted that two designs of coherent mixer are possible using single-ended or balanced-photodiodes at its output. We need to duplicate this mixer to get a polarization diversity receiver, such as illustrated below.

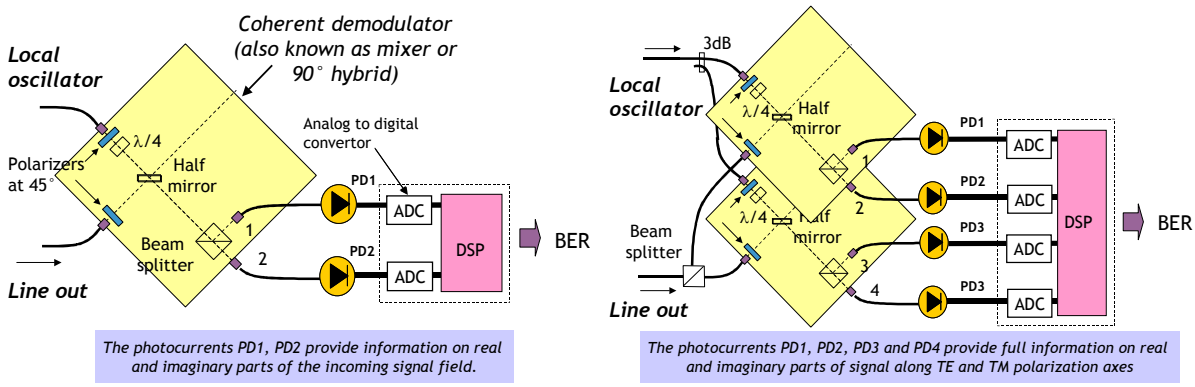

Figure 1-25 : Basic schemes of coherent receivers: polarization sensitive receiver (left) and polarization diversity receiver (right)

Such a polarization diversity receiver is necessary even for signals initially carrying information on a single polarization. Indeed, because of PMD along fibres (due to fibre low birefringence, evolving stochastically with distance and time), the polarization of the signal can not be predicted after propagation and varies with time; the signal can even be partially depolarized; additionally, the resulting birefringence causes different group delays between both components of the signal travelling along the overall principal axes of polarization of the fibre, which is almost similar to multi-paths propagation in radio systems.

The role of digital signal processing, after sampling by Analog to Digital Converters, is then to recover the original signal and mitigate propagation impairments. In case of Polarization Division Multiplexing, those algorithms will also unscramble the two original signals while dealing with PMD. We will not review here the algorithms used in coherent detection since the vast majority of the studies described in this manuscript does not rely on such techniques.

More details can be found in [9] [24] [54] for instance. We will just note that DSP (digital signal processing)-assisted coherent detection has recently brought about a revolution in high-bit rate transmission systems, since the most recent 40 and 100G systems use this technique in combination with polarization multiplexing and QPSK or BPSK.

IV.1.3. Forward Error Correction (FEC) [24]

A transmission is considered "error-free" when BER is smaller than 10^{-13} after propagation. However, the quality of the signal at the receiver end is usually too poor to ensure error-free reception in long-haul systems. This is the reason why forward error correction (FEC) is employed in modern transmission systems. Used in copper-wire radio communication since the 1960s, the application of FEC for the fibre-optic communication systems was not reported until 1988 by Grover [36]. It should be stretched that on shorter distances and lower speed transmissions the fibre-optic channel is almost ideal compared with the traditional copper-based channel.

The principle of FEC is to add redundant information bits within the transmitted signal and to exploit them at the receiver side to detect and correct errors. This extra transmitted information are referred to as FEC overhead and the highest pre-FEC BER that can be corrected to a BER below 10^{-13} after FEC is typically known as FEC limit or threshold.

Different FECs with different characteristics are standardised by the telecommunication standardization sector of the ITU [37]. For ultra long-haul submarine transmissions, FECs with 25% overhead is sometimes employed leading to a FEC limit of $1.31 \cdot 10^{-2}$ as referenced in ITU-T G.975.1-I.7. However, one of today's most widely used FEC for optical systems is referenced in ITU-T G.975.1-I.9. It consists of two interleaved extended Bose-Chaudhuri-Hocquenghem BCH(1020,988) codes with a ten times iterative-decoding. Such FEC requires 7% overhead and the FEC limit is $4 \cdot 10^{-3}$, corresponding to a Q^2 factor about 8.5dB. This means that any transmission resulting in a BER below $4 \cdot 10^{-3}$ can be considered as error-free. This is the FEC considered in the rest of the thesis. Mizuochi [10] gives an overview of FEC in fibre-optic systems where more advanced FECs such as soft-decision FECs are also discussed.

In the following chapters, we consider 7% overhead for 10 and 40Gb/s-modulated systems. We then refer to 10Gb/s and 40Gb/s-modulated systems for actual modulations at 10.7Gb/s and 42.7Gb/s respectively. For 100Gb/s modulated systems including PDM-QPSK and coherent detection as mentioned in Chapter 6, the symbol rate is in fact 28Gbaud and the bit-rate of the modulated signal is in fact 112Gb/s.

IV.2. Optical Amplifiers

We describe here the most usual types of optical amplifiers: the wide-spread Erbium-Doped giber Amplifiers and the principles of distributed Raman amplifiers. More details can be found in [6][8][11].

IV.2.1. Erbium Doped-Fibre Amplifiers

The advent of Erbium-doped fibre amplifiers (EDFA) in the late 1980s has revolutionized the filed of optical communications since it has allowed amplifying optical signals with significant output powers typically as high as 23dBm around 1.55μm over a bandwidth as large as 30nm. Optical amplifiers amplify the incident light through the mechanism of stimulated emission, based on the use of excited states of Er^{3+} ion. To do so, semiconductor optical pumps operating at 1480nm or 980nm bring Er^{3+} ions from the fundamental state $^4I_{15/2}$ to

excited states $^4I_{13/2}$ and $^4I_{11/2}$. All those energy levels are in fact non-degenerated due to Stark effect. After fast non-radiative partial des-excitations, the pumped ions accumulate in the lowest energy level of the $^4I_{13/2}$ state. They can then come back to the energy levels of the $^4I_{15/2}$ state by two means, spontaneous emission or stimulated emission of photons in the range of wavelengths typically between 1500 and 1600nm. In practice, the incoming signal is amplified by the propagation into a 10-20m-long section of Erbium Doped Fibre in which the outputs of 1480 and or 980nm laser diodes are coupled and are co- or contra-propagating with the signal. Depending on the amount of pumping and thus the created inversion of population between fundamental and excited Er^{3+} states, signal amplification is possible in the range of ~[1529-1565] nm (C-band, requiring high population inversion) or [1570-1605]nm (L-band, requiring low population inversion). In addition to the signal amplification, spontaneous emission yields noise over the same spectral range. Due to the presence of multiple optical amplifiers, we usually refer to as spontaneous noise emission. Typical noise figures of EDFAs are in the range of 4 to 8dB. In order to provide a flat spectral gain and noise response over the amplification spectral window, the Erbium-doped fibre is generally followed by a gain flattening optical filter.

Besides, repeaters generally incorporate sections of dispersion compensating fibres (DCFs) located between two EDFA(s). These DCFs have dispersion characteristics opposite to that of the transmission fibre, such that any detrimental waveform distortions due to chromatic dispersion can be contained. However, a proper repeater design demands that the power decay within these fibre sections does not bring significant OSNR degradation. Guidelines to optimize this design are explained in Chapter 5.

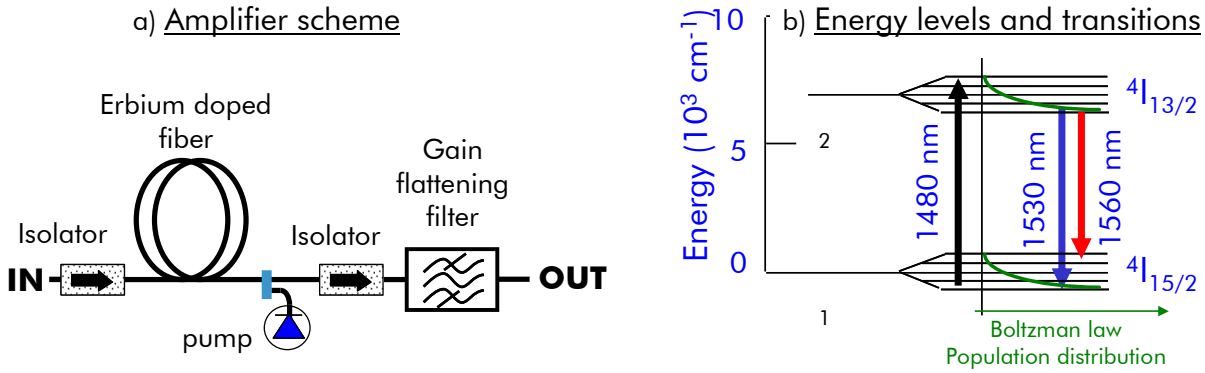

Figure 1-26 : a) typical EDFA scheme; b) energy levels of Er^{3+} and transitions enabling amplifier gain in the C-band.

IV.2.2. Distributed Raman amplification

Stimulated Raman Scattering (SRS) can be used to provide amplification in optical fibres [51][8][6][52]. Contrary to EDFA, it does not require any special fibre since SRS exploits the vibration modes of silica, thus amplification is possible in transmission fibres. To do so, a strong continuous wave is launched (generally backwards) into the fibre. Through SRS, this wave serves as a pump to amplify the WDM channels propagating in the opposite direction, provided that its frequency is approximately 13.2THz higher (or its wavelength 100nm smaller) than the spectral region where gain is needed. Even though full Raman amplification of transmission fibre is possible, hybrid Raman and EDF amplification is often preferred as shown in Figure 1-27. The use of Raman amplification can improve the SNR because it is a distributed process, in contrast to the lumped scheme involved in EDFAs. A better insight into this phenomenon can be obtained by computing the relative change in signal power along a

100 km span, as drawn in Figure 1-27a. In the presence of 15 dB Raman amplification (full line), the power decay resulting from fibre loss is stopped at about 20 km before the next repeater. At this point, the power level is δP=6 dB higher than at the input of a regular EDFA (dotted line). This minimum power level in the span P_{min} mainly sets the amount of noise generated by the overall amplification process. Therefore, deploying Raman amplifiers effectively reduces the span loss by several dB (~δP), or else effectively increases the SNR by the same amount. Naturally, SRS provides a gain only over a limited wavelength region, with gain flatness around 10nm with one pump [52]. Usually gain flatness is generally extended by sending several pumps at different wavelengths simultaneously into the transmission fibre. For instance, in a 6.3Tbit/s C+L-bands experiment [20][21][22], we use three pumps at 1427nm, 1439nm 1450nm providing gain to the C band, and one pump at 1485nm providing gain to the L band, all sent backwards in each fibre span.

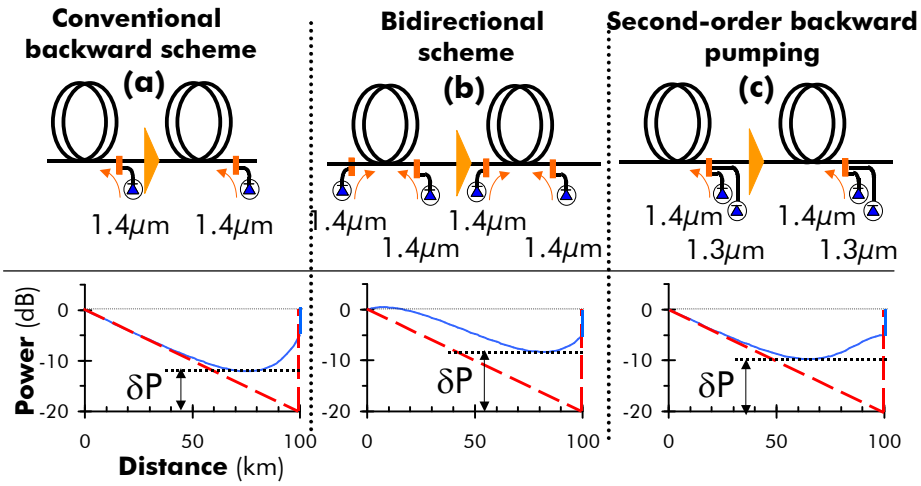

Figure 1-27 : Schematics of Raman-assisted EDFAs (top) in the conventional configuration (a), improved by bidirectional pumping (b) or second-order Raman pumping (c). Assuming 100km-long fibre spans and 15dB total Raman gain, the signal power evolution has been computed (full line) as compared to a lumped EDFA (dotted line).

Two approaches can be used to further improve the noise performance of such Raman-assisted EDFAs. The first one consists in sending the Raman pumps not only in the backward direction but also in the forward direction (Figure 1-27b). The second consists in sending along with all the other pumps, the light from a fibre laser at wavelength 1346nm (in Figure 1-27c). This light act as a secondary pump for the other pumps (here, mostly at 1427 and 1439nm) limiting their decay along the fibre. In both approaches, the minimal power level in the span P_{min} is increased (i.e. δP is increased), as computed in Fig. 6b and 6c. This reduces the noise generated by the overall repeater. We estimate at 1dB the gain on the signal-to-noise ratio obtained using the second-order pumping technique. Naturally, the two approaches (b) and (c) are not contradictory and could be mixed together.

Additionally, the design of Raman or hybrid Raman + EDF amplification has to account for extra loss stemming from the DCF. The loss of the DCF could also be compensated by Raman amplification as in the 6.3Tbit/s C+L-bands experiment [20][21][22]. To this end, four other pumps at 1423nm and 1455nm in C Band, and 1470nm and 1500nm in L band also provide Raman gain in the DCFs. The resulting repeater configuration is summarized in Figure 1-28.

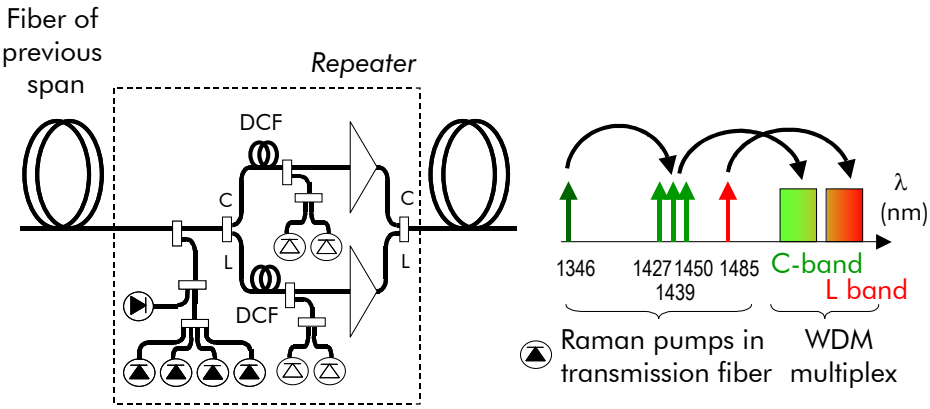

Figure 1-28 : Schematic of an experimental C+L bands repeater (left) involving three successive stages: Raman amplification in the transmission line according a specific wavelength allocation (right), followed by individual Raman amplifier in DCF and EDFA for each of two wavelength bands.

IV.3. Optical Fibres

We review here the characteristics of typical transmission optical fibres, following the introduction of their differences in GVD in section III.3. Table 1 , based on measurements detailed in [38], summarizes the characteristics of SMF fibre (G652), NZDSF fibre types (G655: LEAF™ and TeraLight™) and Pure Silica core Fibre (PSCF) in terms of chromatic dispersion, ratio between chromatic dispersion and chromatic dispersion slope (derivative of chromatic dispersion with angular frequency) , effective area and nonlinear index (based on analytical computation [38] and measurements [39]) at 1550nm. Examples of Dispersion Compensating Fibres are also given. Note that today's DCFs are almost exclusively single-mode. Their chromatic dispersion ranges between -70 and -150ps/nm/km. They are designed to compensate for the dispersion of specific types of fibre over the amplification window since the dispersion over dispersion slope ratio has to be almost equal between DCF and transmission fibre.

In addition to the parameters listed in Table 1 , we should mention attenuation and PMD. Typical loss of a transmission fibre is 0.2dB/km in lab conditions, and typically reaches 0.22 to 0.25dB/km in field conditions, essentially due to the cabling of the optical fibres, their ageing, and the numerous splices over transmission fibre sections (approximately every 2 to 5km). Typical loss of a DCF involves 0.5dB/km attenuation of the compensating fibre itself plus extra connection losses stemming from the difference in effective area between DCF and usual transmission fibres. Fibre Bragg Gratings are an alternative to DCF to compensate for dispersion. They exhibit a lower loss than DCF for high values of cumulated dispersion to compensate but suffer from phase and amplitude ripple issues.

Fibre type	Index profile	Dispersion (ps/nm-km)	Disp./Slope (nm)	A_{ef} (µm²)	$n_{2\ fibre}$ Measurement (10^{-20}m²/W)	$n_{2\ fibre}$ Calculation (10^{-20}m²/W)
Pure Silica-Core Fibre	Step	16.8	193	76.3	2.5	2.53
Standard SMF	Step	17	304	80	2.6	2.66
Teralight	3-Clad	8.1	156	64.8	2.7	2.71
LEAF™	3-Clad	4.2	50	73.7	2.7	2.72
Single-mode DCF	3-Clad	-70.4	166	18.8	3.0	3.01
Higher-order-mode DCF	4-Clad	-162	60	64	3.0	3.04

Table 1 : Main characteristics of transmission and compensating fibres (Soruce [38])

As far as PMD is concerned, typical PMD of a transmission fibre goes down to 0.04ps/km$^{1/2}$ for the most recent fibre generations.

IV.4. ROADM architectures

Reconfigurable Optical Add Drop Multiplexers (ROADMs) enable to selectively route and insert wavelengths to multiple directions, and receive wavelengths stemming from multiple possible directions. They require several functions, such as demultiplexing/multiplexing of the wavelengths, blocking wavelengths and switching wavelengths to different directions. Wavelength blockers or wavelength-selective switches (WSS) are the key integrated elements to perform such ROADMs.

A wavelength-blocker consists of a demultiplexer followed by an array of 1x1 switches (in fact variable optical attenuators) then a multiplexer. It enables to selectively block or let transit a series of wavelength. Note that wavelength power equalization is also possible. The wavelength blocker is suitable for simple topologies such as busses or rings (plus add/drop functionalities at nodes), but will not lead to compact solutions when building multi-degree ROADMs for mesh topologies.

The Wavelength-Selective Switch is today the favoured element to build ROADM: this integrated device enables not only to selectively block a wavelength but to direct it to a set of N possible directions (typically 9 today). It is basically composed of a wavelength-demultiplexer followed by an array of 1xN switches then by N multiplexers. Note that additional wavelength power equalization can also be integrated. Integrated solutions exist today, and the switching and attenuation stage is essentially based on MEMs (Micro-Electromechanical Mirrors) or LCOS (Liquid Crystal on Silicon) technologies, such as solutions provided by JDSU or Finisar respectively. A schematic diagram of a MEMs-based WSS is detailed in Figure 1-29. The WSS is particularly interesting since it enables to redirect any input channel to any output port with adjustable loss. The possible structure of a WSS-based ROADM enabling to add/drop or let pass wavelengths is depicted in Figure 1-30-Left. The extension to a N-degree ROADM (or optical cross connect) enabling to interconnect multiple fibres from multiple directions is depicted in Figure 1-30-Right. More details can be found in [40].

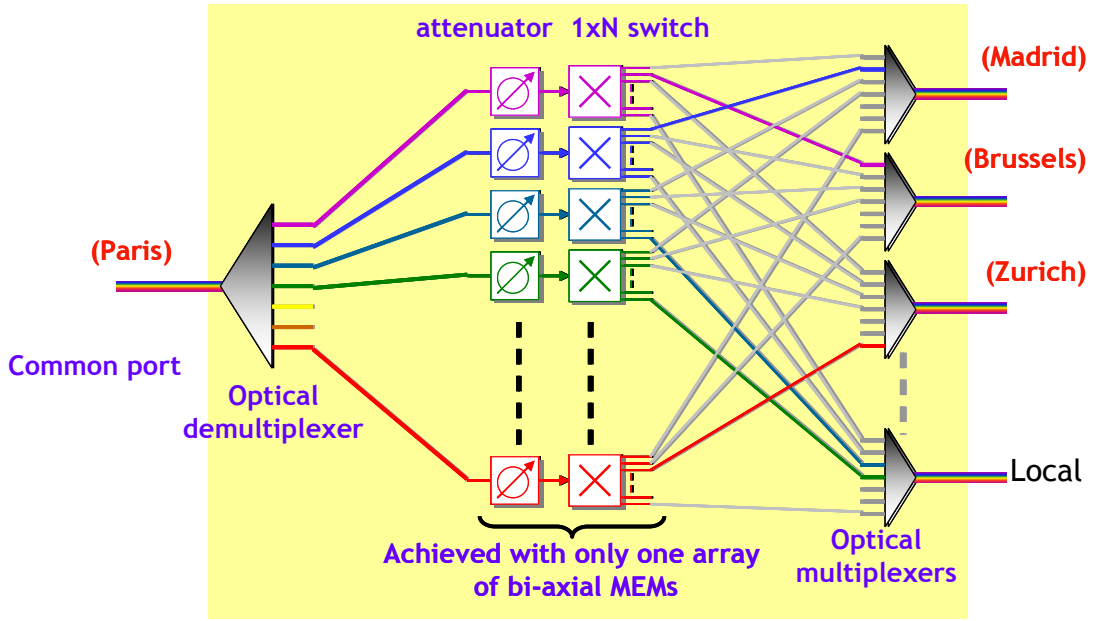

Figure 1-29 : Schematic of a MEMs-based WSS

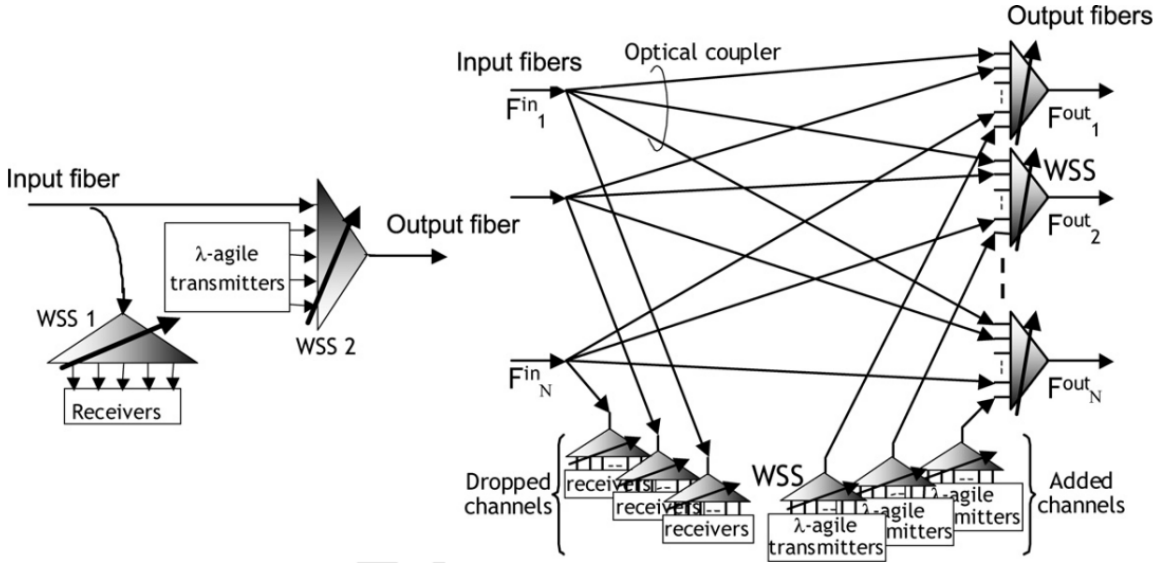

Figure 1-30 : schematic diagram of a WSS-based ROADM (left) and a N-degree WSS-based optical cross-connect (right)

1.V. Optical System Modelling and Domains of validity

We describe here the usual numerical and experimental tools able to emulate optical transmission systems. We then explain the chosen methodology applied in this manuscript to characterize optical networks impacted by multiple sources of impairments, based on the principle of the separation of effects.

V.1. Numerical emulation of transmission systems

The role of numerical simulation is key to understand physical phenomena occurring along the fibres as well as to get insight into the physics behind heterogeneous transmission systems. With simplified or sophisticated models, one can emulate a myriad of configurations much more easily than by experiments, and thus capture the general interactions between the parameters describing the propagation. For that purpose, we generally use an internal tool that aims to emulate transmission links and called OCEAN (Optical Communication Emultator of Alcatel-lucent Networks). We will not explain hereafter the way this tool works, but introduce the basics behind numerical emulation of communication systems.

The principle of a numerical simulation emulating a transmission link is the following: we emulate the generation, then the propagation into transmission sections and the reception of optical channels; eventually we analyze the quality of the received signals by means of OSNR measurements or estimation, or by estimation of the eye opening or the BER.

V.1.1. Emulation of the transmission line thanks to the Split-Step Fourrier Method

In order to emulate numerically the propagation of a signal, time and distance become discrete parameters. The complex amplitude of signals is generally encoded by a 1xN dimension vector representing its evolution with time or frequency, with N generally being a power of 2. In the time domain, the signal samples correspond to a duration δT, and the emulated total temporal window has a duration of $\Delta T = N\ \delta T$. In the frequency domain, this correspond to an emulated spectral window of width $\Delta F = 1/\delta T$ and with samples of width $\delta F = 1/\Delta T$. We generally assume that the central frequency of this vector corresponds to a given reference wavelength.

The numerical generation of modulated signals mimics experimental ways to proceed: a periodic binary sequence of finite period L is generally converted into an analog signal varying with discrete time, with N_{spb} samples per bit time, thus leading to a total length of $N=L*N_{spb}$ samples. Setting the bit time to T_b (equal to the inverse of the bit-rate), this vector emulates a time-frame of $\Delta T=L\ T_b$, with a duration of time samples equal to $\delta T=T_b / N_{spb}$. A Fast Fourier Transform (FFT) of this vector will allow getting the signal in the frequency domain, with frequency samples of size $\delta F = 1/\Delta T=N_{spb}/T_b$ and a total emulated spectral window of $\Delta F= 1/\delta T = N_{spb} / T_b$. This time-varying signal will then undergo modulation similar to experiments, first in base-band, around the central frequency, and then this modulation will be offset to the desired wavelength.

To generate a WDM multiplex, several channels are modulated around different carrier wavelengths and combined directly or after passing through optical multiplexers. The different channels are often encoded with the same modulation and with the same binary sequences (generally 2^n-bit-long De Bruijn sequences) but may experience different phase shifts and time shifts before combination.

In the optical domain, the signal essentially propagates through three types of devices, optical amplifiers, filtering functions and optical fibre sections. Depending on the device, the computation of the evolution of the signal vector is performed in the time or frequency domain. In addition to the signal vector, a second vector containing the noise power spectral density profile may be updated after each crossed element.

Optical amplifiers are characterized by their gain profile in the spectral domain as well as by their noise characteristics. Then either noise random samples are added to the amplified signal in the spectral domain, or the signal vector is simply impacted by the amplifier gain while the noise power spectral density profile is updated. Optical filters are best characterized by their transfer function, thus the evolution of signal and noise vectors after crossing such elements in performed in the frequency domain.

To emulate the propagation of signals into optical fibre, one has to numerically solve the nonlinear Schrödinger equation (NLSE). The NLSE is a nonlinear partial differential equation that does not generally has any analytic solution. A numerical approach is therefore necessary. One of the most widespread methods is known as the Split-Step Fourier Method (SSFM) [6], which is a finite-difference method.

To understand the philosophy of this approach, we can rewrite the NLSE from Equation (1-7) as:

$$\frac{\partial A}{\partial z}(z,T) = (\hat{D} + \hat{N}).A, \; with$$
$$\begin{cases} \hat{D} = -\frac{\alpha}{2} - \frac{i}{2}\beta_2 \frac{\partial^2}{\partial T^2} + \ldots \\ \hat{N} = i\gamma |A|^2 + \ldots \end{cases} \qquad (1\text{-}17)$$

where $\hat{D}$ is a differential operator accounting for dispersion and attenuation in a linear medium, and $\hat{N}$ is a nonlinear operator accounting for nonlinear effects along the fibre (Kerr and Raman effects).

Should signal propagation be governed separately by $\hat{D}$ and $\hat{N}$ operators, the integration of the equation would be straightforward.

The operator $\hat{D}$ accounts for the linear response of the medium and the medium response is therefore well characterized by its infinitesimal transfer function $H(\omega,z).dz = \exp\left(dz.\tilde{\hat{D}}(z,\omega)\right) = \exp\left(\left(-\frac{\alpha(z,\omega)}{2} + \frac{\beta_2(z,\omega)}{2}(\omega-\omega_0)^2 + ..\right).dz\right)$.

The infinitesimal response of the fibre when governed by the nonlinear operator can be computed in the time domain: $\frac{A(z+dz,T)}{A(z,T)} = \exp\left(dz.\hat{N}(z,T)\right) = \exp\left(i\gamma|A|^2(z,T).dz + \ldots\right)$.

In general, dispersion and nonlinear effects act together along the fibre. The split-step Fourier method yields therefore an approximate solution of the NLSE by assuming that in propagating the optical filed over a sufficiently small distance dz, the dispersive and nonlinear effects can act independently. The method thus consists in integrating sequentially the impact of dispersive then nonlinear effects on the signal.

The propagation equation can then be integrated as:

$$A(z+dz,T) = \exp\left(dz.(\hat{D}+\hat{N})\right).A(z,T)$$
$$\approx \left\{FFT^{-1}.\exp\left(\frac{dz}{2}.\tilde{\hat{D}}(z,\omega)\right).FFT\right\}\cdot\exp\left(dz.\hat{N}(z,T)\right)\cdot\left\{FFT^{-1}.\exp\left(\frac{dz}{2}.\tilde{\hat{D}}(z,\omega)\right).FFT\right\}\cdot A(z,T)$$

Such a relationship is approximate since $\hat{D}$ and $\hat{N}$ operators do not actually commute, the error being in third order with dz. Usually the integration step size is set to vary proportionally with $L_{Kerr} = \frac{1}{\gamma.|A|^2}(z,T)$ along the fibre, accounting for reduced nonlinearities due to fibre attenuation. A typical proportionality coefficient is 1% for single-channel propagation and down to 10^{-3} for WDM propagation where Four-Wave Mixing impact is not negligible. The computation time scales proportionally with N $\log_2$ N qnd the number of spatial steps per fibre, with N being the size of the signal vector.

Note that in WDM propagation, the NLSE governing the evolution of the total optical field can be decomposed in several coupled equations corresponding to the evolution of the different channels composing the multiplex. Each equation is impacted by linear effects and nonlinear effects coming from the channel itself (SPM) and the other channels (XPM and FWM). It is therefore possible to compute those separate equations instead of the global equation and study / overlook the impact of one propagation effect. A possible benefit of using coupled equations is computation time: since referring to channels of spectral bandwidth significantly lower than the whole multiplex bandwidth, the NLSE per equation could be computed with reduced spectral window and number of samples N. For instance, when we can neglect Four Wave Mixing the computation time when using coupled equations can be significantly reduced since each equation referring to one of the n channels contains only n nonlinear terms.

To illustrate that section dedicated to the numerical generation and the propagation of signals, we can give an example of the type of simulations performed: in [7], we aimed to capture the evolution with distance and power of the signal impairments due to nonlinear and dispersive effects. We emulated a singly-periodic dispersion-managed terrestrial transmission 40Gb/s system composed of N sections of 100km transmission fibre followed by DCF at the inter-stage of dual-stage EDFAs. With this simulation tool, we were able to vary the transmission distance, dispersion map, input powers into the transmission fibre and DCF before processing the data, amounting to emulating more than a thousand different propagation configurations. Such a parametric study enabled to demonstrate that for optimized dispersion-management strategies, the induced signal degradation varied as a biunivocal function of the nonlinear phase shift (Equation (1-15)) no matter the input power into the transmission fibre or in the DCF, or the number of sections.

V.1.2. Receiver models

There exist several methods to estimate the BER by analytical means or by error counting. Analytical methods rely on the modelling of the optoelectronic receiver and of the statistics of electrical noise at decision time. They usually require the (noiseless) optical signal vector as well as the power spectral density of optical noise at receiver input. The electrical signal is then computed as well as the characteristics of electrical noise at decision time. Further assumptions on the nature of electrical noise enable to get a BER estimate: Gaussian assumptions may lead to Q-factor estimations as in II.2. for each bit or group of bits, then to BER; in direct-detection or balanced differential detection schemes not relying on coherent receivers, the approximation that the optical noise is Gaussian rather leads to consider a non-centred Chi-2 distribution of electrical noise, leading to BER estimates based on Kahrunen-Loewe expansion method [45].

However, in configurations where inline signal-noise nonlinear interaction cannot be neglected, these methods may fail since they require separate inputs for signal and noise. In such configurations and in case of less-conventional receiver types such as coherent receivers, BER can be estimated through a Monte-Carlo–type method. Such a method consists in counting the number of errors out of the reception of a myriad of noisy data samples. To get an estimation of BER with 10% accuracy, it typically requires the detection of a few 100s errors. Thus, the detection of BER around 10^{-3}, 10^{-5} or 10^{-9} would require some 100000, 10^{7} or 10^{11} noisy samples, which can consume significant computation times. Computation times could be reduced by assuming that optical signal and noise do not interact along the fibre sections, resulting in the noiseless propagation of shorter De Bruijn-encoded sequence (in the order of 128 to 2048 bits depending on the link characteristics) and in the repetitive receptions of noisy samples consisting of this optical field plus random optical noise seeds, so as to reach the necessary amount of noisy samples to estimate the BER [46][47].

V.2. Experimental tools

Beside numerical simulations, experimental tools can be used to emulate optical networks and optical transmission systems with devices (fibres, transmitters, receivers, amplifiers…) and propagation issues closer to the conditions of deployed systems. Even though they enable to approach the field conditions, most experimental setups do not aim to mimic exactly deployed systems.

An experimental setup usually consists of a transmitter module, a transmission module and a receiver module.

At transmission input, predetermined pseudorandom sequences are generally encoded into optical signals coming from laser sources in driving electro-optic modulators. As in simulations, the choice of predetermined sequences enables to count the errors at receiver end. WDM systems are often emulated with independent modulations on consecutive channels, so as to prevent interchannel nonlinear artefacts. One way to do so is to generate two separate combs multiplexing each the laser sources of one channel over two, then to modulate independently the outputs of each comb before combining them. At receiver end, an optical filter generally precedes the receiver itself to select the channel to detect.

The transmission section mainly consists of a concatenation of optical amplifiers and optical fibres. One way to emulate long reach systems with limited equipment consists in using a recirculating loop: as shown in Figure 1-31, the transmitter side feeds the loop through an acousto-optic injection switch then an optical 2x2 coupler, the loop itself starts at one output of the 2x2 coupler, then mainly consists of a few hundred kilometres fibre and a few amplifiers followed by a loop acousto-optic switch and ends at the second input of the 2x2 coupler; the second output of the 2x2 coupler is connected to the receiver side. This way, it is possible for an incident signal entering the loop to propagate over multiple loop laps before detection, thus enabling long distances. The control mechanism of the acousto-optic switches is the following: at injection step, the injection switch is in the passing state and the loop switch is in blocking state, so that the modulated signals stemming from the transmitters fill the loop, for typically 1 or 2ms; the injection switch is then in the blocking state and the loop switch is in passing state, so that the previously injected signal circulates inside the loop and feeds the receiver at the same time, with typically 1ms-long detection periods corresponding to different loop laps. The receiver and the loop control must be synchronized so as to enable the error detection. The duration of this process depends on the reach to emulate. The cycle injection and recirculation is then repeated at a frequency of a few tens of Hz. Note that the management of amplification has to ensure lossless loop cycles.

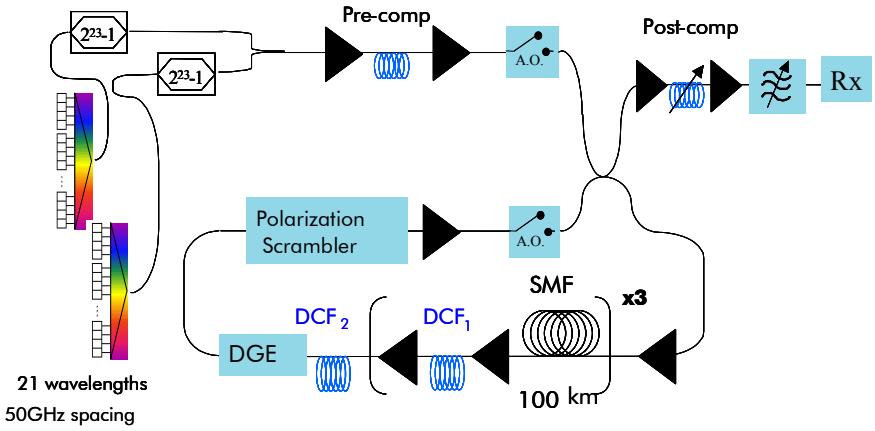

Figure 1-31: Experimental set-up of a recirculating loop.

One of the advantages of the recirculating loop is that it allows the measurement of signal quality after each loop lap. However, it is limited to the repetition of a periodic pattern. This can be of particular importance as soon as polarization effects come into play. One way to approach field conditions is to insert polarization scramblers inside the loop. Improvements of this tool have been reported to better emulate the heterogeneity of actual systems: some utilize the possibility to switch from one loop to another after each lap, individual loops possibly based on different line fibre types [48]; some offer the possibility to add / drop some channels after each loop lap [49].

The following example describes the experimental set-up used in [50] to build a Quality of Transmission estimator for 10Gb/s-modulated systems.

This experimental set-up is based on a 10.7 Gbit/s SMF-based WDM transmission system that is emulated by means of a recirculating loop (see Figure 1-31). It is made of three 100km-long spans of SMF fibre. An in-line Dispersion Compensation Fibre (DCF_1 in Figure 1-31) spool under-compensates each span, in order to maintain a target residual dispersion per span of +100 ps/nm at 1550 nm (i.e. the cumulated dispersion of the line fibre span plus the following in-line DCF). After a loop section, comprising 3-spans sections, a DCF spool (DCF_2 in Figure 1-31) enables to zero the accumulated dispersion at 1550nm over one loop lap. The accumulated dispersion of the pre-compensation DCF (at transmission input) is –860ps/nm at 1550 nm. Eventually, residual dispersion D_{res} is varied at the receiver side using a tuneable dispersion compensation module (referred to as Post-comp).

We have thus propagated 21 channels spaced by 50 GHz and measure the performance of the central wavelength channel (1550.12 nm). Such an approach is representative of the performance of the whole C-band multiplex since the DCF modules do compensate well for the chromatic dispersion of SMF over the whole C-band and since the local chromatic dispersion of the line fibre slightly varies (by less than 10%) over the C-band. The channels have been modulated with Non Return to Zero (NRZ) format and pseudo-random binary sequence of 2^{23}-1 bits.

The nominal power per channel is varied from 1 to 4dBm and is measured at the input of each line fibre span and at every loop lap. The input power per channel into DCF modules is set 7 dB lower than the input into SMF sections. The total transmission distance varies from 300 to 2400 km (1 to 8 loop laps). The PMD measured over a loop lap is 1.45 ps. A polarization scrambler has been introduced into the loop in order to reduce the loop polarization effects so as to only consider the penalties induced by the chromatic dispersion and the nonlinear phase. PMD induced penalties will be considered independently.

V.3. Methodology used in this manuscript: physical effects decoupling

Designing optical transmission systems as well or predicting the quality of transmission is a complex issue: we have previously seen that a transmission link is composed of the concatenation of a myriad of individual subsystems. For instance, a 1600km-long link composed of 80-km sections of transmission fibre is likely to comprise 20 non-identical sections of transmission fibre, probably the same amount of dispersion compensating modules, more than 20 dual-stage amplifiers, intermediate ROADMs, and a certain number of transmitters and receivers operating at given bit rate(s) with given modulation format(s) and channel spacing. Besides, one has to account the system heterogeneity due to the non-negligible uncertainties related to the deployed subsystems or due to the history of the evolution of the installed networks. Eventually, we have seen that propagation is affected by numerous physical effects occurring at the same time, some of which are time-varying while others are nonlinear.

Therefore, it becomes crucial to identify some main aggregated sources of impairments that could simply describe the signal propagation while dealing only with these main sources and the related parameters that help to describe their impact. This is the main goal of this manuscript. For that purpose, one constant direction is to assess whether the impacts of different propagation effects can be considered as decoupled, and build the design or performance prediction tools based on that assumption.

The first assumption being made in that direction is to separate (nonlinear) signal propagation from noise accumulating along the links. All the studies to come emulate the impact of ASE noise by partially or totally adding noise after signal propagation. We have investigated this approximation by theoretical, numerical or experimental ways for 10Gb/s NRZ-modulated systems in [43]. The resulting OSNR penalties due to the nonlinear interaction between noise and signal rarely happen to produce more than 0.5dB penalty. The net impact is expected to fade with high chromatic dispersion fibres and at higher symbol rates. Other studies have showed that for 40Gb/s-modulated systems, the impact of such noise-signal interaction remained low compared to other signal-signal nonlinear interactions, even for phase-modulated systems [44]. Allowing the separation of noise and other propagation effects enables to characterize their impact separately through estimations of OSNR on the one hand, and measurements of OSNR sensitivities or penalties.

Based on this principle of effects decoupling, we first investigate in Chapter 2 and 3 the sole impact of Kerr-like nonlinearities and chromatic dispersion, overlooking other sources of signal degradations. Then in Chapter 4, we investigate the impact of other propagation effects such as PMD or inline optical filtering and investigate how to combine their impact with the impact of nonlinearities and noise to build an accurate estimator of the quality of transmission.

1.VI. Summary

We have presented in this chapter the fundamentals of optical transmission systems that will be necessary to understand the following work. We have introduced the main building blocks of optical transmission systems and networks, then the main physical effects coming into play. We have then described the means to emulate transmission systems both by numerical or experimental means as well as the methodology that will be used throughout this manuscript. In the following, we will now investigate the accumulation of nonlinear effects, their system impact and quality of transmission estimators.

Eventually, we have experimentally characterized the nonlinear coefficients of typical optical fibres that will serve as references for the emulation of transmission systems in this manuscript and the subsequent building of design and prediction tools. Such results, shown here in the following Appendix, were presented at ECOC conference in 2001 [39].

1.VII. Appendix: Experimental estimation of nonlinear index and effective areas of optical fibres, and assumption of constant n2 over C+L band

Here the original contributions to this manuscript start with an experimental characterization of the nonlinear coefficient of most used optical fibres that had been published at ECOC conference in 2001 [39] and will serve as a reference for the studies in the following chapters.

The nonlinear index coefficient n_2 is one key parameter that is needed to characterize the strength of the Kerr nonlinearity. All of the techniques that have been proposed for measuring n_2 provide indirect estimation through one of the Kerr-related phenomena. A large number of them resort to the measurement of the nonlinear phase, be it the result of SPM or XPM [55]. These techniques mostly use interferometric devices, which are subject to environmental instability, a potential cause for large uncertainties. In other approaches, the distortions caused by SPM are analyzed through spectral measurements [56], which requires a good knowledge of the initial waveform. The simplest time-dependent waveform is probably a wave of sinusoidal envelope. Such a wave can be generated through the beating of two continuous-wave (cw) lasers, as in [56]. However, in this case, measuring the relative power of the harmonic components induced by SPM amounts to measuring the relative power of the inter-modulation products induced by Four-Wave Mixing (FWM) as two cw tones propagate, a method described earlier in ref. [57]. The nonlinear index n_2 can be derived from these power measurements through an analytical formula, but a better accuracy is obtained through numerical simulations. Only DSF was tested this way, but one key advantage of the FWM approach is that it can be extended to any fibre type with the same apparatus.

Here, this technique is applied to the measurement of n_2 over C+L bands for two typical terrestrial fibres (Standard Single-Mode Fibre, and TeraLight™, a non-zero dispersion shifted fibre (NZDSF)), demonstrating that n_2 is independent on wavelength. Then, we measured for the first time a large and representative panel of fibres at 1550 nm with the same technique, ranging from highly negative to highly positive dispersion fibres.

Experimental set-up and principle

The experimental set-up for the nonlinearity strength measurements is shown in Figure 1-32. For a given central wavelength, two cw signals emitted by temperature-controlled DFB (Distributed FeedBack) lasers with 0.25 nm spacing are sent into two booster amplifiers of variable power. The output powers are equalised within 0.01 dB. The polarizations of the cw waves after the amplifiers are adjusted until parallel to each other using polarization controllers and a polarizer. The pump signals are then combined into the fibre. After propagation, the output signal is fed to an optical spectrum analyser of 0.02 nm resolution to get the power ratio I0/I1 between the power of the pumps I0 and the power of the harmonics I1 generated by four-wave mixing (see Figure 1-32.b-c).

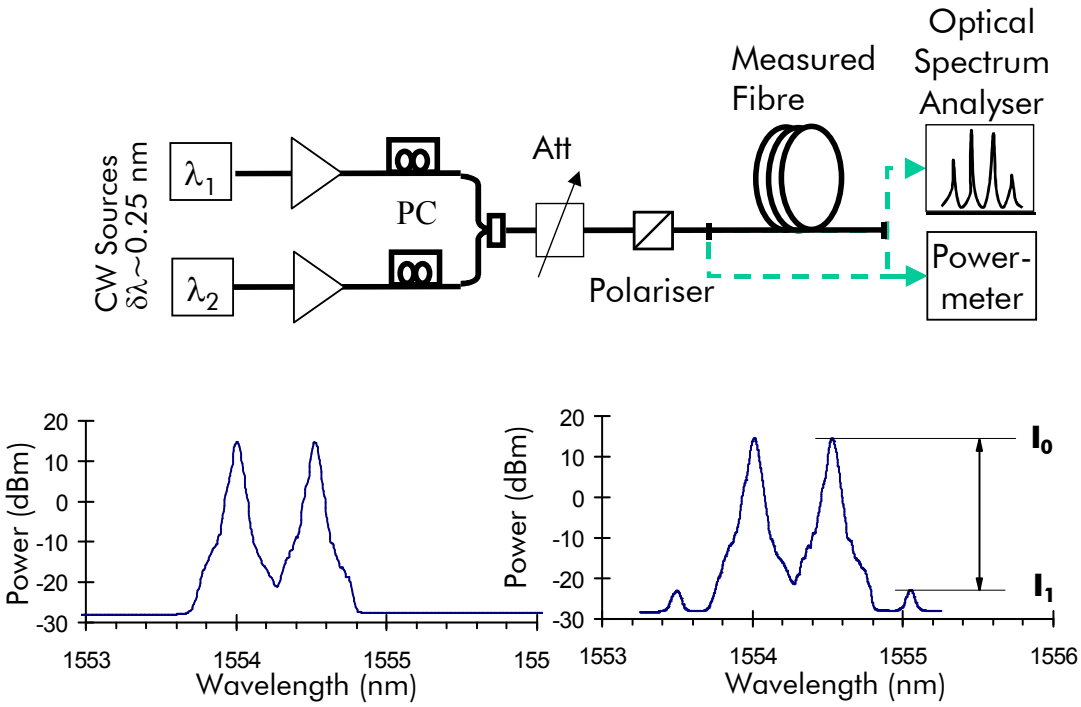

Figure 1-32 : Experimental set-up (top, a) and typical input and output spectra (bottom left and right b,c) with the effect of FWM.

Then the nonlinear coefficient n_2/A_{eff} (A_{eff} being the fibre effective area) is recovered when this experimental power ratio I_0/I_1 matches that obtained after some numerical integration of the nonlinear Schrödinger equation. The knowledge of A_{eff} at the specified wavelength finally leads to n_2.

To assert a good accuracy and FWM efficiency at the same time, the fibre length was carefully chosen for each type of fibre, because of the phase-matching condition governing the FWM process [59]. Besides, the power of the generated harmonic components had to remain significantly higher than the amplifier noise, requiring high input powers, though low enough to avoid noticeable Brillouin effects, and finely controlled. Eventually, the fine adjustment of those parameters leads us to an excellent accuracy (estimated around 3%) on the Kerr nonlinear coefficient for all kinds of fibre.

In actual fibres, averaging over all polarization states is taken into account in numerical simulations by an effective nonlinear coefficient, 8/9 lower than the material coefficient [58]. The results presented in this paper correspond to the material nonlinear coefficient.

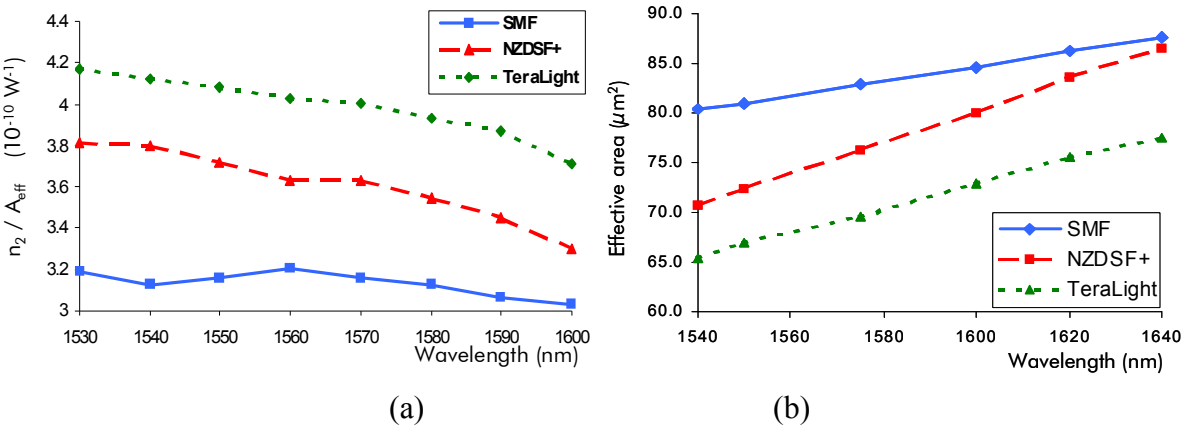

Figure 1-33 : nonlinear coefficient n2/Aeff (a) and effective area (b) measurements vs. Wavelength

Results:

Figure 1-33-a represents the nonlinear coefficient n_2/A_{eff} from 1530 to 1600 nm for two typical terrestrial fibres: Standard Single Mode Fibre, TeraLight™, and LEAF™ fibre (see parameters in Table 1). Every point on the graph represents the fitted nonlinear coefficient corresponding to the measured FWM efficiency, for several input powers. The reproducibility of the nonlinear coefficient determination is within 1%. For every fibre, the nonlinear coefficient is found to decrease with wavelength.

To extract the nonlinear index, we measured the effective areas of the fibres in study over C+L bands (Figure 1-33-b), using the direct far-field method according to the TIA/EIA Standard [60]. The effective area is found to vary as a linear increasing function of wavelength with a good accuracy for any fibre.

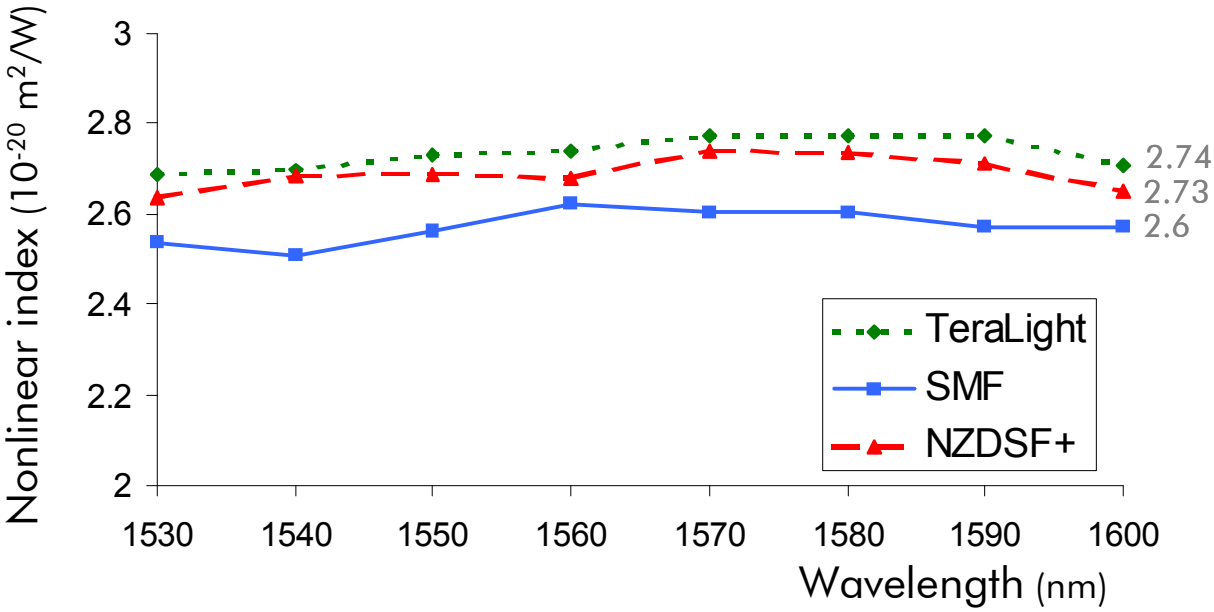

Figure 1-34 : Nonlinear index vs. wavelength for SMF, TeraLight™ and LEAF™ fibres.

The nonlinear index n_2 is then deduced from those measurements. On Figure 1-34, n_2 is plotted over C and L bands, showing its weak sensitivity with wavelength: for every fibre, its variations remain within the 3% error margin. Therefore, the variation of the nonlinear coefficient comes only from the effective area dependence on wavelength.

	Length (km)	**D** (1550 nm) (ps/nm.km)	**n2/Aeff** 10^-10 W^-1	**Aeff** (μm_2)	**n2** 10^-20 m2/W
PSCF	1.00	16.8	**3.3**	76.3	**2.5**
SSMF	1.76	17.0	**3.2**	80	**2.6**
TeraLight	2.00	7.9	**4.1**	66.9	**2.7**
NZDSF +	2.00	4.2	**3.6**	73.7	**2.7**
NZDSF - 1	2.00	-2.1	**3.6**	75.4	**2.7**
NZDSF - 2	1.84	-2.9	**4.9**	56	**2.7**
NZDSF - 3	1.27	-4.0	**5.6**	49	**2.7**
DCF 1	0.71	-50.9	**16.5**	18.1	**3.0**
DCF 2	0.51	-70.4	**16.0**	18.8	**3.0**

Table 2 : n2/Aeff and n2 measurement results for PSCF, SSMF, various NZDSF and DCF

We also measured a wide range of typical fibres (see Table 2) at 1550 nm, corresponding to commercially available products from different suppliers for terrestrial or submarine systems: Dispersion Compensating Fibres (DCF), various NZDSF with positive or negative dispersion, SSMF and Pure Silica Core Fibre.

Nonlinear index is 2.5 10^{-20} m^2/W for PSCF, 2.6 for SMF, whereas all NZDSF have a n_2 of 2.7 10^{-20} m^2/W and DCF index is 3 10^{-20} m^2/W, confirming that Germanium concentration increases the value of the nonlinear index coefficient [61].

Conclusion:

We experimentally demonstrated that the nonlinear index coefficient does not depend on wavelength at least on C+L bands and measured all sorts of submarine or terrestrial fibres ranging from SMF to DCF with a FWM technique, which offers high accuracy and repeatability. Such results have been published at ECOC conference [39] and further confirmed by analytical models estimating the nonlinear index of fibres based on the concentration of doping ions such as Germanium [38].

1.VIII. References

[1] J.-X. Cai, Y. Cai, Y. Sun, C. R. Davidson, D. G. Foursa, A. Lucero, O. Sinkin, W. Patterson, "112x112 Gb/s Transmission over 9,360 km with Channel Spacing Set to the Baud Rate (360% Spectral Efficiency)", in Proc. European Conference on Optical Communications Conference (ECOC'11), paper PD2-1, September 19-23, 2010, Torino, Italy

[2] G. Charlet, M. Salsi, H. Mardoyan, P. Tran, J. Renaudier, S. Bigo, M. Astruc, P. Sillard, L. Provost, F. Cérou, "Transmission of 81 channels at 40Gbit/s over a Transpacific-Distance Erbium-only Link, using PDM-BPSK Modulation, Coherent Detection, and a new large effective area fibre", in Proc. European Conference on Optical Communications Conference (ECOC'O8), paper Th3E3, September 21-25, 2008, Brussels, Belgium

[3] J.-X. Cai, Y. Cai, C. Davidson, A. Lucero, H. Zhang, D. Foursa, O. Sinkin, W. Patterson, A. Pilipetskii, G. Mohs, N. Bergano, "20 Tb/s capacity transmission over 6,860km", in Proc. Optical Fibre Communications Conference (OFC'11), paper PDPB4, March 6-10, 2011, Los-Angeles (California), USA

[4] D. Qian, M.-F. Huang, E. Ip , Y.-K. Huang, Y. Shao, J. Hu, T. Wang, "101.7 Tb/s (370×294- Gb/s) PDM- 128QAM- OFDM Transmission over 3×55- km SSMF using Pilot- based Phase Noise Mitigation," in Proc. Optical Fibre Communications Conference (OFC'11), paper PDPB5, March 6-10, 2011, Los-Angeles (California), USA

[5] J. Sakaguchi, Y. Awaji, N. Wada, A. Kanno, T; Kawanishi, T. Hayashi, T. Taru, T. Kobayashi, M. Watanabe, "109Tb/s (7x97x172Gb/s SDM/WDM/PDM) QPSK transmission through 16.8km homogeneous multi-core fibre", in Proc. Optical Fibre Communications Conference (OFC'11), paper PDPB6, March 6-10, 2011, Los-Angeles (California), USA

[6] G.P. Agrawal, "Nonlinear fibre optics", third edition, Academic Press, 2001

[7] J.-C. Antona et al, "Nonlinear cumulated phase as a criterion to assess performance of terrestrial WDM systems", in Proc. Optical Fibre Communications Conference (OFC'02), paper WX5, March 18-22, 2002, Anaheim, California, USA

[8] E. Desurvire et al, « Erbium-doped fibre amplifiers, Device and System Developments », Wiley & sons, Chapter 7, New York, 2002

[9] G. Charlet, "Coherent detection associated with Digital Signal Processing for Fibre Optics Communications", C. R. Physique 9 (9-10) (2008) 1012-1030

[10] T. Mizuochi, "Recent progress in forward error correction and its interplay with transmission impairments", IEEE Journal of Selected Topics in Quantum Electronics, Vol. 12, No. 4, July/August 2006, pp.544 - 554

[11] I. P. Kaminow, T. Li, "Optical Fibre Telecommunications IV-B: Systems and Impairments", Academic Press; 1st edition (April 15, 2002)

[12] S. D. Personick, "Receiver Design for Digital Fibre Optic Communications Systems," Bell System Technical Journal, Vol. 52, No. 6, pp. 843-886, 1973

[13] A.R. Chraplyvy et al, "8x10Gb/s transmission through 280km of dispersion-managed fibre", IEEE Photon. Technol. Lett., vol. 5, n°10, pp. 1233-1235 (1993).

[14] C. Kurtzke, "Suppression of fibre nonlinearities by appropriate dispersion management", IEEE Photon. Technol. Lett., Vol. 5, n°10, pp. 1250-1253 (1993)

[15] S. Bigo et al, "Design of multi-terabit/s terrestrial transmission systems facilitated by simple analytical tools", in 'Optical Communications 2. Transmission systems and

networks' (Annales des Télécommunications Tome 58 N° 11-12 Novembre-Décembre 2003), pp.1757-1784
[16] C. Xie, "A Doubly Periodic Dispersion Map for Ultralong-Haul 10- and 40-Gb/s Hybrid DWDM Optical Mesh Networks", IEEE Photonics Technology Letters, Vo. 17, No. 5, May 2005
[17] A. Färbert et al, "Optimised dispersion management scheme for long-haul optical communication systems",IEE Electronic Letters, Vol35, No21, Oct 1999,pp 1865-1866
[18] A. Morea et al, "New transmission systems enabling transparent network perspectives", C. R. Physique 9 (9-10) (2008), 985-1001
[19] M. Joindot, S. Gosselin, "Optical Fibre Transport Systems and Networks: Fundamentals and Prospects", C. R. Physique 9 (9-10) (2008), 914-934
[20] G. Charlet, J.-C. Antona, S. Lanne, P. Tran, W. Idler, M. Gorlier, S. Borne, A. Klekamp, C. Simonneau, L. Pierre, Y. Frignac, M. Molina, F. Beaumont, J.-P. Hamaide, S. Bigo, "6.4Tb/s (159x42.7Gb/s) Capacity over 21x100km using Bandwidth-Limited Phase-Shaped Binary Transmission", ECOC'02, Post-Deadline paper PD 4.1, Copenhagen (Denmark), Sept 2002
[21] G. Charlet, J.-C. Antona, S. Lanne, S. Bigo, "From 2100 to 2700km distance using Bandwidth-Limited Phase-Shaped Binary Transmission at 6.3Tb/s capacity", Proc. OFC'2003, paper WE3, Atlanta (Georgia), USA, March 2003
[22] S. Bigo, Y. Frignac, J.-C. Antona, G. Charlet, "Design of multi-terabit/s terrestrial transmission systems facilitated by simple analytical tools", Annales des Télécommunications, Nov-Dec 2003
[23] P. M. Krummrich, R. E. Neuhauser, and G. Fischer, "Experimental Comparison of Raman Thresholds of Different Transmission Fibre Types," in Proc. of European Conference on Optical Communication ECOC 2000, Munich, Germany, Sept. 2000, paper 4.4.1.
[24] O. Bertran Pardo, Thèse de doctorat "On coherent detection for optical transmissions at 40 Gb/s and 100 Gb/s", Télécom ParisTech, September 2010
[25] A. R. Chraplyvy, "Limitations on Lightwave Communications Imposed by Optical-Fibre Nonlinearities," Journal of Lightwave Technology, vol. 8, no. 10, pp. 1548–1557, Oct 1990.
[26] K.-P. Ho, "Statistical Properties of Stimulated Raman Crosstalk in WDM Systems," Journal of Lightwave Technology, vol. 18, no. 7, pp. 915–921, Jul. 2000.
[27] S. Bigo, S. Gauchard, J.-P. Hamaide, "Experimental investigation of Stimulated Raman Scattering limitation on WDM transmission over various types of fibre infrastructures", IEEE Photon. Technol. Lett., vol 11, No.6, pp. 671-673, 1999
[28] M. Zirngibl, "Analytical model of Raman gain effects in massive wavelength division multiplexed transmission systems", Electronics letters, vol. 34, No. 8, pp. 789-790, 1998
[29] S. Bigo, A. Bertaina, Y. Frignac, S. Borne, L. Lorcy, D. Hamoir, D. Bayart, J.-P. Hamaide, W. Idler, E. Lach, B. Franz, G. Veith, P. Sillard, L. Fleury, P. Guénot, P. Nouchi, "5.12 Tbit/s(128x40Gbit/s WDM) transmission over 3x100 km of TeraLight Fibre", ECOC'00, post-deadline paper 1.2, Sept. 3-7 2000, Munich (Germany)
[30] P. J. Winzer and R. J. Essiambre, "Advanced Optical Modulation Formats," Proceedings of the IEEE, Vol. 94, No. 5, May 2006
[31] D. Penninckx, "Etudes des liaisons numériques terrestres sur fibres optiques dispersives : du codage duobinaire aux transmissions binaires à profil de phase controlée (PSBT)", Thèse de doctorat, Mars 1997, ENST.
[32] H. Bissessur, L. Pierre, D. Penninckx, J.-P. Thiéry, and J.-P. Hamaide, « Enhanced phase-shaped binary transmission for dense WDM systems", Electron. Letters, vol. 37, No. 1, pp. 45-46 (2001).

[33] J.-C. Antona, D. Penninckx, “Enhanced phase-shaped binary transmission modulation format for dispersion-managed WDM systems”, Proc. of ECOC’00 (European Conf. on Optical Communications), 8.3.4, München (Germany), Sept 2000
[34] G. Charlet, J.-C. Antona, S. Lanne, P. Tran, W. Idler, M. Gorlier, S. Borne, A. Klekamp, C. Simonneau, L. Pierre, Y. Frignac, M. Molina, F. Beaumont, J.-P. Hamaide, S. Bigo, “6.4Tb/s (159x42.7Gb/s) Capacity over 21x100km using Bandwidth-Limited Phase-Shaped Binary Transmission”, Proc. of ECOC’02, Post-Deadline paper PD 4.1, Copenhagen (Denmark), Sept 2002
[35] A.H. Gnauck, et al., “2.5 Tb/s (64 × 42.7 Gb/s) Transmission over 40x100km NZDSF using RZ-DPSK format and all-Raman amplified spans”, in: OFC’02, Anaheim, CA, March 17–22, FC2-1
[36] W. D. Grover, “Forward Error Correction in Dispersion-Limited Lightwave Systems,” Journal of Lightwave Technology, vol. 6, no. 5, pp. 643–654, May 1988.
[37] ITU-T G.975.1, “Forward Error Correction for High Bit Rate DWDM Submarine Systems”, Feb. 2004
[38] P. Sillard, P. Nouchi, J-.C. Antona, S. Bigo, “Modeling the nonlinear index of optical fibres”, Proc. of OFC’05, paper OFH4, Anaheim, February 2005
[39] J.-C. Antona, S. Bigo, S. Kosmalski, “Nonlinear index measurement of various fibre types over C+L bands using four-wave mixing”, Proc. of ECOC’01, We. L.1.2, Amsterdam (Netherlands), 2001
[40] A. Morea et al, “New transmission systems enabling transparent network perspectives”, C. R. Physique 9 (9-10) (2008), 985-1001
[41] D. Penninckx et al, “Relation between spectral bandwidth and the effects of chromatic dispersion in optical transmissions”, Electronics Letters, vol.32, No. 11, pp. 1023-1024, 1996
[42] D. Penninckx et al, “The phase-shaped binary transmission (PSBT): a new technique to transmit far beyond the chromatic dispersion limit”, IEEE Photon. Tehcn Lett., vol. 9, pp 259-261, 1997
[43] P. Serena, A. Bononi, J.-C. Antona and S. Bigo, “Parametric Gain in the Strongly Nonlinear Regime and its Impact on 10 Gb/s NRZ Systems with Forward-Error Correction”, IEEE Journal of Lightwave Technology, Volume 23, Issue 8, Aug. 2005, pp. 2352 – 2363
[44] A. Bononi, P. Serena, N. Rossi, and D. Sperti, ``Which is the Dominant Nonlinearity in Long-haul PDM-QPSK Coherent Transmissions?" in Proc. ECOC 2010, paper Th10E1, Torino, Italy, Sept. 2010
[45] E. Forestieri, “Evaluating the error-probability in lightwave systems with chromatic dispersion, arbitrary pulse shape and pre- and postdetection filtering”, IEEE Journal of Lightwave Technology, Volume 18, Issue 11, pp. 1493-1503, Nov. 2000
[46] J.-C. Antona, E. Grellier, A. Bononi, S. Petitrenaud, S. Bigo, “Revisiting Binary Sequence Length Requirements for the Accurate Emulation of Highly Dispersive Transmission Systems”, Proc. of ECOC 2008, Paper We 1.E.3, Brussel (Belgium), September 2008
[47] E. Grellier, J.-C. Antona, S. Bigo, “Are multilevel pseudorandom sequences really needed to emulate highly dispersive optical transmission systems?”, in Proc. of ECOC 2010, Paper We 6.A.1 , September 19-23, Torino (Italy)
[48] P. Peloso, M. Prunaire, L. Noirie, and D. Penninckx “Optical transparency of a heterogeneous pan-European network,” J. Lightwave Technology, vol. 22, no. 1, pp. 242–248, Jan. 2004
[49] T. Zami, P. Henri, L. Lorcy, C. Simonneau, "Impact of the optical routing on the transmission in transparent networks," Optical Communication, 2009. ECOC '09. 35th

European Conference on , vol., no., pp.1-2, 20-24 Sept. 2009
[50] B. Lavigne, F. Leplingard, L. Lorcy, E. Balmefrezol, J.-C. Antona, T. Zami, D. Bayart, "Method for the determination of a Quality-of-Transmission estimator along the lightpaths of partially transparent networks", in Proceedings IEEE ECOC07, paper 08.5.2, Berlin (Germany), September 2007
[51] R.H. Stolen and E.P. Ippen, "Raman gain in glass optical waveguides", Applied Physics Lett., 22(6), 276 (1973)
[52] D. Bayart, "Undersea Fibre Communication Systems – Chapter 4", editor J. Chesnoy, Elsevier Science (USA), 2002
[53] C. Fludger et al., "10x111Gbit/s, 50GHz spaced, POLMUX-RZ-DQPSK transmission over 2375km employing coherent equalization", Proc. of OFC'07, paper PDP22, March 2007, Anaheim (California)
[54] E. Grellier, "Etude des effets non-linéaires à l'œuvre dans les systèmes de transmissions optiques fortement dispersifs", Thèse de doctorat, Université de Besançon, July 2011
[55] Y. Namihira: 'Nonlinear coefficient round robin measurements for various DSF in Japan and UK'. European Conference on Optical Communication, ECOC'00, Munich, 2000, We 8.2.5.
[56] A. Boskovic et al.: 'Direct continuous-wave measurement of n_2 in various types of telecommunication fibre at 1.55 μm'. Optics Letters, vol. 21, No. 24, 1996, pp 1966-1968
[57] L. Prigent et al: 'Measurement of fibre nonlinear Kerr coefficient by Four-Wave Mixing'. IEEE Photonics Technol. Lett., vol. 5, 1993, pp. 1092-1095
[58] S.V. Chernikov et al., Optics Letters, vol. 21, No. 19, 1996, pp. 1559-1561.
[59] S. Bigo et al: 'Measurement of the impact of fibre nonlinearities on high data rate, dispersion-managed WDM systems' (invited paper). Symposium on Optical Fibre Measurements, Symposium on Optical Fibre Measurements SOFM'98 , Boulder, 1998, pp 77-82
[60] Standard TIA/EIA-455 - FOTP 132, 1998
[61] D.L. Philen et al: 'Measurement of the nonlinear index of refraction; n_2, for various fibre types'. Optical Fibre Commincation Conf., OFC'00, Baltimore, 2000, Th L.5, pp. 184-186

Chapter 2 : SIMPLE CRITERION TO PREDICT THE IMPACT OF NONLINEAR EFFECTS IN IDEAL DISPERSION-MANAGED SYSTEMS

Contents

2.I. Motivation and outline

The capability to predict how accumulated nonlinear effects impact signal distortions is paramount to design long haul optical transmission systems. Indeed, while low signal power transmission systems suffer from the accumulation of noise stemming from the inline optical amplifiers, high signal power transmission systems suffer from the accumulation of detrimental nonlinear effects. Thus system reach is most of the time determined by the power trade-off between the impacts of noise and nonlinear Kerr effects. However, the simple determination of how nonlinear effects can accumulate is not trivial due to their complex interaction with chromatic dispersion, and because of the highly heterogeneous nature of terrestrial optical networks. By essence, a dispersion-managed transmission link consists of a non-obvious concatenation of line fibre sections and dispersive compensating modules with alternate signs of chromatic dispersion; the distance between amplifier sites may significantly vary from one amplifier to the other, from 10 to 150km; the local characteristics of fibre sections may vary from one section to the other. Besides, since most optical networks have been deployed and improved for years and decades, it has become common to consider signal propagation over a hybrid transmission link presenting different types of line fibre installed at different periods of time.

In that prospect, the chapters 2 and 3 aim to build a tool that predicts the impact of nonlinear Kerr effect on signal quality with reasonable accuracy and computation time. Chapter 2 focuses on optical transmission systems operated in ideal, academic conditions with one type of line fibre and optimized, periodic, dispersion-management while Chapter 3 will aim to assess the domain of validity of the tools developed in Chapter 2 and to adapt them to real-life conditions of deployed optical networks.

Here, in section 2.II. , we particularly revisit the simple nonlinear cumulated phase parameter from Equation (1-15) and numerically demonstrate that we can build a locally bi-univocal relationship with excellent accuracy between transmission penalties and the nonlinear phase for a terrestrial WDM system impacted by Group Velocity Dispersion and Kerr effects whatever the fibre input powers and distance. Such studies are conducted for multiple bit-rates and multiple types of transmission fibre.

Then in section 2.III. , we investigate more sophisticated analytical models derived from the propagation equation and discuss their ability to predict nonlinear / dispersion induced signal distortions system performance. We show that they enable to get more insight into physics, to simplify the optimization of the dispersion management but do not appear particularly more accurate than the simple nonlinear phase-based prediction tool, despite a substantial increase in the computation complexity. Yet such models enable to confirm that the signal distortions could vary as a function of a linear combination of the nonlinear phases stemming from each fibre section, which can be further simplified under certain assumptions of bit-rate and of dispersion management so as to comfort the use of the total nonlinear phase proposed in section 2.II. .

2.II. Nonlinear phase shift to account for Kerr / GVD interaction for single line-fibre type systems

This section focuses on the determination of a simple parameter accounting for the joint impact of Kerr nonlinear effects and Group Velocity Dispersion in the case of periodic dispersion managed transmission systems with only one type of line fibre and optimized dispersion management conditions.

In fibres with zero chromatic dispersion, the sole impact of Kerr effect is a time-varying phase shift given by Equation (1.15) on the propagating optical field, proportional to instantaneous signal power. From a system point of view, the transmission of an intensity modulated signal into such a medium could ideally suffer from no penalty after direct detection of intensity through a photodiode. In a multi-channel environment though, Kerr effect also causes detrimental transfer of energy between independently detected channels through Four-Wave Mixing. This effect is maximized for zero chromatic dispersion (cf Chapter 1). Propagation on fibres with very low values of chromatic dispersion is therefore best avoided, and most transmission systems involve non-zero dispersion fibres, while the combined impact of nonlinear effects and chromatic dispersion can be mitigated through optimized dispersion management, but up to a certain point only. Due to the complex Kerr / chromatic dispersion interaction, finding a relevant parameter accounting for the accumulation of nonlinearities, and directly linked to the impact on the system, is not straightforward for dispersion-managed systems.

II.1. Nonlinear phase shift as criterion to simply describe WDM optical transmission systems with optimized dispersion management scheme at 40 and 10Gb/s

In 2002, we introduced the concept of nonlinear phase shift for 40G dispersion-managed systems [62].

Prior to that work, to rate nonlinear effect accumulation in dispersion managed systems, simple criterions such as the span number of a link, or the input power into the line fibre [67][68] had first been investigated. We describe hereafter two synthetic tools: firstly the product MxP_{line} [69][70] between number of spans M and input power into line fibre P_{line} proposed by A. Färbert in 1999 or by [94], and secondly, the nonlinear phase, that we first introduced in [62]. It has the additional advantage of taking into account the impact of nonlinearities in the dispersion-compensating fibre as well as in the line fibre. We rely for that purpose on numerical simulations emulating a singly-periodic dispersion-managed, terrestrial, multi-channel, Nx40Gbit/s, SMF-based system affected not only by Self-Phase Modulation but also by Cross-Phase Modulation and Four-Wave Mixing.

After describing the concept of nonlinear phase and its possible utilization, we verify its applicability to various configurations at 40Gb/s and 10Gb/s, over multiple types of fibres.

II.2. Principle of nonlinear phase shift criterion to describe 40Gb/s optical systems based on SMF-fibre with optimized dispersion-management

II.2.1. System under study

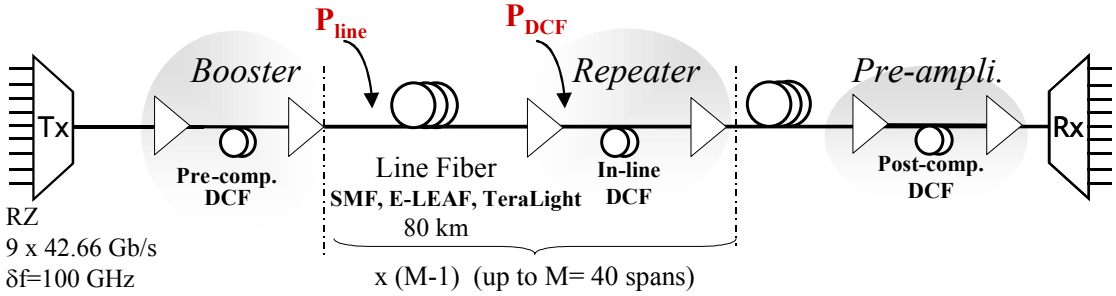

Figure 2-1: simulated set-up for assessment of impact of nonlinearities

The system under study is depicted in Figure 2-1. It is a WDM 9x42.66 Gbit/s dispersion-managed, terrestrial, ultra-long haul link, based on return-to-zero (RZ) modulation format. The transmitter consists of nine channels spaced 100GHz apart, centered on 1550 nm, with the same polarization. Each channel is modulated by a 128-bit long De Brujn sequence, decorrelated with that of the other channels by introducing a random delay. The basic transmission link consists of up to 35 sections of 80km-long line fibre (Standard Single Mode Fibre (SMF), TeraLight™, or LEAF™ [62], essentially characterized by their chromatic dispersion at 1550nm, of 17, 8, and 4.25ps/(nm.km) respectively) with discrete, dual-stage erbium-based repeaters. Chromatic dispersion is compensated for within each amplifier following a singly-periodic scheme at the link input (pre-compensation), along the link (in -line compensation) and at the link output (post-compensation) by sections of DCF, as illustrated by Figure 2-2. In addition, the dispersion slope of DCF modules is assumed to fully compensate for that of the line fibre.

As we focus on the ultimate impact of nonlinear impairments, noise limitations are overlooked here and dispersion management is assumed optimized. To assess the accuracy of the nonlinear phase as performance estimator, we investigate next the correlation between this estimator and a more conventional one obtained through numerical simulations, the OSNR penalty for a Bit Error Rate of 10^{-5}. Here, we always consider an average penalty over the five central channels of a nine-channel multiplex, after full optimization of the dispersion map.

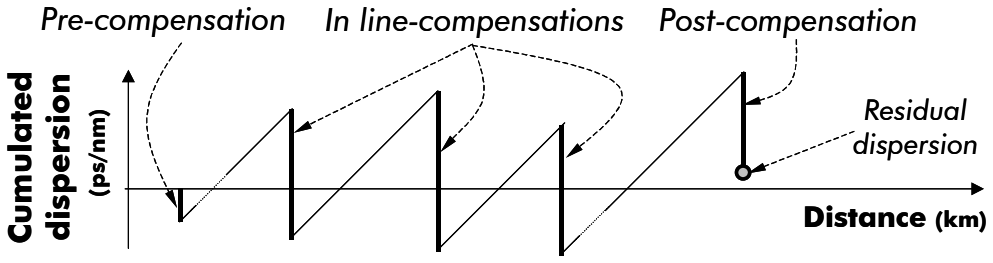

Figure 2-2: Dispersion management scheme

To investigate the performance of such a system, we varied all the parameters of the dispersion maps for any transmission distance or input powers. The cumulated dispersion of the pre -compensation module was varied between 0 and –720ps/nm (40ps/nm step) for SMF, and between 0 to –300ps/nm (20ps/nm step) for TeraLight and LEAF. Post-compensation was added for every channel at the end of the link so that the residual dispersion varied between -50 and 100ps/nm (5ps/nm step). In-line compensation was not varied from one simulation to another. It was set to fully compensate for the cumulative dispersion of one transmission fibre span (100% in-line compensation), but on average only. The actual value was randomly picked with [90%, 110%] according to a uniform distribution, in order to emulate installation constraints. The optimization of the dispersion map is the following: for each combination of pre-compensation, powers and distance, the post-compensation is optimized for each channel so as to maximize the eye aperture (cf Chapter 1); then for each set of distance and powers, the pre-compensation is optimized so as to minimize the averaged penalty over the five central channels.

II.2.2. Product MxP_{line} and Integrated Power

First, we investigate the dependence of the penalty on the transmission distance and the input power P_{line} into one type of line fibre (SMF), assuming that the input power into the DCF P_{DCF} is proportional to P_{line}, but 8 dB lower. The curves of Figure 2-3.a show the optimum OSNR penalty results as a function of P_{line} for different transmission distances (Mx80 km, M being 10, 20 or 30). P_{line} is varied within [–4 dBm; +4 dBm] by 2dB step. At each point, only the penalty corresponding to optimal dispersion map is shown. Not surprisingly[65][66][68][71], the penalty is found to increase with both parameters M and P_{line}, in an exponential-like manner. If we now express it as a function of the number of spans times power MxP_{line} product, the former set of points plus additional ones (the transmission distance is varied here between 5 and 35 spans by steps of 5 spans) gathers in a single curve (cf Figure 2-3.b) for a total of 35 points coming from 103075 receptions. The penalty depends here bi-univocally on the MxP_{line} product, as already shown by Färbert in [69]. A natural extension of this synthetic parameter to the case of fibre input powers P_{line} different from fibre section to another is the sum of those input powers along the transmission link; it can be referred to as the **integrated power** (IP):

$$IP = \sum_{\substack{line \\ fiber\ k}} P_{line}^{(k)} \qquad (2\text{-}1)$$

The integrated power is usually either expressed in mW or in dBm, similar to conventions on optical power.

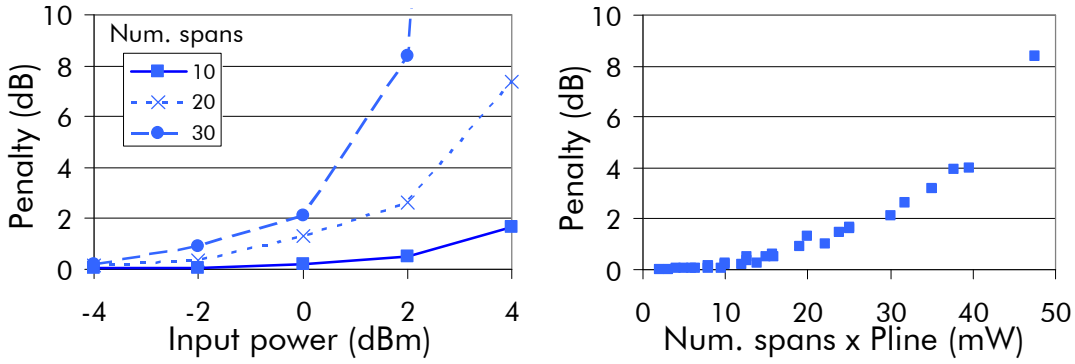

Figure 2-3: (a) Penalty vs input power P_{line} into line fibre after M=10, 20 or 30 spans. (b): Penalty vs MxP_{line} for variable powers and distances (from 5 to 35 spans).

II.2.3. Nonlinear phase shift

To assess the relevance of using the integrated power to describe the accumulation of nonlinearities and overcome its limitations, we investigate the dependence of the penalty on the MxP_{line} product (still over SMF), assuming that the amount of nonlinear effects in the DCF is increased, which is obtained by changing the ratio between P_{DCF} and P_{line} from 8 dB to 6 and 4 dB. This corresponds to 105 optimized configurations of distance and powers, stemming from 309225 signal receptions[1]. As depicted in Figure 2-4.a, the penalty is found to increase with the power into the DCF, which indicates that the product MxP_{line} does not fully assess the nonlinear limitations of the system.

The penalty thus depends on the contributions to nonlinear effects coming from both the line fibres and the DCFs and is most probably a function of MxP_{line} and MxP_{DCF}. We propose to investigate then whether the penalty could depend on a linear combination of MxP_{line} and MxP_{DCF}. Obviously, the line fibre and the DCF are two types of fibres that differ in terms of effective area A_{eff} and nonlinear index n_2. Their respective contributions should therefore be weighted by the nonlinear strength n_2/A_{eff} of the involved fibre types, which suggests using the nonlinear phase shift Φ_{NL} as a more accurate criterion for performance assessment, as defined after Equation (1.15).

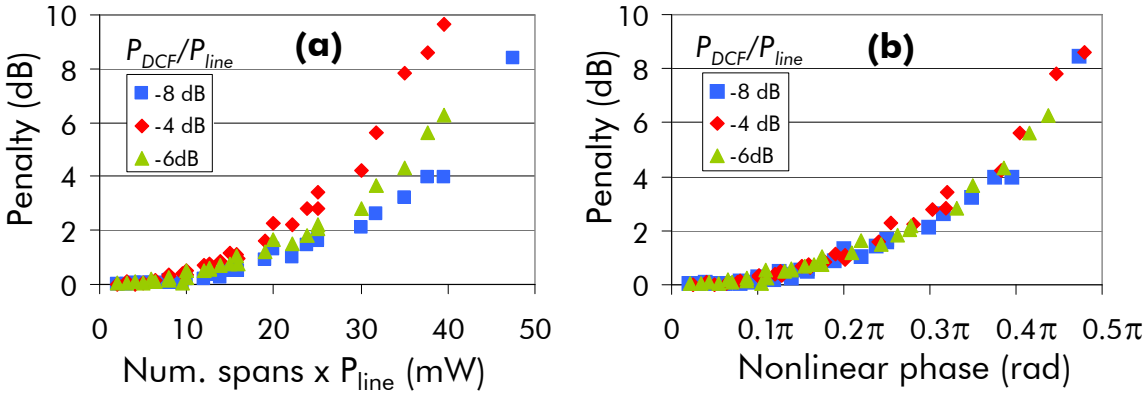

Figure 2-4: impact of nonlinearity in the DCF for an SMF-based 40Gb/s system:
a) penalty vs MxP_{line}, with P_{DCF} 4, 6 or 8dB lower than P_{line}, P_{line} varied between -4 and 4dBm, and distances ranging from 5x80km to 35x80km
b) penalty versus nonlinear cumulated phase for the same investigated configurations.

By overlooking its time-dependence and keeping only the mean contributions, we obtain the following formula:

$$\Phi_{NL} = \frac{2\pi}{\lambda}\int_{link}\left(\frac{n_2.P}{A_{eff}}\right)(z).dz = \frac{2\pi}{\lambda}M\left(\left.\frac{n_2.P.L_{eff}}{A_{eff}}\right|_{\substack{line\\fiber}} + \left.\frac{n_2.P.L_{eff}}{A_{eff}}\right|_{DCF}\right) \qquad (2\text{-}2)$$

λ being the current wavelength, P the mean input power into the considered fibre sections, and L_{eff} the effective length of a fibre section of length L and attenuation α:

$$L_{eff} = \frac{1}{P(z=0)}\int_0^L P(z).dz = \frac{1-e^{-\alpha L}}{\alpha} \qquad (2\text{-}3)$$

Note that ϕ_{nl} is indeed a linear combination of the integrated powers derived from the line fibres and the DCFs as:

[1] 19 values of pre-compensation x 31 values of residual dispersion x 5 channels x 7 distances x 5 input powers into SMF x 3 relative input powers into DCF vs SMF = 309225 signal receptions.

$$\Phi_{NL} = c_{line}.M.P_{line} + c_{DCF}.M.P_{DCF}, \quad with \quad c_{line/DCF} = \frac{2\pi}{\lambda}\frac{n_2.L_{eff}}{A_{eff}}\bigg|_{line/DCF} \tag{2-4}$$

Figure 2-4.b shows the penalties of Figure 2-4.a expressed as a function of the nonlinear phase. It can be seen that all the points gather along one single curve in very good approximation. The relationship between penalty and nonlinear phase appears as bi-univocal.

Note that the nonlinear phase parameter rates fairly well the impact of FWM and XPM that are present in those simulations, even though these effects do not appear explicitly in the expression of Φ_{NL}.

II.2.4. Correlation between penalty and nonlinear phase

We characterize here the correlation between the observed penalties and the nonlinear phase parameter and show that it is possible to describe the evolution of penalty by a simple function of nonlinear phase in very good approximation.

To do so, we interpolate the plots of Figure 2-4-b by a 2nd order polynomial function of ϕ_{nl}. We find the estimated penalty function equal to: $Pen_{est}^{dB}(\phi_{nl})=38.51\ \phi_{nl}^2-2.48\ \phi_{nl}$.

Figure 2-5 highlights then the very small discrepancies between the estimated penalty with the polynomial function of ϕ_{nl} and the measured penalties for all the previous configurations of distance and fibre input powers: they remain lower than +/-0.6dB for penalties lower than 3.5dB (in practice a penalty of 3.5dB will be far beyond what is generally acceptable).

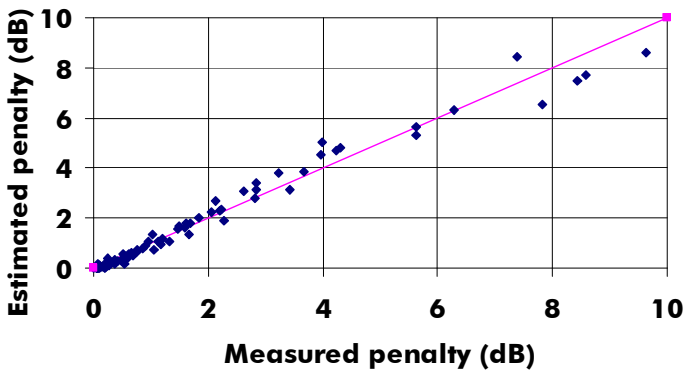

Figure 2-5 : Estimated penalty using a 2nd order polynomial function of nonlinear phase vs measured penalty for the previous configurations of distances, and powers into SMF and DCF

Range of measured penalties	[0-0.5] dB	[0.5-1] dB	[1-1.5] dB	[1.5-2.5] dB	[2.5-4] dB	[4-10] dB
Standard deviation of the difference between estimated and measured penalties	0.11 dB	0.15 dB	0.22 dB	0.27 dB	0.52 dB	0.75 dB

Table 2-1 : standard deviation of the difference between measured and estimated penalties (using 2nd order polynomial function of ϕ_{nl}) for the different configurations of distance, power into SMF and DCF

In order to estimate the correlation between penalties and ϕ_{nl}, we compute the standard deviation of the difference (in dB) between the measured penalty and the estimated penalty for the 105 points. Provided a limitation to the configurations where the penalty is lower than 10dB, this standard deviation is as low as 0.34dB. In detail, the standard deviation increases with the amount of nonlinearities and the penalty, as summarized by Table 2-1.

II.2.5. Nonlinear phase criterion

From the latest results, it appears tempting to describe system penalties based on a single function of Φ_{NL}. A practical way to proceed is to fit the penalty versus nonlinear phase relationship from a few measurements, usually thanks to a 3rd-4th order polynomial function, and to use this fit to predict the performance in other configurations. For instance measurements taken at a constant distance with various line fibre input powers could enable to build this function. Note that the nonlinear phase shift is an aggregate parameter that cannot be measured directly: it is calculated from the knowledge of the characteristics of the traversed fibres and the measurement of fibre input powers.

The obtained fitting function could then be used to **predict system performance** for other configurations with arbitrary distance and input powers into the line fibres or DCF sections. Depending on the applications, one is interested in average predictions or worst-case predictions (accounting for the finite accuracy related to the prediction) of the penalty.

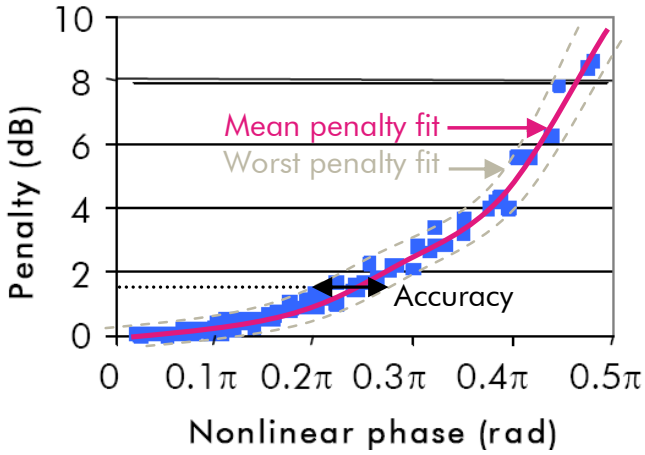

Figure 2-6 : Penalty vs nonlinear cumulated phase, for SMF fibre. Square blue symbols: numerical simulation results coming from various configurations of distances and powers; solid magenta curve: average penalty fit (typically a 4th order polynomial function); dashed curves: worst and best-penalty fits.

In the following, the **nonlinear phase criterion** is referred to as the action to predict system penalty as a function of the nonlinear phase shift as expressed in Equation (2-2).

We define the **accuracy** of the nonlinear phase criterion as $10\log_{10}$ of the ratio between the maximum and minimum estimated values of nonlinear phase (in radians) leading to a given penalty threshold. It is thus expressed in dB. It characterizes somehow the correlation between the nonlinear phase and the penalty around a specific region of interest.

In the following, we set the **acceptable level of accuracy** for system design as equal to **1.5dB** for 40Gb/s-modulated systems. It can be compared in practice with the precision of the knowledge of the measured fibre input powers around 0.5-1dB.

The abovementioned **penalty threshold** is representative of the tolerated nonlinearity-induced impairments. As such, it varies depending on the system-design or research teams or depending on the system under study. It is typically chosen between 1dB and 3dB. It can also be specified by analytical means, e.g. such that the derivative of the relationship between penalty and nonlinear phase is high enough, around 1dB/dB, so as to enable maximal reach of transmission systems. We will detail that point in more details in Chapter 5. Note that with this choice, estimates of the accuracy in terms of nonlinear phase or penalty will be almost identical.

From a system perspective, the knowledge of the accuracy of the nonlinear phase criterion as it is defined is meaningful: the penalty threshold is usually related to the reach and/or the

feasibility of a transmission; then the accuracy of the nonlinear phase criterion corresponds to the uncertainty on the estimated maximum tolerable amount of nonlinearities. For a fixed distance, it is equal to the uncertainty on the maximum tolerated fibre input power. Besides, the uncertainty in the maximum achievable distance (in dB scale) happens to be half the accuracy of the nonlinear phase criterion, should we consider a transmission system with identical spans (see Chapter 5).

For the studied SMF-based system, and for a reference penalty of 1.5dB (in line with the recommendations of Chapter 5), we can observe in Figure 2-6 that the values of nonlinear phase leading to 1.5dB penalty range between 0.21π and 0.26π radians. This corresponds then to an accuracy of 0.9dB. By comparison, the accuracy of the equivalent criterion based on the integrated power rather than on the nonlinear phase would be as high as 1.7dB.

The nonlinear phase criterion thus appears as accurate enough to describe SMF-based systems operated at 40Gb/s with RZ format provided optimized dispersion management.

II.3. Accuracy of the nonlinear phase criterion for various 10 and 40Gb/s WDM systems

We expect that the relationship between Φ_{NL} and penalty depends on the chromatic dispersion of the transmission fibre, the bit-rate, the modulation format and the channel spacing, and therefore should be re-estimated any time one of these parameters is changed. In the following we show that the nonlinear phase criterion can be generalized to most conditions is and not limited to the SMF 40Gb/s case. In details, we show the good correlation between penalties and nonlinear phase in verifying that accuracy of the nonlinear phase criterion is lower than 1.5dB for various configurations of fibres (SMF, LEAF, TeraLight) and bit-rates (10Gb/s single-channel and WDM, 40Gb/s). For that purpose, the same protocol is used for each configuration. The reference penalty to assess this accuracy is chosen equal to 1.5dB for 40Gb/s-modulated systems and 2dB for 10Gb/s-modulated systems (in line with the recommendations of Chapter 5).

II.3.1. Nonlinear phase shift criterion to describe 40Gb/s optical systems over SMF, LEAF or TeraLight fibre type

The formerly described results obtained at 40Gb/s over SMF fibre type have been extended to other types of fibres with the same conditions of transmission: Figure 2-7 shows the penalty versus the nonlinear phase computed over SMF, TeraLight or LEAF-based systems. For each fibre, it corresponds to 105 configurations of distance and input powers into line fibre and DCF with optimized dispersion management, stemming from 309225 (respectively 260400) signal receptions with different dispersion map settings for SMF line fibre (respectively TeraIlght or LEAF line fibre).

For TeraLight transmission fibre, the estimated values of nonlinear phase leading to 1.5dB penalty range between 0.24π and 0.31π radians; this corresponds then to an accuracy of 1.1dB.

For LEAF transmission fibre, the estimated values of nonlinear phase leading to 1.5dB penalty range between 0.24π and 0.3π radians; this corresponds then to an accuracy of 0.9dB.

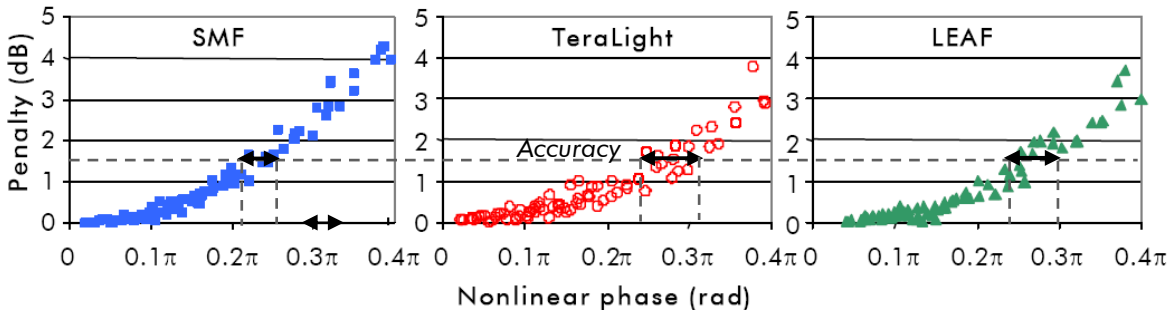

Figure 2-7: Assessment of nonlinear phase as performance estimator: impact of line fibre type

Whatever the fibre type at 40Gb/s; the accuracy of the nonlinear phase criterion is found at most as high as 1.1dB. We can therefore the nonlinear phase criterion as accurate enough to describe most 40Gb/s systems with RZ format.

II.3.2. Nonlinear phase shift criterion to describe 10Gb/s optical systems over SMF, LEAF or TeraLight fibre type

To complete this study, we show that the nonlinear phase criterion remains accurate enough for 10Gb/s transmissions in the same conditions as previously, for single-channel as well as WDM transmission systems, based on numerical simulations and experiments. To do so, we assess the accuracy of the nonlinear phase for a reference penalty of 2dB. This work has been achieved jointly with my colleagues Emmanuel Seve and Bruno Lavigne, who respectively performed the numerical simulations and the experiments.

Details of the transmission set-up

The system under study is a typical 10.7Gb/s dispersion-managed, terrestrial, ultra-long haul link. The transmitter consists of either a single channel at 1550nm or a WDM multiplex of 15 channels regularly spaced (50GHz) around 1550nm according to the ITU grid. For both cases, a NRZ modulation format with a 64-bit long sequence has been considered. For the WDM signal, each channel has the same polarization and the bit sequence is decorrelated with respect to the other channels with a random delay. The transmission link is singly periodic-dispersion managed: it consists of a pre-compensation, a successive repetition of a 100km line fibre-section followed by a DCF fibre (D=-80ps/nm/km) and finally a post-compensation fibre. SMF (and LEAF) fibre will be used as the line fibre. To compare the performance of such a system for different power ratio between the line and the DCF fibre, the dispersion map has been, in a first step, fully optimized: pre-, post- and in-line compensation have been optimized for each combination (line fibre power/distance).

For the corresponding experiment, a 15-channels WDM 10Gbit/s NRZ signal coded with 2^{23}-1 PRB sequence is launched in a system composed of 100 km SMF line fibre sections followed by a DCF fibre. The measurement of the OSNR penalty is carried out on the central channel only for a fixed bit-error-rate (BER) of 10^{-5}.

Results

Figure 2-8 represents the transmission penalty as a function of the nonlinear phase for different number of spans, different input powers into the **SMF** and the DCF, sorted into different powers ratios P_{line}/P_{DCF}, issued from single-channel (left plot) and WDM (right plot) systems with 50GHz channel spacing (numerical simulations). The considered power ratios

P_{line}/P_{DCF} range between 2 and 10dB, which covers typical ranges in optical systems between 5 and 10dB (see Chapter 5).

At first sight, there is still a good correlation between penalty and nonlinear phase. More precisely, we can assess the accuracy of the nonlinear phase criterion. In single channel-configuration, the estimated values of nonlinear phase leading to 2dB penalty range between 11.1 and 12$dB_{0.1\pi}$[2]; this corresponds then to an accuracy of 0.9dB. In WDM configuration, the estimated values of nonlinear phase leading to 2dB penalty range between 8.1 and 8.6$dB_{0.1\pi}$; this corresponds then to an accuracy of 0.5dB.

Similarly, loop experiments were conducted to emulate WDM 15x10Gb/s, SMF-based transmission systems with various fibre input powers, relative input powers into line fibre with respect to DCF, and transmission distances, in the same conditions previously. In Figure 2-9, we observe that the accuracy of the nonlinear phase criterion is similar to the one in numerical simulations: the estimated values of nonlinear phase leading to 2dB penalty range here between 8.8 and 9.7$dB_{0.1\pi}$; this corresponds then to an accuracy of 0.9dB.

[2] A nonlinear phase ϕ_{NL} expressed in unit $dB_{0.1\pi}$.means 10 $Log_{10}(\phi_{NL}[rad]/(0.1\pi))$

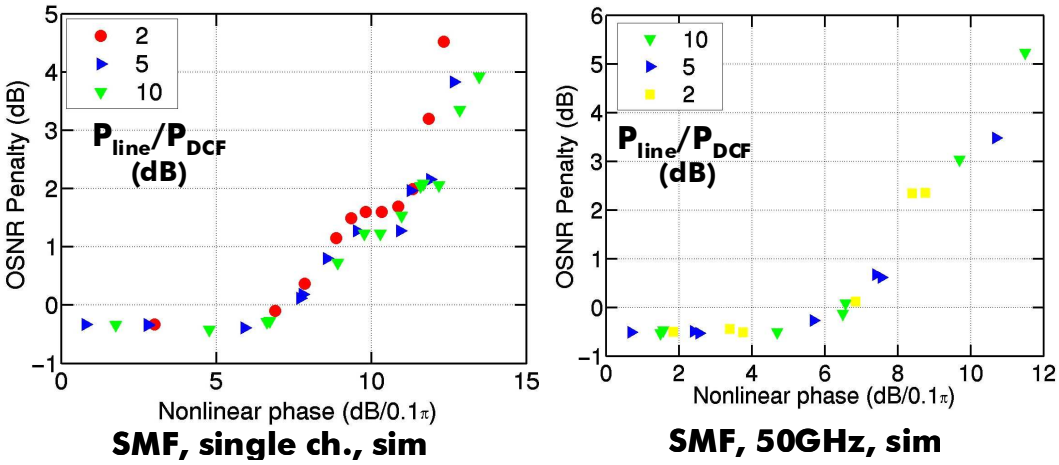

Figure 2-8: OSNR penalty versus nonlinear phase (in $dB_{0.1\pi}$[3]) for different DCF input powers (from 15dB below to 10 above the SMF input power). The left and right figures correspond to single channel and WDM transmission, respectively. Numerical simulations.

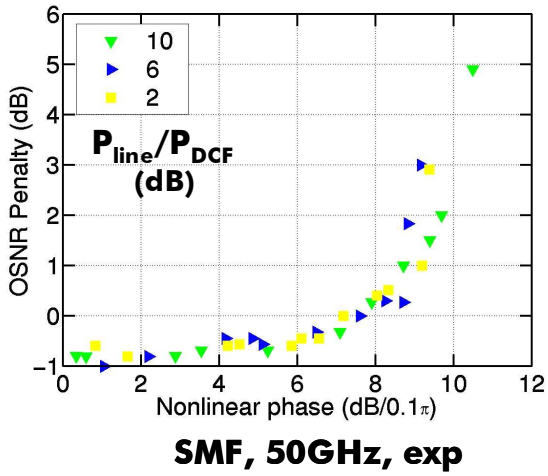

Figure 2-9: Experimental plots showing OSNR penalty vs nonlinear phase for various DCF input powers ([2-10]dB lower than SMF input power), for SMF-based 15x10Gb/s systems with 50GHz ch. Spacing

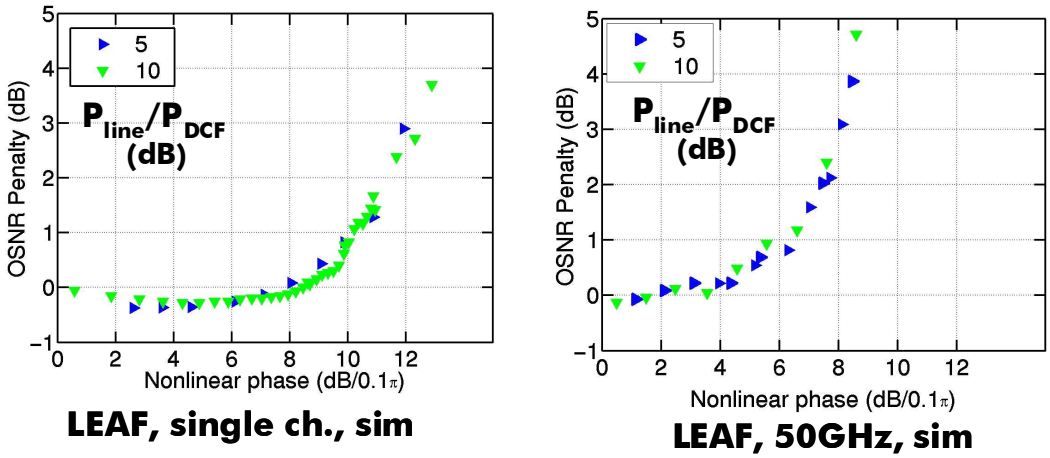

Figure 2-10: OSNR penalty versus the nonlinear phase with realistic DCF input powers ([5-10]dB lower than LEAF input power), for LEAF-based single channel (on the left) systems and WDM systems with 50GHz spacing (on the right). Numerical simulations

[3] ϕ_{NL} in unit $dB_{0.1\pi}$ means $10\ Log_{10}(\phi_{NL}[rad]/(0.1\pi))$

Eventually, Figure 2-10 represents the transmission penalty as a function of the nonlinear phase for a **LEAF fibre**-based transmission system, for numerically-emulated single-channel and WDM systems, following the same protocol (different line fibre input powers, different distances, and input power into DCF 5 or 10dB lower than into LEAF). Here again the correlation between nonlinear phase and penalty is fairly good up to the nonlinear regime. Precisely, in single channel-configuration, the estimated values of nonlinear phase leading to 2dB penalty range 11.1 and 11.6dB$_{0.1\pi}$; this corresponds then to an accuracy of 0.5dB. In WDM configuration, the estimated values of nonlinear phase leading to 2dB penalty range between 7.4 and 7.9dB$_{0.1\pi}$; this corresponds then to an accuracy of 0.5dB.

In summary, those results confirm that the nonlinear phase criterion can be considered as applicable for optimized 10Gb/s systems over low-chromatic dispersion as well as high dispersion line fibres, whatever the number of line fibre spans or the typical input powers into line fibre or DCF sections. In all the investigated configurations, the accuracy of the nonlinear phase criterion is very good, lower than 1dB for a reference penalty of 2dB.

One can also notice that the penalty versus nonlinear phase function is no longer bi-univocal at 10Gb/s contrary to 40Gb/s systems. Indeed, the nonlinear phase captures fairly well the impact of distance and power, but the resulting penalty curve is not monotonous: for low values of nonlinear phase, the penalty remains rather constant and even possibly negative (the joint impact of nonlinearities and dispersion causing here pulse compression and increasing the eye opening), before increasing for higher values of nonlinear phase.

II.3.3. Other bit-rates and impact of power profile

Similar studies were conducted in 2004 at **160Gb/s** by S. Vorbeck and M. Schneiders from T-Systems [72]: the authors considered a single-channel transmission with RZ modulation, over a dispersion-managed link with full inline dispersion compensation. Several types of line fibre type were studied, with chromatic dispersion ranging from 4 to 17ps/nm/km. They varied the number of line fibre spans, the input power into line fibre and DCFs, and even the amplification scheme (based on localized, assumed nonlinear free, EDFAs, or distributed, nonlinear impacting, **Raman** amplification). They concluded on the good correlation between penalty and nonlinear phase to tackle the accumulation of nonlinearities over the link, whatever the amplification scheme, distance or power distribution.

II.3.4. Conclusion on the nonlinear phase shift concept

In summary, we have shown through extensive numerical simulations that the cumulated nonlinear phase is a simple and accurate enough parameter that can be used to assess the performance of dispersion-managed WDM terrestrial systems modulated at 10, 40 or 160Gb/s, provided that we have fixed line fibre type, modulation format and channel spacing and that dispersion management has been optimized. We have demonstrated a very strong correlation between transmission penalties and the nonlinear cumulated phase from Equation (1-15) and an almost bi-univocal relationship whatever distance or the power distribution along transmission links. The main benefit stems from the fact that this relationship can be estimated out of a few transmission measurements and be in turn used to predict system tolerance to nonlinearities in other configurations, thereby defining the nonlinear phase criterion. The accuracy of the nonlinear phase criterion has always been found below an acceptable limit of 1.5dB for system design (in practice observed below 1.1dB).

Next we propose to make a connection between the nonlinear phase criterion and some analytical theories that will help us get more insight into physics then set the limits of the criterion and improve it in Chapter 3.

2.III. Nonlinear phase and more advanced analytical models

III.1. Introduction

We showed in the previous section that the proposed concept of nonlinear phase appears as quite interesting to describe the accumulation of nonlinearities in dispersion-managed systems, based on a very simple model.

More sophisticated models to capture the evolution of nonlinearity-induced signal distortions have been developed in the literature, based on theoretical analyses of weakly-nonlinear dispersion managed optical transmission systems. A first family of models is based on a perturbative approach from the NLSE, such as the regular-perturbation or logarithmic perturbation analyses from [74] (by A. Bononi, P. Serena, A. Orlandini and A. Vanucci) or the application of Volterra series [75][76][80] (by J. K. Fischer, H. Louchet, C. A. Bunge and K. Petermann). Others are based on small-signal approaches [73] (by Y. Frignac, J.-C. Antona and S. Bigo) or [79] (by R. I. Killey, H. J. Thiele, V. Mikhailov, and P. Bayvel).

Their computation complexity does not make such models particularly suitable for fast and accurate performance prediction but they enable to capture the most significant scaling laws in the physics of dispersion managed systems. As a result, they reveal useful to optimize the dispersion management. They also enable to make the connection with the nonlinear phase criterion. More particularly, investigations of systems with periodic dispersion management schemes (possibly including some random fluctuations) have been performed and they show that the Kerr effect-induced perturbations are a function of least the nonlinear cumulated phase in line fibre sections, in DCFs, and of the dispersion management parameters. Under certain conditions, these perturbations appear as a linear combination of the nonlinear phase shift coming from the transmission fibres and of the nonlinear phase shift coming from the dispersion compensation fibres.

In the following, we briefly present one of these models, the Phase to Intensity Conversion (PIC) small-signal model from [73], discuss its utilization to set the dispersion management, its limitations to predict system performance and make the connections with the nonlinear phase.

Regular perturbation models will be presented and investigated as well in Appendix 2.V. . They essentially enable to draw the same conclusions as the PIC model.

III.2. Phase to Intensity Conversion Criterion

III.2.1. General formulation of the small signal model

In [65][73], we introduced the so-called Phase to Intensity Conversion model (PIC), which is an easy-to-handle-tool enabling to get good physical intuition on dispersion management at 10 and 40Gb/s. The PIC model is in fact a simple estimation of the intensity noise at receiver end coming from the conversion of nonlinear phase shifts (SPM/XPM) into intensity due to Group Velocity Dispersion (GVD) along the line. Here is the principle.

Let us consider an input optical signal characterized carried by a central angular frequency ω_0, by its power $P_{in}(t)$ and phase $\phi_{in}(t)$ at time t.

$$E_{in}(t) = \sqrt{P_{in}(t)}.e^{-j\omega_0 t + j\phi_{in}(t)} \quad (2\text{-}5)$$

In the Fourier domain, the field can be rewritten as

$$\widetilde{E}_{in}(\omega) = \int_{-\infty}^{+\infty} E_{in}(t).e^{j\omega t}dt \quad (2\text{-}6)$$

Let us now model the impact of chromatic dispersion and Kerr effect.

To begin with, chromatic dispersion is a linear effect and can thus be characterized by a transfer function: an optical signal characterized by its complex amplitude $E_{in}(\omega)$ traverses a medium characterized by a cumulated group velocity dispersion $\beta_{2,cum}$. $\beta_{2,cum}$ is referring to physics notations, i.e. the derivative of the group delay with respect to angular frequency; it is related to the cumulated dispersion in optics notation, D_{cum}, with $\beta_{2,cum} = -\frac{\lambda^2}{2\pi c} D_{cum}$, around wavelength λ (cf Chapter 1). Then the signal output complex amplitude is, assuming the abovementioned Fourier Transform convention.

$$E_{out}(\omega) = E_{in}(\omega).e^{j\frac{\beta_{2,cum}}{2}\omega^2} \quad (2\text{-}7)$$

Signal power can be described as the sum of signal average power <P> and power variations $\Delta P_{in}(t)$, so that:

$$P_{in}(t) = < P > + \Delta P_{in}(t) \quad (2\text{-}8)$$

Let us assume that signal power fluctuations are very small with repect to average power, such that:

$$\sqrt{P_{in}(t)} \approx \sqrt{\langle P \rangle}\left(1 + \frac{\Delta P_{in}(t)}{2\langle P \rangle}\right) \quad (2\text{-}9)$$

Under such small-signal model assumptions, it is possible to derive an expression of this transfer function of accumulated chromatic dispersion in the 2D space (relative power fluctuations and phase), such that:

$$\begin{pmatrix} \frac{\Delta\widetilde{P}_{out}}{2 < P >}(\omega) \\ \widetilde{\Phi}_{out}(\omega) \end{pmatrix} = \begin{pmatrix} H_{IM-IM} & H_{PM-IM} \\ H_{IM-PM} & H_{PM-PM} \end{pmatrix} \cdot \begin{pmatrix} \frac{\Delta\widetilde{P}_{in}}{2 < P >}(\omega) \\ \widetilde{\Phi}_{in}(\omega) \end{pmatrix}, \quad (2\text{-}10)$$

where H_{IM-IM}, H_{PM-IM}, H_{IM-PM} and H_{PM-PM} respectively refer to the Intensity Modulation to Intensity Modulation filter, the Phase Modulation to Intensity Modulation filter, the Intensity Modulation

to Phase Modulation filter and the Phase Modulation to Phase Modulation filter. In [81], the authors expressed this small-signal group velocity dispersion transfer function as:

$$H_{Dcum}(\omega)=\begin{pmatrix} H_{IM-IM} & H_{PM-IM} \\ H_{IM-PM} & H_{PM-PM} \end{pmatrix}=\begin{pmatrix} \cos\left(\beta_{2cum}\frac{\omega^2}{2}\right) & -\sin\left(\beta_{2cum}\frac{\omega^2}{2}\right) \\ \sin\left(\beta_{2cum}\frac{\omega^2}{2}\right) & \cos\left(\beta_{2cum}\frac{\omega^2}{2}\right) \end{pmatrix}$$
$$=\begin{pmatrix} \cos\left(\frac{\omega^2\lambda^2}{4\pi.c}D_{cum}\right) & \sin\left(\frac{\omega^2\lambda^2}{4\pi.c}D_{cum}\right) \\ -\sin\left(\frac{\omega^2\lambda^2}{4\pi.c}D_{cum}\right) & \cos\left(\frac{\omega^2\lambda^2}{4\pi.c}D_{cum}\right) \end{pmatrix} \quad (2\text{-}11)$$

Let us now extend that theory to the case of dispersion-managed systems impaired by chromatic dispersion and Kerr effects.

The sole impact of Kerr effect on signal between propagation distances z and z+dz is to produce a nonlinear phase shift, equal to:

$$d\varphi_{NL}=\gamma\,P(z,t)\;dz \quad (2\text{-}12)$$

with γ referring to the nonlinear coefficient. In the frequency domain, we get

$$d\varphi_{NL}(\omega)=\gamma\,\widetilde{P}(z,\omega)\;dz \quad (2\text{-}13)$$

The proposed model assumes that the signal perturbations after propagation result from the sum of the contributions due to the nonlinear phase shifts occurring at any distance z and converted into intensity perturbations after transmission due to chromatic dispersion.

We focus now in more details on the resulting intensity distortions.

The nonlinear phase shifts generated by Kerr effect at distance z will undergo a phase to intensity conversion due to the accumulated dispersion between z and transmission end, i.e. D_{res}-$D_{cum}(z)$ if D_{res} refers to the residual dispersion at receiver end and if $D_{cum}(z)$ refers to the accumulated dispersion at distance z. The resulting infinitesimal relative intensity distortion dPIC(z,ω) can be written as:

$$dPIC(z,\omega)=\frac{d\widetilde{P}(z,\omega)}{2\langle P\rangle}=H_{PM-IM}\left(D_{res}-D_{cum}(z)\right).d\varphi_{NL}(z,\omega)=\sin\left[\frac{\omega^2\lambda^2}{4\pi c}\left(D_{res}-D_{cum}(z)\right)\right].d\varphi_{NL}(z,\omega) \quad (2\text{-}14)$$

One typical assumption concerning the calculation of the nonlinear phase shift at distance z is to consider that the signal power at distance z is primarily impacted by the cumulative losses from transmission input to distance z, and possibly by chromatic dispersion through phase to intensity or intensity to intensity filters.

$$\begin{aligned} d\varphi_{NL}(z,\omega)&=\gamma.\widetilde{P}(z,\omega)\;dz=\gamma.\left(<P(z)>\delta(\omega)+\Delta\widetilde{P}(z,\omega)\right)dz \\ &=\gamma\,Loss(0\to z).\left[H_{IM-IM}\left(D_{cum}(z)\right).\widetilde{P}(0,\omega)+2<P(0)>H_{PM-IM}\left(D_{cum}(z)\right).\widetilde{\phi}(0,\omega)\right]dz \end{aligned} \quad (2\text{-}15)$$

The simplest models only consider the impact of loss to calculate $d\phi_{nl}$, i.e. assuming $H_{IM\text{-}IM}=1$ and $H_{PM\text{-}IM}=0$ (a more advanced model, compatible with phase modulation is detailed in V.2.

$$d\varphi_{NL}(z,\omega)\approx\gamma\,\widetilde{P}(0,\omega).Loss(0\to z).dz=\gamma\,\widetilde{P}(0,\omega)\frac{<P(z)>}{<P(0)>}\;dz \quad (2\text{-}16)$$

The resulting relative intensity distortion due to SPM-induced phase shifts occurring at distance z and chromatic dispersion from distance z to distance L_{tot} thus becomes:

$$dPIC(z,\omega)=\frac{d\widetilde{P}(z,\omega)}{2\langle P(L_{tot})\rangle}=\gamma\,\widetilde{P}(0,\omega)\frac{<P(z)>}{<P(0)>}\sin\left[\frac{\omega^2\lambda^2}{4\pi c}\left(D_{res}-D_{cum}(z)\right)\right]..dz \quad (2\text{-}17)$$

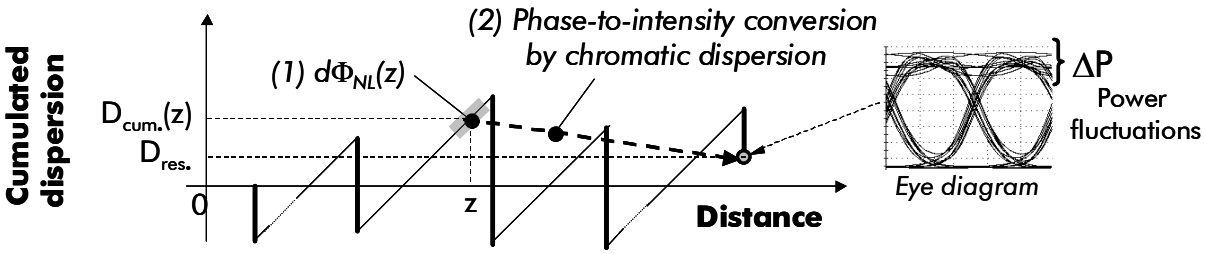

Figure 2-11: Principle of Phase to Intensity Conversion, with SPM-induced phase shift at distance z, converted into intensity noise by chromatic dispersion from distance z to transmission end.

The contributions of all the spatial steps of the link can then be added to get an integrated expression of the resulting relative intensity perturbation PIC(ω).

$$PIC(\omega)=\frac{\Delta\widetilde{P}(L_{tot},\omega)}{2\langle P\rangle}=\int_{\hat{a}}^{Ltot}\sin\left[\frac{\omega^2\lambda^2}{4\pi c}\left(D_{res}-D_{cum}(z)\right)\right].d\varphi_{NL}(z,\omega) \tag{2-18}$$

Note also that the same theory could be applied to XPM-induced phase shifts such as in [82] or [83].

We now consider a N-fibres transmission: let $\alpha_{(k)}$, $D^{(k)}$, $L_{(k)}$ and γ_k be the attenuation, the chromatic dispersion, the length and the nonlinear coefficient of fibre k; let $\phi_{nl,(k)}$ be the average accumulated nonlinear phase shift over span k and $D_{cum,input}^{(k)}$ be the cumulated dispersion at the input of fibre index k. Equation (2-18) becomes:

$$PIC(\omega)=\frac{\Delta\widetilde{P}(L_{tot},\omega)}{2\langle P\rangle}=\sum_{k=1}^{N}\gamma_k\,\widetilde{P}(0,\omega)\frac{<P_{in,(k)}>}{<P(0)>}\int_0^{L_{(k)}}\sin\left[\frac{\omega^2\lambda^2}{4\pi c}\left(D_{res}-D_{cum,input}{}^{(k)}-D_{(k)}z\right)\right]e^{-\alpha_{(k)}z}dz \tag{2-19}$$

If we define:

$$A=\frac{\omega^2\lambda^2}{4\pi c} \tag{2-20}$$

Then Equation (2-19) can be integrated and becomes:

$$\begin{aligned}PIC(\omega)&=\sum_{k=1}^{N}\gamma_k\,\widetilde{P}(0,\omega)\frac{<P_{in,(k)}>}{<P(0)>}.\mathrm{Im}\left[e^{j.A.\left(D_{res}-D_{cum,input}{}^{(k)}\right)}\int_0^{L_{(k)}}e^{-\left(\alpha+j.A.D_{(k)}\right)z}\,dz\right]\\&=\frac{\widetilde{P}(0,\omega)}{<P(0)>}.\sum_{k=1}^{N}\frac{\gamma_k<P_{in,(k)}>}{\alpha_{(k)}}.\mathrm{Im}\left[e^{j.A.\left(D_{res}-D_{cum,input}{}^{(k)}\right)}\frac{1-e^{-(\alpha+j.A.D_{(k)})L_{(k)}}}{1+j.\frac{A.D_{(k)}}{\alpha_{(k)}}}\right]\end{aligned} \tag{2-21}$$

Eventually, we get this generic expression of the response of the dispersive and nonlinear medium with respect to the input signal power:

$$PIC(\omega)=H_{\substack{PIC\\SPM}}(\omega).\widetilde{P}(0,\omega)=\frac{\widetilde{P}(0,\omega)}{<P(0)>}.\sum_{k=1}^{N}\phi_{nl,k}.\mathrm{Im}\left[\frac{1-e^{-(\alpha+j.A.D_{(k)})L_{(k)}}}{1-e^{-\alpha_{(k)}L_{(k)}}}\frac{e^{j.A.\left(D_{res}-D_{cum,input}{}^{(k)}\right)}}{1+j\frac{A.D_{(k)}}{\alpha_{(k)}}}\right] \tag{2-22}$$

We can observe that **the estimated perturbation appears quite naturally as a linear combination of the nonlinear phase shifts induced by each fibre section**. Note that the weighting factors $a_k(\omega)$ depend here on fibre dispersion, on dispersion management, on frequency and slightly on fibre section length:

$$PIC(\omega) = \underset{SPM}{H_{PIC}}(\omega).\widetilde{P}(0,\omega) = .\sum_{k=1}^{N} a_k(\omega)\phi_{nl,k}$$

$$with\ \ a_k(\omega) = \frac{\widetilde{P}(0,\omega)}{< P(0) >} \mathrm{Im}\left[\underbrace{\frac{1-e^{-(\alpha+j.A.D_{(k)})L_{(k)}}}{1-e^{-\alpha_{(k)}L_{(k)}}}}_{\substack{typic.\ within[1;1.2] \\ for\ L_{(k)}>2.4/\alpha_{(k)}}} \frac{e^{j.A.\left(D_{res}-D_{cum,input}{}^{(k)}\right)}}{1+j\dfrac{A.D_{(k)}}{\alpha_{(k)}}} \right] \tag{2-23}$$

The expression of the weighting factors can also be rewritten as:

$$a_k(\omega) = \frac{\widetilde{P}(0,\omega)}{< P(0) >} \frac{\sqrt{1-2e^{-\alpha L_{(k)}}\cos\left(A.D_{(k)}.L_{(k)}\right)+e^{-2\alpha L_{(k)}}}}{\left(1-e^{-\alpha_{(k)}L_{(k)}}\right)}$$
$$* \frac{\sin\left(A.\left(D_{res}-D_{cum,input}{}^{(k)}\right) - \arctan\left(\dfrac{A.D_{(k)}}{\alpha_{(k)}}\right) + \arctan\left(\dfrac{e^{-\alpha L_{(k)}}\sin\left(A.D_{(k)}.L_{(k)}\right)}{1-e^{-\alpha L_{(k)}}\cos\left(A.D_{(k)}.L_{(k)}\right)}\right)\right)}{\sqrt{1+\left(\dfrac{A.D_{(k)}}{\alpha_{(k)}}\right)^2}} \tag{2-24}$$

At receiver end, provided a direct detection receiver and signal filtering essentially achieved by the electrical filter (of transfer function $H_e(\omega)$), we can assess the photo-detected intensity perturbation ΔI around the mean intensity $<I>$ in the frequency domain as

$$\Delta I(\omega) = 2.< I >.H_e(\omega).PIC(\omega) = 2.< I >.H_e(\omega).\underset{SPM}{H_{PIC}}(\omega).\widetilde{P}(0,\omega) \tag{2-25}$$

We can eventually obtain the perturbation in the time domain by applying an inverse Fourier transform.

$$\Delta I(t) = \frac{1}{2\pi}\int_{-\infty}^{+\infty} \Delta I(\omega).e^{-j\omega t}d\omega = 2\langle I\rangle \sum_{k=1}^{N} \phi_{nl,k}.\frac{1}{2\pi}\int_{-\infty}^{+\infty} H_e(\omega).a_k(\omega).e^{-j\omega t}d\omega \tag{2-26}$$

It is possible to get a simpler expression of Equation (2-22) if we focus on small enough angular frequencies and/or values of inline cumulated dispersion.

Indeed, if for each span k and if the angular frequency ω is such that:

$$\frac{\omega^2\lambda^2}{4\pi c}\left(D_{res}-D_{cum,input}{}^{(k)}(z)\right) << 1 \ \text{ and } \frac{\omega^2\lambda^2}{4\pi c}\left(D_{res}-D_{cum,input}{}^{(k)}(z)\right) << \arctan\left(\frac{\omega^2\lambda^2}{4\pi c}\frac{D_{(k)}}{\alpha_{(k)}}\right) \tag{2-27}$$

Then $a_k(\omega)$ could be rewritten as:

$$a_k(\omega) = \frac{\widetilde{P}(0,\omega)}{< P(0) >} \mathrm{Im}\left[\frac{1-e^{-(\alpha+j.A.D_{(k)})L_{(k)}}}{1-e^{-\alpha_{(k)}L_{(k)}}} \frac{1}{1+j\dfrac{A.D_{(k)}}{\alpha_{(k)}}} \right] \tag{2-28}$$

And if we further assume identical line fibre spans and identical DCFs along the transmission linkn then:

$$PIC(\omega)=\sum_{k=1}^{N} a_k(\omega)\phi_{nl,k}=\frac{\widetilde{P}(0,\omega)}{<P(0)>}\left(a_{line\,fibre}(\omega).\phi_{nl,line,total}+a_{DCF}(\omega).\phi_{nl,DCF,total}\right) \quad (2\text{-}29)$$

Under those assumptions, the relative intensity distortion for such frequencies is a linear combination of the total nonlinear phase shift accumulated over line fibre sections and of the total nonlinear phase shift accumulated over DCF sections.

More generally, if the angular frequencies are such that:

$$\frac{\omega^2\lambda^2}{4\pi c^2}D_{cum}(z)<<1 \quad (2\text{-}30)$$

for each distance z where optical power is significant, then:

$$PIC(\omega)\approx-\frac{\omega^2\lambda^2}{4\pi c^2}\frac{\widetilde{P}(0,\omega)}{<P(0)>}\sum_{span\ k}\phi_{nl,k}\left(D^{(k)}{}_{cum,input}-D_{res}+\frac{D^{(k)}{}_{loc}}{\alpha_{(k)}}\left(1-\frac{L_{(k)}e^{-\alpha_{(k)}L_{(k)}}}{L_{eff,(k)}}\right)\right) \quad (2\text{-}31)$$

with, for each fibre (k), the effective length $L_{eff,(k)}$ (following Equation (2-3)).

In case of identical line fibre sections and identical DCF sections, Equation (2-31) becomes:

$$PIC(\omega)\approx-\frac{\omega^2\lambda^2}{4\pi c^2}\frac{P(0,\omega)}{<P(0)>}\left(\begin{array}{l}\phi^{total}{}_{nl,line}\left(\frac{D_{line,loc}}{\alpha_{line}}\left(1-\frac{L_{line}e^{-\alpha_{line}L_{line}}}{L_{eff,line}}\right)-D_{res}+\frac{1}{N}\sum_{span\ k=1}^{N}D^{(k)}{}_{cum,input}\right)\\+\phi^{total}{}_{nl,DCF}\left(\frac{D_{DCF,loc}}{\alpha_{DCF}}\left(1-\frac{L_{DCF}e^{-\alpha_{DCF}L_{DCF}}}{L_{eff,DCF}}\right)-D_{res}+\frac{1}{N}\sum_{DCF\ k'=1}^{N}D^{(k')}{}_{cum,input}\right)\end{array}\right) \quad (2\text{-}32)$$

with the number of line fibre sections N, $\phi^{total}{}_{line/DCF}$ the total nonlinear phase shift accumulated over line fibre / DCF sections, $D_{line/DCF,loc}$ the local dispersion of line fibre/DCF, $\alpha_{line/DCF}$ the attenuation of line fibre/DCF, $L_{line/DCF}$ the lengths of sections of line fibre/DCF and the corresponding effective lengths $L_{eff,\ line/DCF}$.

Here again, we can observe that the induced perturbation appear as a linear combination of the total nonlinear phase shifts accumulated over line fibres and DCFs provided the variations with N of $\frac{1}{N}\sum_{span\ k=1}^{N}D^{(k)}{}_{cum,input}$ remain small with respect to $\frac{D_{line,loc}}{\alpha_{line}}\left(1-\frac{L_{line}e^{-\alpha_{line}L_{line}}}{L_{eff,line}}\right)-D_{res}$ for the line fibres sections and the equivalent assumption for the DCFs.

Relevant range of frequencies

One can assume that only the frequencies lower than the cut-off frequency

$$F_e=\eta_e R \quad (2\text{-}33)$$

of the electrical filter (with R the symbol rate and η_e a scaling factor, typically around 0.7) are likely to play a significant role.

Besides, the term in $1/(1+j\frac{A.D_{(k)}}{\alpha_{(k)}})$ in Equation (2-22) suggests a 3dB cut-off frequency of the PIC filter at:

$$F_{PIC}=\sqrt{\frac{\sqrt{3}\,c}{\pi.\lambda^2}\frac{\alpha_{(k)}}{D_{(k)}}} \quad (2\text{-}34)$$

Typically, F_{PIC} is 14GHz for an SMF based system (assuming 0.22dB/km fibre attenuation), 28GHz for LEAF based systems around 1550nm.

Therefore the only frequencies with a significant impact will be lower than F_{max} with

$F_{max} = \min(F_e; F_{PIC})$. (2-35)

Note that with the previous examples, F_{max} is limited by the bit-rate for 10Gb/s modulated systems and by the fibre characteristics for 40Gb/s modulated systems.

Thus, since D_{res} is usually close to zero (typically below 1000ps/nm and 100ps/nm for 10Gb/s and 40Gb/s-modulated systems respectively), a sufficient condition to the low frequency approximation from Equation (2-30) becomes

$$\frac{\pi \lambda^2}{c}.F_{\max}{}^2 D_{cum}(z) << 1$$

i.e. (2-36)

$$\min\left(\frac{\pi \lambda^2}{c} F_e^{\,2};\ \sqrt{3}.\frac{\alpha_{(k)}}{D_{(k)}}\right).\left|D_{cum}(z)\right| << 1$$

whatever distance z, as mentioned in [64] [87] [88].

Therefore, typical limit values of $|D_{cum}(z)|$ would be around 800 ps/nm for 10Gb/s-modulated systems, 200ps/nm for 40Gb/s modulated systems over SMF and 50ps/nm for 40Gb/s modulated systems over LEAF™ fibre.

III.2.2. Application to periodic dispersion management strategies

We briefly explain here the possible applications of the PIC models from Equation (2-22) and (2-26) or from Equation (2-32) (low frequency approximation) in terms of help for the optimization of dispersion management, in terms of performance prediction or in terms of insight into the relevant physical parameters. For simplicity, we focus on optical systems with periodic dispersion management strategies: particularly we essentially consider formulations of the model for doubly-periodic dispersion maps that include the case of singly-periodic dispersion maps.

Dispersion map optimization

As far as dispersion management is involved, one way to optimize dispersion management is to minimize the absolute value of the relative intensity perturbation. Such a rule, that easily relates the parameters of the dispersion management, can be referred to as the **PIC criterion**. For the low frequency model Equation (2-32), it amounts to ensuring that $PIC(\omega) \sim 0$ [73]. The PIC criterion can therefore be very convenient to simplify the optimization of dispersion management, all the more as very simple expressions can be extracted to the usual cases of singly- or doubly-periodic maps.

For instance, we can consider doubly-periodic dispersion maps, such as in [63], with N spans composed of Nb_{subdiv} subdivisions (or node sections) of $N_{spans\ per\ subdiv}$ spans each (such that $N = Nb_{subdiv} * N_{spans\ per\ subdiv}$), and negligible nonlinearities stemming from DCFs . Equation (2-21) can then be rewritten (after a few calculations) as:

$$PIC(\omega) = -\frac{\tilde{P}(0,\omega)}{<P(0)>}\frac{N*\phi_{nl,span}}{\sqrt{1+A^2 {D_{loc}}^2/\alpha^2}}\frac{\sqrt{1+e^{-2\alpha L}-2e^{-\alpha L}\cos(A.D_{loc}L)}}{(1-e^{-\alpha L})}$$
$$*\frac{\sin\left(\frac{A.Nb_{spans/subdiv}.D_{res/span}}{2}\right)}{Nb_{spans/subdiv}.\sin\left(\frac{A.D_{res/span}}{2}\right)}.\frac{\sin\left(\frac{A.Nb_{subdiv}.D_{res/subdiv}}{2}\right)}{Nb_{subdiv}.\sin\left(\frac{A.D_{res/subdiv}}{2}\right)} \qquad (2\text{-}37)$$
$$*\sin\left(A\left(\begin{array}{l}\Pr e-Dres+\frac{Nb_{spans/subdiv}-1}{2}D_{res/span}+\frac{Nb_{subdiv}-1}{2}D_{res/subdiv}\\+\frac{1}{A}\arctan\left(\frac{A.D_{loc}}{\alpha}\right)-\frac{1}{A}\arctan\left(\frac{e^{-\alpha L}\sin(A.D_{loc}.L)}{1-e^{-\alpha L}\cos(A.D_{loc}.L)}\right)\end{array}\right)\right)$$

Where $\phi_{nl,span}$ refers to the total cumulated nonlinear phase per span, D_{loc} to local chromatic dispersion of line fibre spans, Pre to the cumulated dispersion of the pre-compensation module at transmitter side, $D_{res,span}$ to the residual dispersion per span, including the accumulated dispersion over one line fibre span and the following inline DCF after each span but the last one of a subdivision, and $D_{res,subdiv}$ refers to the cumulated dispersion per subdivision.

Naturally this equation can be simplified in the low frequency-dispersion regime. Let us define $<D_{res/span}>=\frac{D_{res/subdiv}}{Nb_{span/subdiv}}$.

Then provided $\frac{\omega^2\lambda^2}{4\pi.c}N.\langle D_{res/span}\rangle<<1$ and $\frac{\omega^2\lambda^2}{4\pi.c}Nb_{span/subdiv}.D_{res/span}<<1$, Equation (2-37) becomes:

$$PIC(\omega)\approx -\frac{\tilde{P}(0,\omega)}{<P(0)>}\frac{\phi_{nl,span}}{\sqrt{1+A^2 {D_{loc}}^2/\alpha^2}}\frac{\sqrt{1+e^{-2\alpha L}-2e^{-\alpha L}\cos(A.D_{loc}L)}}{1-e^{-\alpha L}}.$$
$$.\sin\left(A\left(\begin{array}{l}\Pr e-Dres+\frac{Nb_{spans/subdiv}-1}{2}D_{res/span}+\frac{Nb_{subdiv}-1}{2}D_{res/subdiv}\\+\frac{1}{A}\arctan\left(\frac{A.D_{loc}}{\alpha}\right)-\frac{1}{A}\arctan\left(\frac{e^{-\alpha L}\sin(A.D_{loc}.L)}{1-e^{-\alpha L}\cos(A.D_{loc}.L)}\right)\end{array}\right)\right) \qquad (2\text{-}38)$$

Eventually, if ω is small enough, such that $\frac{\omega^2\lambda^2}{4\pi.c}D_{loc}.L<<1$ or if $L>2/\alpha$, we get the very simple expression:

$$PIC(\omega)\approx -\phi_{nl,tot}\left(\Pr e-Dres+\frac{Nb_{spans/subdiv}-1}{2}D_{res/span}+\frac{Nb_{subdiv}-1}{2}D_{res/subdiv}+\frac{D_{loc}}{\alpha}\left(1-\frac{Le^{-\alpha L}}{L_{eff}}\right)\right).\frac{\tilde{P}(0,\omega)}{<P(0)>}.\frac{\omega^2\lambda^2}{4\pi.c} \qquad (2\text{-}39)$$

Note that Equation (2-39) concerns here only contributions to PIC(ω) coming from line fibres. The equivalent contribution coming from DCFs is straightforward, and the overall PIC(ω) is simply the sum of the contributions coming from both types of fibres.

$$\begin{aligned}PIC(\omega)&\approx PIC_{line}(\omega)+PIC_{DCF}(\omega)\\&\approx \phi_{nl,tot}^{\ line}\left(Dres-\Pr e-\frac{Nb_{spans/subdiv}-1}{2}D_{res/span}-\frac{Nb_{subdiv}-1}{2}D_{res/subdiv}-\frac{D_{line,loc}}{\alpha_{line}}\left(1-\frac{L_{line}e^{-\alpha_{line}L_{line}}}{L_{eff,line}}\right)\right).\frac{\tilde{P}(0,\omega)}{<P(0)>}.\frac{\omega^2\lambda^2}{4\pi.c}\\&+\phi_{nl,tot}^{\ DCF}\left(Dres-\Pr e-D_{line,loc}L_{line}-\frac{Nb_{spans/subdiv}-1}{2}D_{res/span}-\frac{Nb_{subdiv}-1}{2}D_{res/subdiv}-\frac{D_{DCF,loc}}{\alpha_{DCF}}\left(1-\frac{L_{DCF}e^{-\alpha_{DCF}L_{DCF}}}{L_{eff,DCF}}\right)\right).\frac{\tilde{P}(0,\omega)}{<P(0)>}.\frac{\omega^2\lambda^2}{4\pi.c}\end{aligned} \qquad (2\text{-}40)$$

Here again, we find that provided low values of the product between inline dispersion compensation and the square of the symbol rate, the PIC-induced degradation linearly depends on the nonlinear phase shift of each fibre type.

Zeroing this equation in case of sufficiently long spans (longer than 30-40km) amounts then to link dispersion map parameters such that:

$$\mathrm{Pre} - D_{res} + \frac{N_{\substack{\text{spans} \\ \text{per subdiv}}} - 1}{2} D_{res,span} + \frac{Nb_{\text{subdiv}} - 1}{2} D_{res,subdiv} + \frac{D_{loc}}{\alpha} = 0 \qquad (2\text{-}41)$$

The PIC criterion and particularly this formula have been successfully used to optimize dispersion management [73][84][85], especially at 40Gb/s and higher bit-rates, for multiple distances, powers, fibres, in absence or in presence of distributed Raman amplification [92]. Without entering the details of the existing studies Figure 2-12 (from [65]) illustrates that point. It depicts some contour plots of the OSNR penalty versus pre-compensation and residual dispersion per span for a numerically-emulated 40Gb/s channel propagating over a 5x100km SMF-based transmission system with single-period dispersion management and optimized post-compensation at receiver end. The different graphs correspond to different modulation formats: NRZ, RZ, PSBT, DPSK and RZ-DPSK.

We can observe the excellent agreement between the predictions of the PIC criterion using Equation (2-41) with 1 subdivision, $N_{spans/subdiv}$ =5, D_{res}=0, (red diamonds) and the optimal values of pre-compensation leading to minimum computed OSNR penalty according to simulations (blue circles).

In practice the PIC criterion enables to find the optimum value of pre-compensation fibre of a dispersion managed system with an accuracy around +/-100ps/nm for 40Gb/s-modulated systems, one slight adjustment appearing as helpful for phase-modulated systems [79].

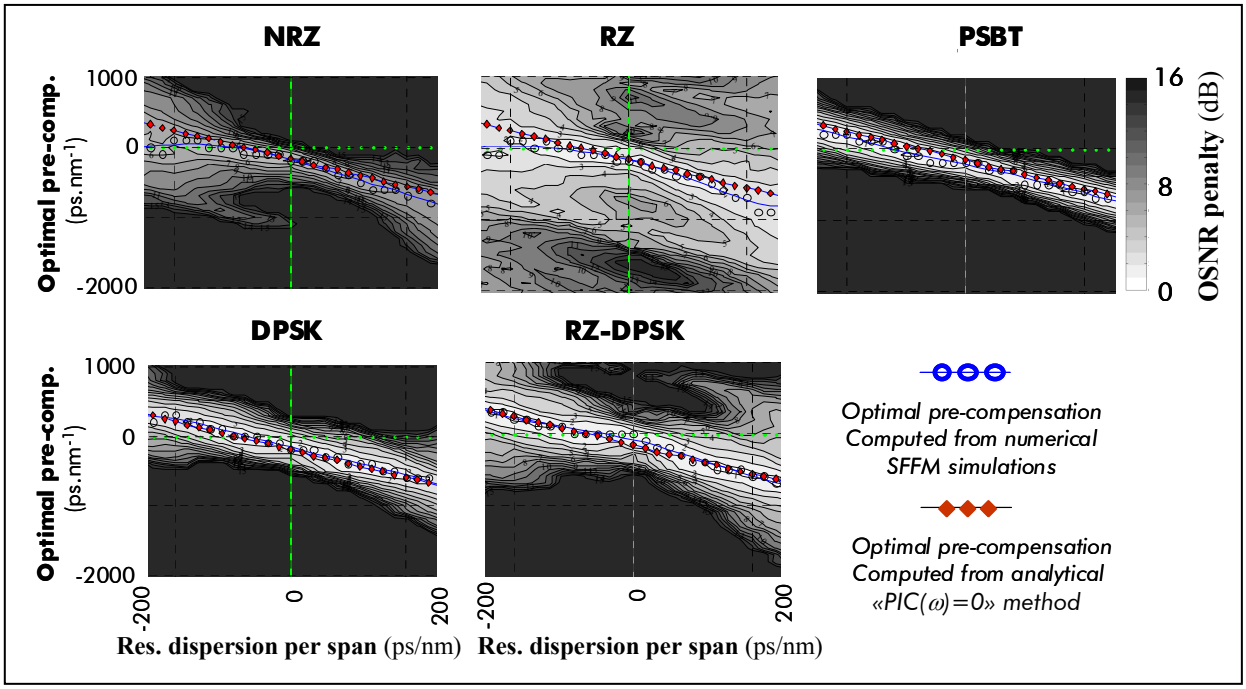

Figure 2-12: Contour plots of OSNR penalty as a function of dispersion management parameters such as pre-compensation and residual dispersion per span for a single-channel 40Gb/s transmission over 5x100km SMF fibre, using a singly-periodic dispersion map, for various modulation formats. Red plots correspond to PIC predictions, blue circles to optimal values of pre-compensation for each value of inline residual dispersion.

Performance prediction

Despite their interest for dispersion management optimization or to capture physics of propagation, both mathematical models from Equation (2-22) and (2-26) or from Equation (2-32) (low frequency approximation), whatever their assumption on frequencies, have not proved sufficient to help predict performance accurately for 10 and 40Gb/s-modulated systems. Indeed, we performed some studies to investigate a possible correlation between the estimated related intensity distortion from Equation (2-26) and transmission penalties but they did not appear as quite satisfactory. As an example to illustrate that statement, we assessed the ability of this analytical tool to predict performance for 10Gb/s WDM systems operating over LEAF™ fibre with various conditions of dispersion management and power. We reported on Figure 2-13 the measured transmission penalties and the calculated relative intensity perturbation at sampling time t=0 (center of bit time) derived from Equation (2-25). We also varied here the dispersion management conditions since the PIC model proposes to account for it.

In details, we considered a 10Gb/s WDM system consisting of 15 channels (50GHz-spaced) propagating around 1530nm over 15 spans of 100km LEAF™ fibre and following an aperiodic dispersion management scheme typical of optical networks with irregularly spaced nodes: between two adjacent nodes, the dispersion map is singly-periodic and is characterized by -400ps/nm pre-compensation at 1530nm, 60ps/nm residual dispersion per span (at 1530nm) and adjustment of the DCF at node input ensuring that the residual dispersion between adjacent nodes is equal to 0ps/nm at 1550nm (around 1530nm, it means an average dispersion of -0.045ps/nm/km). Then we varied the location of the nodes and the fibre input powers and numerically emulated the link accordingly.

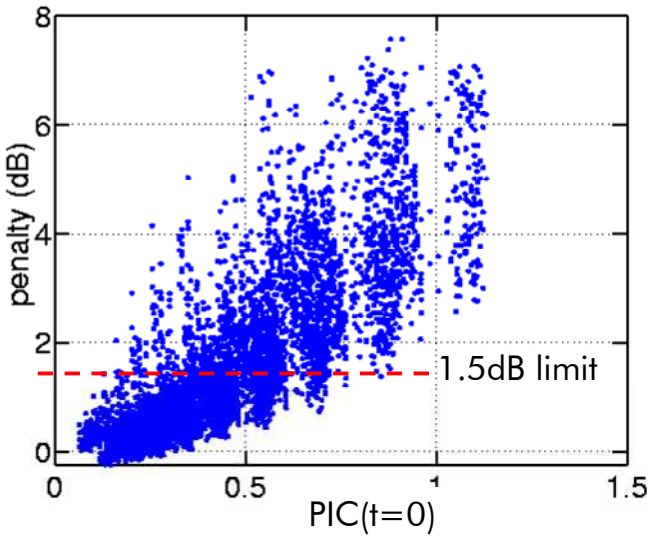

Figure 2-13 : Relationship between the relative intensity distortion calculated after Equation (1-25) and OSNR penalties for a 10Gb/s NRZ modulated system over LEAF fibre, for different conditions of power and dispersion management typical of optical networks with irregular node spacing.

We can observe that the correlation between transmission penalty and the observed relative intensity distortion does not look excellent. We can quantify that and note that 1.5dB reference penalty is associated to relative intensity distortions ranging from 0.2 to 0.85 (in dB scale, it corresponds to 6.3dB). Conversely, for a value of relative intensity perturbation in the middle of this range, equal to 0.5, the expected penalties range between 0.5 and 5.5dB. Such a

behaviour suggests that the PIC tool will not bring any benefit with respect to the sole nonlinear phase when it comes to build a tool that predict nonlinear induced penalties for 10Gb/s-modulated systems. Similar studies consisting in adapting this theory to XPM-induced relative intensity distortions after [82] or [83] lead to the same conclusion.

PIC and nonlinear phase

From Equations (2-37) to (2-39), we find as in the previous section that the relative intensity distortion is proportional to a linear combination of the nonlinear phase shifts induced by line fibres and the nonlinear phase shifts induced by DCFs provided low values of the product between total inline dispersion (e.g. the product between number of spans and average residual dispersion per span) and the square of the maximum frequency F_{max} (from Equation (2-35)).

If we further imagine ideal transmission systems with optimized dispersion management or such that $\frac{Nb_{spans/subdiv}-1}{2}D_{res/span}+\frac{Nb_{subdiv}-1}{2}D_{res/subdiv}$ varies weakly with distance with respect to $\Pr e+\frac{D_{line,loc}}{\alpha_{line}}\left(1-\frac{L_{line}e^{-\alpha_{line}L_{line}}}{L_{eff,line}}\right)-D_{res}$ for any power or distance, it becomes conceivable that the weighting factors of this linear combination remain the same for various conditions of power and distances., which is consistent with the nonlinear phase criterion proposed in section 2.II. The specificity of the nonlinear phase criterion as proposed in section 2.II. remains that the observed transmission penalties are highly correlated to the simple addition of the nonlinear phase stemming from line fibre sections and of the nonlinear phase stemming from line DCF sections.

However, one can anticipate from the PIC model that if the abovementioned conditions are not fulfilled, the nonlinear phase criterion will need to be adjusted or reinforced in several directions. For instance, the linear combination of the nonlinear phases coming from each fibre sections that would make sense to describe system distortions might differ from the simple addition of the nonlinear phases. In case of non-optimized maps with high values of average residual dispersion per span, the weighting factors might depend on distance, or at least the product between number of spans and average residual dispersion per span.

One can also expect from Equations (2-32) and (2-39) that the distortions will depend on the nonlinear phase shifts, but also on the local dispersion of the transmission fibre and possibly on the fibre section length when span length is lower than $2/\alpha$.

Such early considerations will be confronted with experimental and numerical studies in Chapter 3 to comfort and consolidate the nonlinear phase criterion.

III.3. Regular perturbation models

Besides the PIC model, more advanced models, based on a linearization of the Dispersion-Managed Nonlinear Schrödinger Equation have been developed for the last 15 years [74] [80]. Similarly, they aim to predict system degradation and enable dispersion map optimization, and very similar expressions can be obtained, unfortunately sometimes out of their strict mathematical domain of validity. They indeed assume very few nonlinearities on the whole link, and their utilization must therefore be considered cautiously and systematically validated by numerical or experimental simulations, otherwise possibly leading to erroneous prediction tools [76][80]. In practice, they cannot be used for pure performance estimation due to accuracy and computation time issues: computation time is comparable or even higher than SSFM numerical simulations if we require accuracy on the predictions. However they provide guidance into the physics of dispersion-managed systems and relevant scaling laws.

In Appendix V.1. we describe the regular perturbation method from [74] [80] in more details and analyze its validity.

We will simply recall here that the signal distortions due to nonlinear effects and chromatic dispersion can appear as a linear combination of the nonlinear phase shifts induced by each fibre section, with expressions similar to the PIC model, and weighting factors depending on dispersion management parameters, local fibre dispersion and length.

Indeed, the multi-span perturbation approach described in the Appendix leads to this expression of the evolution of the optical field E(z,t) (or $\widetilde{E}(z,\omega)$ in the frequency domain):

$$\widetilde{E}(Rx,\omega)=\sqrt{\frac{\left\langle |E|^2(Rx)\right\rangle}{\left\langle |E|^2(z=0)\right\rangle}}\left(\widetilde{E}(0,\omega)-j\sum_{\substack{fibre\\ section\\ k=1..N}}\int_{\omega_1,\omega_2}S(0,\Omega)\,\Phi_{nl,k}\,\frac{e^{j\beta_{2,cum}(z=0_{span\,k})\Omega^2}}{1-j\dfrac{\beta_{2,loc,k}\,\Omega^2}{\alpha}}\right).e^{-j\frac{\beta_{2,cum}(Rx)}{2}\omega^2} \qquad (2\text{-}42)$$

With $S(0,\Omega)=\widetilde{E}_1(0,\omega_1)\widetilde{E}_1(0,\omega_2)\widetilde{E}_1^{\,*}(0,\omega_1+\omega_2-\omega)$, Rx meaning transmission end (before receiver), and $\Omega=(\omega-\omega_1)(\omega-\omega_2)$

We can therefore easily understand that under conditions of frequency and inline cumulated dispersion similar to the conditions appearing with the PIC model, the signal distortions can appear as a linear combination of the total nonlinear phase shift coming from the line fibre sections and of the total nonlinear phase shift coming from the DCFs as mentioned by Fischer et al in [75].

The overall field perturbation using the multi-span perturbation approach can be expressed for doubly-periodic maps (overlooking here the contributions of DCF) as:

$$\widetilde{E}(Rx,\omega)=\sqrt{\frac{\left\langle |E|^2(Rx)\right\rangle}{\left\langle |E|^2(z=0)\right\rangle}}.\left(\widetilde{E}(0,\omega)-j\int_{\omega_1,\omega_2}S(0,\Omega').K(\Omega).d\omega_1.d\omega_2\right).e^{-j\frac{\beta_{2,res}}{2}\omega^2}$$

With the nonlinear kernel K(Ω): (2-43)

$$K(\Omega)=(N.M.\Phi_{nl,1\,span}).\frac{e^{j\left(\beta_{2,pre}+\frac{N-1}{2}\beta_{2,res\,span}+\frac{M-1}{2}\beta_{2,res\,node\,sec.}\right)\Omega^2+j.\arctan\left(\frac{\beta_{2,loc}\Omega^2}{\alpha}\right)}}{\sqrt{1+\left(\dfrac{\beta_{2,loc}\Omega^2}{\alpha}\right)^2}}\frac{\sin\left(\dfrac{N\beta_{2,res\,span}\Omega^2}{2}\right)}{N.\sin\left(\dfrac{\beta_{2,res\,span}\Omega^2}{2}\right)}\frac{\sin\left(\dfrac{M\beta_{2,res\,node}\Omega^2}{2}\right)}{M.\sin\left(\dfrac{\beta_{2,res\,node}\Omega^2}{2}\right)}$$

assuming N as the number of spans per subdivision (that can be a node section), M the number of subdivisions and other obvious notations detailed in the Appendix.

2.IV. Summary

This Chapter is the first step towards a tool able to simply predict the impact of nonlinear effects and chromatic dispersion with a reasonable accuracy. We have introduced the nonlinear phase criterion and shown its interest and accuracy for transmission systems with optimized dispersion management. Then we have investigated more advanced perturbative models that comfort this criterion and highlight a few expected directions of improvements when transposing this tool to real-life conditions. Chapter 3 will aim to address more specifically that topic with an improved nonlinear phase tool adapted to deployed systems.

In details, we have first shown that the average nonlinear phase shift from Equation (2-2) theoretically applicable for zero chromatic dispersion is in fact a very good metrics to characterize the accumulation of Kerr-related effects (SPM, XPM) in single channel and WDM transmission systems characterized by non-zero dispersion fibres and optimized dispersion management. Such a metrics enables to capture the power-related impact of line fibre sections and DCF sections as well as the number of spans. In particular, we have experimentally and numerically shown a strong correlation between transmission penalties and such nonlinear phase shift whatever distance or powers for 10 and 40Gb/s transmission systems, while similar results have been observed also at 160Gb/s. We have defined the nonlinear phase criterion as the ability to describe system penalties through the knowledge of the total nonlinear phase shift and have shown an excellent accuracy below 1.1dB in various cases. We can further note that for transmission systems with high symbol-rates such as 40Gb/s, the optimization of residual chromatic dispersion before receiver may only depend on the nonlinear phase shift whatever the distance or the dispersion map [91], thus highlighting the key role of this metrics.

We have then investigated more advanced models derived as perturbations from the propagation equations such as the small-signal phase-to-intensity conversion models (or perturbative expansions of the nonlinear Schrödinger equation in the Appendix).

Such models are not practical or accurate enough to be used for pure performance prediction during the design or the operation of optical networks, but they enable to get more physical insight into signal propagation and understand better the relevant parameters over a dispersion-managed transmission system. As such they enable to derive very interesting laws to ease the optimization of the dispersion management, and they can be used to comfort and consolidate the nonlinear phase criterion.

We have thus made the connection between this nonlinear phase criterion and such perturbative theories. In all the described models, the predicted nonlinearity induced perturbation can appear as a linear combination of the nonlinear phase shifts of the different fibre sections.

We have further shown that provided sufficiently low values of the total cumulated inline dispersion and/or symbol rate, the predicted perturbation appears as a linear combination of the total nonlinear phase coming from the line fibre sections and of the total nonlinear phase coming from the DCFs. In more details, one condition appears as sufficient to enable the natural emergence of the total nonlinear phase parameter out of the latter models, apart from the domain of validity of such models: the product between total accumulated inline dispersion in physical notations and the square of the symbol-rate has to remains sufficiently low with respect to 1. This is particularly the case for 10Gb/s modulated systems. We mentioned that in 2008 in [64] and this appears in the equations of the regular perturbation models as well [74],[78]. One other emerging sufficient condition for dispersion-managed transmission

systems is that the total inline cumulated dispersion remains below the accumulated dispersion over a few times the effective length of the line fibre as in Equation (2-36) and mentioned by Fischer et al in 2009 [75] or in [87][88][89]. This is particularly the case for systems with symbol rates higher than 10Gbaud. One last possible sufficient condition would be to optimize dispersion management for each distance, which would be consistent with the observations of such an ideal, asymptotic case in section 2.II. Under such conditions, one can expect that the signal distortions depends on a linear combination of the total nonlinear phase shift coming from the line fibre sections and of the total nonlinear phase shift coming from the DCF sections. *We will numerically and experimentally confront the nonlinear phase criterion with realistic dispersion management conditions in Chapter 3*.

What is even more remarkable with the nonlinear phase criterion as emerging from the observations in section 2.II. is that the signal distortion depends on the simple sum of the total nonlinear phase shift coming from the line fibre sections and of the total nonlinear phase shift coming from the DCF sections, i.e. a simple sum of the nonlinear phase shift coming from each fibre section rather than a linear combination. This is probably because DCF-induced nonlinearities are generally two to four times lower than line-fibre-induced nonlinearities (input power into DCF 10 to 4dB lower than into line fibre) and therefore can be treated as perturbations. *We will thus numerically and experimentally investigate the domain of validity/accuracy of the total nonlinear phase criterion in Chapter 3 by substantially varying the relative powers into line fibres and DCFs far outside the usual conditions of operation.*

More generally, in the former perturbative models the contribution of each fibre section to signal distortion depends not only on nonlinear phase shift but also on fibre local dispersion and on fibre length when low enough [90]. This raises the question of the accuracy of the nonlinear phase criterion and its possible consolidation beyond the simple sum of the nonlinear phase shifts of each fibre section when dealing with typically deployed transmission systems presenting a mix of line fibre section lengths and chromatic dispersions.

In conclusion, the nonlinear phase criterion tool can be of high interest to design a system or predict performance. Indeed, we can imagine calibrating the relationship between nonlinear phase shift and penalty out of a few experiments and configurations, and use that calibrated relationship to predict the penalty in many other configurations of distance or power, with possibly line fibre sections of different lengths. We have shown here that this nonlinear phase criterion is particularly adapted to catch the asymptotic performance of ideal systems with optimized dispersion management conditions. With the guidance of the analytical models developed here, Chapter 3 will be dedicated to the domain of validity /accuracy of the nonlinear phase criterion and to its generalization for real-life conditions characterized by non-fully optimized dispersion maps and heterogeneity in line fibre span lengths and types.

The nonlinear phase criterion developed here can also be part of an even more ambitious estimator of the quality of transmission as in Chapter 4 including multiple sources of system degradation; it could serve as well to set the input powers into fibre sections or the optical amplifier schemes in order to maximize the achievable reach of optical transmission systems as a trade-off between nonlinear- and noise-related issues as in Chapter 5.

Most of the work on this topic has been published in [62][64][65].

2.V. Appendix

V.1. Pertubative models based on the Dispersion –Managed NLSE

V.1.1. Introduction

In this section, we investigate the relevance of alternative models based on a perturbative approach of the Nonlinear Schrödinger Equation, accounting for Dispersion-Management. Such models have been proposed by the University of Parma [86] and the Technical University of Berlin [80].

We will first explain the common basis of such models, before recalling the numerically observed validity domain of this basis, and conclude on the relevance of the models proposed by the Universities.

V.1.2. The perturbative NLSE model

Let us explain the common foundations of models from Universities of Parma and Berlin, that we could call the "Perturbative DM NLSE" (for Dispersion Managed NLSE): in the (ωt -kz) phase convention, the propagation equation (in the time domain) can be written as:

$$\frac{\partial E(z,t)}{\partial z} = j\frac{\beta_2}{2}\frac{\partial^2 E}{\partial T^2} - j\gamma(z)\left|E\right|^2 E - \frac{\alpha}{2}E \qquad (2\text{-}44)$$

with the envelope E of the signal field, time t and distance z, the local group velocity dispersion β_2 of the fibre, the local attenuation α, and local nonlinear coefficient γ.

With usual change of variable $E = \sqrt{P}e^{\frac{-\int_0^z \alpha(z')dz'}{2}}E_0(z,t)$, we get (in the frequency domain):

$$\frac{\partial \widetilde{E}_0}{\partial z}(z,\omega) = -j\frac{\beta_2(z)}{2}\omega^2\widetilde{E}_0 - j\gamma(z)P(z)\int_{\omega_1}\int_{\omega_2}\widetilde{E}_0(\omega_1)\widetilde{E}_0(\omega_2)\widetilde{E}_0{}^*(\omega_1+\omega_2-\omega)\frac{d\omega_1}{2\pi}\frac{d\omega_2}{2\pi} \qquad (2\text{-}45)$$

We can eventually make a second change of variable accounting for the sole impact of accumulated Group Velocity Dispersion on the signal, $\beta_{2,cum}(z)$:

$$\widetilde{E}_0(z,\omega) = e^{-j\frac{\beta_{2,cum}(z)}{2}\omega^2}\widetilde{E}_1(z,\omega) \qquad (2\text{-}46)$$

and get a dispersion-managed NLSE with only one term:

$$\frac{\partial \widetilde{E}_1}{\partial z}(z,\omega) = -j\gamma(z)\overline{P}(z)\int_{\omega_1}\int_{\omega_2}\widetilde{E}_1(z,\omega_1)\widetilde{E}_1(z,\omega_2)\widetilde{E}_1^*(z,\omega_1+\omega_2-\omega)e^{+j\beta_{2,cum}(z)(\omega-\omega_1)(\omega-\omega_2)} \qquad (2\text{-}47)$$

In absence of nonlinearities, the new field E_1 is unchanged by transmission. The perturbative approach assumes weak enough nonlinearities over one span such that $E_1(z,\omega)$ does not depend on z within a transmission span.

Thus, we can integrate the previous equation over 1 span, which leads to:

$$\widetilde{E}_1(z_{span},\omega) = \widetilde{E}_1(0,\omega) + \delta_{nl} \qquad (2\text{-}48)$$

with

$$\delta_{nl} = -j\int_{\omega_1}\int_{\omega_2} \widetilde{E}_1(0,\omega_1)\widetilde{E}_1(0,\omega_2)\widetilde{E}_1^{\,*}(0,\omega_1+\omega_2-\omega)\int_{z=0}^{z_{span}} \gamma(z)\,\overline{P}(z)e^{+j\beta_{2,cum(z)}(\omega-\omega_1)(\omega-\omega_2)} \qquad (2\text{-}49)$$

The nonlinear perturbation δ_{nl} can itself be expressed as:

$$\delta_{nl} = -j\int_{\omega_1}\int_{\omega_2} S(0,\Omega)\,c(\Omega) \qquad (2\text{-}50)$$

With

- $S(0,\Omega) = \widetilde{E}_1(0,\omega_1)\widetilde{E}_1(0,\omega_2)\widetilde{E}_1^{\,*}(0,\omega_1+\omega_2-\omega)$ (2-51)
- $\Omega = (\omega-\omega_1)(\omega-\omega_2)$ (2-52)
- And the kernel c

$$c(\Omega) = \int_{z=0}^{z_{span}} \gamma(z)\,\overline{P}(z)e^{+j\beta_{2,cum(z)}(\omega-\omega_1)(\omega-\omega_2)} \sim \gamma P_0 \frac{e^{j\beta_{2,cum}(z=0_{span})\Omega^2}}{\alpha - j\beta_{2,loc}\,\Omega^2} = \Phi_{nl}{}^{1\,span}\frac{e^{j\beta_{2,cum}(z=0_{span})\Omega^2}}{1-j\dfrac{\beta_{2,loc}\,\Omega^2}{\alpha}} \qquad (2\text{-}53)$$

for long spans, so that after one span, we get.

$$E_0(z_{span},\omega) = \left(E_0(0_{span},\omega) - j\int_{\omega_1,\omega_2} S(0_{span},\Omega)\,\Phi_{nl}\frac{e^{j\beta_{2,cum}(z=0_{span})\Omega^2}}{1-j\dfrac{\beta_{2,loc}\,\Omega^2}{\alpha}} \right).e^{-j\frac{\beta_{2,cum}(z_{span}\ or\ Rx)}{2}\omega^2} \qquad (2\text{-}54)$$

To model the propagation after N spans, we can consider two strategies:

- the "**1-span perturbation model**", which consists in recalculating the signal after each span before feeding Equation (2-54) corresponding to another span
- the "**multi-span perturbation model**", which consists in extending the perturbative approach to the whole transmission link, and which leads, after N spans, to the following equation:

$$E_0(Rx,\omega) = \left(E_0(0,\omega) - j\sum_{k=1..N}\int_{\omega_1,\omega_2} S(0,\Omega)\,\Phi_{nl,k}\frac{e^{j\beta_{2,cum}(z=0_{span\,k})\Omega^2}}{1-j\dfrac{\beta_{2,loc,k}\,\Omega^2}{\alpha}} \right).e^{-j\frac{\beta_{2,cum}(Rx)}{2}\omega^2} \qquad (2\text{-}55)$$

which can be expressed for doubly-periodic maps as:

$$E_0(Rx,\omega) = \left(E_0(0,\omega) - j\int_{\omega_1,\omega_2} S(0,\Omega')\Phi_{nl,1\,span}\frac{e^{j\left(\beta_{2,pre}+\frac{N-1}{2}\beta_{2,res\,span}+\frac{M-1}{2}\beta_{2,res\,node\,sec.}\right)\Omega^2}}{1-j\dfrac{\beta_{2,loc}\Omega^2}{\alpha}}\frac{\sin\left(\dfrac{N\beta_{2,res\,span}\Omega^2}{2}\right)}{\sin\left(\dfrac{\beta_{2,res\,span}\Omega^2}{2}\right)}\frac{\sin\left(\dfrac{M\beta_{2,res\,node}\Omega^2}{2}\right)}{\sin\left(\dfrac{\beta_{2,res\,node}\Omega^2}{2}\right)} \right).e^{-j\frac{\beta_{2,res}}{2}\omega^2} \qquad (2\text{-}56)$$

with N as the number of spans per subdivision (that can be a node section), M the number of subdivisions (or node sections), and explicit terms of local fibre dispersion, residual dispersion per span or subdivision (or node section).

From this point on, the signal field can be calculated (after a certain time due to presence of the double integral in ω) after transmission using this approach, enabling direct investigation of the validity domain of those approximations through comparison of system performance with usual Split-Step Fourier Method-based simulations.

Additionally, this approximation can be the basis for derived, intuitive and less-time consuming models, focusing on the overall kernel, its phase, imaginary part, or module.

Indeed, the perturbation after NxM spans will be:

$$\widetilde{E}_1(z_{Rx},\omega)=\widetilde{E}_1(0,\omega)+\delta_{nl} \quad with \quad \delta_{nl}=-j\int_{\omega_1}\int_{\omega_2} S(0,\Omega)\,K(\Omega) \tag{2-57}$$

where the kernel K(Ω) is:

$$K(\Omega)=\Phi_{nl}^{1span}\frac{e^{j\left(\beta_{2,pre}+\frac{N-1}{2}\beta_{2,res\,span}+\frac{M-1}{2}\beta_{2,res\,node\,\mathrm{sec.}}\right)\Omega^2}}{1-j\dfrac{\beta_{2,loc}\,\Omega^2}{\alpha}}\frac{\sin\left(\dfrac{N\,\beta_{2,res\,span}\,\Omega^2}{2}\right)}{\sin\left(\dfrac{\beta_{2,res\,span}\,\Omega^2}{2}\right)}\frac{\sin\left(\dfrac{M\,\beta_{2,res\,node}\,\Omega^2}{2}\right)}{\sin\left(\dfrac{\beta_{2,res\,node}\,\Omega^2}{2}\right)} \tag{2-58}$$

or

$$K(\Omega)=\Phi_{nl}^{1span}\frac{e^{j\left(\beta_{2,pre}+\frac{N-1}{2}\beta_{2,res\,span}+\frac{M-1}{2}\beta_{2,res\,node\,\mathrm{sec.}}+\frac{1}{\Omega^2}\arctan\left(\frac{\beta_{2,loc}\,\Omega^2}{\alpha}\right)\right)\Omega^2}}{\sqrt{1+\left(\dfrac{\beta_{2,loc}\,\Omega^2}{\alpha}\right)^2}}\frac{\sin\left(\dfrac{N\,\beta_{2,res\,span}\,\Omega^2}{2}\right)}{\sin\left(\dfrac{\beta_{2,res\,span}\,\Omega^2}{2}\right)}\frac{\sin\left(\dfrac{M\,\beta_{2,res\,node}\,\Omega^2}{2}\right)}{\sin\left(\dfrac{\beta_{2,res\,node}\,\Omega^2}{2}\right)} \tag{2-59}$$

Looking for a **purely real Kernel** (for a certain frequency, or integrated…) leads to similar requirements as **PIC criterion** [73] with a tiny difference in the arctan() term. This way, the perturbation δ_{nl} could be in quadrature with the signal (e.g. if we assume that the incident field E_1 and S are real in the frequency domain). It would correspond to a minimization of the perturbation of the in-phase component of the signal. Note that for a modulation format including multilevel phase modulation, the benefit of having a real kernel may vanish [89].

Alternatively, focusing only on the module of the Kernel, such as the work from [80], appears of little use since we lose track of the pre-compensation term, (which term has a clear impact on the optimum value of inline compensation, since it follows PIC rules very strictly at least at 40G) and of the sign of the inline residual dispersion (also in contradiction with PIC criterion).

We can further observe in Equation (2-56) that the **term in residual dispersion** cannot be so easily subtracted from the Pre-compensation term as in the simplified PIC criterion since each term is here multiplied by a different frequency component.

In fact the observed small differences between both PIC and regular perturbation models regarding either the arctan() term or the residual dispersion essentially come from the approximation in Equation (2-15) that $H_{IM\text{-}IM}(D_{cum}(z))=1$ rather than $\cos(\omega^2\lambda^2/(4\pi c)^* D_{cum}(z)/2)$. Such differences naturally vanish in the low frequency approximation.

In conclusion, up to now and after a few equations, we have two models, the one-span and the multi-span perturbation models, that enable to approximate the distorted signal after propagation. Such models are time-consuming, but they are relevant. They can be the basis for derived simpler and intuitive models, such as considering the Kernel of the perturbation, which phase zeroing almost amounts to applying the PIC criterion.

The next section recalls the domains of validity of both "basic"-models

V.1.3. Validity domains of the 1-span and multi-span perturbation models

Naturally, the approximations behind the 1-span and multi-span perturbation (respectively) models are based on the assumptions of weak amounts of nonlinearities, per span and per transmission link (respectively).

Figure 2-14 highlights the fact that the accuracy of the 1-span perturbation model to predict performance and optimized dispersion maps improves rapidly with the number of spans: at 40Gb/s, the NLT can be estimated with less than 1dB error after 10 spans (here of SMF fibre, similar conclusions can be drawn using LEAF fibre) for NRZ and PSBT formats (15-20 spans at 10Gb/s), whatever the pre-compensation of the singly-periodic dispersion managed tested system. Conversely, the multi-span perturbation model does not appear reliable, at any transmission distance, for NLT estimation, and even for the prediction of the right dispersion map, where it appears less accurate than PIC criterion (which is somehow unexpected since the derivation of such a criterion leads, after other approximations, to the PIC criterion, as abovementioned). Nonetheless, the multi-span approach enables to catch the fact that the optimal residual dispersion does not depend on dispersion map at 40Gb/s, while it follows the directions of the PIC at 10Gb/s. Maybe the derivation of higher order perturbative terms of such a model will make it more usable.

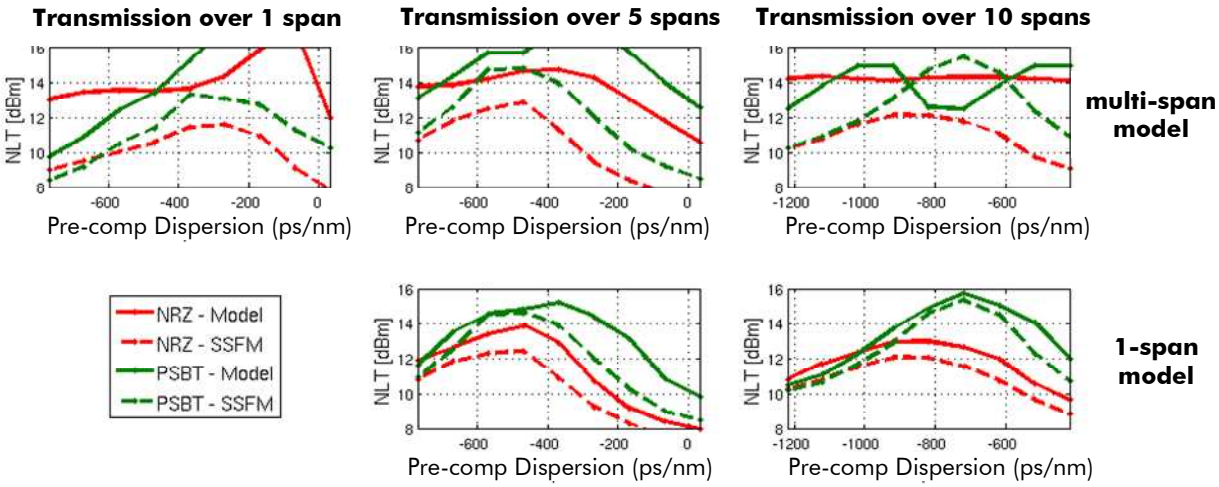

Figure 2-14: 1.5dB penalty nonlinear threshold (integrated power) estimation for NRZ/PSBT 40Gb/s systems over SMF and singly periodic dispersion maps (varying Pre, inline residual dispersion set to 100ps/nm, and optimized residual dispersion, for 1, 5 and 10 spans), using standard split-step Fourier method (SSFM) simulations, or signal computation with 1-span/multi-span perturbation models.

In conclusion, the 1-span perturbation model enables to emulate correctly signal distortions along the line as soon as the number of amplified spans is high enough (10 at 40Gb/s, 15-20 at 10Gb/s), but at the expense of the calculation time, while the simpler multi-span perturbative approach is not usable to predict performance. Note that choosing a logarithmic multi-span perturbation approach [78] rather than the multi-span regular perturbation brings better results in terms of emulation of nonlinear systems. Yet the computation time still remains a practical issue and the models have more value to understand the underlying physics laws of the dispersion-managed systems.

V.1.4. Advanced model from the University of Parma

The University of Parma proposed a median way between the single-span and multi-span perturbation models. They try to get the best of both, and simplify the problem when possible.

The problem can indeed by simplified as soon as dispersion management becomes regular. Suppose for instance singly periodic dispersion management. The multi-span-perturbation approach sees only a regular change of the kernel for each span due to the regular accumulation of dispersion (due to inline compensation), while the one-span-perturbation model also catches the progressive signal distortions.

The approach from the University of Parma is slightly different from the "one-term" Dispersion-managed NLSE expression in Equation (2-47), due to a different change of variable. Instead of considering the linear impact of cumulated dispersion, they consider the net impact of cumulated dispersion minus the average inline cumulated dispersion, resulting in this change of variable for the power-averaged NLSE

$$\frac{\partial \widetilde{E}_0}{\partial z}(z,\omega) = -j\frac{\beta_2(z)}{2}\omega^2 \widetilde{E}_0 - j\,\gamma(z)\,P(z)\int_{\omega_1}\int_{\omega_2} \widetilde{E}_0(\omega_1)\widetilde{E}_0(\omega_2)\widetilde{E}_0{}^*(\omega_1+\omega_2-\omega)\frac{d\omega_1}{2\pi}\frac{d\omega_2}{2\pi} \qquad (2\text{-}45)$$

With

$$E_0(z,\omega) = e^{-j\frac{\beta_{2,cum}(z)-<\beta_2>z}{2}\omega^2} E'_1(z,\omega) \qquad (2\text{-}60)$$

and with $<\beta_2>$ equal to the inline residual dispersion per span divided by span length. This allows to get the new DM NLSE:

$$\frac{\partial \widetilde{E}'_1}{\partial z}(z,\omega) = -j\frac{<\beta_2>\omega^2}{2}E_1 - j\,\gamma(z)\,\overline{P}(z)\int_{\omega_1}\int_{\omega_2} \widetilde{E}'_1(z,\omega_1)\widetilde{E}'_1(z,\omega_2)\widetilde{E}'_1{}^*(z,\omega_1+\omega_2-\omega)e^{+j\Delta\beta_{2,cum(z)}(\omega-\omega_1)(\omega-\omega_2)} \qquad (2\text{-}61)$$

with $\Delta\beta_{2,cum}(z) = \beta_{2,cum}(z) - <\beta_2>z$, the cumulated dispersion profile in addition to the average inline dispersion profile.

Then, after averaging each coefficient over a span (method of the multiple scales, detailed in [74] and equivalent to the 1-span perturbation model approximation), the kernel of the nonlinear perturbation is the same after all the spans of the link.

$$\frac{\partial E_1}{\partial z}(z,\omega) = -j\frac{<\beta_2>\omega^2}{2}E_1 - j\frac{1}{L_{span}}\int_{\omega_1}\int_{\omega_2} d\Omega.\widetilde{E}_1(z_{0,span},\omega_1)\widetilde{E}_1(z_{0,span},\omega_2)\widetilde{E}_1{}^*(z_{0,span},\omega_1+\omega_2-\omega).c(\Omega) \qquad (2\text{-}62)$$

$$\text{with kernel } c(\Omega) = \int_0^{z_{span}} dz'\gamma(z')\overline{P}(z')e^{j\Delta\beta_{2,cum}(z')\Omega^2} \approx \phi_{nl,1\,span}\frac{e^{j\beta_{2,pre}\Omega^2}}{1-\frac{\Delta\beta_{2,loc}}{\alpha}\Omega^2} \qquad (2\text{-}63)$$

for long spans.

Thus, the coefficients of this span-averaged Dispersion-Managed NLSE remain the same from span to span, which allows us to describe the system impact of the dispersion management of the system using these synthetic parameters, with the accuracy of the previously described one-span perturbation model.

From this equation, the University derived a few scaling factors that will rule system performance at any rate, distance, fibre:

- The ratio between the total length of the link and the **average dispersion length** $L_{<D>} = \frac{d^2}{R^2 <\beta_2>}$ (with bit-rate R and duty cycle d): it amounts to the value: $\boxed{L/L_{<D>} = \frac{R^2}{d^2}<\beta_2>L_{span}N_{span}}$, which corresponds to the slowly varying linear effect.

- The product between the total nonlinear phase and the **map strength S = L_{eff} / L_{Δ}**, with the differential dispersive length $L_{\Delta} = \frac{d^2}{R^2 \Delta\beta_{2,loc}}$, and $L_{eff} = 1/\alpha$. It amounts to

$$\phi_{nl,total} * S = \phi_{nl,total} * \frac{R^2}{d^2} \Delta\beta_{2,loc} L_{eff}$$

- The phase rotation induced by dispersion **pre-compensation**.

The first two scaling factors set the amplitude of the perturbations to the signal, while the last one sets the phase shift between the nonlinear perturbation and the incoming signal. This is rather in agreement with results of Chapter 3 showing that tolerance to nonlinearities, is a function of the Pre-compensation value and total inline cumulated dispersion $NxD_{res/span}$, for one constant type of fibre.

To derive more explicit rules between the different factors, the University somehow reinserted the average GVD term into the kernel and did the multi-span perturbation approximation, to look for the zeroing of the kernel phase, leading to the abovementioned close-to-PIC formula.

In conclusion, the scaling laws derived by the University of Parma for singly periodic dispersion maps have the intrinsic validity domain of the one-span perturbation approach, that is to say ~10 spans for 40Gb/s. Similar laws can be obtained when considering doubly-periodic maps, but we would require at least 10 subdivisions to get the same relevance. Such laws can therefore be very useful to design and predict performance of submarine systems at various bit-rates. For non-periodic terrestrial systems, and especially for metropolitan systems, PIC criterion and the 1-span perturbation approach still remain the most-suitable approaches, even though suffering from strong lack of accuracy. Investigations on the refinement of the multi-span perturbation model should be a solution in the future, but at the expense of the simplicity.

V.2. PIC model: accounting for IM-IM and PM-IM filters in P(z,ω) for any kind of modulation format

Here we generalize the single-span PIC model from section III.2. to cases where modulation formats and dispersion maps are arbitrary. In other words, we do not assume any longer that $H_{IM-IM}=1$ and $H_{PM-IM}=0$ to simplify Equation (2-15) into Equation (2-17).

Thus we have:

$$\begin{aligned} dPIC(z,\omega) &= \frac{d\widetilde{P}(z,\omega)}{2\langle P(L_{tot})\rangle} \\ &= \gamma\frac{<P(z)>}{<P(0)>}.dz.\left(\widetilde{P}(0,\omega)\cos\left[\frac{\omega^2\lambda^2}{4\pi c}(D_{cum}(z))\right]+2.\langle P(0)\rangle.\widetilde{\phi}(0,\omega).\sin\left[\frac{\omega^2\lambda^2}{4\pi c}(D_{cum}(z))\right]\right).\sin\left[\frac{\omega^2\lambda^2}{4\pi c}(D_{res}-D_{cum}(z))\right] \end{aligned} \quad (2\text{-}64)$$

Note that if the input signal is intensity modulated, and $D_{res}=0$, then we get

$$dPIC(z,\omega)=-\gamma\frac{<P(z)>}{<P(0)>}.\frac{\widetilde{P}(0,\omega)}{2}\sin\left[\frac{\omega^2\lambda^2}{2\pi c}D_{cum}(z)\right].dz$$

All the calculations from section III.2. apply except that A should be replaced by $A' = \sqrt{2}*A$.

Coming back to arbitrary modulation, Equation (2-64) becomes:

$$\begin{aligned} dPIC(z,\omega,D_{res}) &= \gamma\frac{<P(z)>}{<P(0)>}.dz.\left(\widetilde{P}(0,\omega)\cos\left[\frac{\omega^2\lambda^2}{4\pi c}(D_{cum}(z))\right]+2.\langle P(0)\rangle.\widetilde{\phi}(0,\omega).\sin\left[\frac{\omega^2\lambda^2}{4\pi c}(D_{cum}(z))\right]\right).\sin\left[\frac{\omega^2\lambda^2}{4\pi c}(D_{res}-D_{cum}(z))\right] \\ &= \gamma\frac{<P(z)>}{<P(0)>}.dz.\left(\widetilde{P}(0,\omega)\cos\left[\frac{\omega^2\lambda^2}{4\pi c}(D_{cum}(z))\right]+2.\langle P(0)\rangle.\widetilde{\phi}(0,\omega).\sin\left[\frac{\omega^2\lambda^2}{4\pi c}(D_{cum}(z))\right]\right) \\ &\quad *\left(-\sin\left[\frac{\omega^2\lambda^2}{4\pi c}(D_{cum}(z))\right]*\cos\left[\frac{\omega^2\lambda^2}{4\pi c}(D_{res})\right]+\cos\left[\frac{\omega^2\lambda^2}{4\pi c}(D_{cum}(z))\right]*\sin\left[\frac{\omega^2\lambda^2}{4\pi c}(D_{res})\right]\right) \end{aligned}$$

then

$$\begin{aligned} dPIC(z,\omega,D_{res}) &= dPIC(z,\omega,D_{res}=0)*\cos\left[\frac{\omega^2\lambda^2}{4\pi c}(D_{res})\right] \\ &\quad +\underbrace{\gamma\frac{<P(z)>}{<P(0)>}.dz.\left(\widetilde{P}(0,\omega)\cos\left[\frac{\omega^2\lambda^2}{4\pi c}(D_{cum}(z))\right]+2.\langle P(0)\rangle.\widetilde{\phi}(0,\omega).\sin\left[\frac{\omega^2\lambda^2}{4\pi c}(D_{cum}(z))\right]\right)*\cos\left[\frac{\omega^2\lambda^2}{4\pi c}(D_{cum}(z))\right]*\sin\left[\frac{\omega^2\lambda^2}{4\pi c}(D_{res})\right]}_{dB_{PIC}} \end{aligned}$$

In a first step, let us assume that $D_{res}=0$ps/nm, before calculating the additional B_{PIC} term.

$$\begin{aligned} dPIC(z,\omega,D_{res}=0) &= \frac{d\widetilde{P}(z,\omega)}{2\langle P(L_{tot})\rangle} \\ &= -\gamma\frac{<P(z)>}{<P(0)>}.dz.\left(\frac{\widetilde{P}(0,\omega)}{2}\sin\left[\frac{\omega^2\lambda^2}{2\pi c}(D_{cum}(z))\right]+2.\langle P(0)\rangle.\widetilde{\phi}(0,\omega).\sin^2\left[\frac{\omega^2\lambda^2}{4\pi c}(D_{cum}(z))\right]\right) \end{aligned} \quad (2\text{-}65)$$

We then integrate over distance 0 to L, and get:

$$\begin{aligned} PIC(z,L,\omega,D_{res}=0) &= \int_0^L dPIC(z,\omega)=-\gamma\int_0^L dz.e^{-\alpha z}.\left(\frac{\widetilde{P}(0,\omega)}{2}\sin\left[\frac{\omega^2\lambda^2}{2\pi c}(D_{cum}(z))\right]+2.\langle P(0)\rangle.\widetilde{\phi}(0,\omega).\sin^2\left[\frac{\omega^2\lambda^2}{4\pi c}(D_{cum}(z))\right]\right) \\ &= PIC_{IM-IM}+PIC_{PM-IM} \end{aligned} \quad (2\text{-}66)$$

with

$$PIC_{IM-IM}=-\gamma\int_0^L dz.e^{-\alpha z}.\left(\frac{\widetilde{P}(0,\omega)}{2}\sin\left[\frac{\omega^2\lambda^2}{2\pi c}(\Pr e+D_{loc}*z)\right]\right)=-\gamma\frac{\widetilde{P}(0,\omega)}{2.\alpha}\mathrm{Im}\left[e^{j\frac{\omega^2\lambda^2}{2\pi c}\Pr e}\frac{1-e^{-\left(\alpha-j\frac{\omega^2\lambda^2}{2\pi c}D_{loc}\right)L}}{1-j\frac{\omega^2\lambda^2}{2\pi c}\frac{D_{loc}}{\alpha}}\right] \quad (2\text{-}67)$$

If we further define the kernel K(ω) such that

$$K(\omega)=\frac{e^{j\frac{\omega^2\lambda^2}{2\pi c}D_{cum,input}(0)}}{1-j\frac{\omega^2\lambda^2}{2\pi c}\frac{D_{loc}}{\alpha}}\frac{1-e^{\left(-\alpha+j\frac{\omega^2\lambda^2}{2\pi c}D_{loc}\right)L}}{1-e^{-\alpha L}}$$
$$=\frac{e^{j\left(\frac{\omega^2\lambda^2}{2\pi c}D_{cum,input}(0)+\arctan\left(\frac{\omega^2\lambda^2}{2\pi c}\frac{D_{loc}}{\alpha}\right)-\arctan\left(\frac{e^{-\alpha L}\sin\left(\frac{\omega^2\lambda^2}{2\pi c}D_{loc}L\right)}{1-e^{-\alpha L}\cos\left(\frac{\omega^2\lambda^2}{2\pi c}D_{loc}L\right)}\right)\right)}}{\sqrt{1+\left(\frac{\omega^2\lambda^2}{2\pi c}\frac{D_{loc}}{\alpha}\right)^2}}\frac{\sqrt{1-2e^{-\alpha L}\cos\left(\frac{\omega^2\lambda^2}{2\pi c}D_{loc}L\right)+e^{-2\alpha L}}}{1-e^{-\alpha L}} \quad (2\text{-}68)$$

then:

$$PIC_{IM-IM}=-\phi_{nl}\frac{\widetilde{P}(0,\omega)}{2.\langle P(0)\rangle}\mathrm{Im}[K(\omega)] \quad (2\text{-}69)$$

Similarly we can calculate $PIC_{PM\text{-}IM}$

$$PIC_{PM-IM}=-\phi_{nl}.\widetilde{\phi}(0,\omega).(1-\mathrm{Re}[K(\omega)]) \quad (2\text{-}70)$$

In details:

$$PIC_{PM-IM}=-2.\gamma\langle P(0)\rangle.\widetilde{\phi}(0,\omega).\int_0^L dz.e^{-\alpha z}.\sin^2\left[\frac{\omega^2\lambda^2}{4\pi c}D_{cum}(z)\right]$$
$$=-2.\gamma\langle P(0)\rangle.\widetilde{\phi}(0,\omega).\int_0^L dz.e^{-\alpha z}\frac{1-\cos\left(\frac{\omega^2\lambda^2}{2\pi c}D_{cum}(z)\right)}{2}$$
$$=-2.\gamma\langle P(0)\rangle.\widetilde{\phi}(0,\omega).\int_0^L dz.e^{-\alpha z}\frac{1-\mathrm{Re}\left[e^{j\frac{\omega^2\lambda^2}{2\pi c}D_{cum}(z)}\right]}{2}$$
$$=-\gamma\langle P(0)\rangle.\widetilde{\phi}(0,\omega).\left(L_{eff}-\mathrm{Re}\left[\int_0^L dz.e^{-\alpha z+j\frac{\omega^2\lambda^2}{2\pi c}D_{cum}(z)}\right]\right)$$
$$=-\gamma\langle P(0)\rangle.\widetilde{\phi}(0,\omega).\left(L_{eff}-\frac{1}{\alpha}\mathrm{Re}\left[e^{j\frac{\omega^2\lambda^2}{2\pi c}D_{cum,input}(0)}\frac{1-e^{\left(-\alpha+j\frac{\omega^2\lambda^2}{2\pi c}D_{loc}\right)L}}{1-j\frac{\omega^2\lambda^2}{2\pi c}\frac{D_{loc}}{\alpha}}\right]\right)$$
$$=-\left(\gamma\langle P(0)\rangle.L_{eff}\right)\widetilde{\phi}(0,\omega).\left(1-\mathrm{Re}\left[\frac{e^{j\frac{\omega^2\lambda^2}{2\pi c}D_{cum,input}(0)}}{1-j\frac{\omega^2\lambda^2}{2\pi c}\frac{D_{loc}}{\alpha}}\frac{1-e^{\left(-\alpha+j\frac{\omega^2\lambda^2}{2\pi c}D_{loc}\right)L}}{1-e^{-\alpha L}}\right]\right)$$

The overall nonlinear induced relative power distortion is therefore:

$$PIC(\omega,L,D_{res}=0)=\frac{\Delta\widetilde{P}(L_{tot},\omega,D_{res}=0)}{2\langle P(L_{tot})\rangle}=-\phi_{nl}\left(\frac{\widetilde{P}(0,\omega)}{2.\langle P(0)\rangle}\mathrm{Im}[K(\omega)]+\widetilde{\phi}(0,\omega).(1-\mathrm{Re}[K(\omega)])\right) \quad (2\text{-}71)$$

Let us now add the impact of D_{res} and calculate dB_{PIC} then B_{PIC}

$$dBPIC(z,\omega)=\gamma\frac{<P(z)>}{<P(0)>}.dz.\left(\frac{\tilde{P}(0,\omega)}{2}\left(1+\cos\left[\frac{\omega^2\lambda^2}{2\pi c}\left(D_{cum}(z)\right)\right]\right)+\langle P(0)\rangle.\tilde{\phi}(0,\omega).\sin\left[\frac{\omega^2\lambda^2}{2\pi c}\left(D_{cum}(z)\right)\right]\right)$$

The integration of B_{PIC} over distance yields :

$$B_{PIC}(L,\omega)=\phi_{NL}.\left(\frac{\tilde{P}(0,\omega)}{2.\langle P(0)\rangle}\left(1+\mathrm{Re}[K(\omega)]\right)+\tilde{\phi}(0,\omega).\mathrm{Im}[K(\omega)]\right)$$

In summary :

$$PIC(L,\omega,D_{res})=\frac{\Delta\tilde{P}(L,\omega)}{2\langle P(L)\rangle}$$

$$=-\phi_{nl}\left(\frac{\tilde{P}(0,\omega)}{2.\langle P(0)\rangle}\mathrm{Im}[K(\omega)]+\tilde{\phi}(0,\omega).(1-\mathrm{Re}[K(\omega)])\right)*\cos\left[\frac{\omega^2\lambda^2}{4\pi c}\left(D_{res}\right)\right]$$

$$+\phi_{nl}.\left(\frac{\tilde{P}(0,\omega)}{2.\langle P(0)\rangle}\left(1+\mathrm{Re}[K(\omega)]\right)+\tilde{\phi}(0,\omega).\mathrm{Im}[K(\omega)]\right)*\sin\left[\frac{\omega^2\lambda^2}{4\pi c}\left(D_{res}\right)\right]$$

In other words:

$$PIC(L,\omega,D_{res})=\phi_{nl}*\left(\begin{array}{l}\frac{\tilde{P}(0,\omega)}{2.\langle P(0)\rangle}*\left(-\mathrm{Im}[K(\omega)]*\cos\left[\frac{\omega^2\lambda^2}{4\pi c}\left(D_{res}\right)\right]+\left(1+\mathrm{Re}[K(\omega)]\right)*\sin\left[\frac{\omega^2\lambda^2}{4\pi c}\left(D_{res}\right)\right]\right)\\+\tilde{\phi}(0,\omega).\left(-\left(1-\mathrm{Re}[K(\omega)]\right)*\cos\left[\frac{\omega^2\lambda^2}{4\pi c}\left(D_{res}\right)\right]+\mathrm{Im}[K(\omega)]*\sin\left[\frac{\omega^2\lambda^2}{4\pi c}\left(D_{res}\right)\right]\right)\end{array}\right)$$

$$=\phi_{nl}*\left(\frac{\tilde{P}(0,\omega)}{2.\langle P(0)\rangle}H_{PIC,power}(\omega)+\tilde{\phi}(0,\omega)H_{PIC,phase}(\omega)\right)\text{ with implicit notations}$$

$$K(\omega)=\frac{e^{j\frac{\omega^2\lambda^2}{2\pi c}D_{cum,input}(0)}}{1-j\frac{\omega^2\lambda^2}{2\pi c}\frac{D_{loc}}{\alpha}}\frac{1-e^{\left(-\alpha+j\frac{\omega^2\lambda^2}{2\pi c}D_{loc}\right)L}}{1-e^{-\alpha L}}$$

$$=\frac{e^{j\left(\frac{\omega^2\lambda^2}{2\pi c}D_{cum,input}(0)+\arctan\left(\frac{\omega^2\lambda^2}{2\pi c}\frac{D_{loc}}{\alpha}\right)-\arctan\left(\frac{e^{-\alpha L}\sin\left(\frac{\omega^2\lambda^2}{2\pi c}D_{loc}L\right)}{1-e^{-\alpha L}\cos\left(\frac{\omega^2\lambda^2}{2\pi c}D_{loc}L\right)}\right)\right)}}{\sqrt{1+\left(\frac{\omega^2\lambda^2}{2\pi c}\frac{D_{loc}}{\alpha}\right)^2}}\frac{\sqrt{1-2e^{-\alpha L}\cos\left(\frac{\omega^2\lambda^2}{2\pi c}D_{loc}L\right)+e^{-2\alpha L}}}{1-e^{-\alpha L}}$$

$$\Delta P(z,t)=\frac{1}{2\pi}\int_{-\infty}^{+\infty}\Delta\tilde{P}(z,\omega).e^{-j\omega t}d\omega$$

$$=2\langle P(L_{tot})\rangle\sum_{k=1}^{N}\phi_{nl,k}.\frac{1}{2\pi}\int_{-\infty}^{+\infty}\left(H_{PIC,power,k}(\omega).\frac{\tilde{P}(0,\omega)}{2.\langle P(0)\rangle}+H_{PIC,phase,k}(\omega).\tilde{\phi}(0,\omega)\right).e^{-j\omega t}d\omega$$

If Dres=0,

$$\Delta P(L_{tot},t)=-2\langle P(L_{tot})\rangle\sum_{k=1}^{N}\phi_{nl,k}.\frac{1}{2\pi}\int_{-\infty}^{+\infty}\left(\mathrm{Im}[K_k(\omega)].\frac{\tilde{P}(0,\omega)}{2.\langle P(0)\rangle}+\left(1-\mathrm{Re}[K_k(\omega)]\right).\tilde{\phi}(0,\omega)\right).e^{-j\omega t}d\omega$$

2.VI. References

[62] J.-C. Antona, S. Bigo, J.-P. Faure, "Nonlinear cumulated phase as a criterion to assess performance of terrestrial WDM systems", in Proc. Optical Fibre Communications Conference (OFC'02), paper WX5, March 18-22, 2002, Anaheim, California, USA

[63] J.-C. Antona, M. Lefrançois, S. Bigo, G. Le Meur, "Investigation of Advanced Dispersion Management Techniques for Ultra-Long Haul Transmissions", Proceedings of ECOC'05, paper Mo.3.2.6, 2005, Glasgow (Scotland)

[64] J.-C. Antona, S. Bigo, "Physical Design and performance estimation of heterogeneous optical transmission systems", C.R. Physique 9 (2008), 963-984

[65] S. Bigo, Y. Frignac, J.-C. Antona, G. Charlet, "Design of multi-terabit/s terrestrial transmission systems facilitated by simple analytical tools", in 'Optical Communications 2. Transmission systems and networks' (Annales des Télécommunications Tome 58 N° 11-12 Novembre-Décembre 2003), pp.1757-1784

[66] R.I. Killey, H.J. Thiele, V. Mikhailov, and P. Bayvel, "Prediction of Transmision Penalties due to Cross-Phase Modulation in WDM Systems Using a Simplified Technique", IEEE Photon. Techn. Lett., vol 12, No.7, July 2000

[67] G. Bellotti et al, "Dependence of self-phase modulation impairments on residual dispersion in 10 Gbit/s based terrestrial transmissions using standard fibre", IEEE Photon. Technol. Lett., Vol. 11, n°7, pp. 824 -826 (1999)

[68] S. Bigo et al, "Investigation of self-phase modulation limitation on 10-Gbit/s transmission over different types of fibre", in Proc. Optical Fibre Communications (OFC'98), San Jose, FC2, pp. 389-390, Feb. 1998

[69] A. Färbert et al, "Optimised dispersion management scheme for long-haul optical communication systems",IEE Electronic Letters, Vol35, No21, Oct 1999,pp 1865-1866

[70] J.-P. Elbers, A. Färbert, C. Scheerer, C. Glingener, and G. Fischer, "Reduced model to describe SPM-limited fibre transmission in dispersion-managed lightwave systems," *IEEE J. of Selected Topics on Quantum Electron.*, vol. 6, pp.276–281, Mar./Apr. 2000.

[71] C. Kurtzke, "Suppression of fibre nonlinearities by appropriate dispersion management", IEEE Photon. Technol. Lett., Vol. 5, n°10, pp. 1250-1253 (1993)

[72] S. Vorbeck, M. Schneiders, "Cumulative nonlinear phase shift as engineering rule for performance estimation in 160-Gb/s transmission systems", IEEE Photonics Technology Letters, Volume: 16, Issue: 11, Nov. 2004, page(s): 2571 – 2573.

[73] Y. Frignac, J.-C. Antona, S. Bigo, "Enhanced analytical engineering rule for fast optimization of dispersion maps in 40 Gbit/s-based transmission systems", in Proceedings Optical Fibre Communications OFC'04, Los Angeles (Ca), paper TuN3, 2004

[74] A. Bononi, P. Serena, A. Orlandini, "A unified framework for single channel dispersion managed terrestrial systems", IEEE Journal of Lightwave Technology, vol. 26, No 22, November 15th 2008

[75] J.K. Fischer, C.A. Bunge, K. Petermann, "Equivalent single span model dor dispersion-managed fibre optics transmission systems", IEEE Journal of Lightwave Technology, vol. 27, No 16, August 15th 2009

[76] H. Louchet, A. Hodzic, K. Petermann, A. Robinson, and R. Epworth, "Analytical Model for the Design of Multispan DWDM Transmission Systems", IEEE Photon. Technol. Lett., Vol 17, No1 (2005), pp. 247-249, Jan 2005.

[77] G.P. Agrawal, "Nonlinear Fibre Optics", Third Edition. 2001, Academic Press, NY

[78] A. Bononi, P. Serena, M. Bertolini "Unified analysis of weakly-nonlinear dispersion-

managed optical transmission systems using a perturbative approach", C.R. Physique 9 (2008), pp 947-962

[79] R. I. Killey, H. J. Thiele, V. Mikhailov, and P. Bayvel, "Reduction of Intrachannel nonlinear distortion in 40Gb/s-based WDM transmission over standard fibre", IEEE Photon. Technol. Lett., 12 (2000), pp 1624-1626.

[80] H. Louchet, A. Hodzic, K. Petermann, A. Robinson, and R. Epworth, "Simple Criterion for the characterization of nonlinear impairments in dispersion-managed optical transmission systems", IEEE Photon. Technol. Lett., 17 (2005) 2089-2091.

[81] J. Wang and K. Petermann, "Small signal analysis for dispersive optical fibre communication systems", IEEE J. of Lightwave Technol., vol. 10, n° 1, pp. 96-100, Jan. 1992

[82] G. Bellotti, M. Varani, C. Francia and A. Bononi, "Intensity Distortion Induced by Cross-Phase Modulation and Chromatic Dispersion in Optical fibre Transmissions with Dispersion Compensation", in IEEE Photonics Technology Letters, vol. 10, No.12, pp. 1745-1747, Dec. 1999

[83] A.V.T. Cartaxo, 'Cross-Phase Modulation in Intensity Modulation-Direct Detection WDM Systems with Multiple Optical Amplifiers and Dispersion Compensators", in IEEE J. of Lightwave Technology, vol. 17, No. 2, pp178-190, Feb 1999

[84] Y. Frignac, "Contribution à l'ingénierie des systèmes de transmissions terrestres sur fibre optique utilisant le multiplexage en longueur d'onde de canaux modulés au débit de 40 Gbit/s", Thèse présentée devant l'ENST, Paris (2003)

[85] Y. Frignac, J.-C. Antona, S. Bigo and J.-P. Hamaide, "Numerical optimization of pre- and inline-dispersion compensation in dispersion-managed systems at 40Gb/s", Proceedings Optical Fibre Communications OFC'02, Paper ThFF5, Anaheim (Ca), 2002

[86] P. Serena, A. Orlandini, A. Bononi; "Scaling Laws for Weakly-nonlinear WDM Dispersion Managed OOK Systems", European Conf. Optical Comm., ECOC'06, We3.P.129

[87] E. Grellier, J.-C. Antona, and S. Bigo, "Revisiting the evaluation of non-linear propagation impairments in highly dispersive systems," in Proc. ECOC'09, paper 10.4.2,Vienna, September 2009

[88] E. Grellier, J.-C. Antona, S. Bigo, "Global criteria to account for tolerance to nonlinearities of highly dispersive systems," IEEE Photon. Tech. Letters, Vol 22, No 10, May 15th 2010

[89] E. Grellier, "Etude des effets non-linéaires à l'œuvre dans les systèmes de transmissions optiques fortement dispersifs", Thèse de doctorat, Université de Besançon, July 2011

[90] A. Cauvin, Y. Frignac, S. Bigo, "Nonlinear impairments at various bit-rates in single-channel dispersion-managed systems", Electronics Letters, Nov 13th 2003, vol. 39, No23

[91] Y. Frignac, S. Bigo, "Numerical optimization of residual dispersion in dispersion-managed systems at 40 Gbit/s", Optical Fibre Communication Conference and Exhibit, 2000. OFC 2000, Baltimore (MD), Vol.1, Page(s): 48– 50, paper TuD3.1

[92] I. Joindot, "Dispersion map optimization in hybrid Raman/Erbium-doped fibre amplifier-based 40Gb/s link", IEEE Photonics Technology Letters, Vol. 17, No. 7, July 2005

[93] G. Bellotti, S. Bigo, "Cross-Phase Modulation Suppressor for multi-span dispersion-managed WDM transmissions", IEEE Photonics Technology Letters, vol 12, No6, June 2000

[94] C. Fürst, G. Mohs, H. Geiger, and G. Fischer, "Performance limits of nonlinear RZ and NRZ coded transmission at 10 and 40 Gb/s on different fibres," in *Tech. Dig. Optical Fibre Communication (OFC 2000)*, Baltimore, MD, 2000, Paper WN31.

Chapter 3 : Domain of Validity of Nonlinear Phase Criterion and Extension to Practical Transmission Systems

CONTENTS

3.I. Introduction

In Chapter 2, we have shown that the nonlinear cumulated phase shift from Equation (1-15) appears as a promising, simple candidate to capture the impact of nonlinearities and their interplay with chromatic dispersion for WDM dispersion-managed transmission systems. More particularly, we have shown a very strong correlation between the total nonlinear phase shift and transmission penalties for a periodic transmission system composed of a variable number of dispersion-managed line fibre sections and for various input powers into line fibre and/or DCF, provided optimum dispersion management for each condition of power or distance.

We have then introduced the nonlinear phase criterion as the ability to predict OSNR penalties of a WDM system based on the knowledge of the nonlinear phase whatever the reach and input powers into the line fibres and DCFs (assuming realistic power values), and we have shown that the criterion accuracy remains below an acceptable limit of 1.5dB for a representative bunch of configurations of bit-rates, fibres, formats, channel spacing, still provided optimized dispersion management. Such a tool has revealed particularly fruitful to achieve exploratory studies to determine the ultimate limits of transmission systems, or in support to record lab experiments I have contributed to [100][118][120][121][122].

Eventually, we have also established in Chapter 2 the connection between the nonlinear phase criterion and perturbative analytical models describing the evolution of signal distortions due to Kerr effect and Group-Velocity Dispersion. Such models have enabled to expect limitations to the nonlinear phase criterion and directions of improvement when it comes to adapt the criterion to deployed system-like configurations.

In that prospect, the present chapter discusses the domain of validity of the nonlinear phase criterion and proposes to generalize its formulation in the case of typical, heterogeneous transmission systems, taking advantage of the intuitions we can gain from those analytical models.

In section 3.II. , we numerically and experimentally assess the domain of validity of the nonlinear phase criterion: we particularly investigate the impact of the number of transmission fibre sections, the impact of the heterogeneity between transmission and dispersion compensating fibres beyond the typical configurations, and the impact of the length of transmission fibre sections.

Then, in section 3.III. , we investigate the accuracy and the validity of the nonlinear phase criterion in the cases of non-fully optimized dispersion-management schemes for 10 and 40Gb/s-modulated transmission systems.

Eventually section 3.IV. addresses the issue of line fibre type heterogeneity and the necessary extensions of the nonlinear phase criterion so as to get a criterion adapted to any configuration.

3.II. Limits of the nonlinear phase criterion

In order to assess whether the nonlinear phase criterion can be reliably used for the design of actual systems and to help deciding whether a connection is feasible, its accuracy and domain of application have to be refined.

From a fundamental point of view, several directions need to be investigated:

- Applicability of the nonlinear phase shift criterion for multi-span systems and single-span systems with a single relationship between penalty and nonlinear phase.
- Impact of the heterogeneity in fibre type between line fibre and DCF sections with alternated dispersion signs
- impact of span length, attenuation

II.1. Nonlinear phase shift and correlation between single-span and multi-span transmission systems

This section investigates the tolerance to nonlinearities of single-span and multi-span systems and is based on simulations done by my colleague Emmanuel Sève. Having in mind the results from Chapter 2 related to multi-span systems with more than 3 spans, it is natural to wonder whether the nonlinear phase criterion originally calibrated for multi-spans systems can predict anything in single-span systems and vice versa. If so, a calibration of the penalty versus nonlinear phase relationship made for multi-span terrestrial systems could be used to design single-span unrepeatered undersea systems. Conversely, one could more easily calibrate the penalty versus nonlinear phase relationship for a single-span system and extend the prediction to multi-span systems.

However, we want to stress here the fact that the nonlinear phase criterion is not meant to predict performance based on a single relationship between penalty and nonlinear phase for single span and multi-span systems.

II.1.1. State of the art and predictions of the perturbative models

So far, a few articles [102][103][104] mentioned the possibility to make the bridge between single-span and multi-span systems and reported measurements for single-span 40Gb/s systems, based on more or less concordant results with multi-span configurations, or even sometimes in absence of verification. We can however observe in [103][104] relatively large discrepancies: indeed, single-span and multi-span systems happen to yield up to 2dB difference in terms of nonlinear phase shift values leading to 1dB penalty.

A possible explanation could be the following: assuming a given nonlinear phase shift leading to a moderate transmission penalty, the amount of nonlinearities per span in a multi-span configuration may be low enough to consider the nonlinear induced impairments per span as perturbations. The perturbative theories evoked in Chapter 2 in relation with the nonlinear phase may then apply. In a single-span configuration however, the perturbative approach might no longer hold because of the too high fibre input power resulting from all nonlinearities concentrated into a single span.

An additional explanation resides in the fact that the dispersion-management schemes that we can apply for single-span or multi-span systems are not equivalent. For a single-span system indeed, there are at most two degrees of freedom to manage the dispersion distribution along

the link, based on inserting DCM before the line fibre section (pre-compensation) and after the line-fibre section (post-compensation). For a multi-span transmission system, there is at least one extra-degree of freedom to manage the dispersion distribution along the link: the inline dispersion compensation. We can therefore wonder whether the nonlinear phase versus penalty relationships could be identical for a single-span system and a multi-span system for a specific configuration of inline dispersion compensation. Candidate configurations could correspond to full inline dispersion compensation from span to span or even optimized inline dispersion compensation.

If we refer to perturbative models such as the PIC model, the Kerr induced perturbation arising after 1 span is the following (after Equation (2-37)):

$$PIC\left(\omega, N=1, \left\langle P(z=0)\right\rangle\right) = -\phi_{nl,span} * \left.\begin{aligned} & \frac{\widetilde{P}(0,\omega)}{< P(0) >} \frac{1}{\sqrt{1+A^2 {D_{loc}}^2/\alpha^2}} \frac{\sqrt{1+e^{-2\alpha L}-2e^{-\alpha L}\cos\left(A.D_{loc}L\right)}}{\left(1-e^{-\alpha L}\right)} \\ & * \sin\left(A\left(\Pr e - Dres + \frac{1}{A}\arctan\left(\frac{A.D_{loc}}{\alpha}\right) - \frac{1}{A}\arctan\left(\frac{e^{-\alpha L}\sin\left(A.D_{loc}.L\right)}{1-e^{-\alpha L}\cos\left(A.D_{loc}.L\right)}\right)\right)\right) \end{aligned}\right\} \begin{array}{l} independent\ of \\ < P(0) > \end{array}$$

Let (3-1)

$$H(\omega) = -\frac{\widetilde{P}(0,\omega)}{< P(0) >} \frac{1}{\sqrt{1+A^2 {D_{loc}}^2/\alpha^2}} \frac{\sqrt{1+e^{-2\alpha L}-2e^{-\alpha L}\cos\left(A.D_{loc}L\right)}}{\left(1-e^{-\alpha L}\right)} * \sin\left(A\left(\begin{aligned} & \Pr e - Dres + \frac{1}{A}\arctan\left(\frac{A.D_{loc}}{\alpha}\right) \\ & - \frac{1}{A}\arctan\left(\frac{e^{-\alpha L}\sin\left(A.D_{loc}.L\right)}{1-e^{-\alpha L}\cos\left(A.D_{loc}.L\right)}\right)\end{aligned}\right)\right)$$

Then $PIC\left(\omega, N=1, \left\langle P(z=0)\right\rangle\right) = \phi_{nl,span} * H(\omega)$

After N spans Equation (2-37) becomes, provided a zero residual dispersion per span ($D_{res/span}=D_{res/subdiv}=0$ps/nm):

$$PIC\left(\omega, N, \left\langle P(z=0)\right\rangle\right) = -N * \phi_{nl,span} * \left.\begin{aligned} & \frac{\widetilde{P}(0,\omega)}{< P(0) >} \frac{1}{\sqrt{1+A^2 {D_{loc}}^2/\alpha^2}} \overbrace{\frac{\sqrt{1+e^{-2\alpha L}-2e^{-\alpha L}\cos\left(A.D_{loc}L\right)}}{\left(1-e^{-\alpha L}\right)}}^{\approx 1 \text{ if long span or } A.D_{loc}L \ll 1s} \\ & * \sin\left(A\left(\Pr e - Dres + \frac{1}{A}\arctan\left(\frac{A.D_{loc}}{\alpha}\right) - \frac{1}{A}\arctan\left(\frac{e^{-\alpha L}\sin\left(A.D_{loc}.L\right)}{1-e^{-\alpha L}\cos\left(A.D_{loc}.L\right)}\right)\right)\right) \end{aligned}\right\} \begin{array}{l} independent\ of \\ N \text{ and } < P(0) > \end{array} \quad (3\text{-}2)$$

Thus

$$PIC\left(\omega, N, \left\langle P(z=0)\right\rangle\right) = N * PIC\left(\omega, N=1, \left\langle P(z=0)\right\rangle\right) = N * \phi_{nl,span} * H(\omega) = \phi_{nl,total} * H(\omega)$$

As a result, provided zero residual dispersion per span, the nonlinear induced signal distortion as estimated by the PIC model (or by multi-span perturbative theories) varies as a function of the total nonlinear phase whatever the number of spans N, equal to or higher than 1.

Yet assessing the nonlinear tolerance to a single-span system means high optical power per channel and therefore such perturbative analyses may fail, as illustrated by the following numerical study

II.1.2. Numerical study

To show that despite the predictions of the perturbative models, the extension of the nonlinear phase criterion to single-span systems is not straightforward, we considered one example. We numerically investigated the transmission of a 40Gb/s-modulated single-channel over a SMF-based terrestrial link with different number of spans, different singly-periodic dispersion management settings and for two modulation formats, NRZ-DPSK and CS-RZ-DPSK. In

particular, we considered for each format two possible number of spans: 1 and 3 spans for the NRZ-DPSK case, and 1 and 15 spans for the CS-RZ-DPSK case. We then determined the nonlinear threshold, i.e. the value of nonlinear phase corresponding to 1dB OSNR penalty (for a BER of 10^{-5}), for single-span and multi-span configurations. While details of this study can be found in the next inset, the main results can be summarized as follows.

For NRZ-DPSK, the nonlinear threshold for the single-span configuration was found identical to the one corresponding to the 3-span configuration provided full inline dispersion compensation (i.e. 0ps/nm average residual dispersion per span), but 1.2dB lower than the nonlinear threshold for the 3-span system with optimized inline dispersion compensation. This sounds in agreement with the predictions of the perturbative models. Further studies could be done to establish whether the domain of validity (in terms of nonlinearities) of the perturbation approaches is improved for NRZ-DPSK format because of its very limited amplitude fluctuations.

For CS-RZ DPSK, the nonlinear threshold for the single span configuration appeared 1.2dB higher than for the 15-span configuration with full inline dispersion compensation, and 1.4dB lower than for the 15-span configuration with optimized inline dispersion compensation.

Such measurements illustrate that **there is no clear correlation between the penalty versus nonlinear phase relationships obtained for single span and multi-span transmission systems**. The correlation is weak between the single-span configuration and the multi-span configuration with full inline dispersion compensation. Even though analytical perturbative models tend to suggest that there could be equivalence, the perturbative assumption is probably no longer valid for the single-span configuration due to the very high optical powers required to degrade significantly the signal. The correlation is even weaker when comparing single-span configuration with multi-span configurations with optimal dispersion management.

As a conclusion, we recommend to use one relationship between nonlinear phase and penalty for multi-span configurations with more than 3 spans, and another relationship (if required) for single span configurations.

Details on single vs multi-span numerical experiments

a) Set-up: the transmission link under study is similar to the one utilized for the previous studies with 100km-long spans of SMF. We varied the number of spans, the dispersion management parameters (pre-, inline and post-dispersion compensation), and the input powers into line fibres (with DCF input power set 7dB lower) We used an 1.2nm-wide band-pass optical filter with Gaussian profile before a balanced receiver (Mach-Zehnder interferometer extinction ratio of 25dB). A single-ended photodiode has been considered to detect DPSK and a differential photodiode has been considered for CSRZ-DPSK. Before the receiver, some optical noise is added to the signal so as to estimate the required OSNR to get a BER of 10^{-5}. In the following, we only present OSNR penalty results corresponding to optimized pre- and post-compensation fibres for any power, distance or setting of the inline dispersion compensation.

b) Results: for **DPSK** format, single-span transmission systems yield a nonlinear threshold, NLT (defined here as the nonlinear phase shift ϕ_{NL} such that the penalty is equal to 1 dB), of 0.22π rad (a differential photodiode would have led to a nonlinear threshold of 0.32π rad). Figure 3-1-a represents a contour plot of the penalty versus nonlinear phase and inline-compensation (here the absolute value of the ratio of the cumulated dispersion over line fibre and DCF) after 3 spans: for 100% inline compensation, the NLT is 0.22π, identical to the single span measurements; this value is about 1.2dB lower than the highest possible NLT values obtained for optimized inline compensation, i.e. 0.29π and 0.27π rad for 110 % and 90 % inline compensation respectively. With a differential photodiode, relative conclusions (in dB) are identical.

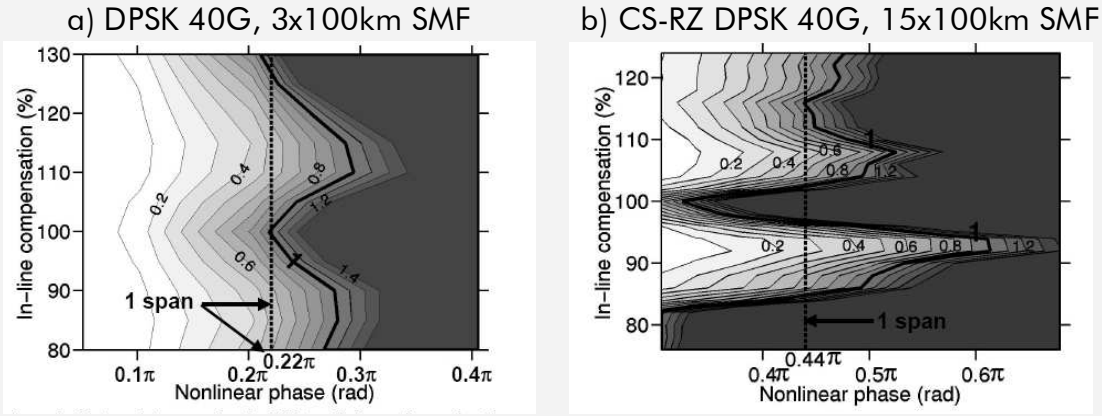

Figure 3-1: Contour plot of the OSNR penalty versus nonlinear phase and inline compensation ratio for singly-periodic dispersion managed transmission system with optimized pre/post compensation DCM.
a) 3x100km SMF transmission system using single channel 40Gb/s DPSK format
b) 15x100km SMF transmission system using single channel 40Gb/s CS-DPSK format.
Contours correspond to different values of OSNR penalty by steps of 0.1dB.
Black solid curve corresponds to 1dB penalty. Vertical dashed line corresponds to the nonlinear phase leading to 1dB penalty for single span configuration.

To further check whether the system impact of nonlinear phase is systematically identical for single-span configurations and multi-span configuration with full inline compensation, we performed another set of simulations with **CS-RZ DPSK** format. Single-span transmission systems yield a NLT of 0.44π rad. Figure 3-1-b shows the penalty contour plots after 15 spans versus ϕ_{nl} and inline-compensation. We see that for 100% inline compensation, the NLT is 0.33π, i.e. 1.2dB lower than for the single-span. The highest possible NLT value for optimized inline compensation is 0.61π for 92% inline compensation. It is 1.4dB higher than for the single-span and 2.6dB higher than for the 15span configuration with full inline compensation.

II.2. Limits of the nonlinear phase criterion stemming from line fibre / DCF heterogeneity

Motivation

We have previously shown the relevance of the nonlinear phase criterion for single-line fibre type transmission systems with typical configurations of signal power into line fibre and DCF sections and optimized dispersion management. This means that the transmission penalty induced by chromatic dispersion and nonlinear effects can be seen as a function of the nonlinear phase shift, whatever the distance and powers into line fibre sections, provided one choice of transmission fibre, one choice of modulation format at a given bit-rate, and one choice of channel spacing.

Under such conditions, despite the system heterogeneity due to the cohabitation of two types of fibre (line fibre and DCF) with very different chromatic dispersion characteristics, the total nonlinear phase captures both the impact of line and dispersion compensating fibres. For such systems, some 15-40% of the accumulated nonlinearities come from the DCF (as long as the input power into DCF sections is some 4-10dB lower than in the line fibre).

However, we can infer that the situation might be different under other circumstances. For instance, we can anticipate that for systems where most of the nonlinearities come from the DCF, system degradation should rather depend at some point on the local dispersion of the DCF than on the local dispersion of line fibre.

Besides, the analysis of the perturbative models from Chapter 2 tells us that the signal degradation is expected to vary (under certain assumptions) as a function of a linear combination of the nonlinear phase induced by line fibre spans and of the nonlinear phase induced by DCF sections, but not necessarily as a function of the total nonlinear phase, as expressed in Equation (2-40).

For those reasons, we would like here to assess the domain of validity of the nonlinear phase criterion outside typical configurations. We could imagine very different situations where the impact of nonlinearities in the DCF is negligible (e.g. when using Fibre Bragg Gratings for dispersion compensation) or conversely very high (e.g. when applying very strong distributed Raman amplification in the DCF), or when changing DCF technologies, leading to different chromatic dispersion values. Should the nonlinear phase criterion remain accurate enough for multiple configurations, no further calibration of the penalty vs nonlinear phase is required when changing configuration.

Therefore, we addressed the issue of the limits of the nonlinear phase criterion through an extensive investigation of the impact of DCF input power as well as chromatic dispersion, beyond conventional configurations, for 10Gb/s transmission systems. This work has been achieved jointly with my colleague Emmanuel Seve, from Bell-Labs, who performed the numerical simulations.

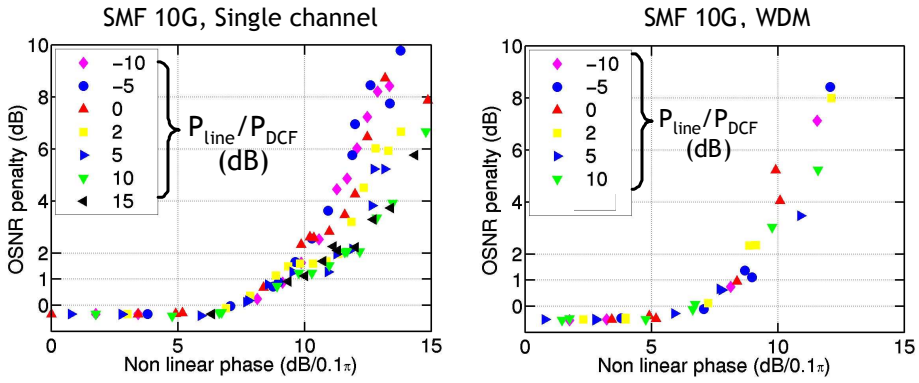

*Figure 3-2: OSNR penalty versus nonlinear phase (in dB with respect to 0.1π, ie 10*Log10(ϕ_{NL}/0.1π)) for different DCF input powers (from 15dB below to 10 above the SMF input power). The left and right figures correspond to single channel and WDM transmission, respectively. Numerical simulations.*

Numerical study and discussion

For that purpose, we numerically addressed the issue of the relative input powers and amounts of nonlinearities stemming from DCF and line fibre (SSMF) and determined the accuracy of the nonlinear phase criterion for 2dB penalty in single channel and WDM configurations. Detailed setup and observations are given in the following inset. In essence, Figure 3-2 shows the penalty vs nonlinear phase shifts plots for both configurations. We can observe that while the accuracy of the nonlinear phase criterion appears as quite satisfactory for 10Gb/s WDM systems using SMF fibre (accuracy within 1dB in any conditions), larger inaccuracy appears for single-channel configurations (accuracy evolving from 1dB for typical configurations up to 2.5dB for all the investigated cases). It reveals that sometimes a better linear combination between the nonlinear phases arising from DCF and line fibres (enabling to reduce the accuracy down to 1.5dB as shown in Figure 3-3) than the mere sum can be found to capture the impact of the overall nonlinearities.

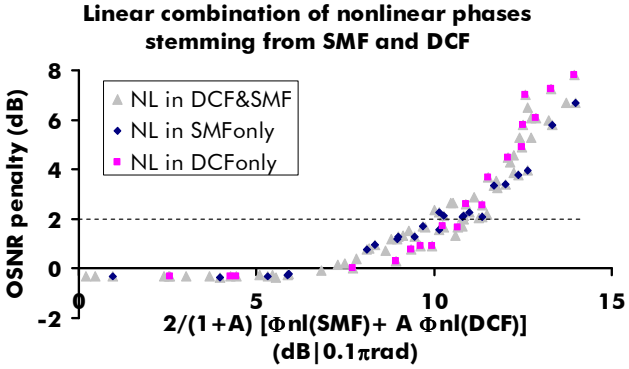

Figure 3-3 : OSNR penalty versus one linear combination of nonlinear phases stemming from SMF and DCF sections $\frac{2}{1+A}\left(\phi_{nl,SMF} + A.\phi_{nl,DCF}\right)$ *with A=1.16 (eventually expressed in dB with respect to 0.1π).*

Numerical simulation representing a 10Gb/s NRZ single channel propagating over SMF fibre-based system with optimized singly-periodic dispersion management and multiple conditions of distances and powers into SMF and DCF. Relative DCF input powers range from from 15dB below to 10dB above the SMF input powers. Measured accuracy at 2dB penalty:1.5dB.

Details on the numerical study to assess the impact of DCF input power into 10G SMF-based systems

The transmission set-up is identical to the one from Chapter 2: we considered a typical 10.7Gb/s dispersion-managed, terrestrial, ultra-long haul link with either 1 or 5 NRZ-modulated 50GHz-spaced-channels. The transmission link consists in a concatenation of sections of 100km-long spans of SMF and DCF (D=-80ps/nm/km chromatic dispersion) modules following an optimized singly-periodic dispersion management scheme whatever the conditions of distance and powers. We varied the transmission distance, the input powers into line fibre and DCF such that the power ratio P_{line}/P_{DCF} ranges between -10 and 10dB, and measured the OSNR penalties corresponding 10^{-5} BER on the central channel.

Figure 3-2 represents the transmission penalty as a function of the nonlinear phase for different number of spans, different input powers into the **SMF** and the DCF, sorted into different powers ratios P_{line}/P_{DCF}, issued from single-channel (a) and WDM (50GHz spacing) (b) systems (numerical simulations).

We can observe in **single channel configuration** that the estimated values of nonlinear phase leading **to 2dB reference penalty** range between 9.5 and $12dB_{0.1\pi}$[4]; this corresponds then to a **2.5dB accuracy of the nonlinear phase criterion**. This highlights the fact that the nonlinear phase criterion is not accurate enough when applied to truly heterogeneous systems (with potentially all the nonlinearities focused in the line fibre, or in the DCF), at least in single-channel configuration. It can be noted that configurations with nonlinearities mainly stemming from DCF yield the highest penalties. We can see here an agreement with single-channel simulations from Frignac & Cauvin [105] or Conrad & Petermann [106]: the authors showed that the nonlinear induced penalties increase with the chromatic dispersion of the line fibre (when overlooking DCF-induced nonlinearities). Here the absolute value of DCF chromatic dispersion is much higher than that of SMF, also resulting in higher sensitivity to nonlinearities. **In WDM configuration** though, both extreme cases show a similar resistance to nonlinearities, resulting in **a satisfactory accuracy of the nonlinear phase criterion, below 1dB, whatever the relative power into the line fibre** (wrt DCF), below the 1.5dB threshold of acceptability defined in Chapter 2.

Of course, as stated in Chapter 2, with a more realistic range of relative powers (DCF input powers 2 to 10dB lower than line fibre input powers), the correlation between nonlinear phase and penalty remains totally acceptable, with an accuracy of the nonlinear phase criterion for to 2dB reference penalty lower than 1dB in all cases.

Such results stress the limits of the nonlinear phase criterion in its simplest formulation, here quite far out of the typical conditions of system operation.

If we refer then to the abovementioned 1st order approximations based on perturbative models suggesting that nonlinearity-induced signal degradations may depend on a linear combination of nonlinear phase shifts stemming from DCF and line fibres, we can think of another linear combination than the sum of DCF and line fibre contributions to extend the accuracy of the nonlinear phase criterion.

As an illustration, the previous single-channel results are represented in Figure 3-3 with OSNR penalty plots as a function of a linear combination of nonlinear phase shifts stemming from SMF and DCF, proportional to the sum of the SMF-nonlinear phase shift and 1.56 times the DCF-induced nonlinear phase shift. In dB scale, the spread of the "weighted" nonlinear phase values leading to 2dB penalty falls below 1.5dB, instead of 2.5dB when using the original nonlinear phase. We will see in section II.3.3. and section III. how it is possible to simply propose some linear combinations that make sense when necessary.

[4] A nonlinear phase ϕ_{NL} expressed in unit $dB_{0.1\pi}$.means $10\ Log_{10}(\phi_{NL}[rad]/(0.1\pi))$

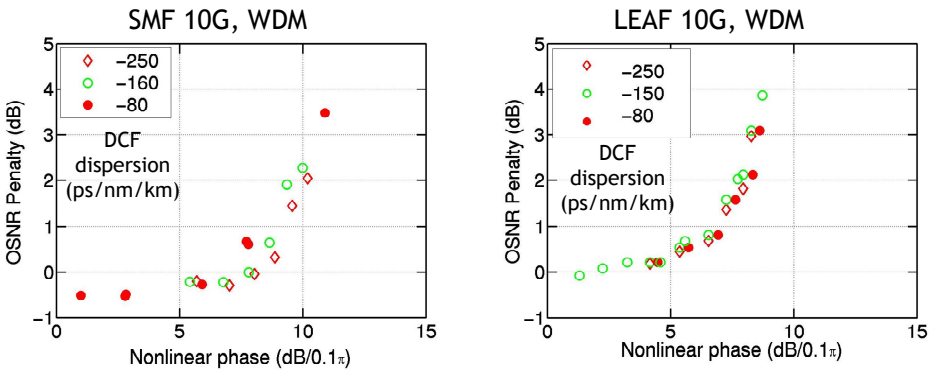

Figure 3-4: WDM transmission penalty versus the nonlinear phase for different DCF dispersions: –80,–160 and –250ps/(nm.km) for SMF (a) and –80, -150 and –250ps/(nm.km) for LEAF (b). DCF input power set 5dB lower than line fibre input power.

In a second step, we numerically assessed the impact of a change of DCF local chromatic dispersion for 10G systems based on SMF or LEAF transmission fibre. We observed that a change of DCF chromatic dispersion from -80 to -250ps/nm was negligible on the accuracy of the nonlinear phase criterion, resulting in less than 0.5dB inaccuracy. We can then conclude that measurements of system performance using one kind of DCF can be safely extrapolated to predict the impact of another technology of DCF, provided we do not totally suppress the nonlinearities (see in Appendix VI.1.).

In summary, the nonlinear phase criterion is shown here as totally sufficient to capture accurately the impact of DCF and line fibre heterogeneity for 10Gb/s-modulated systems in typical conditions of exploitation (and beyond), even though a better linear combination between the contributions coming from line fibres and DCFs would further improve this accuracy and make the adapted criterion suitable for extreme conditions of operation, as suggested by the perturbation theories from Chapter 2.

II.3. Impact of span length and attenuation

II.3.1. Accuracy of nonlinear phase criterion

This section investigates the impact of span length and fibre attenuation on the Kerr-induced signal impairments, and assesses the limits of the sole nonlinear phase shift to handle this.

In [105][107][108], Y. Frignac and A. Cauvin established the duality between chromatic dispersion, symbol rate and span length in terrestrial dispersion managed single-channel transmission systems. More particularly, the authors showed that for a given nonlinear phase and an appropriate dispersion management strategy; the transmission penalty induced by the interplay of Kerr effect and Chromatic Dispersion depends on the product between line fibre chromatic dispersion, the square of the symbol rate and the effective span length (depending on line fibre span length as defined in Equation (2-3)). One can therefore expect that the relationship between penalty and nonlinear phase also depends on span length in a similar way to the way it depends on fibre chromatic dispersion. A lower line fibre span length could thus be interpreted as a lower value of the absolute value of the fibre chromatic dispersion.

Additionally, the perturbative models from Chapter 2 suggest that the nonlinear phase criterion may not be sufficient to capture the impact of a diversity of line fibre lengths.

Therefore we report here numerical simulation results quantifying the loss of accuracy of the simple nonlinear phase criterion due to the diversity of line fibre lengths for a representative panel of line fibres types, bit-rates and fibre lengths.

		Accuracy of nonlinear phase criterion (dB) *(range of nonlinear phases yielding 2dB penalty)*	
Bit rate	Fibre	Single-Channel	WDM
10.7Gb/s	SMF: 10-100km	1.8dB	1.7dB
	LEAF: 25-100km	0.5dB	1.8dB
42.7Gb/s	30-100km SMF: 20-100km 10-100km	1.6dB 3dB 5dB	
	LEAF: 30-100km	2dB	

Table 3-1 : Numerical assessment of the impact of span length on the inaccuracy of the nonlinear phase criterion for 2dB OSNR reference penalty (for 10^{-5} BER), for various bit-rates and line fibre types.

We considered for that purpose SMF- and LEAF-based transmission systems with a single-channel or multiple 50GHz-spaced channels modulated at 10.7Gb/s with NRZ format, or a single-channel modulated at 40Gb/s with NRZ format. We fixed the input fibre into line fibre spans, and for each span length we varied the transmission distances until nonlinear-induced penalties appear significant. While the details of the simulations and results are given in Appendix VI.2. , Table 3-1 summarizes here the observed accuracy of the nonlinear phase criterion when varying the line fibre section length for 2dB reference OSNR penalty.

We can first observe that the span-length induced inaccuracy remains lower than 1.8dB at 10Gb/s for SMF span lengths higher than 10km or LEAF span lengths higher than 25km. Such inaccuracy is higher than the acceptable 1.5dB limit proposed in Chapter 2, but the system impact of such an inaccuracy will be mitigated in practice by the statistical distribution of the span lengths over a transmission system, such that the probability that most of the

nonlinearities come from the contributions of 10km-long spans in ultra-long haul system is very low.

At 40Gb/s, we can observe that the span-length induced inaccuracy remains lower than 2dB for spans lengths higher than 30km; a focus on span lengths higher than 50km leads to an inaccuracy lower than 1dB over LEAF fibre at 40G and lower than 0.5dB for other configurations. Under such conditions, and for the same reason as abovementioned at 10Gb/s, this inaccuracy could be statistically affordable for the design of ultra-long haul systems.

However Table 3-1 also stresses that for 40Gb/s systems with spans lengths ranging between 10 and 100km, the inaccuracy of the nonlinear phase criterion becomes unacceptable: as high as 3dB for 20km-long spans, and as high as 5dB for 100km-long spans. In that case, extensions to the nonlinear phase concept could be very helpful. In the Appendix VI.2. , we propose an analytical extension of the nonlinear phase based on the Phase to Intensity Conversion theory and regular perturbation model from Chapter 2 to account for the duality between span length and fibre chromatic dispersion.

$$Adapted\ \ nonlinear\ \ phase = \sum_{\substack{fiber\\ \text{sec}tions\\ k}} \phi_{nl,k}\beta_{2,loc,k}\widetilde{L}_{eff,k}.B^2 \qquad (3\text{-}3)$$

(with B being the symbol rate and $\phi_{nl,k}$, $\beta_{2,k}$, $\widetilde{L}_{eff,k}$ respectively corresponding to the nonlinear phase shift, the local chromatic dispersion and an effective length of span k).

This adapted nonlinear phase allows reducing the 2dB-penalty deviation in nonlinear phase between 20 and 100km-long spans down to 1dB for 40Gb/s systems, but appears of little use for 10Gb/s WDM systems.

II.3.2. Tolerance to nonlinearities and impact of span length, attenuation and bit-rate

More generally, beside the attempt of Equation (3-3), there is no obvious formula accounting simultaneously for symbol rate, fibre length, attenuation, chromatic dispersion and nonlinear phase shift at the same time for both single-channel and WDM transmission systems.

One way to account for the diversity of possible transmission systems is to build the relationship between penalty, nonlinear phase ϕ_{nl} and the product $\left|\beta_2\mathbf{B}^2L_{eff}\right|$ between the line fibre chromatic dispersion the square of symbol rate and an effective length characterizing line fibre, as in [105][106] for single channel configuration. The improved nonlinear phase criterion will thus consist of a prediction of penalty as a function of ϕ_{nl}, $\left|\beta_2\mathbf{B}^2L_{eff}\right|$, and of conditions of channel spacing, choice of modulation format and strategy of dispersion management.

One simplification is to measure system tolerance to nonlinearities as a function of the product between the square of the symbol rate, the fibre chromatic dispersion and the line fibre section effective length.

We will see in section 3.IV. how to combine this information to build a tool predicting the impact of nonlinearities applicable to heterogeneous configurations with different characteristics per fibre section.

For that purpose, we numerically emulated different dispersion-managed transmission systems with different bit-rates, number of channels, different line fibre chromatic dispersion and line fibre span lengths. We varied power and distance so as to get the nonlinear threshold, i.e. the

value of nonlinear phase shift leading to 2.5dB OSNR penalty (for 10^{-5} BER). Details of the numerical simulations are shown in the following inset.

Set-up

The transmission set-up is similar to the abovementioned ones. The transmitter consists of a single channel NRZ-modulated either at 10.7Gb/s or 42.7Gb/s at 1550nm or a WDM multiplex of 15 channels (10.7Gb/s-NRZ-modulated) regularly spaced (50GHz) around 1550nm. We considered a 64-bit long (resp. 128bit-long) De Bruijn sequence for 10Gb/s (resp. 40Gb/s) systems. For the WDM signal, each channel has the same polarization and the bit sequence is decorrelated with respect to the other channels with a random delay. The transmission link consists of a pre-compensation, a successive repetition of a fixed length line fibre-section followed by a DCF fibre (D = 80 ps/nm/km) and finally a post-compensation fibre. Whatever the distance or power considered, the dispersion map was optimized for best BER measurement. Three different types of line fibre have been considered: SMF, TeraLight and LEAF fibres with chromatic dispersions of 17, 8 and 4.25ps/nm/km respectively. Span lengths were varied between 10 and 100km. Nonlinearities coming from the DCF have been overlooked.

Figure 3-5 shows the correlation between the nonlinear threshold and the product $\left|\beta_2 \mathbf{B}^2 L_{eff}\right|$ for all those configurations, for either single-channel or WDM system configurations (with β_2, B and L_{eff} respectively referring to the chromatic dispersion, the bit-rate and the effective length of the transmission span). This extends the validity of the work of [105][106] to WDM configurations.

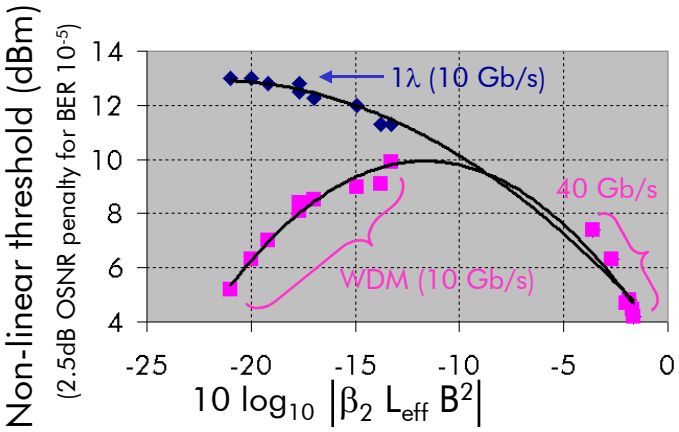

Figure 3-5 : Evolution of the nonlinear threshold as a function of the product between the line fibre effective length L_{eff}, the chromatic dispersion β_2 and the square of the symbol rate B (in dB scale: $10\log\left|\beta_2 \mathbf{B}^2 L_{eff}\right|$), for 10 or 40G single channel or WDM NRZ-modulated systems, for different line fibre chromatic dispersions (4.25, 8, 17ps/nm/km) and different span lengths (from 10 to 100km)

From a practical point of view:

From Figure 3-5 we can make the approximation that, for a fixed bit rate, the nonlinear threshold scales linearly with the product $\left|\beta_2 \mathbf{B}^2 L_{eff}\right|$ when all terms are expressed in dB. At 40Gb/s, the nonlinear threshold scales linearly with the product $\left|\beta_2 \mathbf{B}^2 L_{eff}\right|$ with a slope of -1dB/dB; this means that for constant penalty, the product between nonlinear phase and $\left|\beta_2 \mathbf{B}^2 L_{eff}\right|$ is constant, which is consistent with the proposed concept of adapted nonlinear

phase. At 10Gb/s, the slope of this linear approximation is about -0.2dB/dB for the single-channel case and +0.66dB/dB for the WDM case. We can additionally notice that a stronger correlation was generally found between nonlinear threshold and the product $\left|\beta_2 \mathbf{B}^2 L_{eff}\right|$ than between the nonlinear threshold and the product $\left|\beta_2 \mathbf{B}^2 \widetilde{L}_{eff}\right|$ as previously introduced.

3.III. Impact of dispersion management

III.1. Introduction: practical limitations of the optimization of dispersion maps

In the previous sections, we showed the relevance and assessed the accuracy of the nonlinear phase criterion for transmission systems with optimized dispersion management. Doing so enables to get an estimation of the ultimate nonlinear limits of a transmission system. This section addresses the accuracy and limitations of this criterion for possibly under-optimized dispersion maps, closer to actual deployed systems constraints.

Indeed, for deployed terrestrial systems, some trade-offs are necessary regarding the optimization of the dispersion management. The personalization of dispersion compensation at receiver side for each wavelength is today limited to systems with bit rates higher than 40Gb/s using tuneable optical or electrical dispersion compensation strategies, and to a few point to point connections. The personalization of dispersion compensation at the emitter side is limited to a few long-reach point to point connections and to few 10Gb/s systems based on electronic signal pre-distortion [123][123] [124]. Eventually, the personalization of inline dispersion compensation for each wavelength is even scarcer for point to point systems, and almost impossible to achieve for reconfigurable transparent networks. In summary, most 10Gb/s systems are usually deployed with a constant strategy of chromatic pre/inline/post-dispersion compensation whatever the wavelength or whatever the reach of a lightpath. This strategy is often set to maximize the reach of the systems, making shorter connections more sensitive to nonlinearities than their ultimate limit even though these short connections remain feasible. The per-channel optimization of systems modulated at 40Gb/s or higher is generally limited to the optimization of the dispersion compensation at receiver end: indeed the very limited tolerance to residual dispersion is generally shorter than the uncertainties regarding the knowledge of the cumulated dispersion after transmission.

In the following, we investigate the applicability and the accuracy of the nonlinear phase criterion for such systems: we first consider 10Gb/s-modulated systems with fixed strategies of inline dispersion compensation and optimized pre-and post compensation over widespread LEAF then SMF fibres types; then we fix pre- and post-compensation fibres as in typically deployed systems. Eventually we consider 40Gb/s-modulated systems and highlight the need for additional parameters so as to capture correctly the accumulation of nonlinearities, as suggested in Chapter 2 using the perturbative models.

III.2. Limits of nonlinear phase criterion with non fully optimized dispersion maps at 10Gb/s

III.2.1. Numerical investigation of LEAF-based transmission systems with fixed inline compensation strategy and optimized pre- and post-compensation

In this section, we investigate the applicability of the nonlinear phase criterion through the study of a 10Gb/s **WDM** transmission system with fixed inline compensation strategies, and optimized dispersion adjustment at both emitter / receiver sides. We consider different strategies of inline dispersion compensation following a singly-periodic or doubly-periodic

pattern. We numerically emulated WDM transmission over E-LEAF fibre with 50-GHz-spaced NRZ channels.

We reported these results at ECOC conference in 2005, as part of an article dealing more generally with singly- and doubly-periodic dispersion management schemes (cf Chapter 1) at 10Gb/s [98]. We investigated each scheme then assessed the relevance of the nonlinear phase criterion for the optimal configuration of each scheme.

Some details about the set-up and the physical performance of the dispersion management strategies are given in the following inset.

Details on the dispersion management study over LEAF fibre at 10Gb/s

The simulated link applies to terrestrial Ultra-Long Haul systems, as depicted by Figure 3-6: it consists of up to 6 subdivisions of 5 spans of 100km-long NZDSF fibre (E-LEAF fibre with 4.25ps/nm/km chromatic dispersion at 1550nm), separated by DCM located within dual-stage EDFAs. The transmitter consists of 21 NRZ-modulated channels (decorrelated De Bruijn sequences of 64bits), with a channel bit rate of 10.66Gb/s and 50GHz channel spacing, in the C band. For simplicity reasons, we overlooked Four Wave Mixing. Noise accumulation is also overlooked as we focus on the transmission penalty. We derived such penalty from the average eye opening over the 11 central channels of the multiplex.

Dispersion management is achieved using DCM (being either Dispersion Compensating Fibre, DCF or Standard Single Mode Fibre, depending on the type of dispersion compensation). The maps under study have a two period-pattern: within a 5-span subdivision, per span inline compensating modules are adjusted to maintain a given residual dispersion per span (accumulated over the line fibre span and the following module), while at the end of the subdivision, we authorize another Dispersion Compensating Module (DCM), as illustrated by Figure 3-6 and Figure 3-7, to maintain a target "residual dispersion per subdivision" (cumulated dispersion over the whole subdivision). The map is thus composed of a pre-DCM (optimized after the PIC criterion from Chapter 2), then of a concatenation of subdivisions of 5 spans and DCM, and eventually of post-DCM.

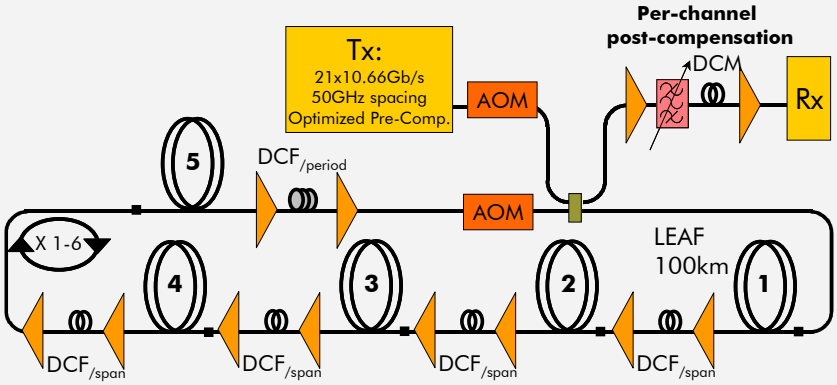

Figure 3-6: Simulated transmission set-up

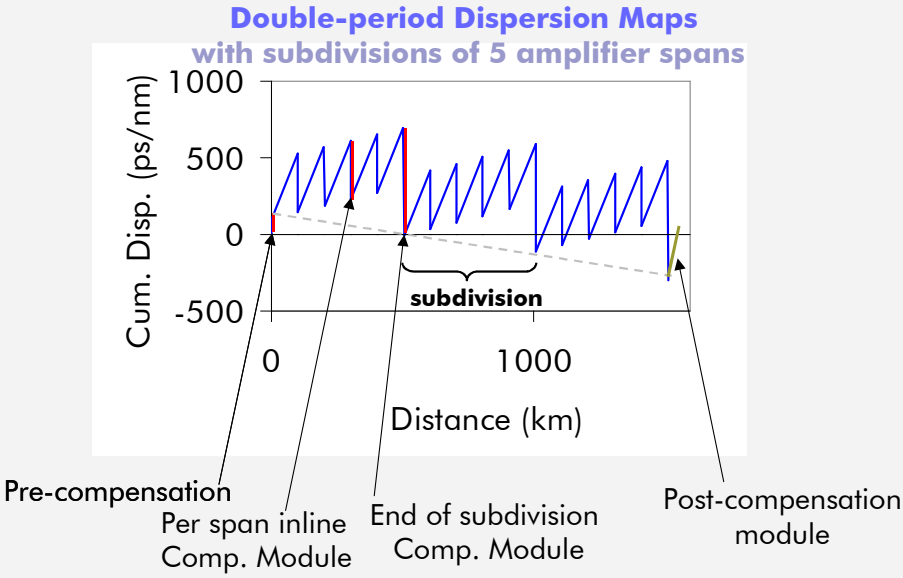

Figure 3-7: Typical double-period dispersion map with subdivisions of 5 spans

Figure 3-8 represents contour plots of the transmission penalty versus the residual dispersions per span and per subdivision, after 4x500km transmission with 2dBm per channel input power into the line fibre (-5dBm into the DCMs), and optimized pre- and post-DCM. The lighter the area, the lower the penalty.

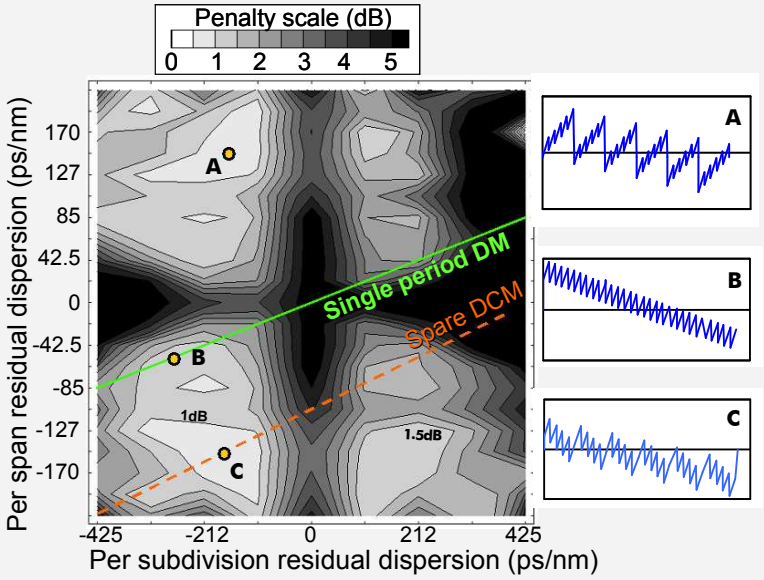

Figure 3-8 : Transmission penalty contours versus per span and per subdivision residual dispersion, after 4x500km transmission with optimal pre- and post-DCMs. Maps A and C represent the best double-period maps. Map B is the best single-period map.

Without discussing in details the different dispersion maps as in article [98], globally decreasing dispersion maps (with negative residual dispersion per subdivision) offer slightly lower penalties (0.5dB) than increasing maps. As for the choice between locally increasing or decreasing maps, there is no significant difference. Note that the multi-span perturbation models from Chapter 2 would suggest no real difference between globally or locally, decreasing or increasing map, provided optimized pre-compensation. The two best

dispersion maps, yielding the same transmission penalty, are referred to as A and C in Figure 3-8 for locally increasing and decreasing maps respectively. While solution A might appear less interesting as it requires quite a long DCF every five spans (even though additional studies show a weak impact on the Optical Signal to Noise Ratio), solution C is rather remarkable: indeed, it corresponds to the strategy of sparing (or skipping) one DCM every five spans, while distributing the compensation per subdivision only over four out of five spans. The straight line entitled "Spare DCM" in the same Figure 3-8 corresponds to this strategy.

The straight line entitled "Single Period DM" corresponds to single period maps, with a "per subdivision residual dispersion" five times as large as "per span residual dispersion". Case B is the best single period map, yielding an extra–penalty of 0.7dB with respect to best double period maps.

After optimizing the inline dispersion compensation for singly-periodic and doubly-periodic strategies at a fixed distance, we assessed the relevance of the nonlinear phase criterion, for conventional optimized Single-Period (case B in Figure 3-8) and Double-period, periodically uncompensated dispersion maps (case C) in agreement with the protocol detailed in chapter 2 (that is various distances and fibre input powers, with optimized pre- and post-compensation modules for each configuration).

Figure 3-9 highlights the good correlation between penalty and nonlinear phase for both dispersion map strategies: the accuracy of the nonlinear phase criterion for a 2dB reference penalty is found lower than 0.5dB.

It also stresses that doubly-periodic dispersion maps are about 1dB more tolerant to nonlinearities than singly-periodic dispersion maps, which translates into 1dB extra power margin, for system design.

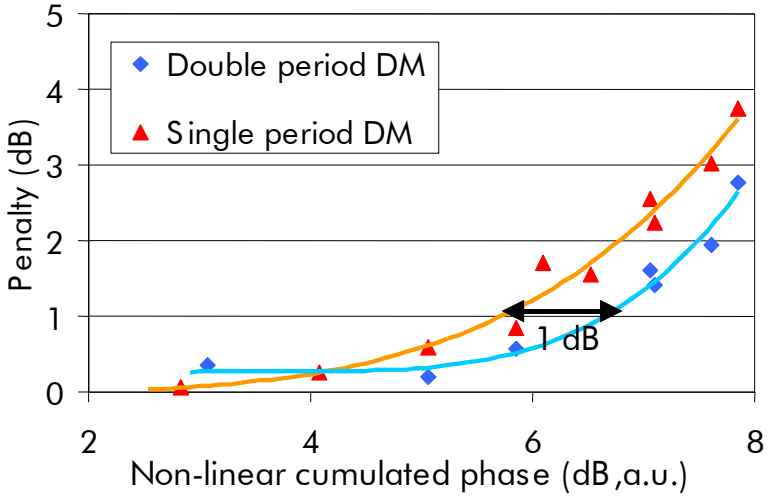

Figure 3-9: Relationship between transmission penalty and nonlinear phase for optimal dispersion maps, following two strategies: single-period (case B), or double-period, periodically uncompensated (case C).

The nonlinear phase criterion appears thus here as still relevant for WDM transmissions based on 10Gb/s bit rate and LEAF fibre provided one good fixed strategy of singly-periodic or doubly-periodic inline dispersion management with adjustment of pre-compensation at transmitter output and residual dispersion at receiver input to distance and power. In the following section, we will pursue the estimation of the accuracy of the nonlinear phase criterion for not-optimized maps at 10Gb/s with a similar study performed over SMF fibre.

III.2.2. Experimental investigation of SMF-based transmission systems with fixed inline compensation strategy and optimized pre- and post-compensation

In order to pursue the investigations of the accuracy of the nonlinear phase criterion for 10Gb/s systems using a fixed inline dispersion compensation strategy, we report here experiments over SMF fibre, mainly achieved by B. Lavigne and E. Balmefrezol in 2004.

Set-up

The transmitter side consists of 5 channels centred around 1550nm and separated by 50GHz. Each channel is NRZ-modulated channels with a 2^{23}-1 pseudorandom binary sequence. The signals are multiplexed then sent into a dispersion pre-compensation fibre (within an amplifier site) and into a recirculating loop composed of two sections of 100km SMF followed by DCF at the inter-stage of optical amplifiers. At the output of the loop; the signals pass through a dispersion post-compensation stage before detection and BER measurement of the central channel. The input powers into SMF (respectively DCF) sections are varied between 0 and 10dBm (respectively between -6 and 10dBm). The number of loop laps before reception is varied between 1 and 15. The emulated dispersion map is singly periodic with two configurations of residual dispersion par span, either 0 or 100ps/nm/span, and optimized pre-compensation and post-compensation for any combination of distance and power.

Results

Figure 3-10 depicts the OSNR penalty corresponding to 10^{-5} BER as a function of nonlinear phase for both configurations of residual dispersion per span and various conditions of powers and distances. The increasing dispersion map (with 100ps/nm/span residual dispersion per span) appears more resistant to nonlinear impairments than the full inline compensation scheme, as illustrated by the tolerable nonlinear phase corresponding to 2dB penalty, respectively 2.8rad instead of 1.8rad (corresponding to an improvement of 1.9dB) mainly because of a better mitigation of Cross-Phase Modulation [111][112].

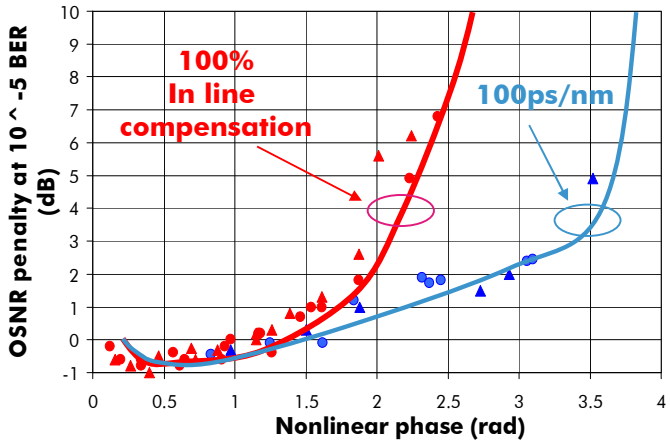

Figure 3-10 : Experimental assessment of penalty vs nonlinear phase relationship for a WDM 10.7Gb/s transmission system over SMF fibre with fixed residual dispersion per span (either 100% inline compensation, ie 0ps/nm/span or +100ps/nm/span) and optimized pre- and post-dispersion compensation.

In both configurations of residual dispersion per span, the accuracy of the nonlinear phase criterion, as measured for a reference 2dB penalty, is fine, about 0.8dB (lower than the 1.5dB limit), which is comparable to the case of a fully optimized map (see in Chapter 2).

III.2.3. Extension to dispersion maps typical of deployed 10Gb/s systems, with fixed pre-, inline and post-compensation strategies

The previous results suggest that the nonlinear phase criterion is relevant for 10Gb/s-modulated transmission systems provided a good fixed inline dispersion strategy combined optimized dispersion pre- and post- compensation for different configurations of distance or power.

In fact, for 10Gb/s systems, tolerance to pre-compensation is such that it is possible to get the same level of accuracy for the nonlinear phase criterion with one fixed pre-compensation whatever the distance. To a larger extent, if the residual dispersion per span is not too high in absolute values, the post-compensation module may also be kept constant whatever the reach for limited impact without degrading too severely the accuracy of the nonlinear phase criterion.

To illustrate that point, we report here one experiment achieved by Bruno Lavigne, Elodie Balmefrezol, Pierre Peloso and Magali Prunaire in 2005 for a WDM system representative of terrestrial optical networks with node sections of 4 spans.

Set-up

40 channels from the C-band and spaced by 100GHz are NRZ-modulated at 10.7Gb/s with 2^{23}-1-long PRBS, multiplexed and sent into a recirculating loop emulating a link between two consecutive nodes. A loop lap includes a pre-compensating fibre, set to -800ps/nm, a concatenation of four spans of SMF followed by DCF such that the residual dispersion per span is either 50, 100 or 130ps/nm depending on the chosen configuration; eventually a post-compensating module ensures that the residual dispersion per loop lap (or node section) is close to zero. The loop also includes one power equalizer and optical amplifiers before each fibre section. Different fibre input powers and loop laps are investigated, before reception of the central channel at 1545nm.

Results

Figure 3-11(b) depicts measurement points of the OSNR penalty (for 10^{-5} BER) as a function of nonlinear phase, for all evoked configurations. We observe the good matching between penalty and nonlinear phase whatever the residual dispersion per span, the powers and distances.

The accuracy of the nonlinear phase criterion is found about 1dB for a reference 2dB penalty. Choosing 1dB reference penalty would lead to the same accuracy. In summary, the nonlinear phase criterion originally defined for fully optimized dispersion managed systems appears also relevant at 10Gb/s for dispersion maps typical of deployed systems. This is consistent with the recommendations of the PIC theory in Chapter 2 requiring that the absolute value of the cumulated dispersion at the input of each span remains lower than 800ps/nm.

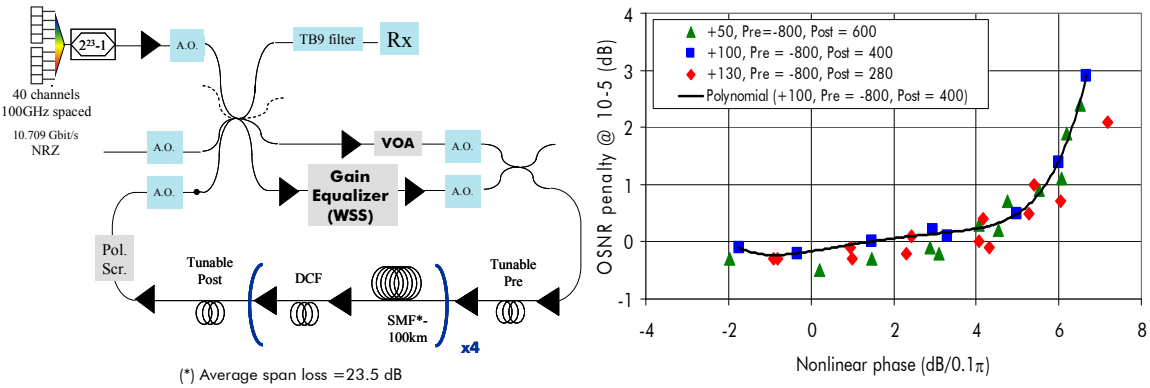

Figure 3-11 : 10Gb/s transmission over SMF fibre, dispersion map typical of transparent optical networks with sections of 4 spans. Left: exp. set-up. Right: penalty vs nonlinear phase plots

III.3. Applicability of the nonlinear phase criterion at 40Gb/s

The PIC theories from Chapter 2 suggest that they are consistent with the nonlinear phase criterion for a strongly reduced maximum value of inline cumulated dispersion when moving from 10 to 40Gb/s.

Here we assess the accuracy of the nonlinear phase criterion for 40Gb/s-modulated systems using fixed inline dispersion compensation strategies and we propose a possible improvement of the criterion in accounting for the total inline cumulated dispersion in addition to the nonlinear phase.

To do so, we report here numerical studies of single-channel transmission systems with either NRZ or PSBT modulation format over SMF or LEAF fibre. This study has been achieved when supervising the student Alexandros Pitilakis in 2007.

Set-up

The transmission link consists of a variable number (5 to 20) of line fibre (SMF or LEAF fibre) sections and DCF located within dual-stage amplifiers, arranged according to a typical singly-periodic dispersion map, with fixed inline dispersion compensation strategy (residual dispersion per span being either -100, -50, 0, 50, or 100ps/nm) and optimized pre- and post-compensation modules whatever the investigated reach of the system or input power into the line fibre. Nonlinearities in the DCF are neglected. The transmitter consists of one NRZ or PSBT-modulated channel with a 256 bit-long De Brujn sequence.

The goal of such a study is to assess the accuracy of the nonlinear phase criterion for an OSNR penalty for 10^{-5} BER equal to 1.5dB. To do so and to speed up computation, we add noise to the incoming signal at receiver side such that the OSNR is 1.5dB higher than the required OSNR to get 10^{-5} BER in back to back configuration ($OSNR_{ref} = ROSNR_{10^{-5}}^{(btb)} + 1.5dB$), and measure the Q factor. This way, when transmission impairments are such that the observed Q^2 -factor is equal to 12.6dB (i.e. BER is 10^{-5}), the OSNR penalty will be 1.5dB by construction. Figure 3-12 depicts such results for multiple configurations of fibre, modulation formats, residual dispersion per span, and shows for each graph some plots of the Q-penalty with respect to the nonlinear phase as a result of various transmission distances (from 5 to 20) and fibre iput powers. The Q-penalty is here defined as

$$Q_{penalty,dB} = Q^{10^{-5}\,BER}{}_{dB} + 1.5 - Q_{dB}(after\ propagation) \qquad (3\text{-}4)$$

It is equal to 1.5dB when the OSNR penalty for a BER of 10^{-5} is 1.5dB, by definition.

Observations

The observation of Figure 3-12 shows that the correlation between penalty and nonlinear phase is excellent when the residual dispersion per span is null, while it becomes weaker when the ratio of the absolute value of the residual dispersion per span over the local fibre dispersion becomes higher. In more details, for NRZ format, over SMF fibre for instance, the accuracy of the nonlinear phase criterion for 1.5dB reference penalty is below 0.4dB for 0ps/nm residual dispersion per span (RDPS), 0.7dB for +/- 50ps/nm RDPS, and 1 to 1.1dB for +/-100ps/nm RDPS. Over LEAF fibre, the inaccuracy becomes as high as 3.5dB for +50ps/nm RDPS. Additional measurements of the nonlinear phase criterion accuracy are reported in Table 3-2 with grey cells representing acceptable accuracies lower than 1.5dB.

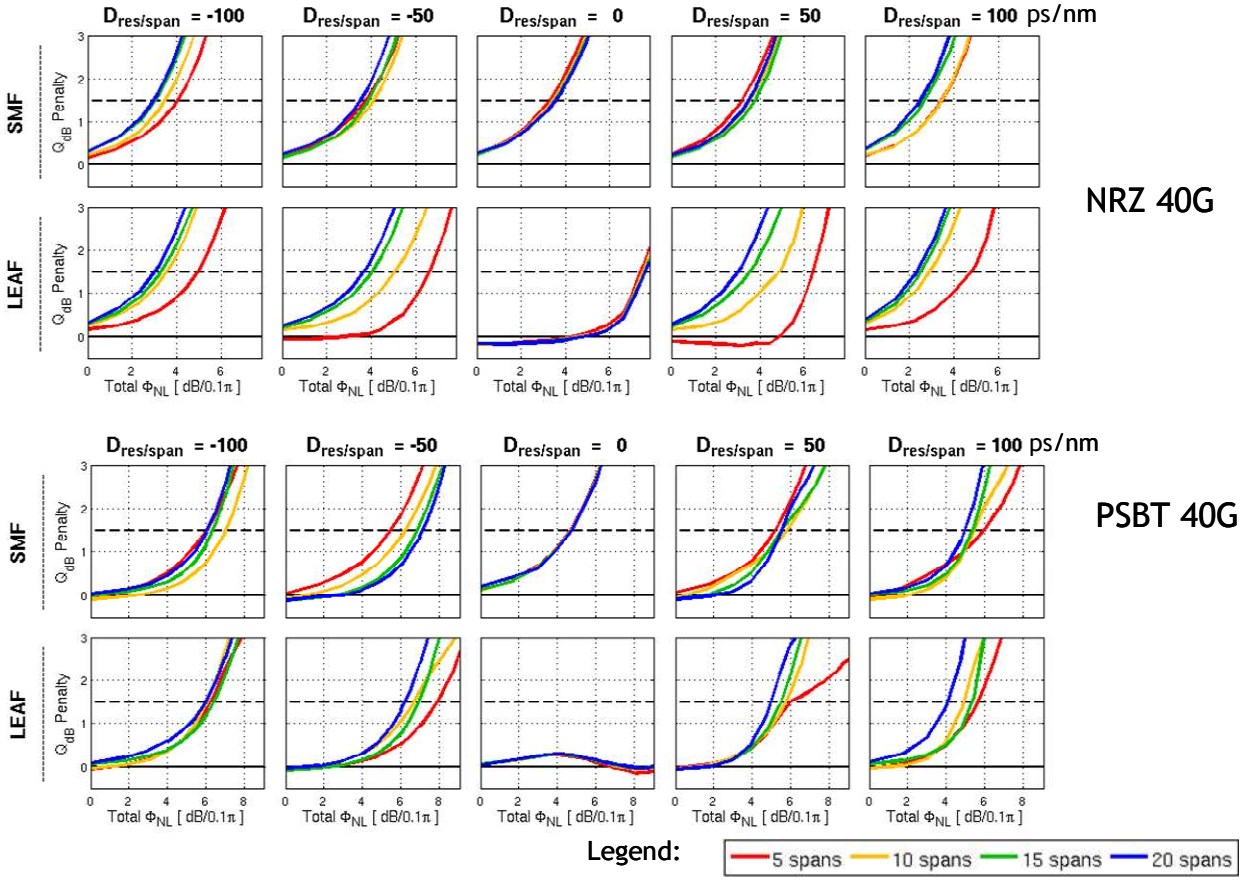

Figure 3-12 : Penalty vs nonlinear phase plots using various fibre input powers and transmission distances, for different configurations of 40Gb/s single-channel transmission systems: NRZ or PSBT modulation formats (upper and lower series of graphs, resp.), with SMF or LEAF line fibre (top graphs, resp. bottom graphs for each format), and singly-periodic dispersion maps with per-channel optimized pre- and post-compensation and fixed residual dispersion per span (-100, -50, 0, 50, 100ps/nm).

This illustrates the fact that for suboptimal maps the nonlinear phase criterion does not allow to capture the impact of accumulated nonlinearities at 40Gb/s as well as 10Gb/s, except when the residual dispersion per span is close enough to zero. This is rather in agreement with the perturbative models previously described in Chapter 2: the lower the product between the residual dispersion per span and the square of the symbol rate, the more naturally the nonlinear phase parameter comes out of the equations.

	Residual dispersion per span (ps/nm)

		-100	-50	0	50	100
Format	*Line fibre*	*Accuracy of the nonlinear phase criterion at 1.5dB OSNR penalty (dB)*				
NRZ	*SMF*	1	0.7	0.4	0.7	1.1
	LEAF	2	3	0.4	3.5	2.5
PSBT	*SMF*	1.2	1.8	0.2	0.8	1
	LEAF	0.5	1.8	0.2	1.1	1.8

Table 3-2 : accuracy of nonlinear phase criterion for 40Gb/s systems with fixed strategy of inline dispersion compensation. Grey cells corresponds to an accuracy lower than 1.5dB limit.

When this assumption is no longer feasible, Equation (2-37) to (2-39) suggest that the degradations will depend on the nonlinear phase and the product between the number of spans and the average residual dispersion per span, as well as the optimal pre-compensation will depend on such a product.

To emphasize that point, Figure 3-13 shows contour plots of the nonlinear phase values leading to 1.5dB penalty for PSBT-based systems, as a function of the product between span number and RDPS versus the relative accumulated dispersion of the pre-compensation module with respect to the predictions of the PIC criterion (cf Chapter 2); dispersion post-compensation is still optimized at receiver end. Four graphs are represented for different transmission distances: 5, 10, 15 and 20 spans. The contour plots corresponding to 10, 15 and 20 spans look very much alike, stressing the fact that system performance essentially depends on nonlinear phase and on the total inline cumulated dispersion.

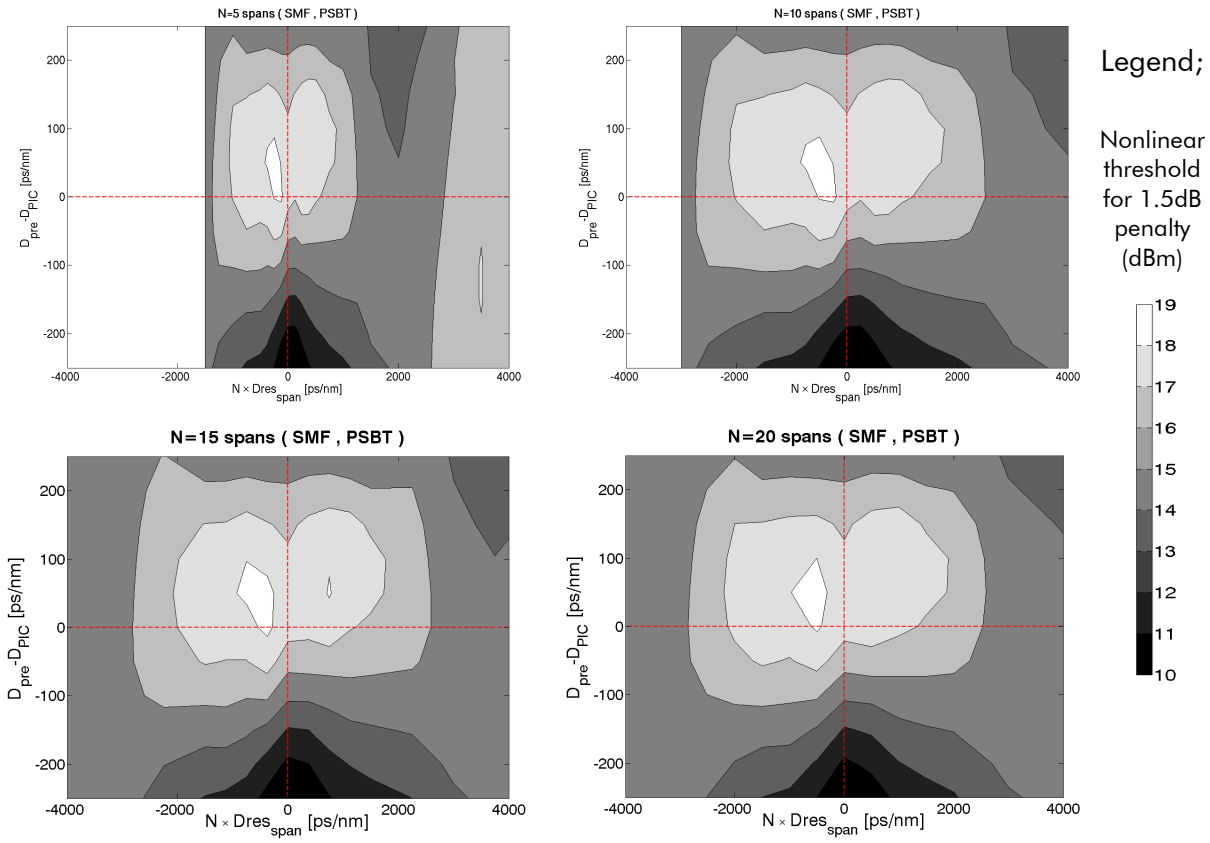

Figure 3-13: contour plot of 1.5 dB penalty nonlinear threshold of 40G PSBT – modulated vs product between number of spans N and inline residual dispersion per span, and the difference between the optimal pre-compensation and the PIC value.

Figure 3-14 is even more explicit: it represents the nonlinear phase leading to1.5dB penalty for PSBT format for the four investigated distances 5, 10, 15 and 20 spans, as a function of the product between number of sans and RDPS, with optimized pre-compensation (following PIC rules) and post-compensation whatever distance and power. It clearly shows that system tolerance to nonlinear phase is a function of the product between number of spans and residual dispersion per span. The highest tolerance is obtained for relatively low values of this product at + or -600ps/nm: if we anticipate a maximum reach of 20 spans, it corresponds to a residual dispersion per span of + or -30ps/nm. For a number of spans between 5 and 20 the spread of nonlinear phase values leading to 1.5dB penalty is as wide as 0.5dB for positive RDPS and below 1dB for negative RDPS.

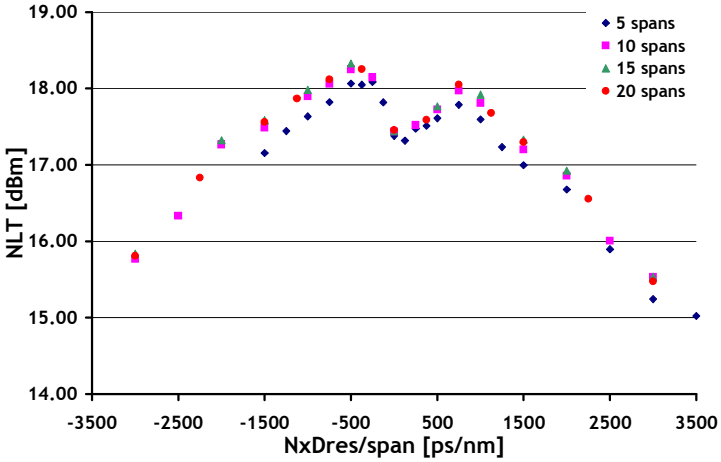

Figure 3-14 : Evolution of 1.5dB penalty NonLinearThreshold (NLT, here the value of integrated power corresponding to 1.5dB penalty) of 40Gb/s NRZ-modulated, singly-periodic dispersion maps, vs product between number of spans N and inline residual dispersion Dres/span, assuming optimized residual dispersion and Pre-compensation following PIC criterion rules.

Even if the relation between penalty and nonlinear phase criterion also depends on the total inline residual dispersion, the optimal values of residual dispersion per span are here so low for the chosen formats that the nonlinear phase criterion can still be used without any modification and with a fair accuracy. Besides, if the product between residual dispersion per span and number of spans remains low with respect to the accumulated dispersion over twice the effective length of line fibre spans, the perturbation theories from Chapter 2 tell us that the optimal pre-compensation is expected to remain almost constant with distance, which relaxes design constraints.

We will see in Chapter 6 that for polarization multiplexed signals with multilevel phase modulation and coherent detection, the optimum values of residual dispersion per span are so high that the nonlinear phase criterion will need to be rethought or at least adapted.

III.4. Conclusion on the impact of dispersion map

We have shown that even if the nonlinear phase criterion is particularly suitable for fully optimized dispersion maps, it remains fairly accurate for typical, under-optimized, transmission systems.

For 10Gb/s-modulated terrestrial systems, provided a good dispersion management strategy, a very good accuracy can be obtained (below 1dB). This is particularly the case if we can adapt the post-compensation module to the distance (which is not the case in practice for deployed multi-reach optical networks) or if the need for distance-dependent post-compensation adjustment is not too stringent (which can be ensured by targetting zero accumulated dispersion between nodes).

For 40Gb/s-modulated terrestrial systems, per-channel dispersion post-compensation is a prerequisite because of the much lower tolerance to accumulated dispersion and of the multiple sources of variation of the accumulated dispersion before the post-compensation module (dispersion matching between line fibre and DCF over a full spectral band, partial knowledge of the accumulated dispersion, fluctuations with temperature, distance dependence on a per channel basis in optical networks). However the accuracy of the nonlinear phase criterion is limited by the fact that the optimal optimal setting for dispersion pre-compensation strongly depends on the total accumulated inline dispersion, and by the fact that the penalty versus nonlinear phase also strongly depends on total accumulated inline dispersion. Such double-dependences are attenuated for lower bit-rates, in agreement with perturbative models suggesting dependence to the product between inline accumulated dispersion and the square of the symbol rate. The solutions for high-bit-rate systems are either to include this additional parameter in the model and to calibrate its impact, or to design dispersion maps with relatively small values of possible inline accumulated dispersion whatever the distance. Fortunately, such configurations are optimal for most classic formats, but we will see in Chapter 6 that it is no longer the case for the most recent PDM-QPSK format used for 100Gb/s transmission.

In addition to the abovementioned studies, the reader can find additional validations of the nonlinear phase criterion in our papers [96] and [97] for singly- and doubly-periodic dispersion maps, at 10 and 40Gb/s channel bit-rates.

3.IV. Generalization of the nonlinear phase criterion to tackle hybrid systems with mixed-line-fibre types and span lengths: towards the concepts of weighted nonlinear phase

IV.1. Introduction to line fibre type heterogeneity

The recent introduction of transparency, as well as the necessity to re-use legacy fibre as much as possible, brings new challenges in the efficient design of meshed optical networks, for instance coping with line fibre type heterogeneity. Indeed, it has now become almost common to deal with light-paths between two points of the network involving at least two different line fibre types [96][97][113][114][115][116][117] with different values of chromatic dispersion, and it has therefore become crucial to use simple tools in order to predict accurately light-path feasibility. The problem is similar to the case of the diversity of line fibre section lengths as evoked in section.1.II. One of the most critical issues is to determine the tolerance to Kerr-like nonlinear impairments, without requiring customized simulations or experiments for each possible configuration.

We proposed in [96][97] a simple tool, the weighted nonlinear criterion, to predict the penalties induced by nonlinearities for an heterogeneous system composed of the concatenation of two homogeneous subsystems (each of which involving only one fibre type) from the sum of the nonlinear contributions of both homogeneous subsystems, weighted by their own tolerance to nonlinearities. Such an approach is fully inline with the PIC or perturbation theories developed in Chapter 2. Its potential was illustrated in an NRZ system at 10Gb/s consisting of G.652 Standard Single-Mode fibre (SMF) and G.655 Large Effective Area Fibre (LEAF), assuming singly-periodic dispersion mapping for each subsystem: two calibration measurements of the tolerance to a given level of penalty for each SMF or LEAF system were sufficient to predict the tolerated amount of nonlinear phase leading to this same amount of penalty in an heterogeneous SMF+LEAF system.

In [97], we reported on an extensive investigation of the accuracy of this criterion at both 10Gb/s and 40Gb/s, for various modulation formats (NRZ, Phase-Shaped-Binary Transmission PSBT, Differential Phase-shift Keying DPSK [112][118]), over numerous system configurations using doubly periodic dispersion management schemes, typical of meshed networks. All these systems involved a combination of SMF and LEAF line fibres, since these fibre types are the most widespread and lead to very different propagation behaviours due to their different dispersions characteristics. Eventually, in [101], we performed an experimental assessment of the accuracy of the proposed criterion.

The weighted nonlinear phase approach is general and is particularly adapted to replace the nonlinear phase to tackle the impacts of fibre dispersion, length.

The following sections summarize such studies through the numerical investigation of mixed line fibre type systems, the introduction of the weighted nonlinear phase parameter, then numerical and experimental assessments of the related accuracies.

Note that the weighted nonlinear phase criterion depends on the choice of a reference penalty, and so does slightly the resulting accuracy of this new criterion. That point is particularly addressed in Appendix VI.3.

IV.2. Nonlinearity /GVD interaction and weighted nonlinear phase

IV.2.1. Set-up

We define a homogeneous (sub-) system as a transmission (sub-) system involving only one line fibre type. By contrast, we define a heterogeneous, or mixed, system, as a transmission system involving at least two different line fibre types, and thus composed of the concatenation of at least two homogeneous subsystems. The mixed system under study here is here composed of the concatenation of two homogeneous subsystems, each involving either SMF or LEAF line fibre and a doubly-periodic dispersion map, with zero residual dispersion per subdivision or 5 spans, as illustrated by Figure 3-15. The number of subdivisions for each subsystem is varied, enabling distances up to 30x100km, as well as the input powers into line fibre spans within [-10;+10]dBm, and the subsystem arrangement (SMF then LEAF subsystems, or LEAF, then SMF subsystems). Typical residual dispersion per span is set to 50ps/nm, while Pre-compensation into each subsystem is optimized for the homogeneous propagation. At receiver end, post-compensation DCF is optimized on a per channel basis. NRZ is considered here for single-channel 40Gb/s simulations. All these investigated configurations amounted to a total of over 50,000 simulations runs.

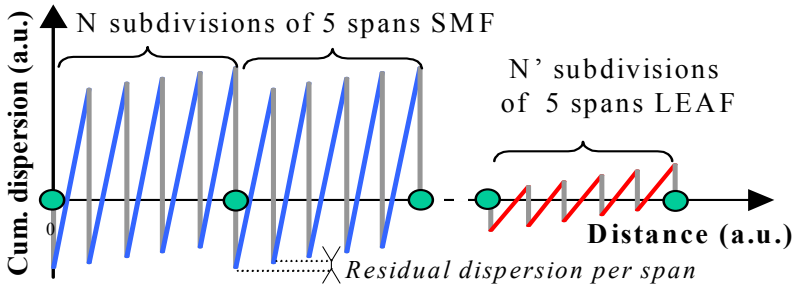

Figure 3-15: Typical dispersion map of mixed system composed of SMF, then LEAF subsystems, each w/ doubly periodic map (N=2 subdivisions of 5 spans SMF, then N' subdivisions of 5 spans LEAF, with null residual disp. per subdivision, and 50ps/nm residual disp. per span).

IV.2.2. Weighted nonlinear phase criterion and numerical validation at 10 and 40Gb/s

We first emulate homogeneous systems based on LEAF or SMF fibre, then heterogeneous systems mixing the two line fibre types. Figure 3-16-a/b represents the computed penalties of reference homogeneous transmission configurations, for LEAF, or for SMF systems, as a function of total cumulated nonlinear phase.

For each fibre type, the tolerance to nonlinearities is assessed by measuring the nonlinear threshold (NLT) that is the nonlinear phase leading to a reference 1.5dB penalty. The relationship between penalty and nonlinear phase is almost bi-univocal regardless of distances and power, in agreement with the results of the previous sections. The accuracy of the nonlinear phase criterion is assessed through the spread of the total nonlinear phases corresponding to 1.5dB-penalty: it is lower than 0.4dB for SMF and 0.8dB for LEAF systems. The minimum NLT (mNLT) value, ensuring a penalty lower than the reference penalty in all conditions, corresponds to short transmissions over a single 5-spans subdivision: mNLT is

equal to $3.2dB_{0.1\pi}$[5] (=0.66rad) for SMF and $6.4dB_{0.1\pi}$ (=1.37rad) for LEAF-based homogeneous systems.

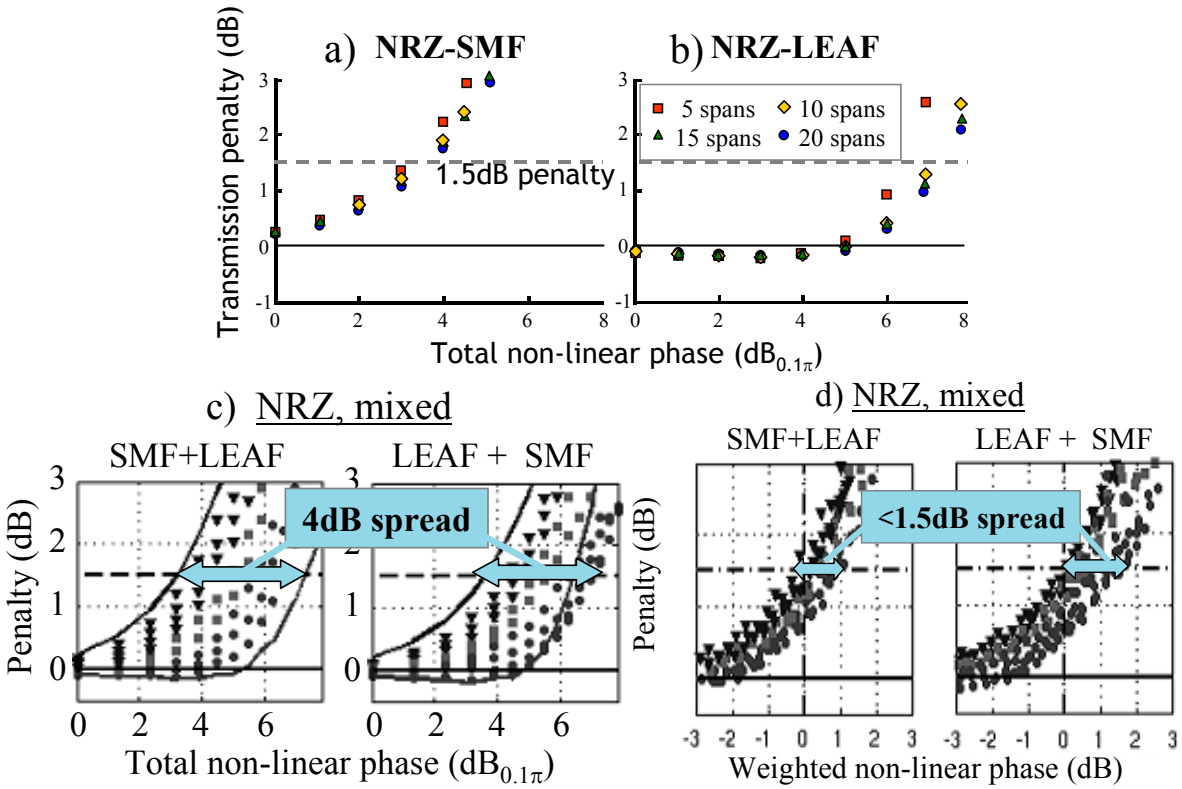

Figure 3-16:a and b plots: penalty vs total nonlinear phase, for SMF (a) and LEAF (b) homogeneous systems, w/ doubly periodic disp. maps Various distances within [5; 20] spans, powers within [–10; +10] dBm. NRZ format, 40Gb/s.
c: Penalty for mixed SMF/LEAF system consisting of concatenations of subsystems of a and b, vs total nonlinear phase.
d: Evolution of penalty for mixed SMF/LEAF system, vs weighted nonlinear phase.

Figure 3-16-c represents all the computed transmission penalties of NRZ-heterogeneous LEAF/SMF systems, such as abovementioned. As we had already observed in [96] at 10Gb/s, the performance of heterogeneous systems based on a combination of different line fibre types almost always lies in between the performance of the corresponding homogeneous systems based on those line fibre types (full lines), for a given total nonlinear phase. Across all mixed systems, the spread of total nonlinear phases corresponding to 1.5dB-penalty is found as large as 4dB, with values ranging from $3.2dB_{0.1\pi}$ and $7.2dB_{0.1\pi}$. The accuracy of the nonlinear phase criterion is clearly not sufficient.

Weighted nonlinear phase

In [96], we proposed a new nonlinear estimator that would be linearly dependent on the nonlinear phase shifts induced by the different subsystems: we proposed to sum the contributions to nonlinear phase $\Phi_{NL,A}$, resp. $\Phi_{NL,B}$ coming from each subsystem A resp. B, weighted by their own tolerance to nonlinearities. (i.e. minimum nonlinear threshold $mNLT_A$, resp. $mNLT_B$ at a given reference penalty, e.g. at 1.5dB here), leading to a new variable called **weighted nonlinear phase**:

[5] By convention, a nonlinear phase of x rad, expressed in $dB_{0.1\pi}$ scale is defined as $10\log_{10}\left(x_{rad}/0.1\pi\right)$.

$$\Phi_W = \frac{\Phi_{NL,A}}{mNLT_A} + \frac{\Phi_{NL,B}}{mNLT_B} \quad (3\text{-}5)$$

If the whole system is homogeneous, based on a single line fibre type, A or B, the penalty is lower than the reference provided that the total nonlinear phase is lower than the minimum nonlinear threshold of this subsystem, thus as long as the weighted nonlinear phase ϕ_W is lower than 1 (i.e. 0dB when converted into dB scale).

By analogy with the definition of the NLT for homogenous systems, we can define the Weighted Nonlinear Threshold (WNLT) as the value of ϕ_W yielding the same reference 1.5dB penalty, and we expect it to remain close to 1 (i.e. 0dB) for heterogeneous systems. Under such assumptions, we can easily derive the expected total nonlinear phase corresponding to the reference penalty for the mixed system (still denoted as NLT in the following), as a function of the ratio α of cumulated nonlinear phase induced by one of the subsystems (e.g. subsystem A in our two-subsystems model) over the total nonlinear phase:

$$NLT_{A+B}(\alpha) = \frac{1}{\frac{\alpha}{NLT_A} + \frac{1-\alpha}{NLT_B}}, \quad with\ \alpha := \frac{\Phi_{NL,A}}{\Phi_{NL,A} + \Phi_{NL,B}} \quad (3\text{-}6)$$

Such an expected NLT value thus varies in between the NLTs of pure systems A and B alone, depending on the relative amount of nonlinearities in the different subsystems A&B, in agreement with Figure 3-16-c. Figure 3-16-d shows the computed penalties of Figure 3-16-c but the x-axis has been converted into the weighted nonlinear phase. It can be observed that the resulting weighted nonlinear leading to 1.5dB penalty for heterogeneous systems are equal or higher than 0dB in all the investigated configurations. In other words, the feasibility of heterogeneous systems is very likely ensured with respect to nonlinear issues provided that the weighted nonlinear phase is lower than the weighted threshold of 0dB. To get insight on the resulting benefits, it should be emphasized that, in an industrial environment, the feasibility of a light-path usually relies on the worst-case scenario. Hence, with the conventional nonlinear phase, the feasibility would be stemming from that of the worst performing fibre, in absence of specific experimental or numerical trial. Although an expected 0dB-weighted nonlinear threshold appears also pessimistic with respect to actual system behaviour, it always predicts (by construction) a better resistance to nonlinear effect over the heterogeneous system than over the homogeneous system of the same length, based on the worst performing fibre. Hence, using the weighted nonlinear phase instead of the nonlinear phase alleviates the need for power margin provisioning and results in even fewer rejections of actually feasible systems. Additionally, Figure 3-16-d also shows that the range of weighted nonlinear threshold values leading to 1.5dB penalty (thereby defining the accuracy of the weighted nonlinear phase criterion) covers less than 1.5dB. It is substantially lower than the accuracy of the nonlinear phase criterion corresponding to 1.5dB-penalty estimated around 4dB. The tolerance to nonlinear effects is hence better assessed, which also results in fewer rejections of actually feasible systems. By analogy with the nonlinear criterion, we can now also talk of the **weighted nonlinear phase criterion** and of its accuracy estimated for the same level of penalty as that enabling to calibrate the weighted nonlinear phase criterion.

			Nonlinear phase	*Weighted nonlinear phase*	
Bit-rate	*Reference penalty (dB)*	*Modulation Format*	*Accuracy for ref. penalty (dB)*	*Accuracy for ref. penalty (dB)*	*Min value leading to ref. penalty (dB)*
40Gb/s	1.5dB	NRZ	4dB	1.5dB	0dB
		PSBT	5dB	2.5dB	0dB
		DPSK	1dB	0.5dB	0dB
10Gb/s	2.5dB	NRZ	2.5dB	1dB	-0.2dB

Table 3-3 : Nonlinear phase vs weighted nonlinear phase criteria over SMF+LEAF heterogeneous systems

In order to be comforted in the use of the weighted nonlinear phase concept, additional simulations have been performed at 40Gb/s with PSBT or DPSK format and at 10Gb/s with NRZ format under similar transmission conditions. Results are summarized in Table 3-3. We can observe that in any case, the weighed nonlinear threshold is close to 0dB (higher than -0.2dB) and that the accuracy of the weighted nonlinear phase criterion is always better than half the accuracy of the nonlinear phase criterion. Details of such simulations and results are given in the following inset.

Details on PSBT/DPSK results at 40Gb/s and NRZ results at 10Gb/s

Similarly to the NRZ at 40Gb/s case, we observed [97] for PSBT format, under the same conditions, a spread of total nonlinear phases corresponding to 1.5dB-penalty as large as 5dB. Conversely; weighted nonlinear threshold values were found equal to, or higher than 0dB, with a reduced spread, as low as 2.5dB. For DPSK formats, similar simulations enabled to show that the spread of total nonlinear phases corresponding to 1.5dB-penalty is as high as 1dB, whereas weighted nonlinear threshold values are higher than 0dB, with a spread as low as 0.5dB.

Similarly, for 10Gb/s NRZ systems with 50GHz channel spacing, the spread of total nonlinear phases corresponding to 2.5dB-penalty (2.5dB leading to the maximization of reach for homogeneous LEAF or SMF systems, with a BER of 10^{-5}, as explained in Chapter 5) is as high as 2.5dB, whereas weighted nonlinear threshold values at 2.5dB-penalty were always found equal to or higher than –0.2dB, quite close to the 0dB expected target, with a spread as low as 1dB.

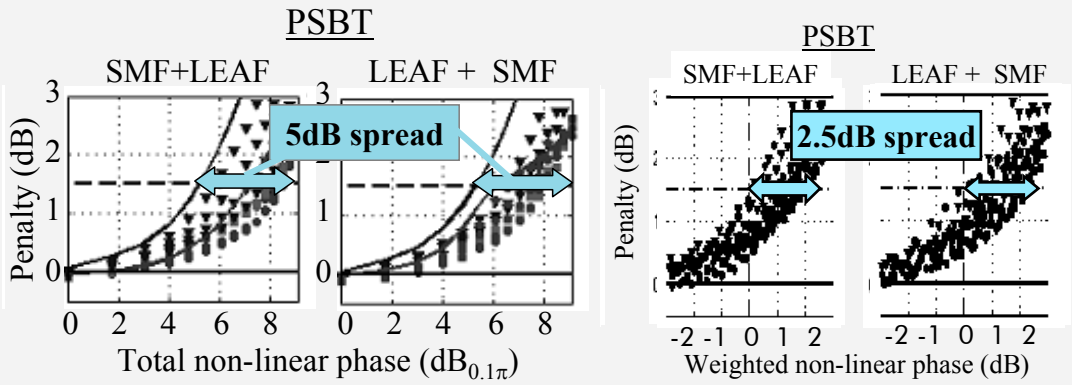

Figure 3-17: Penalty vs total (left) or weighted (right) nonlinear phase for heterogeneous SMF+LEAF, LEAF+SMF 40Gb/s systems with PSBT format, for various sets of fibre input powers, and length of each SMF or LEAF subsystems. Full lines correspond to homogeneous LEAF, or SMF, systems.

This conclusion extends to all the investigated systems configurations simulated at 40Gb/s. Figure 3-17 shows another example of results, obtained with PSBT format. Across all mixed systems, the spread of total nonlinear phases corresponding to 1.5dB-penalty is found as large as 5dB, with values between $4.7dB_{0.1\pi}$ and $9.6dB_{0.1\pi}$. Conversely; weighted nonlinear threshold values are always found equal to, or higher than 0dB, with a reduced spread, as low as 2.5dB. For DPSK formats, similar simulations enabled to show weighted nonlinear thresholds higher than 0dB, with a spread as low as 0.5dB whereas the spread of NLT values is as high as 1dB.

Additionally, we performed similar simulations for fifteen **10Gb/s NRZ**-modulated channels around 1530nm with 50GHz channel spacing, in simulation conditions identical to [96], but now with concatenation of doubly periodic maps (here with subdivisions of 4 spans with 0ps/nm residual dispersion per subdivision at 1550nm, and realistic DCF modules). Fig 5 (from top to bottom plots) illustrates the benefits of the weighted nonlinear approach in LEAF+SMF / SMF+LEAF configurations (up to 24 total spans, and same power variations as above): weighted nonlinear threshold values at 2.5dB-penalty are always found equal to or higher than –0.2dB, quite close to the 0dB expected target, with a spread as low as 1dB, whereas the spread of NLT values at 2.5dB-penalty is as high as 2.5dB.

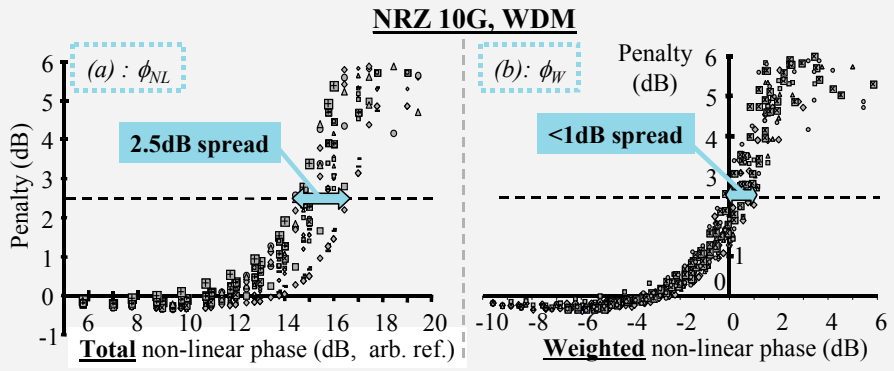

Figure 3-18: NRZ, 10Gb/s, WDM. Penalty vs total (left) or weighted nonlinear phase (right), for different configurations of LEAF+SMF / SMF+LEAF mixed systems, with various input powers and distances into line fibre spans.

Extension to multi-fibre links.

The use of the weighted nonlinear approach can be easily extended to higher degrees of heterogeneities: if we consider a mixed system composed of concatenation of k homogeneous subsystems, the weighted nonlinear phase becomes:

$$\Phi_w = \sum_{i=1-k} \frac{\Phi_i}{NLT_i} \qquad (3\text{-}7)$$

with ϕ_i being the cumulated nonlinear phase over subsystem i, with nonlinear threshold NLT_i. Note that the nature of heterogeneity can either be a change of chromatic dispersion or span length, which is equivalent as explained in section II.3.

Preliminary simulations performed with three types of fibre (D=2, 4, 17ps/(nm/km)) confirmed the relevance of this approach, with weighted nonlinear threshold values always found equal to or higher than 0dB.

In summary, we carried out here an extensive numerical assessment of the accuracy of the weighted nonlinear criterion for predicting the tolerance to nonlinearities, over heterogeneous systems, over a wide range of mixed SMF/LEAF configurations at 10 and 40Gb/s, for several modulation formats (NRZ, PSBT, DPSK), thus highlighting its high potential to easily design heterogeneous meshed networks with mixed fibre types.

This proposal is consistent with the perturbative models described in Chapter 2. Indeed, according to such models, the signal perturbation should depend on a linear combination of the nonlinear phase shifts induced by each span. Besides, the weighting factor associated to the nonlinear phase shift of a fibre section essentially depends on the product between frequency and input cumulative dispersion and the characteristics of the section, not really on the nature of the previous or next sections. As a result, given a dispersion map strategy; if the nonlinear phase criterion applies for each of the different types of fibres involved, then the weighted nonlinear phase appears as a natural candidate for the heterogeneous system.

This model may appear as empiric since it has been built to match observations in the homogeneous configurations. However it is easy to use starting from the determination of the penalty vs nonlinear phase in the homogeneous configurations. Moreover the pure application of perturbative models has proved less accurate than that simple model, at least for the intensity modulated formats for which the discrepancies in nonlinear threshold between LEAF

and SMF-based systems appeared consistent. In Appendix VI.3. , we discuss the impact of the arbitrary choice of the reference penalty for the determination of the NLTs that are required for the calculation of the weighted nonlinear phase

Next section focuses on an experimental validation of this concept.

IV.2.3. Experimental evidence

In this section, we report an experimental investigation [101] of the performance of WDM Nx10Gb/s transmission systems based on mixed SMF and LEAF infrastructures with various distances and fibre input powers, without then with optimized chromatic dispersion at receiver. As a result, we experimentally assess the accuracy of the weighted nonlinear phase criterion. These studies have been achieved in 2009 by P. Henri, C. Simonneau, L. Lorcy, F. Leplingard and myself and published at OFC conference in 2010.

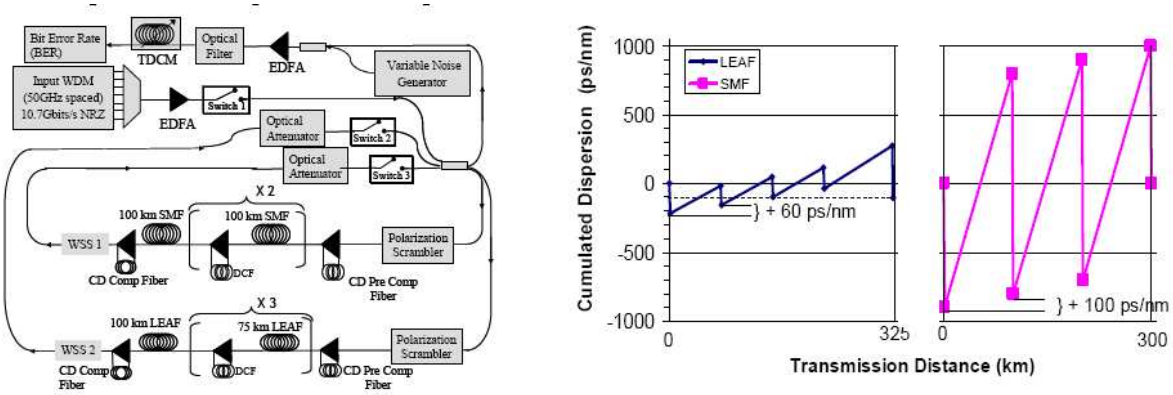

Figure 3-19: Experimental set-up.
Left: description of the physical set-up with the dual-arm recirculating loop.
Right: dispersion map of the 300km-long SMF-based and 325km-long LEAF-based arms at 1530.7nm

IV.2.3.1. *Set-up*

The experimental set-up is depicted in Figure 3-19. The transmitter consists of a multiplex of either 21 or 41 channels modulated at 10.7 Gb/s with NRZ format. Two combs of 100 GHz-spaced channels are encoded with 2^{23}-1 long pseudo-random binary sequences, fed by two independent pattern generators, and are interleaved. The resulting multiplex is passed in an acousto-optic switch and injected into a dual-arm recirculating loop. The loop has two possible paths which emulate different combinations of line fibre types, depending on the state of two other acousto-optic switches, one along each path. Each path emulates a node-to-node link with sections of only one fibre type (either SMF or LEAF) and incorporates a Wavelength-Selective Switch (WSS) which equalizes the channel powerlevels. The SMF-based arm is made of up three spans of 100km SMF, while the LEAF-based arm consists of three spans of 75 km and one of 100 km. Dispersion Compensation Modules (DCMs) are inserted within dual-stage erbium-doped fibre amplifiers after each line fibre spans, and for the pre- and post-compensation of the link, ensuring a dispersion management, with almost zero residual dispersion between two nodes. In the LEAF-based arm, the residual dispersion per lap is set to 0ps/nm at 1550nm and -100ps/nm at 1530.7nm while the residual dispersion per span is 60ps/nm. In the SMF-based arm, the residual dispersion per lap is set to 15ps/nm at 1550nm and 0ps/nm at 1530.7nm while the residual dispersion per span is 100ps/nm at (Fig. 2). At loop output, after a given number of laps, a Tunable Dispersion Compensation Module (TDCM) may be used for performance optimization. Eventually noise is added before

reception so as to measure the required Optical Signal to Noise Ratio (OSNR) to ensure a 10^{-5} bit error rate. We then derive the OSNR penalty.

IV.2.3.2. *Experimental results*

To focus our investigation field on the worst propagation case, we measure the OSNR penalty at 1530.7nm, based on experiments performed over LEAF and SMF fibre at several wavelengths and showing detrimental inter-channel effects in the lower C-band. To ease the reading a WDM comb propagating alternatively in one loop arm of SMF followed by one loop arm of LEAF is noted SL so that an SLSL scenario repeats the basic pattern SL alternating loop sections of SMF (S) and of LEAF (L) as long as we can match the 10^{-5} bit error ratio.

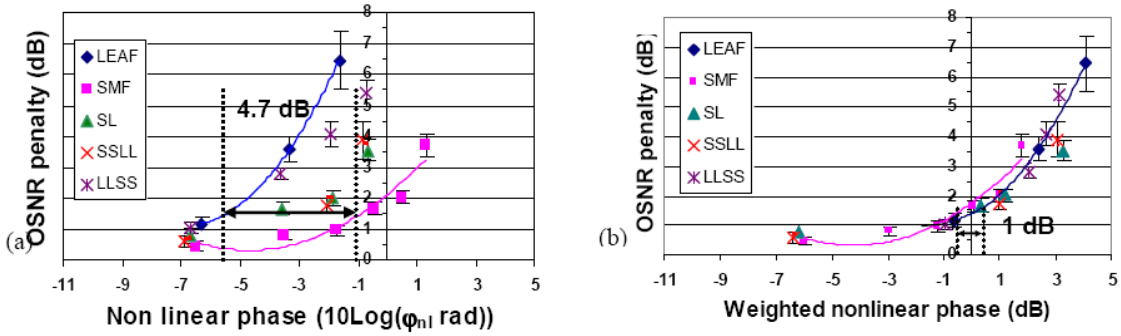

Figure 3-20 : (a) OSNR penalty for 10-5 BER as a function of nonlinear phase (b) OSNR penalty for 10-5 BER as a function of weighted nonlinear phase. Different mixed fibre scenarios; ***3dBm per channel*** *into line fibre spans;* ***no adjustment of dispersion compensation at receiver***

Figure 3-20 (a) depicts the OSNR penalty for homogeneous and heterogeneous scenarios with 21 propagating channels (3dBm per channel line fibre input power) for various loop laps. We do not use here any TDCM. Similar to the numerical results, the OSNR penalties for the mixed fibres scenarios appear bounded by the penalties for homogeneous LEAF and SMF scenarios, at a given nonlinear phase shift. The SMF case exhibits the lowest penalties. We can observe that the scenarios beginning with LEAF loop sections yield more penalties than scenarios beginning with SMF sections. It can be seen that the accuracy of the nonlinear phase criterion (i.e. the range of nonlinear phases which leads to 1.5dB OSNR penalty) is as high as 4.7dB, which is well beyond any reasonable limit. Hence, the nonlinear phase criterion is clearly not sufficient to capture the signal distortions in heterogeneous light-paths.

Therefore, as in the previous study, we compute the weighted nonlinear phase based on the determination of the 1.5dB-penalty nonlinear thresholds for SMF-only or LEAF-only links. Applying the variable change from nonlinear phase shift to weighted nonlinear phase, the measures are rescaled into Figure 3-20 (b). By definition, the weighted nonlinear phase is equal to 0dB for pure SMF and LEAF systems at 1.5dB OSNR penalty. For mixed systems, the values of weighted nonlinear phase corresponding to 1.5dB penalty are all higher than -0.5dB, quite close to the 0dB target, with an accuracy of the weighted criterion reduced down to 1dB. This is in good agreement with the theoretical and numerical results showed in the previous section. Thanks to the weighted nonlinear phase we are able to predict with a pretty good accuracy the performance of any mixed system once we know the penalty curves on homogeneous SMF and LEAF systems.

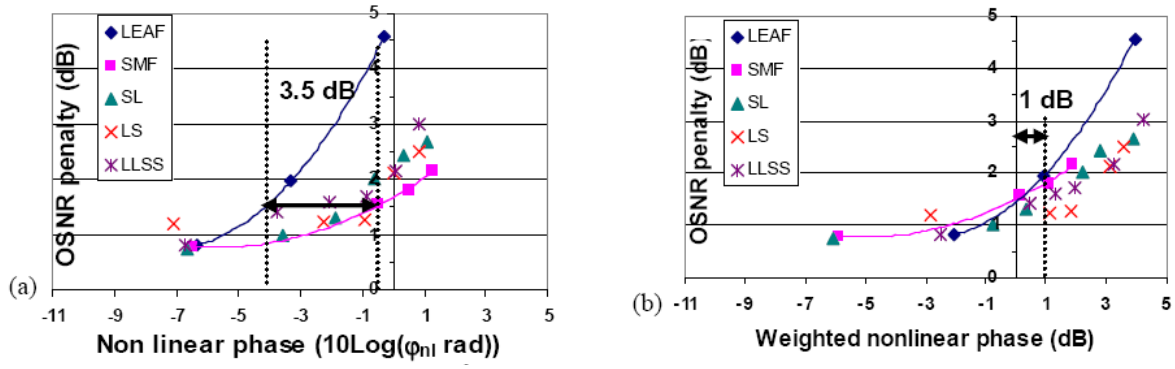

Figure 3-21 : (a) OSNR penalty for 10-5 BER as a function of nonlinear phase
(b) OSNR penalty for 10-5 BER as a function of weighted nonlinear phase. Different scenarii of fibre-mix; 3dBm input power per channel into line fibre spans; per-channel adjustment of dispersion compensation at receiver

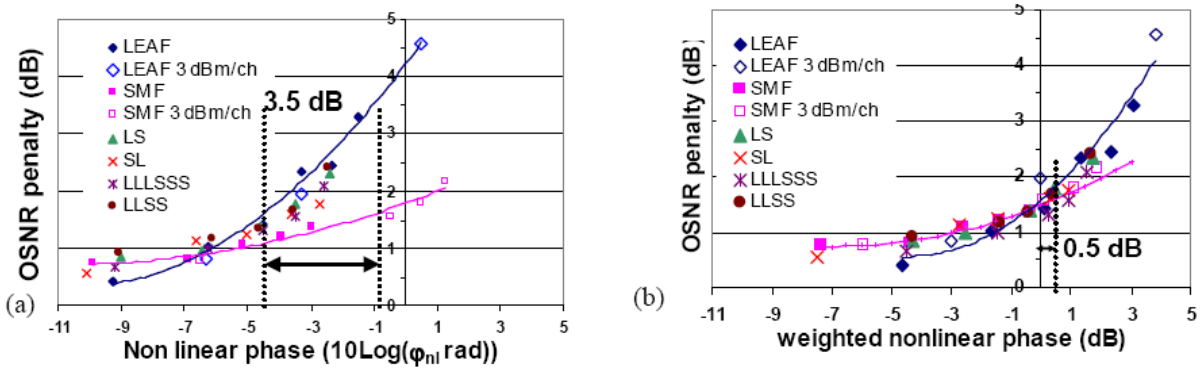

Figure 3-22(a) OSNR penalty for 10-5 BER as a function of nonlinear phase
(b) OSNR penalty for 10-5 BER as a function of weighted nonlinear phase. Different scenarii of fibre-mix; 0dBm input power per channel into line fibre spans; per-channel adjustment of dispersion compensation at receiver

Next, we further investigate heterogeneity when using the TDCM to optimize the residual dispersion. Figure 3-21 and Figure 3-22 respectively represent the penalty measurements in mixed systems for 3dBm and 0dBm input powers per channel into line fibre sections, as a function of either the nonlinear phase (left graphs, labelled as a) or the weighted nonlinear phase (right graphs, labelled as b). We observe though Figure 3-21-a and Figure 3-22-a that the accuracy of the nonlinear phase criterion for 1.5dB penalty is about 3.5dB, and that the penalty of mixed systems still appears as bounded by pure LEAF and SMF penalty curves (such penalty versus nonlinear phase relationships being independent on the fibre input power in fairly good approximation). After converting nonlinear phases into weighted nonlinear phases based on the measured nonlinear thresholds corresponding to 1.5dB penalty, Figure 3-21-b and Figure 3-22-b show that the values of weighted nonlinear phase corresponding to 1.5dB penalty are all higher than 0dB, with an accuracy of the weighted criterion reduced down to 1dB.

This experiments highlight that the weighted nonlinear phase criterion can be used with an acceptable accuracy for typical 10Gb/s-modulated WDM systems.

IV.2.4. Conclusion on the weighted nonlinear phase concept

In summary, we have introduced the weighted nonlinear phase concept as a first order approximation that captures rather well fibre heterogeneity in a heterogeneous transmission system in usual conditions of operations, although some more in-depth analytical studies might lead to more accurate predictions provided system complexity is not too high. We showed by numerical and experimental means that it was applicable to dispersion-managed transmission systems presenting an heterogeneity of line fibre dispersion, but the same concept can be applied to deal with line fibre/DCF heterogeneity or span length diversity more accurately than nonlinear phase. More particularly, this concept is fully in line with the evoked issue in Chapter 2 and extends the proposed analytical concepts based on a few calibration measurements rather than analytical guesses. To complete this study the impact of the reference penalty necessary to estimate a nonlinear threshold and thus the weighted nonlinear phase is investigated in Appendix VI.3.

3.V. Summary

In this chapter, we have investigated the domain of validity and the accuracy of the nonlinear phase criterion introduced in Chapter 2.

We have first considered the impact of the number of spans, the DCF input power and span length in the same dispersion map configurations as in Chapter 2, then we have considered the impact of realistic dispersion maps and eventually we have generalized the nonlinear phase criterion so as to fully tackle fibre diversity.

Therefore, we have first shown that the nonlinear phase criterion is not meant to be applied for single-span and multi-span systems with a single relationship linking penalty and nonlinear phase.

We have then shown that the nonlinear phase criterion is accurate enough to deal with line fibre / DCF heterogeneity in usual conditions of utilisation, even though the sum of the nonlinear phase shifts coming from line fibres and from the DCFs is not the best linear combination of the contributions coming from line fibres and from the DCFs that would enable an excellent accuracy of an adapted criterion in the most exotic configurations.

We have assessed the accuracy of the nonlinear phase criterion when accounting for line fibre span length and we have shown the need for different relationships between penalty and nonlinear phase depending on the product between square of symbol-rate, line fibre chromatic dispersion and effective length.

After those studies with optimized dispersion management conditions, we have shown that the nonlinear phase criterion remains accurate enough for non-fully optimized dispersion maps, yet with almost full inline dispersion compensation, especially for 40Gb/s modulated systems. Otherwise the total inline dispersion should be an input parameter to the penalty estimator in addition to the nonlinear phase, in agreement with the perturbation theories from Chapter 2.

Eventually, we have introduced the weighted nonlinear phase criterion to predict the nonlinear induced distortions for heterogeneous transmission systems. It is based on a few calibration measurements of tolerance to nonlinearities for the homogeneous subsystems and on a linear combination of the nonlinear phases induced by each fibre weighted by the tolerance of the homogeneous system corresponding to such fibre. This approach is general and enables to account for diversity in line fibre dispersion or span length. It is fully consistent with the PIC and perturbation theories and the dispersion management considerations are the same as with the nonlinear phase criterion.

The results presented in this Chapter have been published in [96][97][98][99][101].

At this stage, we have now elaborated a simple tool that enables to predict nonlinear induced distortions with reasonable accuracy in almost any usual configuration. In Chapter 4, we will elaborate on that tool in order to build an “easy-to-use yet accurate” quality of transmission estimator accounting for additional sources of degradation. And in Chapter 5, we will rely on the existence of the (weighted) nonlinear phase criterion to build simple reach estimators accounting for nonlinearities and noise, and then guidelines to optimize subsystems and input powers into the fibres.

3.VI. Appendix

VI.1. Impact of DCF nonlinearities into 40Gb/s-modulated SMF-based systems

We performed similar types of numerical simulations for 40Gb/s single-channel transmission systems based on 100km-long spans of SMF line fibre and using NRZ modulation format, with optimized dispersion management, for different distances and fibre input powers. Here, we considered two configurations, accounting for or overlooking nonlinearities coming from the DCF in the numerical tool. In presence of nonlinearities in the DCF, we chose fibre modules with a chromatic dispersion of -100ps/nm/km, and the DCF input power was set 7dB lower than the line fibre input power.

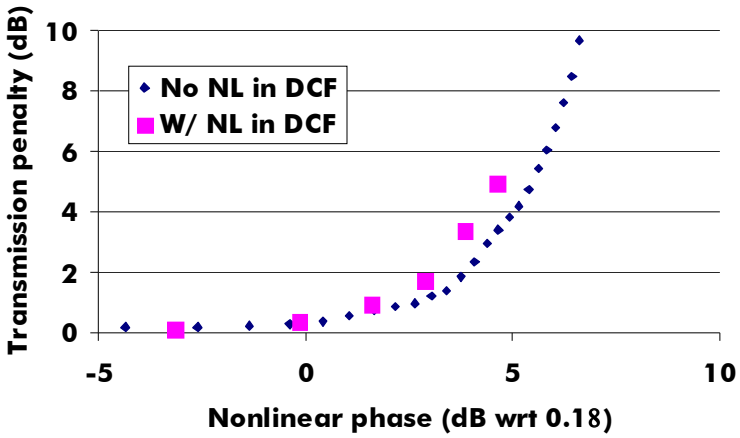

Figure 3-23: Impact of nonlinearities originating froom the DCF fibre: plots of the OSNR penalty for 10^{-5} BER as a function of nonlinear phase for a Nx100km SMF system based on single-channel 42.7Gb/s NRZ-modulated channel.

Figure 3-23 shows OSNR penalty versus nonlinear phase plots for both types of configurations. We can observe that the values of nonlinear phase leading to 2dB penalty differ from 1dB depending on the presence of absence of nonlinearities in the DCF, with higher tolerance to nonlinear phase in absence of DCF-nonlinearities, similar to the 10G single-channel case. We can have the following interpretation: in presence of nonlinearities into the DCF, the equivalent line fibre dispersion regarding nonlinearities is inbetween the dispersion of the SMF (17ps/nm/km) and the absolute dispersion of the DCF (100ps/nm/km), thus higher than SMF dispersion and resulting in lower tolerance to nonlinearities as in Cauvin & Frignac [105] or Petermann & Conrad [106].

This means that when using a Dispersion Compensating Module without nonlinearitiy instead of a standard DCF for a transmission system with fixed distance and fibre input powers, the Kerr-induced impairements are expected to be reduced for two cumulative reasons, first because of the reduced overall nonlinear phase shift, then because the penalty versus nonlinear phase relationship has changed towards more tolerance.

VI.2. Impact of span length on the accuracy of the nonlinear phase criterion at 10 and 40Gb/s

We report here 10 and 40Gb/s studies that enable to determine the impact of span length on the accuracy of the nonlinear phase criterion.

The experimental set-up is here identical to the one chosen for assessing the impact of DCF in Chapter 2 and section II.2. It represents a singly-periodic dispersion-managed, terrestrial, ultra-long haul link.

The 10Gb/s transmitter consists of a single channel at 1550nm or a WDM multiplex of 15 channels regularly spaced (50GHz) around 1550nm according to the ITU grid. For both cases, a NRZ modulation format with a 64-bit long De Bruijn sequence has been considered. For the WDM signal, each channel has the same polarization and the binary sequence is decorrelated with respect to the other channels with a random delay.

For the 40Gb/s studies, we have considered a single-channel configuration with NRZ format since for such a symbol rate, SPM is the predominant effect even for WDM configurations.

The transmission link consists of a concatenation of sections of line fibre and DCF separated by optical amplifiers, organized in an optimized singly-periodic dispersion-management scheme whatever power and distance. Two different types of line fibre have been considered : SMF, and LEAF fibres. The power into the DCF fibre has been chosen such that the nonlinearity can be neglected. The power into the line fibre has been fixed, and span length and number of spans are varied.

VI.2.1. 10Gb/s-modulated systems

Figure 3-24 represents different relationships between transmission penalty (OSNR penalty to get 10^{-5} BER) and nonlinear phase for different line fibre span lengths ranging between 10 and 100km, for single-channel and WDM 10Gb/s NRZ modulated transmission systems over dispersion-managed LEAF or SMF fibre sections.

Let us characterize for each fibre / channel configuration the inaccuracy of the nonlinear phase criterion due to span length in estimating the range of nonlinear phase values leading to 2dB penalty. For SMF-based transmission systems, this range amounts to 1.7dB in WDM configuration and 1.8dB in single-channel configuration. For LEAF based transmission systems, this range amounts to 1.8dB in WDM configuration and below 0.5dB in single-channel configuration. This clearly shows the dependence of those relationships on span length except for LEAF-based single-channel systems (using lower chromatic dispersion values for the line fibre would have lead to identical results as well).

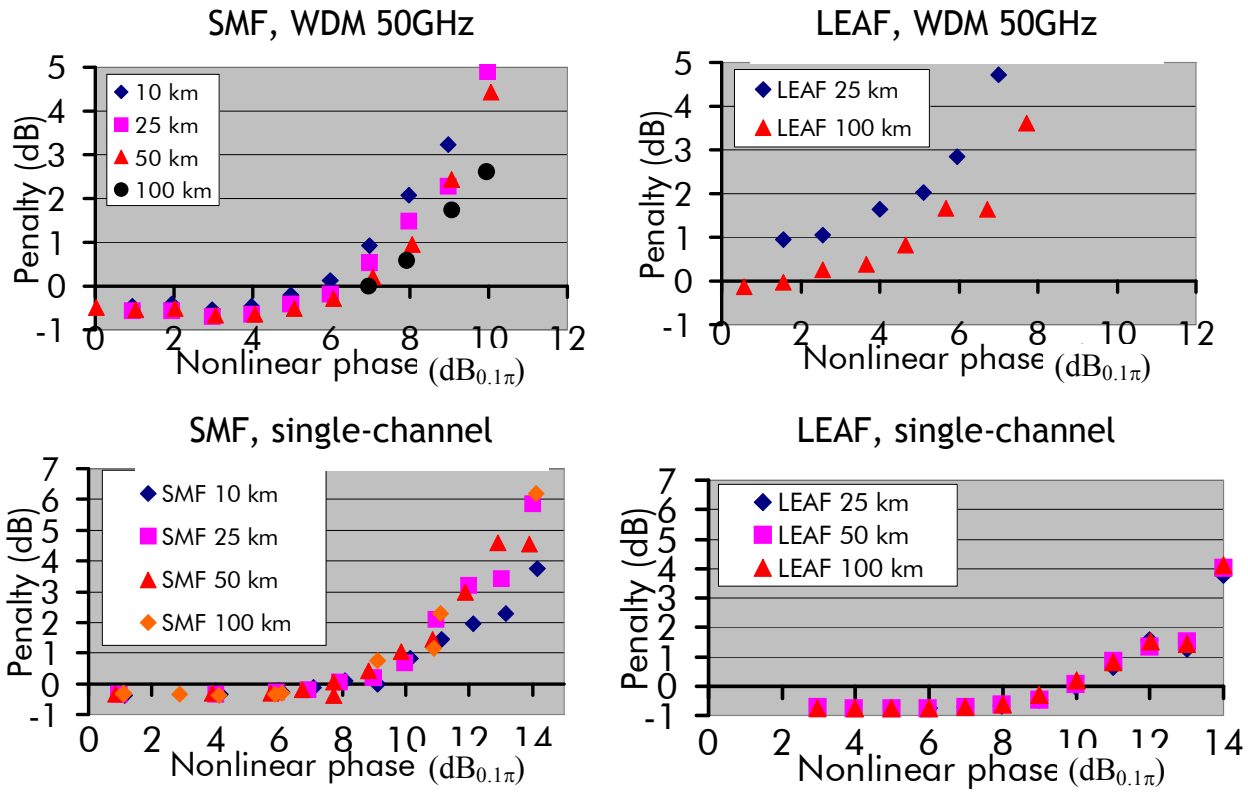

Figure 3-24: OSNR penalty (within 0.1nm for 10^{-5} BER) plots versus nonlinear phase(dB scale with respect to 0.1π) for different line fibre span lengths for 10.7Gb/s NRZ-modulated signals. Top figures correspond to WDM configurations, bottom figures to single-channel configurations ; left figures correspond to SMF line fibre type, right figures to LEAF line fibre type.

VI.2.2. 40Gb/s-modulated systems

As far as 40Gb/s systems are concerned, we investigate first SMF-based transmissions then LEAF-based transmissions.

Figure 3-25 represents the different relationships between penalty (OSNR penalty for 10^{-5} BER) and nonlinear phase for SMF-based transmission systems with optimized singly-periodic dispersion map whatever the distance; for SMF span lengths ranging between 10 and 80km, assuming 0.22dB/km fibre attenuation plus one extra configuration with 50km span length and 0.15dB/km attenuation. Such relationships have been obtained by fixing the fibre input power depending on span length and varying the transmission distance up to 30 spans, so as to ensure a constant range of investigated values of nonlinear phase for each span length (in detail, the SMF input power were respectively set to 8,6,5,4, 3 or 4dBm for span lengths of 10, 20, 30, 50 to 80, and 100km respectively). It appears that the lower the span length, the more tolerant to nonlinear phase the system becomes. The impact of span length appears much stronger than at 10Gb/s: the range of nonlinear phase values leading to 2dB OSNR penalty is already as wide as 3dB for span lengths between 20 and 100km. For the configuration with 10km-long SMF spans, the impact of nonlinearities is significantly different from the configurations with longer line fibre spans and we did not reach any positive penalty (in dB) even after 30 spans.

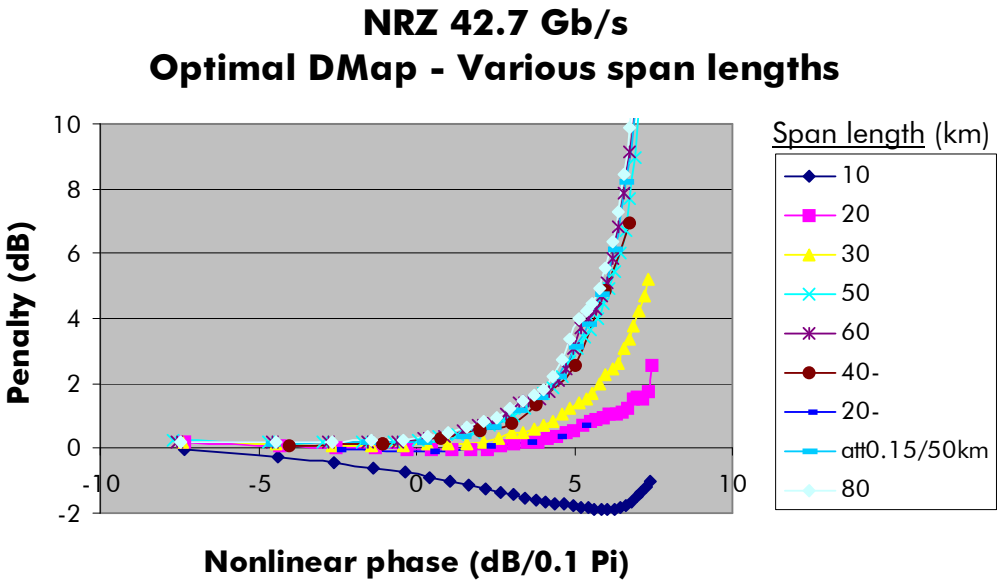

Figure 3-25 : Impact of span length for SMF-based 40G NRZ-modulated single-channel systems. OSNR penalty versus nonlinear phase for spans with attenuation 0.22dB/Km and lengths between 10 and 80km, and one span configuration with 0.15db/km attenuation and 50km length.

Figure 3-26 shows similar results for LEAF-based systems: it represents the impact of LEAF-span length (from 30 to 100km) on the relationship between penalty and nonlinear phase (obtained in varying the transmission distance from 3 to 39 spans with constant input powers into LEAF and DCF sections, respectively 2 and -5dBm). The range of nonlinear phase values leading to 2dB OSNR penalty appears to be as wide as 2dB for span lengths between 30 and 100km.

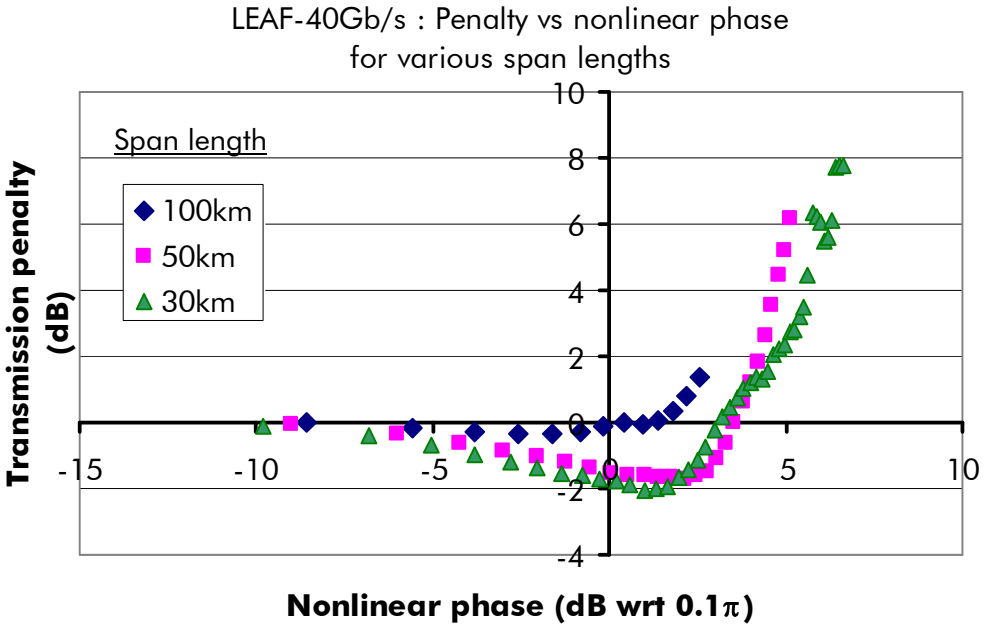

Figure 3-26 : Impact of span length for LEAF based 40G NRZ-modulated single-channel systems. OSNR penalty versus nonlinear phase for span lengths of 30, 50 and 100km.

Now that we have set the impact of span length on the deviation of the penalty versus nonlinear phase relationship, we will explain in the following how we can cope with that based on analytical consideration or using calibrations.

VI.2.3. Small-signal model-inspired adapted nonlinear phase for single-channel transmission systems

Model

If we refer to perturbative analyses such as the Phase to Intensity Conversion small-signal model yielding pretty good insight for the optimization of dispersion maps when considering low frequencies, one can analyze Equation (2-39) and see that for low pulsations ω the phase to intensity converted signal distortion corresponding to line fibre spans is proportional to the product between the nonlinear phase and a sum of parameters describing the dispersion map plus the product between local dispersion and an effective length:

$$PIC(\omega) \approx -\phi_{nl,tot} * \left(f(Dispersion\ Map) + D_{loc} \widetilde{L}_{eff} \right) \frac{P(z,\omega)}{\overline{P}} . \frac{\omega^2 \lambda^2}{4\pi . c}$$

$$with \begin{cases} \widetilde{L}_{eff} = \frac{1}{\alpha}\left(1 - \frac{Le^{-\alpha L}}{L_{eff}}\right), \\ f(Dispersion\ Map) = \Pr e - Dres + \frac{Nb_{spans/subdiv} - 1}{2} D_{res/span} + \frac{Nb_{subdiv} - 1}{2} D_{res/subdiv} \end{cases} \quad (3\text{-}8)$$

We can therefore infer that for optimized dispersion maps, the Kerr + Chromatic disperson may depend on the product between the nonlinear phase and the product $D_{loc}.\widetilde{L}_{eff}$. Such adapted nonlinear phase (in fact homogeneous to cumulated chromatic dispersion) that could be named as "nonlinear cumulated dispersion" could be summed for each fibre type (line fibre or DCF).

$$Nonlinear\ cumulated\ dispersion = \sum_{\substack{fiber\ sections \\ k}} \phi_{nl,k} D_{loc,k} \widetilde{L}_{eff,k} \quad (3\text{-}9)$$

In order to create a dimensionless parameter, we can consider the local dispersion in physical units (in ps^2/km) rather than in optical units (in ps/nm/km) and multiply by the square of the symbol rate B such that we get a normalized adapted nonlinear phase:

$$Adapted\ nonlinear\ phase = \sum_{\substack{fiber\ sections \\ k}} \phi_{nl,k} \beta_{2,loc,k} \widetilde{L}_{eff,k} . B^2 \quad (3\text{-}10)$$

This new parameter appears promising to catch the impact of cumulated nonlinearities in **single channel configurations**.

For instance, if we reconsider the **10Gb/s SMF**-based transmission systems studied in section II.2. accounting for the impact of DCF, we showed that the optimized linear combination of the nonlinear phases coming from SMF and DCF enabled to reduce the spread of modified nonlinear phase values leading to 2dB penalty from 2.5dB to less than 1.5dB whatever the input powers into the fibre types. For such optimal linear combination, a nonlinear phase value stemming from SMF is equivalent to 1.56 times the nonlinear phase stemming from DCF. When applying the proposed adapted nonlinear phase, we find a quasi-optimal configuration: for a model, a nonlinear phase value stemming from SMF is equivalent to 1.59 times the nonlinear phase stemming from DCF. This corresponds to the same minimum spread of phase values leading to 2dB penalty.

Let us now reconsider the **40Gb/s** transmission systems studied in the previous section. If we come back to the **SMF-based systems** with span lengths ranging from 20 to 100km and add results from section VI.1. including the impact of DCF nonlinearities for 100km-long spans, the range of nonlinear phases leading to 2dB penalty is as high as 4dB, as illustrated by Figure 3-27(left). This corresponds to a 4dB accuracy of the nonlinear phase criterion. When representing this penalty plots with respect to the adapted nonlinear phase, the spread

of phase values leading to 2dB penalty falls below 0.5dB, as illustrated by Figure 3-27(right), thus stressing the excellent accuracy of this new tool in such a configuration.

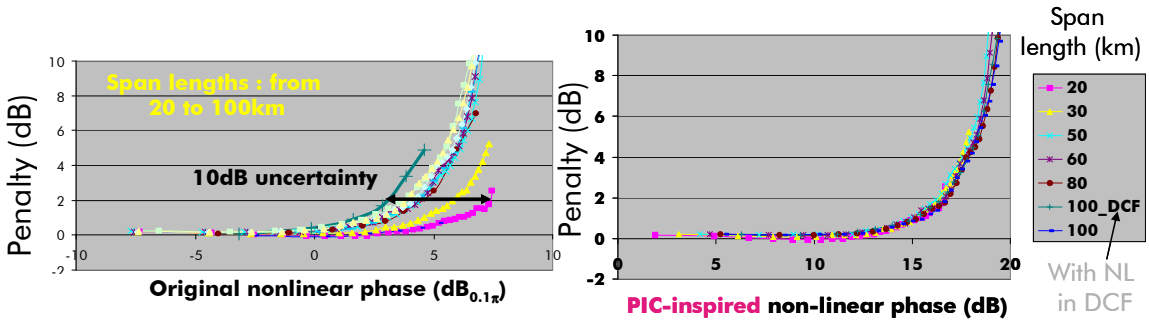

Figure 3-27 : SMF 40Gb/s, impact of span of span length and nonlinearities.
Left: Penalty vs nonlinear phase. Right: penalty vs PIC-inspired nonlinear phase from Eq. (3-10)

However the penalty curve corresponding to a span length of 10km does not match the other curves even when plotted against the adapted nonlinear phase: indeed the equivalent dispersion regime becomes significantly different such that strong negative penalties (downto -2dB, meaning signal quality improvement) can be observed for nonlinear phases lower than $\pi/2$ rad, while for higher span lengths, nonlinearities always cause detrimental effects and positive penalties. One reason for such discrepancies may come from the fact that for long spans, the propagation regime can be considered as highly dispersive: two frequencies separated by a 40GHz (corresponding to the bit-rate) are temporally shifted by dispersion over the effective length by 6 bit periods for 10km-long spans while they are decorrelated by 28 bit periods for 100km-long spans, where inter-pulse nonlinear interactions are dominant [105][109][110].

For the **LEAF-based transmission systems** with span lengths between 30 and 100km, the use of the **adapted nonlinear phase enables to reduce the spread of phase values leading to 2dB penalties from 2dB to 0.95dB** as illustrated by Figure 3-28. However, as for SMF-based transmissions with span lengths of 10km, the relationships between adapted nonlinear phase and penalty for the different LEAF span lengths tend to converge only in the moderately to highly nonlinear regime in presence of detrimental effect of nonlinearities while in the weakly nonlinear regime the adapted nonlinear phase cannot capture the larger signal improvements when span length becomes shorter, with measured negative penalties downto -0.3dB observed for 100km-long line fibre spans and downto -2dB for 30km-long spans. The explaination proposed for SMF-based transmission systems still stands here. Let us first consider the 100km-long transmission systems. Two frequencies separated by a 40GHz are temporally shifted by dispersion by 6 bit periods over the effective length (i.e. when signal power suffers from 4.3dB loss); in addition, if we also consider the nonlinear impact of DCF, we must take into account the fact that there is a balance between the 7dB reduction in the input power set into the DCF relative to line fibre and the 6.8dB increased confinement of light in DCF with respect to LEAF, as characterized by the ratios of the effective areas (resp. 15 and 72μm^2); thus the temporal shift over the length of DCF such that the power is reduced by the same loss as in the effective length of line fibre amounts to 30 bit-periods; here the regime highly dispersive can still be considered as highly dispersive because of the nonlinearities coming from DCF. For 30km-long spans of line fibre, we estimate that this temporal shift representative of the number of neighbouring bits impaired by nonlinear interactions is 4 bits over line fibre and 10 bits over DCF. The propagation regime is thus weakly dispersive both for line fibre and DCF.

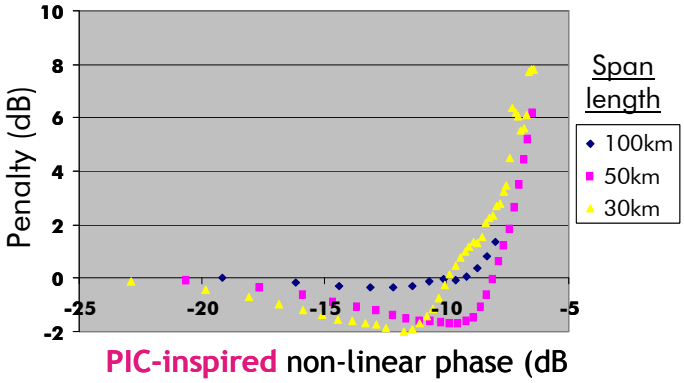

Figure 3-28 : LEAF 40Gb/s; impact of span of span length (30, 50, 100km) and nonlinearities. Penalty vs PIC-inspired nonlinear phase from Eq. (3-10)

All such results demonstrate the interest of such an adapted nonlinear phase parameter for single-channel transmission systems, essentially in the moderately-to-highly nonlinear regime that is often the critical regime that limits the reach of systems. The action of such a parameter is to linearly combine the nonlinear phase shifts from the different fibre sections with an increased detrimental impact of sections with longer length or higher dispersions, which is quite in line with the behaviour of single-channel transmission systems. **Conversely, 10G WDM transmission systems suffer from more penalties when fibre dispersion (in absolute values) or section length are lower (as can be deduced from Figure 3-24), and thus this "adapted" nonlinear phase is not adapted at all**.

VI.3. Impact of the choice of the threshold penalty in the definition of the weighted nonlinear phase

In order to complete the study around the weighted nonlinear phase we address here the impact of the reference penalty that leads to the determination of the nonlinear thresholds and enables to calculate a weighted nonlinear phase. The motivation lies in the fact that the choice of the reference penalty is arbitrary according to the definition and that different values can be considered in the literature. Sometimes such reference penalty values are also related to the maximum reach of transmission systems (as detailed in Chapter 5) as a trade-off between noise and nonlinearities and depend on the bit rate, modulation format, and dispersion management optimization schemes.

In order to address that issue, we reconsider the numerical study of section IV.2.2. for mixed SMF+LEAF systems using NRZ modulation format at 40Gb/s and resume from the measurements of Figure 3-16 (a-b-c).

On the one hand, we can measure the nonlinear thresholds for single-line-fibre type systems (SMF or LEAF) corresponding to reference penalies among 1, 1.5, 2, and 2.5dB. Then we can switch to mixed systems, apply the weighted nonlinear phase theory and estimate the expected nonlinear phase leading to one of those reference penalties depending on the relative nonlinear phase accumulated over SMF fibre sections with respect to the total accumulated nonlinear phase, following Equation (3-6). Such relationships are illustrated by the grey curves of *Figure 3-29* for reference penalties of 1, 1.5, 2, and 2.5dB from left to right plots respectively. On the other hand, the plots of Figure 3-16(c) are reprocessed: for each configuration of fibre arrangement and relative input power into SMF and LEAF fibres, we determine the total nonlinear phase yielding one of the abovementioned reference penalties. For each reference penalty, we then report the value of such nonlinear threshold against the relative nonlinear phase accumulated over SMF fibre sections with respect to the total accumulated nonlinear phase in *Figure 3-29*.

In a weak nonlinear regime (1dB penalty), the total nonlinear threshold of mixed systems directly stemming from simulation results follows a linear evolution with the relative nonlinear phase in SMF sections; this threshold is higher than the expected values derived from the weighted nonlinear criterion. For stronger nonlinear regimes (1.5dB or more penalties), we can observe discrepancies between SMF+LEAF systems (SMF line fibre sections followed by LEAF sections) and LEAF+SMF systems (LEAF line fibre sections followed by SMF sections): the nonlinear threshold of SMF+LEAF systems becomes lower than the predicted linear evolution and rather corresponds to the predictions of the weighted nonlinear criterion. It must be noted that in the strongest nonlinear regime (2.5dB penalty), the predictions of nonlinear threshold deduced from the weighted nonlinear criterion appear rather optimistic with respect to the LEAF+SMF case.

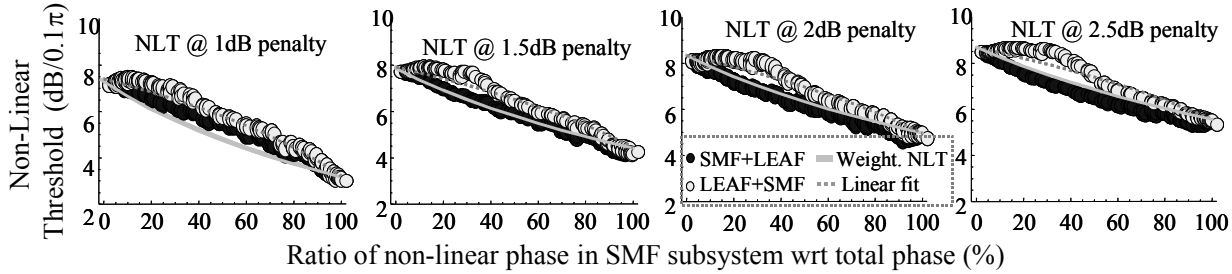

Figure 3-29: Evolution of total nonlinear phase leading to x dB-penalty for 40G NRZ SMF/LEAF heterogeneous systems as a function of the ratio of nonlinear phase coming from SMF sections

over the total nonlinear phase, for various distances, and input powers into SMF and LEAF sections, and for several reference penalty values x=1, 1.5, 2, 2.5dB (resp. plots a, b, c, and d)

For all choices of reference penalty and investigated configurations, the differences between the measured nonlinear threshold and the expected value derived from the weighted nonlinear criterion do not exceed 1dB (the differences range at most between -0.5 and +1dB).

This illustrates that the weighted nonlinear phase approximation can be used with confidence to estimate the tolerance to nonlinearities of mixed systems for different reference values of penalty.

3.VII. References

[95] J.-C. Antona, S. Bigo, J.-P. Faure, "Nonlinear cumulated phase as a criterion to assess performance of terrestrial WDM systems", in Proc. Optical Fibre Communications Conference (OFC'02), paper WX5, March 18-22, 2002, Anaheim, California, USA

[96] J.-C. Antona, S. Bigo, A.-S. Jehanno, "Performance Evaluation of WDM Transparent Networks Incorporating Various Fibre Types", Proceedings of ECOC'06, We.3.P.141, Sept. 2006, Cannes (France)

[97] J.-C. Antona, E. Seve, A. Pitilakis, P. Ramantanis, "Design and Performance Prediction in Meshed Networks with Mixed Fibre Types", in Proc. Optical Fibre Communications Conference (OFC'08), paper JThA48, February 24-28, 2008 San Diego, California, USA

[98] J.-C. Antona, M. Lefrançois, S. Bigo, G. Le Meur, "Investigation of Advanced Dispersion Management Techniques for Ultra-Long Haul Transmissions", Proceedings of ECOC'05, paper Mo.3.2.6, 2005, Glasgow (Scotland)

[99] J.-C. Antona, S. Bigo, "Physical Design and performance estimation of heterogeneous optical transmission systems", C.R. Physique 9 (2008), 963-984

[100] S. Bigo, Y. Frignac, J.-C. Antona, G. Charlet, "Design of multi-terabit/s terrestrial transmission systems facilitated by simple analytical tools", in 'Optical Communications 2. Transmission systems and networks' (Annales des Télécommunications Tome 58 N° 11-12 Novembre-Décembre 2003), pp.1757-1784

[101] P. Henri, C. Simonneau, F. Leplingard, J.-C. Antona, L. Lorcy, "Experimental investigation of the quality of transmission in transparent mesh networks with mixed fibre types", Proceedings of OFC 2010, paper JThA1, March 2010, San Diego (Ca)

[102] A. Klekamp, R. Dischler, W. Idler, "Impairments of bit-to-bit alternate-polarization on nonlinear threshold, CD and DGD tolerance of 43 Gb/s ASK and DPSK formats", Optical Fibre Communication Conference, 2005. Technical Digest. OFC/NFOEC, Volume: 5, paper OFN3

[103] R Dischler, A. Klekamp, J. Lazaro, W. Idler , "Experimental comparison of nonlinear threshold and optimum pre dispersion of 43 Gb/s ASK and DPSK formats", in Proc. OFC 2004, 23-27 Feb. 2004, Vol. 1, paper TuF4

[104] W. Idler, A. Klekamp, R. Dischler, B. Wedding, "Advantages of frequency shift keying in 10 Gb/s systems", 2004 IEEE/LEOS Workshop on Advanced Modulation Formats, 2004 , Page(s): 51 – 52, paper FD3.

[105] A. Cauvin, Y. Frignac, S. Bigo, "Nonlinear impairments at various bit-rates in single-channel dispersion-managed systems", Electronics Letters, Nov 13th 2003, vol. 39, No23

[106] B. Konrad and K. Petermann, "Optimum fibre dispersion in high-speed TDM systems," IEEE Photon. Technol. Lett., vol. 13, no. 4, pp. 299–301, Apr. 2001

[107] Y. Frignac et al, "Variations avec le débit de modulation de la performance de transmission sur fibre optique", Journées Nationales d'Optique Guidée, JNOG'2004

[108] Y. Frignac, "Contribution à l'ingénierie des systèmes de transmissions terrestres sur fibre optique utilisant le multiplexage en longueur d'onde de canaux modulés au débit de 40 Gb/s", Thèse présentée devant l'ENST, Paris (2003)

[109] L.K. Wickham, R.-J. Essiambre, A.H. Gnauck, P.J. Winzer, A.R. Chraplyvy, "Bit pattern length dependence of intrachannel nonlinearities in pseudolinear transmission", Photonics Technology Letters, IEEE, Vol 16 (2004), No 6, pp 1591-1593

[110] M. Lefrançois, E. Barnasson, G. Charlet, J.-C. Antona, S. Bigo, "Relative impact of the different intrachannel nonlinear effects over 43 Gb/s transmissions with varying fibre dispersion", Proceedings of ECOC 2005, Page(s): 133 - 134 vol.2.

[111] G. Bellotti, S. Bigo, “Cross-Phase Modulation Suppressor for multi-span dispersion-managed WDM transmissions”, IEEE Photonics Technology Letters, vol 12, No6, June 2000

[112] E. Desurvire et al, « Erbium-doped fibre amplifiers, Device and System Developments », Wiley & sons, Chapter 7, New York, 2002

[113] S. Pachnike et al, “Experimental investigation of XPM-induced birefringence in mixed-fibre transparent optical networks”, Proceedings of OFC’06, paper JThB9; March 2006, Anaheim (Ca)

[114] S. Pachnike, E. Voges, E. De Man, E. Gottwald, and J. Reichert, “Experimental investigation of XPM-induced birefringence in mixed-fibre transparent optical networks”, Proceedings of OFC’06, paper JThB9; March 2006, Anaheim (Ca)

[115] D. Breuer, N. Hanik, C. Caspar, F. Raub, G. Bramann, M. Rohde, E.-J. Bachus, S. McLeod, M. Edwards, “Mixed Fibre Infrastructures in Long Haul WDM-Transmission”, OSA Journal of Optical Communications, 2004, Issue 1, pp 10-13

[116] D. Z. Chen, G. Wellbrock, S. J. Penticost, D. Patel, C. Rasmussen, M. C. ChiIders, X. Yaog, M.Y. Frankel, “World's first 40 Gbps overlay on a field-deployed, 10 Gbps, mixed-fibre, 1200 km, ultra long-haul system”, Proceedings of OFC’05, paper OTuH4, March 2005, Anaheim (Ca)

[117] M.H. Eiselt, L. D. Garrett, J. M. Wiesenfeld, W. D. Bragg, J. L. Cox, A. D. Hill, K. L. Sharp, B. T. Teipen, R. J. Baca, M. R. Young, R. W. Tkach, “Field trial of a 1250-km Private Optical Network Based on a Single-Fibre, Shared-Amplifier WDM System”, Proceedings of OFC’06, paper NThF3, March 2006, Anaheim (Ca)

[118] P. J. Winzer and R. J. Essiambre, “Advanced Optical Modulation Formats,” Proceedings of the IEEE, Vol. 94, No. 5, May 2006

[119] S. Bigo, W. Idler, J.-C. Antona, G. Charlet, C. Simonneau, M. Gorlier, M. Molina, S. Borne, C. de Barros, P. Sillard, P. Tran, R. Dischler, W. Poehlmann, P. Nouchi, Y. Frignac; “Transmission of 125 WDM channels at 42.7Gbit/s (5 Tbit/s capacity) over 12x100 km of TeraLightTM Ultra fibre”, Proc. of ECOC’01, Post-Deadline session, vol.6, , pp. 2- 3 , Amsterdam (Netherlands), September 2001

[120] G. Charlet, W. Idler, R. Dischler, J.-C. Antona, P. Tran, S. Bigo, “3.2Tbit/s (80x42.7Gb/s) C-Band transmission over 9x100km of TeraLightTM fibre with 50GHz channel spacing”, in Optical Amplifiers and Their Applications, J. Nagel, S. Namiki, and L. Spiekman, eds., Vol. 77 of OSA Trends in Optics and Photonics Series (Optical Society of America, 2002), paper PD1, Vancouver, Canada, July 2002

[121] G. Charlet, J.-C. Antona, S. Lanne, P. Tran, W. Idler, M. Gorlier, S. Borne, A. Klekamp, C. Simonneau, L. Pierre, Y. Frignac, M. Molina, F. Beaumont, J.-P. Hamaide, S. Bigo, “6.4Tb/s (159x42.7Gb/s) Capacity over 21x100km using Bandwidth-Limited Phase-Shaped Binary Transmission”, Proc. of ECOC’02, Post-Deadline paper PD 4.1, Copenhagen (Denmark), Sept 2002

[122] G. Charlet, J.-C. Antona, S. Lanne, S. Bigo, “2100 to 2700km distance using Bandwidth-Limited Phase-Shaped Binary Transmission at 6.3Tb/s capacity”, Proc. of OFC’2003, paper WE3, Atlanta (Georgia), USA, March 2003

[123] R. I. Killey, P. M. Watts, V. Mikhailov, M. Glick, and P. Bayvel, "Electronic dispersion compensation by signal predistortion using digital signal processing and a dual-drive Mach–Zehnder modulator", IEEE Photon. Technol. Lett., vol. 17, no. 3, pp.714 -716 , 2005.

[124] D. McGhan , C. Laperle , A. Savchenko , C. Li , G. Mak and M. O.Sullivan, "5120-km RZ-DPSK transmission over G.652 fibre at 10 Gb/s without optical dispersion compensation", IEEE Photon. Technol. Lett., vol. 18, pp.400 2006

Chapter 4 : Quality of Transmission Estimators

Contents

4.I. Introduction

I.1. Motivation

The physical infrastructure of a terrestrial optical network is usually quite complex due to its intrinsically high heterogeneity and the number of physical effects jointly impairing the signal. Such heterogeneity mainly stems from network topology and topography issues (likely to lead to unequal node or amplifier spacing), from the partial knowledge of the characteristics of the deployed links and from the evolutions and extensions of the network during its lifetime (involving the interconnection of different generations and types of fibres and network elements). Moreover, multiple sources of degradation jointly affect the signal propagation such as the accumulation of noise, optical nonlinearities, chromatic dispersion issues, polarization issues, and phenomena related to the crossing of wavelength-selective optical nodes such as inline optical filtering and crosstalk induced by insufficient isolation between the signals entering the nodes from multiple directions.

Due to such complexity, design tools, based on numerical simulations, experiments and theoretical back-up, are essential to predict system performance accurately, and to guide the choices of components arrangements and settings for optimal performance. Besides, hybrid transparent networks have the additional requirement that the feasibility of a connection has to be known before its establishment. This allows a determination of where to regenerate the signal if required. Since it is impossible to consider a priori all the connections that will be established in the network, a simple scheme is necessary to obtain the required information. Eventually, accurate and simple performance prediction tools are also crucial for dynamic transparent networks for the possibly dynamic assignment of new light-paths over operational networks [126].

It is therefore key to benefit from an accurate, easy to compute quality of transmission (QoT) estimator. In order to remain useful when ruling an optical network, where the number of possible connections grows supra-linearly with the number of nodes, the set of information to collect for QoT estimator should be reduced. One practical way to do so is to choose "cumulative" information. We mean by "cumulative" that the information may be updated after each amplifier span or node section of the connection without losing information. For instance, the OSNR (Optical Signal to Noise Ratio) is a cumulative parameter but not the BER (Bit Error Rate). We suggest to use few parameters, the bunch of which we can call the QoT vector [135][136]. From such a QoT vector, we can estimate the BER through a quality of transmission estimation function (or QoT function). The accuracy of the BER predictions will depend on the inherent accuracy of the QoT function: such accuracy will particularly depend on the relevance of the components of the QoT vector, on their number; it will also depend on the accuracy of the measurements done to build the QoT function, and on the engineering rules applied to build the different transmission links of the network (dispersion management, heterogeneity, etc). Additionally, the accuracy of the BER predictions will also depend on how accurate the QoT vector is known prior to setting a connection or dimensioning a network (field measurements or not, statistical knowledge coming from product datasheets, evolution with time…).

Computation time is also a very serious issue. It is particularly stringent in the operation phase of a network, when demands of reconfiguration may arrive to follow an evolution of the traffic or in order to quickly restore connections after detection of a failure in one or several network sections. The time constraint may seem less stringent in the planning phase of a network but it remains an important issue. Indeed, the planning phase actually corresponds to the

dimensioning of a whole network with a possibly high number of nodes and connections to establish, thus the overall computation time may be substantial. Besides, the planning phase is most often part of the phase consisting in establishing a detailed bid for the carrier, following a request proposed to multiple system-vendors. Hence time becomes a valuable asset: an overall computation time lower than an hour or even a few hours is usually required for the whole network dimensioning. Conversely, a computation time of one day is not affordable.

Here, we propose to build a QoT estimator that goes beyond the (weighted) nonlinear phase criterion from Chapters 2 and 3, which QoT vector includes not only the Kerr-induced non-linear phase ϕ_{NL}, but also the OSNR, the residual dispersion Dres (accumulated dispersion along a transmission link), the PMD coefficient. We also consider the number of nodes in a lightpath, to account for their filtering impact on performance as well as the inband crosstalk due to unperfect isolation of blocked signals with the same wavelength as the considered signal.

I.2. Outline of the chapter

In this chapter, we propose to build a simple, versatile and accurate enough model of quality of transmission estimation based on numerical and experimental investigations about possibility to decouple the impact of physical effects. The typical application is to help deciding on the optical feasibility of connections at the planning stage of optical networks but also during the operation of reconfigurable, GMPLS-controlled optical networks. We will not address here the issue of the overall accuracy of the BER prediction that also depends on measurement conditions for the establishment of the QoT function and on the knowledge on the QoT vector in field operations. Insight on such issues is given in [144][145][146][147][138] where the notions of confidence levels associated with a predictions are defined and used to manage an optical network.

Here, we first describe the prerequisites of a good QoT estimator and describe the usual solutions proposed in the literature.

In a second step, we assess the evolution of the Q-factor with the OSNR in presence of other propagation effects and derive a preliminary quality of transmission estimator enabling to separate amplifier noise contributions from other sources of signal impairments.

In a third step, we will explain a method to assess the joint impact of non-noise-related propagation effects in order to build a modular and accurate quality of transmission estimator enabling to separate as much as possible the contributions of all the sources of signal impairments. We mainly consider in this section transmission systems with single type of line fibre but will present as well a natural extension of the quality of transmission estimator to the mixed-line-fibre-type configurations based on the use of the weighted nonlinear phase detailed in Chapter 3.

In a fourth step, we will discuss the required complexity of the models of quality of transmission estimator depending on their planned utilization. We will first focus on the proposed model, then will give a partial example of experimental establishment of the estimator, then will compare this model with other existing models from simple models (maximum reach estimation based on worst case calibration, use of the sole OSNR parameter) to complex ones (such as [127]).

4.II. Litterature on QoT estimators and limitations

In this paragraph, we discuss the existing types of physical performance estimation models and their benefits and limitations depending on the application (physical design of a network prior to an installation, live operation of the network) and on the degree of heterogeneity of the considered network.

Today, most studies regarding network planning, routing and wavelength assignment are considering physical impairments using different kinds of physical performance estimators. A detailed overview of the possible performance estimators can be found in [154]. One of the simplest ways to account for that is to consider the transmission reach [155], or the OSNR degradation [156] that can be compared to a pre-established threshold enabling to decide whether the connection is optically feasible or not [154]. A combination of thresholds corresponding to different physical impairments can be considered as well [157][158][160][161]. More advanced QoT estimators aim to predict a Q factor [127][152][153][159][164][162][163]. For instance the model from [127] calculates a Q factor based on a few calibrations and analytical calculations of the impact of several effects (cross-channel nonlinear effects, PMD...). The modular QoT model that we will detail in the following also enables to account quite simply and accurately for multiple effects after a calibration phase.

Generic models of QoT estimators

Besides the two obvious models based on maximum reach or minimum OSNR, two models are generally considered to predict the BER (or rather Q factor) in the literature: a first model [127] [148], denoted as Gaussian-Q model, aims to calculate an analytic expression of the Q factor, based on perturbations of Equation (1-2), and a second model [126], denoted as QoT-model, based on the addition of OSNR penalties stemming from the different physical effects.

In the Gaussian-Q model [127], the Q factor expression is calculated after separation between deterministic signal degradations (through the estimation of an eye opening penalty as a function of Dispersion, SPM, and one condition of Differential Group Delay, i.e. an instantaneous realization of PMD), and noise-like perturbations, including ASE noise, but also models for XPM/GVD-induced phase and intensity noises, FWM-induced noise, crosstalk, … Deterministic impairments lead to an estimation of the difference between mean intensities from marks or spaces in Equation (1-2), while noise-like processes impact the calculation of standard deviations of marks and spaces, enabling to calculate a Q factor. PMD impact can be accounted for by the estimation of the mean PMD value of the link, as well as the assumption of Maxwellian distribution for possible instantaneous PMD values. This way, it is possible to weigh Q factor by the distribution of possible PMD instantaneous values to obtain the outage probability (probability that Q factor is lower than a reference value Q_{ref}). The transmission link will therefore be considered as feasible provided the Q factor is higher than Q_{ref} and the outage probability lower than a reference value such as 10-5, i.e. Q higher than Q_{ref} with a probability of $(1\text{-}10^{-5})$.

$$Q = \frac{"\mu_1 - \mu_0"\left(\overline{P}, \Phi_{nl}, D_{cum}, DGD, ...\right)}{"\sigma_1 + \sigma_0"\left(\overline{P}, OSNR, XPM, FWM\right)} \Rightarrow \text{Outage Probability} = \int_0^{Q_{ref}} pdf(Q).dQ \qquad (4\text{-}1)$$

In Equation (4-1), "μ_1-μ_0" is the relative power of marks versus spaces at sampling time, that depends on the average signal power $\overline{P}$, the non-linear phase shift ϕnl, the accumulated (or residual) dispersion over the link Dres, and the Differential Group Delay DGD (i.e. PMD instantaneous value); σ_1 and σ_0 respectively correspond to the standard deviations of signal power for marks and spaces at sampling time, include Amplified Spontaneous Emission-

related contributions, estimates of the intensity noise regarding XPM and FWM, and depend on the signal power distribution of each channel, optical signal to noise ratio OSNR … From the calculation of Q factor for each value of DGD, and from the known distribution of DGD, one obtains the power density function (pdf) of Q factor, thus allowing to derive the outage probability that Q is lower than Q_{ref}. The expression of Equation (4-1) is meant for intensity-modulated signals with direct detection. Equivalent models exist for intensity [152] or phase-modulated signals with differential detection [129].

The usual alternative model, that we describe in more details in the following chapter and in [126], is not based on the analytical expression of Q factor since its connection with BER assumes Gaussian distributions of the received intensities at receiver side, which is an assumption that does not hold in many configurations. The QoT-model is rather based on the separation between actual OSNR and required OSNR for a reference Q factor Qref, as proposed in Chapter 1:

$$Q(\Phi_{nl}, D_{res}, OSNR, PMD, XTalk, ...) = Q_{ref} + \zeta(\Phi_{nl}, D_{res}).\left(OSNR - ROSNR_{Q_{ref}}(\Phi_{nl}, D_{res}, PMD, XTalk, ...)\right) \quad (4\text{-}2)$$

Here, the assessment of lightpath feasibility corresponds to estimating whether the actual OSNR is higher than the required OSNR corresponding to modulation limitations and system impairments. Particularly, $ROSNR_{Q_{ref}}$ corresponds to the required OSNR after transmission, to guarantee a Q factor equal to Q_{ref}, and depends on non-linear phase, residual dispersion, PMD and crosstalk terms. The function $\zeta(\Phi_{nl}, D_{res})$ is related to the observation that Q factor (in dB) generally scales proportionally with OSNR (in dB) with a slope ζ lower than 1 in usual conditions of OSNR, due to pattern effects [126].[128].

Equation (4-2) can be rewritten in terms of OSNR penalties:

$$Q(\Phi_{nl}, D_{res}, OSNR, PMD, XTalk, ...) = Q_{ref} + \zeta(\Phi_{nl}, D_{res}).\left(OSNR - ROSNR_{Q_{ref},btb} - Pen_{Q_{ref}}(\Phi_{nl}, D_{res}, PMD, XTalk, ...)\right) \quad (4\text{-}3)$$

with Pen_{Qref} (…) being the OSNR penalty after propagation, for reference Q factor Qref, equal to the difference in the required OSNR for reference Qref, after propagation ($ROSNR_{Q_{ref}}$) and without propagation $ROSNR_{Q_{ref},btb}$.

Eventually, assuming that the joint induced penalty due to the different sources of degradation is equal to the sum of the induced penalties of each source, we get:

$$Q(\Phi_{nl}, D_{res}, OSNR, PMD, XTalk, ...) = Q_{ref} + \zeta(\Phi_{nl}, D_{res}).\left(OSNR - OSNR^{Q_{ref}}_{req,btb} - Pen^{Q_{ref}}(\Phi_{nl}, D_{res}) - Pen^{Q_{ref}}(PMD) - Pen^{Q_{ref}}(XTalk)\right) \quad (4\text{-}4)$$

This assumption enables to separately characterize the impact of the different phenomena, and get an overall estimation of system performance. It must be noted that the non-linear and dispersive terms cannot be treated separately, due to their strong interplay.

The model can be refined by dealing differently with deterministic and time-varying or statistical effects (due to PMD, or partial knowledge of some system features for instance). The easiest simplification of the QoT model consists in estimating a tolerable amount of penalty for each physical effect, thus a maximum amount of the quantifier for this effect and an overall tolerated penalty, or minimum required OSNR; feasibility assessment consists in checking that the limit is not crossed for each effect, and that the actual OSNR is higher than the minimum required OSNR.

For both models, a performance estimator can be built based on analytical considerations and measurements stemming from experiments or numerical simulations, such as evolution of the eye opening or penalty with non-linearities, for a pre-defined dispersion management scheme, evolution with PMD, crosstalk, accumulated dispersion….

Limitations of the physical performance estimators

The maximum reach or minimum OSNR-based estimators are by far the simplest QoT estimators that can be computed in routing algorithms. Simplicity is their main advantage.

However, as mentioned earlier, networks are intrinsically heterogeneous. One first cause of heterogeneity comes from length of inter-amplifier line fibre section which usually varies from one section to another between 10 and 130km. This source of heterogeneity makes the reference to any achievable distance irrelevant in practice. Indeed, let us assume a network composed of WDM dispersion-managed links always using the same type of line fibre. Let the fibre attenuation be 0.23dB/km and the span length either 100km or 50km (leading to 23 or 11.5dB span loss respectively). Eventually we consider here that the limiting impairments are noise and optical nonlinearities. Then, if we optimize the input power into each span according to the rules of Chapter 5, we can expect that the total achievable reach can be obtained with Equation (5-5). It comes that using 50km-long spans instead of 100km-long spans will enable increase the number of traversed spans by $(Loss_{100km,dB}\text{-}Loss_{50km,dB})/2 = 5.75dB$, which translates into an increase of reach by 2.75dB, i.e. 88%. Under such assumptions, the reach of optical connections using short spans can be 88% higher than the reach of optical connection using long spans. As a consequence, even if a "maximum-reach" estimator [155] is easy to use in most Routing and Wavelength Assignment algorithms, it can not be considered for practical systems due to its inability to account for the span loss variations.

In other publications, comparing the OSNR with a threshold OSNR target is often referred as a standalone candidate to enable the decision regarding the feasibility of a connection [154][156]. By definition, this estimation accounts for noise accumulation. In first order, it can account as well for the nonlinearities: if we overlook other signal degradation sources than noise and nonlinearities, or consider the induced penalty as constant, we can ideally optimize the power into each line fibre span depending on its length, as abovementioned. Under such assumptions, we show in Chapter 5 that nonlinear and noise constraints become equal. However such model does not allow any power imbalance from the optimum value and does not allow releasing or tightening the constraints on the target OSNR depending on the actual PMD of the traversed fibre or the actual filtering of the nodes… The power imbalance issue is particularly limiting since in practice the power cannot be optimized for all the channels, due to spectral variations of the gains of the optical amplifiers, due to Raman-induced tilt causing the depletion of low wavelength channel and the amplification of high-wavelength channels in each fibre span. The imbalances can be predicted after calibration of the amplifiers responses but are not necessarily corrected.

It is thus preferable to be account for the joint impact of multiple propagation effects with a method preferably different from the setting of fesibility thresholds to each source of propagation impairment. Therefore, the model from [127][148] appears as much more complete than the previous models. The main limitations come from the nature of the model and possibly from the complexity and time of computation of the variances [152] (but the model can be simplified provided assumptions on dispersion management [150], naturally at the expense of accuracy). Fundamentally, such a model is based on the assumption of a two states-signal impacted by Gaussian noise. The Q factor is assessed by the difference in the mean intensities of the two detected states for marks and spaces, divided by the sum of the standard deviations of noise over marks then spaces. The difference in the mean intensities of the two detected states 1 or 0 accounts may be calibrated by measurements of the eye opening penalties induced by Self-Phase Modulation, Chromatic Dispersion, filtering and to a certain extent Polarization Mode Dispersion. The Gaussian noise is composed of beatings between signal and Amplified Spontaneous Emission for marks and spaces, of crosstalk arising when traversing optical nodes and of a calculation of XPM [151] and FWM-induced

intensity noise [148] stemming from the different channels, based on small-signal models similar to the PIC described in Chapter 2.

From an accuracy point of view, the model from Pachnicke [127] [148] may look like the basic QoT model as defined in Equation (4-4) as far as SPM, filtering or PMD are concerned. Yet it does not account for the evolution of the derivative ζ of Q versus OSNR (in dB/dB scale) induced by the non-Gaussian distribution of detected marks and spaces because of SPM, filtering or PMD. Such a derivative, as we will show in the following, could be reduced by 30-40% due to propagation impairments: it means that a 3dB variation in the OSNR may correspond to a 3dB variation of the Q factor in absence of signal degradations while it may correspond to only 2dB variation of the Q factor in presence of signal degradations. Such behaviour is not captured by [127]. For the same reasons, the model will miss the possibly substantial variations of the Non-Linear Threshold with OSNR and/or Q; for instance, the NLT may vary over 2.8dB for bit error rates between 10^{-7} and 10^{-3} for 10Gb/s LEAF-based system (as shown in Figure 4-2). Such inaccuracies could be limiting when actually designing a system, leading to too optimistic predictions or provisioning of unnecessary system margins.

From a computation point of view, the use of analytical expressions to assess the FWM/XPM terms depending on the position and power of each possible neighbouring channel and requiring integrations variances considerably slows down the calculation speed of a performance estimator compared to the QoT estimator proposed in Equation (4-4). This can be particularly critical when applying such tools to the process of lightpath establishment and resource allocation when designing a network or even more when reconfiguring a network already in operation. For each requested connection between distant nodes corresponding, the performance will be assessed for all paths imagined by the Routing and Wavelength Assignment algorithms, such that the computation time of the dimensioning process is likely to become limited by the computation time of the physical performance estimations [162]. As a result, approximate estimations of the variances based on simplified models and/or interpolations from a few measurements may be necessary to keep computation time manageable [150].

The model from Equation (4-4) can be seen as an attempt to bring accurate estimates of the Q factor with low computation time, thanks to a strong analysis of the degradation of the Q factor with multiple sources of impairments enabling to build a simple model, and thanks to a limited number of calibration experiments.

Now we will explain how to build such an estimator.

4.III. Evolution of Q factor and OSNR and set-up of a QoT estimator separating noise from other sources of impairments

With respect to the goal of this Chapter to build a QoT estimator accounting for multiple propagation effects, this section focuses on the first step towards this goal: build a QoT estimator enabling to separate amplifier noise from other sources of impairments.

To do so, we analyse the relationship between the Q factor and the OSNR, through numerical and analytical studies before proposing a QoT model. We first derive a basic QoT model based on Gaussian noise distribution showing that the Q factor (in linear scale) may scale proportionally to the square root of the OSNR as mentioned in Chapter 1. Then we compare this model with numerical simulations and show that a reasonable assumption for 10Gb/s modulated systems is to consider that the Q factor rather scales proportionally with a power of the square root of the OSNR because of the non-degenerated levels of detected "1s" and "0s" stemming from linear and nonlinear distortions. This will enable us to build this first QoT model separating noise from other sources of signal distrortions.

III.1. Basic model linking Q-factor and OSNR

This section aims to come back to the basic model proposed by D. Penninckx in [130][131] linking the Q factor, the OSNR and the eye aperture for a basic transmission system with on-off keying modulation. From such an expression we derive a first relationship between Q, OSNR and OSNR penalties induced by non-noise propagation effects.

III.1.1. Link between Q, OSNR and Eye aperture

Let us consider an intensity-modulated optical field $E_{in}(t)$ and white Gaussian noise generated by the optical amplifiers (described by N_{ASE} as the noise power spectral density per polarization) being sent into before a direct-detection photoreceiver. The direct-detection receiver can be seen as an optical filter (characterized by pulse response $h_o(t)$), followed by a perfect photodiode, an electrical filter (characterized by pulse response $h_e(t)$), and a perfect decision circuit that periodically sorts the received signals into "1s" and "0s" depending on their relative amplitude with respect to a decision threshold. We can assume that for OSNR higher than 10dB within 0.1nm and extinction ratios lower than 13dB, the electrical noise mainly consists of Gaussian signal-ASE beating on the received "1" and "0" symbols.

The signal voltage $\mu(t)$ before the decision circuit can be expressed as (assuming perfect optoelectronic conversion efficiency):

$$\mu(t) = h_e * |h_o * E_{in}|^2 (t_i), \quad \text{or } \mu(t) = h_e * |E|^2 (t) \tag{4-5}$$

with E(t) the optically filtered signal, before the photodiode and * stands for the convolution product.

Let μ_i be the electrical signal amplitude of the bit i at decision time, σ_i be the standard deviation due to the electrical noise on the received bit i at the decision time, P_i be the occurrence probability of bit i, and D be the decision threshold. Then the Bit Error Rate (BER) can be easily calculated as:

$$BER = \frac{1}{2}\sum_{bit\ i} P_i \times Erfc\left(\left|\frac{D-\mu_i}{\sqrt{2}\sigma_i}\right|\right) \quad (4\text{-}6)$$

where Erfc() is the complementary error function.

If the eye diagram is homogeneous, i.e. if the received symbols "1" (resp. "0") have the same intensity μ_1 (resp. μ_0) and standard deviation σ_1 (resp. σ_0), and assuming identical occurrence probabilities of symbols "1" and "0", Equation (4-3) becomes:

$$BER = \frac{1}{4}\sum_{i=0,1} Erfc\left(\left|\frac{D-\mu_i}{\sqrt{2}\sigma_i}\right|\right) = \frac{1}{2}Erfc\left(\frac{Q}{\sqrt{2}}\right) \quad (4\text{-}7)$$

with

$$Q = \frac{\mu_1 - \mu_0}{\sigma_1 + \sigma_0} \quad (4\text{-}8)$$

Noise mainly comes from the beating of Amplified Spontaneous Emission (ASE) with itself or with the signal. The total electrical signal + noise voltage is indeed equal to:

$$\mu(t) + \underbrace{n_{el}(t)}_{\substack{electrical\\noise}} = h_e * \left|E + h_o * n\right|^2(t) = \mu(t) + \underbrace{h_e * \left|h_o * n\right|^2(t)}_{ASE-ASE\ beating} + \underbrace{2h_e * \Re e\left(E^*.\left(h_o * n\right)\right)(t)}_{signal-ASE\ beating} \quad (4\text{-}9)$$

The variance of signal-ASE beating noise can be derived after a few calculations as:

$$\sigma_{Sig-Ase}{}^2(t) = 2N_{ASE}\,\Re e\iint d\tau_1 d\tau_2\, h_e(t-\tau_1)h_e{}^*(t-\tau_2)\,E(\tau_1)\,E^*(\tau_2)\left(h_o{}^*(-) * h_o\right)(\tau_2-\tau_1) \quad (4\text{-}10)$$

with the function "$h_o(-)$" such that "$h_o(-)$"(t) = $h_o(-t)$.

The variance of ASE-ASE beating noise, independent on time, can be expressed as well:

$$\sigma_{Ase-Ase}{}^2 = 2N_{ASE}{}^2 \int d\tau\, h_e{}^*(\tau)\left(h_e * \left|h_o(-) * h_o\right|^2\right)(\tau) \quad (4\text{-}11)$$

where the factor 2 accounts for the 2 polarization modes.

In most of the cases, the extinction ratios of signals being less than 13dB and the OSNR larger than 10dB, one can assume the beating between signal and ASE being the dominant noise contribution for both marks and spaces.

If we normalize the field after optical filtering as $E(t) = \sqrt{\overline{P}}\,e(t)$, with $\overline{P}$ the average power, $\sigma_{sig\text{-}ase}$ can be re-written as:

$$\sigma_{Sig-Ase}{}^2 = \overline{P}\,N_{ase}\,B_{elec}\,s^2{}_{sig-ase} \quad (4\text{-}12)$$

with $B_{elec} = \frac{1}{2}\int_{-\infty}^{+\infty}\left|h_e\right|^2(t)\,dt$, the electrical bandwidth and a dimensionless $s_{sig\text{-}ase}$, depending on signal distortions:

$$s_{Sig-Ase}{}^2(t) = \frac{2}{B_{elec}}\,\Re e\iint d\tau_1 d\tau_2\, h_e(t-\tau_1)h_e{}^*(t-\tau_2)\,e(\tau_1)\,e^*(\tau_2)\left(h_o{}^*(-) * h_o\right)(\tau_2-\tau_1) \quad (4\text{-}13)$$

We can notice that for NRZ format, neglecting the role of optical filtering leads to $s_{sig\text{-}ase}=2$ and the well known formula.

$$\sigma^2{}_{sig-Ase,k=0,1} = 4N_{Ase}B_{elec}P_k \quad (4\text{-}14)$$

The expression of Q factor can then be derived as:

$$Q = \frac{\overline{P}}{\sqrt{N_{Ase}\overline{P}.B_{elec}}}\left(\frac{h_e * |e|^2(\text{sampling time bit 1}) - h_e * |e|^2(\text{sampling time bit 0})}{s_{sig-ase,1} + s_{sig,ase,0}}\right) \quad (4\text{-}15)$$

$$Q = \sqrt{\frac{OSNR\,B_{ref}}{B_{elec}}}\underbrace{\left(\frac{h_e * |e|^2(\text{sampling time bit 1}) - h_e * |e|^2(\text{sampling time bit 0})}{s_{sig-ase,1} + s_{sig,ase,0}}\right)}_{Q_1} \quad (4\text{-}16)$$

with B_{ref} as the bandwidth in which the Optical Signal to Noise Ratio (OSNR) is given.

Therefore, Q factor expression can be split in an OSNR contribution and another contribution describing the eye distortion and the way the optical noise (dimensionless) is filtered in the receiver, called Q_1.

In most cases, the optical bandwidth is considered larger than the electrical bandwidth, and the expressions can be simplified:

$$\sigma^2{}_{sig-Ase} = 2N_{Ase}|h_e|^2 * |E|^2(t) \text{ , or } s^2{}_{sig-Ase} = 2\frac{|h_e|^2 * |e|^2(t)}{B_{elec}} \quad (4\text{-}17)$$

If we then assume that the time response of the electrical filter is short with respect to the variations of E(t) in the vicinity of the decision time, E(t) can be considered as constant equal to $\sqrt{P_{1,0}}$ and then $\mu(t) = E^2(t)$ and $\sigma^2{}_{sig-Ase} = 4N_{Ase}B_{elec}|E|^2(t)$, so that:

$$Q = Q'\sqrt{\frac{OSNR\,B_{ref}}{B_{elec}}} \quad (4\text{-}18)$$

Where

$$Q' := \frac{\sqrt{P_1} - \sqrt{P_0}}{\sqrt{2\overline{P}}} \quad (4\text{-}19)$$

Q' corresponds to an eye aperture assessment and is called geometrical eye aperture [130][131].

As for the assumption of the predominance of the beating between ASE and Signal, simple calculations of the Q factor including variances of Ase-Ase beating as well as Signal-Ase beating show that Q' model tends to overestimate the Q factor by less than 5% in the case of NRZ format at 10Gb/s, with 13dB extinction ratio and OSNR of 13dB in 0.1nm: lower extinction ratios, or larger OSNR and/or bit rates will quickly diminish the uncertainty of the model.

III.1.2. Towards a basic QoT estimator

We have shown with a simple model that Q factor appears as the trade-off between the orthogonal contributions of noise and signal distortion. A candidate for a quality of transmission estimator describing the joint impact of OSNR and effects x,y,z could therefore exploit this and be based on the following model:

$$Q(x,y,z,OSNR) = \sqrt{\frac{OSNR\,B_{ref}}{B_{elec}}}.Q'(x,y,z) \quad (4\text{-}20)$$

This equation can be rewritten in dB scale, as:

$$Q^2{}_{dB}(x,y,z,OSNR) = OSNR_{dB} + 10\log\left(\frac{B_{ref}}{B_{elec}}\right) + Q'^2{}_{dB}(x,y,z) \quad (4\text{-}21)$$

In a more generic way, if we define Q° as a reference Q factor, and $ROSNR_{Q°}$ the required OSNR to ensure a Q factor equal to Q°, then:

$$Q^2{}_{dB}(x,y,z,OSNR) = Q° + OSNR_{dB} - ROSNR_{Q°,dB}(x,y,z) \quad (4\text{-}22)$$

with

$$ROSNR_{Q°,dB}(x,y,z) = Q° - Q'^2{}_{dB}(x,y,z) - 10\log\left(\frac{B_{ref}}{B_{elec}}\right) \quad (4\text{-}23)$$

This formulation is particularly interesting since the required OSNR to get a given Q factor can be experimentally estimated through measurements of the OSNR and the bit-error-rate after propagation and addition of noise at receiver end. The main task will then reside in the determination of the evolution of the required OSNR with the non-noise-related propagation effects.

We can derive from Equation (4-23) the OSNR penalty:

$$\begin{aligned} Pen_{Q°,dB}(x,y,z) &= ROSNR_{Q°,dB}(x,y,z) - ROSNR_{Q°,dB}(0,0,0) \\ &= Q'^2{}_{dB}(0,0,0) - Q'^2{}_{dB}(x,y,z) \end{aligned} \quad (4\text{-}24)$$

And we notice that the penalty is independent on the target Q factor.

Equation (4-22) can then be rewritten as:

$$Q^2{}_{dB}(x,y,z,OSNR) = Q° + OSNR_{dB} - Pen_{Q°,dB}(x,y,z) - ROSNR_{Q°,dB}(0,0,0)$$

or equivalently

$$Q^2{}_{dB}(x,y,z,OSNR) = OSNR_{dB} - Pen_{Q°,dB}(x,y,z) + Q'^2{}_{dB}(btb) + 10\log\left(\frac{B_{ref}}{B_{elec}}\right) \quad (4\text{-}25)$$

Such a relationship is the first brick enabling to build a QoT estimator. As such, it is the starting point of the original studies we have conducted.

III.2. Towards a refined QoT estimator.separating contributions from noise and other sources of impairments

The QoT estimator that we have just proposed in Equation (4-25) is really basic. In this section, we investigate its relevance through comparisons with numerical simulations and propose an advanced version of this QoT estimator as well as physical interpretation of the necessary adjustments.

III.2.1. Numerical studies

In order to test the validity of the previous model, we first performed numerical simulations of 10Gb/s WDM terrestrial transmission systems over SMF or LEAF™ fibre around 1550nm.

The transmitter side consists of 16 NRZ channels modulated at 10.7Gb/s with randomly decorrelated 128-bit long De Bruijn sequences, and spaced by 50GHz. The transmission link consists of a concatenation of subdivisions of four 80km-long spans of SMF or LEAF. Each subdivision is dispersion-managed so that the residual dispersion per subdivision is zero at 1550nm (which is typical of transparent optical networks) and consists of a dispersion pre-compensation section of -800ps/nm (resp. 0ps/nm) and inline dispersion compensation modules such that the residual dispersion per span is +100ps/nm/span (resp. -100ps/nm/span) for the SMF fibre transmission system (resp. the LEAF fibre transmission system). For sake of simplicity, the wavelength-dependence of chromatic dispersion is overlooked.

The number of transmitted subdivisions is varied as well as the line fibre input power (from -4 to +4dBm), while the DCF input power is kept 7dB below the line fibre input power. At receiver end, the residual dispersion is set to 0ps/nm. Noise is added to signal only before the receiver, so that the OSNR (within 0.1nm) is adjusted between 10 and 24dB. Bit-error rate is measured for the 10 central channels, then averaged, before the equivalent Q factor is derived.

Figure 4-1 represents the Q-factor as a function of nonlinear phase shift, for different conditions of power, distances and OSNR, for LEAF-based transmission systems. Nonlinear phase shifts are here expressed in dB scale with respect to an arbitrary reference R° as $\phi_{nl,dB,R°}=10\log_{10}(\phi_{nl,rad}/R°)$, with R° corresponding here to the nonlinear phase shift accumulated after one span of transmission fibre and DCF with 0dBm line fibre input power. In other words, the x-axis corresponds to the integrated power expressed in dBm (see Chapter 2), i.e. $\phi_{nl,dB,R°}=10\log_{10}(N) + P_{in,dBm}$ with N representing the number of transmission sections and $P_{in,dBm}$ the transmission fibre input power (in dBm).

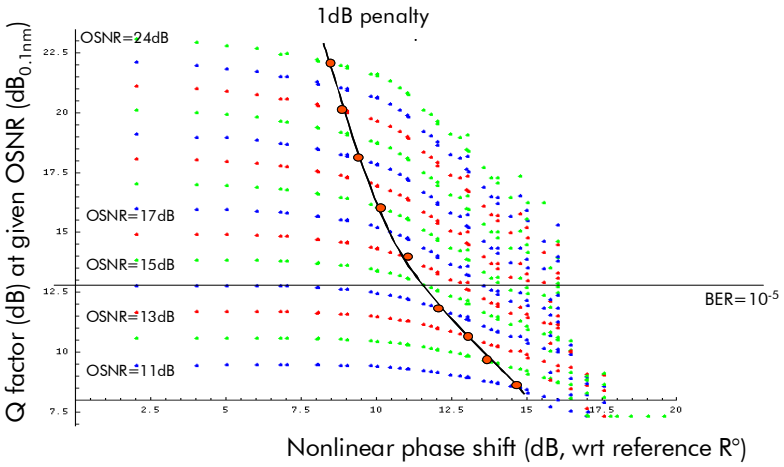

Figure 4-1 : Q factor versus nonlinear phase shift and OSNR for a LEAF-based WDM 16x10Gb/s terrestrial transmission system. Nonlinear phase shift is expressed in dB scale with respect to an arbitrary reference R° ($\phi_{nl,dB,R°}=10\log_{10}(\phi_{nl,rad}/R°)$. R° is here chosen such that $\phi_{nl,dB,R°}=0$dB for transmission over 1 span LEAF with 0dBm input power into LEAF fibre.

We can first observe the bi-univocal relationship between Q factor and nonlinear phase, for a given OSNR, whatever the distance or fibre input power. Such relationships can not be superposed from one condition of OSNR to another. Indeed, in the weak nonlinear regime , for a nonlinear phase shift 2.5dB higher than R°, a 10dB change of OSNR (from 11 to 21dB) results in a 9.8dB variation of the Q factor (from 10.3 to 20.1 dB); this almost corresponds to the ratio of 1dB Q variation per dB of OSNR change predicted by the previously proposed model. Conversely, in a stronger nonlinear regime, for a nonlinear phase shift 15dB higher than R°, a 10dB change of OSNR (from 11 to 21dB) results in a 6dB variation of the Q factor

(from 8.4 to 14.4dB), corresponding to a ratio of 0.6dB of Q variation per dB of OSNR change.

We can conclude that the ratio between variations of Q factor and OSNR, $\partial Q_{dB} / \partial OSNR_{dB}$, named as ζ in the following, is not constant and depends at least on the nonlinear phase shift. Consequently, the OSNR penalties are expected to depend on the reference Q factor, thus highlighting the limitations of the basic model predictions. This point is illustrated by Figure 4-2 representing the required OSNR to ensure given BERs (10^{-3}, 10^{-5}, 10^{-7}) as a function of the nonlinear phase shift; particularly, the nonlinear phase shift values leading to 1dB penalty range over almost 3dB depending on the reference BER: 11.1dB higher than R° for a BER of 10^{-7}, 13.9dB higher than R° for a BER of 10^{-3}. This highlights that the notions of required OSNR penalties or nonlinear threshold cannot be dissociated from the reference BER.

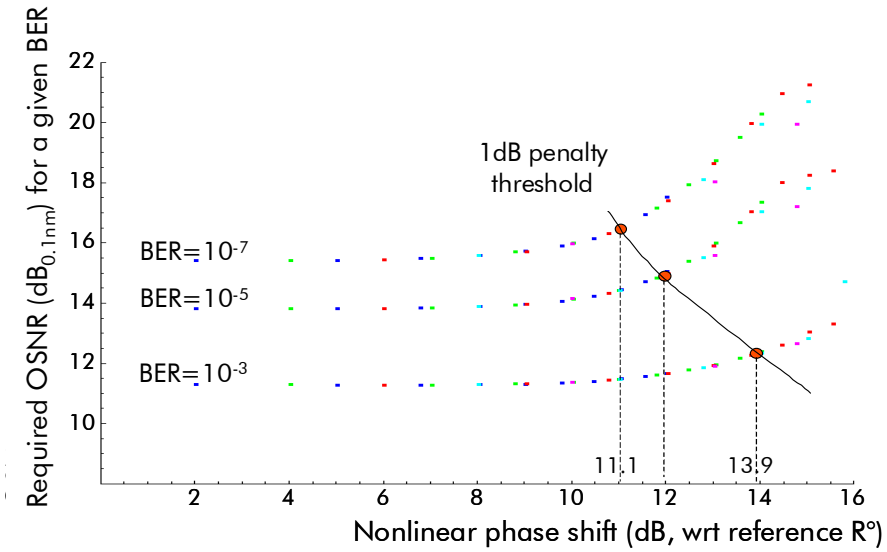

Figure 4-2 : LEAF-based Nx10Gb/s WDM transmission system: required OSNR (within 0.1nm) to get BERs of 10^{-3}, 10^{-5}, or 10^{-7} as a function of nonlinear phase shift.

Now we investigate more thoroughly the relationship between Q factor and OSNR for a few representative values of nonlinear phase shift from 5dB to 15dB higher than R°, respectively corresponding to propagation regimes with no transmission penalty and with an OSNR penalty to get 10^{-5} BER higher than 2dB. We can observe on Figure 4-3-Left that whatever the nonlinear phase shift, the relationship between Q factor (in dB) and OSNR (in dB) can be considered as linear over the range of OSNR between 11 and 22dB (within 0.1nm). As abovementioned, this plot illustrates that the derivative of Q versus OSNR (in dB/dB scale) is 1 for weak values of nonlinear phase, and falls to 0.5 for higher values. The same behaviour can be observed on SMF-based terrestrial systems, as illustrated by Figure 4-3-Right: Q factor (in dB) still varies linearly with the OSNR and the derivative ζ of Q versus OSNR decreases as nonlinear phase shift grows, but remains closer to 1 than for LEAF-based systems: ζ is 0.75dB/dB for SMF systems with a nonlinear phase shift 17.5dB higher than $R°_{SMF}$, while it amounts to 0.5dB/dB for LEAF systems with a nonlinear phase shift 15dB higher than $R°_{LEAF}$. Note here that due to its definition, R° values are different for SMF or LEAF configurations.

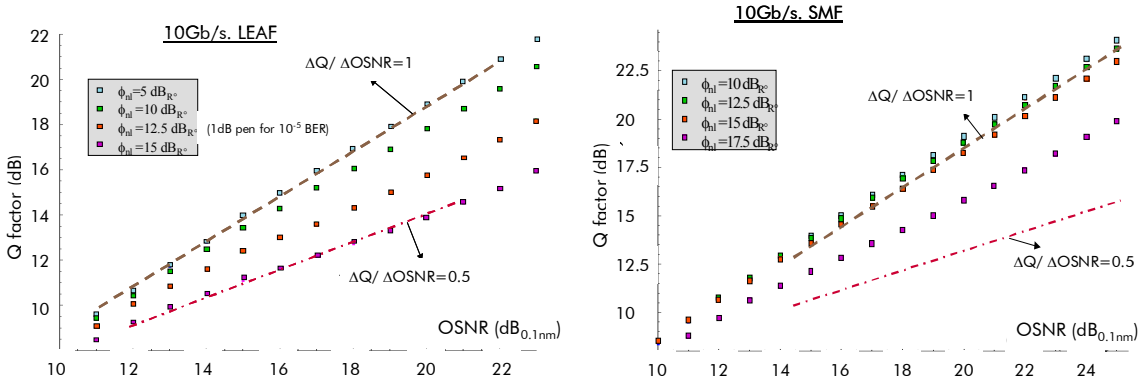

Figure 4-3 : Q factor versus OSNR, for given amounts of nonlinear phase shifts.
Left: WDM Nx10Gb/s systems based on LEAF fibre. Right: WDM Nx10Gb/s systems based on SMF fibre

The observed quasi-linear relationship between Q and OSNR (in dB scales) within the usual range of OSNR (between 11 and 22dB) has been confirmed for other types of transmission systems involving different bit-rates of fibres than the one considered here, such that this characteristic could be exploited to build a quality of transmission estimator. However, contrary to the predictions of Equation (4-22), the slope ζ of this relationship does not remain equal to 1 whatever the propagation effects, but is found to be a decreasing function of the nonlinear phase shift. It was also found to depend on fibre type and dispersion map.

and refinement of the Q versus OSNR relationship

III.2.2. QoT estimator expression

Extrapolating from the previous results, we can build a QoT estimator based on the observed linear evolution of Q (in dB) with OSNR (in dB). Equation (4-22) can then be generalized accounting for this slope ζ as:

$$Q^2{}_{dB}(x,y,z,OSNR) = Q^\circ + \zeta(x,y,z).\left(OSNR_{dB} - ROSNR_{Q^\circ,dB}(x,y,z)\right) \qquad (4\text{-}26)$$

(where x,y,z are representative of non-noise propagation effects such as nonlinear phase shift, residual dispersion, polarization mode dispersion, in-band crosstalk and the number of cascaded filters)

It can be rewritten in terms of OSNR penalties:

$$Q^2{}_{dB}(x,y,z,OSNR) = Q^\circ + \zeta(x,y,z).\left(OSNR_{dB} - ROSNR_{Q^\circ,dB}(0,0,0) - Pen_{Q^\circ,dB}(x,y,z)\right) \qquad (4\text{-}27)$$

(where $ROSNR_{Q^\circ,dB}(0,0,0)$ stands for the required OSNR in back to back to ensure a Q factor equal to Q°, in absence of detrimental propagation effects).

The proposed formulation of the evolution of Q factor in presence of multiple effects enables to separate the impact of noise from other transmission effects. The impact of noise is accounted for the required OSNR to ensure a target Q factor, while the impacts of the other transmission effects are accounted for by the transmission penalty and ζ function.

III.2.3. Interpretation of the linear relationship between Q and OSNR

In order to support the numerical observations, we propose an interpretation to the quasi-linear relation between Q factor and OSNR as well as the origin of this slope ζ lower than 1 in presence of nonlinearities, inspired by discussions with Prof. A. Bononi. The above-described model corresponding to the detection of NRZ symbols 1 and 0 with well defined intensities in presence of Gaussian ASE-Signal beating predicts this linear relationship with a slope ζ=1. To

understand why this slope decreases in presence of nonlinearities, we propose first to analyze the eye diagrams after transmission: Figure 4-4 represents a series of noiseless eye diagrams obtained for the central channel after transmission over the LEAF-based system for different values of nonlinear phase shifts ranging from 5dB to 15dB higher than R°, as well as the corresponding ζ factor.

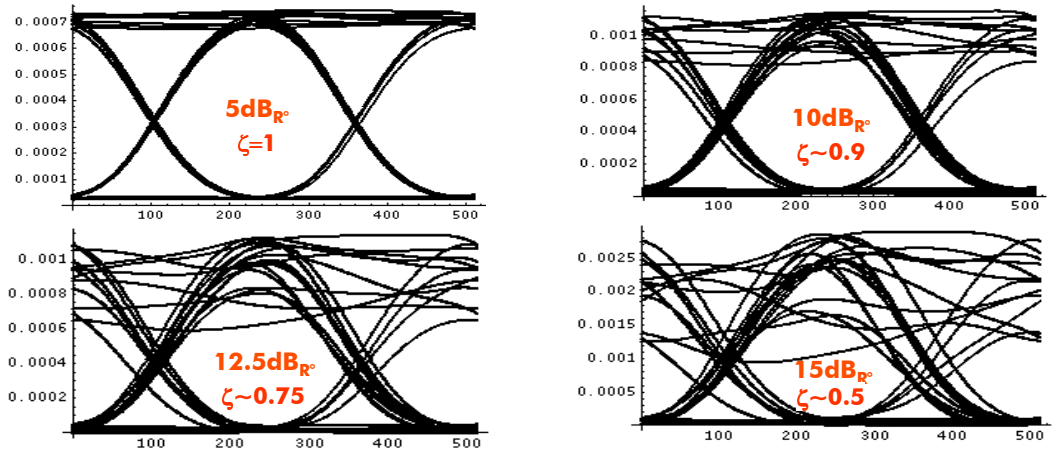

Figure 4-4 : Evolution of the eye diagrams and $\zeta = \partial Q_{dB} / \partial OSNR_{dB}$ *for different amounts of nonlinear phase shifts expressed in dB$_{R°}$ scale (as in Figure 4-1). LEAF-based Nx10Gb/s transmission system.*

We can observe a correlation between the decrease of the slope ζ and the degradation of the eye opening, or more precisely a correlation with an inhomogeneous degradation of the eye opening due to patterning effects leading to non-degenerate levels of detected 1s and 0s. At 10Gb/s, the intra-channel nonlinear effects concern interactions within only a few neighbouring bits (that can be estimated using [165]), such that the main sources of pattern-dependent distortions are Four-Wave Mixing and Cross-Phase Modulation. If confirmed, this hypothesis could explain why ζ varies less for SMF-based transmissions rather than LEAF-based transmissions since cross-channel effects have a weaker impact over the highly-dispersive SMF fibre. Such an assumption can be supported by a basic model and numerical simulations.

Indeed, let us come back to the BER model from the beginning of this section, with incoming on-off keying modulated signal and additive Gaussian noise into a direct detection photoreceiver.

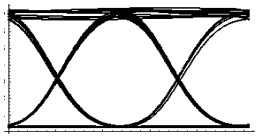

We previously showed that if the eye is homogeneous, i.e. if the noiseless intensities of marks (resp. spaces) are identical, then the BER is directly linked to the Q factor by Equation (4-7) and the Q factor (in dB) is shown to vary linearly with the OSNR (in dB) with a slope ζ=1dB/dB, as illustrated by Equation (4-22).

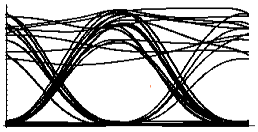

Let us now consider an inhomogeneous eye with non-degenerate levels for the marks and the spaces. Intuitively, two extreme regimes are of particular interest: for very high and very low OSNR values. For very high OSNR values, we expect the BER to be essentially determined by the error rate related to the mark with the lowest detected (noiseless) intensity and the space with the highest noiseless intensity. Such error rate associated to the worst traces can be calculated analytically as done previously, and we expect the same conclusions, i.e. a linear evolution of Q with OSNR with a slope of 1dB/dB, associated to the worst-trace eye aperture. The total BER will be the product of this worst-trace error rate and the probability of occurrence of this worst case. The derived Q-factor from the total BER (following Equation (4-7)) is also expected to follow the same evolution with the OSNR. Conversely, for very low values of OSNR, we can

expect the distribution of noise to be larger than the dispersion of the noiseless detected intensities for marks or spaces, so that the calculation of the BER can be essentially determined by an equivalent 2-level system characterized by the average intensities of the marks and spaces. Thus we should also expect a linear evolution of Q with OSNR with 1dB/dB slope, associated to the average eye aperture. We therefore expect that the curve describing the Q factor evolution with OSNR is between both mentioned parallel asymptotes, with a slope lower than 1, as illustrated by Figure 4-5-Left.

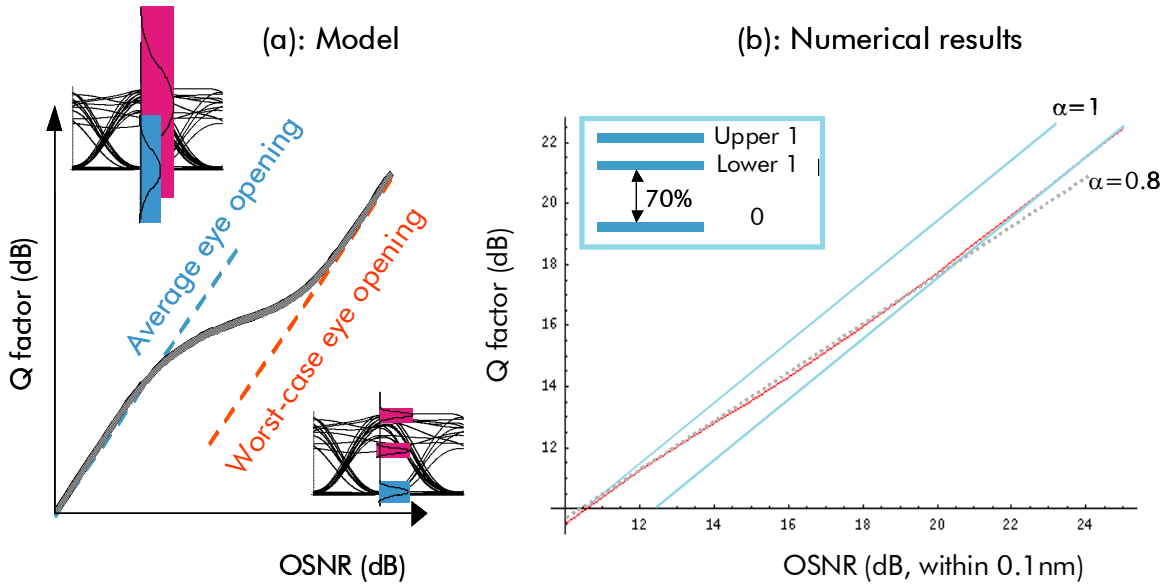

Figure 4-5: Q factor versus OSNR for an inhomogeneous eye diagram.
(a): Basic model with unity slope asymptotes corresponding to low OSNR and high OSNR behaviours, resp. linked to average and worst case eye opening; captions represent noiseless eye diagrams in such regimes along with distribution of noise for marks and spaces.
(b): numerical results obtained for a three state-eye diagram (one level for the spaces with reference power P° and probability of occurrence 0.5, and two levels for the marks with powers 20P° and 14P° and probabilities of occurrence of 0.45 and 0.05). Red curve: derived Q factor from computed BER. Blue curves: slope-1 asymptotes. Dashed grey line: linear approximation of computed Q factor vs OSNR with slope 0.45.

In order to check this hypothesis, we computed the BER of a modulated signal characterized by 13dB extinction ratio, with 10 spaces with identical power, 9 marks with identical power plus one additional mark with 30% less power. Figure 4-5-b represents then the derived Q factor from the computed BER as a function of the OSNR for this system, and clearly shows the two unit-slope asymptotes corresponding to average and worst-case eye openings, as well as the transition region that can be easily approximated by a linear curve with ζ=0.8dB/dB slope for OSNRs between 11 and 21dB.

As a consequence, considering a linear behaviour of Q versus OSNR (in dB) for OSNRs between 11-21dB (within 0.1nm) seems a fair enough approximation with a strong likelihood to exploit it in the constuction o a QoT estimator. We must however keep in mind that the slope of this linear evolution depends on pattern-dependent signal degradations induced by physical effects quantified by the nonlinear phase shift such as Cross-Phase Modulation, Four-Wave Mixing, Self-Phase Modulation in highly dispersive transmission regimes (high symbol rates and/or high values of average residual dispersion per span); we also expect an impact of total accumulated dispersion, Polarization Mode Dispersion and filtering issues. Figure 4-6 stresses that particular point: it depicts the evolution of the slope ζ as a function of nonlinear phase shift for the LEAF-based transmission system and for two values of residual dispersions, 0 and 400ps/nm. More particularly, let us consider a nonlinear phase shift 12.7dB higher

than R°. While it corresponds to 1dB penalty (within 0.1dB accuracy) for both values of residual dispersion (in agreement with Figure 4-2 for zero residual dispersion), Figure 4-6 shows that ζ is 0.74, respectively 0.84dB/dB for a residual dispersion of 400, respectively 0ps/nm.

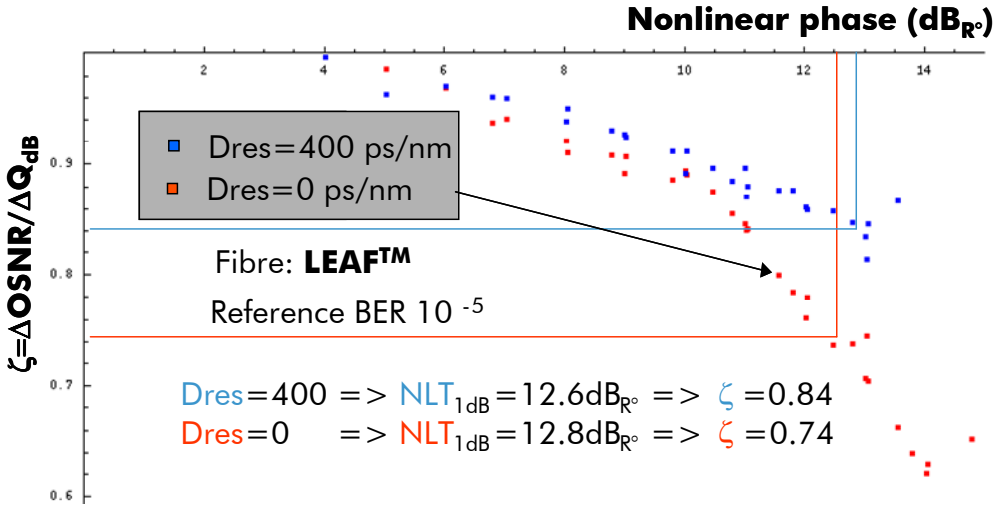

Figure 4-6 : Evolution of the slope ζ of the relation Q / OSNR as a function of the nonlinear phase for residual dispersions of 0 (red dots) or 400ps/nm (blue dots). Type of fibre: LEAF. Bit Rate: 10.7Gb/s

III.2.4. Conclusion

We have proposed a QoT model enabling to capture the evolution of Q factor in presence of multiple effects and particularly enabling to separate the impact of noise from other transmission effects. The impact of noise is accounted for the required OSNR to ensure a target Q factor, while the impacts of the other transmission effects are accounted for by the transmission penalty and ζ functions.

In the following section, we propose to develop further the QoT model so as to account simply for the impact of non-noise sources of signal degradation, which amounts to build models to estimate the penalties and the ζ function influenced by a mix of propagation effects. Then we will discuss the accuracy and complexity of the final proposition of QoT model.

4.IV. Joint impact of non-noise-related propagation impairments and establishment of a modular quality of transmission estimator

After building a QoT model enabling to separate noise from other sources of impairments, we propose now a method to come up with a QoT estimator enabling to separate the impact of non-noise-related signal degradations. In particular, we investigate in a first step the separate impact of nonlinearities, PMD or inline filtering on the penalty and on the ζ function. In a second step we investigate their joint impact in order to come out with a proposal of a "separated effects"-QoT estimator. We do not claim that the few examples that enable here to build this QoT estimator are sufficient to ensure a total confidence in the tool but the method will remain valid with more in-depth investigations.

Such results were obtained in 2009 through the training period of a 6-month student, Pascal Mahou, that I have supervised in association with Florence Leplingard.

IV.1. Investigation of the impact of a single propagation effect on the QoT estimator

Here we investigate the separate impact of nonlinearities, PMD and inline filtering on the quality of transmission of a WDM 43Gb/s PDPSK-modulated transmission link, by numerical as well as experimental means. We first consider the evolution of penalty, then of the ζ function.

The system under study consists of the transmission of eleven PDPSK-modulated channels at 43Gb/s with 50GHz spacing over a typical dispersion-managed terrestrial link including 100km-long SSMF spans and dual-stage Erbium-doped fibre amplifiers.

IV.1.1. Evolution of penalty with nonlinearities, inline filtering or PMD

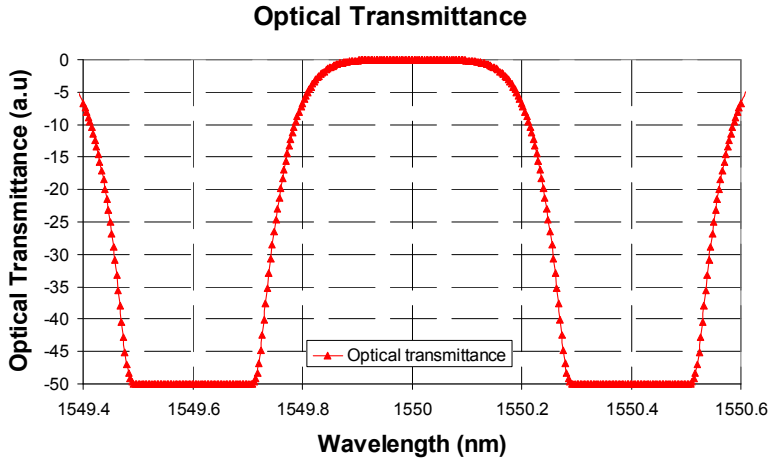

Figure 4-7 : Typical filtering function of a WSS for passing central channel at 1550nm and blocked neighbouring channels at 1549.6 and 1550.4nm

The isolated impact of filtering is illustrated by Figure 4-8-a with the description of the set-up on the left plot, and the numerically-estimated evolution of the OSNR penalty for BER of 10^{-5} and 10^{-3} as a function of the number of cascaded filtering functions. Each filtering function

corresponds to the most impairing response of one JDSU Wavelength-Selective Switch (WSS) typical of the ROADMs used in optical networks that emulates the separation of each channel from each neighbours (here we separated odd and even channels then recombined them after inserting random phase and delay shifts). It typically takes 12 WSS to get 1dB penalty for a BER of 10^{-5}. The tolerance to 1dB penalty increases up to 15 WSS for a BER of 10^{-3}. This tolerance is quite high for usual 40G systems. In order to further assess the joint impact of filtering and nonlinearities, we will consider narrower filtering functions every 3 spans so as to get 1dB penalty for 10^{-5} BER with 8 filtering functions.

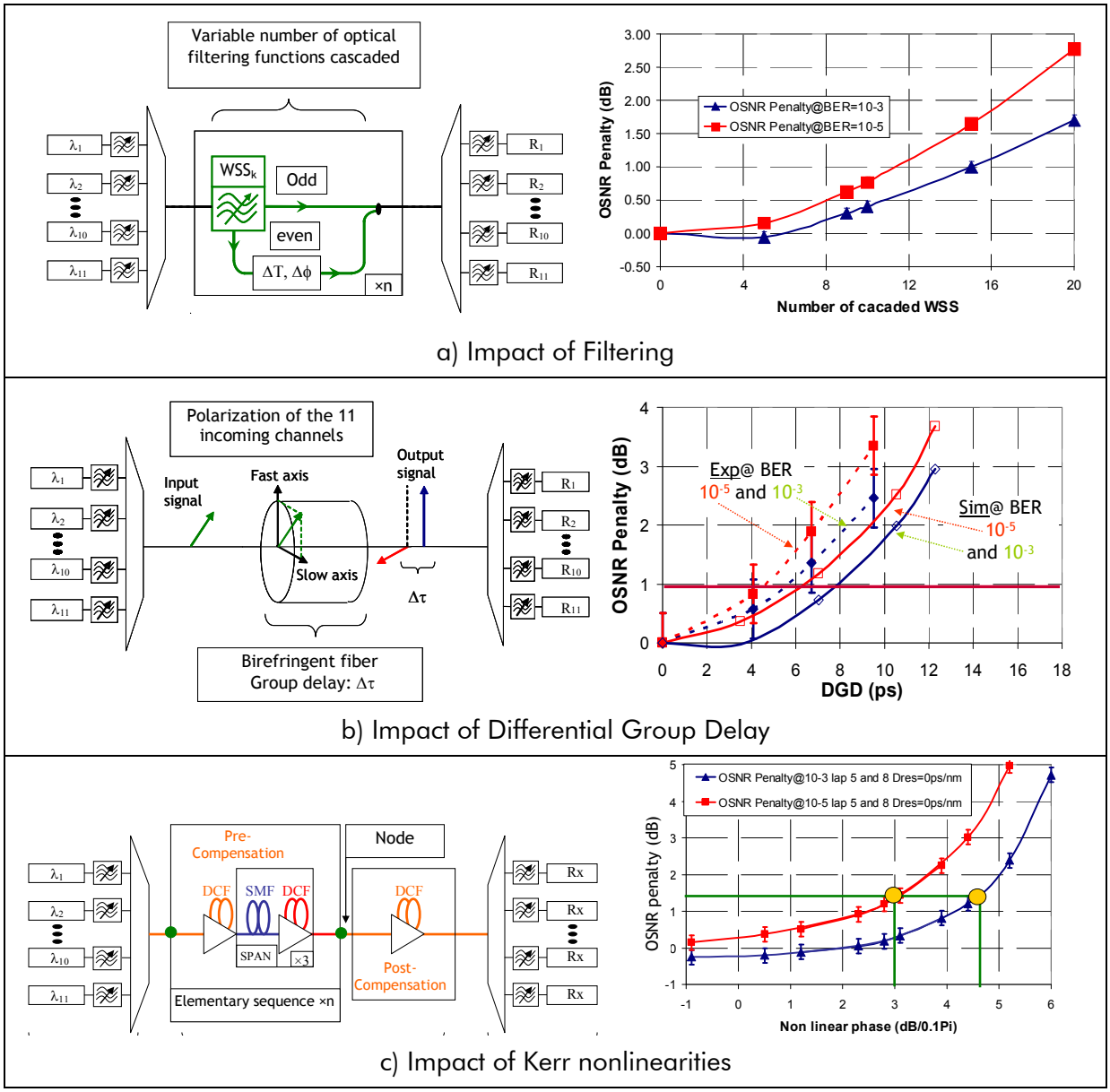

Figure 4-8 : Set-up (left plots) and evolution of OSNR penalty (right plots) when varying the number of cascaded wavelength-selective switches (top, a), the differential group delay (middle, b), or the nonlinear phase (bottom, c).

The isolated impact of PMD is illustrated by Figure 4-8-b with the description of the set-up on the left plot, and the numerically-estimated evolution of the OSNR penalty for BER of 10^{-5} and 10^{-3} as a function of the Differential Group Delay (DGD). To do so, we sent the signals into a birefringent fibre of variable DGD with an input polarization state 45° from the principal states

of polarization of the birefringent medium. We measured that it takes 4ps (respectively 7ps) DGD to get 10^{-5} BER through experimental (respectively numerical) investigations for a BER of 10^{-5}. The tolerance to 1dB penalty increases up to 5.5 (respectively 8ps) for a BER of 10^{-3}.

The isolated impact of Chromatic Dispersion and Kerr effects is illustrated by Figure 4-8-c with the description of the set-up on the left plot, and the numerically-estimated evolution of the OSNR penalty for BER of 10^{-5} and 10^{-3} as a function of the nonlinear phase shift. To do so, we emulated a doubly-periodic dispersion-managed system consisting of a variable number of subdivisions of 3 spans SMF emulating different node sections; at receiver end, some post-compensation DCF was set to zero the residual dispersion. We measured through numerical simulations and experiments the nonlinear thresholds associated to 1.5dB OSNR penalty to get a BER of respectively 10^{-5} and 10^{-3} with values respectively amounting to 3 and 4.5$dB_{0.1\pi}$.

IV.1.2. Evolution of ζ function with nonlinearities, inline filtering or PMD

In this section, we focus on the evolution of the ζ function corresponding to the derivative of the Q factor with respect to the OSNR as a function of one source of impairments such as nonlinearities, PMD or filtering functions.

As aforementioned and illustrated in case of Kerr effects-induced impairments, ζ tends to decrease in presence of physical effects causing inter-symbol interference. Such observation also applies in presence of filtering of Polarization Mode Dispersion, as illustrated by Figure 4-9: it represents the evolution of an estimated ζ as a function of the number of cascaded WSS, the Differential Group Delay or nonlinear phase, in the same conditions of emulation as in Figure 4-8. Here, ζ is estimated by varying the OSNR at receiver end around the value corresponding to the required OSNR to ensure a given BER. Estimations of ζ for a BER of 10^{-5} are roughly 9% higher than estimations for a BER of 10^{-3}. In the following, estimations of ζ are given for a BER of 10^{-3} in experiments, 10^{-5} in simulations.

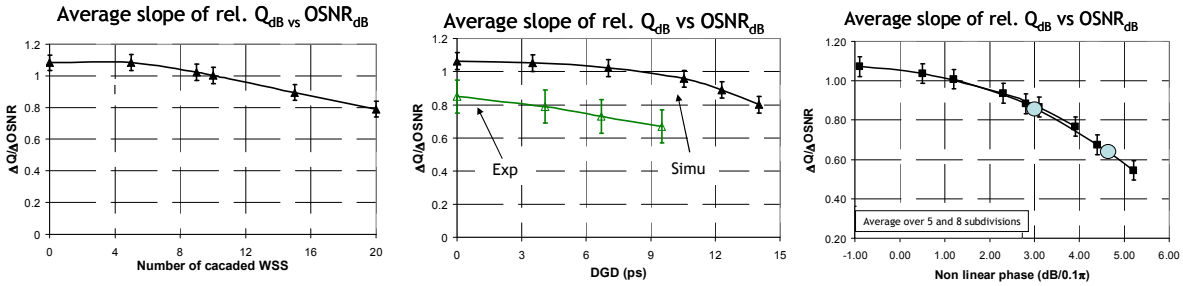

Figure 4-9 : Evolution of ζ, the average derivative of Q versus OSNR (dB vs dB scale), as a function of the number of the chosen cascaded wavelength-selective switches (left plot), of the differential group delay (center plot), or of the nonlinear phase (right plot) following conditions of Figure 4-8. Error bars on the plots correspond to the accuracy of the estimations of ζ..

IV.2. Investigation of the impact of combined effects on the QoT estimator

After investigating the evolution of the QoT estimator (though the evolution of penalty and ζ functions) as a function of a single source of signal degradation, we study here the joint evolution of the QoT estimator in presence of two combined sources of signal degradation in order to come up with an approximate of the QoT estimator enabling to decouple the impacts of propagation effects.

IV.2.1. Impact of combined effects on OSNR penalty

Signal degradations can be divided into two classes: the ones that distort signal pulses (chromatic dispersion , PMD, nonlinear phase, filtering), and the ones that increase noise around marks, "1," and spaces, "0," (ASE, Amplified Spontaneous Emission and Crosstalk). The latter types of degradation can be considered independent from each other and justify the penalty separation of Crosstalk and ASE from other effects, as a first approximation. Crosstalk penalties and OSNR can be separated, as the resulting power distributions are different [132]. Zyskind et al [133] showed that penalties due to chromatic dispersion are related to nonlinear phase values; furthermore, in a first-order approximation these penalties could be considered as independent from PMD values [134]. With these assumptions, we can consider that the overall penalty could be fairly well estimated by the sum of the penalties due to isolated propagation effects and we rewrite Equation (4-27) as follows:

$$Q^2{}_{dB}(x,y,z,OSNR) = Q^\circ + \zeta(\phi_{nl}, D_{res}, PMD, Xtalk, Filter). \cdot \begin{pmatrix} OSNR_{dB} - ROSNR_{Q^\circ,dB}(0,0,0) - Pen_{Q^\circ,dB}(\phi_{nl}, D_{res}) \\ - Pen_{Q^\circ,dB}(PMD) - Pen_{Q^\circ,dB}(Xtalk) - Pen_{Q^\circ,dB}(Filter) \end{pmatrix} \quad (4\text{-}28)$$

We propose here to discuss here the accuracy of such an assumption that is the estimation of the OSNR penalty induced by joint propagation effects through the sum of the penalties induced by separate effects.

The joint impact of filtering and nonlinearities is first assessed by inserting the filtering functions of Figure 4-8-a-left at the end of each subdivision of three spans as depicted in Figure 4-8-c-left. Figure 4-10 then represents the OSNR penalty for a BER of 10^{-5} as a function of nonlinear phase for 2, 5 and 8 crossed subdivisions and filtering functions (also called laps in the Figure). In absence of filtering, the penalty plots are aligned along a single curve, which is no longer the case with the distance-dependent impact of filtering. We can notice two regimes: for lower values of nonlinear phase, the filtering impact is dominant and the penalty curves are well separated from a distance to another, while for high values of nonlinear phase, the impact of filtering fades and the penalty curves tend to converge. The curve representing the sum of the penalties induced by nonlinearities and filtering after 5 subdivisions happens to be always higher than the joint penalty curve, showing discrepancies up to 0.7dB for nonlinear phases higher than the 1.5dB penalty NLT due to the sole impact of Kerr effect. This trend was confirmed in additional (not presented here) configurations.

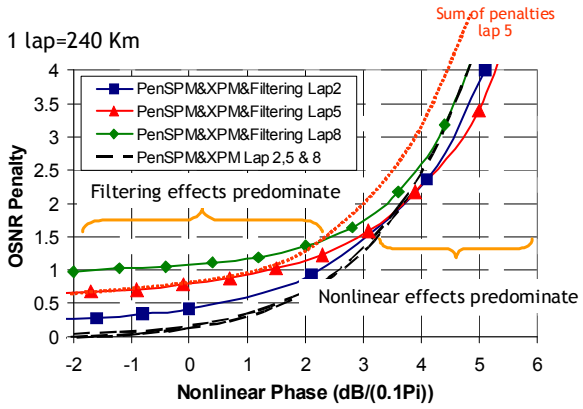

Figure 4-10 : Joint impact of nonlinearities and filtering on transmission OSNR penalty (for reference BER = 10^{-5}. Numerical simulations for different distances: 2, 5, 8 node sections (or laps) of 3 dispersion-managed spans of SMF followed by WSS filter. Dashed black line without symbol: impact of nonlinearities only, for different distances; lines with symbols: joint impact of nonlinearities and WSS-induced filtering on penalty for different distances; dotted line without symbol: sum of individual penalties stemming from nonlinearities and filtering for 5 node sections.

The joint impact of PMD and nonlinearities is assessed by inserting the DGD emulator of Figure 4-8-b-left at the beginning, at the end of the transmission link, or after each span. Figure 4-11 then represents the OSNR penalty as a function of DGD for various values of nonlinear phase. The measurements come from numerical results (Figure 4-11-left) and experiments (Figure 4-11-right) and penalties are calculated for reference BERs of 10^{-5} and 10^{-3} respectively.

The numerical study included nonlinear phases between -1dB$_{0.1\pi}$[6] and +4.5dB$_{0.1\pi}$, leading penalties within 0 and 3.8dB penalty in absence of DGD. In all conditions, the sum of individual penalties coming from DGD and nonlinearities appears as an upper-bound of the measured overall penalty with discrepancies up to 0.5dB for the case of distributed DGD along the line, and up to 1dB in the case of all the DGD located at the transmitter side. For 6ps DGD, leading to typically acceptable 1dB penalty in absence of nonlinearities, these discrepancies do not exceed 0.5dB.

The experimental study included nonlinear phases[7] between -2 and +2.5dB$_{0.1\pi}$, leading to penalties between 0.8 and 3dB penalty in absence of DGD. For practical reasons, the addition of DGD in the line was not achieved but only at the transmitter and the receiver. Similar to the numerical study, the sum of individual penalties coming from DGD and nonlinearities appears as an upper-bound of the measured overall penalty with discrepancies up to 0.5dB for the case of DGD located at the receiver, and up to 1dB in the case of all the DGD located at the transmitter side. For 6ps DGD, leading to 1dB penalty in absence of nonlinearities, these discrepancies do not exceed 0.5dB.

[6] Nonlinear phase $\phi_{dB,0.1\pi}$ expressed in dB$_{0.1\pi}$ means here $10\log_{10}(\phi_{nl,rad}/(0.1\pi))$ when $\phi_{nl,rad}$ corresponds to nonlinear phase shift expressed in rad.

[7] Nonlinear phases are here derived from the measurements of the fibre input powers and the knowledge of the characteristics of the traversed fibres.

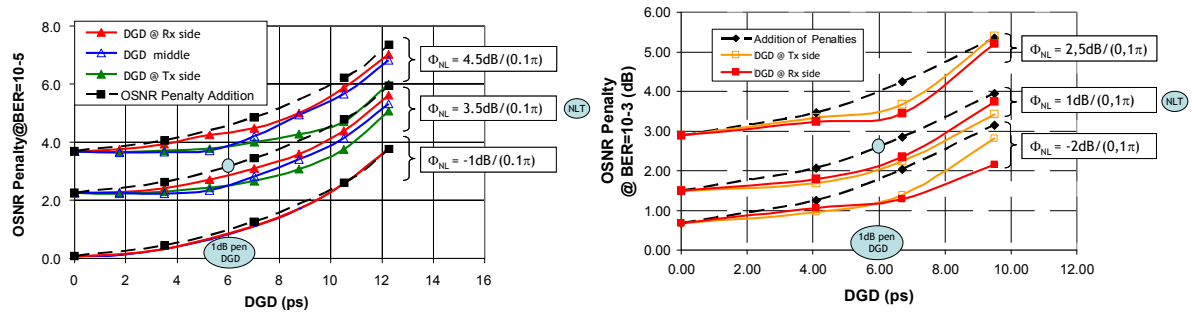

Figure 4-11 : OSNR penalty versus Differential Group Delay (DGD) in presence of nonlinear effects accumulating over the transmission link.
Left graph: numerical data; reference BER = 10^{-5}; nonlinear phases of -1, 3.5 and 4.5dB$_{0.1\pi}$[6]; lines with triangles: measurements with DGD inserted at begin, mid- or end-transmission; dashed lines with square symbols: sum of individual penalties stemming from nonlinearities and DGD.
Right graph: experimental data, reference BER= 10^{-3}; nonlinear phases of -2, 1 and 2.5dB$_{0.1\pi}$; lines with square symbols: measurements with DGD inserted at begin or end-transmission; dashed lines with diamond symbols: sum of individual penalties stemming from nonlinearities and DGD.

In summary, we investigated both numerically and experimentally various configurations of a mix of propagation effects and showed that the penalty induced by the sum of two effects is upper-bounded by the sum of the penalties induced by isolated effects, with discrepancies up to 0.7dB in usual conditions of operation. We can then imagine to build the QoT estimator based on this concept of summation of penalties with limited inaccuracy.

Note that the use of such upper-bound into a quality of transmission estimator is then expected to lead to an under-estimation of the Q factor by down to 0.5dB (accounting for the conversion factor between OSNR variations into Q variations).

IV.2.2. Impact of combined effects on the ζ function

Now we investigate the evolution of ζ in presence of combined effects, first nonlinearities and filtering then nonlinearities and DGD, as previously done for the evolution of penalties.

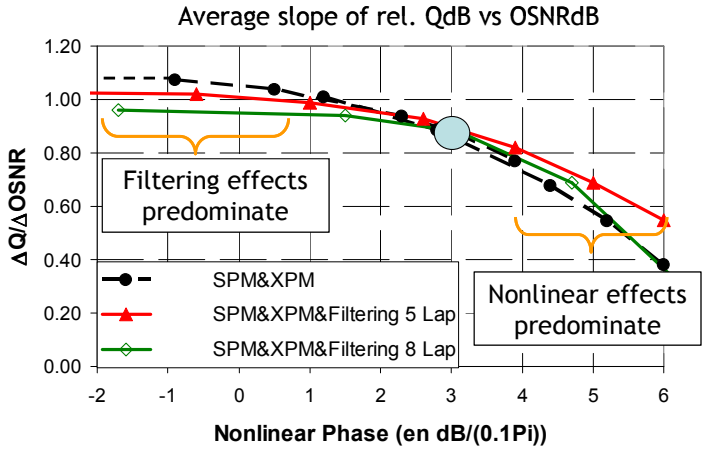

Figure 4-12 : Evolution of ζ function (i.e. derivative of Q vs OSNR in dB/dB scale) with nonlinear phase and filtering issues for 5 and 8 transmission subdivisions (including 5 and 8 inline filters resp.).

Figure 4-12 represents the evolution of ζ as a function of nonlinear phase after five and eight node sections including WSS filtering functions similar to the conditions of Figure 4-10. The sole impact of the cascade of five or eight nodes results in a penalty of 0.6 or 1dB respectively

(for a BER of 10^{-5}), and a decrease of ζ from 1.08 (in absence of any impairment) to 1.02 or 0.96 resepctively. In the weak nonlinear regime, with nonlinear phases lower than the 1.5dB-penalty NLT, ζ is rather constant and essentially depends on the number of cascaded WSS. However, for nonlinear phases close to the NLT or higher ζ is lower bounded by the estimation stemming from the sole impact of nonlinearities. It appears then that in fairly good approximation, the estimation of ζ in presence of combined effects is always lower-bounded by the minimal estimation coming from isolated effects, which can be expressed as:

$$\zeta(\phi_{nl}, filtering) \geq Min\{\zeta(\phi_{nl},0), \zeta(0, filtering)\} \quad (4\text{-}29)$$

The discrepancy between the actual ζ and the lower-bound never exceed 15% in presence of filtering penalties lower than 1dB or nonlinear penalties lower than 5dB. Using such a lower-bound to ζ is of particular interest for a Q-estimator since it amounts to having a lower-bound to the estimation of the Q factor.

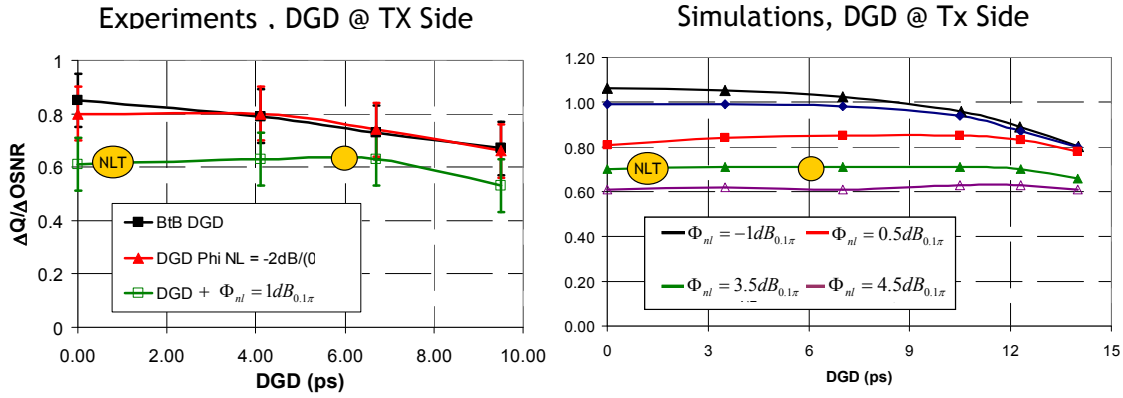

Figure 4-13 : Evolution of ζ function (i.e. derivative of Q vs OSNR in dB/dB scale) with nonlinear phase and differential group delay, by experimental (left) or numerical (right) means.

Similarly, we conducted numerical simulations and experiments to assess the joint impact of nonlinearities and PMD over the evolution of ζ, following the conditions of Figure 4-11. Figure 4-13 then represents the evolution of ζ as a function of DGD and for different values of nonlinear phase, assuming that all the DGD is injected at transmission input (which corresponded to the worst case penalty in Figure 4-11). Here again, for DGD values lower than 6ps (leading to 1dB OSNR penalty for a BER of 10^{-3} in experiments and 10^{-5} in numerical simulations), the measured ζ in presence of combined effects appears lower-bounded by the minimal estimation coming from isolated effects. The domain of validity of this assumption can be extended for DGD values up to 8ps according to experimental measurements. This corresponds to 2dB OSNR penalty and is usually beyond the tolerated values of DGD in deployed systems.

In summary, in presence of two combined effects the estimation of ζ appears lower-bounded by the minimal estimation coming from isolated effects, in usual conditions of system operation, through the investigation of joint nonlinear phase and PMD effects, and joint nonlinear phase and filtering effects. From those simple examples, it appears reasonable to consider this assumption in presence of more than two combined effects, such that a lower-bound estimation of ζ could be ζ_{min} with:

$$\zeta(\phi_{nl}, D_{res}, filtering, PMD, XTalk) \geq \zeta_{\min}(\phi_{nl}, D_{res}, filtering, PMD, XTalk)$$
$$with \quad \zeta_{\min}(\phi_{nl}, D_{res}, filtering, PMD, XTalk) := Min\begin{Bmatrix}\zeta(\phi_{nl}, D_{res},0,0,0), \zeta(0,0, filtering,0,0),\\ \zeta(0,0,0, PMD,0), \zeta(0,0,0,0, XTalk)\end{Bmatrix} \quad (4\text{-}30)$$

In the following section, we will come back to the final QoT model that we can build.

4.V. Final proposition of QoT estimator and required complexity

V.1. General formulations of the quality of transmission estimator

To summarize the previous studies, we first proposed a model for the estimation of the Quality of Transmission which consisted in separating noise contribution to signal degradations from the other contributions (depending on a few cumulative parameters), taking advantage of the observed quasi-linear evolution of the Q factor with the OSNR (in dB/dB scale). The obtained relationship between the estimation of the Q factor and the QoT vector was expressed by equation (4-27):

$$Q^2{}_{dB}\left(\phi_{nl}, D_{res}, PMD, XTalk, filter, OSNR\right) = Q^\circ + \zeta(\phi_{nl}, D_{res}, PMD, XTalk, filter). \\ * \begin{pmatrix} OSNR_{dB} - ROSNR_{Q^\circ,dB}(0,0,0) \\ - Pen_{Q^\circ,dB}(\phi_{nl}, D_{res}, PMD, XTalk, filter) \end{pmatrix}.$$

With such a relationship, a prediction of the Q factor requires the knowledge (through direct measurements or interpolations from measurements) of the required OSNR to get a given Q factor Q° in absence of signal degradations, the evolution of the OSNR penalty for this same given Q factor, and the estimate derivative ζ of Q with OSNR, as functions of the non-EDFA-noise-related parameters of the QoT vector. The complexity lies here in the determination of such functions of combined parameters.

The second step was then to simplify this model and investigate whether the combined impacts of the different sources of degradations on penalty or on ζ could be estimated from their isolated impacts. We particularly showed that the OSNR penalty (in dB scale) induced by combined propagation effects can be practically approximated by the sum of the OSNR penalties induced by almost each propagation effect (we chose not to separate Kerr effects from Chromatic Dispersion due to their strong interaction). Such an approximation happens to be a lower bound to the overall penalty in the investigated configurations. One can thus determine the overall penalty function from measurements and interpolations of the penalties induced by isolated effects, with an accuracy of typically 0.7dB, as shown in section 4.IV.

$$Pen_{Q^\circ,dB}\left(\phi_{nl}, D_{res}, PMD, XTalk, filter, OSNR\right) \le Pen_{Q^\circ,dB}(\phi_{nl}, D_{res}) + Pen_{Q^\circ,dB}(PMD) \\ + Pen_{Q^\circ,dB}(Xtalk) + Pen_{Q^\circ,dB}(Filter) \qquad (4\text{-}31)$$

Consequently, this enables to get a lower estimate Q_e of the Q factor:

$$Q^2{}_{dB}\left(\phi_{nl}, D_{res}, PMD, XTalk, filter, OSNR\right) \ge Q_e\left(\phi_{nl}, D_{res}, PMD, XTalk, filter, OSNR\right) \qquad (4\text{-}32)$$

with Q_e expression given by Equation (4-28):

$$Q_e{}^2{}_{dB}\left(\phi_{nl}, D_{res}, PMD, XTalk, filter, OSNR\right) = Q^\circ + \zeta(\phi_{nl}, D_{res}, PMD, Xtalk, Filter). \\ \cdot \begin{pmatrix} OSNR_{dB} - ROSNR_{Q^\circ,dB}(0,0,0) \\ - Pen_{Q^\circ,dB}(\phi_{nl}, D_{res}) - Pen_{Q^\circ,dB}(PMD) \\ - Pen_{Q^\circ,dB}(Xtalk) - Pen_{Q^\circ,dB}(Filter) \end{pmatrix}$$

Let us now define the OSNR margin $m_{Q°}$ for a reference Q factor Q° as:

$$m_{Q°,dB}(\phi_{nl}, D_{res}, PMD, XTalk, filter, OSNR) = \begin{vmatrix} OSNR_{dB} - ROSNR_{Q°,dB}(0,0,0) - Pen_{Q°,dB}(\phi_{nl}, D_{res}) \\ - Pen_{Q°,dB}(PMD) - Pen_{Q°,dB}(Xtalk) - Pen_{Q°,dB}(Filter) \end{vmatrix} \quad (4\text{-}33)$$

then the Q factor estimate becomes

$$Q_e{}^2{}_{dB}(\phi_{nl}, D_{res}, PMD, XTalk, filter, OSNR) = Q° + \zeta(\phi_{nl}, D_{res}, PMD, Xtalk, Filter) * m_{Q°,dB}(\phi_{nl}, D_{res}, PMD, Xtalk, Filter, OSNR). \quad (4\text{-}34)$$

We have previously shown that the $\zeta(.)$ function is a decreasing function of its input parameters, and that in good approximation, we could assume the Equation (4-30), i.e.

$$\zeta(\phi_{nl}, D_{res}, filtering, PMD, XTalk) \geq \zeta_{\min}(\phi_{nl}, D_{res}, filtering, PMD, XTalk)$$
$$with \ \ \zeta_{\min}(\phi_{nl}, D_{res}, filtering, PMD, XTalk) := Min \begin{Bmatrix} \zeta(\phi_{nl}, D_{res}, 0,0,0), \zeta(0,0, filtering, 0,0), \\ \zeta(0,0,0, PMD, 0), \zeta(0,0,0,0, XTalk) \end{Bmatrix} \quad (4\text{-}35)$$

and that

$$\zeta(\phi_{nl}, D_{res}, filtering, PMD, XTalk) \leq \zeta_{\max}(\phi_{nl}, D_{res}, filtering, PMD, XTalk)$$
$$with \ \ \zeta_{\max}(\phi_{nl}, D_{res}, filtering, PMD, XTalk) := Max \begin{Bmatrix} \zeta(\phi_{nl}, D_{res}, 0,0,0), \zeta(0,0, filtering, 0,0), \\ \zeta(0,0,0, PMD, 0), \zeta(0,0,0,0, XTalk) \end{Bmatrix} \quad (4\text{-}36)$$
$$\leq \zeta(0,0,0,0,0)$$

Thus a final lower bound estimate of the Q factor is Q_{est} with:

$$Q_{est}{}^2{}_{dB}(\phi_{nl}, D_{res}, PMD, XTalk, filter, OSNR) =$$
$$\begin{cases} . \ Q° + \zeta_{\min}(\phi_{nl}, D_{res}, PMD, Xtalk, Filter) * m_{Q°,dB}(\phi_{nl}, D_{res}, PMD, Xtalk, Filter, OSNR), \ if \ \ m_{Q°,dB} \geq 0 \\ . \ Q° + \zeta_{\max}(\phi_{nl}, D_{res}, PMD, Xtalk, Filter) * m_{Q°,dB}(\phi_{nl}, D_{res}, PMD, Xtalk, Filter, OSNR), \ if \ \ m_{Q°,dB} < 0 \end{cases} \quad (4\text{-}37)$$

Such a final quality of transmission estimator enables to account fairly well for the joint impact of multiple effects and is based on the sole measurements of the evolutions of penalties and ζ with isolated effects. Such an estimator is by construction a lower-bound of the Q-factor such that very good accuracies can be obtained in usual conditions of operation.

In some cases though, the determination of ζ is not even necessary. Indeed, if the role of such a quality of transmission estimator is to help planning tools or the control plane to decide whether the quality of transmission of a path between distant nodes is good enough for the establishment of a connection without optoelectronic regeneration, then the decision will depend on the Q factor being higher or lower than a given Q factor target Q_{target}. Such Q factor target depends straightforwardly on the performance of the embedded error correction functions in the transponders. Equivalently, the decision will depend on the sign of the OSNR margin determined for this Q factor $Q°=Q_{target}$. Should the OSNR margin be positive for $Q°=Q_{target}$, then the connection will be feasible. In that case, provided the OSNR penalties

induced by the different propagation effects are determined for $Q°=Q_{target}$, then the determination of ζ may not necessary. Note that for such an application, the uncertainties associated with the built estimator and the knowledge of the input QoT vector need to be dealt with so as to come up with an overall estimate of the minimum Q factor associated to degrees of confidence (typically higher than 95%).

The knowledge of the Q factor can however be useful complementary information for the system designer or the operator. For instance, when deploying a system one can compare the measurements of the Q factor in the field with an expected average or median estimate of the Q factor with respect to the uncertainties on the QoT vector and possibly overlooking extra-losses provisioned for the ageing of components or fibre sections. For such applications, the determination of ζ is key and Equation (4-37) can be applied. One can also deduce from Equation (4-37) that the lower the OSNR margin becomes and thus the closer to Q° the prediction on Q becomes, then the lower uncertainty we get on the Q factor prediction associated to ζ. Another use of the ζ function is to anticipate possible evolutions of the target Q factor Q_{target} corresponding to the feasibility of an optical connection with the improvements of the optical transmission systems: over the last ten years, the correction capabilities of the implemented Forward Error Correction Codes (FEC) have greatly improved with tolerated uncorrected BERs from $2\ 10^{-4}$ to $4\ 10^{-3}$ with 7% overhead; new-generation soft-decision FEC are likely to enable in the future to tolerate uncorrected BER around $4\ 10^{-2}$ (with 25% overhead). As a result, the thresholds set to establish the feasibility of a connection are likely to evolve with time and will require the knowledge of the $\zeta(.)$ function to avoid successive rounds of measurements and calibrations over time.

V.2. Example of establishment of a QoT estimator based on experiments

In this section, we illustrate the previously described concepts to the construction of a quality of transmission estimator based on experiments for 10.7Gb/s NRZ-modulated systems deployed over SMF line fibre type.

The chosen model is that of Equation (4-28).

The initial studies on that topic were conducted in the frame of the French-funded RNRT collaborative project RYTHME (Réseaux hYbrides Transparents Hiérarchiques Multiplexés En longueur d'onde) [139][140].

In the following, we will particularly explain how to obtain $Pen_{Q°,dB}(\phi_{nl},D_{res})$ and $Pen_{Q°,dB}(PMD)$ as detailed in articles [141] and [142] respectively. The experiments related to the assessment of the impact of nonlinearities were conducted by B. Lavigne and the outputs of such a study were published at ECOC conference in 2007 [141].

Note that for 10G systems, the impact of filtering can be overlooked, and that the crosstalk penalties induced by the traversed optical nodes could be derived from [143].

V.2.1. Method for the interpolation of $Pen_{Q°}(D_{res},\varphi_{nl})$.

We focus our analysis on $Pen_{Q°}(D_{res}, \varphi_{nl})$, the penalty term due to chromatic dispersion and non-linearities. The WDM system is emulated by means of a recirculation loop (described later) enabling to perform a large set of measurements for various fibre input powers and transmission distances. Figure 4-14 gives an example of an OSNR penalty curve (for BER of 10^{-5}) with respect to chromatic dispersion obtained after 18 spans of 100 km SMF and a input power of 3 dBm per channel (corresponding to an integrated power of 17.3dBm or to a nonlinear phase φ_{nl} of 1.27rad, i.e. $6dB_{0.1\pi}$).

We apply a two-step process to derive the relation: in the first step, we approximate each OSNR penalty versus the residual dispersion curve by a quadratic polynomial, as long as the penalty is less than 5 dB. Higher penalties are not considered because the precision of the estimation will be degraded, and for penalties greater than 5 dB no connections are possible.

$$Pen_{Q°,dB}(D_{res},\phi_{nl}) = a_{\phi}.{D_{res}}^{2} + b_{\phi}.D_{res} + c_{\phi}$$

In the second step, the coefficients a_φ, b_φ and c_φ are fitted by a polynomial of second (or fourth) degree as a function of φ_{nl}. The scope of the estimator is to have a good precision and not be too heavy in computation. Precision is obtained by the degree of the polynomial function; the complexity is reduced if such degree is lower. We look for the smaller degree that satisfies the best function precision. The OSNR penalty can be rewritten as:

$$Pen_{Q°,dB}(D_{res},\phi_{nl}) = \sum_{i=0}^{2}\left[\sum_{j=0}^{k}\alpha_{j,i}.\phi_{nl}^{j}\right].{D_{res}}^{i}$$

with $2 \leq k \leq 4$.

This polynomial approximation may simply be interpreted as a Talyor expansion of the penalty with respect to D_{res} and ϕ_{nl}.

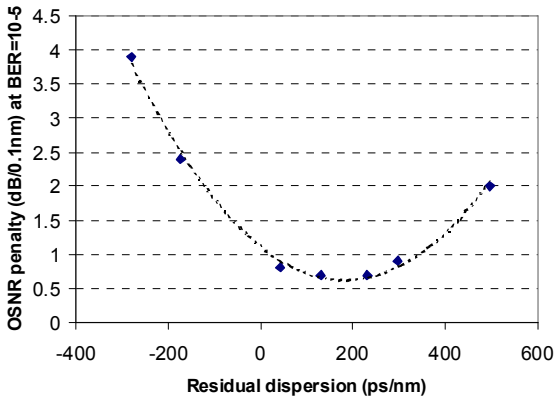

Figure 4-14: Example of OSNR penalty versus the residual dispersion measured for φ_{nl} = 1.27 rad. Diamonds are measured points and the dotted line is the interpolation.

We have applied our method for the establishment of a QoT estimator using an experimental set up. This experimental set-up emulates a 10.7 Gbit/s SMF-based WDM transmission system that is emulated by means of a recirculating loop (see Chapter 1). It is made of three 100km-long dispersion-managed spans of SMF fibre. Details of the set-up and of dispersion-management scheme can be found in [141]. The nominal power per channel is varied from 1 to 4dBm and is measured at the input of each line fibre span and at every loop lap. The input power per channel into DCF modules is set 7 dB lower than the input into SMF sections. The total transmission distance varies from 300 to 2400 km (1 to 8 loop laps).

The coefficients of the polynomial estimator are deduced from a wide number of measurements of the OSNR penalty by a least mean square method. To assess the accuracy of the estimator, its predictions are compared with the measured OSNR penalties in 230 different conditions of power, distance and residual dispersion. Figure 4-15 thus represents a histogram of the difference in penalty (in dB scale) between measurements and estimations. By fitting this distribution with a Gaussian curve, we find that the estimation is within +/-0.5 dB for 91.5% of samples, +/-1 dB for 98.6% and +/-2 dB for 99.97% of the samples. In other words, if the required level of confidence associated with the prediction of feasibility of a connection is 99.97%, some 2dB extra-penalties may need to be provisioned in addition to the mean prediction.

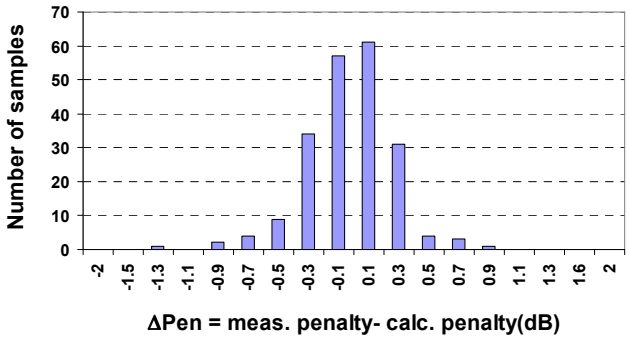

Figure 4-15: Number of lightpaths versus the penalty differences (Pen(measured)-Pen(estimated)) for the experimental set up

To conclude, we have detailed here one method to obtain a representative function of the evolution of the OSNR penalty with cumulative dispersion and nonlinear phase and have applied such a method to the experimental determination of this relationship. The polynomial expression of the relationship makes it particularly easy to compute in embedded tools within

a control plane. We have assessed the accuracy of the derived predictions with respect to a large number of measured system configurations and highlighted the relation between the required level of confidence for those predictions and the extra-margins to provision for system design.
If the reader is interested, the method to estimate the PMD-induced penalties is described in Appendix.

V.3. Extensions towards wavelength-aware and fibre-type-aware QoT estimators

In addition to the determination or not of the ζ function, the estimation of the quality of transmission can be enhanced along at least two directions: the impact of wavelength and the heterogeneity of line fibre types. We will briefly describe such cases in the following paragraphs.

V.3.1. Impact of wavelength

First of all, the signals propagating along transmission systems degrade differently depending on their wavelength, in a possibly predictable manner : for instance optical amplifiers do not have a flat spectral distribution of gains and noise figures; the stimulated Raman scattering process causes energy transfer from the lower-wavelength channels to the higher-wavelength channels resulting in larger OSNR degradations and lower nonlinearities impairing the lower-wavelength channels; some power pre-emphasis of the different channels can be performed at transmitter side to mitigate the role of Raman scattering; fibre chromatic dispersion varies with wavelength, causing discrepancies in the residual dispersion (which can be quite detrimental if the residual dispersion can not be adjusted on a per channel basis at receiver side) and also in the tolerance to nonlinearities such as with LEAF™ G655 fibre yielding chromatic dispersion values between 2.5ps/nm/km in the part of the C-band and 4.5ps/nm/km in the higher part of the C-band. To cope with such discrepancies, different quality of transmission estimators can be obtained for different sets of wavelengths. The benefits of using such a finer quality of transmission estimator were shown in [137] and [138]. In [138], we considered a typical American Backbone Network, based on SMF-line fibre type, 10Gbit/s-modulated NRZ channels, 46 nodes and uniform traffic matrices with loads ranging from 200 to 350 bi-directional 10G demands: this study showed that some 70-80% of the required optoelectronic regenerators over the network could be saved when relying on a wavelength sensitive quality of transmission estimator instead of designing the network relying on the worst-case wavelength. When planning networks resistant to one link failure with optical restoration, the number of saved optoelectronic regenerators remains higher than 50% whatever the traffic demand. This amounts to a reduction of at least 20% optoelectronic interfaces throughout the network. The benefits of having a wavelength-sensitive quality of transmission estimator are thus significant and enable to reduce the over-provisioning of optoelectronic resources. Routing strategies can also take advantage of this knowledge and allocate preferentially low-performance channels to unconstrained shortest connections and reserve high performance channels for longest connections. Obviously the obtained benefits come at the expense of the complexity of the estimator and the time spent to calibrate this estimator. In most cases, a fair trade-off can be obtained calibrating the performance estimator for three representative wavelengths in the C-band with differentiated performance and propose wavelength-sensitive estimates based on interpolations from the Q-estimates for each representative wavelength or based on the estimate corresponding to the reference wavelength closest to the asked wavelength.

V.3.2. Mixed fibre types networks

Another possible refinement of the quality of transmission estimator aims to cope with heterogeneous optical networks comprising mixed line fibre types [166][167][168][169]. We have shown in Chapters 2 and 3 that the tolerance to nonlinearities strongly depends on the type of line fibre type, and thus the penalty induced by the nonlinear phase. A fair estimate of the induced penalty in case of mixed fibre types can be obtained in using the weighted

nonlinear phase instead of the nonlinear phase shift [125], i.e. for each span the ratio of the nonlinear phase shift over the nonlinear threshold leading to a given penalty x dB (for a reference Q factor Q°). Thus for each fibre type mainly characterized by its local chromatic dispersion D_{loc}, the function $Pen_{Q°,dB}^{(Dloc)}(\phi_{nl}, D_{res})$ can be converted into $Pen_{Q°,dB}^{(Dloc)}(\phi_w, D_{res})$ with $\phi_w = \phi_{nl}/NLT_{x\ dB,\ Q°}^{(Dloc)}$. Note that this nonlinear threshold $NLT_{x\ dB,\ Q°}$, expressed here in the same units as ϕ_{NI} i.e. in radians, is likely to depend on the residual dispersion D_{res}. A worst-case estimate of the induced penalty can be obtained by:

$$Pen_{Q°,dB}^{(mix)}(\phi_w, D_{res}) = Max_{D_{loc}}\left(Pen_{Q°,dB}^{(D_{loc})}(\nu.\phi_w, D_{res})\right) \quad (4\text{-}38)$$

with D_{loc} corresponding to the possible chromatic dispersion values of the line fibres spread over the network, and ν corresponding to a margin such that for $\nu.\phi_w<100\%$ and whatever D_{loc}, we could ensure that $Pen_{Q°,dB}^{(Dloc)}<$ x dB. We showed in [125] and Chapter 3 that ν does not exceed 1.1 (i.e. a provisioned 0.5dB margin on the tolerated nonlinearities) for 10G and 40G systems. The accuracy of the resulting quality of transmission estimation is obviously degraded with respect to the case of single-line fibre type systems but it remains much better than the known alternative strategy consisting in keeping the nonlinear phase shift as an input parameter of the prediction function related to the worst-performing fibre. For instance, in [125], the nonlinear thresholds for 1.5dB penalty (10^{-5} BER) between 40Gb/s NRZ-modulated systems based on SMF and LEAF™ fibre differ by 4dB. With a mixed-fibre-type system such that almost all nonlinearities come from the sections with the best line fibre, here LEAF™. We can thus expect that the tolerance to nonlinearities will be almost that of the LEAF™ system. The worse-case strategy will automatically limit the maximum amount of nonlinearities 4dB below the expectable tolerance, while the weighted approach that we propose will authorize a maximum amount of nonlinearities 0.5dB below the expectable tolerance. In terms of reach, the weighted approach allow distances 50% higher than the worse-case approach.

V.4. Conclusion

We have seen how the complexity of the quality of transmission estimator can be adapted to the needs and the type of network and how such complexity improves the accuracy of the estimation.

4.VI. Chapter conclusion

In this chapter, we have thoroughly investigated the individual and combined impacts of propagation effects on the BER through numerical and experimental means, in order to build a modular, simple and rather accurate QoT estimator. Such estimator is of particular interest to design transmission systems and networks since it allows predicting whether a connection can be deployed without intermediate optoelectronic regeneration. We have particularly shown how the impact of noise could be separated from the impact of non-noise related propagation effects, in decoupling the OSNR, the OSNR penalties and the derivative ζ of Q versus OSNR. We have additionally studied how the impacts of non-noise related propagation effects combined in order to propose estimates of the penalties and ζ from the knowledge of individual contributions from those effects. We have discussed the accuracy and the complexity of this QoT estimator and have eventually shown how it could be extended to account for wavelength or mixed-fibre types.

In Chapter 5, we will come back to a simpler QoT estimator model essentially accounting for the impact of Kerr-induced nonlinearities and amplifier noise, so as to build guidelines to optimize subsystems such as amplifier schemes or DCF features an to optimize the fibre input powers in heterogeneous optical networks.

4.VII. Appendix 1: Determination of the relationship between penalty and PMD

Polarization Mode Dispersion (PMD) impact on a system performance can not be correctly emulated in a loop experiment [149]. However, the penalty dependence on PMD can be derived from measurements of the penalty as a function of the differential group delay (DGD), by the means of a PMD emulator with tunable DGD. We have seen in Chapter 1 that the DGD characterizes the instantaneous birefringence of the optical fibre and causes inter-symbol interference. Figure 4-16-Left shows a typical measured OSNR penalty as a function of DGD, for a 10Gb/s NRZ signal (T_0 represents the bit duration). After such a measurement, we can expect that, knowing the DGD of the birefringent material that supports transmission, we can derive the induced penalty and add this to other sources of signal distortions. Since DGD wanders with time and follows a Maxwellian distribution characterized the mean DGD value (i.e. the PMD) we usually consider the outage probability (typically 10^{-5}) that the DGD of the link becomes higher than a given value.

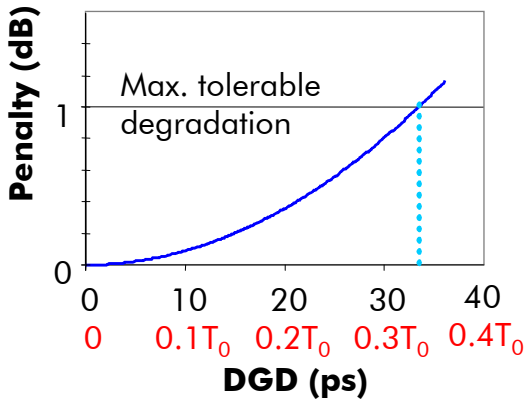

Figure 4-16 : Left: typical OSNR penalty versus DGD for 10Gb/s NRZ signal.

More precisely, if we calculate the DGD threshold such that the cumulated probability of getting a higher DGD is 10^{-5} using the Maxwellian law and the knowledge of PMD, it amounts to 3.2 PMD.

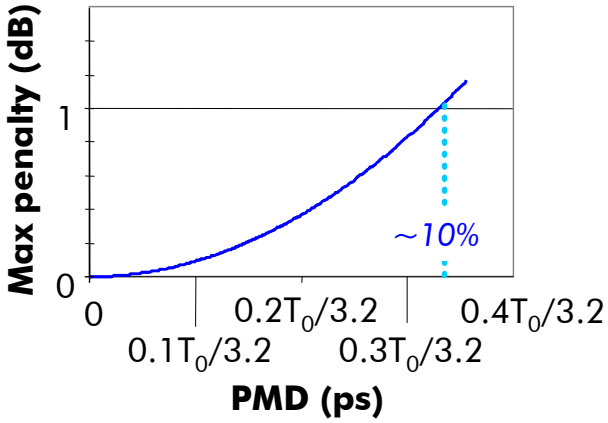

Figure 4-17 : Maximum OSNR penalty for 10^{-5} outage probability as a function of PMD

We can then derive the relationship between the maximum expectable OSNR penalty and the PMD of a system for an outage probability, as illustrated by Figure 4-17 for an outage probability of 10^{-5}: knowing the scaling factor between the maximum expectable DGD and the

PMD, for a given outage probability, it just consists in a change of scales in the relationship between penalty and DGD, to get the relationship between the likely expectable penalty and the PMD.

$$Pen_{OSNR}^{BER=10^{-5}}(PMD,\ ps) = 0.0099\ PMD^2 + 0.0058\ PMD$$

This way, we can assess with quite an honest accuracy what will be the PMD-induced penalty of a system, depending on the value of the cumulated PMD.

4.VIII. References

[125] J.-C. Antona et al, “Design and Performance Prediction in Meshed Networks with Mixed Fibre Types”, in Proc. Optical Fibre Communications Conference (OFC’08), paper JThA48, February 24-28, 2008 San Diego, California, USA

[126] A. Morea, F. Leplingard, T. Zami, N. Brogard, C. Simonneau, B. Lavigne, L. Lorcy and D. Bayart, “New transmission systems enabling transparent network perspectives”, C. R. Physique 9 (9-10) (2008), 985-1001

[127] S. Pachnicke, et al; “Fast analytical assessment of the signal quality in transparent optical networks”, IEEE Journal of Lightwave Technology, Volume 24, Issue 2, Feb. 2006 Page(s):815 – 82

[128] C. J. Anderson et al, “Technique for evaluating system performance using Q in numerical simulations exhibiting intersymbol interference”,IEE Electronics Letters, vol 30, No1, 1994, pp. 71-72

[129] N.S. Avlonitis, I. Tomkos, I., "Fast method for Q factor estimation in delay line demodulated DPSK optical communications systems", in 11th International Conference on Transparent Optical Networks,. ICTON '09., On page(s): 1 - 4, Volume: Issue: , June 28 -July 2 2009

[130] D. Penninckx, O. Audouin : "Optically preamplified systems: defining a new eye aperture", OFC'98, WM36, San Jose, USA, Feb. 1998

[131] D. Penninckx, “Etudes des liaisons numériques terrestres sur fibres optiques dispersives : du codage duobinaire aux transmissions binaires à profil de phase controlée (PSBT)”, Thèse de doctorat, Mars 1997, ENST.

[132] T. Zami, L. Noirie, F. Bruyère, and A. Jourdan, “Crosstalk-induced degradation in an optical-noise-limited detection system,” in Proceedings of IEEE/OSA Optical Fibre Communication Conference (OFC1999) (IEEE, 1999), pp. 255–257.

[133] J. Zyskind, R. Barry, G. Pendock, M. Cahill, and J. Ranka, “High-capacity, ultra-long-haul networks,” in Optical Fibre Telecommunication, IV B, Systems and Impairments, I. Kaminov and T. Li, eds. (Academic, Elsevier Science Imprint, 2002), pp. 198–231.

[134] H. Kogelnik, R. M. Jopson, and L. E. Nelson, “Polarization-mode dispersion,” in Optical Fibre Telecommunication, IV B, Systems and Impairments, I. Kaminov and T. Li, eds. (Academic, Elsevier Science Imprint, 2002), pp. 725–861.

[135] D. Penninckx and C. Perret, "New physical analysis of 10Gbit/s transparent optical networks", IEEE Photonics Technology Letters, Vol. 15, No. 5, 2003.

[136] D. Penninckx and C. Perret, “New physical analysis of 10Gb/s transparent networks”, Conference on Lasers and Electro-Optics 2003, CLEO’03, pp. 1836-1837, June 2003

[137] S. Duhovikov et al., “Dynamic RWA for All Optical Networks Using Linear Constraints for Optical Path Feasibility Assessment”, Proc. of IEEE ECOC06, Sept. 2006.

[138] A. Morea, J.-C. Antona, “Benefits of fine QoT-estimator to dimension spare resources in automatic restorable networks”, Proceedings of ICTON’10 (International Conference on Transparent Optical Networks), invited paper Mo D4.4, Munich (Germany), July 2010.

[139] P. Peloso, J.-C. Antona, “Physical design of hybrid network based on QoT vector featuring 4 parameters”, French RNRT Project RYTHME, Deliverable 2.1, March 2005

[140] J.-C. Antona, B. Lavigne, T. Zami, « Design physique définitif avec un QoT à 4 composantes, perspectives d’évolution », French RNRT Project RYTHME, Deliverable

2.2-2.3, June 2005
[141] B. Lavigne, F. Leplingard, L. Lorcy, E. Balmefrezol, J.-C. Antona, T. Zami, D. Bayart, “Method for the determination of a Quality-of-Transmission estimator along the lightpaths of partially transparent networks”, in Proceedings IEEE ECOC07, paper 08.5.2, Berlin (Germany), September 2007
[142] A. Morea, N. Brogard, F. Leplingard, J.-C. Antona, T. Zami, B. Lavigne, and D. Bayart, “QoT function and A * routing: an optimized combination for connection search in translucent networks”, Journal of Optical Networking, Vol. 6, No. 12, December 2007
[143] J. D. Downie and A. B. Ruffin, “Analysis of signal distortion and crosstalk penalties induced by optical filters in optical networks”, IEEE J. Lightwave Techno., **21**, 1876-1886 (2003)
[144] T. Zami et al.” The relevant impact of the physical parameters uncertainties when dimensioning an optical core transparent network”, paper We. 3.D.2, ECOC’08
[145] F. Leplingard et al., "Interest of an Adaptive Margin for the Quality of Transmission Estimate for Light-path Establishment", Paper OWI6, OFC'2009
[146] T. Zami et al, “A new method to plan more realistic optical transparent networks”, Bell Labs Technical Journal 14(4), 213-226 (2010)
[147] F. Leplingard, T. Zami, A. Morea, N. Brogard, D. Bayart., “Determination of the impact of a quality of transmission estimator margin on the dimensioning of an optical network”, in Proceedings IEEE/OSA OFC08, paper OWA6, March 2008.
[148] S. Pachnicke, T. Gravemann, M. Windmann, and E. Voges, “Physically Constrained Routing in 10Gb/s DWDM Networks Including Fibre Nonlinearities and Polarization Effects”, IEEE J. Lightwave Technol, Vol. 24, No 9, 3418-3425 (2006)
[149] E. Corbel, "Concerns about emulation of polarization effects in a recirculationg loop", in Proc. ECOC'03, Mo.3.7.4, Rimini, Italy, September 2003
[150] S. Pachnicke, S. Spälter, J. Reichert, E. Voges, “Analytical assessment of the Q-factor due to Cross-Phase Modulation (XPM) in Multispan WDM Transmission Systems”, Proceedings of SPIE ITCOM 2003, September 7–11 2003, Orlando
[151] A.V.T. Cartaxo, ‘Cross-Phase Modulation in Intensity Modulation-Direct Detection WDM Systems with Multiple Optical Amplifiers and Dispersion Compensators”, in IEEE J. of Lightwave Technology, vol. 17, No. 2, pp178-190, Feb 1999
[152] I. Tomkos, S. Sygletos, A. Tzanakaki, G. Markidis, “Impairment Constraint Based Routing in Mesh Optical Networks”, in Proc. Optical Fibre Communication and the National Fibre Optic Engineers Conference, 2007. OFC/NFOEC 2007, paper OWR1, Anaheim (Ca), 25-29 March 2007
[153] P. Kulkarni,A. Tzanakaki, C.M. Machuka, I. Tomkos, “Benefits of Q-factor based routing in WDM metro networks”, in Proc. ECOC 2005, paper Th3.5.7, pp. 981 - 982 vol.4, September 2005
[154] S. Azodolmolky et al., "A survey on physical layer impairments aware routing and wavelength assignment algorithms in optical networks", Computer Networks, 53(7), pp. 926-44, May 2009.
[155] E. Marin, S. Sánchez, X. Masip, J. Solé, G. Maier, W. Erangoli, S. Santoni, M. Quagliotti, “Applying prediction concepts to routing on semi transparent optical transport networks”, in: Proceedings of ICTON 2007, Rome, Italy, July 2007, pp. 32–36.
[156] A. Jukan, G. Franzl, “Constraint-based path selection methods for on-demand provisioning in WDM networks”, in: Proc. IEEE INFOCOM 2002, New York, NY, USA, June 2002
[157] N. Zulkifli, C. Okonkwo, K. Guild, “Dispersion optimized impairment constraint based routing and wavelength assignment algorithms for all-optical networks”, in Proc. of ICTON 2006, Nottingham, UK, vol. 3, June 2006, pp. 177–180

[158] Y. Pointurier, M. Brandt-Pearce, S. Subramaniam, “Analysis of blocking probability in noise and crosstalk impaired all-optical networks”, in Proc. IEEE INFOCOM 2007, Anchorage, Alaska, USA, May 2007, pp. 2486–2490.
[159] B. Ramamurthy, D. Datta, H. Feng, J.P. Heritage, B. Mukherjee, “Impact of transmission impairments on the teletraffic performance of wavelength-routed optical networks”, in Journal of Lightwave Technology 17 (10) (1999) 1713–1723.
[160] A. Marsden, A. Maruta, K. Kitayama, “Routing and wavelength assignment encompassing FWM in WDM lightpath networks”, in Proc. IFIP ONDM 2008, Vilanova i la Geltrú, Spain, March 2008.
[161] H.A. Pereira, D.A.R. Chaves, C.J.A. Bastos-Filho, J.F. Martins-Filho, Impact of physical layer impairments in all-optical networks”, in Proc. Microwave SBMO/IEEE MTT-S International IMOC 2007, Salvador, Brazil, November 2007, pp. 536–541.
[162] Y. Zhai, Y. Pointurier, S. Subramaniam, M. Brandt-Pearce, “Performance of dedicated path protection in transmission impaired DWDM networks”, in Proc. IEEE ICC 2007, Glasgow, UK, June 2007, pp. 2342–2347.
[163] J. He, M. Brandt-Pearce, Y. Pointurier, S. Subramaniam, “QoT-aware routing in impairment-constrained optical networks”, in Proc. IEEE GLOBECOM 2007, Washington (USA), November 2007, pp. 2269–2274.
[164] G. Markidis, S. Sygletos, A. Tzanakaki, I. Tomkos, “Impairment aware based routing and wavelength assignment in transparent long haul networks”, in: Proceedings of IFIP ONDM 2007, Athens, Greece, May 2007, pp. 48–57.
[165] L.K. Wickham, R.-J. Essiambre, A.H. Gnauck, P.J. Winzer, A.R. Chraplyvy, “Bit pattern length dependence of intrachannel nonlinearities in pseudolinear transmission”, Photonics Technology Letters, IEEE, Vol 16 (2004), No 6, pp 1591-1593
[166] D. Breuer, N. Hanik, C. Caspar, F. Raub, G. Bramann, M. Rohde, E.-J. Bachus, S. McLeod, M. Edwards, “Mixed Fibre Infrastructures in Long Haul WDM-Transmission”, OSA Journal of Optical Communications, 2004, Issue 1, pp 10-13
[167] D. Z. Chen et al, “World's first 40 Gbps overlay on a field-deployed, 10 Gbps, mixed-fibre, 1200 km, ultra long-haul system”, Proceedings of OFC’05, paper OTuH4, March 2005, Anaheim (Ca)
[168] M.H. Eiselt et al, “Field trial of a 1250-km Private Optical Network Based on a Single-Fibre, Shared-Amplifier WDM System”, Proceedings of OFC’06, paper NThF3, March 2006, Anaheim (Ca)
[169] P. Peloso, M. Prunaire, L. Noirie, and D. Penninckx “Optical transparency of a heterogeneous pan-European network,” J. Lightwave Technology, vol. 22, no. 1, pp. 242–248, Jan. 2004
[170] A. Erhardt, N. Hanik, A. Gladisch, and F. Rumpf, “Field demonstration of a transparent optical 10Gb/s-WDM network based on normalized transmission sections”, OFC’02, TuH2, Anaheim (Ca), February 2002

Chapter 5 : CHARACTERIZATION AND PHYSICAL DESIGN OF OPTICAL NETWORKS

CONTENTS

Introduction

We have previously introduced some key parameters that enable to simply account for the joint accumulation of Group Velocity Dispersion and Kerr effects in dispersion-managed optical transmission systems, such as the nonlinear phase ([171], Chapter 2) and the weighted nonlinear phase ([172], Chapter 3): we have particularly shown that provided a choice of transceiver set-up (modulation format, bit-rate, channel spacing…), infrastructure (types of fibre sections) and relevant dispersion management strategy, the induced transmission penalties essentially accumulate as a function of the total nonlinear phase shift; we also have generalized the concept to heterogeneous infrastructures with the notion of weighted nonlinear phase.

These parameters can be part of more complete physical performance prediction tools accounting for multiple propagation effects (such as Kerr effect, group velocity dispersion, noise accumulation, polarization mode dispersion, optical filtering or in-band crosstalk) in the context of heterogeneous, partially transparent, optical networks, as detailed in Chapter 3. Those performance prediction tools can be used to design systems before installation and to help deciding when and where optoelectronic regeneration is required prior to establish connections operate.

In this chapter, we would like to re-focus on system limitations induced by both noise and nonlinear issues and on the impact on system reach. First of all, we come back to the notion of tolerance to nonlinearities and propose an original definition of nonlinear threshold consistent with the achievable reach of optical transmission systems, as published in [172] in 2008. Then we derive from such notions a simple estimator of achievable reach as well as rules to optimally set the fibre input powers, in the context of homogeneous and heterogeneous infrastructures. Eventually we show how such simple tools can be utilized to compare modulation formats, to compare and design optical amplifier schemes, to compare and design line fibres then dispersion compensation fibres. In particular, these works have been used to design the Raman/Erbium amplification schemes of some record experiments presented in post-deadline sessions at major conferences [173][174][175].

5.I. Towards the definition of a non-linear threshold to quantify system resistance to non-linearities

I.1. From tolerance to nonlinearities to the notion(s) of nonlinear threshold

Nonlinear Kerr effects are a major limitation to the reach of optical transmission systems since reach is always limited by a trade-off between noise and nonlinear induced-limitations whatever the techniques to mitigate the detrimental role of nonlinear effects. Indeed, optical amplifier noise accumulates with distance and the effective OSNR increases with power while decreasing with distance; thus the minimum required fibre input powers to ensure a sufficient quality of transmission increase with distances. Conversely, nonlinear-induced impairments increase with distance and power, so that the maximum tolerable power for a given penalty decreases with distance. At maximum reach, the power will be such that the system is equally limited by both noise and nonlinearities. In that respect the determination of a so-called tolerance to nonlinearities is essential to design optical systems, estimate their reach and draw comparisons.

From Chapters 2 to 4, we know that we can relate the optical power into fibre sections, the number of spans, the product between number of spans and fibre input power, or the nonlinear phase to the transmission penalty or the Bit Error Rate. Such relationships depend on the considered kind of optical systems that are characterized by their transceiver setup (modulation formats, bit-rates, wavelength allocation plan) and their infrastructure (line fibre type; span lengh; dispersion, power and noise management strategy).

Nonlinear threshold usual definitions

When it comes to comparing and designing optical systems with different relationships between nonlinearities and physical performance, it is common to extract from those relations one specific point, the so-called **nonlinear threshold (NLT)**, in order to represent system tolerance to nonlinearities. However, despite this common notion of tolerance to nonlinearities, the definitions of nonlinear threshold are multiple in the literature: some articles relate the nonlinear threshold to a value of fibre input power [183] [184], product between the number of spans and power [185] or nonlinear phase; such a value is chosen to correspond to a given amount of OSNR penalty for a given BER [184] [185] (or Q penalty for a given OSNR), typically arbitrarily chosen between 1 and 3dB depending on the reports, or is related to the power maximizing the Q factor for a given distance and a given amount of noise.

Beyond the choice of metrics to quantify nonlinearities, there are thus two philosophies related to the measurements of penalties while setting the OSNR, or to the measurements of BER while keeping constant the accumulated noise and the distance: the former is consistent with the establishment of quality of transmission estimators relying on penalties, while the latter directly corresponds to the result and the setting of a transmission (lab experiment or deployed) link with no additional artifices like the addition and measurement of extra-noise at receiver end. In all cases, such definitions rely on the choice of an arbitrary reference penalty or an arbitrary system configuration such as distance or noise level.

Towards a new definition of the nonlinear threshold

In [172], we propose to make the connection between both philosophies, with a third definition of the NLT related to the maximum reach of an optical system with a maximum tolerable BER. We define the nonlinear threshold as the amount of nonlinear phase (or integrated power, i.e. the sum of the input powers into all line-fibre sections) related to the maximum reach of an optical system tolerating a given maximum BER value. This amount is equivalent to the nonlinear phase (or integrated power) such that the derivative of the relationship between the OSNR penalty for this same acceptable BER value and the nonlinear phase (or integrated power resp.) is unity (when all terms are expressed in dB scale):

$$\phi_{nl}=NLT \text{ when } \frac{dPen_{dB}}{d\phi_{nl,dB}}(\phi_{nl})=1, \quad i.e.\ \frac{\phi_{nl}}{Pen(\phi_{nl})}\frac{dPen}{d\phi_{nl}}(\phi_{nl})=1 \text{ in linear scale} \tag{5-1}$$

To demonstrate that point, we can come back to the model of Quality of Transmission estimation proposed in Chapter 4. Let us consider a class of homogeneous transmission systems characterized by a given type of transceiver set-up (modulation formats, bit-rates, wavelength allocation plan) and line infrastructure (line fibre type; span length; dispersion management strategy). This class is characterized by one relationship between OSNR penalty (for a given BER) and nonlinear phase. Let us then assume the generic relation between Q factor, OSNR and transmission penalties from Chapter 4 (Equation (4-4)) in dB scale. We assume here that the nonlinear phase ϕ_{nl} and the OSNR are the only varying parameters of such relationship. D_{res}, PMD and XTalk respectively refer here to the residual chromatic dispersion at receiver, the polarization mode dispersion and the linear crosstalk. Q_{ref} is the reference Q factor for which the OSNR penalties are calculated. Eventually, $\zeta()$ refers to the derivative of Q factor with OSNR when non-OSNR parameters are fixed.

$$Q^2_{dB}(\Phi_{nl},OSNR,D_{res},PMD,XTalk,...)={Q_{ref}}^2_{dB}+\zeta(\Phi_{nl},D_{res}).\begin{pmatrix} OSNR_{dB}-OSNR^{Q_{ref}}_{req,btb,dB}-Pen^{Q_{ref}}{}_{dB}(\Phi_{nl},D_{res}) \\ -Pen^{Q_{ref}}{}_{dB}(PMD)-Pen^{Q_{ref}}{}_{dB}(XTalk) \end{pmatrix} \tag{5-2}$$

For simplicity, we consider first a transmission system composed of N identical line fibre sections, with the same power P_{line} at each line fibre span input, identical DCFs with the same input power, proportional to P_{line}, and eventually amplifiers with constant noise figures. We assume that the impact of impairments caused by other sources than noise or nonlinearities is independent on distance.

Let us now consider the maximum reach of such a system while ensuring a minimum Q factor that will be equal to Q_{ref}. This reach is limited by the accumulation of noise and nonlinearities and is such that the maximum Q factor with optimized P_{line} will be equal to Q_{ref}: this means that the derivative of the Q factor (in dB scale) with $P_{line,\,dB}$ is expected to be zero, and that the OSNR will be equal to the required OSNR to ensure Q_{ref} , such that we get from Equation (5-2):

$$\underbrace{\frac{\partial Q^2_{dB}(...)}{\partial P_{dB}}}_{0}=\frac{\partial\zeta(...)}{\partial P_{dB}}\underbrace{\left(OSNR_{dB}-Pen_{NL,dB}(\Phi_{NL,dB},D_{res})-...\right)}_{0 \text{ since } Q=Q_{ref}}+\zeta(...).\left(1-\frac{\partial Pen_{NL,dB}(\Phi_{NL,dB})}{\partial\Phi_{NL,dB}}\right) \tag{5-3}$$

Indeed, OSNR and nonlinear phase ϕ_{NL} are both proportional to P_{line} in linear scale, or equivalently derivatives of the $OSNR_{dB}$ and $\phi_{NL,dB}$ with respect to $P_{line,dB}$ in (dBxdB) scale are equal to 1. This also means that the derivative of penalty with respect to power in (dBxdB) scale is equal to the derivative with respect to the nonlinear phase (in dBxdB) scale.

Therefore, the **optimum power corresponds in fact to an optimum value of non-linear phase such that the derivative of the penalty versus non-linear phase function** $Pen_{NL,dB}(\Phi_{NL,dB},...)$ **(in dBxdB scale) is equal to unity**. This non-linear threshold corresponds to a specific amount of penalty. The same reasoning also applies with use of the

integrated power concept instead of the non-linear phase concept, since here, the integrated power is simply proportional to ϕ_{NL}.

A geometrical interpretation is also possible, as illustrated by Figure 5-1. We consider here a transmission system at two distances with fibre spans characterized by their input powers: one distance (left plots) is lower to the maximum reach of the system characterized by a reference threshold Q_{ref}; the other distance (right plots) is equal to the maximum reach of the system so that at optimized fibre input power the Q factor is equal to Q_{ref}. Top figures depict the evolution of Q factor versus power and bottom figures depict the evolution of the (actual) OSNR after transmission as well as the required OSNR to ensure $Q=Q_{ref}$. In good approximation, the OSNR grows linearly with power in dB scale with a slope of 1dB/dB (assuming amplifiers noise figures independent on power).

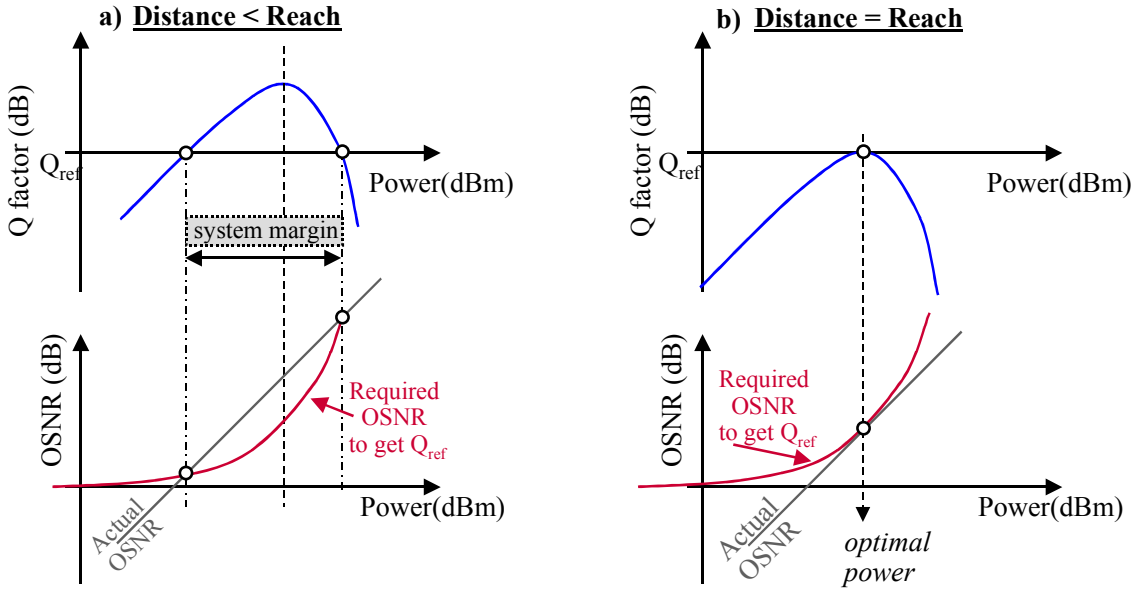

Figure 5-1: optimal power at maximum system reach. Evolution of Q factor (top) and actual OSNR / required OSNR to get $Q=Q_{ref}$ (bottom) as a function of input power into line fibre spans, for two configurations: distance lower than system reach, and distance equal to system reach (i.e. $Q=Q_{ref}$ for optimized power)

When the distance is lower than system reach, the Q factor is higher than Q_{ref} over a finite range of powers allowing system operation; within this range of powers, the actual OSNR is higher than the required OSNR to get Q_{ref}. When distance increases, the actual OSNR curve is shifted down, since OSNR decreases with distance, and the required OSNR curve is shifted to the left, towards lower values of power, since the required OSNR actually depends on the product between power and number of line fibre spans (or nonlinear phase). As a result, at maximum reach, the actual OSNR and required OSNR curve are tangent, corresponding to one single value of power allowing system operation with Q factor equal to Q_{ref}. Thus, for this optimal power value, the power-derivative of the required OSNR to get Q_{ref} is equal to 1dB/dB. It means that a small increase in power would lead to an increase of OSNR exactly compensated by the increase of the required OSNR or the OSNR penalty (in dB scales).

Since the required OSNR can actually be seen as a function of the product between span number and power, or more generally of the non-linear phase shift, this optimum power such that the derivative of penalty is 1dB/dB (Figure 5-2a) in one configuration of transmission (e.g. amplifier scheme or distance) indeed translates into an optimum value of the non-linear phase (or integrated power i.e. product between number of spans and power) that should remain the same for numerous system configurations. It is therefore meaningful to call such value the nonlinear threshold, and it is such that the derivative of the required OSNR with respect to the

integrated power or nonlinear phase is equal to 1dB/dB, as illustrated by Figure 5-2b. This nonlinear threshold must be calibrated (experimentally or numerically) for given fibre, format and channel spacing.

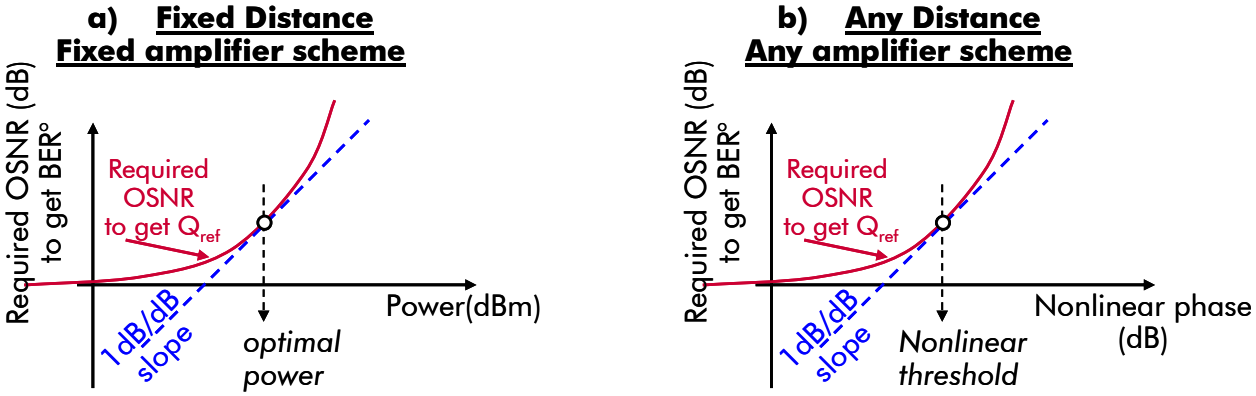

Figure 5-2 : Optimal power (a, left) and optimal nonlinear phase (b, right) corresponding to the unit slope of the curve "required OSNR" vs power (left) or nonlinear phase (right)

We see here that this proposed definition of nonlinear threshold is consistent with the abovementioned definitions: it corresponds to the amount of nonlinearities leading to the maximization of Q factor when this maximum is equal to the feasibility threshold Q_{ref}, for a distance being the maximum reach, and it also corresponds to a special point of the penalty versus nonlinear phase relationship. Moreover, such a definition does not rely any longer on an arbitrary choice of penalty or distance but is focused on the achievable reach of transmission systems, which makes particular sense for system design.

Note that for systems such that the function $\zeta(P_{dBm}, D_{res}...)$ from Equation (5-2) can be considered as constant when varying ϕ_{nl} (ie such that the Q factor scales proportionally to a constant power of the OSNR, then we can derive from Equation (5-3) that the nonlinear threshold is independent on the Q factor and on the reach.

For such NLT, the Q factor would be maximized with respect to power whatever the distance, noise and other sources of system penalties. Then, assuming N identical line fibre spans in the link, and considering the optimal performance with respect to N, we can infer that the optimal power varies proportionally to 1/N, where N is the number of spans, whereas OSNR scales proportionally to $1/N^2$ and the maximum Q factor scales proportionally to $1/N^{\alpha}$.

Generally, such NLT corresponds to penalties within 1 and 3dB depending on the considered classes of optical transmission systems, which is also inline with the choices made in Chapter 2 and 3 to assess the accuracy of the nonlinear phase criterion or define weighted nonlinear phases. In particular, if we refer back to the initial study presenting the nonlinear phase criterion (described in Chapter 2), we can deduce the nonlinear thresholds from the simulation results of the considered 40Gb/s-modulated systems with RZ format and based on SMF, TeraLight or LEAF transmission fibre. Out of the simulation results representing the penalty versus for different configurations of distance or power, we obtained polynomial interpolations of the measured relationships between penalty and nonlinear phase, out of which we measured the NLTs. The NLTs were found equal to 0.27π, 0.32π and 0.32π rad for SMF, LEAF™ and TeraLight™ line fibre type respectively (+4.3, 5.0 and 5.0dB with respect to 0.1π rad reference), with almost identical penalties around 2.3dB, leading to a required OSNR of 22.8dB to ensure 10^{-5} BER.

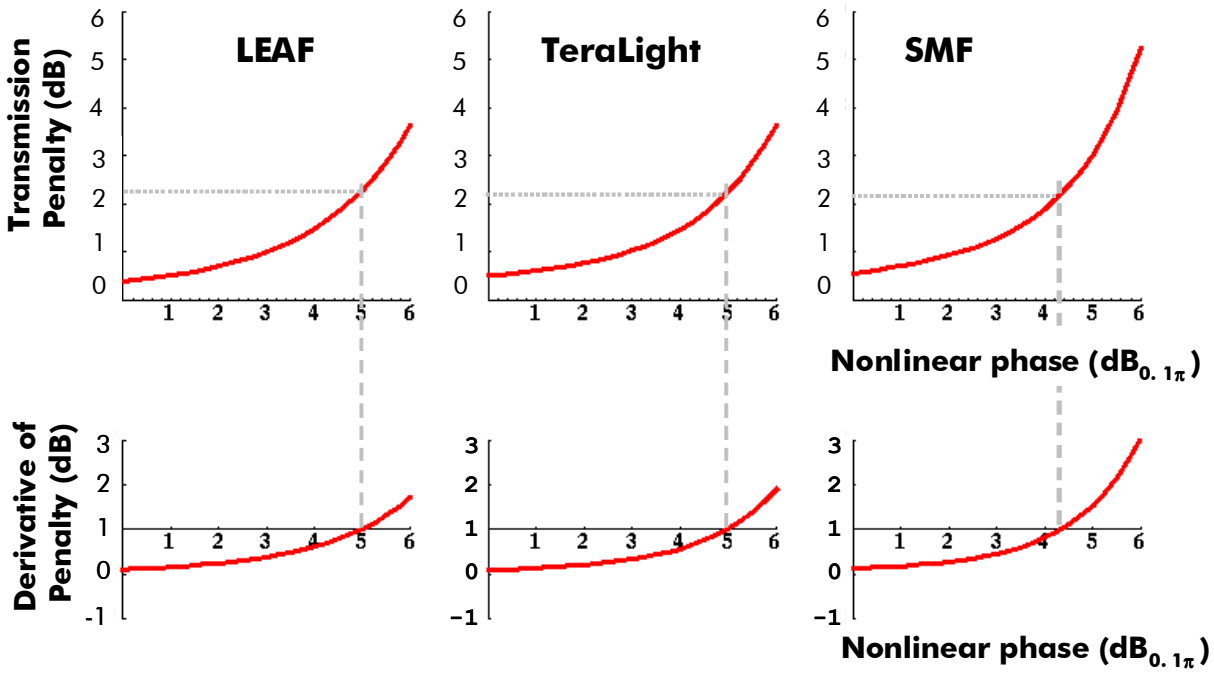

	LEAF	TeraLight	SMF
NLT (rad)	0.32 π / 5.0 $dB_{0.1\pi}$	0.32 π / 5.0 $dB_{0.1\pi}$	0.27 π / 4.3 $dB_{0.1\pi}$
Required OSNR (10^{-5} BER, w/in 0.1nm)	22.8 dB	22.8 dB	22.8 dB

Figure 5-3 : Up: Penalty vs nonlinear phase fitting curves stemming from simulation results of [171] for LEAF, TeraLight and SMF fibres and 40Gb/s RZ modulation format.
Middle: derivative of penalty curve and optimal phase with unit derivative.
Bottom: summary of the maximum-reach NLTs and required OSNRs to ensure 10^{-5} BER.
Nota: nonlinear phase expressed in $dB_{0.1\pi}$ unit means $10\log_{10}$ of the ratio of nonlinear phase in rad unit over 0.1π rad.

In practice the measurements of the nonlinear threshold may be subject to inaccuracy because of the difficulties to measure the exact value of nonlinear phase (or power) such that the derivative of the penalty function is equal to 1dB/dB, or such that the Q factor is maximized; such difficulties essentially lie in the accuracy of the nonlinear phase criterion itself (see Chapter 2), in the accuracy in the measurement of the required OSNR or the Q factor, in the granularity of the investigated series of power or nonlinear phase, and in the accuracy in the determination of an optical power or nonlinear phase. It is often more practical to measure an effective nonlinear threshold for a constant penalty, close to the one corresponding to the true nonlinear threshold. From a system perspective, this inaccuracy has a negligible impact because of the definition of the nonlinear threshold: a small shift of power δP (in dB scale) from the true nonlinear threshold leads to the same shift δP of the actual OSNR and of the required OSNR, so that the Q factor remains constant, at first order.

In conclusion, we have shown that it is possible to characterize a whole class of systems by the knowledge of the non-linear threshold NLT and the corresponding transmission penalty provided the validity of the nonlinear phase criterion. Besides, we have proposed a definition of nonlinear threshold with a true physical meaning since it sets the limits of feasibility of the system. This paves the way to simple rules for reach estimation and power tuning. In the following, we will develop analytical rules exploiting the NLT.

.

5.II. Design rules derived from the definition of a NLT

In this section, we extrapolate the previous results stating that the system reach can be characterized by a nonlinear threshold along with corresponding OSNR penalty for a reference BER and derive simple tools to optimize the input powers into fibre sections and estimate the reach of dispersion-managed optical transmission systems. We will first consider homogeneous transmission systems with identical line fibre and dispersion-compensation sections, then generalize the tools to heterogeneous systems typical of deployed optical networks.

There is a special interest for such tools in addition to complex quality of transmission estimators for mainly three reasons: firstly, they enable to estimate very simply the reach of systems due to noise and Kerr limits; secondly they provide guidance to set the input powers into the different fibre sections; and thirdly they enable to draw comparisons and optimize subsystems such as modulation formats, amplifier schemes, line or compensating fibres.

II.1. Simple reach estimator and optimal power setting rules for homogeneous transmission systems, as a trade-off between noise and nonlinearities

Let us consider here a class of systems characterized by their non-linear threshold NLT, corresponding to a reference penalty, thus to a required OSNR after transmission, denoted S, to obtain a reference BER. This required OSNR S can also include penalties stemming from non-Kerr sources of impairments.

We will consider a transmission system belonging to this class, with M identical line fibre sections, and identical repeaters after each line fibre section (with constant, identical noise figures, identical output per channel power P_{line} and hosting Dispersion Management modules). For simplicity reasons, we overlook in this first step the differences from one Dispersion Compensating Module to the other due to the specific choice of dispersion map and overlook the impact of the pre-compensation module.

To account for the accumulation of non-linearities, we can consider equivalently either the non-linear phase, or the integrated power, simply proportional. In the following, we choose the non-linear phase terminology, ϕ_{NL}. With these assumptions, the OSNR and ϕ_{NL} evolutions with M and P_{line}, as well as system limitations, can be expressed as follows:

$$\begin{cases} .OSNR\left(P_{line}, M\right) = OSNR°\left(P°, M=1\right).\dfrac{P_{line}}{P°.M} & \geq S \\ .\Phi_{NL}\left(P_{line}, M\right) = \Phi_{NL}°\left(P°, M=1\right).\dfrac{P_{line}}{P°}.M & \leq NLT \end{cases} \quad (5\text{-}4)$$

with P° as an arbitrary reference power, OSNR° (resp. ϕ°) as the OSNR (resp. the accumulated non-linear phase) after one section of line fibre and the following inline repeater, for input power P°, assuming infinite OSNR and null non-linear phase at section entry. The set of Equations (5-4) means that the OSNR, which scales proportionally with P_{line} and with the inverse of span number, is expected to remain above the required OSNR limitation S at non-linear threshold, while at the same time, the non-linear phase, which scales proportionally with P_{line} and span number, is expected to remain below the non-linear threshold NLT, as illustrated by Figure 5-4.

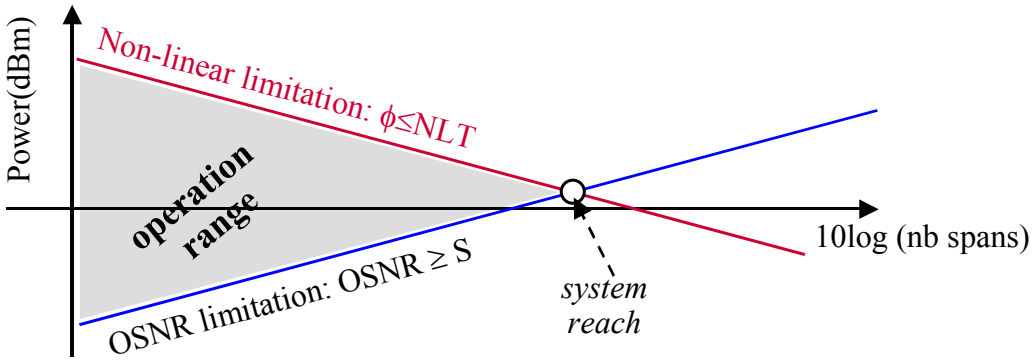

Figure 5-4: Evolution of range of span input powers for system operation with respect to distance.

At maximum reach $M_{max,}$ with optimized power P_{opt}, non-linear phase will be equal to NLT, and the OSNR will be equal to the corresponding required OSNR S. Thus, we get:

$$\begin{cases} M_{\max} = \sqrt{\frac{NLT}{\Phi^\circ}}\sqrt{\frac{SNR^\circ}{S}} \\ P_{line,opt} = P^\circ \cdot \sqrt{\frac{NLT.S}{\Phi^\circ.SNR^\circ}} \end{cases} \text{, or in dB scale: } \begin{cases} M_{\max,dB} = \frac{NLT_{dB} - \Phi^\circ_{dB}}{2} + \frac{SNR^\circ_{dB} - S_{dB}}{2} \\ P_{line,opt,dBm} = P^\circ + \frac{NLT_{dB} - \Phi^\circ_{dB}}{2} + \frac{S_{dB} - SNR^\circ_{dB}}{2} \end{cases} \quad (5\text{-}5)$$

We clearly see the trade-offs between nonlinearities and OSNR to determine the transmission distance. We can observe that an increase of x dB in the NLT or in the OSNR sensitivity respectively will result in an increase, respectively a decrease of x/2 dB in the achievable reach. Up to now, replacing the non-linear phase concept by the integrated power is possible, leading to ad hoc rules.

The proposed reasoning leads to the same tools as the ones proposed by [186][187] to optimize amplifier schemes based on the maximization of the OSNR at constant nonlinear phase or based on the minimization of nonlinear phase shift at constant OSNR degradation.

Such tools are very useful to compare the performance of modulation formats, to compare and optimize amplifier schemes including Erbium and/or Raman amplification [186][187], or to find trade-offs in the design of new line fibres or dispersion-compensating fibres [177][178][179][181].

We will illustrate such applications in section 5.III. in particular with the works related to the optimization of the amplification scheme of transmission experiments [173][174][175][176].

II.2. Simple reach estimator and optimal power setting rules for heterogeneous transmission systems

II.2.1. Introduction

We show in this section how the previously proposed tools to estimate reach and set optical powers can be extended to heterogeneous transmission systems with a mix of fibre sections: this heterogeneity may come from the different losses and lengths of the fibre sections mainly due to the unequal amplifier spacing and to the age of installed fibres, from the difference between line fibre and DCF types, and from different types of line fibre with possibly different chromatic dispersions.

First of all, the notion of achievable reach is well suited for homogeneous transmission systems made of a concatenation of N identical blocks (made of fibre and amplifier sections for instance) such that N is the maximum number of blocks compatible with a reference quality of transmission after transmission. Should we consider heterogeneous transmission systems typical of optical networks, predicting a reach is not feasible. However, it is still possible to predict the feasibility of an optical connection and to build tools to set fibre input powers so as to enable the longest possible optical connections. The degree of heterogeneity that can be tackled by such tools first depends on the used metrics to measure the accumulation of nonlinearities: the integrated power enables to deal with unequal span loss and length; the nonlinear phase additionally enables to deal with DCF versus line fibre heterogeneity, eventually the weighted nonlinear phase additionally enables to deal with the heterogeneity of line fibre type (mainly chromatic dispersion, along with span length and power distribution over a span with more accuracy than nonlinear phase, as explained in Chapter 3).

II.2.2. Positioning of the work

In [191], A. Mecozzi presented in 1998 a method to optimally set the amplifier gain distribution along a line composed of spans with unequal amplifier spacing (leading to span-dependent losses), in order to minimize the average power of the line at constant OSNR, which is equivalent to minimizing the nonlinear phase shift at constant OSNR. He established the equivalence with a strategy consisting in maximizing the OSNR at constant average power, and showed that the optimal distribution of gains was such that the power in the middle of each line fibre span is constant along the line. It means that for spans with x dB extra-loss with respect of reference spans, the input power will be increased by approximately x/2 dB (at the same time the output power will be decreased by approximately x/2 dB as well, such that at mid span, the power is independent on span loss). Such an optimization problem was solved using a Lagrange multiplier technique [193][194] and was based on the assumption that the average power was a good metrics for the accumulation of nonlinearities per span.

From the results mentioned earlier in this manuscript, we can establish the validity of this model. In Chapters 2 and 3, we have shown that the nonlinear phase is a good metrics to capture the accumulation of nonlinearities; thus in case of transmission fibre sections differentiated by their length or attenuation (and overlooking the impact of dispersion compensating fibres), it is proportional to the sum of the span-averaged powers of each section. Based on our work on nonlinear phase from Chapter 2 or [171], S.K. Turytsyn et al extended the work from Mecozzi the case of line fibre and DCF heterogeneity [192]. Moreover, from the previous section, we know that a particular value of nonlinear phase, the NLT, corresponds to the limits of system feasibility, associated to a corresponding required OSNR to ensure the reference BER. Therefore setting powers of a transmission system so as to maximize the OSNR at a given nonlinear phase such as the NLT actually enables to improve

system margins and increase the reach, up to the point when the maximum OSNR becomes equal to the target required OSNR.

In the following, we extend the work from Mecozzi or Turytsyn to multiple types of heterogeneity based on the weighted nonlinear phase criterion and further show that the power setting rules are indeed very simple.

II.2.3. Proposed model

In [172], we extend the study from Mecozzi to other types of heterogeneity with a slightly different approach yet fully compatible. The problem is here to optimize fibre input power distribution in a heterogeneous link where the concepts of integrated power, non-linear phase or weighted non-linear phase are applicable.

Let us consider a dispersion-managed heterogeneous system composed of N sections of fibre followed by an amplifier. The types of transmitters and receivers as well as the spectral distribution of channels are given.

The propagation over each section i=1..N is characterized by the accumulated phase $\phi^\circ_{(i)}$ (weighted nonlinear phase, standard nonlinear phase or integrated power, i.e. fibre input power for one fibre section), and by the degradation of the signal to noise ratio $OSNR^\circ_{(i)}$ (assuming no noise at section input) for a reference section input power P°.

Let NLT_i be the nonlinear threshold (expressed in terms of weighted nonlinear phase, nonlinear phase or integrated power, with same convention as ϕ°) corresponding to the type of fibre section i (mainly the chromatic dispersion and the span length, or the power distribution profile), in the context of an homogeneous transmission system composed of all sections identical to section i; this nonlinear threshold corresponds to a given required OSNR, namely S, to ensure a reference BER. We note here that when considering a weighted nonlinear phase formulation, the nonlinear threshold is equal to 1, by definition. For sake of simplicity, and in good agreement with the results of section I.1. , we assume here that the required OSNR S is independent of fibre type. In a dispersion-managed system, those fibre sections are alternatively made of line fibre sections or Dispersion Compensating Fibres, followed by an amplifier with a noise figure independent on input/output power. For each Dispersion Compensating Fibre, we consider a non-linear threshold identical to that of the preceding line fibre section to compensate for, in agreement with the non-linear phase criterion.

The degree of freedom for each fibre section is the input power P_i Under those assumptions, we expect the OSNR at transmission end to be higher than S, and the sum of the phases of each section weighed by their NLT to be lower than 1, when transmission is feasible. Noise and non-linear constraints can hence be expressed in agreement with the nonlinear phase and weighted nonlinear phase criteria studied in Chapter 2 as:

$$\begin{cases} \dfrac{1}{OSNR(N,P_1,...P_N)} = \displaystyle\sum_{i=1}^{N} \frac{1}{OSNR^\circ_{(i)}} \frac{P^\circ}{P_i} \le \frac{1}{S} \\ \widetilde{\Phi}_{NL}(N,P_1,...,P_N) = \displaystyle\sum_{i=1}^{N} \frac{\Phi^\circ_{(i)}}{NLT_i} \frac{P_i}{P^\circ} \le 1 \end{cases} \qquad (5\text{-}6)$$

System optimization corresponds here to the find optimal set of fibre input powers ($P_{i=1...N}$) to maximize N. We propose the following changes of variables: for each i=1..N, we define

$$\overline{P_i} = P^\circ \sqrt{\frac{NLT_i.S}{\Phi^\circ_{(i)}.SNR^\circ_{(i)}}} \text{ and } \overline{N_i} = \sqrt{\frac{NLT_i}{\Phi^\circ_{(i)}}} \sqrt{\frac{SNR^\circ_{(i)}}{S}} \qquad (5\text{-}7)$$

corresponding to the optimal power and maximum reach of an homogeneous (dispersion-managed) system characterized by all spans identical to spans (i).

We also define:

$$y_i = P_i / \overline{P_i} \tag{5-8}$$

Thus the set of Equations (5-6) can be rewritten as $H_1(N,\underline{y})$ and $H_2(N,\underline{y})$:

$$\begin{cases} H_1(N,\underline{y}) = \sum_{i=1}^{N} \frac{y_i}{\overline{N_i}} \le 1 \\ H_2(N,\underline{y}) = \sum_{i=1}^{N} \frac{1}{\overline{N_i} y_i} \le 1 \end{cases} \tag{5-9}$$

Let us eventually define the function $H(N,\underline{y})$ such that

$$H(N,\underline{y}) = \frac{H_1(N,\underline{y}) + H_2(N,\underline{y})}{2} = \frac{1}{2}\sum_{i=1}^{N} \frac{1}{\overline{N_i}} \left(y_i + \frac{1}{y_i} \right) \tag{5-10}$$

By construction, as long as the transmission is feasible, we have: $H(N,\underline{y}) \le 1$. Besides, for all $\underline{y}$, $H(N,\underline{y}) \ge \sum_{i=1}^{N} \frac{1}{\overline{N_i}}$, with equality between both terms when $\underline{y}=(y_1, \ldots, y_n) = (1,\ldots 1)$. Let us now define N_{max} as:

$$N_{\max} = Max\left\{ N \text{ such that } \sum_{i=1}^{N} \frac{1}{\overline{N_i}} \le 1 \right\} \tag{5-11}$$

The number of fibre sections N cannot be higher than N_{max}, otherwise $H(N,\underline{y}) > 1$, which would mean that the transmission is not feasible. Conversely, for all N lower or equal to N_{max}, then we can choose a set of normalized powers $\underline{y}=(y_1, \ldots, y_n) = (1,\ldots 1)$, such that $H(N,\underline{y}) = H_1(N,\underline{y}) = H_2(N,\underline{y}) = \sum_{i=1}^{N} \frac{1}{\overline{N_i}} \le 1$, which satisfies the feasibility criteria. It can be noted that in doing so, the noise-related (H_1) and non-linear (H_2) constraints are identical. Then, the maximum reach of the system is actually equal to N_{max}. Besides, the dimensionless vector $\underline{y}=(y_1, \ldots, y_n) = (1,\ldots 1)$ is the one enabling the longest reach.

II.2.4. Conclusion

If we look back at our transmission system, we have shown that the optimum combination of powers simply consists in setting the power of each fibre section in order to allow maximum reach of a virtual link composed only of a succession of this replicated section ($P_i = \overline{P_i}$, following Equation (5-7)). Following such rules, the setting of power for one fibre section is independent of the nature of the other fibre sections of the transmission line. With such rules, non-linear and noise constraints become identical, and Equation (5-11) guarantees the feasibility of the connexion.

II.2.5. Practical applications

a) One practical application concerns transmission links with line fibre sections differentiated by their losses: x dB higher loss should result in a fibre input power increased by x/2 dB, in full agreement with the results of Mecozzi.

b) Moreover, we can also note that the chosen formalism makes such rules particularly adapted for line fibre type heterogeneity as well: if we consider for instance a one practical application with a transmission link with line fibre sections differentiated by their nonlinear threshold: a x dB higher nonlinear threshold should result in a fibre input power increased by x/2 dB.

c) One final practical application concerns the heterogeneity between line fibre and DCF. In the case of identical sections of line fibre and DCF, the maximum achievable number of line fibre spans M_{max} becomes:

$$\frac{1}{M_{\max}} = \frac{1}{\overline{N}_{(line\ fiber)}} + \frac{1}{\overline{N}_{(DCF)}} \qquad (5\text{-}12)$$

We established that particular point in [178] and this point is in full agreement with the model from [181].

Besides, the optimum input powers into line fibre and DCF can be derived from Equation (5-7):

$$\overline{P}_{DCF/line} = P^{\circ}\sqrt{\frac{NLT.S}{\Phi^{\circ}_{DCF/line}.SNR^{\circ}_{DCF/line}}} \qquad (5\text{-}13)$$

As a result, we can derive the optimum ratio between input powers into line fibres and DCF, in full agreement with [192]:

$$\frac{\overline{P}_{line}}{\overline{P}_{DCF}} = \sqrt{\frac{\Phi^{\circ}_{DCF}.SNR^{\circ}_{DCF}}{\Phi^{\circ}_{line}.SNR^{\circ}_{line}}} \qquad (5\text{-}14)$$

If we assume localized amplifiers with identical noise figure after each fibre, we get

$$\begin{aligned}
\Phi^{\circ}_{k} &= \frac{2\pi}{\lambda}\frac{n_{2,(k)}}{A_{eff,(k)}}P^{\circ}L_{eff,(k)} \\
OSNR^{\circ}_{(k)} &= \frac{P^{\circ}e^{-\alpha_{(k)}L_{(k)}}}{NF.h\nu.\Delta\nu} \\
\frac{\overline{P}_{line}}{\overline{P}_{DCF}} &= \sqrt{\frac{n_{2,DCF}.L_{eff,DCF}.e^{-\alpha_{DCF}L_{DCF}}}{A_{eff,DCF}}.\frac{A_{eff,line}}{n_{2,line}.L_{eff,line}.e^{-\alpha_{line}L_{line}}}}
\end{aligned} \qquad (5\text{-}15)$$

With such a formula, we can then compare the optimum power ratio and the ones chosen in the numerical and experimental simulations in Chapter 2s and 3, between 4 and 10dB with typical values around 7dB. For that purpose, we consider typical dispersion-managed transmission systems composed of 100km-long sections of SMF or LEAF fibre fully compensated by DCF. The main characteristics of the transmission and compensating fibres are described in Table 5-1. The analytic estimation of the optimum power ratio between input powers into SMF and DCF sections gives 4.8, which amounts to 6.7dB in logarithmic scale. The analytic estimation of the optimum power ratio between input powers into LEAF and DCF sections gives 4.8, which amounts to 8.2dB in logarithmic scale. Such power ratios are fully inline with the ratios considered in Chapters 2 and 3.

Parameter (at 1550nm)	***SMF***	***DCF for SMF***	***LEAF***	***DCF for LEAF***	***Unit***
Nonlinear index	$n2_{line}$ =2.6	$n2_{dcf}$=3.0	$n2_{line}$ =2.7	$N2_{dcf}$=3.0	10^{-20} m^2/W
Attenuation	α_{line} = 0.2	α_{dcf}=0.5	α_{line} = 0.2	α_{dcf}=0.5	dB/km
Chromatic Dispersion	D_{line}=17	D_{DCF}=-100	D_{line}=4.25	D_{DCF}=-150	ps/nm/km
Effective Area	$A_{eff,line}$=80	$A_{eff,DCF}$=20	$A_{eff,line}$=72	$A_{eff,DCF}$=15	μm^2
Fibre length	L_{line}=100	L_{dcf} = 17	L_{line}=100	L_{dcf} = 2.8	km

Table 5-1 : Typical figures representative of line fibres (SMF or LEAF™) and matching DCFs.

II.3. Derived tools to compare the system impact of modulation formats, fibres, and amplifiers

In the previous sections, we proposed rules to predict the system reach and to optimize the input powers into the fibre sections of a transmission link, accounting for the accumulation of nonlinearities and noise, and assuming the validity of the (weighted) nonlinear phase criterion.

More particularly, Equation (5-5) can be rewritten so as to enable to distinguish the impact of the modulation format M_{format} from the impact of the infrastructure (amplifiers, fibres) M_{ampli} as:

$$M_{\max} = \underbrace{M_{\max,format}}_{=} * \underbrace{M_{\max,ampli}}_{=} = \sqrt{\frac{NLT}{S}} * \sqrt{\frac{SNR°}{\Phi°}} \quad \textit{i.e.} \quad M_{\max,dB} = \underbrace{M_{\max,format,dB}}_{=} + \underbrace{M_{\max,ampli,dB}}_{=} = \frac{NLT_{dB} - S_{dB}}{2} + \frac{SNR°_{dB} - \Phi°_{dB}}{2} \qquad (5\text{-}16)$$

Additionally, this separation also enables to make a distinction between contributions that will be obtained from numerical simulations or experiments (M_{format}) and contributions that canbe obtained analytically (M_{ampli}).

Indeed, a change of modulation format (or transceiver, channel spacing) results in a change of the nonlinear threshold NLT and/or the required OSNR S to ensure an acceptable BER, and thus the achievable distance scales proportionally with M_{max} i.e. the ratio $\sqrt{NLT/S}$. Getting back to the original study dealing with the nonlinear phase criterion in Chapter 2 and the extracted NLT and required OSNR in section I.1. , we can deduce M_{format} for 40Gb/s transmission systems over LEAF, TeraLight and SMF fibre types, respectively equal to -11.4dB, -11.4dB and -11.05dB. It means that a transmission on SMF and TeraLight with the same ratio of OSNR over nonlinear phase after one span would lead to a maximum achievable transmission distance on SMF reduced by 0.35dB (8%) with respect to a transmission on TeraLight, due only to the larger dispersion of SMF.

On the other hand, a change of amplifier scheme (localized versus distributed amplification, impact of amplifier noise figure, of gain distribution within the dual-stage amplifier structure) or type of DCF will essentially result in changing the reach proportionally to M_{ampli}, the ratio $\sqrt{SNR°/\Phi°}$ between the OSNR degradation SNR° and the nonlinear phase shift ϕ° accumulated after one line fibre section followed by an amplification site. The amplifier site

can itself include a dual stage-amplifier hosting DCF. A formal decoupling of the impact of line fibre and DCF is also possible using Equation (5-12).

$$\frac{1}{M_{\max}} = \frac{1}{\overline{N}_{(line\ fiber)}} + \frac{1}{\overline{N}_{(DCF)}} = \sqrt{\frac{S}{NLT}}.\left(\sqrt{\frac{\Phi°_{line}}{SNR°_{line}}} + \sqrt{\frac{\Phi°_{DCF}}{SNR°_{DCF}}}\right) \qquad (5\text{-}17)$$

Of course, finely assessing the system impact of a change of a fibre parameter such as length or chromatic dispersion may require considering the induced changed in the $\sqrt{NLT/S}$ ratio. We can account as well for the impact on this ratio when considering the difficulties to manage the dispersion identically over the whole spectrum due for instance to a mismatch of line fibre and DCF chromatic dispersion profiles over the amplification spectral band [177][178][179].

Eventually, note that we can make a similar distinction and similar reasoning concerning the estimation of the optimal input power:

$$\begin{aligned} P_{line,opt} &= P°.\ \underbrace{f_{format}}_{=} * \underbrace{f_{ampli}}_{=} \\ &= P°.\sqrt{NLT.S} * \sqrt{\frac{1}{\Phi°.SNR°}} \end{aligned} \quad \text{i.e.} \quad \begin{aligned} P_{line,opt,dBm} &= P°_{dBm} + \underbrace{f_{format,dB}}_{=} + \underbrace{f_{ampli,dB}}_{=} \\ &= P°_{dBm} + \underbrace{\frac{NLT_{dB} + S_{dB}}{2}}_{f_{format,dB}} + \underbrace{\frac{-\Phi°_{dB} - SNR°_{dB}}{2}}_{f_{ampli,dB}} \end{aligned} \qquad (5\text{-}18)$$

We will illustrate such applications in the following section in particular with the works related to the optimization of the amplification scheme of transmission experiments.

5.III. Application to the design of an ultra-long haul experiment based on hybrid Raman and Erbium amplification

III.1. Introduction

We propose here to apply the formerly presented tools to the design of the amplifier architecture of one of the first ultra-long-haul multi-terabit/s experiments [173] , the transmission of 125 WDM channels modulated at 42.7Gbit/s (5 Tbit/s capacity) over 12x100 km of TeraLight™ Ultra fibre, that was presented at the post-deadline session of ECOC conference in 2001.

If we come back to March 2001 at OFC conference, the 10Tbit/s capacity barrier had just been broken over limited distances (under 120km) [200][201]; at the same conference 1200km distance had been reached while transmitting data at 3Tbit/s [202] based on distributed Raman amplification in the transmission fibre coupled with Erbium-doped fibre amplification (EDFA).

At ECOC conference in September 2011 we demonstrated 5Tbit/s capacity over 1200km. As in the aforementioned record experiments, our 125 WDM channels carried electrically time-division multiplexed (ETDM) data at 40Gbit/s effective rate. These channels were separated alternatively by 50 and 75GHz and de-multiplexed by optical vestigial-side band (VSB) filtering, as proposed in [203], yielding the high spectral efficiency of 0.64bit/s/Hz with regular NRZ format. The transmission was carried out over twelve 100km-long spans of TeraLight™ Ultra fibre, separated by optimized Raman-assisted erbium-doped fibre amplifiers operated in C and L bands. In this experiment, as opposed to [202] [188] [190], Raman amplification was applied in both the transmission fibre and the DCF and the optimization was achieved using the tools that we have introduced in the previous section.

In the following, we describe the analytical process of optimization of hybrid Raman-Erbium amplification used or this experiment, then the experiment itself.

III.2. Design of Raman + Erbium amplifier scheme

The link design of terrestrial transmission systems is usually made of transmission fibre sections separated by discrete optical amplifiers every 80-100km. One way to increase the reach of such a transmission system is to ensure a more distributed amplification along the link. While the reduction of amplifier spacing is not an option in terrestrial system, Stimulated Raman Scattering process can be used to transform the transmission and even the dispersion compensation fibres into distributed amplifiers thanks to the use of pumps operated at wavelengths approximately 100nm lower than the signal wavelength [198][196][197][186][187].

The principles of the calculation of the Raman gain and the generated noise power for backward Raman amplification are detailed in Appendix V.1. By extension, they enable to calculate the OSNR or the nonlinear phase shifts.

Here, we apply the results of the section 5.II. to optimize the amplifier scheme of dispersion–managed systems based on 100km sections of TeraLight™ Ultra fibre with 0.2dB/km attenuation (lab conditions) through a mix of distributed Raman and localized Erbium amplification. To do so, we do a parametric investigation of the distribution of gains stemming from Raman or Erbium amplification in the line fibre and the DCF. At the time this study has

been made, it could be found similar to the works conducted in [188] [190] that used the same tools as the ones introduced in the previous sections, but the specificity of our study was to consider Raman amplification in the DCF and to apply the results directly to a transmission experiment.

Set-up

The transmission scheme of an ultra-long haul system can be seen as basically composed of the accumulation of line fibre sections of 100km, separated by modules of Dispersion Compensation and amplifiers (distributed and/or discrete). Transmission fibre is characterized by 8ps/nm/km chromatic dispersion, 0.2dB/km attenuation, 63μm^2 effective area at 1550nm, 0.283dB/km attenuation at 1450nm; DCF is characterized by a length of 10km, a chromatic dispersion of -80ps/nm/km, 0.6dB/km attenuation, splice losses equal to 0.5dB, 17μm^2 effective area at 1550nm, and 0.7dB/km attenuation at 1450nm.

At the output of each fibre section, backward Raman pumps can be inserted through waveband-multiplexers however bringing 0.5dB additional loss. Eventually, localized optical amplifiers are considered with 6dB noise figures and gains G_1 and G_2 after transmission and dispersion compensating fibres respectively. Figure 5-5 summarizes the main elements of this periodic pattern of fibre sections and amplifiers, and Figure 5-6 illustrates the impact of backward Raman amplification in the channel power evolution with distance within a 100km-long span and following DCF.

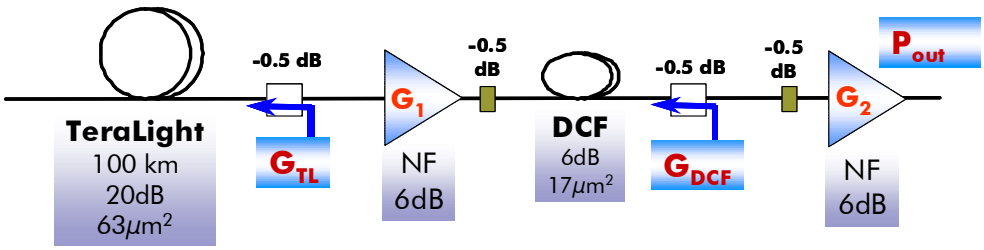

Figure 5-5: Periodic pattern of a line fibre span followed by DCF within a dual-stage amplifier structure for an ultra-long haul transmission system. The amplifier structure possibly includes distributed backward Raman pumping in the line and DCF fibres.

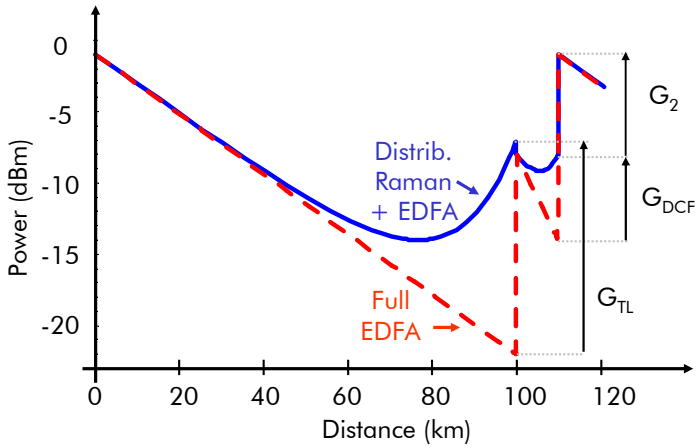

Figure 5-6: Typical power profile with distance for a 100km-span followed by DCF in case of localized EDFA-assisted amplification after each fibre (dashed red line) or in case of distributed backward Raman + localized EDFA amplification (blue solid line) with 15dB OnOff Raman gain in the line fibre and 6dB in the DCF, and EDFA after the DCF.

In the study, the Raman gain in line fibre and in DCF as well as the gain in the first EDFA are varied by steps of 0.5dB from 0dB and up to the necessary and sufficient value to compensate

for the total loss of the periodic pattern. G_2 is adjusted so that the total loss of the pattern is fully compensated for.

Then for each combination gains the nonlinear phase and the OSNR of the periodic pattern are computed assuming unit input power in to the line fibre, thus corresponding to the ϕ_{nl}° and SNR° used in the previous section. Assuming then that we can utilize the nonlinear phase criterion, one can compute the reach impact of a change of amplifier scheme from Equation (5-16), and more particularly M_{ampli}.

Results

In absence of Raman pumping, M_{ampli} is maximized when G_1=14dB and G_2 = 13dB and this maximum is equal to 22.3dB. We can note that this means that the input power into DCF is 6.5dB lower than in line fibre, which is in the same order of magnitude as the studies from Chapter 2 and 3 and is fully consistent with the calculation of the optimum ratio of input powers from Equation (5-15). This optimized configuration, further denoted as "all EDFA" configuration, will be our reference starting from now.

Adding Raman amplification in the line fibre enables to increase M_{ampli} by 2.5dB (up to 24.7dB) and then the maximum achievable distance by 76% with respect to the reference case. This optimum configuration relies on a Raman gain of 18dB in the line fibre, and no first-stage EDFA, as illustrated by Figure 5-7. In details, ϕ_{nl}° increases by 1.5dB but SNR° increases by 6.4dB with respect to the reference. If we focus on the Raman amplified span of TeraLight Ultra and the first stage EDFA, the nonlinear phase at constant input power increases by 0.9dB, which is counterbalanced by a decrease of the effective noise figure (i.e. the noise figure of an equivalent localized amplifier located at fibre end) from 6dB to -1.4dB, which corresponds to an increase of the OSNR at constant fibre input power by 7.4dB. This highlights the net benefit of distributed Raman amplification. We can further observe in Figure 5-7 that for Raman gains equal or higher than 15dB, the first stage EDFA has to be removed to achieve the best performance. From Equation (5-18), we eventually get that the optimal power is decreased down by 3dB with respect to the "all-EDFA" configuration.

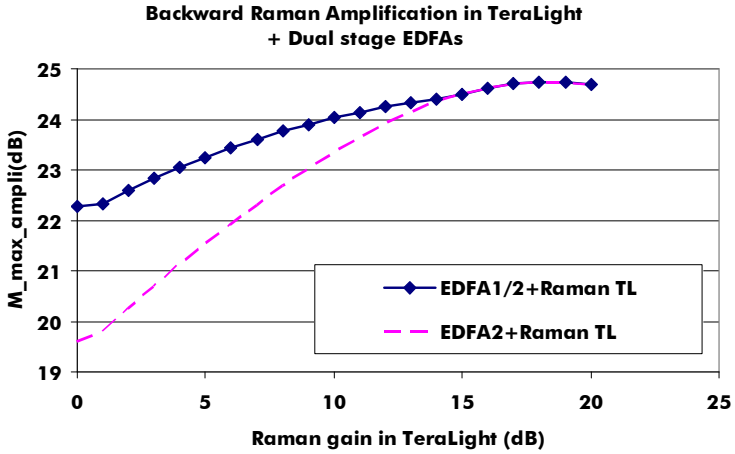

Figure 5-7 : Distributed Raman amplification in the line fibre combined to dual-stage Erbium amplification: evolution of $M_{max,ampli}$ with the backward Raman gain in TeraLight Ultra fibre, provided optimal setting of the amplifier gains, in absence of Raman gain in the DCF, and assuming the presence (blue solid line) or the absence (red dotted line) of a first stage localized amplifier.

Let us now consider the more general case of hybrid amplification with Distributed Raman Amplification in both the line fibre and the DCF. Figure 5-8 shows the relative gain of using combined Raman amplification in line fibre and DCF. For the optimal configuration, M_{ampli}

tops at 24.9dB, which corresponds to 83% increase of reach with respect to the "all-EDFA" scheme and +5% with respect to the hybrid amplification scheme without DCF pumping, with Raman gains in line fibre of 15dB and in DCF of 7dB, while the first stage of the EDFA is suppressed. The optimal power into the transmission fibre is here 3.4dB lower than for the EDFA scheme. Obviously Raman pumping in the DCF brings a negligible advantage from a pure performance perspective, but it enables to relax the constraints on the Raman pumping in the line fibre: reaching successfully 95% of the best achievable distance requires +/- 2.5dB accuracy on the Raman gain in line fibre (from 17 to 22dB) for the configuration without pumping in DCF, while the required accuracy is +/- 4.5dB in presence of DCF Raman pumping (from 12 to 21dB). This feature can be key to guarantee high performance for experiments or for deployed systems. Moreover, the reduced amount of Raman gain in the TeraLight fibre when also Raman-pumping the DCF should help reducing the impact of Double Rayleigh Scattering [182].

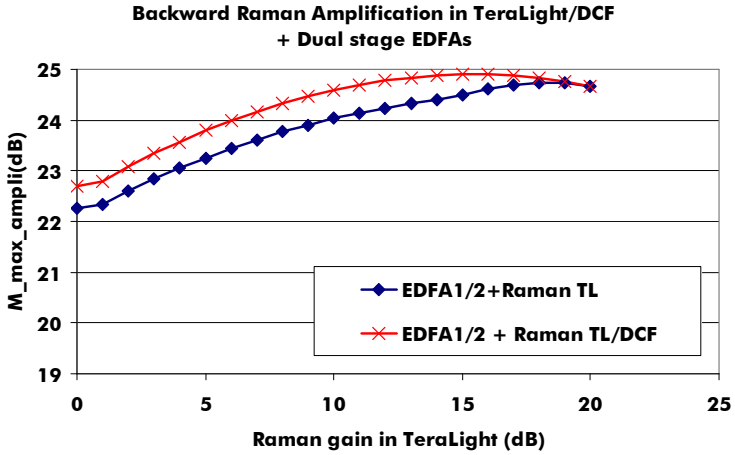

Figure 5-8: Distributed Raman amplification in the line fibre and DCF, combined to dual-stage Erbium amplification: evolution of $M_{max,ampli}$ with the backward Raman gain in TeraLight Ultra fibre, provided optimal setting of the amplifier gains (discrete plus distributed), in presence (blue solid line) or absence (red dotted line) of distributed Raman amplification in the DCF.

Table 5-2 summarizes the abovementioned performance associated with the different amplification schemes. In addition we can notice that using full-Raman amplification through the suppression of the EDFA after the DCF would bring no additional benefit but would lead to the same reach as systems without Raman amplification within the DCF.

	Contra (dB)	G_DCF (dB)	G_EDFA1 (dB)	G_EDFA2 (dB)	Loss (dB)	SNR° (dB)	PhiNL° (dB)	DeltaP (dB)	M_max_ampli (dB)	Distance (a.u.)
Full EDFA	0	0	14	13.0	-27	31.2	-13.4	0	22.3	**1.00**
Contra TL + EDFA	18	0	0	9.5	-27.5	37.6	-11.9	**-3.0**	24.7	**1.76**
Contra TL + Contra DCF + EDFA	15	7	0	6.0	-28	37.5	-12.3	**-3.4**	24.9	**1.83**
Full Raman	15	13	0	0.0	-28	38.2	-11.3	**-2.4**	24.7	**1.77**

Table 5-2 : Summary of performance obtainable with different amplification schemes.

Update of the study when refining the nonlinear phase criterion with the equivalence between effective length and chromatic dispersion

At this point, it is possible to refine these estimations with the results of Chapter 3 (section II.3.2) and [205] showing that the nonlinear impairments in a dispersion-managed transmission system can be described by both the nonlinear phase shift and the product between chromatic dispersion, effective length and the square of the symbol rate.

Indeed, in the case of distributed Raman amplification, the power profile of the fibres is

changed and thus their effective lengths. Assuming here 15dB gain in the transmission fibre due to backward Raman pumping results in an increase of the line fibre effective length by 15%, i.e. 0.6dB. Considering then a bit rate of 40Gb/s for NRZ modulation format, we can expect from Figure 3-5 a resulting decrease of the nonlinear threshold of the system by 0.6dB. This will translate in a reduction of the reach by half (in dB), i.e. 0.3dB, i.e. 7%. The net reach improvement due to Raman amplification instead of full Erbium amplification should therefore be closer to 70% in case of Raman amplification only in the line fibre and 77% in case of Raman pumping in both line and compensating fibres.

In summary, we applied the simple reach estimator model described in the previous section and showed that the combination of backward Raman amplification to Erbium amplification is likely to substantially increase by the transmission reach of a dispersion-managed transmission system based on 100km-long lab-type sections of TeraLight Ultra fibre with respect to a Full-Erbium amplification scheme. In particular, we showed 77% improvement in reach in presence of 15dB Raman gain in the transmission fibre, 7dB in the DCF (i.e. in order to mask the loss of the fibre) and Erbium amplification after the DCF.

III.3. Multiterabit/s experiment

Now that the optimization of the amplification scheme has been explained through analytical means, we come back to the Ultra-Long Haul experiment in [173].

Experimental set-up

Figure 5-9-left shows the set-up of the recirculating loop. The WDM transmitter consists of 125 DFB lasers with wavelengths ranging from 1529.94nm to 1561.22nm in the C-band and 1571.03nm to 1602.53nm in the L-band. In each band, two sets of 125GHz-spaced channels, shifted with respect to each other by 50GHz and corresponding to odd and even channels respectively, are combined through 1x32 array-waveguide multiplexers. They are modulated independently by two Mach-Zehnder modulators (M-Z) fed by a 2^{31}-1 pseudo-random bit sequence (PRBS) for the set including the channel under test and a 2^{23}-1 PRBS for the other set. Both PRBS are generated electrically, out of two separate pattern generators. Such a scheme provides effective decorrelation of the data carried by neighbouring WDM channels. Each generator delivers four sequences at 10Gbit/s with 7% overhead, i.e. at 10.7Gbit/s, to emulate the presence of forward error correction (FEC). The sequences are combined through Si-Ge-based 2:1 MUX circuits for successive 10.7:21.3Gbit/s and 21.3:42.7Gbit/s electrical multiplexing. The resulting complementary outputs at 42.7Gbit/s, forming real PRBS patterns, are amplified in order to drive the M-Zs. Odd and even modulated channels are interleaved with orthogonal polarisations through polarisation beam splitters (PBS), boosted, passed into an acousto-optic switch and sent into the loop via a 3dB coupler.

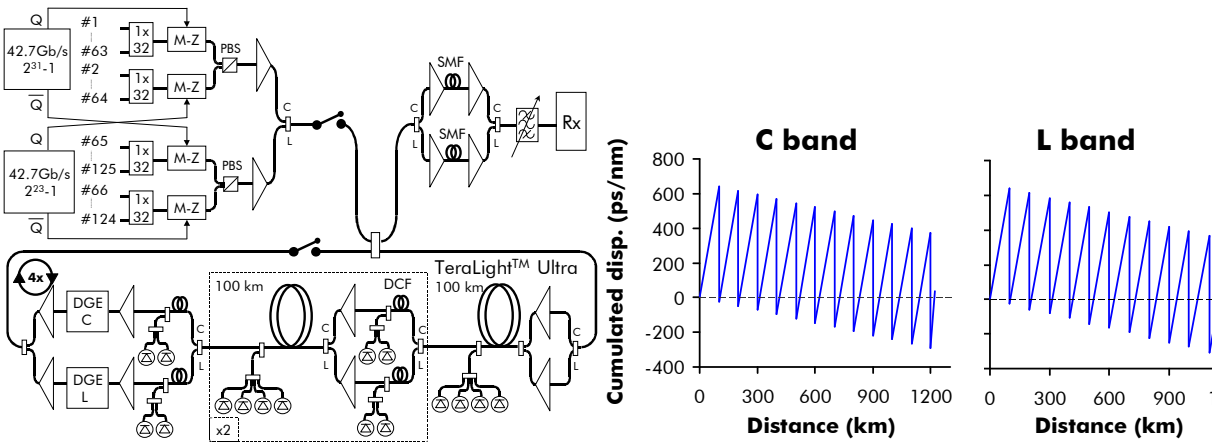

Figure 5-9 : Experimental set-up (left); dispersion map (right)

The loop consists of three 100km-long sections of TeraLight™ Ultra fibre. This non-zero dispersion-shifted fibre complies with all the characteristics of TeraLight™ fibre [203], with a chromatic dispersion of 8ps/nm.km, loss of 0.20dB/km and effective area of 63μm2 at 1.55μm. However, the tighter specifications on PMD (total 1ps per loop round-trip), dispersion slope (0.052ps/nm2.km) and the guaranteed low loss within the wavelength region of Raman pumps (0.25dB/km at 1.45μm) make it particularly suited for transmissions over ultra-long haul distances.

Two sections of dispersion compensating fibre for C and L bands are inserted within each repeater. They provide full dispersion slope compensation, so that the excursion of cumulated dispersion does not exceed 10ps/nm per fibre span along the whole multiplex. The corresponding dispersion maps are represented in Figure 5-9-right at 1545nm and 1585nm. These maps were optimised based on computer simulations, and further verified experimentally. Fine tuning of the residual dispersion is performed on channel-by-channel basis by including a small spool of standard single-mode fibre within the receiver preamplifier, outside the loop.

Each span is separated by repeaters formed of dual-band EDFAs providing a total 18dBm and 16dBm in C and L-band, respectively. In each of them, EDF length was carefully adjusted to deliver higher gain (2dB in C-band, 1dB in L-band) in the lower-wavelength region than in the higher-wavelength one, so as to mitigate self-induced Stimulated Raman scattering spectral distortions [204].

Moreover, in order to improve the overall optical signal-to-noise ratio, four sets of two polarisation-multiplexed semiconductor pumps, of respective wavelengths 1427nm, 1439nm, 1450nm and 1485nm, are sent backwards into the transmission fibre in order to provide extra amplification through stimulated Raman scattering. Similarly, four laser pumps, two in both bands, are sent into the DCFs in order to mask DCF loss and thus improve the noise figure of the EDFAs. These pumps are at wavelengths 1423nm and 1455nm for the C band and 1470nm and 1500nm for the L band. Raman gain is approximately 15dB and 8dB in the TeraLight™ Ultra and in the DCFs respectively, as calculated in the previous section. Note that the last repeater consists of dual-stage EDFAs which incorporate dynamic gain equalisers (DGE) to ensure optimal gain flatness in both bands. Power excursion after 1200km is better than 3dB, as depicted in the spectrum of Figure 5-10. Another acousto-optical switch closes the loop. Like the first switch, it is driven by electrical delay generators which trigger the periodical filling and clearing of the loop, synchronously with the measuring equipment.

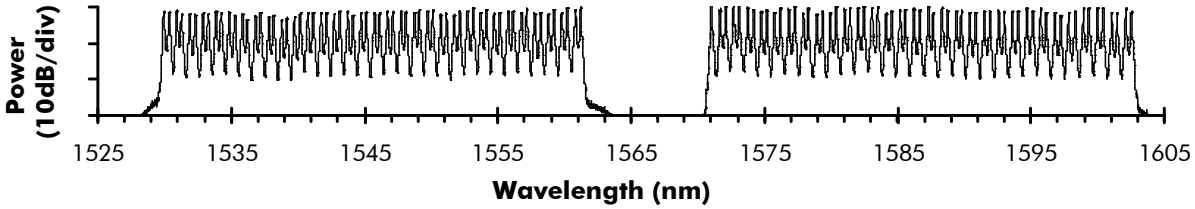

Figure 5-10 : Optical spectrum after 1200km (0.1nm resolution)

In the receiver, each channel is selected with a very narrow (30GHz at 3dB), tuneable filter. This filter performs VSB filtering when tuned off the channel central frequency towards the 75GHz-spaced neighbouring channel. Thus, only the side-band experiencing the smallest overlap with adjacent channels is isolated regardless the crosstalk affecting the other side-band [203]. An EDFA boosts the VSB signal to 12dBm on the pin-photodiode.

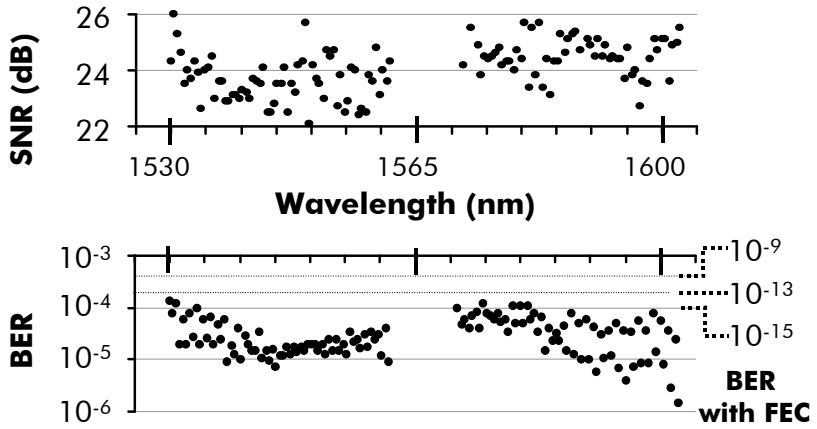

Figure 5-11: Experimental results after 1200km. Top: OSNR within 0.1nm versus wavelength; bottom: BER versus wavelength

Figure 5-11 represents the experimental results at 1200km, after 4 round-trips in the loop. The OSNR at the input of the receiver preamplifier in a 0.1nm bandwidth varies within [22.1dB, 26.0dB] and [22.7dB, 27.6dB] in C-band and L-band, respectively. The BERs of all 125 channels are also shown. Note that in our ETDM receiver, the 42.7-to-10.7Gbit/s demultiplexer uses a phase-locked loop which is automatically reset at each round-trip of the recirculating loop. This randomly changes the measured 10.7Gbit/s tributary and ensures that the BER performance of Figure 5-11 exactly represents the average performance of all four 10.7Gbit/s tributaries. Measured BERs are always better than $1.4.10^{-4}$. With FEC, this would correspond to a BER performance lower than 10^{-13}.

Note that we further managed to improve the reach of this experiment from 1200 to 1500km by tuning even more precisely the dispersion management of the line, in agreement with the observations of Chapter 3 regarding inline dispersion compensation.

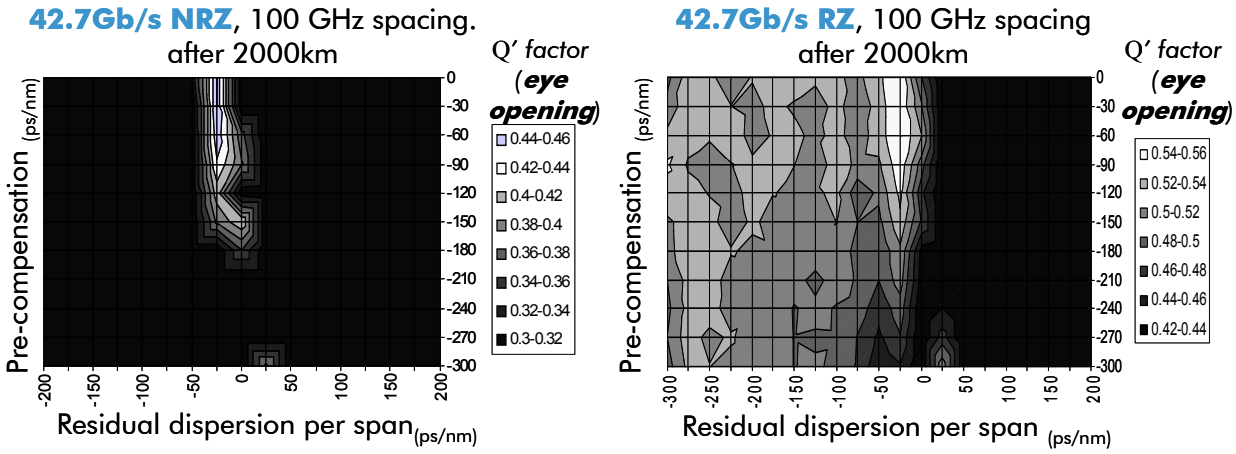

Figure 5-12 : Contour plots of the eye opening for a simulated 2000km-long dispersion-managed transmission link with 11x42.7Gb/s channels modulated with NRZ (left) or RZ right) format and 100GHz-spaced, as a function of the amount of pre-compensation and residual dispersion per span.

Indeed, in the 1200km experiment, the worst performing channels were found in the lower part of the C-band and were mainly limited by optical nonlinearities, as testified by their relatively larger OSNR. Further studies of optimization of the in-line dispersion compensation confirmed its paramount impact on transmission performance: numerical studies showed that for distances longer than 1200km, the optimum value of residual dispersion per span was close to -20ps/nm/span, with a very narrow tolerance of about +/-10ps/nm apart from this optimum value, as illustrated by the penalty contour plots of Figure 5-12. Conversely, the tolerance on the cumulated dispersion of a possible pre-compensation fibre was centered around 0ps/nm and at least as large as 100ps/nm. In our experiment, no pre-compensation fibre was used. Such results are consistent with the results of Chapter 2 and 3. Indeed, the PIC criterion predicts the optimum setting of dispersion management such that the sum of the dispersion pre-compensation and the product between the residual dispersion per span and ~half the number of spans remains constant; this suggests that for long distances, the tolerance to residual dispersion per span decreases. Moreover, we have shown in Chapter 3 that the transmission penalty indeed depends on the nonlinear phase shift and the total inline dispersion (i.e. the product between the number of spans and residual dispersion per span); this suggests that the optimum value of residual dispersion per span (in absolute value) decreases proportionally with the inverse of distance, as well as the range of values enabling low penalty.

Precise measurements of the residual dispersion per span for the dispersion map of [173] revealed a very low excursion of ±5ps/nm around -30ps/nm/span in the C-band after 100km TeraLigt Ultra and the corresponding DCF (due to the mismatch of the dispersion profiles of line fibre and DCF with wavelength over the whole C-band), as illustrated the solid lines of Figure 5-13. In particular, the residual dispersion per span in the lowest-performance region around 1530nm was found close to -35ps/nm, while simulations suggested an optimal range between [-25; -15]ps/nm.

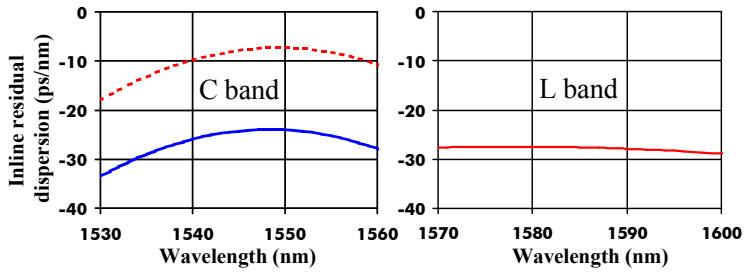

Figure 5-13: Plots of the average residual dispersion per span as a function of wavelength for C- (left) and L-(right) bands. Dashed red line on left plot illustrates the new dispersion map.

Inline compensation in the lower part of the C band was confirmed to be the limiting factor, preventing from reaching longer distance. Tight adjustment of the amount of central inline dispersion compensation around -10ps/nm/span in average (illustrated by Figure 5-13, dashed line) confirmed the extremely narrow range of tolerance, slightly higher than 10ps/nm after 15x100km and allowed the transmission of 5 Terabit/s over 1500 km with a BER better than 1.6 10^{-4} over C and L bands, as shown in Figure 5-14.

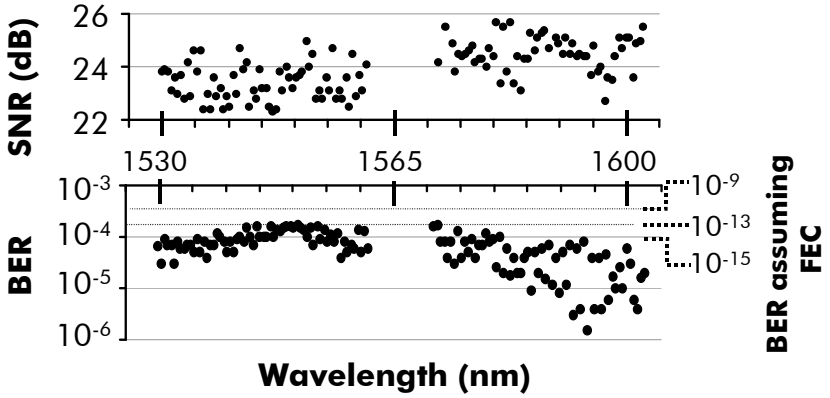

Figure 5-14 : Experimental results after 1500km with the new dispersion map with -10ps/nm/span residual dispersion per span in the C-band.
Top: OSNR within 0.1nm versus wavelength; bottom: BER versus wavelength

Conclusion

This study demonstrated the transmission of data at 5Tbit/s over fifteen 100 km-long spans of TeraLight™ Ultra fibre, yielding 7.5Pbit/s.km capacity times distance product in 2001. This was obtained by sending 125 WDM channels modulated at 42.7Gbit/s and alternatively spaced by 50/75 GHz into a loop including Raman-assisted C and L band EDFAs, as designed in the previous section. VSB filtering was applied at the receiver end. We showed how tightly the dispersion management has to be set for ultra-long haul experiments.

III.4. Applications to longer distances and more elaborated amplification schemes

We showed in the previous section how we applied the nonlinear phase criterion to design optimized hybrid Raman + Erbium amplifier schemes for ultra-long haul hero experiments, based on backward Raman amplification in the line fibre and the DCF. The same kind of tools has been further applied in [174][175][176] in 2002 and 2003 to bridge up to 2700km for a total capacity of 6.3Tb/s (158 channels modulated at 42.7Gb/s with Bandwidth-Limited PSBT format, and 50GHz spaced), using 2nd order Raman pumping: eight polarisation-multiplexed semiconductor laser diodes at wavelengths 1427nm, 1439nm 1450nm and 1485nm were sent backwards in each fibre span to provide approximately 18dB Raman gain; additionally, light from a fibre laser at wavelength 1346nm was sent in the same direction, acting as a secondary pump for the lower-wavelength pumps at 1427 and 1439nm; the hybrid amplification scheme regarding the DCF is similar to the above-described one. We performed similar calculations to the ones done in section III.2 showing that the 2nd order Raman amplification can help further increasing the reach by 20% with respect to schemes exploiting only 1st order Raman pumping. Such calculations can particularly account for Double Rayleigh Back-Scattering that can no longer be neglected, as we showed in [182].

It can be noticed that the dispersion map enabling to bridge the longest distance of 2700km in [176] had to be changed with respect to [175] where only 2100km had been reached: a residual dispersion per span of -25ps/nm was chosen instead of -35ps/nm, in good agreement with the numerical observations in Chapter 2 stating that the nonlinear threshold varied with the product between residual dispersion per span and the number of spans: in these experiments, this product appeared unchanged with 8% accuracy.

5.IV. Summary

In this chapter, we have focused on system limitations induced by both noise and nonlinear issues and on their impact on system reach, assuming the relevance of the (weighted) nonlinear phase criterion from Chapters 2 and 3.

First of all, we have proposed an original definition of nonlinear threshold consistent with the achievable reach of optical transmission systems, as published in [172] in 2008.

Then we have derive from such notions a simple estimator of achievable reach as well as rules to optimally set the fibre input powers, in the context of homogeneous and heterogeneous infrastructures (different types of fibres, of different lengths).

Eventually we have shown how such simple tools can be utilized to compare modulation formats, to compare and design optical amplifier schemes, to compare and design line fibres then dispersion compensation fibres.

In particular, these works have been used to design the Raman/Erbium amplification schemes of some record experiments presented in post-deadline sessions at major conferences [173][174][175] and regular sessions as well [176]. They have also served to account for the impact of double Rayleigh backscattering in Raman-assisted amplifier schemes [182].

Eventually, derivations and extensions of those works and of Chapter 3 have also been used to optimize the design of Dispersion Compensating Fibres [177][178][179], possibly over a full spectral window [180], but they are not presented in this document.

Chapter 6 will show that the introduction of new modulation formats (PDM-QPSK) and coherent detection leads to new trade-offs in terms of dispersion-management and therefore imposes to adapt the nonlinear phase criterion (accounting for the total inline dispersion or the number of spans in addition to the nonlinear phase parameter) and thus the guiding rules developed here, especially concerning fibre input powers.

5.V. Appendix

V.1. Simple method to compute the gain and generated noise power by a distributed Raman amplifier

V.1.1. Principles of distributed amplification

Let $P_{sig}(z)$ be the optical power at distance z of a signal propagating over an amplified medium characterized by a differential on-off gain $g_{onoff}(z)$ and an attenuation $\alpha(z)$.

The basic power propagation equation is thus:

$$\frac{dP_{sig}}{dz}(z) = \left(g_{onoff}(z) - \alpha(z)\right)P_{sig}(z) \qquad (5\text{-}19)$$

Shall we define the net differential gain $g_{net}(z) = g_{onoff}(z)-\alpha(z)$, we get

$$\frac{dP_{sig}}{dz}(z) = g_{net}(z).P_{sig}(z) \qquad (5\text{-}20)$$

If $g_{net}(z)$ is independent of $P_{sig}(z)$, then we can easily calculate the total gain after a distance L:

$$\frac{P_{sig}(L)}{P_{sig}(0)} = G_{net}(0 \to L) = \exp\int_0^L g_{net}(z).dz$$

$$i.e.\ \frac{P_{sig}(L)}{P_{sig}(0)} = G_{onoff}(0 \to L).\exp(-\alpha L), \qquad (5\text{-}21)$$

where $G_{onoff} = \exp\int_0^L g_{onoff}(z).dz$

and assuming constant α over distance

V.1.2. Application to the calculation of the gain induced by Stimulated Raman scattering

The stimulated Raman amplification process involves the frequency down-conversion of an incident photon into a Stokes photon and an optical phonon [195].

Let us consider an incident pump signal at pulsation ω_p characterized by optical power $P_p(z)$ and by a fibre attenuation β and the Stokes amplified signal at pulsation ω_{sig} characterized by optical power $P_p(z)$ and by a fibre attenuation α.

The coupled equation between the pump signal and the amplified signal is thus:

$$\begin{cases} \dfrac{dP_{sig}}{dz} = \underbrace{C_R}_{\substack{Raman\ gain \\ coefficient}} P_p(z)P_{sig}(z) - \alpha P_{sig}(z) \\ \dfrac{dP_{pump}}{dz} = \underbrace{-C_R \dfrac{\omega_p}{\omega_{sig}} P_p(z)P_{sig}(z)}_{\text{negligible if } P_p >> P_{sig}} - \beta P_{sig}(z) \end{cases} \qquad (5\text{-}22)$$

with C_R as the Raman gain of the fibre for the corresponding set of frequencies. C_R is equal to the ratio between the material Raman gain and the effective area of coupling between pump and Stokes signals: in practice, the usual effective area at signal frequency is often considered.

Under the assumption of non-depleted pump, we can separately calculate the pump power profile over distance. Under such assumptions, we have:

$$\begin{aligned} g_{onoff}(z) &= C_R P_p(z) \\ g_{net}(z) &= C_R P_p(z) - \alpha \\ G_{net}(x \to y) &= \exp \int_x^y \left(C_R P_p(z) - \alpha \right) dz \end{aligned} \quad (5\text{-}23)$$

Let us now assume counter-propagating pump and probe signals, then the pump power at distance z can be deduced from its injection power at distance L:

$$P_{pump}(z) = P_p(L).e^{-\beta(L-z)} \quad (5\text{-}24)$$

Then

$$\frac{P_{sig}(L)}{P_{sig}(0)} = G_{net}(0 \to L) = \exp\left(C_R P_p(L) \overbrace{\int_0^L .e^{-\beta(L-z)} dz}^{L_{eff,p}} - \alpha L \right) \quad (5\text{-}25)$$

$$G_{net}(0 \to L) = \exp\left(C_R P_p(L).L_{eff,p} - \alpha L \right)$$

In dB scale, we get

$$\begin{aligned} G_{net}(0 \to L)_{dB} &= \frac{10}{\ln 10} C_R P_p(L).L_{eff,p} - \alpha_{dB/km} L \\ G_{onoff}(0 \to L)_{dB} &= \frac{10}{\ln 10} C_R P_p(L).L_{eff,p} \end{aligned} \quad (5\text{-}26)$$

It is here worth noting that the total on-off gain expressed in dB is proportional to the pump power expressed in linear scale (in W).

Note that the effective length of the amplified section is given by:

$$\begin{aligned} L_{eff} &= \int_0^L G_{net}(0 \to x).dx = \int_0^L \exp\left(\frac{\ln 10}{10} G_{onoff}(0 \to L)_{dB} \frac{L_{eff,p}(0 \to x)}{L_{eff,p}} - \alpha.x \right) .dx \\ with\ L_{eff,p}(w \to x) &= \int_w^x .e^{-\beta(L-z)} dz \end{aligned} \quad (5\text{-}27)$$

This can be further simplified as:

$$L_{eff} = \int_0^L \exp\left(\frac{\ln 10}{10} G_{onoff}(0 \to L)_{dB} \frac{e^{\beta x} - 1}{e^{\beta L} - 1} - \alpha.x \right) .dx \quad (5\text{-}28)$$

V.1.3. Principle of the creation and amplification of noise

The creation of noise coming from an amplifier is distributed aver the full length of the amplifier. We can distinguish the local creation of noise at distance z and the noise amplification until the end of the amplification section.

Let us consider a small fraction dz of the amplifier section at distance z: the spontaneous noise power generated locally can be expressed as Ase(z)*dz, where Ase(z) is most of the time proportional to $g_{onoff}(z)$ (itself most of the time representing the stimulated emission process); such noise will then undergo an amplification process from distance z to distance L, with a net gain $G_{net}(z->L)$.

At amplifier output, the total created noise power P_{ase} of amplified spontaneous emission is then:

$$P_{ASE} = \int_0^L Ase(z).G_{net}(z \to L).dz,$$

solution of the differential equation:

$$\frac{\mathrm{dP_{ASE}}}{\mathrm{dz}} = Ase(z) + g_{net}(z).P_{ASE}(z) \qquad (5\text{-}29)$$

V.1.4. Application to the calculation of noise generated through a distributed Raman amplifier

Following the formalism from the previous paragraphs and applied to Raman amplification processes [196][197][198][199] the power of the noise created spontaneously at the frequency $\nu_{sig}=\omega_{sig}/2\pi$ due to the incident pump signal, and estimated over the spectral bandwidth $\Delta\nu_{ref}$ is:

$$Ase(z).dz = 2.K.h\nu_{sig}.\Delta\nu_{ref}.C_R.P_p(z).dz \qquad (5\text{-}30)$$

where the factor 2 stands for both polarizations, h stands for the Planck constant and K corresponds to the density of optical phonons in the fibre (equal to 1 + the Bose repartition function $K = 1/(1-\exp(-h\nu/kT)$ at temperature T and with k referring to as the Boltzmann constant).

The propagation equation for noise power then becomes

$$\frac{dP_{ase}}{dz} = 2.K.h\nu_{sig}.\Delta\nu_{ref}.C_R.P_p(z) + \left(C_R.P_p(z) - \alpha\right)P_{ase} \qquad (5\text{-}31)$$

After noise creation and amplification at distance L, we get

$$P_{ase}(L) = 2.K.h\nu_{sig}.\Delta\nu_{ref}\int_0^L C_R.P_p(z).G_{net}(z \to L).dz \qquad (5\text{-}32)$$

Getting back to the backward Raman pumping scheme and the assumption of non-depletion of pump signal by probe signal, we get:

$$P_{ase}(L) = 2.K.h\nu_{sig}.\Delta\nu_{ref}.C_R P_p(L)\int_0^L \exp\left(\left(\alpha+\beta\right)\left(z-L\right) + C_R P_p(L)\frac{1-\exp\left(\beta\left(z-L\right)\right)}{\beta}\right).dz \qquad (5\text{-}33)$$

Considering the total OnOff gain $G_{onoff,dB}$ of the amplifier, the equation can be rewritten as:

$$P_{ase}(L) = 2.K.h\nu_{sig}.\Delta\nu_{ref}.\frac{G_{onoff,dB}}{L_{eff,p}}\frac{\ln 10}{10}\int_0^L \exp\left(\left(\alpha+\beta\right)\left(z-L\right) + \frac{\ln 10}{10}G_{onoff,dB}\frac{L_{eff,p}(L-z \to L)}{L_{eff,p}}\right).dz \qquad (5\text{-}34)$$

5.VI. References

[171] J.-C. Antona et al, "Nonlinear cumulated phase as a criterion to assess performance of terrestrial WDM systems", in Proc. Optical Fibre Communications Conference (OFC'02), paper WX5, March 18-22, 2002, Anaheim, California, USA

[172] J.-C. Antona, S. Bigo, "Physical Design and performance estimation of heterogeneous optical transmission systems", C.R. Physique 9 (2008), 963-984

[173] S. Bigo, W. Idler, J.-C. Antona, G. Charlet, C. Simonneau, M. Gorlier, M. Molina, S. Borne, C. de Barros, P. Sillard, P. Tran, R. Dischler, W. Poehlmann, P. Nouchi, Y. Frignac; "Transmission of 125 WDM channels at 42.7Gbit/s (5 Tbit/s capacity) over 12x100 km of TeraLight^{TM} Ultra fibre", Proc. of ECOC'01, Post-Deadline session, vol.6, , pp. 2- 3 , Amsterdam (Netherlands), September 2001

[174] G. Charlet, W. Idler, R. Dischler, J.-C. Antona, P. Tran, S. Bigo, "3.2Tbit/s (80x42.7Gb/s) C-Band transmission over 9x100km of TeraLightTM fibre with 50GHz channel spacing", in Optical Amplifiers and Their Applications, J. Nagel, S. Namiki, and L. Spiekman, eds., Vol. 77 of OSA Trends in Optics and Photonics Series (Optical Society of America, 2002), paper PD1, Vancouver, Canada, July 2002

[175] G. Charlet, J.-C. Antona, S. Lanne, P. Tran, W. Idler, M. Gorlier, S. Borne, A. Klekamp, C. Simonneau, L. Pierre, Y. Frignac, M. Molina, F. Beaumont, J.-P. Hamaide, S. Bigo, "6.4Tb/s (159x42.7Gb/s) Capacity over 21x100km using Bandwidth-Limited Phase-Shaped Binary Transmission", Proc. of ECOC'02, Post-Deadline paper PD 4.1, Copenhagen (Denmark), Sept 2002

[176] G. Charlet, J.-C. Antona, S. Lanne, S. Bigo, "2100 to 2700km distance using Bandwidth-Limited Phase-Shaped Binary Transmission at 6.3Tb/s capacity", Proc. of OFC'2003, paper WE3, Atlanta (Georgia), USA, March 2003

[177] P. Sillard, B. Dany, A. Bertaina, L. Curinckx, C. Bastide, O. Courtois, J-.C. Antona, S. Bigo, "Simple criterion of quality to evaluate DCM impact on WDM system performance", Proc. of Optical Fibre Communication conference OFC'04, paper FA4, Los Angeles (Ca), February 2004

[178] J.-C. Antona, P. Sillard, "Relationship between the Achievable Distance of WDM Transmission Systems and Criterion of Quality for DCM", in Proc. Optical Fibre Communication Conference OFC'06, paper OWJ2, Anaheim (Ca), March 2006

[179] P. Sillard et al, "Optimized Chromatic Dispersion of DCMs in WDM Transmission Systems at 40Gbps", in Proc. Optical Fibre Communication Conference OFC'08, paper JWA13, San-Diego (Ca), 2008

[180] J.-C. Antona, P. Sillard, S. Bigo, "Impact of Imperfect Wideband Dispersion Compensation on the Performance of WDM Transmission Systems at 40 Gbit/s", ECOC'06, Th1.6.4, Cannes (France), Sept 2006

[181] F. Forghieri, R.W. Tkach, A.R. Chraplyvy, "Dispersion Compensating Fibre: is there Merit in the Figure of Merit?", IEEE Photonics Technology Letters, Vol. 9, No. 7, July 1997

[182] C. Martinelli, D. Mongardien, J.-C. Antona, C. Simonneau, D. Bayart, "Analysis if bi-directional and second-order pumping in long-haul systems with distributed Raman amplification", Proceedings of ECOC'02, paper P3.30, Copenhagen (Denmark), September 2002

[183] R. Dischler and F. Buchali, "Experimental Investigation of Non-Linear Threshold of 113Gb/s O-OFDM Signals on DCF Free Transmission Links," in Optical Fibre Communication Conference, OSA Technical Digest (CD) (Optical Society of America,

2009), paper OWW2
[184] J. K. Fischer, M. Winter, and K. Petermann, "Scaling of Nonlinear Threshold with Fibre Type and Channel Spacing in WDM Transmission Systems," in Optical Fibre Communication Conference, OSA Technical Digest (CD) (Optical Society of America, 2009), paper JThA41
[185] E. Grellier, J.-C. Antona, and S. Bigo, "Global Criteria to Account for Tolerance to Nonlinearities of Highly Dispersive Systems," in IEEE Photonics Technology Letters, Vol. 22, No. 10, May 15, 2010
[186] V.E. Perlin, H.G. Winful, "On trade-off between noise and nonlinearity in WDM systems with distributed Raman amplification", Proc. Optical Fibre Communications (OFC'02), WB1, pp. 178-179, March 18-22, 2002, Anaheim, California, USA
[187] A. Carena et al, "On the optimization of hybrid Raman/Erbium doped fibre amplifiers", IEEE PTL Vol 13, No.11, Nov 2001
[188] R. Hainberger, J. Kumasako, T. Terahara, H. Onaka, T. Hoshida, "Optimum span configuration of Raman-amplified dispersion-managed fibres", Proc. of OFC'01, Vol. 2, paper TuA3.1.3, March 2001
[189] R.J. Essiambre, P. Winzer, J. Bromage, C. H. Kim, "Design of bidirectionally puped fibre amplifiers generating double Rayleigh backscattering", IEEE Photonics Technology Letters, vol. 14, No. 7, July 2002
[190] A. Carena, V. Curri, P. Poggiolini, "Comparison between different configurations of hybrid Raman/Erbium-doped fibre amplifiers ", OFC'01, Paper Tu A3-1, March 2001
[191] A. Mecozzi, "On the Optimization of the Gain Distribution of Transmission Lines with Unequal Amplifier Spacing", IEEE Photonics Technology Letters Vol 10, No7, July 1998
[192] S.K. Turitsyn, M.P. Fedoruk, V. K. Mezentsev, E.G. Turitsyna, "Theory of optimal power budget in quasi-linear dispersion-managed fibre links", Electronics Letters, Vol. 39, No. 1, pp 29-30, 2003
[193] H. Goldstein, "Classical Mechanics", 3rd Edition, Addison Wesley (1980)
[194] D.P. Bertsekas, "Nonlinear programming", 2nd Edition, Athena Scientific (1999)
[195] G.P. Agrawal, "Non-linear fibre optics", third edition, Academic Press, 2001
[196] E. Desurvire et al, « Erbium-doped fibre amplifiers, Device and System Developments », Wiley & sons, Chapter 7, New York, 2002
[197] I. P. Kaminow, T. Li, "Optical Fibre Telecommunications IV-B: Systems and Impairments", Academic Press; 1st edition (April 15, 2002)
[198] R.H. Stolen and E.P. Ippen, "Raman gain in glass optical waveguides", Applied Physics Lett., 22(6), 276 (1973)
[199] D. Bayart, "Undersea Fibre Communication Systems – Chapter 4", editor J. Chesnoy, Elsevier Science (USA), 2002
[200] K. Fukuchi et al., "10.92-Tb/s (273x40-Gb/s) triple-band/ultra-dense WDM optical-repeatered transmission experiment", Proc. OFC'01, Anaheim, paper PD-24
[201] S. Bigo et al., "10.2Tbit/s (256x42.7Gbit/s PDM/WDM) transmission over 100km TeraLightTM fibre with 1.28bit/s/Hz spectral efficiency", Proc. OFC'01, Anaheim, paper PD25
[202] B. Zhu et al., "3.08Tb/s (77x42.7 Gb/s) transmission over 1200km of non-zero dispersion-shifted fibre with 100-km spans using C- and L-band distributed Raman amplification", Proc. OFC'01, Anaheim, paper PD23
[203] S. Bigo et al., "5.12Tbit/s (128x40 Gbit/s WDM) transmission over 3x100km of TeraLightTM fibre", Proc. ECOC'00, Munich, paper PD1.2
[204] D. N. Christodoulides and R. B. Jander, "Evolution of stimulated Raman cross-talk in wavelength division multiplexed systems", IEEE Photon. Technol. Lett., vol. 8, n°12, pp.

1722-1724 (1996)
[205] A. Cauvin, Y. Frignac, S. Bigo, “Nonlinear impairments at various bit-rates in single-channel dispersion-managed systems”, Electronics Letters, Nov 13th 2003, vol. 39, No23

Chapter 6 : EXTENSION TO COHERENT SYSTEMS

Contents

Introduction

The advent of coherent detection and 100Gb/s-compatible high-speed numerical electronics (analog to digital converters and digital signal processing capabilities) has recently disrupted the way optical transmission systems had been designed [206][207][208].

First of all the intensity, phase, and polarization-sensitive receivers have enabled the emergence of new modulation formats exploiting multi-level phase modulation and polarization multiplexing. Secondly, heterodyne detection has enabled linear optoelectronic conversion of the incident signal, such that the electronic digital signal processing can efficiently and adaptively mitigate linear propagation effects such as Chromatic Dispersion, Polarization Mode Dispersion, filtering as well as the tracking of the polarizations where the signal is encoded. Thirdly, the speed of analog to digital converters and the digital signal processing capabilities have become compatible with very high symbol-rates around 30Gbaud in 2011. As a result, industrial products have already been developed offering 100Gb/s modulated channels based on 28Gbaud PDM-QPSK format and on 50GHz spacing, in conjunction with real-time DSP assisted coherent detection with unprecedented tolerance to linear propagation effects .

Eventually, the conjunction of those points has led to propose drastically new methods of dispersion management: suppressing inline dispersion compensation has thus happened to be a particularly suitable strategy. Beside some compatibility issues with existing networks operated with simpler modulation formats and dispersion maps, the accumulation of nonlinearities and the prediction performance tools have also been deeply revisited in these new regimes of propagation for the past few years.

Due to my carrier evolution I have not contributed to that revolution as an individual but as the supervisor of a PhD student, Edouard Grellier, and as the manager of a research group within Bell-Labs investigating dynamic optical networks. Thus, this chapter aims to be no more than an introduction to the physics and the design of coherent detection-assisted transmission systems. At least one whole PhD manuscript such as the one from E. Grellier [209] would be necessary to cover the richness of this field. Here we put into perspective the studies of the previous Chapters in the new era of multilevel phase modulated systems using coherent detection.

In section 6.I. we address the domain of validity of the nonlinear phase criterion and its limitations in absence of inline dispersion management, based on an article published in 2010 by E. Grellier, S. Bigo and myself [211]. We discuss a possible evolution of the nonlinear phase criterion in such dispersive regimes as well as the implications on reach prediction tools and power setting rules.

Eventually, in section 6.II. , we recap some numerical and theoretical work from E. Grellier and the experimental work achieved by F. Vacondio, C. Simonneau that showed that nonlinearity-induced distortions can be modelled as an additive Gaussian noise which variance is proportional to the cube of signal power and which span contributions can be considered as independent in absence of inline dispersion management. This paves the way for new ways to consider the accumulation of nonlinearities with a very promising presented model and for new ways to predict the Q factor in a much simpler way than with the QoT model from Chapter 4.

6.I. Limitations and evolution of nonlinear phase criterion

I.1. Nonlinear phase criterion and dispersion-managed systems

Changing the modulation format as well as the detection scheme from non-coherent to coherent systems with multilevel phase modulation and polarization-multiplexing and tracking has changed the rule concerning the main impacting nonlinear effects. Indeed, such systems are more sensitive to nonlinear effects directly impacting the phase or the polarization, such as Cross-Phase Modulation, Cross-Polarization Modulation or nonlinear phase noise (another manifestation of the nonlinear interaction between noise and signal)[215]. Conversely, Self-Phase Modulation appears as relatively less impairing in dispersion-managed systems.

However, the physics of transmission has not changed for each propagation effect. Besides, when looking back to the perturbative models developed for non-coherent systems, there is no reason why they should be less helpful than before. On the contrary, since the new systems are rather phase-modulated the approximations of small intensity perturbations ruling SPM or XPM models could appear as even more applicable than for intensity-modulated systems, as evoked in Chapter 3.

For such reasons, it may sound reasonable that the nonlinear phase criterion from (Chapter 2), its generalization to mixed-fibre types (from Chapter 3) and the derived rules enabling to predict the reach or to set powers (from Chapter 5) remain valid with an accuracy at least as good as for 40Gb/s non-coherent systems.

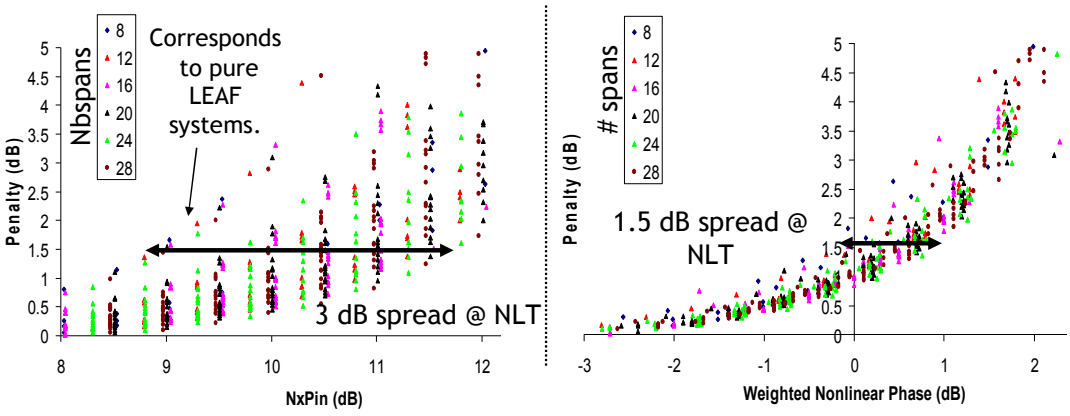

Figure 6-1 : Nonlinear phase criterion (left) and weighted nonlinear phase criterion (right) for WDM transmissions of 100Gb/s PDM-QPSK channels over a mix of SMF and LEAF line fibre sections, provided same dispersion management scheme as section 3.IV. Multiple points correspond to different distances into LEAF and SMF fibres, different fibre input powers, and different ordering of fibres.

Without getting too much into details that are rather described in [209][210][211], we have performed numerical and experimental studies that confirm our intuitions for different formats and over different types of fibres. One example is given below, with a direct estimation of the accuracy of the weighted nonlinear phase criterion for a transmission systems consisting of 50GHz-spaced 100Gb/s PDM-QPSK channels propagating over a dispersion-managed system (similar to Chapter 3 – section IV) consisting of a mix of 100km-long spans of SMF and LEAF™ fibre, for given combinations of distances, fibre input powers and order of fibres. The accuracy of the nonlinear phase criterion, assessed by the range of nonlinear phase values leading to 1.5dB penalty (for a BER of 10^{-3}) is here equal to 3dB, but the accuracy of the weighted nonlinear phase criterion is here equal to 1.5dB with a weighted nonlinear phase of

0dB ensuring that the penalty is higher than 1.5dB. Such results are similar to the accuracy already obtained with 40Gb/s-modulated NRZ format in Chapter 3.

This illustrates that the use of coherent systems over dispersion management schemes optimized for more classical systems does not bring major changes in the way nonlinearities accumulate nor in the way to design systems or predict the reach. As a result, we still recommend the use of the (weighted) nonlinear phase criterion (from Chapter 3) and of the design tools from Chapter 5.

However when coherent channels are used over a classical infrastructure, they most often have to coexist with already deployed non-coherent channels operated at 10 or 40Gb/s. The XPM induced by the existing channels may then be not negligible; this is even truer if those channels are intensity-modulated. Indeed the intensity modulation would then directly transfer into detrimental phase modulation by XPM on the phase-modulated channels and into detrimental fast polarization changes that the coherent receiver might not be able to follow because of Cross-Polarization Modulation (XPolM) [215]. XPM-based small-signal models similar to the PIC model are here very useful to capture the XPM-induced penalties[216]. It is thus quite strategic and challenging to design efficiently such transmission links and optical networks with hybrid bit-rates and technologies.

Eventually, as stated earlier, these coherent systems with advanced modulation formats are more sensitive to inter-channel nonlinear effects than former systems with simpler formats. Thus dispersion management strategies with high absolute values of inline residual dispersion per span have been found to yield better tolerance to nonlinearities [210][211] than conventional dispersion–management strategies with almost full span-to-span dispersion compensation [210][211]. A transmission system with all the chromatic dispersion compensated for at receiver end by numerical means is here one of the best configurations for purely coherent systems. As a result, the region of interest for the future deployment of coherent systems is very likely to become the dispersive region [209] where the nonlinear phase criterion appears less and less accurate (as described in Chapters 2 and 3), thus requiring to revisit the concepts of Chapters 2 and 3.

I.2. Limitations of the nonlinear phase criterion in weakly dispersion-managed systems … and proposed adaptation

In Chapters 2 and 3, we have shown that system penalty can be found to vary as a function of multiple parameters: the nonlinear phase, the total inline cumulated dispersion, and the product between line fibre chromatic dispersion, the square of the symbol rate and the line fibre effective length. Provided low values of total inline cumulated dispersion, the impact of distance is accounted for by the nonlinear phase parameter with a sufficient accuracy, thus justifying the (weighted) nonlinear phase criterion.

The following article [211], published in Photonics Technology Letters, illustrates the limits of the nonlinear phase criterion for coherent systems in the highly dispersive propagation regime. We investigate there the tolerance to nonlinear effects in highly dispersive regime for WDM, singly-periodic dispersion-managed, 100Gb/s PDM-QPSK systems, thanks to numerical simulations and analytical interpretations. In this regime, i.e. for values of inline cumulated dispersion higher than 1200ps/nm, the nonlinear threshold (in rad) is found to increase as a power of the number of spans. Furthermore, we point out here two sub-regimes depending on the ratio between the residual dispersion per span and the accumulated dispersion along the line fibre effective length, going beyond the considerations of Chapter 2: for values lower than

1, the nonlinear threshold actually scales as a power of the inline cumulated dispersion, while for larger values, it only depends on the span number whatever the residual dispersion per span.

IEEE PHOTONICS TECHNOLOGY LETTERS, VOL. 22, NO. 10, MAY 15, 2010

Global Criteria to Account for Tolerance to Nonlinearities of Highly Dispersive Systems

Edouard Grellier, Jean-Christophe Antona, *Member, IEEE*, and Sébastien Bigo, *Member, IEEE*

***Abstract*—We numerically investigate the relevance of criteria such as the nonlinear phase or the inline cumulated dispersion to assess the tolerance to nonlinearities of highly dispersive optical transmission systems. For such systems, we propose and validate new rules to predict the performance of systems with different residual dispersion per span or number of spans.**

***Index Terms*—Coherent detection, dispersion management, nonlinearities, polarization-multiplexed quadrature phase-shift keying (PDM-QPSK).**

I. Introduction

THE ability to predict transmission penalties due to the combined impact of nonlinear effects and chromatic dispersion is of great importance in long-haul wavelength-division-multiplexed (WDM) systems. In [1], the authors recommend the nonlinear phase shift as a useful and simple parameter to assess tolerance to nonlinearities of classic dispersion-managed 40-Gb/s terrestrial systems with almost full inline dispersion compensation.

However, during the last few years, high bit rate transmissions systems have considerably evolved, with the widespread acceptance of new modulation formats, and coherent detection. Besides, new chromatic dispersion mitigation strategies have caught interest, so that highly dispersive systems with sparse or no in-line dispersion compensation are more and more often considered [2], [3]. In such systems, dispersion compensation is generally performed digitally in terminals, as demonstrated up to 140 000 ps/nm · km at 100 Gb/s [3].

In this context, it has become of high interest to find simple criteria and rules to help predict the performance of systems operating in the highly dispersive regime. In [4], we showed that the nonlinear phase shift criterion was insufficient and we introduced another criterion based on the inline cumulated dispersion, for single-channel transmissions. In this letter, we investigate both analytically and numerically the domain of validity of the above-mentioned criteria in both single-channel and WDM configurations, and we numerically derive more accurate rules to predict the performance of systems beyond the domain of validity of the above-mentioned criteria.

Manuscript received November 09, 2009; revised January 06, 2010; accepted February 14, 2010. Date of publication March 01, 2010; date of current version April 16, 2010.

The authors are with the Alcatel-Lucent Bell Laboratories France, Centre de Villarceaux, 91620 Nozay, France (e-mail: Edouard.Grellier@alcatel-lucent.com; Jean-Christophe.Antona@alcatel-lucent.com; Sebastien.Bigo@alcatel-lucent.com).

Color versions of one or more of the figures in this letter are available online at http://ieeexplore.ieee.org.

Digital Object Identifier 10.1109/LPT.2010.2044167

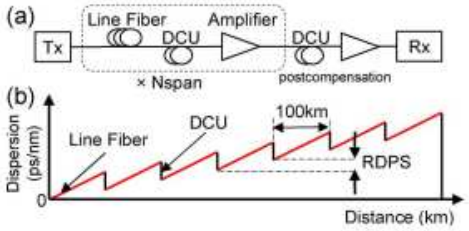

Fig. 1. (a) Setup of the transmission line. (b) Evolution of the accumulated chromatic dispersion along the transmission.

II. System Setup

In the following, the system under study consists of a 112-Gb/s polarization-division-multiplexed quadrature phase-shift keying (PDM-QPSK) transmission link over Nspan (varying from 5 to 30) 100-km-long spans of either standard single-mode fiber (SSMF), or large effective area fiber (LEAF) [1], with singly periodic dispersion maps as described in Fig. 1. The values of the chromatic dispersion D, the nonlinear coefficient γ, and the loss coefficient α are $D = 17$ ps/nm, $\gamma \approx 1.32$ $(\mathrm{W \cdot km})^{-1}$, $\alpha = 0.22$ dB/km for SSMF and $D = 4.25$ ps/nm, $\gamma \approx 1.52$ $(\mathrm{W \cdot km})^{-1}$, $\alpha = 0.22$ dB/km for LEAF. Second-order chromatic dispersion and polarization-mode dispersion were not taken into account. Dispersion compensation is performed at the receiver and (possibly) in the inline repeaters, but not at the transmitter. The residual dispersion per span (RDPS), i.e., the accumulated dispersion in one line fiber span and in the following inline dispersion compensation unit (DCU), is varied between full inline dispersion compensation (i.e., 0 ps/nm) and no inline dispersion compensation (i.e., either 1700 or 425 ps/nm depending on fiber type). The total amount of accumulated dispersion is compensated before reception. Nonlinear effects in DCUs are overlooked. Amplified spontaneous noise is added at receiver to achieve desired optical signal-to-noise ratio (OSNR).

The transmitted signal is either single-channel or composed of seven 50-GHz-spaced WDM channels, all modulated at 112 Gb/s with PDM-QPSK. Ideal 50-GHz bandwidth rectangular filters are used at both transmitter and receiver. At the receiver, each polarization of the signal is mixed with a local oscillator with 200-MHz detuning in a 90° hybrid and then the components of the signal are detected by balanced photodiodes; phase recovery is performed using the method described in [5] with seven taps. Penalties arising from receiver electronics were neglected. Each channel uses a pseudorandom quaternary sequence of 4096 symbols per polarization in order to mimic a 16-level pseudorandom sequence of 2^{14} bits. The bit-error rate (BER) is then estimated by direct error counting with enough

1041-1135/$26.00 © 2010 IEEE

noise samples to detect at least 400 errors; in the WDM case the BER is estimated on the central channel.

For each configuration, we vary the fiber input power P_{IN}, so as to get the power corresponding to 1.5-dB OSNR penalty at 10^{-3} reference BER. To this power P_{NLT}, we associate a nonlinear threshold (NLT) defined as the product Nspan$\times P_{\mathrm{NLT}}$.

III. Limits of Validity of the Nonlinear Phase Criterion

In [1], the authors showed that, for systems with almost full inline dispersion compensation, the penalty due to nonlinearities does not depend on Nspan as long as the nonlinear phase shift Φ_{NL} remains constant. With our chosen setup, $\Phi_{\mathrm{NL}} = \gamma \times \mathrm{Leff} \times \mathrm{Nspan} \times \mathrm{P_{IN}}$; where Leff $\approx 1/\alpha \approx 20$ km is the effective length of the fiber. The product Nspan $\times$ $\mathrm{P_{IN}}$ is thus a useful alternative parameter [6]. As a consequence, the NLT as mentioned above should remain constant when Nspan varies.

The relevance of the Φ_{NL} criterion in dispersion-managed systems can be deduced analytically. Using a first-order perturbation approach such as [7] and [8], the optical field at the receiver can be expressed as a sum of the signal impacted by linear transmission and a perturbation term also accounting for fiber nonlinearity. The influence of the physical parameters of the transmission line on the perturbation is described by the product $\mathrm{P_{IN}} \times \eta(\Omega)$ where the nonlinear transfer function $\eta(\Omega)$ can be expressed in our case as [7]

$$\eta(\Omega) = \gamma L_{\mathrm{eff}} \frac{e^{j\lambda^2\Omega(\mathrm{Nspan}-1)\mathrm{RDPS}/4\pi c}}{1 - j\frac{\Omega}{\Omega_s}} \times \frac{\sin\left(\mathrm{Nspan}\frac{\mathrm{RDPS}}{4\pi c}\lambda^2\Omega\right)}{\sin\left(\frac{\mathrm{RDPS}}{4\pi c}\lambda^2\Omega\right)}. \quad (1)$$

Here, $\Omega_s = 2\pi c\alpha/(\lambda^2 D)$; λ is the optical wavelength and c the light speed. Ω is homogeneous to a product of frequency shifts between two signal spectral components. For small arguments of the sine functions, i.e., for

$$\left|\frac{\lambda^2\Omega}{4\pi c}\mathrm{Nspan} \times \mathrm{RDPS}\right| \ll 1 \quad (2)$$

the product $\mathrm{P_{IN}} \times \eta(\Omega)$ can be approximated as

$$\mathrm{P_{IN}} \times \eta(\Omega) \approx \Phi_{\mathrm{NL}}\left(1 - j\frac{\Omega}{\Omega_s}\right)^{-1}. \quad (3)$$

Thus, within the validity domain of (3) and of the perturbation approach, the performance of systems with various Nspan should be comparable provided that Φ_{NL} remains constant [7].

IV. Inline Cumulated Dispersion and One-Channel Results

In the following though, we focus on highly dispersive systems (with RDPS $\times$ Nspan $> 10^3$ ps/nm) outside condition (3).

In [4], we observed that the NLT of highly dispersive systems increases with the number of spans. Furthermore, it was shown that this increase scales like a power of Nspan [4].

Besides, it was shown that the inline cumulated dispersion $D_{\mathrm{IN}} \equiv$ RDPS $\times$ Nspan is one of the parameters determining the behavior of systems with large inline dispersion compensation

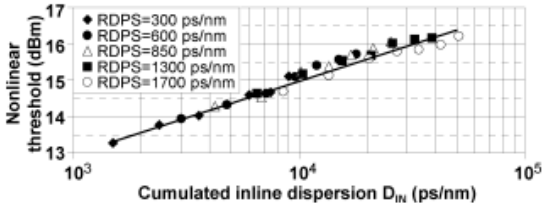

Fig. 2. NLT of a 112-Gb/s coherent PDM-QPSK single-channel transmission on SSMF for different values of residual dispersion per span.

[8]. This can be derived from (1) as long as the argument of the sine function at the denominator is small, i.e., as long as

$$\left|\frac{\lambda^2\Omega}{4\pi c}\mathrm{RDPS}\right| \ll 1. \quad (4)$$

In this case, $\mathrm{P_{IN}} \times \eta(\Omega)$ can be approximated as

$$\mathrm{P_{IN}} \times \eta(\Omega) \approx \Phi_{\mathrm{NL}} \frac{e^{j(\lambda^2\Omega/4\pi c)D_{\mathrm{IN}}}}{\left(1 - j\frac{\Omega}{\Omega_s}\right)} \frac{\sin\left(\frac{\lambda^2\Omega}{4\pi c}D_{\mathrm{IN}}\right)}{\frac{\lambda^2\Omega}{4\pi c}D_{\mathrm{IN}}}. \quad (5)$$

In (5), Φ_{NL} and D_{IN} are the only parameters corresponding to the dispersion map. As a result, within the validity range of (4) and of the perturbation approach, systems with different values of Nspan or RDPS but with the same inline cumulated dispersion should have the same NLT.

Condition (4) would restrict the validity of the D_{IN} criterion to systems with significant inline dispersion compensation (RDPS $\ll 10^3$ ps/nm). However, for single-channel systems, we numerically demonstrated that the predictions of this criterion remain reasonably good even at larger RDPS [4], for QPSK as well as ON–OFF keying. We report in Fig. 2 (markers) the NLT computed using the split step Fourier method as a function of D_{IN} for a single channel transmitted over SSMF in highly dispersive systems. Straight lines in all graphs are intended as guides to the eye. We note that the NLT varies linearly with D_{IN} in logarithmic scale and that the D_{IN} criterion is relevant.

V. Numerical Results for WDM Systems

In this chapter, we investigate how the above concepts can be applied to WDM systems. In Fig. 3, we compute the NLT versus the inline cumulated dispersion for WDM systems over SSMF. For clarity, we chose to represent on separate graphs results obtained with RDPS [50, 600] ps/nm [Fig. 3(a)] and [600, 1700] ps/nm [Fig. 3(b)]. When RDSP $<$ 600 ps/nm, D_{IN} appears as good as in single-channel to biunivocally predict the NLT. Still, two different dispersive regimes can be observed. Below $\sim$ 1200 ps/nm the NLT is constant versus D_{IN}, and above 1200 ps/nm, it increases as a power of Nspan. In contrast, when RDPS $>$ 850 ps/nm, it continues to increase as a power of Nspan (the same for all RDPS), but systems with the same D_{IN} no longer all correspond to a single NLT.

We pursue our study with WDM transmissions over LEAF, the results are reported in Fig. 4. The D_{IN} criterion is biunivocally related to the NLT only when RDPS $<$ 200 ps/nm. This is similar to the SSMF case except that the limit of validity of the D_{IN} criterion is for lower values of RDPS (i.e., between 100

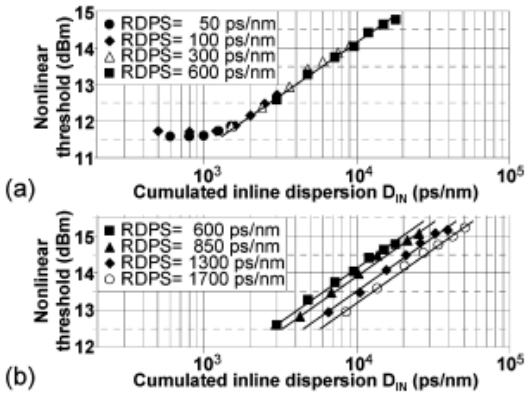

Fig. 3. NLT for a 112-Gb/s PDM-QPSK WDM transmission over spans of 100-km SSMF for different residual dispersion per span. (a) RDPS $\leq$ 600 ps/nm. (b) RDPS $\geq$ 600 ps/nm.

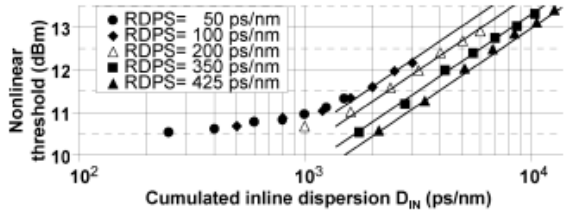

Fig. 4. NLT for a 112-G/bs PDM-QPSK WDM transmission over spans of 100-km LEAF for different residual dispersion per span.

and 200 ps/nm). We can note the existence of an intermediate regime for D_{IN} values between 300 and 1200 ps/nm where the NLT increases with the number of spans but has not completely reached the highly dispersive regime. For values of D_{IN} larger than 1200 ps/nm, as in the previous case over SSMF, we observe an increase of the NLT scaling as a power of Nspan.

VI. Interpretations for Large Values of RDPS

The domain of validity of the D_{IN} criterion can be derived from the above model. We may assume that (5) only needs to be accurate for $\Omega < \Omega s$ since Ωs is an upper bound to the 3-dB bandwidth of $\eta(\Omega)$. Then we get

$$|\mathrm{RDPS}| \ll \left| \frac{2D}{\alpha} \right|. \tag{6}$$

We introduce $D_0 = D \times \mathrm{Leff} \approx D/\alpha$ the amount of dispersion accumulated in the line fiber along its effective length ($D_0 \approx 40$ ps/nm for SSMF, $D_0 \approx 85$ ps/nm for LEAF). For both fiber types, our observations suggest that the limit of validity is $\mathrm{RDPS}/D_0 \sim 1$.

In Fig. 5, we report the data of Fig. 3(b) but versus the sole number of spans. Surprisingly, for RDPS $>$ 850 ps/nm the NLT does not depend on RDPS anymore. The same observation

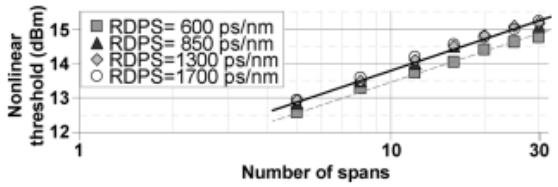

Fig. 5. NLTs of a 112-Gb/s coherent PDM-QPSK transmission over spans of 100-km SSMF for different values of RDPS.

can be made on LEAF for RDPS $>$ 300 ps/nm (not shown here). This suggests that the RDPS does not affect the impact of nonlinearities when $\mathrm{RDPS}/D_0 \gg 1$. At high RDPS, Nspan is, therefore, better suited than D_{IN} to biunivocally determine the NLT.

VII. Conclusion

We have investigated the tolerance to nonlinear effects in highly dispersive regime for WDM, singly periodic dispersion-managed, 112-Gb/s PDM-QPSK systems, thanks to numerical simulations and analytical interpretations. In this regime, i.e., for values of inline cumulated dispersion higher than 1200 ps/nm, the NLT increases as a power of the number of spans. Furthermore, we have pointed out two subregimes depending on the ratio between the residual dispersion per span and the accumulated dispersion along the line fiber effective length. For values lower than 1, the NLT actually scales as a power of the inline cumulated dispersion, while for larger values, it only depends on the span number whatever the residual dispersion per span.

References

[1] J.-C. Antona, S. Bigo, and J.-P. Faure, "Nonlinear cumulated phase as a criterion to assess performance of terrestrial WDM systems," in *Proc. OFC'02*, Anaheim, CA, Mar. 2002, Paper WX5.

[2] S. J. Savory, G. Gavioli, R. I. Killey, and P. Bayvel, "Transmission of 42.8 Gbit/s polarization multiplexed NRZ-QPSK over 6400 km of standard fiber with no optical dispersion compensation," in *Proc. OFC 2007*, Anaheim, CA, Mar. 2007, Paper OTuA1.

[3] G. Charlet, M. Salsi, M. Bertolini, H. Mardoyan, J. Renaudier, O. Bertran-Pardo, and S. Bigo, "72 × 100 Gb/s transmission over transoceanic distance, using large effective area fiber, hybrid Raman-Erbium amplification and coherent detection," in *Proc. OFC 2009*, San Diego, CA, Mar. 2009, Paper PDPB7.

[4] E. Grellier, J.-C. Antona, and S. Bigo, "Revisiting the evaluation of non-linear propagation impairments in highly dispersive systems," in *Proc ECOC'09*, Vienna, Austria, Sep. 2009.

[5] A. Viterbi, "Nonlinear estimation of PSK-modulated carrier phase with application to burst digital transmission," *IEEE Trans. Inf. Theory*, vol. 29, no. 4, pp. 543–551, Jul. 1983.

[6] A. Färbert, C. Scheerer, J.-P. Elbers, C. Glingener, and G. Fischer, "Optimised dispersion management scheme for long-haul optical communication systems," *IEEE Electron. Lett.*, vol. 35, no. 21, pp. 1865–1866, Oct. 1999.

[7] J. K. Fisher, C.-A. Bunge, and K. Petermann, "Equivalent single-span model for dispersion-managed fiber-optic transmission systems," *J. Lightw. Technol.*, vol. 27, no. 16, pp. 3425–3432, Aug. 15, 2009.

[8] A. Bononi, P. Serena, and A. Orlandini, "A unified design framework for single-channel dispersion-managed terrestrial systems," *J. Lightw. Technol.*, vol. 26, no. 22, pp. 3617–3631, Nov. 15, 2008.

From a system design point of view, it is possible to build an interesting model to improve the (weighted) nonlinear phase criterion based on the fact that the NLT scales proportionally to a power of distance, provided a high value of residual dispersion per span is chosen. Such model could then be incorporated into new QoT estimators or could help derive power setting rules and tools similar to the ones developed in Chapter 5.

We explain hereafter one such simple model and the power setting rules that we can derive.

In [211], the NLT increases like a power β of the number of spans N, relatively close for SMF and LEAF fibres (0.31dB/dB and 0.37dB/dB), thus the product between nonlinear phase ϕ_{nl} and $N^{-\beta}$ remains constant when varying distance and fibre input power when we are at the nonlinear limit (here corresponding to an OSNR penalty of 1.5dB).

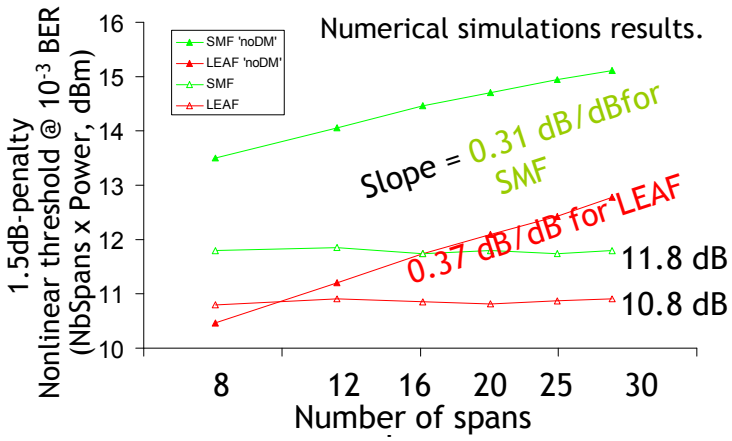

Figure 6-2 : 100Gb/s PDM-QPSK channels with 50GHz spacing. Evolution of the nonlinear threshold , NLT, (for 1.5dB OSNR penalty @BER 10^{-3}) with number of spans, for singly periodic transmission systems composed of 100km-long SMF or LEAF-based spans and residual dispersion per span of zero ps/nm (horizontal curves and plots)) or or in absence of optical dispersion compensation

Said differently, the product between fibre input power and N^{α} is constant when the power is such that we are at the nonlinear limit, where $\alpha=1-\beta$ ($\alpha\sim0.66$ for SMF and LEAF fibres at 100Gb/s in absence of inline dispersion management, $\alpha=1$ for clasically dispersion-managed systems).

We propose then to define the **adapted nonlinear phase** as

$$\bar{\phi} = \left(\sum_{span\ k} \phi_k^{\,1/\alpha} \right)^{\alpha} , \qquad (6\text{-}1)$$

where ϕ_k is the nonlinear cumulated phase shift for the fibre k.

By construction, should all the fibre sections be identical, $\bar{\phi}$ is easily related to the total nonlinear phase $\phi_{nl,tot}$:

$$\bar{\phi} = N^{\alpha}.\phi_1 = N^{-\beta}.\phi_{nl,tot} , \qquad (6\text{-}2)$$

$\bar{\phi}$ is then constant at the nonlinear limit whatever distance and power.

We find that when $\alpha=1$, $\bar{\phi}$ is identical to the standard nonlinear phase. The meaning of $\alpha<1$ could be interpreted as a partial decorrelation between the nonlinear induced distortions coming from each span (if $\alpha=1/2$, $\bar{\phi}$ simply amounts to the quadratic sum of the nonlinear phase contributions coming from each span as if they were statistically independent processes. That point will be discussed in more details in the following section).

Similar to the case of nonlinear phase, we can define an **adapted nonlinear threshold** ANLT (that should depend on fibre type, length, modulation format…) for a reference penalty (typically 1.5dB, preferably 1.76dB as explained in next section) and the concept of **weighted adapted nonlinear phase** for mixed fibre types configurations as:

$$\bar{\phi}_w = \left(\sum_{span\ k} \left(\frac{\phi_k}{ANLT_k} \right)^{1/\alpha} \right)^{\alpha} \qquad (6\text{-}3)$$

Note that we choose with this weighted model a constant α whatever the fibre types and lengths involved. We acknowledge it might represent one point of inaccuracy of the model (even though very weak over 100km –long spans of LEAF or SMF fibres at 100Gb/s).

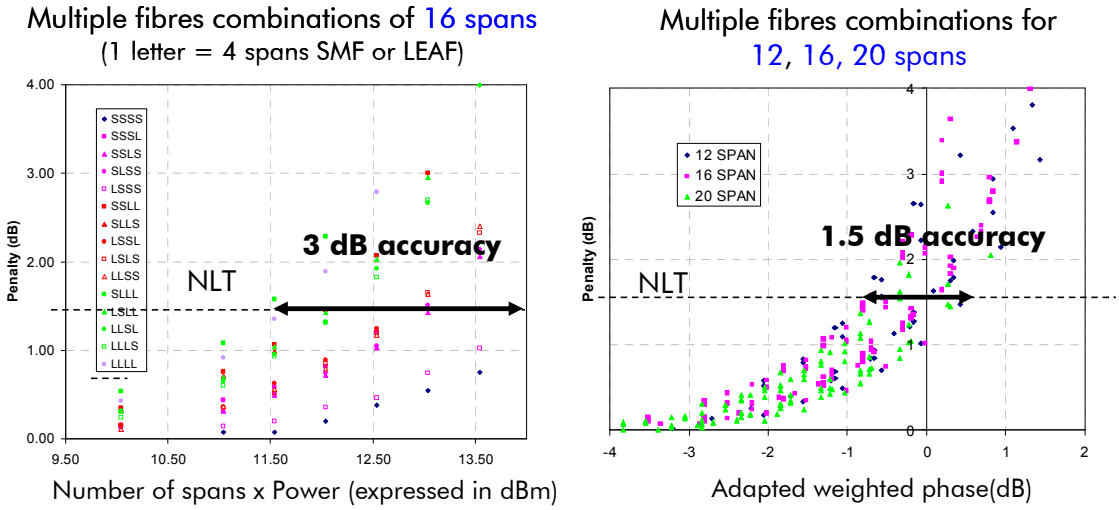

Figure 6-3 : Accuracy of nonlinear phase criterion (left) and weighted nonlinear phase criterion (right) for mixed SMF+LEAF systems without inline dispersion compensation at 100Gb/s.

Eventually, as in Chapter 3, we can eventually define the weighted adapted nonlinear phase criterion as the ability to describe system penalties based on the knowledge of the weighted adapted nonlinear phase and the accuracy of the criterion for the same reference penalty as that of the definition of the ANLTs.

Figure 6-3, coming from [209] and the numerical studies of student A. Laurin supervised by E. Grellier (and myself), illustrates the benefits brought by the weighted adapted nonlinear phase criterion with respect to the weighted nonlinear phase criterion in case of 100Gb/s-modulated, 50GHz-spaced PDM-QPSK channels propagating over hybrid transmission systems composed of sections of 100km SMF or LEAF fibre, without any optical dispersion compensation (but electronic compensation at receiver side): for a given distance (16 spans), the weighted nonlinear phase criterion (calculated with NLTs corresponding to this distance) yields an accuracy (for 1.5dB reference penalty) equal to 3dB; conversely the accuracy of the weighted adapted nonlinear phase criterion is reduced down to 1.5dB, for three different total distances (12, 16, 20 spans). Such accuracy is limited by the inability of the model to capture the arrangement of fibres (which changes the dispersion map). It is however acceptable for system design considerations (equal to the limit proposed in Chapter 2). More advanced models accounting for the arrangement of traversed fibres (such as the one presented in next section) are likely to improve that.

From that new weighted criterion, we can derive power setting rules just as in Chapter 5, assuming that at maximum reach, the weighted adapted nonlinear phase will be equal to 1 and the OSNR equal to a target OSNR S.

Should we consider a homogeneous system composed of identical spans in a dispersion management regime such that the adapted nonlinear criterion is applicable, we get the optimal power equal to:

$$P_{dBm} = P^\circ + \frac{\alpha . S}{1+\alpha} - \frac{\overline{\Phi}_w{}^\circ + \alpha . OSNR^\circ}{1+\alpha} \ (in\ dB\ scale) \qquad (6\text{-}4)$$

And the maximum reach N_{max} equal to:

$$N_{\max} = \left(\frac{1}{\mathrm{S}} \frac{OSNR^\circ}{\overline{\Phi}_w{}^\circ} \right)^{\frac{1}{1+\alpha}}, \qquad (6\text{-}5)$$

with each span characterized by its weighted adapted nonlinear phase $\overline{\phi}_w{}^\circ$ and OSNR degradation OSNR° if input power per channel is P=P°.

Should we consider a heterogeneous transmission system composed of spans of different characteristics and such that the weighted adapted nonlinear criterion is applicable, then the same reasoning as in Chapter 5 (or applying a Lagrange multipliers technique) leads to a similar conclusion: the optimum set of span input powers that maximizes reach amounts to optimizing the input power into each span independently as if we tried to maximize the reach of a system composed of copies of that span.

In details, if each span k is characterized by its weighted adapted nonlinear phase $\overline{\phi}_{w,k}{}^\circ$ and OSNR degradation $OSNR_k{}^\circ$ for P° input power per channel then the optimum power is:

$$\overline{P}_{k,dBm} = P^\circ + \frac{\alpha . S}{1+\alpha} - \frac{\overline{\Phi}_{w,k}{}^\circ + \alpha . OSNR_k{}^\circ}{1+\alpha} \ (in\ dB\ scale) \qquad (6\text{-}6)$$

And if we define $\overline{N}_k = \left(\frac{1}{\mathrm{S}} \frac{OSNR^\circ{}_k}{\overline{\Phi}^\circ{}_{w,k}} \right)^{\frac{1}{1+\alpha}}$, then the transmission is optically feasible if and only if

$$\sum_k \frac{1}{\overline{N}_k} \le 1. \qquad (6\text{-}7)$$

In summary, we have shown that in the weak dispersion management regime particularly suitable for 100Gb/s PDM-QPSK systems, the nonlinear phase criterion needs to be improved. We have shown that the NLT can scale proportionally to a power of distance in such a regime. This enables to propose an adaptation of the (weighted) nonlinear phase criterion from Chapters 2 and 3 that yields a sufficient accuracy for system design purposes and that enables to derive adaptations of the power setting rules and reach estimators proposed in Chapter 5.

6.II. New models to account for nonlinearities and new models for QoT estimation

Here, I would like to recall some recent numerical and theoretical work from collaborators E. Grellier and O. rival and the experimental work achieved by collaborators F. Vacondio, C. Simonneau and L. Lorcy who showed that the nonlinearity-induced distortions can be modelled as an additive Gaussian noise which variance is proportional to the cube of signal power and which span contributions can be considered as independent in absence of inline dispersion management.

For that purpose, I will just propose the reader to dive into the following article [214] that makes a good summary of that work. Such an article follows [209] [212] and [213] and has recently submitted to Optics Express. Such studies pave the way for new ways to consider the accumulation of nonlinearities with a very promising presented model and for new ways to predict the Q factor in a much simpler way than with the QoT model from Chapter 4.

After the article, the reader will find a few recent notes about possibly derived power setting rules.

On nonlinear distortions of coherent systems

Francesco Vacondio[†], Olivier Rival[†], Christian Simonneau[†], Laurence Lorcy[†], Edouard Grellier[†], Jean-Christophe Antona[†], Alberto Bononi[§], Sébastien Bigo[†]

† Alcatel-Lucent Bell Labs, Route de Villejust, 91620, Nozay, France
§ Dipartimento di Ingenieria dell'Informazione, Universitá degli Studi di Parma, Italy
francesco.vacondio@alcatel-lucent.com

Abstract: We investigate via experiments and simulations the statistical properties and the accumulation of nonlinear transmission impairments in coherent systems without optical dispersion compensation. We experimentally show that signal distortions due to Kerr nonlinearity can be modeled as additive Gaussian noise, and we demonstrate that its variance has a supra-linear dependence on propagation distance both for low dispersion and standard single mode fiber. We propose a simple empirical model to account for linear and nonlinear noise accumulation, and to predict system performance for any distance, signal power and optical noise level.

©2011 Optical Society of America

OCIS codes: (060.1660) Coherent communications; (060.4370) Nonlinear optics, fibers.

References and links

1. A. Carena, G. Bosco, V. Curri, P. Poggiolini, M.T. Taiba and F. Forghieri, "Statistical characterization of PM-QPSK signals after propagation in uncompensated fiber links", ECOC 2010.
2. S. J. Savory, "Digital filters for coherent optical receivers," Opt. Express 16, 804-817, 2008.
3. J. J. Filliben, "The probability plot correlation coefficient test for normality", Technometrics, Vol. 17, No. 1, pp. 111-117.
4. S. W. Looney and T. R. Gulledge, "Use of the Correlation Coefficient with Normal Probability Plots", The American Statistician Vol. 39, No. 1, pp. 75-79.
5. E. Grellier and A. Bononi, "Quality parameter for coherent transmissions with Gaussian-distributed nonlinear noise", Optics Express, accepted for publication.
6. G. Bosco, A. Carena, R. Cigliutti, V. Curri, P. Poggiolini and F. Forghieri, "Performance prediction for WDM PM-QPSK transmission over uncompensated links", OFC 2011.
7. P. Poggiolini, A. Carena, V. Curri, G. Bosco and F. Forghieri, "Analytical modeling of non-linear propagation in uncompensated optical transmission links", PTL 2011.
8. A. Bononi, P. Serena, N. Rossi, and D. Sperti, ``Which is the Dominant Nonlinearity in Long-haul PDM-QPSK Coherent Transmissions?" in Proc. ECOC 2010, paper Th10E1, Torino, Italy, Sept. 2010.

1. Introduction

The objective of this paper is to investigate the statistical nature of distortions induced by nonlinear effects, and to clarify how such distortions accumulate with distance in coherent systems without optical dispersion management (NDM), for both standard single mode (SSMF) fiber and nonzero dispersion shifted fiber (NZDSF). We first experimentally assess the behavior of a complete wavelength division multiplexed (WDM-) 100 Gb/s polarization division multiplexed (PDM-) quadrature phase shift keying (QPSK) system, including all propagation impairments, transmitter and receiver imperfections, and realistic digital signal processing. In this scenario, we experimentally confirm that an additive Gaussian noise channel can very well approximate the fiber channel both in linear and nonlinear propagation regimes [1]. We experimentally show the precision of a recently proposed model for evaluating the performance of such systems at a fixed propagation distance, and the dependence of nonlinear noise variance to channel power. We then demonstrate that for both SSMF and NZDSF the nonlinear noise variance has a faster-than-linear dependence on propagation distance. We propose a model accounting for this dependence and assess its precision in predicting performance at any distance. Finally, we turn to simulations to gain

further insight into the mechanism responsible for the accumulation of nonlinear distortions in the propagation of a WDM-PDM-QPSK signal at 100 Gb/s. We show the impact of the cumulated dispersion at the input of each span on the total nonlinear variance, and its importance on the overall supra-linear accumulation on nonlinear distortions.

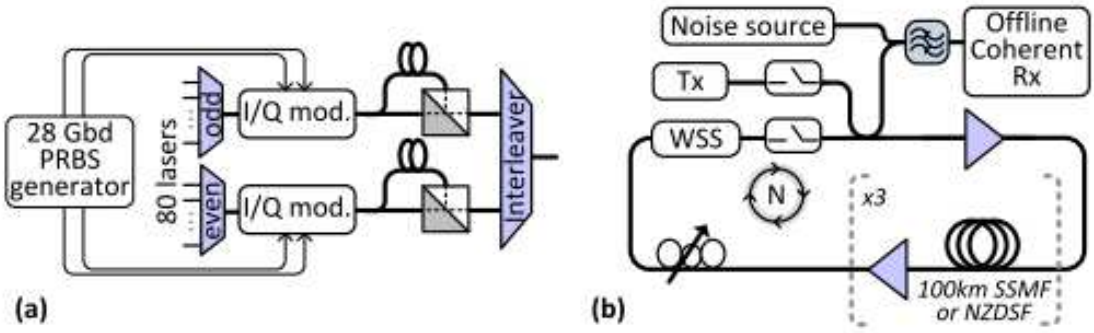

Fig. 1. Experimental setup of (a) transmitter and (b) recirculating loop.

2. Experimental setup

We investigate the respective impact of ASE noise and Kerr nonlinear distortion in a recirculating loop testbed. Figure 1(a) depicts the setup of the transmitter used in the experiment. Two combs of 40 lasers spaced by 100 GHz are independently modulated with I/Q modulators. The I/Q modulators are driven with 28 Gbaud pseudo random bit sequences (PRBS) of length 2^{15}-1. As is customary in laboratory experiments, polarization division multiplexing is emulated by splitting the signal, delaying one branch by several hundreds of symbols, and recombining the signal through a polarization beam combiner. Finally, the two combs are combined using an interleaver to form a single WDM comb of 50GHz-spaced PDM-QPSK signals at 112 Gb/s, accounting for the transport of a 100Gb/s payload with 12% overhead for forward error correction and framing purposes. The experimental setup of the recirculating loop is depicted in Fig. 1(b). Inside the loop light propagates into three spans of 100 km of either SSMF or NZDSF separated by erbium doped fiber amplifiers (EDFAs). The loop also comprises a polarization scrambler and a wavelength selective switch (WSS) for power equalization.

At the loop output, we can load additional noise through an optical noise source. The channel under test is selected with a passband optical filter, and enters a coherent receiver. In the receiver, the signal beats with a local oscillator in a dual polarization downconverter before being photodetected. After photodetection, a 16 GHz, 50 Gsamples/s real time oscilloscope is used to capture traces which are then processed offline. In the offline digital signal processing (DSP), the following steps are applied to the signal: 1) Normalization and resampling to 2 samples/symbol, 2) Chromatic dispersion compensation, 3) Adaptive blind equalization with the constant modulus algorithm [2], 4) Phase and frequency estimation and correction [2], 5) Electrical signal to noise ratio (SNR) evaluation 6) Symbol identification, bit error ratio (BER) evaluation, and conversion to Q^2-factor.

Figure 2(a) shows with markers the measured electrical SNR at the decision gate (expressed in an equivalent two-sided bandwidth of 12.47 GHz) as function of the optical signal to noise ratio before the receiver, measured in 0.1 nm (equivalent to 12.47 GHz). Here and throughout the paper, the signal to noise ratio will be referred to the nominal 0.1 nm bandwidth. As it can be seen, the SNR clearly shows saturation for high values of OSNR, which is a signature of transceiver imperfections or in-band cross-talk. The SNR can therefore be well modeled as

$$1/\mathrm{SNR} = 1/\mathrm{OSNR} + K_{TRX} \quad (1)$$

where K_{TRX} is a suitable constant depending on the particular practical implementation of the transmitter and receiver. In our case, K_{TRX}=1/215 yields very good fit with the measured data,

as can be seen in Fig. 2(a). Therefore, given our transceiver, the maximum achievable electrical SNR at the decision gate is ~23 dB.

The bit error ratio can finally be calculated from the SNR (linear scale) as:

$$\mathrm{BER} = 0.5\,\mathrm{erfc}\left(\sqrt{\eta \cdot \mathrm{SNR}}\right) \tag{2}$$

where erfc(.) is the complementary error function, and η is a suitable constant accounting for all deviations of the receiver from the ideal matched filter and possible errors in the normalization to the reference equivalent bandwidth. With an ideal receiver, η is the ratio of the noise single-sided bandwidth over the signal baud rate, *i.e.* η =(12.47/2)/28=0.22. In our case, η=0.2 gives a very good fit with the measured data, as can be seen in Fig. 2(b). It is important to stress that here, and throughout the paper, the Q²-factor is calculated from the measured bit error ratio as $Q^2 = 20\log10(\sqrt{2}\,\mathrm{erfcinv}(2\cdot\mathrm{BER}))$, where erfcinv is the inverse of the complementary error function.

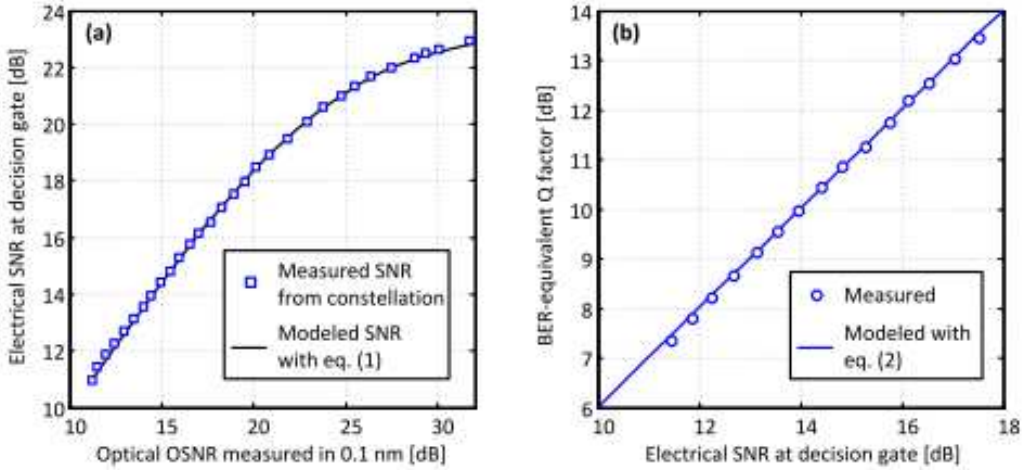

Fig. 2. (a) Measured and modeled electrical SNR at the decision gate as function of the optical signal to noise ratio (b) Measured and modeled BER-equivalent Q²-factor as function of the electrical SNR at the decision gate.

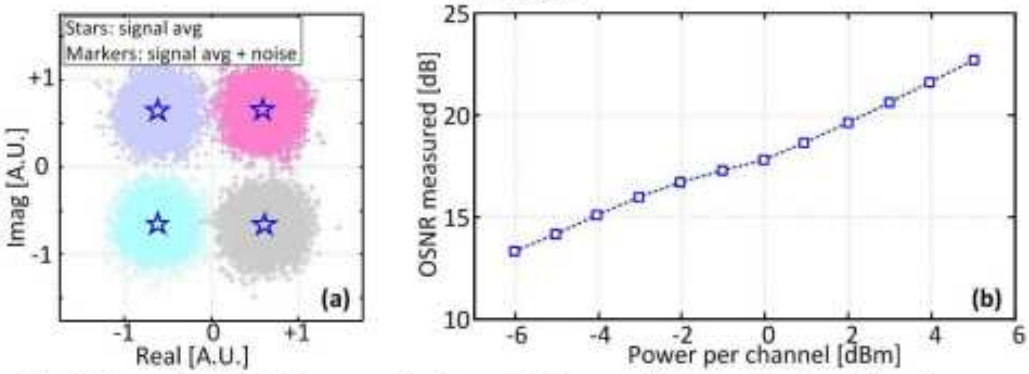

Fig. 3. Measured OSNR in 0.1nm at receiver input after 15 spans of SSMF, as function of channel power (without noise loading).

3. Statistical characterization of measured signals after 15x100km of SSMF

In this section, we characterize the statistics of noise coming from ASE, nonlinear signal distortions, transmitter imperfections, all transmission impairments and realistic receiver and digital signal processing. We measure the noise directly from the received QPSK constellation after propagation over 15x100 km of SSMF. As it is shown in Fig. 3(a), we identify the samples conditioned to the transmitted symbols (different colors), we calculate their average (stars), which we will subtract to the signal, in order to remove modulation and obtain a zero-mean complex noise. We thoroughly tested the statistics of the noise for two exemplary channel powers: P_L = -3 dBm, and P_H = +4 dBm. Fig. 3 shows the measured OSNR at the

receiver input as a function of power per channel after 15x100 km of SSMF propagation without additional noise loading. The noise figure of our EDFAs slightly varies with the optical power level at the amplifier input, therefore the measured OSNR deviates from the ideal 1 dB/dB law. As it can be seen, the OSNR at receiver input is 16dB and 21.6 dB, for P_L and P_H respectively. These power levels have been chosen because they yield the same bit error ratio after transmission, but for the lowest power P_L the system is chiefly limited by OSNR, whereas for the highest power P_H the main source of impairments is fiber nonlinearities.

To study the noise statistics, we have applied Filliben's probability plot correlation coefficient (PPCC) test for normality [3,4]. In this test, for each data set we calculate the correlation coefficient between the quantiles of the measured data and the quantiles of a theoretical Gaussian distribution. With a data set of length 1000 samples, when the correlation coefficient is on average higher than 0.9984 or 0.9979 (shown as red dashed lines in the plots) the hypothesis that the data is normal holds with more than 99% or 95% confidence, respectively.

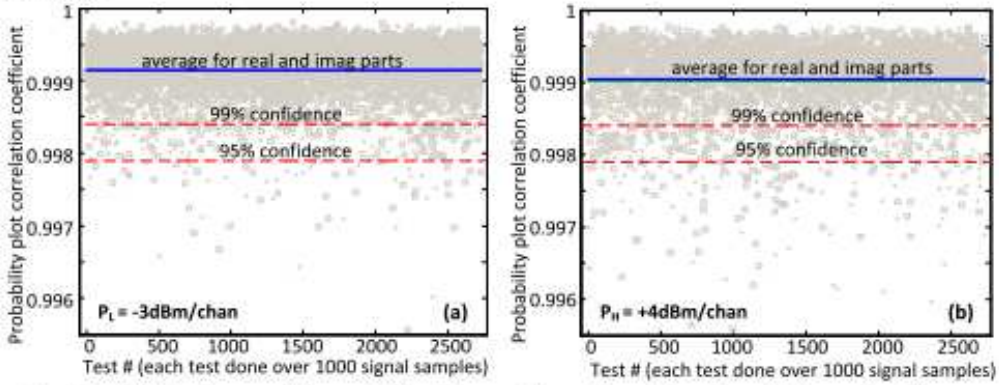

Fig. 4. Probability plot correlation coefficient for normality testing calculated over 1000 samples. The test is repeated more than 2500 times, and for real and imaginary parts. (a) P_L = -3 dBm (b) P_H = +4 dBm

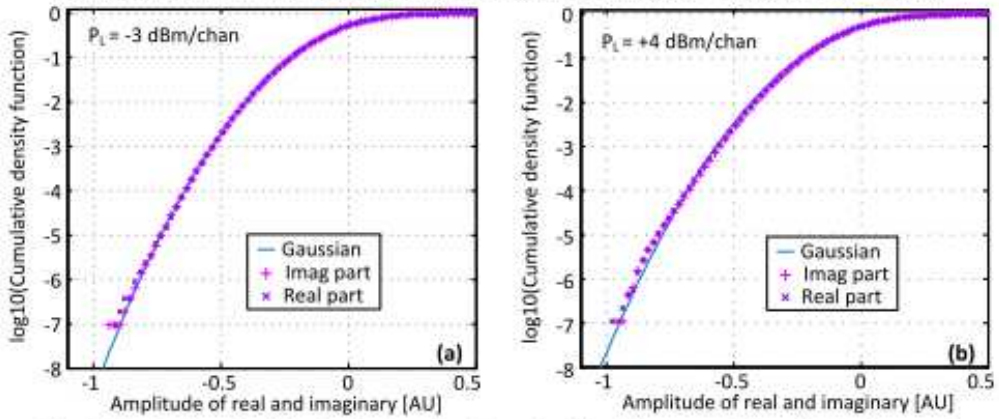

Fig. 5. Cumulative probability density functions for real and imaginary parts of signal noise (measured and theoretical) when modulation is removed. (a) PL = -3 dBm (b) PH = +4 dBm

We have applied the test to more than 2500 different subsets of our signal, of length 1000 samples each (the test has been done independently for the real part and imaginary part of the recovered signal). Figure 4(a) and (b) shows the test results, for P_L and P_H respectively. In our case, the average PPCC is well above the 99% confidence level, therefore proving that for both powers the noise statistics are indeed normal. In conclusion, noise can be considered Gaussian both in the linear and in the nonlinear regime. The normality of the noise is also visually confirmed by the excellent fit over more than 6 orders of magnitude of the cumulative

probability density functions (CDFs) of the measured optical noise (markers) with a theoretical Gaussian CDF, shown in Fig. 5(a) for P_L and Fig. 5(b) for P_H.

The results shown here are for one polarization only, since for the other polarization the results are essentially identical: the normal hypothesis holds with more than 99% confidence, and the PDF fit is again very good. We can therefore conclude that in our transmission experiment noise is Gaussian and identically distributed in the 4D space of the two polarizations in-phase and quadrature components, both in the linear and nonlinear regimes.

4. Performance modeling and prediction after 15x100km

Recent works have proposed that the variance of the nonlinear noise for a given transmission link is well approximated as $a_{NL}P^3$, where P is the channel power and a_{NL} a suitable constant which depends on system parameters and can be obtained numerically or by simple measurements [5-7]. The performance of the system can therefore be characterized by a "total" signal to noise ratio, which, adding the contribution of nonlinearities to eq. (2), can be written as

$$1/\mathrm{SNR}_{tot} = 1/\mathrm{OSNR} + K_{TRX} + 1/\mathrm{SNR}_{NL} \qquad (3)$$

where $1/\mathrm{SNR}_{NL} = a_{NL}P^3/P$ is the inverse of the nonlinear signal to noise ratio and thus depends on the channel power squared.

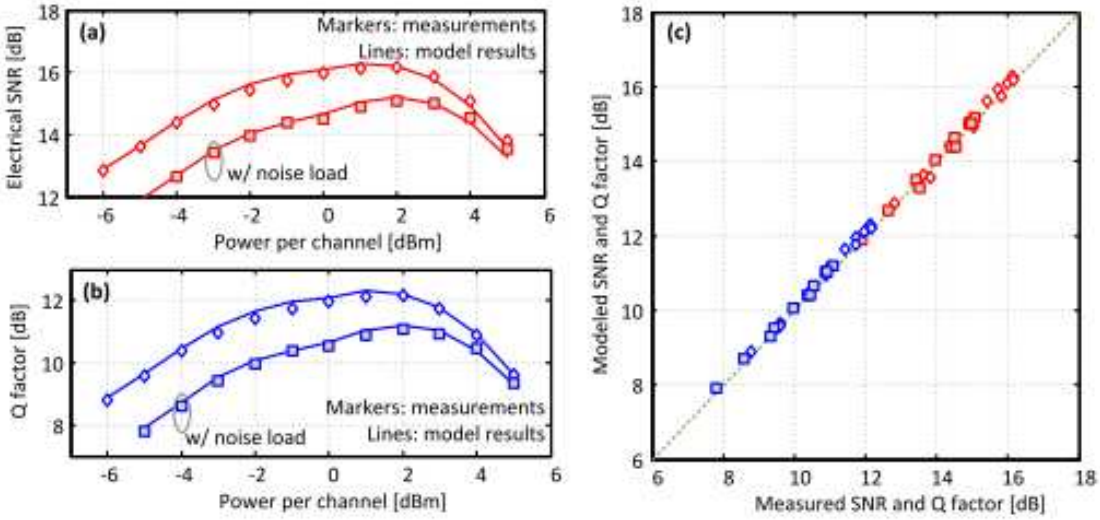

Fig. 6. 15x100km SSMF transmission results with and without noise loading for (a) SNR and (b) Q^2-factor versus power per channel. Solid lines: model, markers: experiment. (c) Modeled versus measured values.

In this section we show how accurately eq. (3) models system performance at a fixed distance. We experimentally measure the signal to noise ratio before the decision gate and the bit error ratio equivalent Q^2-factor after 15x100km of SSMF propagation as a function of channel power, with and without additional noise loading. The results are shown as markers in Fig. 6(a) and 6(b) for SNR_{tot} and Q^2-factor, respectively. The modeled values obtained using (3) and (2) are shown as solid lines. In eq. (3), we have used the measured OSNR, K_{TRX} as characterized in back to back, and a_{NL}=3.3e-3 mW^{-2}. Fig. 6(c) shows the same data, where the modeled values are plotted as function of the measured values for both SNR and Q^2-factor. As it can be seen, all points are within $\pm$0.2 dB of the $y=x$ dashed line, indicating excellent agreement between model and measurements.

We have repeated the same experiment (15x100 km propagation) using nonzero dispersion shifted fiber instead of SSMF. The test channel was at 1546.12 nm, where the local dispersion is ~4 ps/nm/km. The results show a reduced tolerance to nonlinear effects, due to the lower local dispersion and effective area, but the model still holds very well, yielding an error of the modeled Q²-factor with respect to the measured one always within ±0.2 dB.

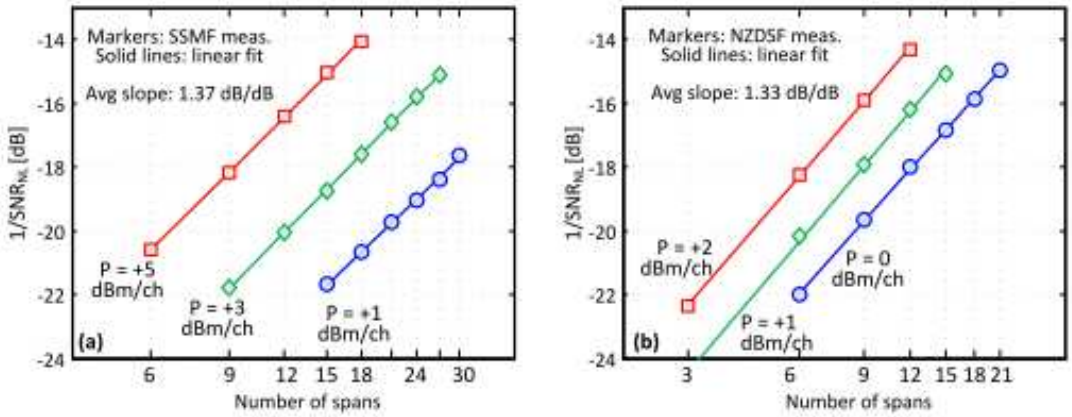

Fig. 7 $1/SNR_{NL}$ calculated from measurements for different channel powers as function of number of spans in dB scale. Solid lines are linear fit. Transmission over (a) SSMF, (b) NZDSF

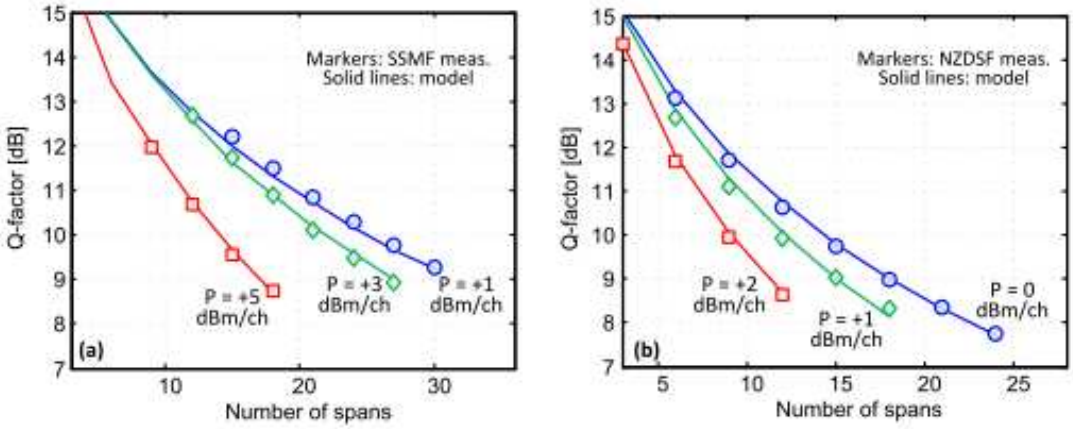

Fig. 8 Measured BER-equivalent Q²-factor is shown as function of the number of spans in linear scale. Solid lines are the results of the model. Transmission over (a) SSMF, (b) NZDSF

5. Performance modeling and prediction for variable distance

In this section, we use eq. (3) to calculate $1/SNR_{NL}$ for a fixed power and variable number of spans, in order to investigate its dependence on propagation distance. In this configuration $1/SNR_{NL}$ is proportional to the nonlinear noise variance so that we can use either quantity to deduce rules on the accumulation of nonlinearity-induced distortions.

Figure 7(a) shows (for SSMF propagation) the values of $1/SNR_{NL}$ calculated with eq. (3) from the measured data (electrical SNR, K_{TX} and OSNR) as function of the number of spans. We repeat the experiment for powers from +1 dBm/channel to +5 dBm/channel. The slope of the linear fit in log-log scale, shown with a solid line, is almost independent of the channel power. The average slope over the investigated powers is 1.37 dB/dB. That means that the nonlinear noise variance grows as $\sim N^{1.37}$, where N is the number of spans. For NZDSF propagation, Fig. 7(b) shows the same type of results. Again, it can be seen that nonlinear noise accumulates almost independently of the power per channel, and the average slope is 1.33 dB/dB. Similarly to SSMF, the nonlinear noise variance therefore grows as $\sim N^{1.33}$.

Recalling from previous section that $1/SNR_{NL} = a_{NL}P^2$, our results therefore suggest that a_{NL} can be written as

$$a_{NL} = \alpha_{NL} N^{1+\varepsilon} \quad (4)$$

where α_{NL} is a constant which in turn does not depend on transmission distance, and the dependence on the number of spans is governed by the exponent $1+\varepsilon$, where ε=0.37 over SSMF and ε=0.33 over NZDSF.

Next, we use the new expression of eq. (4) for a_{NL} in eq. (3), and with eq. (2) we predict system performance as function of distance. Results are shown in Fig. 8(a) for SSFM and Fig. 8(b) for NZDSF. In the figures, markers are experimental results of Q^2-factor versus propagation distance for different optical powers per channel. The solid lines show the results of the proposed model, where ε is used as calculated before. A single free parameter α_{NL} is needed for each fiber type, with which system performance can be predicted accurately for any distance, noise level and channel power. The single parameter actually depends on the characteristics of the optical fiber, as well as on the modulation format which is employed. As it can be seen, there is very good concordance of the model with the measured data.

One would be tempted to speculate that, in NDM systems, the contribution of each span to the total nonlinear noise variance would be independent of, or at least uncorrelated to, the contribution of the other spans, due to the large walk-off and pulse distortions induced by uncompensated chromatic dispersion. If that was the case, and if the same nonlinear noise power was generated in each span, then the total nonlinear noise variance would be directly proportional to the number of spans N: with our formalism, that would mean ε=0. On the contrary, our measurements suggest that, in the systems considered in this study, ε>0. Next section will investigate numerically the origin and the nature of this non-trivial result.

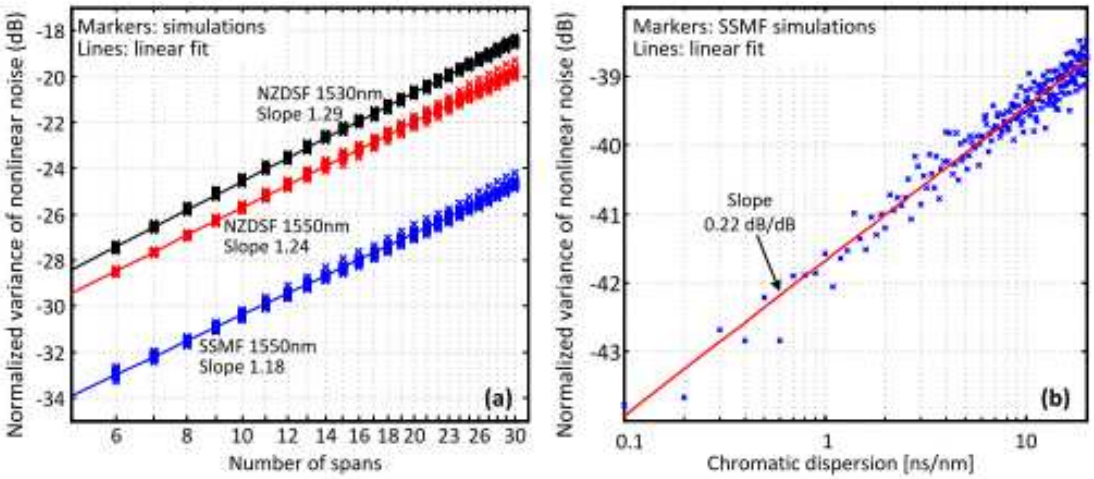

Fig. 9. Numerically calculated variance of nonlinear noise normalized to signal power (a) As function of the number of spans for NZDSF and SSMF, and (b) For a single span as function of chromatic dispersion at the input of the span.

6. Kerr effect-induced signal distortions accumulation

In our simulation setup, we consider 7 channels on a 50 GHz grid modulated with PDM-QPSK at 112 Gb/s. We use independent pseudo-random quaternary sequences of length 4096 symbols on the two polarizations of each channel. The channels states of polarizations (SOPs) and relative delays are random. We do not take into account fiber polarization mode dispersion. Signal propagation is simulated by numerically solving the vector nonlinear Schrödinger equation through the split-step Fourier method with 2^{18} FFT points. The systems under test are based on 100-km spans of SSMF or NZDSF without optical dispersion compensation. The spans are separated by EDFAs which exactly compensate for the optical loss of the preceding fiber. The nonlinear interaction of ASE noise and signal is known to be negligible in NDM systems [8]; we therefore safely neglect ASE noise in our simulations. We are thus able to estimate the distortions induced by the sole Kerr effect by subtracting the (normalized) optical field launched into the transmission link from the (normalized) optical

field at the link output. After having verified that the statistics of such distortions are well approximated by a Gaussian distribution (identically distributed in the 4D space of in-phase and quadrature components for the two polarizations), we express results in terms of the variance of this nonlinear noise.

Fig. 9(a) shows the variance of the nonlinear noise, normalized to unit symbol power and measured over 12.47 GHz, as function of the number of spans for SSMF at 1550 nm and NZDSF at 1550 nm and 1530 nm, assuming -3dBm channel power in all cases. The local dispersion is 17 ps/nm/km, 4.25 ps/nm/km and 2.5 ps/nm/km, respectively. We repeated the simulation 20 times, randomly changing the channels SOPs, relative delays and sequences. These random parameters account for a ~1dB spread in the variance of the nonlinear noise for a given fiber type and number of span. At fixed number of span still, the variance of nonlinear noise is found to increase from SSMF to NZDSF (1550nm) to NZDSF (1530nm).

For a given fiber type and wavelength, Fig. 9(a) shows that the variance of nonlinear noise versus span count can be approximated with excellent accuracy by a linear fit in dB/dB scale with a slope strictly greater than 1, confirming at least qualitatively the findings of the experimental results presented in section 5. Specifically, we find slopes of 1.18, 1.24 and 1.29dB/dB for SSMF, NZDSF (1550nm) and NZDSF(1530nm). These values are somewhat lower than those found experimentally. The slight discrepancy is assigned to the presence of sources of impairments other than Kerr effect in the experimental setup (polarization dependent loss, imperfect DSP, …)

This faster-than-linear growth of the variance of nonlinear distortions may have two (possibly combined) sources:

- Partial (positive) correlation, *i.e.* constructive interference, between the distortions induced by different spans of the transmission links. In the extreme case of all spans creating an identical distortion f, the total distortion after N spans would be $N \cdot f$ and its variance $N^2\mathrm{var}(f)$, thus yielding a 2 dB/dB growth of the total variance of nonlinear distortion with the number of span.

- Increasing of the noise variance generated by the individual spans along propagation, *i.e.*, each span generates a nonlinear noise, the variance of which is greater than the variance generated by the preceding span.

In order to test the latter hypothesis, we present in Fig. 9(b) the variance of the nonlinear distortion created by a single span of 100 km of SSMF with 0 dBm channel power as a function of the cumulated chromatic dispersion at the span input. Besides some scatter (due to random realizations of channels sequences, SOP and delays) a clear linear growth of the variance of nonlinear distortions versus chromatic dispersion in dB/dB scale can be observed. Denoting the average slope ξ, we find ξ~0.22. This result is in line with the intuition that in NDM links, chromatic dispersion gradually distorts the optical signal, increasing the occurrence of short power spikes prone to high nonlinear distortions and increasing the number of interpulse four wave mixing terms.

Assuming complete decorrelation between spans, the variance of the total nonlinear distortion f_{tot} can be written as the sum of the variance of f_k's, where f_k is the nonlinear distortion induced by the span k. Grouping the various results presented in this paper, we can write $\mathrm{var}(f_k)$ as:

$$\mathrm{var}(f_k) = AP^3C_k^{\xi}$$

where P is the channel power, C_k the chromatic dispersion at the input of span k and A is a constant which is independent of the channel power and propagated distance. This model clearly fails for the first span of a transmission link without precompensation as the zero chromatic dispersion at the span input would yield zero nonlinear distortion regardless of the power. Keeping in mind that the first span must be handled separately, the variance of the total nonlinear distortions can thus be written as:

$$\mathrm{var}(f_{tot}) = \mathrm{var}(f_1) + \sum_{k=2}^{N} AP^3C_k^{\xi} = A_1P^3 + AP^3\left(DL_{span}\right)^{\xi}\sum_{k=1}^{N}(k-1)^{\xi} \approx A_1P^3 + \frac{AP^3\left(DL_{span}\right)^{\xi}}{1+\xi}(N-1)^{1+\xi} \quad (5)$$

where A_1 is a constant to account for the first span noise variance var(f_1), D is the local chromatic dispersion, L_{span} is the span length, and we have used $C_k = DL_{span}(k\text{-}1)$, assuming that all spans are of equal length.

The right hand side expression in eq. (5) is obtained through approximation of the discrete sum over the number of span by the corresponding integral. For N large enough, we thus find $\mathrm{var}(f_{tot}) \propto N^{1+\xi}$ with $1+\xi = 1.22$. This value is very close to the 1.18dB/dB slope found in Fig. 9(a) for SSMF links and the small remaining discrepancy is within the accuracy of the simulation.

7. Conclusion

We have experimentally shown that, in the case of a WDM-PDM-QPSK 100 Gb/s system without optical dispersion compensation, the optical fiber channel can be modeled by an additive Gaussian noise channel with high accuracy. We characterized the noise variance with respect to signal power, ASE level and distance. We proposed a simple empirical model to account for the distance dependence of the noise variance, which is shown to be able to predict Q^2-factor with accuracy within $\pm$0.2dB.

Via simulations we have investigated the nature of nonlinear distortions accumulation, showing that not all spans contribute equally to the total nonlinear noise variance, since the nonlinear noise generated in a span is function of the chromatic dispersion at the span input. Finally, we have shown another simple but powerful model that assumes completely uncorrelated nonlinear distortions from span to span and accounts for the increasing chromatic dispersion at the span input along propagation. With such model, the supra-linear dependence of nonlinear noise with propagation distance can be explained with an error which is within simulation accuracy.

Such models capturing how the nonlinear noise variance evolves and how to predict a Q factor are very simple and very powerful. For instance, when setting the fibre input power such that the Q factor is maximized (equal to Q°) assuming a fixed noise power and a given distance, then it comes that the nonlinear noise variance is half the amplifier noise variance. As a result, the resulting OSNR penalty (for the same reference Q factor Q°) is $10\log_{10}(3/2)=1.76$dB [209][213][218]. This means that the NLT as defined in Chapter 5 for a reference Q factor Q° or such that the optical power maximizes the Q factor to Q° at constant noise power (for a given distance) corresponds to an OSNR penalty of 1.76dB whatever the fibre.

The model accounting for the accumulation of nonlinear noise variance from span to span is also quite promising in itself. It is close to perturbative models though much simpler. If we consider a homogeneous system composed of identical spans, such model is also compatible with the adapted nonlinear phase criterion. However, this model inherently accounts for the arrangement of fibres and the dispersion map as opposed to the adapted nonlinear phase criterion. The increase of complexity with respect to the adapted nonlinear phase criterion is not too substantial to imagine utilization in a GMPLS-controlled reconfigurable optical network, but the calculation of the variance further imposes to know the dispersion map.

Eventually this novel model of noise variance estimation can be used to derive power setting rules and reach estimators as well, as in the previous section. Similar reasoning, not detailed here, leads to propose an adaptation of the input power into each span to the cumulated dispersion at span input: actually the optimum power is found to decrease when the absolute value $|Pre|$ of the cumulated dispersion at span input increases (in details almost proportional to $1/|Pre|^{(2\alpha-1)/3}\sim 1/|Pre|^{1/9}$ for SMF or LEAF spans with 100Gb/s PDM-QPSK).

In reconfigurable optical networks, such recommendation is however very likely to be unpractical, the fibre input power per channel generally being identical for channels with the same modulation format whatever the lightpath, thus whatever the position of the fibre in a lightpath. In ultra long-haul submarine applications such recommendation could be applicable: it would to a progressive decrease of fibre input power by about 2 dB over 100 spans at 100Gb/s. However, the reach improvement with respect to the recommendations of the model derived from the adapted nonlinear phase is very limited; it can be analytically calculated and amounts to only 0.85% at 100Gb/s.

On the whole, the proposed average power setting rules derived from the (weighted) adapted nonlinear phase still appear as particularly suitable for 100Gb/s transmission systems.

6.III. Summary

We have covered through two recent articles the most recent advances we have made (within my research group) over the past few years about the transposition of the work of this document to 100Gb/s PDM-QPSK systems employing coherent detection. In a short period, many things have changed, since at such symbol rate (higher than 28Gbaud) and with multilevel phase modulation, the optimal dispersion maps fall in the highly dispersive regime (with very limited or even zero inline dispersion compensation) where the nonlinear phase criterion does not yield enough accuracy. We have thus presented two models to capture the accumulation of nonlinearities in such dispersive regimes, one being a simple adaptation of the (weighted) nonlinear phase criterion and another one rather considering nonlinear induced distortions as uncorrelated noise contributions from span to span, yet depending on the dispersion map. Refinement of the latter model and connection with perturbative models from the NLSE can be found in [209]. We have then proposed derived power setting rules just like in Chapter 5.

Eventually we have shown that with coherent detection, the received signal distortions before symbol identification follow a Gaussian distribution, whether they come from amplifier noise or Kerr-induced nonlinearities. This can considerably ease the design of systems and performance prediction.

6.IV. References

[206] C.R.S. Fludger et al., "10x111 Gbit/s, 50-GHz spaced, POLMUX-RZ-DQPSK transmission over 2375 km employing coherent equalisation," in Proc. OFC/NFOEC, Anaheim, CA, Feb. 2007, paper PDP-22.

[207] G. Charlet, J. Renaudier, H. Mardoyan, P. Tran, O. Bertran Pardo, F. Verluise, M. Achouche, A. Boutin, F. Blache, J.-Y. Dupuy, S. Bigo, "Transmission of 16.4 Tbit/s capacity over 2 550 km using PDM QPSK modulation format and coherent receiver," in Proc. OFC/NFOEC, San Diego, CA, Feb. 2008, paper PDP-3.

[208] G. Charlet, "Coherent detection associated with Digital Signal Processing for Fibre Optics Communications", C. R. Physique 9 (9-10) (2008) 1012-1030

[209] E. Grellier, "Etude des effets non-linéaires à l'œuvre dans les systèmes de transmissions optiques fortement dispersifs", Thèse de doctorat de l'Université de Besançon présentée en Juillet 2011

[210] E. Grellier, J.-C. Antona, and S. Bigo, "Revisiting the evaluation of non-linear propagation impairments in highly dispersive systems," in Proc. ECOC'09, paper 10.4.2,Vienna, September 2009

[211] E. Grellier, J.-C. Antona, S. Bigo, "Global criteria to account for tolerance to nonlinearities of highly dispersive systems," IEEE Photon. Tech. Letters, Vol 22, No 10, May 15th 2010

[212] E. Grellier, A. Bononi, "Quality Parameter for Coherent Transmissions with Gaussian-distributed Nonlinear Noise", in Optics Express, Vol. 19, No. 13, 20 June 2011

[213] F. Vacondio, C. Simonneau, L. Lorcy, J.C.Antona, A. Bononi and S. Bigo, "Experimental characterization of Gaussian-distributed nonlinear distortions", in Proc. ECOC 2011, September 2011, We.7.B.1, Geneva, Switzerland

[214] F. Vacondio, O. Rival, C. Simonneau, L. Lorcy, E. Grellier, J.-C. Antona, A. Bononi, S. Bigo, "On nonlinear distortions of coherent systems", Optics Express, 20, 1022-1032 (2012)

[215] A. Bononi, P. Serena, N.Rossi, and D. Sperti, "Which is the dominant nonlinearity in long-haul PDM-QPSK coherent transmissions?", in Proc. ECOC 2010, paper Th10E1, Torino, Italy, Sept. 2010

[216] M. Bertolini, P. Serena, G. Bellotti, A. Bononi, "On the XPM-Induced Distortion in DQPSK-OOK and Coherent QPSK-OOK Hybrid Systems", in Proc. OFC/NFOEC 2009, paper OTuD4, San Diego, California, USA, March 22-26 2009

[217] V. Curri, P. Poggiolini, G. Bosco, A. Carena, and F. Forghieri "Performance Evaluation of Long-Haul 111 Gb/s PM-QPSK Transmission Over Different Fibre Types", IEEE Photonics Technology Letters, Vol. 22, No. 19, Oct 1, 2010

[218] G. Bosco, A. Carena, R. Cigliutti, V. Curri, P. Poggiolini, F. Forghieri, "Performance Prediction for WDM PM-QPSK Transmission Over Uncompensated Links", in Proc. OFC/NFOEC 2011, paper OThO7, Los Angeles, California, March 2011

OVERALL CONCLUSION

This document has covered many aspects of the models that have been imagined over the past ten years to describe the accumulation of nonlinearities and to predict performance, first in strongly dispersion-managed systems adapted to 10-40Gb/s-modulations in absence of coherent detection, then in weakly dispersion-managed systems adapted to 40-100^{+} Gb/s-modulations taking advantage of DSP-assisted coherent detection.

We have started this work by experimentally characterizing the nonlinear index of a large variety of optical fibres, as a preamble to the necessary numerical simulations for this study.

We have first introduced the (weighted) nonlinear phase criterion in Chapters 2-3 that helps to predict accurately enough transmission penalties induced by Kerr effect and chromatic dispersion in dispersion-managed systems. We have deeply investigated ideal, lab-like, record-experiment-like, configurations as well as realistic configurations, closer to the constraints of deployed heterogeneous networks to come up with a satisfactory proposition which domain of validity is known. We have also developed analytical perturbative tools that help get more insight into the scaling laws of dispersion managed systems.

Once we had enough confidence on the nonlinear phase criterion, we have proposed I Chapter 4 a method to build a quality of transmission estimator predicting the Q factor for a system impaired by multiple propagation effects typical of optical networks.

Then in Chapter 5, we have focused on nonlinear and noise limitations to derive very simple tools that help to capture and to optimize the system benefits of subsystems such as optical amplifiers, dispersion compensating fibres, modulation formats. Such tools have been used among others to optimize the hybrid Raman + Erbium amplification scheme of a few record experiments. Eventually, such tools have brought the ability to predict the optimal setting of fibre input powers over a heterogeneous optical network, which can be of a certain interest.

Eventually Chapter 6 summarizes the most recent advances on the field of 100Gb/s multilevel phase & polarization modulated systems and the revolution they have brought due to coherent detection and the novel ways to manage the dispersion (almost no inline management or not at all). We have shown that in such conditions, the nonlinear induced distortions can be considered as a Gaussian noise, which variance grows with the cube of signal power and supra-linearly with distance (due to uncorrelated noise contributions from span to span and dependence on the dispersion map). This allows revisiting the five first chapters of this document in terms of accumulation of nonlinearities, performance prediction and guidelines to set the powers. Some recent thoughts have been inserted but this subject is far from being closed with the renewal brought by such formats and detection schemes.

In the coming years, the increase of bit-rates, the increased complexity of the modulation formats, the elasticity and the heterogeneity of networks will prevail. In turn, the need for accurate performance prediction tools is likely to become even more stringent than today: we expect that the increase of bit-rate will lead to a decrease of achievable reach thus the more accurate the performance prediction the better, otherwise unnecessary system margins will make systems unpractical. We also expect to make those optical networks evolve towards more autonomy in their decisions to reconfigure themselves, to allocate lightpaths, bit-rates, channels, channel spacing and regenerators at best depending on traffic, energy and physical constraints. This will require particularly clever and flexible tools as well. The tools presented in this document can be seen as a good starting point.

ACKNOWLEDGMENTS

Je tiens à remercier ici ceux sans qui rien n'eût été possible et dont la contribution m'a été précieuse pour réaliser ces travaux et ce manuscript.

Tout d'abord je tiens à remercier vivement Jean-Pierre Hamaide et Sébastien Bigo qui m'ont permis de participer à cette aventure au sein d'Alcatel (aujourd'hui Alcatel-Lucent) et qui m'ont soutenu lors de toutes ces années de recherche et lors de la rédaction de ce manuscrit.

A l'origine et à la conclusion de cette aventure scientifique, je tiens également à remercier vivement Yves Jaouen, qui m'a tout d'abord aiguillé vers les laboratoires d'Alcatel en 1999 alors que j'étais à la recherche d'un stage sur les solitons, et qui, « quelques » années plus tard, a accepté d'être mon directeur de thèse. J'ai particulièrement apprécié les discussions que nous avons eues pour transformer une vaste quantité d'informations accumulée sur 10 ans en un manuscrit qui devienne véritablement « lisible ».

Je tiens également à remercier vivement Michel Joindot, Christophe Finot, Badr-Eddine Benkelfat, Erwan Pincemin et Alberto Bononi qui m'ont fait l'honneur de constituer, avec Sébastien et Yves, le jury de ma thèse.

La plupart des travaux relatés dans ce manuscrit en été réalisés en interaction forte et avec un certain nombre de collègues, tant du coté numérique / théorique (Yann Frignac, Emmanuel Sève durant presque 10 ans, Sandrine Cussat-Blanc, Gaelle Lemeur, Catherine Martinelli, Sébastien Petitrenaud, Florence Leplingard, Edouard Grellier, Olivier Rival) qu'expérimental (Bruno Lavigne, Gabriel Charlet, Elodie Balmefrezol, Pierre Peloso, Denis Penninckx, Christian Simonneau, Pascal Henri, Laurence Lorcy…).

Je remercie également les nombreux stagiaires avec lesquels j'ai eu la chance d'interagir et qui ont participé à ce foisonnement d'idées et de résultats, notamment Mathieu Lefrançois, Anne-Solenn Jehanno, Petros Ramantanis, Alexandros Pitilakis, Patrick Mirault, Pierre Mahou, Sylvain Caze, Antoine Lagré, et Arthur Laurin.

Je pense avoir eu le grand privilège de pouvoir conduire des travaux de recherche ayant une très grande proximité avec les réalisations industrielles tant dans le domaine des fibres optiques que des systèmes de transmissions optiques. A ce titre, les nombreuses discussions et interactions avec Pierre Sillard, Olivier Courtois, Pascal Pecci, Jean-Luc Augé ont été particulièrement enrichissantes et m'ont permis de mesurer toute la complexité d'un véritable système déployé.

Dans le même temps, les travaux que nous avons pu mener ont été constamment enrichis de discussions avancées et passionnées avec des représentants éminents de l'Université de Parme, grands spécialistes des effets non-linéaires dans les systèmes de transmissions optiques, je pense tout particulièrement à Alberto Bononi (encore) et Paolo Serena.

Et pour finir, je tiens à remercier ceux qui m'ont supporté (à tous les sens du terme) ces derniers temps lors de la réalisation de ces travaux et pendant le long processus de maturation du manuscrit, c'est à dire les membres du groupe Réseaux Optiques Dynamiques, mais aussi papa, maman, Carine et ma toute petite Hélène.

LIST OF RELATED PUBLICATIONS AND PATENTS

Journals

1. P. Pecci, S. Lanne, Y. Frignac, J.-C. Antona, G. Charlet and S. Bigo, "Tolerance to dispersion compensation parameters of six modulation formats in systems operating at 43Gbit/s", Electronics Letters, vol. 39, No. 25, 11th December 2003
2. S. Bigo, Y. Frignac, J.-C. Antona, G. Charlet, S. Lanne, "Research trends in terrestrial transmission systems", Compte-Rendus de Physique de l'Académie des Sciences, 4 (2003), 105-113
3. S. Bigo, Y. Frignac, J.-C. Antona, G. Charlet, "Design of multi-terabit/s terrestrial transmission systems facilitated by simple analytical tools", Annales des Télécommunications, Nov-Dec 2003
4. D. Penninckx, G. Charlet, J.-C. Antona, L. Noirie, "Simple engineering rules for a transparent waveband-based optical backbone network", Journal of Optical Networking, Vol. 2 Issue 2, pp.38-45 (2003)
5. P. Serena, A. Bononi, J.-C. Antona and S. Bigo, "Parametric Gain in the Strongly Nonlinear Regime and its Impact on 10 Gb/s NRZ Systems with Forward-Error Correction", Journal of Lightwave Technology, Volume 23, Issue 8, Aug. 2005, pp. 2352 – 2363
6. J. Livas, J.-C. Antona, M. Bortz, R. Dodd, P. Peloso, and A. Saley, "Optical Transmission Evolution: from Digital to Analog to ?: The network tradeoffs between optical transparency and reduced regeneration cost", IEEE Journal of Lightwave Technology, vol. 23, No.3, March 2005
7. M. Lefrançois, E. Barnasson, G. Charlet, J.-C. Antona, S. Bigo, "Numerical discrimination of intrachannel cross-phase modulation and intrachannel four-wave mixing and their respective effect on 40Gb/s transmissions", Optics Letters, Vol 31, No 4, Feb 15, 2006
8. A. Morea, N. Brogard, F. Leplingard, J.-C Antona, T. Zami, B. Lavigne, D. Bayart, "QoT-function and A* routing: an optimized combination for connection search in translucent networks", Journal of Optical Networking, Vol. 7 Issue 1, pp.42-61 (2008)
9. J.-C. Antona, S. Bigo, "Performance & physical design of heterogeneous optical transmission systems", Comptes-Rendus Physique, (10), 2008
10. A. Morea, F. Leplingard, JC. Antona, P. Henri, T. Zami & D. Kilper, "Advanced Test-beds to Validate Physical Estimators in Heterogeneous Long Haul Transparent Optical Networks", in Journal Of Networks, Vol 5, No 11 (2010), 1335-1342, Nov 2010
11. E. Grellier, J.-C. Antona, S. Bigo, "Global criteria to account for tolerance to nonlinearities of highly dispersive systems," IEEE Photon. Tech. Letters, Vol 22, No 10, May 15th 2010
12. F. Vacondio, O. Rival, C. Simonneau, L. Lorcy, E. Grellier, J.-C. Antona, A. Bononi, S. Bigo, "On nonlinear distortions of coherent systems", Optics Express, 20, 1022-1032 (2012)

Conferences

13. J.-C. Antona, Denis Pennninckx, “Enhanced Phase-Shaped Binary Transmission Modulation Format for Dispersion-Managed WDM Systems”, Proc. of ECOC’00 (European Conf. on Optical Communications), 8.3.4, München (Germany), Sept 2000
14. J.-C. Antona, S. Bigo, S. Kosmalski, “Nonlinear index measurements of various fibre types over C+L bands using four-wave mixing”, Proc. of ECOC’01, We. L.1.2, Amsterdam (Netherlands), 2001
15. S. Bigo, W. Idler, J.-C. Antona, G. Charlet, C. Simonneau, M. Gorlier, M. Molina, S. Borne, C. de Barros, P. Sillard, P. Tran, R. Dischler, W. Poehlmann, P. Nouchi, Y. Frignac, “Transmission of 125 WDM channels at 42.7Gbit/s (5 Tbit/s capacity) over 12x100 km of TeraLightTM Ultra fibre”, Proc. of ECOC’01, Post-Deadline session, vol.6, , pp. 2- 3 , Amsterdam (Netherlands), September 2001
16. J.-C. Antona, S. Bigo, J.-P. Faure, “Nonlinear cumulated phase as a criterion to assess performance of terrestrial WDM systems”, Proc. of OFC’02 (Optical Fibre Communications conference), paper WX5, Anaheim (Ca), 2002
17. Y. Frignac, J.-C. Antona, S. Bigo and J.-P. Hamaide, “Numerical optimization of pre- and inline-dispersion compensation in dispersion-managed systems at 40Gb/s”, Proc; of OFC’02, ThFF5, Anaheim (Ca), 2002
18. G. Charlet, W. Idler, R. Dischler, J.-C. Antona, P. Tran, S. Bigo, “3.2Tbit/s (80x42.7Gb/s) C-Band transmission over 9x100km of TeraLightTM fibre with 50GHz channel spacing”, in Optical Amplifiers and Their Applications, J. Nagel, S. Namiki, and L. Spiekman, eds., Vol. 77 of OSA Trends in Optics and Photonics Series (Optical Society of America, 2002), paper PD1, Vancouver, Canada, July 2002
19. C. Martinelli, D. Mongardien, J. C. Antona, C. Simonneau, D. Bayart, “ANALYSIS OF BI-DIRECTIONAL AND SECOND-ORDER PUMPING IN LONG-HAUL SYSTEMS WITH DISTRIBUTED RAMAN AMPLIFICATION”, ECOC’02, paper P3.30, Copenhagen (Denmark), Sept 2002
20. D. Penninckx, G. Charlet, J.-C. Antona, L. Noirie, “Experimental validation of a transparent waveband-based optical backbone network”, Proc. of ECOC’02, paper 6.4.4, Copenhagen (Denmark), Sept 2002
21. G. Charlet, J.-C. Antona, S. Lanne, P. Tran, W. Idler, M. Gorlier, S. Borne, A. Klekamp, C. Simonneau, L. Pierre, Y. Frignac, M. Molina, F. Beaumont, J.-P. Hamaide, S. Bigo, “6.4Tb/s (159x42.7Gb/s) Capacity over 21x100km using Bandwidth-Limited Phase-Shaped Binary Transmission”, Proc. of ECOC’02, Post-Deadline paper PD 4.1, Copenhagen (Denmark), Sept 2002
22. W. Idler, J.-C. Antona, “Record Spectral efficiencies and transmission capacities based on Nx43Gb/s systems”, IEEE LEOS annual meeting, invited paper TuQ1, Glasgow, Nov. 2002
23. C. Martinelli, G. Charlet, L. Pierre, J.-C. Antona, D. Bayart, “System impairment of Double Rayleigh Scattering and dependence on modulation format”, OFC’2003, paper FE3, Atlanta (Georgia), USA, March 2003
24. G. Charlet, J.-C. Antona, S. Lanne, S. Bigo , “From 2100 to 2700km distance using Bandwidth-Limited Phase-Shaped Binary Transmission at 6.3Tb/s capacity”, Proc. of OFC’2003, paper WE3, Atlanta (Georgia), USA, March 2003
25. G. Charlet, S. Lanne, L. Pierre, C. Simonneau, P. Tran, H. Mardoyan, P. Brindel, M. Gorlier, J.-C. Antona, M. Molina, P. Sillard, J. Godin, W. Idler, S. Bigo, “Cost-Optimized 6.3Tbit/s-capacity terrestrial link over 17x100km using Phase-Shaped

Binary Transmission in a conventional all-EDFA SMF-based system", OFC'2003, Post-deadline PD25-1, Atlanta (Georgia), USA, March 2003
26. G. Charlet, J.-P. Thiery, P. Tran, H. Mardoyan, J.-C. Antona, C. Martinelli, S. Bigo; "80x10.7Gbit/s with NRZ, RZ and RZ-DPSK formats over sixty 100-km long terrestrial (non dispersion managed) fibre spans with all-Raman amplification", OAA'03 post-deadline PD1, July 2003
27. P. Serena, J-C. Antona, S. Bigo, A. Bononi, "PARAMETRIC GAIN IMPAIRMENTS IN 10 Gb/s CODED OPTICAL SYSTEMS WORKING AT LOW SIGNAL-TO-NOISE RATIOS", Proc. ECOC'2003, paper Tu4.2.6, Rimini (Italy), Sept 2003
28. P. Pecci, S. Lanne, Y. Frignac, J-C. Antona, G. Charlet and S. Bigo, "Tolerance to dispersion compensation parameters of six modulation formats in systems operating at 43Gb/s", ECOC'03, paper We3.5.5, Rimini (Italy), Sept 2003
29. Y. Frignac, J.-C. Antona and S. Bigo, "Enhanced analytical engineering rule for fast optimization of dispersion maps in 40 Gbit/s-based transmission systems", OFC'04, paper TuN3, Los Angeles (Ca), February 2004
30. P. Sillard, B. Dany, A. Bertaina, L. Curinckx, C. Bastide, O. Courtois, J-.C. Antona, S. Bigo, "Simple criterion of quality to evaluate DCM impact on WDM system performance", OFC'04, paper FA4, Los Angeles (Ca), February 2004
31. P. Peloso, D. Penninckx, M. Prunaire, J-C. Antona, "Relevant pre and/or post compensation strategies for implementing transparency in heterogeneous backbone networks", ECOC'04, Tu 1.6.5, Stockholm, September 2004
32. T. Zami, J.-C. Antona, P. Peloso, E. Le Rouzic, A. Morea, M. Joindot, B. Fracasso, P. Gravey, M. Gagnaire, "Dimensioning of WDM transparent networks based on the Quality of Transmission in the framework of the french RYTHME project", Broad-Band Europe '04 Conference
33. A. Bononi, P. Serena, J.-C. Antona and S. Bigo, "Revisiting Nonlinear Interactions Between Signal and Noise in Presence of FEC", LEOS'04 Conference. Invited Paper, 2004
34. P. Sillard, P. Nouchi, J-.C. Antona, S. Bigo, "Modeling the non-linear index of optical fibres", OFC'05, paper OFH4, Anaheim, February 2005
35. A. Bononi, P. Serena, J.-C. Antona and S. Bigo, "Implications of Nonlinear Interaction of Signal and Noise in Low-OSNR Transmission Systems with FEC", OFC'05, Invited Paper OThW5, Anaheim (Ca), February 2005
36. L.A. de Montmorillon, P. Sillard, M. Astruc-Bigot, B. Dany, P. Nouchi , B. Lavigne, E. Balmefrezol, J.-C. Antona, O. Leclerc, "Transmission fibre optimized for metro optical network", OFC'05, paper OFH1, Anaheim (Ca), February 2005
37. J.-C. Antona, M. Lefrançois, S. Bigo, G. Le Meur, "Investigation of Advanced Dispersion Management Techniques for Ultra-Long Haul Transmissions", ECOC'05, Mo.3.2.6, Sept 2005, Glasgow (Scotland)
38. M. Lefrançois, E. Barnasson, G. Charlet, J.-C. Antona, S. Bigo, "Relative Impact of the Different Intrachannel Nonlinear Effects over 43 Gb/s Transmissions with Varying Fibre Dispersion", Ecoc'05, Tu1.2.7, Sept 2005, Glasgow (Scotland)
39. J.-C. Antona, P. Sillard, "Relationship between the Achievable Distance of WDM Transmission Systems and Criterion of Quality for DCM", OFC'06, paper OWJ2, Anaheim (Ca), March 2006
40. J.-C. Antona, S. Bigo, A.S. Jehanno, "Performance Evaluation of WDM Transparent Networks Incorporating Various Fibre Types", ECOC'06, paper We3.P.141, Cannes (France), Sept 2006

41. J.-C. Antona, P. Sillard, S. Bigo, “Impact of Imperfect Wideband Dispersion Compensation on the Performance of WDM Transmission Systems at 40 Gbit/s”, ECOC’06, Th1.6.4, Cannes (France), Sept 2006
42. E. Seve, J.-C. Antona, T. Zami, “Do’s and Don’ts for the Emulation of Four-Wave Mixing in 10Gb/s WDM Systems Based on Low-Dispersion Fibre”, ECOC’07, paper P096, Berlin (Germany), Sept 2007
43. B. Lavigne, F. Leplingard, L. Lorcy, E. Balmefrezol, J.-C Antona, T. Zami, , D. Bayart, “Method for the determination of a Quality of Transmission Estimator along the lightpaths of partially transparent networks”, ECOC’07, paper We 08.5.2, Berlin (Germany), Sept 2007
44. J.-C. Antona, G. Charlet, S. Bigo, “Next Generation Terabit/s-class transmission systems”, SPIE APOC’07 (Asia-Pacific Optical Communication conference), invited paper, Wuhan (China), Nov 2007
45. J.-C. Antona, E. Sève, A. Pitilakis, P. Ramantanis, S. Bigo, “Design and Performance Prediction in Meshed Networks with Mixed Fibre Types”, OFC’08, paper JThA49, San Diego
46. P. Sillard, J.C. Antona, S. Bigo, “Optimized Chromatic Dispersion of DCMs in WDM Transmission Systems at 40Gbps”, OFC’08, paper JWA13, San-Diego
47. J.-C. Antona, E. Grellier, A. Bononi, S. Petitrenaud, S. Bigo, “Revisiting Binary Sequence Length Requirements for the Accurate Emulation of Highly Dispersive Transmission Systems”, Proc. of ECOC 2008, Paper We 1.E.3, Brussel (Belgium), September 2008
48. E. Grellier, J.-C. Antona, S. Bigo, A. Bononi, “REEXAMEN DES LONGUEURS DE SEQUENCES PSEUDO-ALEATOIRES BINAIRES NECESSAIRES A L’EMULATION PRECISE DES SYSTEMES DE TRANSMISSIONS OPTIQUES FORTEMENT DISPERSIFS”, in Proc. JNOG 2008 (Jounées Nationales de l’Optique Guidée), Lannion (France), October 2008
49. E. Grellier, J.-C. Antona, S. Bigo, A. Bononi, “Revisiting Binary Sequence Length Requirements for the Accurate Emulation of Highly Dispersive Optical Transmission Systems”, in SPIE Proc. APOC 2008, Asia-Pacific conference on Optical Commnications, November 2008
50. J.-C. Antona, G. Charlet, S. Bigo, “Long-Haul 100Gb/s Coherent Transmission Experiments”, invited paper, in SPIE Proc. APOC 2008, Asia-Pacific conference on Optical Commnications, November 2008, Hangzhou, China.
51. E. Grellier, J.-C. Antona, and S. Bigo, “Revisiting the evaluation of non-linear propagation impairments in highly dispersive systems,” in Proc. ECOC’09, paper 10.4.2,Vienna, September 2009
52. J.-C. Antona, “Key technologies for current and future optical networks”, plenary talk at TWEPP’09 (Topical Workshop on Electronics for Particle Physics), September 2009, Paris, France
53. J.-C.Antona, T. Zami, F. Leplingard, A Morea, “Physical impairment-aware transparent optical networks”, invited paper, in SPIE Proc. APOC 2009, Asia-Pacific conference on Optical Commnications, Nov 09, Shanghai, China
54. P. Henri, C. Simonneau, F. Leplingard, JC Antona, “Experimental investigation of the quality of transmission in transparent mesh networks with mixed fibre types”, in Proc. OFC 2010, JThA1, San Diego, California, March 2010
55. A. Morea, J.-C. Antona, “Benefits of fine QoT-estimator to dimension spare resources in automatic restorable networks”, in Proc. ICTON 2010, Munich, July 2010

56. E. Grellier, J.-C. Antona, S. Bigo, “Are multilevel pseudorandom sequences really needed to emulate highly dispersive optical transmission systems?”, in Proc. of ECOC 2010, Paper We 6.A.1 , September 19-23, 2010, Torino (Italy)
57. E. Grellier, J.-C Antona, S. Bigo, “INTERET DE LA GESTION DE DISPERSION CHROMATIQUE PAR CANAL POUR LES SYSTEMS MODULES EN 100G PDM-QPSK”, in Proc. JNOG 2010 (Jounées Nationales de l’Optique Guidée), Lannion (France), October 2010, Besançon (France).
58. F. Vacondio, C. Simonneau, L. Lorcy, J.-C.Antona, A. Bononi and S. Bigo, “Experimental characterization of Gaussian-distributed nonlinear distortions”, in Proc. ECOC 2011, September 2011, paper We.7.B.1, Geneva, Switzerland

Active Patents

6 active patents

Ctry	Title	Inventor(s)	File Date	Issue Date	Expiry Date	Patent No
US	Adaptive Pre/Post compensation rules for Intelligent transponder applied to systems migration to higher bit rates than 10Gb/s.	ANTONA, Jean-Christophe; LAVIGNE, Bruno	09/04/2007	07/12/2010	10/02/2029	7848656
DE	ROADM architecture for multi-bit-rates operation	ANTONA, Jean-Christophe; COURTOIS, Olivier	19/06/2008	21/04/2010	19/06/2028	2007049
GB	ROADM architecture for multi-bit-rates operation	ANTONA, Jean-Christophe; COURTOIS, Olivier	19/06/2008	21/04/2010	19/06/2028	2007049
FR	ROADM architecture for multi-bit-rates operation	ANTONA, Jean-Christophe; COURTOIS, Olivier	19/06/2008	21/04/2010	19/06/2028	2007049
DE	Advanced dispersion map for DSF transmission system	CHARLET, Gabriel; ANTONA, Jean-Christophe	04/01/2005	10/03/2010	04/01/2025	1677444
FR	Advanced dispersion map for DSF transmission system	CHARLET, Gabriel; ANTONA, Jean-Christophe	04/01/2005	10/03/2010	04/01/2025	1677444
GB	Advanced dispersion map for DSF transmission system	CHARLET, Gabriel; ANTONA, Jean-Christophe	04/01/2005	10/03/2010	04/01/2025	1677444
FR	Optical network with self learning of its quality	CHARLET, Gabriel; ANTONA, Jean-Christophe; PELOSO, Pierre	08/01/2008	18/12/2009	08/01/2028	2926174
FR	Rule for operating amplifiers output power	ANTONA, Jean-Christophe; BIGO, Sébastien; CHARLET, Gabriel	10/08/2006	14/10/2009	10/08/2026	1887718
DE	Rule for operating amplifiers output power	ANTONA, Jean-Christophe; BIGO, Sébastien; CHARLET, Gabriel	10/08/2006	14/10/2009	10/08/2026	1887718
GB	Rule for operating amplifiers output power	ANTONA, Jean-Christophe; BIGO, Sébastien; CHARLET, Gabriel	10/08/2006	14/10/2009	10/08/2026	1887718
GB	Method of operating and optimising a WDM transmission system amd computer program product	ANTONA, Jean-Christophe; LAVIGNE, Bruno	08/05/2006	26/08/2009	08/05/2026	1855399
DE	Method of operating and optimising a WDM transmission system amd computer program product	ANTONA, Jean-Christophe; LAVIGNE, Bruno	08/05/2006	26/08/2009	08/05/2026	1855399
FR	Method of operating and optimising a WDM transmission system amd computer program product	ANTONA, Jean-Christophe; LAVIGNE, Bruno	08/05/2006	26/08/2009	08/05/2026	1855399

+ 7 filed applications

Nouveaux outils pour l'estimation de la qualité de transmission et l'optimisation de réseaux optiques modulés à 10, 40 et 100Gb/s

RESUME : Ces dernières décennies, la fibre optique est devenue le support privilégié pour transporter des données numériques sur des distances allant de quelques kilomètres à une dizaine de milliers de kilomètres. Les systèmes de transmissions optiques de recherche autant que commerciaux offrent aujourd'hui des capacités de transport multi-Térabit/s sur plus de 1000km pour répondre à l'augmentation vertigineuse du trafic de données, et sont basés sur l'utilisation en parallèle de canaux modulés à 10, 40 ou 100Gb/s. Pour autant, la conception efficace de tels systèmes ou de réseaux optiques à capacité toujours plus grande et à coût maitrisé n'est pas chose aisée : cette activité requiert une fine connaissance de l'interaction entre de multiples effets physiques linéaires et non-linéaires et de leur impact sur la propagation de signaux optiques modulés. En outre, l'infrastructure d'un réseau optique terrestre est généralement fortement hétérogène en raison de contraintes géographiques ou topologiques, ou du besoin de réutiliser les infrastructures préexistantes. Enfin, cette étape de conception doit tenir compte du caractère partiel de la connaissance des paramètres physiques de l'infrastructure déployée. Pour maîtriser une telle complexité en un temps raisonnable et acquérir une vision globale du système, il est indispensable de s'appuyer sur des outils issus de la physique et de l'observation. Dans cette optique, ce manuscrit s'appuie sur des études menées entre 2000 et 2010 pour comprendre et quantifier l'accumulation des effets non-linéaires de type Kerr sur les systèmes de transmission modulés à 10, 40 et 100Gb/s. Nous introduisons ici de nouveaux outils permettant de prédire rapidement et avec précision la qualité de transmission de réseaux optiques terrestres hétérogènes affectés par de multiples effets de propagation ainsi que des outils permettant d'optimiser le réglage de la ligne de transmission (gestion de la dispersion, réglage des amplificateurs optiques).

Mots clés : réseaux optiques WDM, effet Kerr, 10Gb/s, 40Gb/s, 100Gb/s, détection cohérente

Novel design tools enabling to predict the quality of transmission and to design optical networks modulated at 10, 40 and 100Gb/s

ABSTRACT : Over the last few decades, optical fibre has become the preferred medium for conveying data across cities, regions, nations, continents, oceans. Laboratory but also commercial Wavelength-Division Multiplexed systems offer multi-Terabit/s capacity based on 10, 40 or even 100Gb/s-modulated channels propagating at different wavelengths over more than a thousand kilometres in order to cope with the increase of the data traffic. Yet, an efficient design of high speed optical transmission systems or optical networks at lowest cost with ever increased throughput or reach is a big challenge. It requires a very subtle knowledge of the interplay of multiple linear and nonlinear physical phenomena. Besides, the infrastructure of optical networks is highly heterogeneous with a high impact of legacy systems. Eventually, when building a novel network or upgrading a network, the system designer has only a partial knowledge of the physical features of the deployed infrastructure. To master such complexity in a reasonable time scale, the design and the expected physical performance of transmission systems generally strongly rely on tools derived from physics laws and observations. This manuscript particularly addresses such issues: based on studies conducted over the years 2000 to 2010 to understand and quantify the accumulation of Kerr nonlinearities in transmission systems with bit-rates ranging from 10 to 100Gb/s, we introduce novel tools that aim to rapidly and accurately predict the quality of transmission of heterogeneous terrestrial optical networks impacted by multiple propagation effects and to help optimizing the system design such as the setting of optical amplifiers or dispersion management over the links.

Keywords : optical networks, WDM, Kerr effect, 10Gb/s, 40Gb/s, 100Gb/s, coherent detection

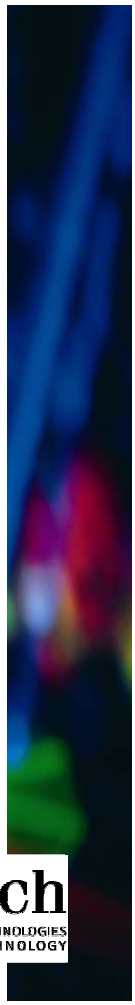

TELECOM ParisTech

ParisTech
INSTITUT DES SCIENCES ET TECHNOLOGIES
PARIS INSTITUTE OF TECHNOLOGY